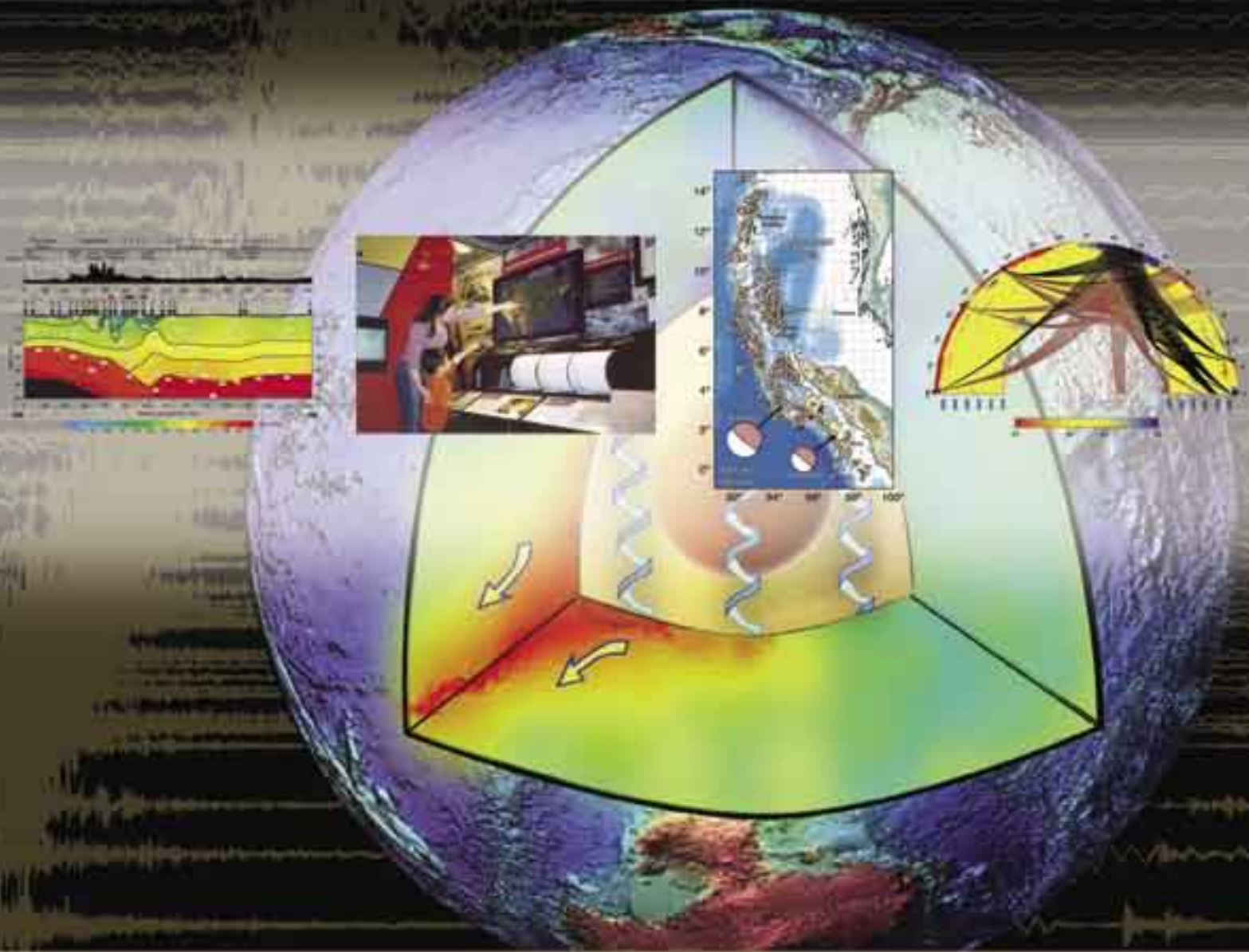




IRIS

Cornerstone Facilities for Seismology and Earth Sciences



About the Cover

From the innermost inner core, which influences the evolution of the magnetic field that protects us from cosmic radiation, to the outermost crust, from which we extract resources and where we build foundations for our structures, the cover illustrates recent discoveries about the solid Earth that are enabled by IRIS facilities.

Velocity Profile: A two-dimensional P-wave velocity model running from southern Austria across eastern Slovakia and Poland and into Belarus based on data from the Central European Lithosphere Experiment Based on Refraction (CELEBRATION 2000). CELEBRATION is one of a series of seismic refraction experiments conducted between 1997 and 2003 that were possible only with international cooperation in logistics and data openness that is unprecedented for geophysical field experiments of this type. Together these experiments constitute a network of seismic profiles from Lithuania to Austria. The results have provided new information to resolve questions about mountain building and large-scale crustal deformation that geologists have been studying since the 18th century. (Source: Grad, M, A. Gutereh, G.R. Keller, T. Janik, E. Hegedus, J. Vozár, A. Ślaczka, T. Tiira, J. Yliniemi, and CELEBRATION 2000 Working Group, Lithospheric structure beneath trans-Carpathian transect from Precambrian platform to Pannonian basin - CELEBRATION 2000 seismic profile CEL05, *J. Geophys. Res.*, submitted, 2005).

Museum Visitors: The IRIS museum display at the Smithsonian Institution's Museum of Natural History captivates audiences of all ages and interests. (Courtesy of Jason Mallett.)

About this Proposal

This proposal was produced by the IRIS Planning Committee and IRIS staff members on behalf of the IRIS Board of Directors, who represent the full membership of the Consortium, and thus the collective scientific interests of 102 research institutions. The proposal consists of two volumes, including the Project Description, Budget and Program Descriptions in volume 1 and the Review of Accomplishments in volume 2.

The Project Description includes an overview of the IRIS Consortium and facilities, the role of IRIS in supporting research and education, a description of our resource needs, and a brief outline of our five-year funding request.

The Budget is an explication of our estimates of costs to carry out the activities that are summarized in the Project Description and detailed in the Program Descriptions.

Map of Sumatra-Andaman: Aftershocks for the December 26, 2004 M_w 9.3 thrust, including the, M_w 8.6 thrust on March 28, 2005, show the extraordinary extent of the rupture zone. As the largest earthquake by far, since high-dynamic range, broadband seismometers began to become widespread in the 1980s, this event suggested new analysis methods for rapidly determining the disaster potential of an earthquake, provided new insights about rupture dynamics and tsunami generation, and resulted in unprecedented free oscillation records for studying Earth's deep structure. (Reprinted with permission from Lay, T., H. Kanamori, C. J. Ammon, M. Nettles, S. N. Ward, R. C. Aster, S. L. Beck, S. L. Bilek, M. R. Brudzinaki, R. Butler, H. R. DeShon, G. Ekström, K. Satake and S. Sipkin, The Great Sumatra-Andaman earthquake of 26 December 2004, *Science*, 308, 1127-1133. Copyright 2004 AAAS.)

Ray Paths: Seismic waves from widely distributed source regions sample the deep mantle en route to the Kaapvaal, Tanzania, and Ethiopia/Kenya PASSCAL experiments. Those ray paths shown in red exhibit travel time delays that could not be accounted for with even the best global tomography models from before the time of the experiment, and thus are the basis for discovering the "Africa anomaly," an extraordinary low-velocity region extending 1300 km up from the core-mantle boundary. The thickness, sharp edges, and magnitude of the velocity anomaly show that a reasonable understanding of mantle convection requires consideration of compositional as well as thermal variability. (Source: Wang, Y. and L. Wen, Geometry and P- and S- velocity structures of the "African anomaly," *J. Geophys. Res.*, submitted, 2005).

The Program Descriptions are synopses of the core IRIS facilities and the programs that operate them. Each synopsis includes an overview of the development and evolution of the facility and a detailed description of plans and resources requested for the IRIS program.

The Review of Accomplishments is comprised principally of more than 200 one-page vignettes contributed by the research community that have been enabled by IRIS, in most cases through use of one or more of the core IRIS facilities.

Cornerstone Facilities for Seismology and Earth Sciences

The IRIS Proposal

July 1, 2006 – June 30, 2011

Submitted to
National Science Foundation
Division of Earth Sciences
Instrumentation and Facilities Program

By
Incorporated Research Institutions for Seismology
1200 New York Avenue, NW, Suite 800
Washington, D.C. 20005

On behalf of
Board of Directors
and 102 Member Research Institutions
of the IRIS Consortium

August 2005

Board of Directors

Thorne Lay (Chair) University of California, Santa Cruz
Thomas Owens (Vice Chair)..... University of South Carolina
Andrew Nyblade (Secretary) Pennsylvania State University
Gregory Beroza Stanford University
Karen Fischer Brown University
Arthur Lerner-Lam..... Columbia University
Kate Miller University of Texas at El Paso
David Okaya University of Southern California
Brian Stump Southern Methodist University

Planning Committee

Arthur Lerner-Lam (Chair) Columbia University
Göran Ekström Harvard University
Alan Levander Rice University
Thorne Lay University of California, Santa Cruz
Anne Meltzer Lehigh University
Barbara Romanowicz University of California, Berkeley
Michael Wyssession Washington University in St. Louis
David Simpson IRIS
Raymond Willemann IRIS

Standing Committee Chairs

Jeffrey Park GSN Yale University
David James PASSCAL Carnegie Institution of Washington
Guust Nolet DMS Princeton University
Richard Aster E&O New Mexico Institute of Mining and Technology

Senior Staff

David Simpson President
Raymond Willemann Director of Planning
Shane Ingate Director of Operations
Candy Shin Director of Finance & Administration
Rhett Butler GSN Program Manager
James Fowler PASSCAL Program Manager
Timothy Ahern DMS Program Manager
John Taber E&O Program Manager

Contents

Introduction.....	1
SEISMIC SUMMARIES	
Earthquake Seismology and IRIS	4
The Continental Lithosphere and Seismology.....	6
Subduction and Seismology	8
Investigating Earth's Dynamic Mantle and Core	10
IRIS Education and Outreach.....	12
EARTHQUAKES	
Long-period Global Detection and Location of Earthquakes Using the GSN	15
The Great Sumatra-Andaman Earthquake of 26 December 2004	16
Rupture Process of the 2004 Sumatra-Andaman Earthquake	17
Imaging the Rupture Process of the 2004 Sumatra-Andaman Earthquake Using Deconvolved Surface Wave Source Time Functions	18
Ultra-long-period Characteristics of the December 2004 Sumatra Earthquake	19
IRIS Data Allowed Rapid Public Information About Sumatra Earthquake and Tsunami.....	20
Multiple Source Analysis of the 2004 Sumatra Earthquake	21
Global Seismographic Network Recording of the Sumatra-Andaman Earthquake.....	22
Rapid Imaging of Large Earthquake Rupture Zones with P waves: Application to the 28 March 2005 Sumatra Mw 8.7 Earthquake Suggests Bilateral Rupture	23
Regional Monitoring of the Aftershock Sequence of the 2002 M 7.9 Denali Fault, Alaska, Earthquake	24
The 2003 Mid-Indian Ocean Earthquake: An Unusual Earthquake in Oceanic Lithosphere	25
Relocations and Focal Mechanisms Determined from Waveform Cross-Correlation of Seismic Data from the Nicoya Peninsula, Costa Rica	26
Seismogenic Zone Processes at the Costa Rica Convergent Margin	27
Aftershock Study of the Subduction to Strike-Slip Transition of the North American-Caribbean Plate Boundary in the Dominican Republic.....	28
Exploring Subduction Zone Earthquake Rupture ...	29
Observational Constraints on the Fracture Energy of Subduction Zone Earthquakes	30
Remote Triggering of Deep Earthquakes: Insight from the 2002 Tonga Sequences	31
Coupled Seismic Slip on Adjacent Oceanic Transform Faults.....	32
The Use of Waveform Shapes to Automatically Determine Earthquake Focal Depth.....	33
MONITORING OTHER SEISMIC SOURCES	
Broadband Recording of the First Historical Eruption of Anatahan Volcano, Mariana Islands	34
Use of Multiple Small Aperture Arrays to Study Deep Subduction-Related Tremor in Cascadia	35
Excitation of Earth's Incessant Free Oscillations by Atmosphere-Ocean-Sea-floor Coupling	36
Kinematic Modeling and Complete Moment Tensor Analysis of the Anomalous, Vertical CLVD Bardarbunga, Iceland, Event.....	37
Ambient Earth Noise: A survey of the Global Seismographic Network	38
A Real-time Seismic Noise Analysis System for Monitoring Data Quality and Station Performance	39
Four Anomalous Episodes in the Late 2003 Microseism Band Offshore Southern California	40
Ambient Seismic Noise Monitoring in North-Central Illinois	41
Strong Directivity of Ocean-Generated Seismic Noise	42
Glacial and Climate Controls on Tide-Water Glacier Calving Dynamics:A PASSCAL Seismic Experiment on the Columbia Glacier, Southeast Alaska	43
Mid-Ocean-Bottom and Land-based Microseism Correlations	44
Ocean Drilling at the Hawaii-2 Observatory (H2O) ..	45
Nanoearthquakes at H2O.....	46
The May 18, 1998, Indian Nuclear Test Seismograms at Station NIL	47

Transfer Functions and Seismic Discrimination: a KNET Case Study	48
Lg-Wave Cross Correlation and Double-Difference Location.....	49
Strong LG Attenuation in Tibet.....	50
Repeating Seismic Events in China	51
A Comprehensive Database for Mining Explosion Discrimination	52
Intermediate Period Surface Waves from Mining Explosions.....	53
Source Scaling of Single Fired Mining Explosions with Different Confinement and Explosive Size at a Copper Mine in Arizona.....	54
SIGNALS AND SYSTEMS	
Quality Control of GSN Sensor Response Information.....	55
GSN Station Operator Training	56
Data Requirements from Low-Frequency Seismology and the Dearth of STS-1 Sensors.....	57
Development of a New Broadband Optical Seismometer	58
Earthquake and Ambient Vibration Monitoring of the 17-Story Steel Frame UCLA Factor Building	59
Passive Crustal Refraction Experiments Using IRIS/PASSCAL Facilities:New Surveys Show Variable Crustal Thickness in the Western Great Basin	60
Signal Restoration Through Deconvolution Applied to Deep Mantle Seismic Probes	61
The Mantle Magnitude Mm and the Slowness Parameter Q: Five Years of Real-time Use in the Context of Tsunami Warning	62
SAC Availability for the IRIS Community	63
ISC On-line Bulletin and IRIS DMC Waveform Retrieval	64
Web Services at the IRIS DMC	65
The Uniform Product Distribution System	66
SURFACE OF THE EARTH: NORTH AMERICA	
The North American Upper Mantle: Density, Composition, and Evolution.....	67
Tomography of the North American Upper Mantle Using Global and Regional Datasets	68
High-Resolution 3D Anisotropic Structure of the North American Upper Mantle from Inversion of Body and Surface Waveform Data	69
High-Resolution Surface Wave Tomography From Ambient Seismic Noise	70
Imaging the Fine Structure of the San Andreas Fault at Seismogenic Depths Using an Archived PASSCAL Dataset	71
A Multi-Institutional, Multi-Disciplinary, Multi-Facility Experiment in Garner Valley, CA.....	72
Brittle-Ductile Interactions in California.....	73
Steep-Dip Seismic Imaging of the Shallow San Andreas Fault Near Parkfield	74
Foundering Lithosphere Imaged Beneath the Southern Sierra Nevada, California, USA	75
Using Marine Seismic Data to Investigate Active Plate Boundary Deformation: The California Continental Borderland and the Marmara Sea.....	76
CANOE: A Broadband Array in Northwestern Canada	77
A Refraction/Reflection/Teleseismic Survey of the Northwestern Basin and Range Transition Zone	78
Passive Shallow Seismic Experiments Using IRIS/PASSCAL Facilities: Shear-Velocity Assessments at Over 300 Urban Sites.....	79
Lithospheric Structure of the Rio Grande Rift	80
A Simple Approach for the Joint Tomographic Inversion of Seismic Body and Surface Waves.....	81
Upper-Crustal Structure in SE Arizona from P and Rg Phases Generated by Explosions	82
Probing the Structure and Evolution of the Rocky Mountains	83
Modern Basalt Extraction Structures in the Southern Rocky Mountains: Multi-band Images from the Jemez Lineament	84
Crustal Structure of the Basin and Range, Colorado Plateau, Rocky Mountains, and Great Plains.....	85
Investigating Crust and Mantle Structure with the Florida-to-Edmonton Broadband Array	86
Numerical Analysis of Overpressure Development in the New Madrid Seismic Zone	87
Imaging the Earth With Dense Arrays of Broadband Seismometers.....	88
Imaging Upper Mantle Structure Beneath the Illinois Basin	89

A Surface-Wave Analysis of Seismic Anisotropy Beneath Eastern North America	90
Scattered Wave Imaging of a Sharp Lithosphere-Asthenosphere Boundary Beneath Eastern North America	91
Subduction Potential at the Eastern Margin of North America	92
SURFACE OF THE EARTH: GLOBAL STUDIES	
BOLIVAR & GEODINOS: The SE Caribbean Continental Dynamics Project	93
The Reflections Under the Scottish Highlands (RUSH) EXPERIMENT: Mapping Fine-Scale Heterogeneities within the Continental Mantle Lithosphere Beneath Scotland, Combining Active- and Passive-Source Seismology	94
(quasi)-Love Found in Tuscany: US-European Seismic Array in Italy Catches the Big Wave	95
PASSCAL Experiments in Central Europe Target Lithospheric Structure	96
Origin and Tectonic Evolution of Active Continental Lithospheric Delamination in the Vrancea Zone, Romania: Project DRACULA	97
The Eastern Turkey Seismic Experiment: The Study of a Young Continent-Continent Collision	98
Systematic High-Resolution Imaging of the Karadere-Düzce Branch of the North Anatolian Fault	99
Tectonic Structure and Surface Wave Dispersion in Eurasia and North Africa	100
Upper Mantle Q and Thermal Structure Beneath Tanzania, East Africa from Teleseismic P Wave Spectra	101
Structure and Evolution of the Main Ethiopian Rift	102
The Upper Mantle P Wave Structure Beneath Ethiopia and Kenya	103
Crustal Structure Beneath Ethiopia and Kenya: Implications for Rift Development in Eastern Africa	104
Small-Scale Variations in Seismic Anisotropy Near Kimberley, South Africa	105
Xenolith Constraints on Seismic Velocities in the Upper Mantle Beneath Southern Africa	106
S-Wave Velocity Structure Beneath the KAAPVAAL Craton	107
Kyrgyz Seismic Network KNET: Application of KNET Data in Scientific Researches	108
Characterizing Crustal Deformation in the North Tien Shan Using Geodetic and KNET Seismic Data	109
High-Resolution Surface Wave Slowness Tomography in Central Asia	110
Seismic Imaging of the Himalayan Collision Zone	111
Receiver Function Imaging of the Eastern Syntaxis of Tibet	112
Shear-Wave Splitting Beneath the Eastern Syntaxis Tibetan Experiment	113
Structure and Deformation of the Tibetan Lithosphere	114
Lithospheric Deformation within a Continental Strike-Slip Fault Zone: Marlborough Fault System, South Island, New Zealand	115
Seismically Imaging the East Antarctica/West Antarctica Boundary with TAMSEIS	116
Upper Mantle Velocity Structure Beneath the TAMSEIS Network, Antarctica	117
Cooling History of the Pacific Lithosphere: Evidence for Thermal Boundary Layer Instabilities and Dislocation Creep	118
Advances in Active-Source Seismic Imaging Using Traveltime and Waveform Tomography	119
High-Resolution Waveform Tomography at a Ground Water Contamination Site	120
Hunting for Ocean Island Moho: The Snipe Bites Back	121
UPWELLING AND DOWNWELLING	
Seismic Hazards Investigations in Puget Sound (SHIPS): I	122
Seismic Hazards Investigations in Puget Sound (SHIPS): II	123
Subduction-Zone Anisotropy Beneath Corvallis, Oregon: A Serpentinite Skidmark of Trench-Parallel Terrane Migration?	124
Imaging Subduction Beneath Alaska: Results From BEAAR	125
The TUCAN Broadband Seismic Experiment: Imaging the Central America Subduction Factory	126
Receiver Function Analysis of the Nicoya Peninsula, Costa Rica	127
Crustal and Upper Mantle Structure in the Flat Slab Region of Central Chile and Argentina	128
Imaging Shallow Subduction Zones With Surface Waves	129
Detailed Structure and Sharpness of Upper Mantle Discontinuities in The Tonga Subduction Zone	130
Evidence of Mid-Mantle Deformation From Shear-Wave Splitting	131
Seismic Anisotropy in the Izu-Bonin Subduction System	132
Finite Difference Synthetic Test for Kirchhoff Migration of Receiver Function on Subducting Slab	133

Observations of Shear Wave Birefringence in Subduction Zones: A Guide to Mantle Flow?	134
Deep Plumes in the Earth's Mantle	135
Plume Heat Flux Estimates	136
Detection of Upper Mantle Flow Associated with the African Superplume	137
Structural Features and Velocity Structures of the "African Anomaly"	138
Seismic Evidence for Hotspot-Induced Buoyant Flow Beneath the Reykjanes Ridge	139
Imaging Seismic Velocity Structure Beneath the Iceland Hotspot – A Finite-Frequency Approach	140
Crustal and Uppermost Mantle Structure Beneath Iceland from Local Earthquake Tomography	141
The Origin of Hotspot Volcanism in the Pacific Northwest	142
Shear Wave Splitting in the Great Basin Solves the Elevation Problem: It Was a Simple Plume-like Upwelling All Along	143
Collaborative Research: Geodynamics of the Yellowstone Hotspot Constrained by Seismic and GPS Imaging	144

GLOBAL MANTLE STRUCTURE

A Three-Dimensional Radially-Anisotropic Model of Shear Velocity in the Whole Mantle	145
Global Anisotropy and the Thickness of Continents	146
Imaging the Anisotropic Shear-wave Velocity Structure of the Earth's Mantle	147
Global Analysis of Upper Mantle Anisotropy Using Automated SKS Splitting Measurements	148
Investigating Attenuation and Velocity Structure from Surface-Wave Amplitudes	149
Global Tomographic Model of Q in the Upper Mantle Obtained Using Long-period Waveform Data	150
Compressional-Wave Studies on the Frequency Dependence of and Lateral Variations in Mantle Attenuation	151
Using IRIS Digital Data to Determine the Radial Attenuation Structure of the Lower Mantle	152
Whole-Mantle 3D Seismic Attenuation: Evidence for Global Mass Flux	153
New Measurements of Radial Mode Eigenfrequencies	154
The Global Short-Period Wavefield Modeled with a Monte Carlo Seismic Phonon Method	155
Discovery of Strong Upper Mantle Reflectors From Back-Scattering of Near-Podal PKPPKP Waves Using Data Acquired From IRIS	156
SH Velocity and Compositional Models Near the 660-km Discontinuity Beneath South America	157
Seismic Evidence for Accumulated Oceanic Crust Above the 660-km Discontinuity Beneath Southern Africa	158
Seismic Investigation of Upper and Lower Mantle Boundary Layering	159
Study of Earth's Layered Structure on a Global Scale Using Broadband Seismic Datasets	160
Probing the Earth's Interior by Stacking Stacked Short-Period Seismic Array Data	161

CORE-MANTLE BOUNDARY

Finite-Frequency Tomography of D" Shear Velocity Heterogeneity Beneath the Caribbean	162
A Seismological Determination of the Temperature Gradient in D" Beneath the Western Pacific	163
Sharp Lateral Boundaries in the D" Region	164
D" Shear Velocity Heterogeneity, Anisotropy, and Discontinuity Structure Beneath the Caribbean	165
Using Array Methods to Investigate Possible Causes for PKP Deviations	166
Lateral Variation of the D" Discontinuity Beneath the Pacific	167
Lateral Variation of the D" Discontinuity Beneath the COCOS Plate	168
Migration of the Lowermost Mantle Structure Under the COCOS	169
Lateral Variation of P- and S-Wave Velocity Discontinuities in the Lower Mantle Beneath the Cocos Plate	170
Observation of P-Wave Velocity Discontinuities in D" Beneath Southeast Asia Using Migration Techniques	171
A Step in the D" Discontinuity Imaged by Kirchoff Migration Through 3D Tomographic Models	172
Lowermost Mantle Anisotropy Beneath the Central Pacific	173
D" Anisotropy From Lamellae and Transverse Isotropy	174
Azimuthal Anisotropy in the D" Layer Beneath the Caribbean Sea	175
Isotropy or Weak Vertical Transverse Isotropy in D" Under the Atlantic	176
A Strong Lateral Shear Velocity Gradient and Anisotropy Heterogeneity in the Lowermost Mantle Beneath the Southern Pacific	177
Detection of an Ultralow Velocity Zone at the CMB Using Diffracted PKKPab Waves	178
Examining the Base of the Mantle Using IRIS FLED PASSCAL Data	179

INNER CORE

An Observation of PKJKP: Inferences on Inner Core Shear Properties	180
Constraints on Density and Shear Velocity Contrasts at the Inner Core Boundary	181
Waveform Search for the Innermost Inner core	182
Near-Podal Observations of PKPPKP Waves and Implications for Central Inner Core Structure	183
Non-linear Waveform and Delay Time Analysis of Triplicated Core Phases: A New Method to Extract Differential Travel Times From Interfering Data	184
Velocity and Attenuation in the Earth's Inner Core	185
Anisotropy of the Inner Core	186
Slowness Anomalies of PKP Phases Recorded in Alaska: Implications for Inner Core Anisotropy	187
Transition From Isotropic Upper Inner Core to Anisotropic Lower Inner Core: The Importance of Anisotropic Ray Tracing	188
Inner Core Anisotropy From PKP Travel Times at Near Antipodal Distances	189
Hemisphericity and Regional Seismic Anisotropy in the Top 80 km of the Earth's Inner Core	190
Uppermost Inner Core Attenuation From PKP Data Observed at Some South American Seismological Stations.....	191
Hemispherical Transition of Seismic Attenuation at the Top of the Earth's Inner Core	192
Differential Inner Core Superrotation From Earthquakes in Alaska Recorded at South Pole Station	193
Support for Inner Core Super-Rotation from High-Quality Waveform Doublets	194
The Earth's Free Oscillations and the Differential Rotation of the Inner Core.....	195

EDUCATION AND OUTREACH

The U.S. Educational Seismology Network.....	196
IRIS and Geological Society of America	197
Global Seismicity Monitor as an Interactive Museum Display	198
IRIS/USGS Seismology Displays at the American Museum of Natural History, New York.....	199
Experiences with the IRIS E&O Lecture	200
A Real-Time Interactive Educational Seismology Exhibit	201
A Suite of Educational Computer Programs for Seismology	202
Educational Seismograph Teaching Modules	203
The Global Earthquake Explorer: A Versatile Tool for Science Education	204
The Use of IRIS Instrumentation in Undergraduate Education.....	205
Seismic Reflection Processing Workshop	206
IRIS and PASSCAL INTERN.....	207
Seismology Education Programs at the University of Portland.....	208
Influence of IRIS on the Construction of a College-Level Seismology Course.....	209
Collaborative Teacher Workshops at the Visualization Center at Scripps Institution of Oceanography (San Diego) ...	210
Project SLAM: A Flexible Field Seismology and Earthquake Studies Teaching Module.....	211
The Boston College Educational Seismology Project: Inviting Students Into the World of Science Research.....	212
Seismographs in Schools.....	213
Earth and Space Science Professional Development Project.....	214
The IRIS Education Program in Support of the National Earth Science Teachers Association.....	215
Impact of a School Seismograph on a Rural Illinois Middle School: Bringing Real Time Recordings Into the Classroom	216
Seismographs in Schools: Shaking Things Up in the 5th Grade	217

Introduction

Michael Wyession • *Washington University*

The scope of research facilitated by IRIS is truly remarkable. This section of the proposal provides an exciting scientific exercise: the assembly of a sample of the broad variety of topics directly influenced and enabled by IRIS facilities. As you look through the following “1-pagers,” observe not only the enormous progress that has been achieved in addressing many long-standing questions in geophysics, but also the large number of new areas of research that have begun since this exercise was last carried out five years ago. A few words of explanation are appropriate here. The 1-pagers have been divided up into several categories for the convenience of handling the more-than-200 entries. However, this categorization is arbitrary: many of the 1-pagers could easily be placed into several different categories, and there are many different choices of categories that could have been used. In addition, a set of five “2-pager” essays are included in order to provide some context for under-

□

Earthquakes

The value and importance of IRIS was never better demonstrated than with the success in recording and disseminating high-quality data from the Sumatra-Andaman earthquake of December, 2004. This earthquake and the devastating tsunami it caused captured the whole world’s full attention. The rapid availability of GSN data demonstrated to world governments that a real-time tsunami warning system could have saved more than a hundred-thousand human lives, and is providing the basis and justification for new tsunami warning systems in both the Indian and Atlantic Oceans. A fundamental part of IRIS-facilitated research will continue to focus on earthquakes and understanding the rupture process. This is important, not only for providing the best advice for earthquake hazard mitigation efforts, but also for addressing fundamental questions concerning seismotectonics, crustal deformation, and the state and composition of the lithosphere.

Monitoring Other Seismic Sources

Lots of things make waves. An increasing number of studies are using IRIS data to examine sources that generate seismic energy other than earthquakes. An important part of this has been the ongoing efforts to improve our ability to monitor nuclear tests and other man-made explosions. The reasons include the political, making sure that there are no clandestine nuclear tests, and the forensic, trying to understand the causes of an accidental explosion. Scientifically, however, IRIS data have allowed for significant new discoveries in the interpretation of seismic signals that have traditionally been considered “noise.” The continuous low-level excitation of normal modes is now being analyzed in terms of interactions between the atmosphere, oceans, and solid earth. Array data are now being used to understand the connection between ocean storms and the ubiquitous microseismic noise. In volcanic regions, a new form of seismic tremor is being studied, and unusual CLVD sources may be related to caldera collapse. In glacial regions, PASSCAL experiments are examining the dynamics of glacial calving and of the seafloor scraping of giant ice sheets. There are now whole new areas of interdisciplinary research being pursued with IRIS data.

Signals and Systems

For research to be done and for the public (and that includes governments!) to remain informed, it is vital for seismic signals to be generated, transmitted, processed, archived, retrieved, analyzed, interpreted, and the lessons learned distributed in efficient and standardized means. IRIS has, and will continue to play the leading role in the oversight of these activities for the field of seismology. This means that IRIS is involved in discussions on the creation of the next generation of seismometers. IRIS has been at the forefront of bringing satellite communications to many parts of the world in order to provide reliable real-time access to seismograms. IRIS is at the technological vanguard in the area of database management and web services in order to provide scientists with instant and user-friendly access to a huge amount of data. And through the E&O, IRIS is increasingly involved in distributing the scientifically, socially, and politically important information that has been obtained from the seismic data.

Surface of the Earth: North America

“North American” seismology is at a very exciting point in time, gearing up for the deployment of the USArray component of EarthScope, which will rectify the long-standing lack in sufficient seismic coverage for most of the U.S. Several excellent recent PASSCAL experiments have made preliminary investigations of the lithosphere of North America, and as

is typical for a new area of research, have raised more questions than given answers. IRIS is providing and will continue to provide the guiding hand for USArray, and the data from this project will provide an important basis for addressing questions like the structure of fault systems, the current state of stress of the North American lithosphere, the composition and layer-

□

slab in the formation of the western U.S., the reasons that North America is moving westward, the connection between deep tectosphere structure and crustal geology, and the assessment of seismic hazards.

Surface of the Earth: Global Studies

There are as many 1-pagers studying the lithosphere outside of the U.S. as there are studying areas within it. This is a remarkable feat, given that funding for PASSCAL experiments goes to PIs who reside at universities within the U.S. Seismology is one of the most successfully international sciences, and this is a very important direction for IRIS to continue. IRIS PASSCAL research over the past 5 years has spanned all of the continents, including Alaska, and has addressed important

□

these experiments have forged important scientific and educational bonds between scientists of many different countries, to every country's benefit. IRIS is also playing an increasingly important role in the establishment of IRIS-like programs in other countries, sharing the technical and scientific knowledge that has been gained. One very important direction for continental studies has been in the use of telemetered arrays, such as in South Africa, where data are recorded and monitored for quality in a real-time mode, and this will likely see a greatly expanded use over the next several years.

Upwelling and Downwelling

Plate tectonics is the surface expression of mantle dynamics, and seismology is addressing the nature of vertical mass flow in several important directions. Because so many earthquakes occur within subduction zones, great advances are being made in using migrated array data to image the structures of plate collisions, increasing our understanding of water cycles, mineral phase changes, mantle flow, and magma generation in these regions. We are still missing a complete explanation for deep earthquakes, however, as rupture seems to occur outside of the cold wedge of the subducted plate. While seismic tomography has shown unequivocally that subducted lithosphere then proceeds to sink into the lower mantle, the question of how mass is returned to the upper mantle is still very actively debated, and the nature and ubiquity of hotspot mantle plumes is currently a topic for much discussion. Imaging mantle plumes is a challenge for seismology, due to a lack of seismic sources in most of these regions and to the process of waveform annealing through low-velocity regions. However, more creative ways of using the seismic wave field (e.g., finite-frequency sensitivity kernels, attenuation, anisotropic splitting for flow directions) have begun to allow for the identification of regions of upward flow between the lower and upper mantles, and these techniques will play an increasingly important part within future seismic analyses of mantle convection.

Global Mantle Structures

Whole-mantle seismic tomography is more than 20 years old, and for most of it the studies involved two elastic parameters. Current global studies are now quantifying the degree to which the mantle is neither isotropic nor elastic. This can be seen in the large number of 1-pagers in this section that involve either anisotropy or attenuation (and in some cases, both!). The mantle is now viewed not as a static onion-like layered spherical shell, but as a fluid, mobile body. Mantle discontinuities are

□
attenuation and anisotropy are being interpreted as indicators of mantle flow. For many years, seismic tomography provided us with a scalar field of three-dimensional variations in elastic parameters. Currently, however, the diversity of seismic techniques is moving toward providing all of Earth sciences with a vector field of mass flow, and therefore significant clues as to the history and evolution of plate tectonics.

Core Mantle Boundary Region

The very base of the mantle continues to be a remarkably rich area for seismological discovery, with a variety of structures and textures varying significantly over short distances. As such, seismologists are taking advantage of the close station spacing of PASSCAL arrays and regional networks in order to quantify these variations, and significant advances are being made using array migration techniques. It seems to be the case that we observe lateral variations at spatial scales as fine as we are able to resolve, reinforcing our idea that the core-mantle boundary is a thermal and chemical boundary layer that rivals

the surface in complexity. Perceptions of this region were greatly altered by the recent mineral physics discovery of the transformation of perovskite to a higher-pressure phase, leading to the possibility of a means of detecting lateral temperature variations and the strength of the thermal boundary layer. Another area of recent interest is the giant megaplume of seismically-slow rock that extends upward from the core beneath Africa, and many efforts are underway to interpret this in terms of mantle dynamics.

Inner Core

At 7/10 of one percent of the volume of the earth, the inner core attracts more than its fair share of attention because of its unusual nature. In spite of the remarkable challenge of viewing this small, frozen ball of iron across two passes through a very heterogeneous mantle, some very unusual results are emerging. The inner core has long been thought to be anisotropic, with an axis-parallel fast direction, but it now seems that this anisotropy may only occur in the eastern hemisphere, and below an isotropic layer at the inner core boundary. The means by which such hemisphere-scale variation could occur is still unclear, especially if conclusions about the inner core's super-rotation are correct. The big challenge for inner core studies

□ distance requirements of PKP waves and the surface distribution of earthquakes and continents. With an increase in global station coverage, particularly in places like Antarctica, there will be significant advances in our understanding of the inner core in the near future.

Education and Outreach

We live in a challenging time for science education. The incredible expansion of media information provides many distractions and sources of competition for people's attention, particularly that of the students we would most like to reach. Science used to be able to rest upon the laurels of its inherent "coolness," but now realizes that it must communicate to the

□ intellectualism that includes an anti-scientific attitude, tied to the focused agendas of certain political and religious interests. As the E&O 1-pagers show, IRIS is meeting these challenges across a wide variety of fronts, often taking advantage of the very technologies that can also be distractions. IRIS is involved with educating students, teachers, and the general public through web-based programs and services, museum displays, lectureships, video formats, teacher training workshops, school programs, teaching materials, curriculum development, and textbooks. Earthquakes are, and always will be, inherently "cool," but the IRIS E&O program is making sure in a wide variety of ways that everybody knows this.

Earthquake Seismology and IRIS

Göran Ekström • *Harvard University*

Earthquake seismology is a broad and diverse field, encompassing both abstract and theoretical work, as well as directly-applied investigations related to earthquake hazards. In between this range lies the broad spectrum of observational earthquake seismology that is focused on the characterization of seismic sources and their interpretation in terms of tectonic and other geophysical processes. IRIS facilities were designed and developed by the academic community that represents this latter field of intellectual inquiry. The impact of IRIS has also been, and will continue to be, significant for the broader scientific field represented by physicists, mathematicians, engineers, and social scientists.

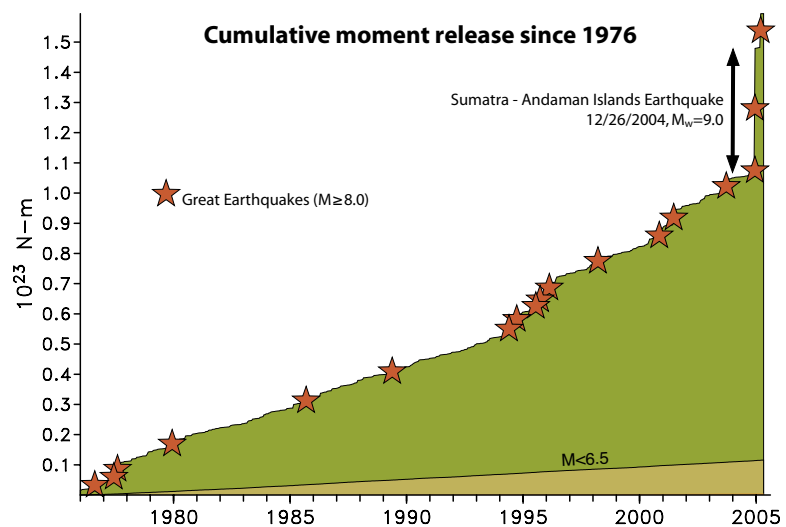
To a large extent, the broader impact that data and observations from IRIS facilities have made stems from the high level of our ignorance. We are still far from reaching a comprehensive understanding of earthquakes based on first principles, and have little opportunity to perform controlled experiments that can isolate the specific physical conditions that control their occurrence. Observations from individual earthquakes are therefore essential for constraining theoretical models, both of the earthquake phenomenon and of the relationships to geophysical processes such as tectonism and volcanism. Similarly, experiences learned from individual earthquakes are still essential for understanding and mitigating their societal effects.

The importance of individual events for furthering our understanding is characteristic for our science, and this is one context in which the value of IRIS facilities can be evaluated. The unpredictability of the events that we wish to study makes targeted hypothesis testing difficult. For example, while many important earthquake-science results come from PASSCAL deployments, motivated by specific scientific questions, other discoveries and unique observations obtained with IRIS instrumentation come as the indirect result of the existing observational infrastructure. The last several years have provided several examples of unanticipated observations that provide added justification for the significant investments in IRIS facilities.

The quality and value of IRIS facilities and the data they produce were demonstrated by the recording of the M_w 9.0 Sumatra-Andaman earthquake of December 26, 2004, and the earthquake sequence that followed. The ability to record an earthquake of this size on-scale and with high fidelity was one of the goals specified when the GSN was designed 20 years ago. This was achieved for the Sumatra-Andaman earthquake, even at stations closest to the earthquake. In addition, data from most GSN stations were available in near-real time via the internet, and were used immediately by operational agencies and academic researchers to provide an initial assessment of this major event.

With nearly all of the seismological data available immediately, scientific investigations started quickly, and research results have arrived nearly continuously since the earthquake occurred. Many reported characteristics of the earthquake have now reached the point of being the consensus view: the earthquake initiated in the south, rupture spread essentially unilaterally to the north for nearly 1300 km, most of the slip occurred in the area near the hypocenter, and the moment magnitude of the event is in the range of 9.0-9.3. Also, the slip direction in the earthquake is consistent with slip partitioning and a very large amount of strike-slip and extensional deformation occurring in the upper plate.

Beyond these basic observations, much still needs to be learned about this earthquake. It is clear that while the tools and techniques that exist today are adequate for getting zeroth- and first-order information about this earthquake, new methods need to be developed to analyze fully an event of this size. This is not surprising, given that the seismic moment of the Sumatra-Andaman earthquake is likely to be 10 to 30 times larger than any event that has occurred since the deployment of the first digital seismograph network in the 1970s (see the Figure). Many seismologists were simply not prepared or equipped



The Sumatra-Andaman earthquake was 10-30 times larger than any other event in the past 30 years, and accounts for roughly a third of the total moment release during this time.

with the appropriate analysis tools to investigate an earthquake of this size, which had a duration of nearly 10 minutes. Newly-developed techniques, some applied for the first time, have already produced important results such as the imaging of the moving rupture area using regional and global short-period recordings and array-processing algorithms.

A key question regarding the Sumatra-Andaman earthquake is the nature of the slip in the northern half of the rupture, where much of the tsunami was generated. Was the character of the rupture different from elsewhere on the fault? Was there a slow component to the slip and the deformation? Is there a connection between some special characteristic of the earthquake and the large tsunami, especially in light of the lack of a large tsunami following the M_w 8.6 aftershock on March 28, 2005? These questions will find answers over the next few years as the result of more-detailed seismological studies. Many of these questions will also be addressed most productively in joint analyses of seismological, geodetic, and geologic data.

In addition to providing a wealth of seismological data directly relevant to the source process of the Sumatra-Andaman earthquake, this earthquake generated a number of observations of related but poorly-understood phenomena. A dramatic example is the intense and geographically-focused earthquake swarm that occurred near the Nicobar Islands one month after the mainshock. A second example is the seismic activity in volcanic areas as much as 10,000 km away that was triggered by the passage of surface waves from the mainshock. It is likely that additional phenomena will be discovered as seismologists examine the data from the earthquake in greater detail. Given that we are still seeing effects of the $M = 9.5$ 1960 Chile earthquake in the distribution of current earthquakes off the coast of southern Chile and in the geodetic deformation measured on land, we should expect the effects of the 2004 earthquake to be seen for decades to come.

Over the last few years we have also seen several discoveries in seismic-source seismology that have resulted from analysis and reanalysis of massive datasets that originally were collected for other purposes. In many cases these investigations have involved the characterization and analysis of noise. The low-frequency ‘hum’ of the Earth was discovered in the late 1990s and is still awaiting a convincing explanation, though it seems likely to involve land-ocean interaction. High-frequency ‘chatter’ has now been observed in several subduction zones, and in the Pacific northwest subduction zone is associated with periodic slip transients that were first observed a few years ago. Array analysis of intermediate-period surface waves has led to the discovery of $M = 5$ slow seismic slip events associated with outlet glaciers in Greenland, and other glaciers in Antarctica and Alaska. Of these three newly-observed phenomena, the subduction-zone chatter is the one that now seems most directly relevant to the traditional field of earthquake seismology and, specifically, to the question of seismic and aseismic slip in subduction zones. The other two illustrate the range of geophysical phenomena that can be observed and investigated with IRIS instrumentation. Equally important are the facts that they demonstrate how discovery is possible with the tools we have developed, and that discovery frequently is unpredictable.

Related to the discoveries to be made in the massive volumes of high-quality data IRIS has collected is the growing trend among seismologists to reuse and reprocess data stored at the IRIS DMC with new algorithms and increasingly capable computers. This is necessary when the goal is to find signals and sources in the noise, and also when the objective is to determine better source parameters and refine images of seismicity. Very impressive relocation results are currently resulting from massive cross-correlations of broad-band waveforms. One can expect that this type of processing, involving computations that would have been impossible a few years ago, will be the normal way to deal automatically with the enormous volume of data now being generated by IRIS facilities and networks all over the world.

In conclusion, it is likely that over several years significant advances of our understanding of both the tectonic processes which result in seismicity and of the earthquake rupture process will result from the analysis of the unprecedented volume of high-quality data generated and distributed by IRIS facilities. Some of this progress will be incremental and will come as the simple result of the accelerating accumulation of seismological observations. However, judging by recent developments, it seems probable that dramatic improvements will also occur in the estimation of earthquake parameters, the imaging of the earthquake source process, and the interpretation of seismic “noise” as the result of new and innovative approaches to the processing of broad-band data.

The Continental Lithosphere and Seismology

Alan Levander, Adrian Lenardic • Rice University

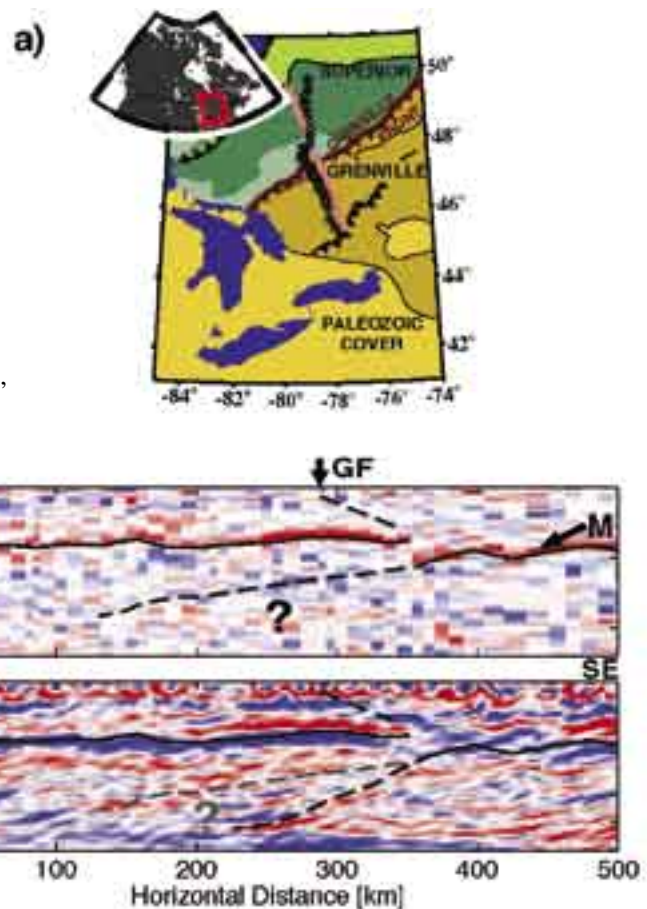
Karl Karlstrom • University of New Mexico

The success of plate tectonics in describing the evolution of the ocean basins lies in the regular progression of oceanic lithosphere from its generation at spreading ridges to its consumption at subduction zones, and the simple description of the tectonics of oceanic lithosphere in terms of translation, rotation, and consumption of large “rigid,” nearly uniform plates obeying fairly simple geometric laws at their boundaries. This process dominates global tectonics at scales of hundreds to thousands of kilometers and durations of ~ 0.2 Ga and is often taken as the surface expression of mantle convection, with the crust and mantle forming the upper thermal boundary layer. Differentiation processes at ocean ridges are also relatively simple, creating plate-wide layered structures that are largely recycled by subduction, and the relationships between the age of the lithosphere, its thickness, thermal state, and density are well known.

The Earth, unique among the planets, has a bimodal distribution of topography, with $\sim 40\%$ of its surface made up of continents, whose surfaces reside above to slightly below sea level, and $\sim 60\%$ oceans with average elevation of ~ -4 km. This is the most obvious difference between the continents and oceans, but there are equally profound differences extending to depths of 200–400 km first recognized seismologically almost 30 years ago. In contrast to the 60% of the Earth forming

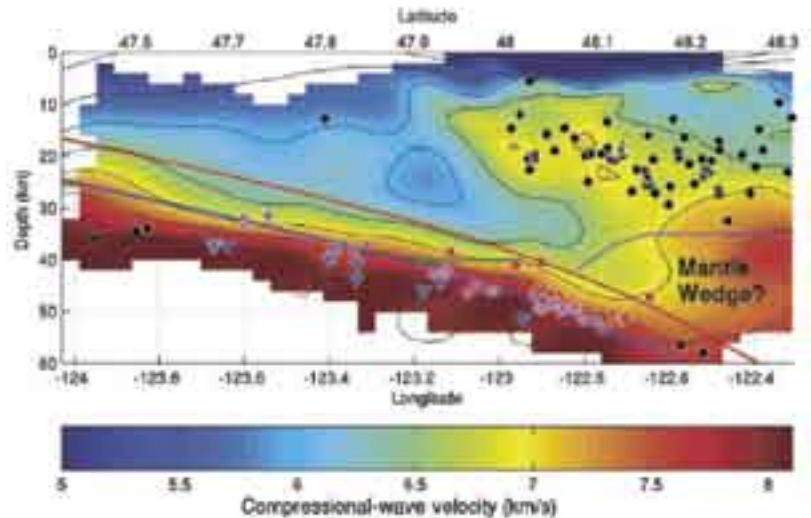
the oceanic plates, the 40% comprising the continents has grown over the last ~ 4.5 Ga through a complex sequence of differentiation and deformation processes that operate on scales of hundreds of kilometers and smaller, including highly localized, phenomena such as faulting and pluton emplacement. The resulting continental lithosphere consists of a complex collage of fragments of various tectonic affinities. While these fragments can be collected to form supercontinents or dispersed by the same convection system that creates and recycles oceanic plates, the development of continental lithosphere itself, unlike the oceanic lithosphere, cannot be viewed in terms of the creation of a thermal boundary layer in the convecting mantle system, and continental tectonics cannot be simply described by translation, rotation, and consumption of large, “rigid,” nearly-uniform plates obeying fairly simple geometric laws at their boundaries. In general, continental crust does not participate in global mantle overturn and this also appears to be the case for the subcontinental mantle beneath many cratons. Thus, the continental lithosphere is not a simple active upper thermal boundary layer within the convecting mantle system, and understanding the structure of continents requires understanding the cumulative products of magmatic and deformational processes that have acted over billions of years of Earth’s history. The thickness and chemical buoyancy of continental crust makes continents resistant to subduction. That this could effect large-scale mantle dynamics was proposed almost 70 years ago by Pekeris (1935).

Continents represent the products of repeated differentiation cycles whereby less-dense, intermediate-to-felsic, crust is upwardly stratified by combinations of tectonomagmatic processes. Accretion of uniquely continental materials takes place above subduction zones in magmatic arcs and orogenic plateaus, but formation of



High-resolution, teleseismic imaging of the lithosphere beneath the Abitibi 1996 broadband array (IRIS-PASSCAL, Lithoprobe). a) Map of study area. b) CCP receiver function profile. Red and blue pulses denote discontinuities with positive and negative downward velocity gradients, respectively. Black lines show interpretation. Abbreviations: GF = Grenville Front, M = Moho. c) S-velocity perturbation profile obtained by 2D Generalized Radon Transform inversion (Rondenay et al., 2005), with red to blue colour scale representing negative (slower) to positive (faster) velocity perturbations.

true continental lithosphere requires multiple differentiation events to reach the average composition of continents. These events take place during plate convergent events such as collisions of arcs with arcs, arcs with continents, and continents with continents. They can also take place during incipient rifting of continents via interactions between lithosphere and asthenosphere. In terms of the differentiation processes that make continental crust over time, the important physical quantities are heat sources, both mantle and crustal, magma sources within the mantle (i.e. fertile mantle), other fluid sources in the crust and mantle (e.g., H_2O and CO_2), and migration pathways provided by existing fractures and shear zones, or in the case of highly-pressured magmas, the regional stress field that controls the orientations and locations of hydrofracturing. It is generally believed that the radiogenic heat production in the crust is inadequate to produce crustal magmas, except in the greatly thickened, probably hydrated, crust occurring near or within orogenic plateaus. Most crustal melting results from heat originating in the mantle that is advectively transferred to the crust in the form of mantle-derived mafic melts, with the melting process facilitated by other fluids residing in the crust, or transferred to the crust from the mantle: for example, hydration melting above subduction zones.



Interpreted cross section showing compressional velocities (contoured at 0.5-km/s intervals), relocated seismicity (black circles: continental crustal events; colored symbols: intraslab events), and Moho reflector (blue line). Interpreted top of subducting plate (red line) is drawn 7 km above reflector. The region between these lines is interpreted to be the subducting oceanic crust, composed of basalt above 40-km depth (horizontal green line) and beginning to transform to eclogite below. Subducting mantle is below the blue line. Low velocities in the mantle wedge imply the presence of serpentinite. There is no vertical exaggeration.

Seismology has played a transformational role in our understanding of the continents and the ocean basins, particularly so in the search for hydrocarbon reserves and (more recently) groundwater, in the recognition and mitigation of earthquake hazards, and in our understanding of Earth's structure, processes, and history. Modern detailed seismic investigations image details of structural and sedimentary geology, identify magmatic and other fluids in the crust, map details of structure within fault zones, and image migration of the seismicity associated with volcanic eruptions and volcanic systems. Seismic investi-

g□
to make the links between brittle and ductile deformation in the crust. Discussion of the deformation of the continental crust is virtually impossible without consideration of the mantle underneath it, part of the remote Earth that is only accessible to seismic and electromagnetic probing. In both ancient cratonic and active modern provinces, surface structures appear to be highly correlated with various mantle structures, giving structural geologists constraints on large-scale lithospheric processes that formed and stabilized the continents. In particular, recent seismic results around the peripheries of the North American craton have led to a thrust-stacking model for the growth and stabilization of the cratonic lithosphere in the late Archean and early Proterozoic. The density of recording in modern seismic experiments, both active and passive, permits wavefield imaging to provide unprecedented resolution of the crust and mantle throughout the transition zone. (Such direct imaging is even being applied to D'' and the Core-Mantle Boundary). Seismic heterogeneities observed in the mantle resulting from subduction, delamination or rifting can be used to infer some of the forces driving modern crustal deformations, providing a vital link to surface deformation measurements provided by modern geodesy.

Seismology, and by inference IRIS, is one of the drivers in modern Earth science, providing images interpreted jointly by a wide variety of researchers investigating virtually every aspect of the continental system. The expanding PASSCAL instrument base permits use of seismic imaging techniques drawing on the most advanced aspects of practices in the petroleum industry, medical imaging fields, and astronomy. This pool of seismometers will continue to provide the primary means by which we will discover the true nature of the structure and evolution of the continents.

Subduction and Seismology

Geoffrey Abers • Boston University

Material that forms at mid-ocean ridges descends into the mantle at subduction zones, along with mineralogically bound fluids and sea floor sediments. Some of the fluid leaves rapidly as pressure and temperature increase, while some migrates into the mantle wedge to fuel arc volcanism, and some descends to great depth. Hence, subduction zones form the primary site of material return into the Earth's mantle, controlling the behavior of subcrustal earthquakes, triggering and feeding most of the planet's destructive volcanism, and regulating the long-term budgets of the atmospheric gases. The anomalous buoyancy of subducting plates also exerts the primary control on mantle circulation. Seismology has provided several important advances in the last five years. Until recently, the seismological tools for studying subduction zones remained crude compared to the characteristic scale of many problems, making it difficult to address even basic questions. For example, subducted oceanic crust is 6 km thick, but traditional body-wave tomography rarely resolves mantle structures to better than 25-50 km. The advent of digital broadband seismology, and its deployment through the GSN and PASSCAL programs, has revolutionized our understanding of these systems. High-fidelity recordings at a range of frequencies are critical for resolving features at the scale of subducted crust, which are turning out to be some of the largest seismic velocity anomalies within the earth's mantle.

Seismology provides constraints on a suite of elastic parameters (V_p , V_s , Q , reflectivity) that bear only passing resemblance to those needed to actually interpret critical processes (e.g., chemical composition, pressure, temperature, melt and fluid abundance). Mineral physics measurements are beginning to remove ambiguity from interpreting seismic data, and petrologists and geodynamacists have begun working directly with seismologists to understand the conditions at which intermediate-depth earthquakes occur, the thermal structure and geodynamic regime of the mantle wedge, and have begun relating seismic images of the sub-arc mantle to magma chemistry. Large interdisciplinary collaborations are now leading to a new level of understanding.

The December 26, 2004, Sumatra earthquake served as a sobering reminder of the broader significance of earthquake source studies. Our methods for analyzing slip on "normal" $M < 8$ earthquakes clearly are inadequate for events of this size, as considerable energy is expended at frequencies below those accessible with body wave methods. Reconciling seismic and tsunami excitation seems possible although challenging, and it remains to be seen whether significant aseismic slip is necessary to explain the tsunami and geodetic signals observed. At greater depth, the very existence of subduction-zone earthquakes below brittle-ductile transition remains a mystery. At intermediate depths, many recent papers have appealed to dehydration embrittlement an enabler of seismicity. Most intermediate-depth seismicity correlates well in distribution with that predicted for water release from dehydration reactions at the top of the slab, although the mechanism by which dehydration triggers earthquakes remains poorly understood. However, the well-documented existence of double seismic zones requires that at least some intermediate-depth earthquakes occur 20-40 km into the mantle, where the presence and release of water remains uncertain. Either another mechanism triggers earthquakes here, some process must deliver water to great depths in oceanic lithosphere. Seismology addresses this problem both by describing these intraslab earthquakes, and by imaging the environment in which they occur.

The triggers for deep earthquakes seem even less clear. Ten years ago, much excitement surrounded the theory that the transformation of metastable olivine to spinel structure could occur catastrophically and generate seismic shear instabilities. However, careful examination of seismic observations from PASSCAL experiments show that some deep earthquakes nucleate outside of the region where olivine should be metastable, and theoretical work has questioned the presence of widespread metastability in most subduction zones. One possibility is that deep earthquakes occur because of fluid release, either H_2O or CO_2 . Alternatively, deep earthquakes may be runaway ductile shear instabilities, an exotic phenomenon rarely observed in rock-forming materials but theoretically possible. A major challenge will be to find diagnostic seismic signals to distinguish this mechanism from others.

In the last five years, several fundamentally new signals have been discovered. One of the most exciting is non-volcanic tremor, a high-frequency signal documented in southern Japan and Cascadia subduction zones, associated with the down-dip limit

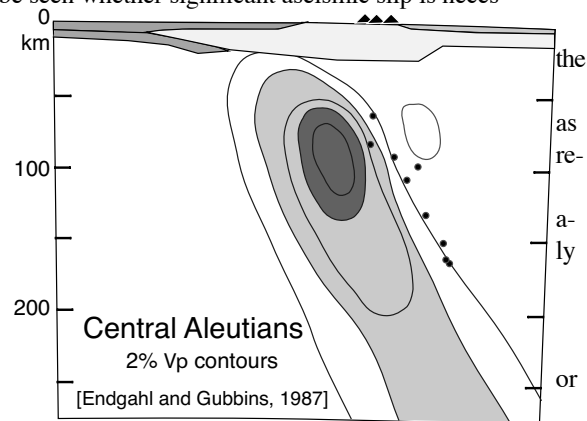
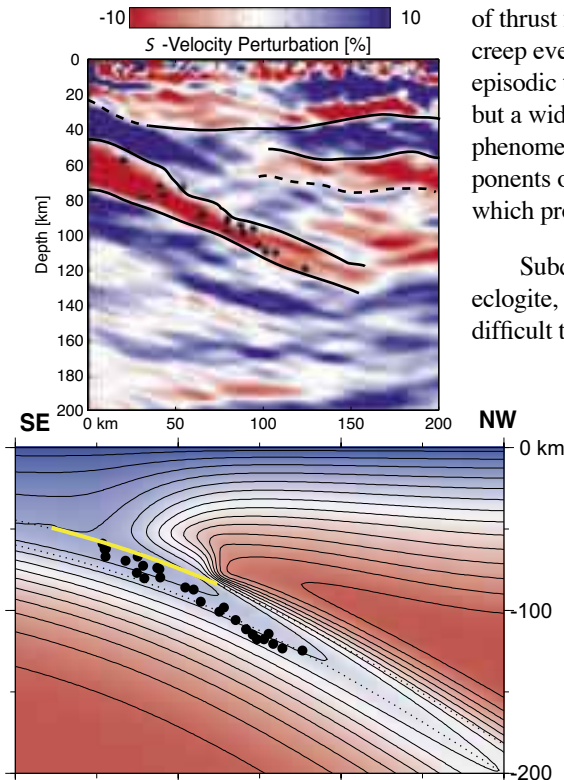


Figure 1. State-of-the-art seismic modeling of the subduction zone modeling two decades ago.



Two examples of current attempts at modeling the structure of the Alaskan subduction zone. (Top) Rondey, Abers and Ferris (2004). (Bottom) Abers, van Keken, Kneller, Ferris, and Stachnik (2005).

of thrust faulting. This tremor correlates closely in space and time with aseismic creep events on the plate interface, contributing to a coupled phenomenon called episodic tremor and slip (ETS). The physics behind ETS remains poorly understood, but a wide range of new experiments and analyses are now underway to explore this phenomenon. These experiments take advantage of both the PBO and USArray components of Earthscope and the flexible telemetered arrays developed by PASSCAL, which provide new tools to characterize the tremor.

Subducting basaltic crust should eventually metamorphose to high-density eclogite, which has seismic properties very similar to mantle peridotites and hence difficult to observe. Several studies have shown that a low-velocity layer persists to depths of 150 km or more at the top of subducting plates, which likely corresponds to hydrated, subducted oceanic crust. If these layers are indeed hydrated, their presence places constraints on the large-scale transport of water into and through the lower mantle, and the physical conditions at which intraslab earthquakes operate. In the last several years, IRIS facilities have made it possible to find the traces of subducted crust throughout the planet. Strategically placed GSN stations on arcs have provided signals from regional and teleseismic events that interact with the downgoing plate. These signals form the basis for a global sample of subduction structure. Recently, dense broadband arrays have begun to show striking images of subducting plates, resolving features a few kilometers thick. Apparently, subducted crust remains slower than mantle to depths of 150 km beneath many arcs. Slow crust has not yet been imaged at greater depths, although some very deep sources of scattered energy may be metamorphosed gabbro.

Applying scattered-wave migration, Bostock and colleagues imaged the apparent dehydration of the Cascadia slab directly below a low-velocity portion of the hydrating mantle. This and subsequent work has indicated

that serpentinization of the cold lithosphere may constitute a significant global reservoir for water. It is less clear how water is transported into the deeper, hotter portions of the wedge, where it plays a critical role in melt generation. In the melt generation region, collaborative, interdisciplinary research will be needed to address first-order questions such as where melt is generated, how it is transported, what regulates eruptive volatile content, and why volcanic fronts form at all. Seismic experiments are finding that the rapid flux of cold lithosphere into the transition zone raises and lowers the 410 and 660 km discontinuities, respectively, in accordance with expectations based upon the mineralogy of the olivine phase changes. However, the results of shear-wave splitting studies have not been easy to interpret in terms of mantle chemistry. In many tectonic environments, shear-wave splitting measurements have been found to be consistent with mantle flow through the induced alignment of olivine crystallographic axes, and flow patterns appear simple over large regions. In subduction zones, however, the fast axes often lie parallel to the arc within the mantle wedge, but exceptions are numerous enough to make any generalization difficult. Interpretation of these data has been complicated by discoveries of new microstructural mechanisms for producing anisotropy, through water- and stress-controlled activation of other crystal slip systems, and through the alignment of melt or fluid conduits. Until recently, sparse networks provided spot measurements that probably spatially alias the flow field in the wedge, but the PASSCAL facility now has begun to support multiple dense arrays, at sufficient density to sample mantle flow.

The next five years should see significant advances. Through EarthScope, Continental Dynamics and the MARGINS program, several large field experiments are now underway in subduction zones around the world, and will produce significant new observations. Among the enduring questions this new generation of experiments should help address: What causes deep and intermediate depth earthquakes? (phase changes, dehydration embrittlement, plastic instabilities or something else?) How much H_2O and CO_2 are deeply subducted, how do they descend, and where do they reside? What triggers melting below arc volcanoes, and what produces the volcanic front? How does slip on the thrust zone, both seismic and aseismic, affect other dynamic phenomena? What happens between the downdip end of the seismic thrust zone and the flowing part of the mantle wedge? What is the pattern of flow in the mantle wedge? How do slabs interact with transition-zone discontinuities, and what is the ultimate fate of subducted material? Answers to these questions, and the formulation of new ones, will come about through partnership between laboratory and theoretical practitioners and the analysis of new signals coming out of the Earth that the IRIS facility will provide.

Investigating Earth's Dynamic Mantle and Core

Edward J. Garnero • Arizona State University

Seismologists have long sought to decipher the Earth's inaccessible and enigmatic interior through detailed interrogation of deeply penetrating seismic energy. As we approach the 100th anniversary of the discovery of Earth's core, we are rapidly moving beyond the characterization of Earth's first-order radial stratification that dominated the decades that followed detection of the core. In fact, an explosion in the availability of broadband data from a variety of agencies and organizations over the last decade has permitted both global and regional analyses of the interior at unprecedented spatial detail. Conclusions using the remote sensing tool of seismology now regularly reach well beyond solution models of Earth's internal elastic structure, and extend to the characterization of Earth's dynamic, thermal, and chemical states (Figure 1). Advancements in our understanding of the interior have been primarily and fundamentally facilitated through the efforts and successes of the IRIS mission. Data are now easily available through a variety of method, to anyone in the world.

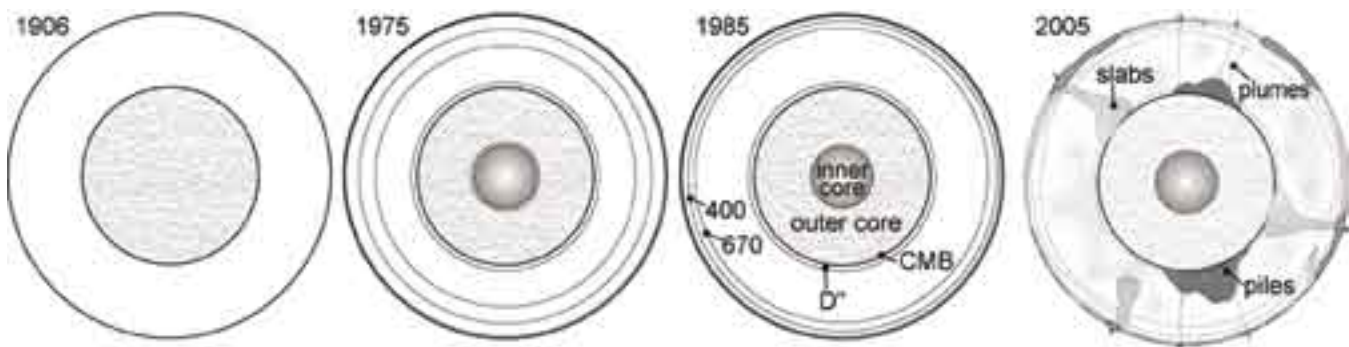


Figure 1. Seismic data provided by IRIS continues to allow for rapid changes in our models of Earth's deep interior.

Mantle Heterogeneity: The Global Picture

In convective systems, diversity in structures can occur near the boundary layers. The core-mantle boundary (CMB), in fact, contains Earth's largest absolute density contrast within the planet, and thus continues to receive significant attention in high-resolution modeling at a variety of spatial scales. The next largest density contrast is between surface rock and air or water, and while large-scale surface tectonics have been appreciated for some time, constraining the role of upper and/or lower mantle structure and the dynamic processes responsible for shaping the surface remains a challenge.

Certainly, tracing subducting slabs to their final resting place or deep plume roots upwards to hot spot volcanism have been a focus of global mantle travel-time tomography. Some recent successes in imaging the apparent connectivity of higher-than-average velocities from the crust to core beneath Mexico, presumably from the ancient Farallon slab, and possibly beneath Japan, have played into the long-standing debate about whether or not the boundary between the upper and lower mantle demarks chemical stratification. Transition zone structure and discontinuity topography may similarly provide important constraints on mantle temperature and dynamics. Several research groups can now boast 3-D global P- and S-wave mantle models, largely owing to data availability through IRIS. Attributing global heterogeneity to a solely thermal versus thermal and chemical origin is regularly pursued. Often significant holes in data coverage are still present, however, which requires future deployment and densification of instruments. EarthScope's USArray will significantly help in the study of the deep Earth that is in the hemisphere containing North America.

Mantle Heterogeneity: High-Resolution Imaging and Short-scale features

Forward-modeling waveform studies augment the global images, often revealing a variety of phenomena not yet available through the tomographic approach. These include discontinuous layering or reflectors near dominant boundary layers, such as layering some 200-300 km above the CMB (the D'' layer), ultra-low velocity (10's of percent reductions from global reference structures) layering right at the CMB, and vertical boundaries between low-velocity structures and neighboring mantle which, beneath southern Africa, are mapped as extending up to 1000 km above the CMB. These features may be intimately related to ultralow velocity zone genesis from partial melt of lowermost mantle material, which can give rise to

instabilities that result in the birth of whole-mantle plumes. Both forward and inverse methods now almost routinely document seismic wave speed anisotropy, anelasticity, and scattering in the mantle, particularly near the surface and CMB, where analyses utilizing reference seismic waves are most easily permitted owing to the existence of the highly reflective Earth's surface and CMB.

The Outer and Inner Core

The relatively rapidly convecting fluid iron-alloy outer core is responsible for the generation of Earth's magnetic field. Lateral heterogeneity in outer core elastic properties is generally assumed absent, based on dynamic arguments. However, the possibility for small-scale structures right at the underside of the CMB, or at the topside of the inner core boundary are possible. Certainly, high-resolution seismic studies have suggested short-scale variability (e.g., km scale) of each. Larger arrays, e.g., USArray, will help to further illuminate these possibilities in the near future.

The solid inner core is but a fraction of a percent of Earth's volume, yet continues to attract significant attention from seismologists, often in collaboration with a variety of geophysicists from other disciplines. Better constraints of the depth and lateral distribution of inner core heterogeneity, anelasticity, and anisotropy (as well as their magnitudes), and inner core super-rotation, likely hold important keys for core (and thus Earth) formation, as well as the nature of the generation of Earth's magnetic field. Global and regional arrays, PASSCAL experiments, and traditional short-period seismic arrays all have the potential to advance our knowledge in these important areas.

Of particular relevance in imaging Earth structure at depths below the CMB is properly accounting for contaminating effects of mantle structure, especially the strong heterogeneities now widely accepted to exist at the base of the mantle. This will certainly receive ever-increasing attention as the deepest mantle comes into sharper focus and our ability to incorporate 3-D wave propagation in our imaging studies improves.

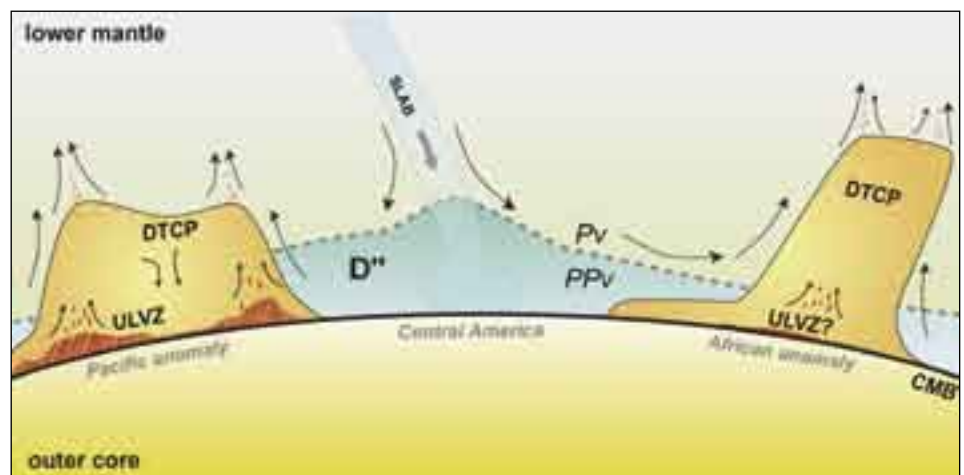


Figure 2. A current representation of the core-mantle boundary region, incorporating many of the structures that have been identified by recent seismological investigations.

Looking to the Future: New Data, New Methods, New Disciplines

We have come a long way since the band-limited digitized recordings from analog instruments (e.g., WWSSN) of the 1960's that were pervasive in studies of the following couple decades. Significant densification of seismic station coverage has also occurred. Thus we are now afforded interrogation methods of Earth's deep interior that once were previously only enjoyed by exploration and crustal seismologists: traditional seismic array techniques, which augment waveform modeling of region studies, as well as global waveform and travel-time tomography. However, future work should more fully utilize the rich bandwidth of information in the recorded wave field. Continued availability and expansion of data made available by IRIS will enable advances on these fronts, which will specifically enhance the connection between seismic results and those from other Earth interrogation disciplines: for example, geodynamics, mineral physics, geochemistry, geomagnetism, geotectonics, and petrology. The multi-disciplinary research approach is important, as it will be a principle method in reducing uncertainty in our often large solution model spaces. More and better data permit better seismic models for this process.

IRIS Education and Outreach

Larry Braile • *Purdue University*

The IRIS E&O program and participating scientists and educators have developed a range of activities and resources designed to effectively reach a wide audience of interested people, from students and teachers, to college and university faculty, to the general public. Interested people can investigate a single topic or question, find a teaching lesson on seismology, Earth

Table 1. "Science Interest Starts Early: More than half of science professionals with a PhD say their first interest in science came at age 5-10. What they say influenced their science interest in childhood."*	
People (parent, teacher)	45%
Experiences	11%
Toys/books/equipment (chemistry set)	10%
Other (class, science on TV)	6%
No significant influence	13%
Don't know	15%
* Source: Roper Starch Worldwide for Bayer, National Science Foundation, as reported in the USA Today, September 10, 1998.	

The IRIS E&O resources and programs provide opportunities for students and teachers (or other interested people) to experience or do science (with real data, in near-real time, with on-line or easily accessible materials and classroom activities) rather than just read about science. Earthquakes, seismology and plate tectonics also provide exciting and relevant science topics that can be used to motivate students for science learning and develop quantitative and critical thinking skills.

During the last century, the United States has made dramatic progress in advancing the educational level of its population, such that today about 85% of the U.S. population (age 25+) has completed 4 years of high school or greater, about 65% of high school graduates enter college within

one year of high school graduation, and about 25% of the population (age 25+) has completed 4 years of college or greater. These educational achievement rates are as high, or higher, than those of any other country. High school and college graduates from around the world compete for entrance to U.S. colleges and universities and for admission to graduate and professional schools. However, over the past 15 years there has been increasing concern about the performance of graduates from our educational system. Much of the criticism has focused on apparent underachievement in science and mathematics in both high school and college graduates. Another area of concern is the failure to attract significant numbers of people to science and technology careers, especially women and minorities. Increasingly, citizens of foreign countries populate our graduate programs in science and technology. In this age of rapid advances in science and technology, there is a great need for all Americans to be scientifically literate to ensure that the US maintains its leadership role in science and the global economy and is able to conduct scientifically informed policies.

IRIS and its member institutions are contributing to solving these problems by:

- Making advances in science and technology knowledge and skills more accessible to all;
- More effectively preparing current and future K-12 teachers to teach science and technology;
- Encouraging and preparing the next generation of scientists and broadening career paths available to them.

Due to the importance of science learning at an early age (Table 1) and the tradition of teaching Earth science primarily in middle school grades, providing materials and training for K-12 teachers is an important part of the IRIS E&O program.

Over 600 K-12 teachers and college faculty have participated in IRIS-sponsored one-day intensive workshops on earthquakes and seismology at national



Figure 1. Modeling the seismic shear wave using the human wave demonstration. In addition to the human wave demos, seismic waves are also investigated using slinky activities and computer animations.



Figure 2. Investigating earthquake hazards by constructing a model building that will withstand earthquake shaking. The model buildings are then tested using a simple shake table with accelerometer output to monitor the input shaking and the building response. Well designed model buildings often can withstand over 75% g accelerations. Comparison of modes of failure (soft first story, building resonance, etc.) of the model buildings with actual building damage caused by earthquakes (using photographs of damage) contributes to understanding of earthquake hazards.

sored one-hour workshops at national and state-level science teacher meetings in which one or more seismology activity has been demonstrated. Distribution of IRIS publications (posters, one pagers, etc., Figure 3) at these meetings and elsewhere has also impacted many thousands of educators.

However, there are many different ways that the excitement and information of science can be conveyed to the public, and so the IRIS E&O program is involved in many different kinds of activities. Millions of people go to science museums each year, and while most science museums have some sort of display on the earth and earthquakes, well-designed displays can reach enormous numbers of people. The IRIS/USGS real-time earthquake display at museums like the American Museum of Natural History and Smithsonian are very popular. Earthquakes have an easy appeal to the public because of their potentially violent and destructive nature, and the displays show that with some good software and attractive design, they can be one of the most successful components of a science museum.

Science museums are also a good site for educating people about earthquakes and seismology through lectures. The newly-begun IRIS-SSA Lectureship has brought research seismologists with a strong interest in public education to many different museums, with a tremendously enthusiastic response. Many of the people who attend these lectures are themselves teachers, and are now using power-point versions of these IRIS-SSA lectures in their own classes.

One important new direction for IRIS E&O is in the area of seismology education for seismologists. The IRIS Intern program continues to be very successful, giving undergraduate students the chance to participate in active seismological research. Some have now gone on to be seismology graduate students. IRIS also plans to be more involved with undergraduate curricula, though the development of technological web-based displays, the development of undergraduate teaching materials, and through its Educational Affiliate program, which is bringing together people and ideas on how to do a better job teaching seismology and geophysics at the undergraduate level.

Education occurs on many different fronts, and the IRIS E&O program is expanding to take advantage of opportunities in many of these. It is important for the IRIS E&O program to maintain its high level of technological competency needed to keep up with the increasing opportunities for science education, but there will also be a continued need for broader participation by its members in the education of the public, whether this is in the form of lectures, hands-on workshops, or one-on-one mentoring.

and state-level science meetings. During these workshops, the teacher/participants learn and experience effective hands-on activities that explore seismic waves (Figure 1), the cause of earthquakes, earthquake occurrences, plate tectonics, the structure and properties of the interior of the Earth, and earthquake hazards (Figure 2). Participant assessments of these workshops and of the learning activities used in the workshops and implemented in the classroom by the teachers have been very positive. Several thousand additional teachers have attended IRIS-spon-

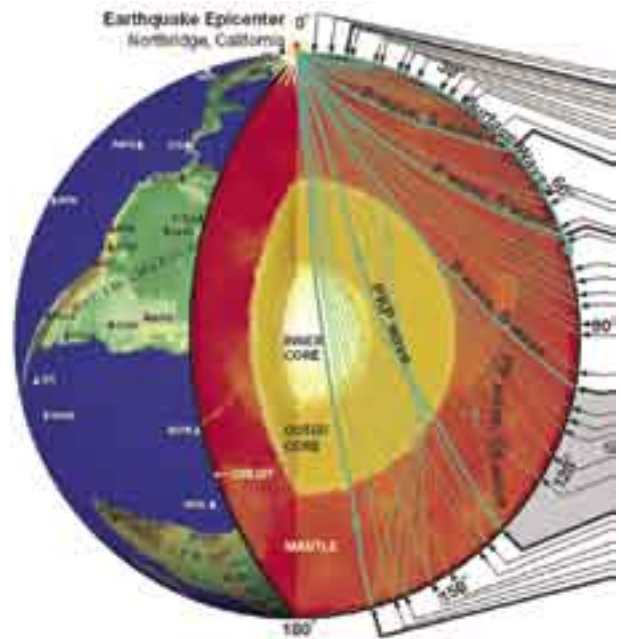


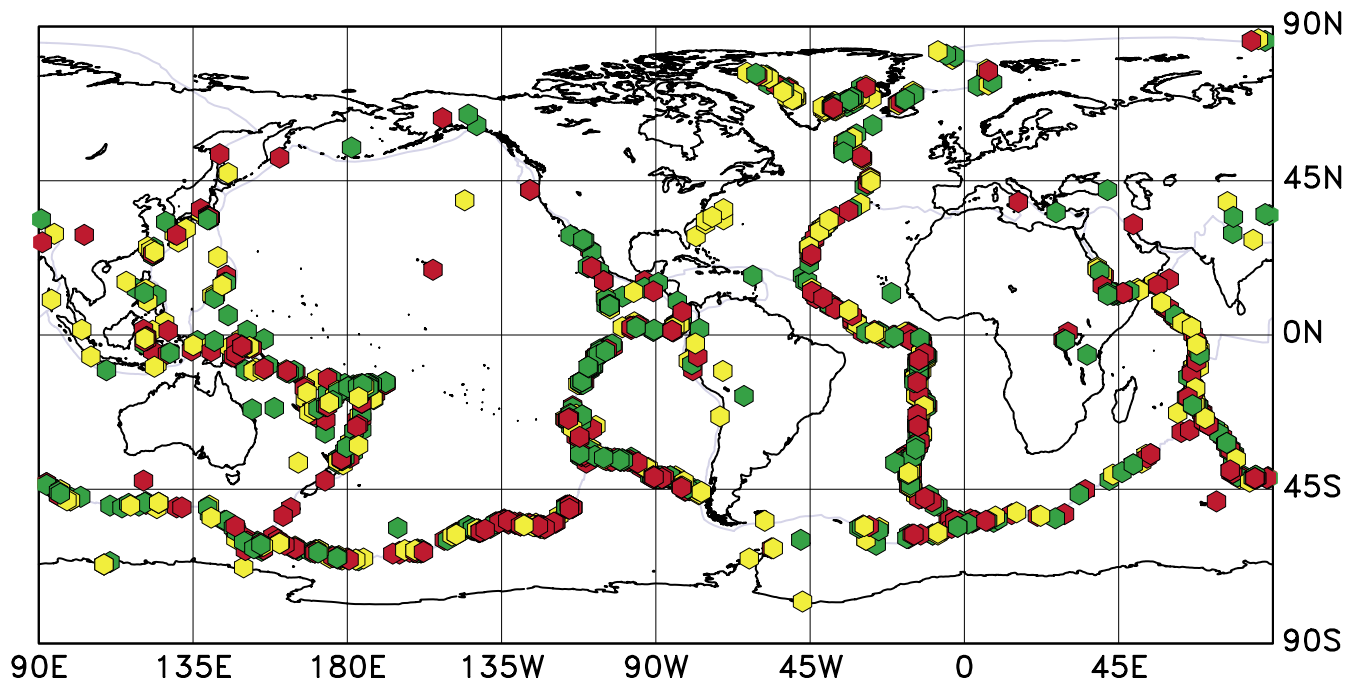
Figure 3. Portion of the IRIS poster "Exploring the Earth Using Seismology". Additional posters, one-pagers describing a specific seismology topic, and other E&O publications have been produced by the IRIS E&O Program.

Long-period Global Detection and Location of Earthquakes Using the GSN

Göran Ekström, Meredith Nettles • Harvard University

We use long-period data from the Global Seismographic Network in an array-processing mode to detect and locate shallow earthquakes globally. A global grid of target locations is monitored continuously for detections of sources of Rayleigh wave energy in the 35–150 s period band. The tuning of the array for each target location is accomplished by calculation of frequency-dependent path corrections using detailed global phase-velocity maps. The detection algorithm uses a matched filter to look for source pulses on reverse-dispersed and stacked seismograms. In addition to analyzing real-time data, we have applied the algorithm in a systematic fashion to continuous archived data from the IRIS GSN and other global networks for a period of 11 years, 1993–2003. For this period, we detect and locate approximately 25,000 earthquakes. The smallest earthquake detected has a magnitude $M = 4.6$. 1,860 of the events are not correlated with any earthquake reported by the NEIC, ISC, or the IDC (based on the REB bulletins). We believe that fewer than 1% of our new events are false detections, and that our analysis identifies around 150 new $M \sim 5$ earthquakes per year. The map below shows the locations of the 1,860 previously unknown earthquakes. The quality of the detection is indicated by the color: red indicates the best quality, green is very good, and yellow is good.

Most of the new events fall along ridges and transform faults, and relatively few in subduction zones; many events associated on the map with subduction zones are located in back-arc basins. More than 100 of the newly detected events are located in areas away from regions that are considered seismically active. In particular, a very large number of earthquakes can be seen along the coast of Greenland. These events, first described by Ekstrom, Nettles, and Abers (*Science*, 2003), belong to a new class of earthquakes associated with the sliding of glaciers. These glacial earthquakes are not detected by traditional methods owing to their very slow slip. The typical duration for an $M = 5$ glacial event is 30–60s. Other previously undetected events may also be unusually slow or may be associated with geophysical phenomena that generate elastic waves by processes other than standard fault motion. For example, several events in central Africa are associated with volcanic eruptions, and the events off the east coast of North America may be related to submarine sliding. Real-time results from our surface-wave detector can be seen at <http://www.seismology.harvard.edu/~ekstrom/Research/SWD/>.



The Great Sumatra-Andaman Earthquake of 26 December 2004

Thorne Lay, Steven N. Ward • *University of California, Santa Cruz*

Hiroo Kanamori • *California Institute of Technology*

Charles J. Ammon • *The Pennsylvania State University*

Meredith Nettles, Goran Ekstrom • *Harvard University*

Richard C. Aster, Susan L. Bilek • *New Mexico Institute of Mining and Technology*

Susan L. Beck • *University of Arizona*

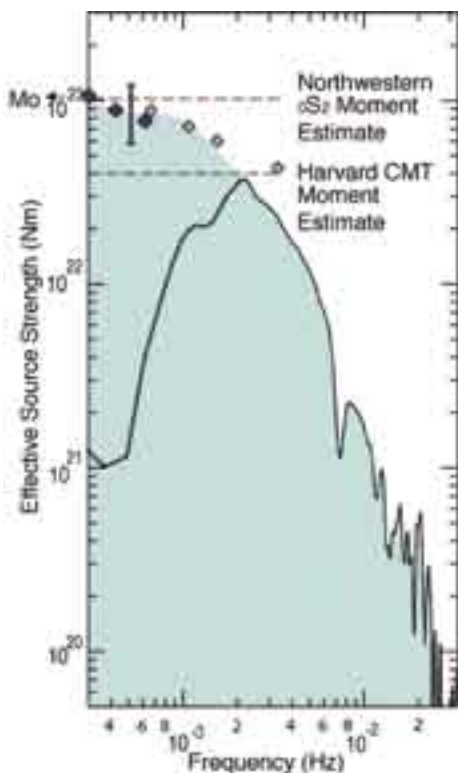
Michael R. Brudzinski, Heather R. DeShon • *University of Wisconsin, Madison*

Rhett Butler • *IRIS Consortium*

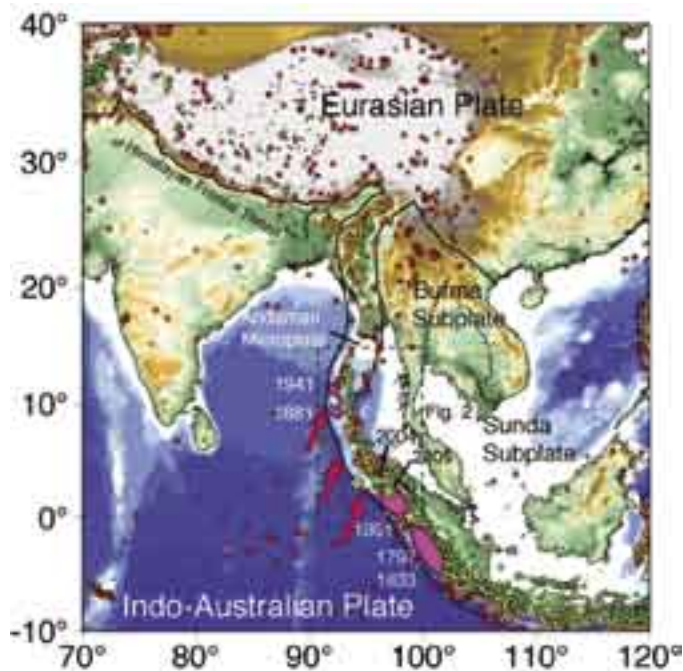
Kenji Satake • *Geology Survey of Japan*

Stuart Sipkin • *U.S. Geological Survey*

An overview of the tectonics and faulting process of the 26 December 2004 rupture and its tsunamigenesis is presented. This earthquake is the largest event in the world in 40 years, and produced the most devastating tsunami in recorded history. Slip during the 10 minute-long rupture along the plate boundary varied systematically toward the north, decreasing from about 15 m near Banda Aceh to only a meter or two near the Andaman Islands. It appears that additional, slower slip occurred in the northern portion of the



Effective source strength for normal modes and Rayleigh waves for the 2004 event, obtained from GSN observations.



Regional tectonic map of the 2004 earthquake, showing earthquakes with magnitudes > 5.0 from 1965 to 25 December 2004. The arrows indicate the relative plate motions between the Indian and Eurasian plates for model NUVEL-1. The location of prior large events in the area are shown.

rupture zone, possibly on a time-scale of one hour or more. This is indicated by modeling of the ocean surface displacements observed by the JASON altimeter. The overall energy release of the earthquake is measured at 1.1×10^{18} J. The seismic moment is $0.65\text{--}1.0 \times 10^{23}$ N-m, with some uncertainty being due to weak constraint on the dip of the fault segments along the rupture. An increasing component of obliquity in the slip is found along-strike. The rupture extended about 1300 km from the epicenter, and an additional 300 km of the fault boundary failed in the March 28, 2005 earthquake.

Lay, T., et. al., The Great Sumatra-Andaman earthquake of 26 December 2004, *Science*, 308, 1127-1133, 2005.

Supported by NSF grants EAR-0125595, EAR-0337495, EAR-0207608, and Cooperative Agreement EAR-0004370.

Rupture Process of the 2004 Sumatra-Andaman Earthquake

Charles J. Ammon • *The Pennsylvania State University*

Chen Ji, Vala Hjorleifsdottir, Hiroo Kanamori, Don Helmberger • *California Institute of Technology*

Hong Kie Thio, Gene Ichinose • *URS Corporation*

David Robinson, Shamita Das • *University of Oxford*

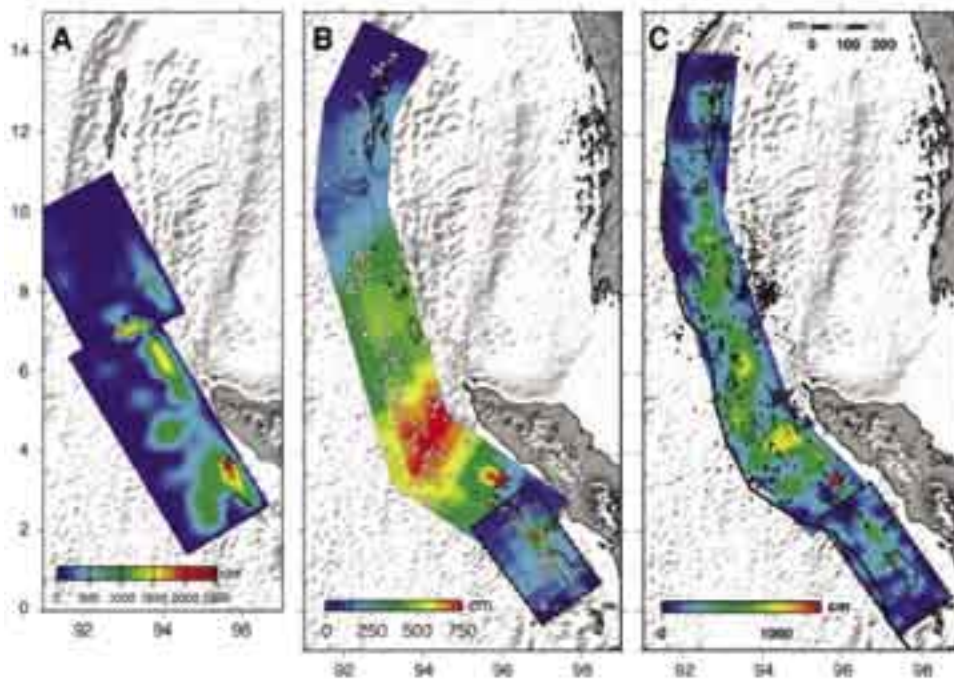
Sidao Ni • *Chinese Academy of Science*

Thorne Lay • *University of California, Santa Cruz*

Jascha Polet • *University of California, Santa Barbara*

David Wald • *U.S. Geological Survey*

An extensive data set of broadband body wave and surface wave observations from IRIS GSN stations is used to constrain the rupture process of the 26 December 2004 rupture. The rupture initiated slowly, with small slip and a slow rupture speed for the first 40 to 60 seconds. Then the rupture expanded at a speed of about 2.5 km/s toward the north northwest, extending 1200 to 1300 km along the Andaman trough. Peak displacements reached about 15 m along a 600-km segment of the plate boundary offshore of northwestern Sumatra and the southern Nicobar islands. Slip was less in the northern 400 to 500 kilometers of the aftershock zone, and at least some slip in that region may have occurred on a time scale beyond the seismic band.



(A) Fault slip 168s after rupture initiation estimated by using 20 azimuthally distributed teleseismic SH waveforms. The rupture model consists of two faults, the first having a strike of 329° and a dip of 8° and the second having a strike of 333° and a dip of 7° . (B) Slip distribution from analysis of intermediate period surface waves and long-period seismograms. While small-scale features are averaged out, this model provides an excellent fit to all long period seismic observations for the event. (C) Slip distribution obtained using teleseismic body waves (50 to 200 s), intermediate period three component regional waves (50 to 500 s) and long-period teleseismic waves (250 to 2000 s).

Ammon, C., et. al., Rupture process of the 2004 Sumatra-Andaman earthquake, *Science*, 308, 1133-1139, 2005.

Supported by NSF grants EAR-0125595, EAR-0337491.

Imaging the Rupture Process of the 2004 Sumatra-Andaman Earthquake Using Deconvolved Surface Wave Source Time Functions

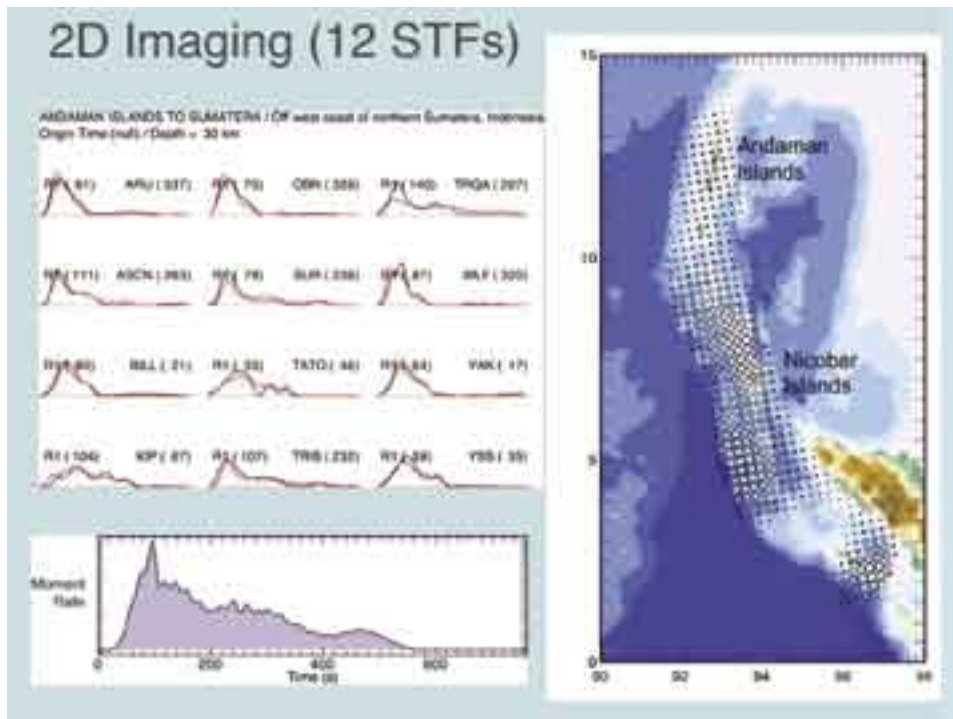
Charles J. Ammon • *The Pennsylvania State University*

Aaron Velasco • *University of Texas, El Paso*

Thorne Lay • *University of California, Santa Cruz*

Rapid determination of the slip distribution for great earthquakes is important for the assessment of their tsunamigenic potential. While analysis of high frequency radiation offers good potential for rapidly constraining total rupture duration, it is important to characterize the magnitude of slip on the fault using longer period signals. This was demonstrated by the tsunami excitation for the 2004 Sumatra-Andaman earthquake, for which reduced slip in the northern portion of the fault plane results in weak tsunami excitation near the Andaman Islands. We have developed a rapid analysis procedure that requires relative

interplate fault. This involves deconvolution of global GSN recordings of long-period Rayleigh waves by theoretical Green's functions for an interplate thrust mechanism, followed by either inverse radon transform for a one-dimensional slip distribution or inversion of the surface wave source time functions for a two-dimensional slip distribution. This procedure can be applied to the full surface wave recordings at relatively short distances from the earthquake to extract a first-order characterization of the earthquake rupture within 20-30 minutes after the event.



Inversion of surface wave source time functions for a two-dimensional slip distribution on the fault for the 2004 Sumatra-Andaman earthquake. Observed and modeled (red) surface wave source time functions for 12 GSN stations are shown on the upper left. The overall source time function for the rupture obtained from the finite source model is shown on the lower left. The distribution of slip along the interplate fault is shown in map view on the right, with larger symbols indicating larger dip-slip sliding on the fault.

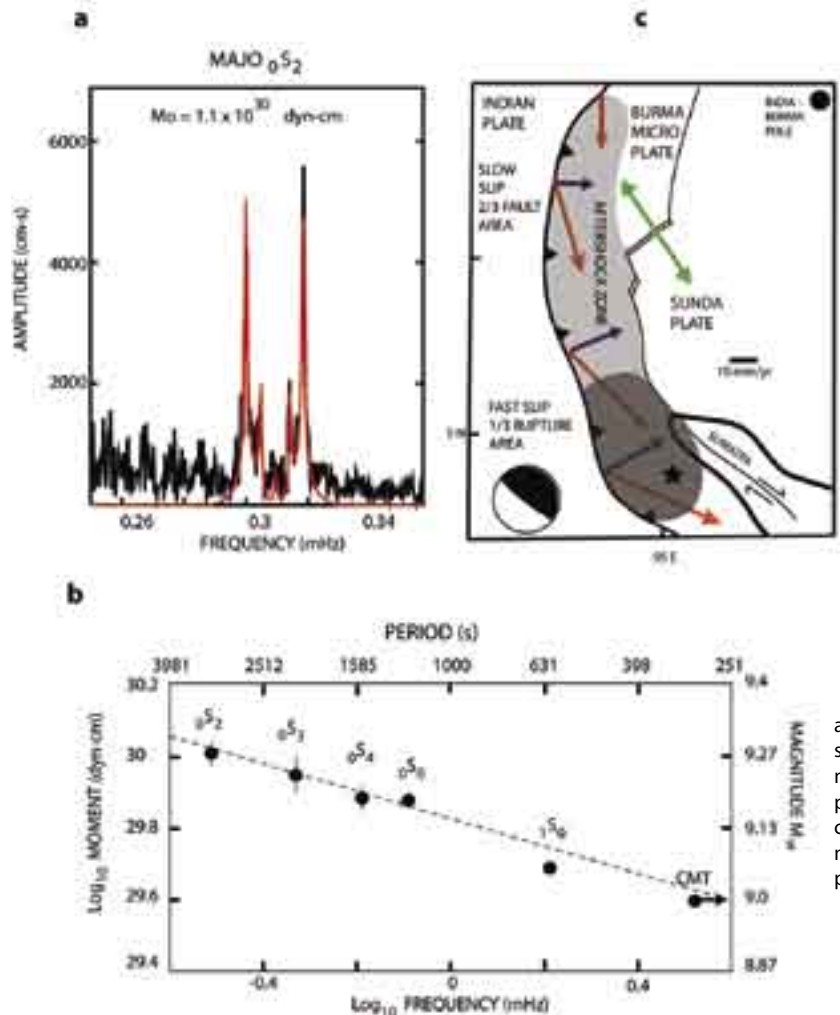
Ammon, C., et al., Rupture process of the 2004 Sumatra-Andaman earthquake, *Science*, 308, 1133-1139, 2005.

Supported by NSF grant EAR-0125595.

Ultra-long-period Characteristics of the December 2004 Sumatra Earthquake

Seth Stein, Emile A. Okal • Northwestern University

What we are learning about the recent December 26, 2004, Sumatra earthquake has important implications for understanding the subduction process, for both scientific and hazard mitigation purposes. Analysis of long period normal modes from IRIS GSN data shows that the earthquake was even bigger than first appeared. The earth's longest period normal mode, ${}_0S_2$, shows a seismic moment of 1.1×10^{30} dyn-cm, or moment magnitude $M_w = 9.3$, approximately 2.5 times larger than initially reported, making the earthquake the second largest ever instrumentally recorded. The larger magnitude likely reflects slip along the entire rupture zone suggested by aftershocks, a much larger area than previously inferred, which is comparable to a rupture of most of the Cascadia subduction zone. These observations have various important implications. It is the first time we have observed seismic moment systematically increasing with period at such long periods. Hence methods normally used to assess earthquake size dramatically underestimate it. This has not been previously observed, raising important issues about



the physics of faulting, notably at what period the moment stabilizes. Although this issue will be difficult to resolve for Sumatra, it illustrates the need to integrate seismology with GPS. Another surprising implication for tsunami physics is that the tsunami observations are in accord with our model in which the entire fault rupture contributed to the tsunami, raising the question of how slow slip could do so. Finally, the larger area indicates that strain on the entire rupture zone has been released, leaving no immediate danger of a comparable tsunami being generated on this part of the plate boundary. This rupture zone is larger than observed in earlier earthquakes along this boundary segment, indicating the variable mode of subduction zone rupture.

a, Observed (black) and predicted (red) amplitude spectrum for a ${}_0S_2$ multiplet, showing best-fitting seismic moment. b, Variation in seismic moment and M_w with period. "CMT" denotes result from 300-s surface waves. c. Schematic illustration comparing aftershock zone to minimum area of fast slip estimated from body waves and possible area of slow slip inferred from normal modes.

S. Stein and E. A. Okal, Speed and size of the Sumatra earthquake, *Nature*, 434, 581-582, 2005.

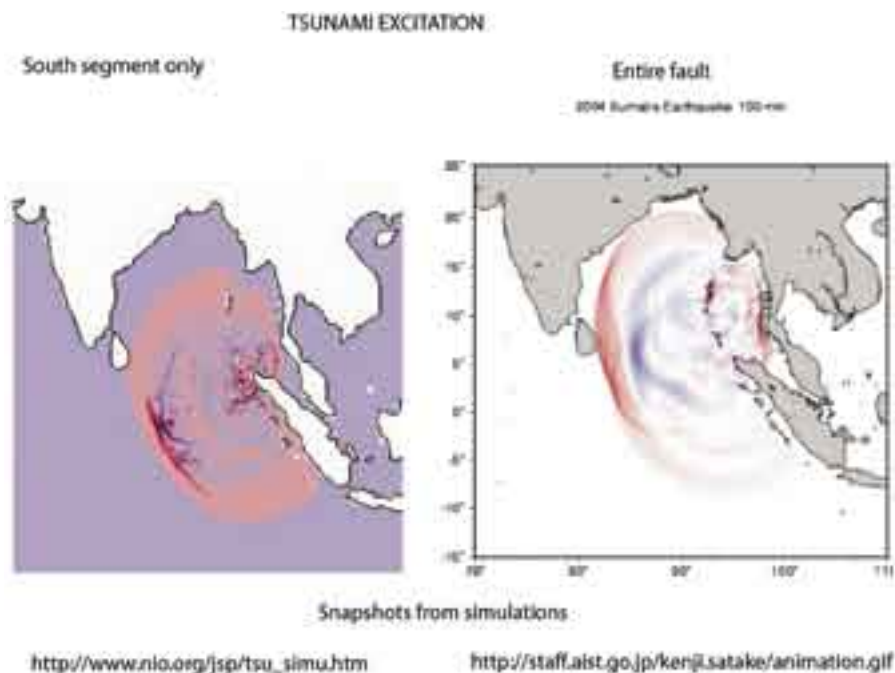
IRIS Data Allowed Rapid Public Information About Sumatra Earthquake and Tsunami

Seth Stein, Emile A. Okal • Northwestern University

The devastation caused by the December 26, 2004 Sumatra earthquake and resultant tsunami caused worldwide public interest and hence provided a “teachable moment” to inform the public about a variety of scientific and hazard issues. However, until recently, such opportunities after major earthquakes were limited because the time required to acquire and analyze seismic data was longer than the period of intense public interest. As a result, although earthquake locations, magnitudes, and mechanisms are available during this “news window”, the most interesting scientific information about the underlying tectonics and physics of major earthquakes often emerges after public interest waned. As a result, the public often gets little feel for how earthquake studies are addressing exciting and unresolved science questions which have great societal import.

The availability of IRIS GSN data immediately following the earthquake made it possible for exciting science to be reported by investigators worldwide. For example, within six weeks (February 7) of the earthquake we reported publically an analysis of ultra-long period normal mode data showing that the earthquake was even bigger than first appeared. These results were disseminated on the WWW and reported worldwide and drew great interest. Thus we were able to explain through the media a number of surprisingly sophisticated concepts. We explained the often-confusing concepts of different magnitude scales yielding different results at different periods. We further explained that these results indicated that slip occurred along the entire rupture zone suggested by aftershocks, a much larger area than previously inferred. We were then able to explain that these seemingly-arcanic seismological issues had important implications.

First, the long rupture played a key role in generating the devastating tsunami. In particular, as shown here, the large tsunami amplitudes in Sri Lanka and India result from rupture on the northern, north-trending, segment because tsunami amplitudes are largest perpendicular to the fault. Second, because the entire rupture zone slipped, strain accumulated from subduction of the Indian plate beneath the Burma microplate has been released, leaving no immediate danger of a large tsunami being generated by slip on this segment of the plate boundary. However, we explained that the danger of a large tsunami resulting from a great earthquake on segments to the south remained. When such an earthquake occurred in March, in the week our paper was published, the media again responded with interest. We used this opportunity to explain both the concept that the first earthquake may have loaded the segment to the south, and that the March earthquake, though large enough to generate a major tsunami, did not do so because the rupture did not extend updip to the sea floor. Throughout this processes we were gratified by the often-sophisticated questions we were able to explore with the media.

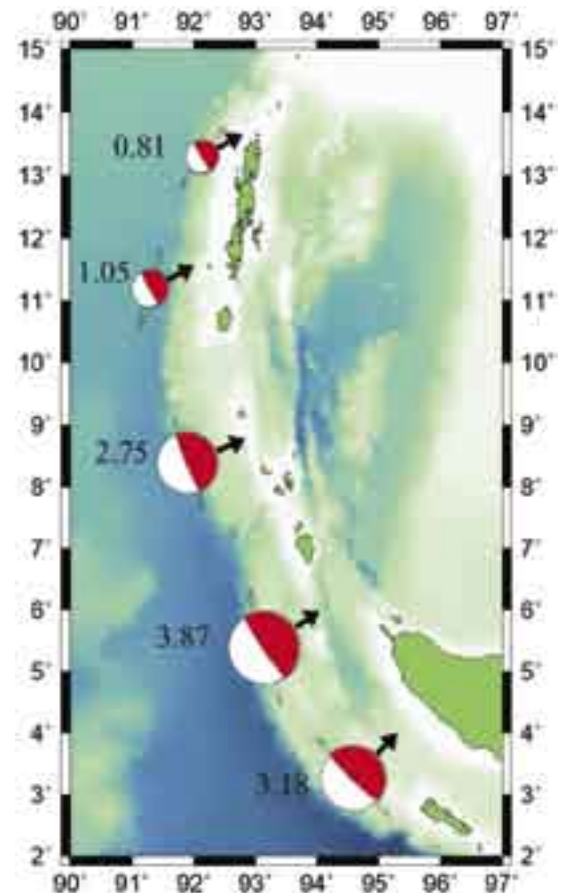


Comparison of predicted tsunami amplitudes assuming the entire fault ruptured or only the southern segment did. The largest tsunami waves would have missed Sri Lanka if only the southern segment of the fault had ruptured.

Multiple Source Analysis of the 2004 Sumatra Earthquake

Victor C. Tsai, Meredith Nettles, Göran Ekström, Adam M. Dziewonski • Harvard University

While it is agreed that the great Sumatra earthquake of December 26, 2004, was among the largest earthquakes of the past century, there has been disagreement on how large it was, which part of the fault ruptured, and how the rupture took place. We carried out a centroid-moment-tensor (CMT) analysis of the earthquake in which multiple point sources were used in the inversion to mimic a propagating slip pulse. Moment-tensor elements and centroid locations for a set of five sources were determined simultaneously. We used waveforms from the IRIS Global Seismographic Network (GSN) filtered in the pass band of 200 to 500 s in the inversion. The multiple-source inversion resulted in a 56% improvement in the fit to the waveforms compared with the original CMT analysis. The strong directivity towards the northwest observed in the data is successfully modeled by the five sources. The total moment for the five sources is 1.17×10^{30} dyne-cm, which corresponds to a moment magnitude $M_w = 9.3$, significantly larger than the $M_w = 9.0$ obtained in the standard single-source CMT analysis, but in agreement with reported long-period normal-mode amplitudes. The figure shows the locations and focal mechanisms of the five sources. The southernmost source ruptured first, and the remaining four sources ruptured in northward succession with a total duration for the earthquake of approximately 500 s. The focal mechanisms of the five sources change systematically from south to north. The strikes of the mechanisms (indicated by the needles) rotate clockwise, in agreement with the geometry of the subduction zone, and the slip vectors (indicated by black arrows) rotate from nearly pure thrust to oblique slip with a large strike-slip component. Most of the moment release occurred in the southern portion of the fault. The numbers in the figure give the individual seismic moments of each source in units of 10^{29} dyne-cm. The seismic data analyzed in this study do not appear to require a slow component of slip for the Sumatra earthquake.



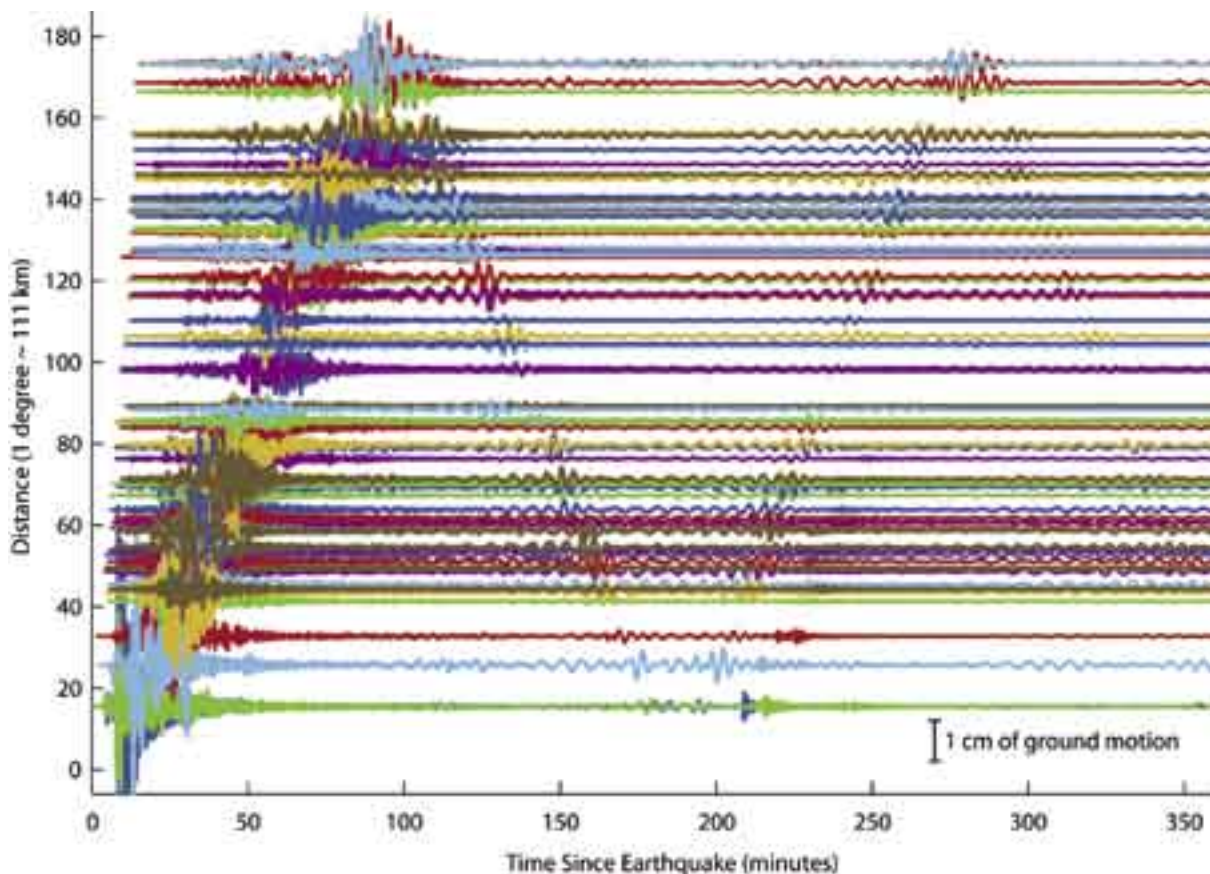
Global Seismographic Network Recording of the Sumatra-Andaman Earthquake

Rick Aster • *New Mexico Institute of Mining and Technology*

Kent Anderson • *New Mexico Institute of Mining and Technology, The IRIS Consortium*

Rhett Butler • *The IRIS Consortium*

The $M_w = 9.0$ Sumatra-Andaman Islands earthquake of December 26, 2004 was among the largest earthquakes of the past century, and the first such earthquake to be recorded by modern digital seismometry with its broad bandwidth and high dynamic range. The wavefield recorded by and real-time telemetered from the Global Seismographic Network (Butler et al., 2004) and from the observatories of the broader Federation of Digital Seismographic Networks (FDSN; Dziewonski, 1994) exceeded 1 cm (Park et al., 2005; Lay et al., 2005). Data were available to the international research and general user communities in real time from the IRIS Data Management Center.



Global vertical-component displacement record for the Sumatra-Andaman earthquake using data from 109 GSN stations retrieved from the IRIS DMC. Velocity seismograms were high-pass filtered at 120 s prior to integration. The time interval of 6 hours is sufficient to show two global circuits of the Rayleigh waves.

Butler R., Lay, T., Creager, K., Earle, P., Fischer, K., Gaherty, J., Laske, G., Leith, W., Park, J., Ritzwoller, M., Tromp, J., and L. Wen, The Global Seismographic Network Surpasses its Design Goal, *EOS Trans. AGU*, 85, 225-229, 2004.

Park, J., K. Anderson, R. Aster, R. Butler, T. Lay, and D. Simpson, Global Seismographic Network Records the Great Sumatra-Andaman Earthquake, *EOS Transactions AGU*, 86(6), 57, 60-61, 2005.

Lay, T., Kanamori, H., Ammon, C., Nettles, M., Ward, S., Aster, R., Beck, S., Bilek, S., Brudzinski, M., Butler, R., DeShon, H., Ekström, G., Satake, K., Sipkin, S., The Great Sumatra-Andaman Earthquake of December 26, 2004, *Science*, 308, 1127-1133, doi:10.1126/science.1112250, 2005.

Rapid Imaging of Large Earthquake Rupture Zones with P waves: Application to the 28 March 2005 Sumatra M_w 8.7 Earthquake Suggests Bilateral Rupture

Kris Walker, Miaki Ishii, Peter Shearer • *University of California, San Diego*

Paul Earle • *U.S. Geological Survey*

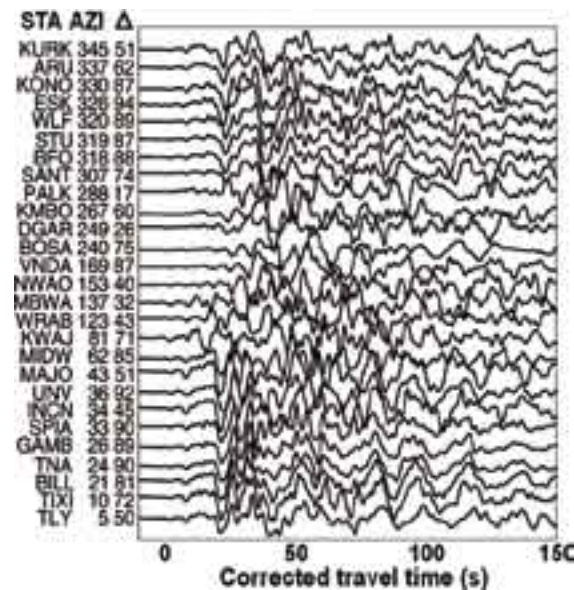
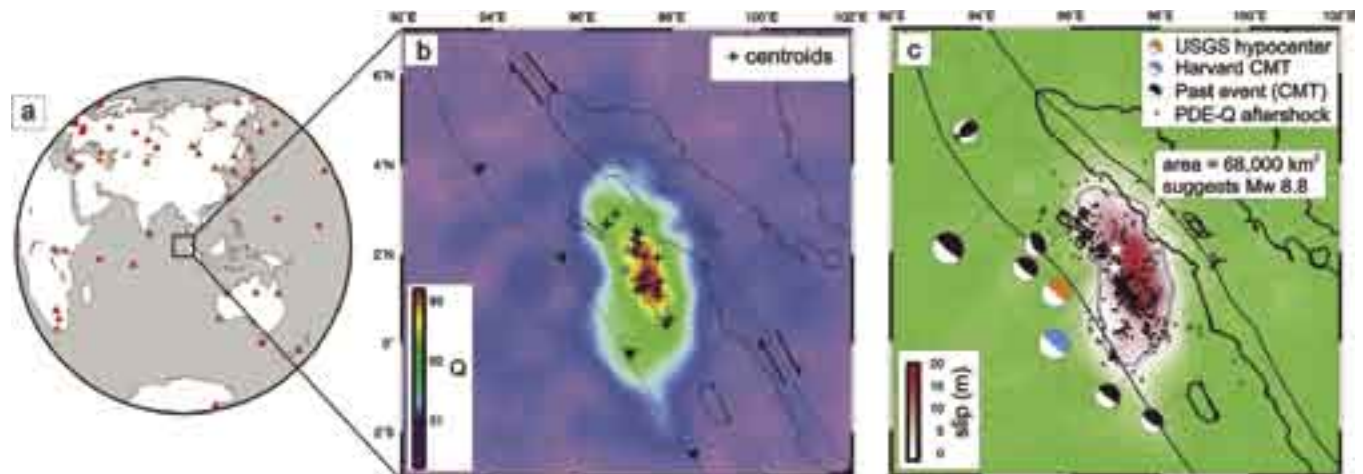


Figure 2. P-waves used to create the image in Figure 1. These seismograms were recorded on vertical component stations of the Global Seismic Network. Traces are sorted by station azimuth from the epicenter and aligned with a waveform cross-correlation method using a 15 s window beginning at the predicted IASP91 travel time.

Figure 1. Images of back-projected P-wave energy for the March 28, 2005, $M_w = 8.7$ Sumatra earthquake. (a) The GSN station distribution with respect to the epicenter. (b) Estimated relative seismic energy release with plus symbols showing spatial centroids at different times. (c) Estimated slip using a simple energy/moment scaling relationship. Aftershock locations and selected focal mechanisms are also plotted. The thick gray contour outlines our estimate of the fault plane.

We image the rupture zone of the March 28, 2005, Sumatra M_w 8.7 earthquake by directly back-projecting teleseismic P waves to their source. We use broadband, vertical-component seismograms recorded by the Global Seismic Network and the Japanese Hi-net network. Our resulting images agree favorably with the aftershock distribution and the location of the Harvard centroid moment tensor. The back-projected energy suggests that the rupture was 120 s long and propagated at 2.9-3.3 km/s from the hypocenter in two directions delayed by about 50 s: first towards the northeast for about 100 km and then toward the southeast for about 200 km. The seismic radiation throughout the rupture zone is characterized by periods between 2-10 s. However, the southern half of the rupture zone generated additional longer-period energy between 10-30 s. The rupture occurred over a surface area of about 70,000 km^2 , which is fairly consistent with a M_w 8.7 event on a nearly horizontal fault plane. It appears that this earthquake is similar to the 1861 M_w 8.3-8.5 thrust event in its location, size, and geometry.

NSF Grant Number: EAR0229323

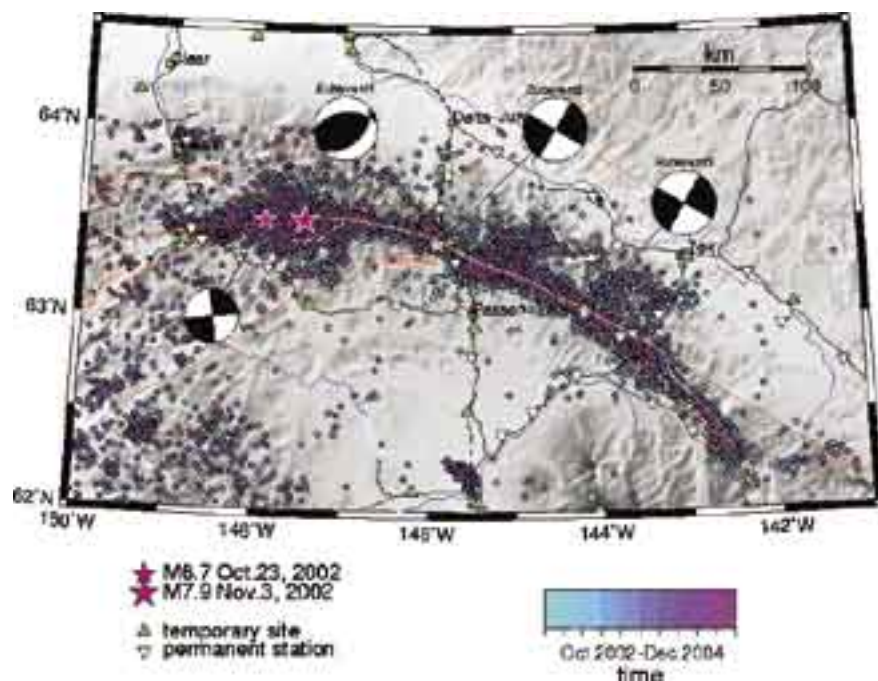
Regional Monitoring of the Aftershock Sequence of the 2002 M 7.9 Denali Fault, Alaska, Earthquake

Natalia A. Ruppert, Roger A. Hansen, J.C. Stachnik, Steve Estes • University of Alaska, Fairbanks

The 2002 Denali fault, Alaska, earthquake sequence provides an exciting opportunity to study major continental strike-slip events. The sequence began with the magnitude Mw 6.7 Nenana Mountain event on October 23, 2002. The source mechanisms from teleseismic and regional data indicate right-lateral strike-slip faulting on a vertical fault plane. Ten days later, on November 3, 2002, the magnitude Mw 7.9 Denali Fault earthquake ruptured for nearly 340 km along the three different faults. It initiated as a thrust event on the previously unrecognized Susitna Glacier Thrust fault, a splay fault located south of the main DF strand. The rupture then transferred onto the main DF strand and continued as a predominately right-lateral strike-slip event for ~220 km until it reached the Totschunda fault (TF) near 143°W longitude. At that point, it right-stepped onto the more south-easterly trending TF strand and stopped after rupturing nearly 70 km. A team of geologists surveyed the total length of the ruptured faults and reported maximum vertical and horizontal offsets of 2.8 m and 8.8 m, respectively, west of the DF and TF junction.

Following the Mw 6.7 event, the Alaska Earthquake Information Center (AEIC) installed a network of seven instruments west and south of its aftershock zone. This initial network consisted of three strong motion and four broadband stations. From this portable network two strong motion and three broadband instruments recorded the Mw 7.9 mainshock. The nearest site was 34 km from its epicenter. Within a few days of the mainshock an additional nineteen temporary sites were installed for monitoring the central and eastern segments of the rupture zone. The temporary installations greatly improved regional station coverage around the DF and provided valuable data. The temporary network consisted of a mixture of strong motion and broadband instruments. The sites were serviced every three to four weeks, when the data were retrieved from the instruments and

brought back to the AEIC to be merged with the permanent network data. Data recovery continued throughout the difficult Alaska winter leading to a recovery rate of less than 75%. The temporary sites were dismantled in June, 2003. The AEIC located ~30,000 aftershocks through the end of 2004. The aftershock sequence provides valuable information on the characteristics of the rupture zone.



Ratchkovski, N.A., A. Hansen, J.C. Stachnik, T. Cox, O. Fox, L. Rao, E. Clark, M. Lafeyers, S. Estes, J.B. MacCormack, and T. Williams, Aftershock sequence of the MW 7.9 Denali, Alaska, earthquake of 3 November 2002 from regional seismic network data, *Seism. Res. Lett.*, 74, 743-752, 2003.

Ratchkovski, N.A., Change in stress directions along the central Denali fault, Alaska after the 2002 earthquake sequence, *Geophys. Res. Lett.*, 30, 2017, doi:10.1029/2003GL017905, 2003.

N.A. Ratchkovski, S. Wiemer, and R.A. Hansen, Seismotectonics of the Central Denali Fault, Alaska and the 2002 Denali Fault Earthquake Sequence, *Bull. Seis. Soc. Am.* 6B, S156-S174, 2004.

USGS contract #01HQAG0138 and NSF grant #EAR-0328043

The 2003 Mid-Indian Ocean Earthquake: An Unusual Earthquake in Oceanic Lithosphere

Michael Antolik • *Quantum Technology Services, Inc.*

Rachel E. Abercrombie • *Boston University*

Göran Ekström • *Harvard University*

We analyze the source process of the large earthquake (Mw 7.6) that occurred in the central Indian Ocean on July 15, 2003. This earthquake ruptured a fossil fracture zone within the Indian Plate. Its epicenter lies within 20 km of the Carlsberg Ridge separating the Somalian and Indian plates, but the rupture directivity was unilateral away from the spreading ridge. Although the earthquake occurred in a remote area far from land, the density and quality of stations within the current IRIS Global Seismographic Network is sufficient to resolve many details of the rupture process.

Analysis of broadband body waves (P and SH) at 1-150 s period reveal an unusual rupture process. The source duration of longer than a minute is more than twice as long as expected from earthquake scaling relations, yet ~80% of the moment release occurred in two energetic asperities near the end of the rupture (see figure). Very little slip occurred near the hypocenter, or close to the Carlsberg Ridge. The two energetic asperities are located in lithosphere with an age of 7 Ma or greater as estimated from the spreading rate of 36 mm/yr.

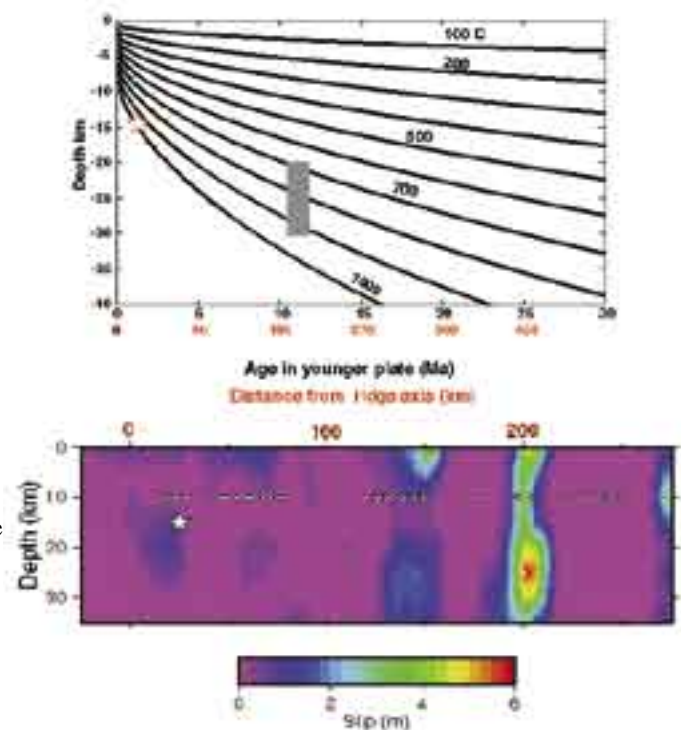
The rupture process of the 2003 earthquake is strikingly similar to the March 20, 1994, earthquake that occurred along the Romanche transform in the central Atlantic Ocean. While some studies have concluded that oceanic strike-slip earthquakes are characterized by high apparent stress (e.g., Choy and McGarr, 2002), Perez-Campos et al. (2003) analyzed several oceanic earthquakes with unusually long source durations (including the Romanche earthquake) and suggested that these long-duration events are the result of a slow slip process and low apparent stress. They concluded that the average apparent stress of oceanic strike-slip earthquakes is not significantly higher than those occurring within continents. We searched for a slow rupture component to the 2003 Mid-Indian earthquake using long-period spectra and the method of Abercrombie and Ekström (2001) and could find no evidence for slow slip.

We suggest that the long source duration of the 2003 earthquake is due only to nucleation close to the active Carlsberg Ridge in very young lithosphere. Young oceanic lithosphere may be unable to sustain slip in a large event due to steady release of strain in aseismic creep events, and large strike-slip earthquakes may occur only in the central portions of long transforms or intraplate regions (in lithosphere with an age larger than 7 Ma). These earthquakes typically rupture energetic asperities like those which failed in the 2003 earthquake, and lead to the observation that oceanic strike-slip earthquakes have the largest apparent stresses among the global population of shallow earthquakes (Choy and McGarr, 2002).

Abercrombie, R.E., and G. Ekström, Earthquake slip on oceanic transform faults, *Nature*, 410, 74-77, 2001.

Choy, G.L., and A. McGarr, Strike-slip earthquakes in the oceanic lithosphere: Observations of exceptionally high apparent stress, *Geophys. J. Int.*, 150, 506-523, 2002.

Perez-Campos, X., J.J. McGuire, and G.C. Beroza, Resolution of the slow earthquake/high apparent stress paradox for oceanic transform fault earthquakes, *J. Geophys. Res.*, 108(B9), 2444, doi: 10.1029/2002JB002312, 2003.



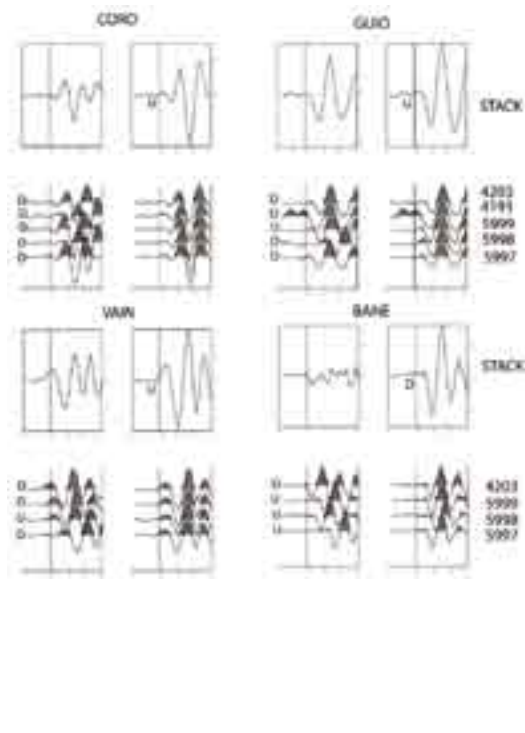
(Top) Isotherms (at 100° C intervals) for a simple half-space cooling model of the Indian Plate lithosphere. The horizontal axis is plotted in terms of age of the younger side of the fracture zone and distance from the Carlsberg Ridge (red). The age and depth range of the strongest asperity of the 2003 earthquake is indicated by the gray rectangle. (Bottom) Slip distribution of the 2003 Mid-Indian Ocean earthquake obtained from inversion of teleseismic body waves, plotted as distance from the Carlsberg Ridge and depth below the seafloor. The hypocenter position is shown by the star.

Relocations and Focal Mechanisms Determined from Waveform Cross-Correlation of Seismic Data from the Nicoya Peninsula, Costa Rica

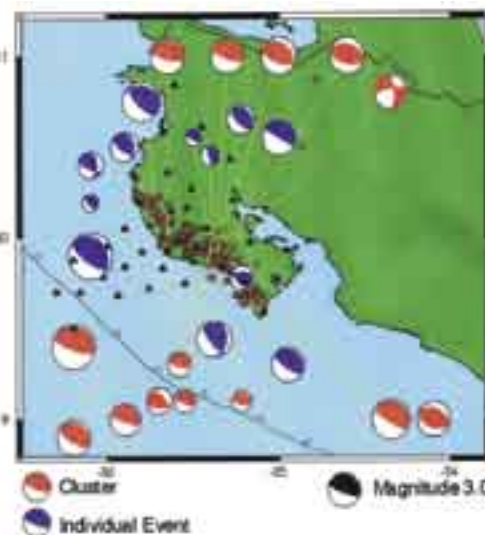
Samantha Hansen, Susan Schwartz • University of California, Santa Cruz

Heather DeShon • University of California, Santa Cruz, now at University of Wisconsin, Madison

The Nicoya Peninsula in Costa Rica lies directly over the seismogenic zone of the Middle America Trench, making this an ideal location for geophysical investigations. As part of the collaborative Costa Rica Seismogenic Zone Experiment, a seismic transect consisting of twenty land and fourteen ocean bottom seismometers was operated across the Nicoya Peninsula from December, 1999, to June, 2001. Waveform cross-correlation and clustering techniques have been employed to examine event similarity and to compute adjustments for P-wave arrival times. The corrected picks were then used to determine cross-correlated relocations as well as more reliable focal mechanisms. Large-scale differences between the cross-correlated relocations and the previously-determined simultaneous inversion relocations were not observed. It is believed that since low-error events were used to begin with and since most of the P-wave shifts were small, the cross-correlated picks did not lead to regional-scale differences in earthquake locations. However, the focal mechanism determinations using the cross-correlated picks were significantly enhanced. For events believed to be interplate, over 95% of the focal mechanisms computed are consistent with underthrusting. Focal mechanisms were also computed for intraplate events in the overlying and subducting plates. In the overlying plate, evidence for dextral strike-slip motion is observed in the more northerly part of the peninsula while extensional, normal motion is seen at the southern tip of the peninsula. These motions are most likely associated with oblique convergence and seamount subduction, respectively. In the subducting plate, the steep P- and T-axes of events at depth are consistent with unbending of the slab.



Cross-Correlated Waveforms. The panels show the waveforms at four different stations for a cluster of correlated events. The left panels show stacked (top) and individual (bottom) waveforms aligned on the original hand picks while the right panels show picks stacked (top) and individual (bottom) waveforms aligned on the cross-correlated picks. The 'U' and 'D' labels indicate 'up' or 'down' first motion, respectively.



Interplate Focal Mechanisms. Map showing events believed to be interplate seismicity (red dots) as well as focal mechanisms for some of these events. Focal mechanisms were computed for both correlated and clustered events (red beach balls) as well as individual events (blue beach balls). About 95% of the computed focal mechanisms are consistent with underthrusting.

DeShon, H.R., S.Y. Schwartz, A.V. Newman, V. González, M. Protti, L.M. Dorman, T.H. Dixon, E.O. Norabuena, and E.R. Flueh, Seismogenic zone structure beneath the Nicoya Peninsula, Costa Rica, from 3D local earthquake P- and S-wave tomography, *Geophys. J. Int.*, in review, 2004.

Rowe, C.A., R.C. Aster, B. Borchers, and C.J. Young, An Automatic, Adaptive Algorithm for Refining Phase Picks in Large Seismic Data Sets, *Bull. Seismol. Soc. Am.*, 92, 1660-1674, 2002a.

Rowe, C.A., R.C. Aster, W.S. Phillips, R.H. Jones, B. Borchers, and M.C. Fehler, Using Automated, High-precision Repicking to Improve Delineation of Microseismic Structures at the Soultz Geothermal Reservoir, *Pure Appl. Geophys.*, 159, 563-596, 2002b.

Seismogenic Zone Processes at the Costa Rica Convergent Margin

Susan Y. Schwartz, Daniel E. Sampson, Kevin M. Brown • *University of California, Santa Cruz*

Heather R. DeShon • *University of Wisconsin*

Andrew V. Newman • *Los Alamos National Laboratory*

Leroy M. Dorman • *Scripps Institution of Oceanography*

Timothy H. Dixon • *Edmundo Norabuena, University of Miami*

Marino Protti, Victor Gonzalez • *Universidad Nacional, Costa Rica*

Ernst Flueh • *GEOMAR, Germany*

The Costa Rica Seismogenic Zone Experiment (CRSEIZE) was a large international effort conducted in 1999-2001 to collect GPS, fluid flow and seismic observations in Costa Rica in order to better understand the mechanical behavior of the seismogenic zone. The seismic component consisted of two OBS and PASSCAL deployments, one primarily recording aftershocks of the 1999, Mw 6.9 underthrusting earthquake in central Costa Rica and the other on and offshore the Nicoya Peninsula (Figure 1). Using arrival time data from our local seismic array and 3D absolute and relative earthquake location techniques, we precisely located seismicity defining the seismogenic zone geometry and up and down dip limits. For northern Costa Rica, well-located earthquakes beneath the Nicoya Peninsula reveal significant along-strike variation. Shallowing of the up dip limit of microseismicity from ~20 to ~15 km occurs where the origin of subducting oceanic crust changes from East Pacific Rise (EPR) to Cocos-Nazca Spreading Center (CNS). The geodetically locked region of the plate interface locates up dip of the onset of microseismicity, while the more freely slipping regions have abundant microseismicity (Figure 2). Research supported by NSF's Margins and Geophysics programs; land instrumentation provided by IRIS PASSCAL.

Newman, A.V., S. Y. Schwartz, V. Gonzalez, H.R. DeShon, J. Protti, L. M. Dorman, Along-strike variability in the seismogenic zone below the Nicoya Peninsula, Costa Rica, *Geophys. Res. Lett.*, 29, doi10.1029/2002GLO15402, 2002.

DeShon, H.R. S.Y. Schwartz, S.L. Bilek, L.M. Dorman, V. Gonzalez, J.M. Protti, T. H. Dixon, and E.R. Flueh, Seismogenic zone structure of the southern middle America Trench, Costa Rica, *J. Geophys. Res.*, 108, doi10.1029/2002JB002294, 2003.

Norabuena, E., T.H. Dixon, S.Y. Schwartz, H. DeShon, M. Protti, L. Dorman, E. R. Flueh, P. Lundgren, A. Newman, F. Pollitz, D. Sampson, Geodetic and seismic constraints on some seismogenic zone processes in Costa Rica, *J. Geophys. Res.*, 109, doi10.1029/2003JB002931, 2004.

DeShon, H.R. and S.Y. Schwartz, Evidence for serpentinization of the forearc mantle wedge along the Nicoya Peninsula, Costa Rica, *Geophys. Res. Lett.*, 31,doi:10.1029/2004GL021179, 2004.

Schwartz, S.Y. and H.R. DeShon, Distinct up-dip limits to geodetic locking and microseismicity at the northern Costa Rica seismogenic zone: Evidence for two mechanical transitions, in *Interplate Subduction Zone Seismogenesis*, eds. T. Dixon and J.C. Moore, Columbia University Press, New York, in press. 2005.

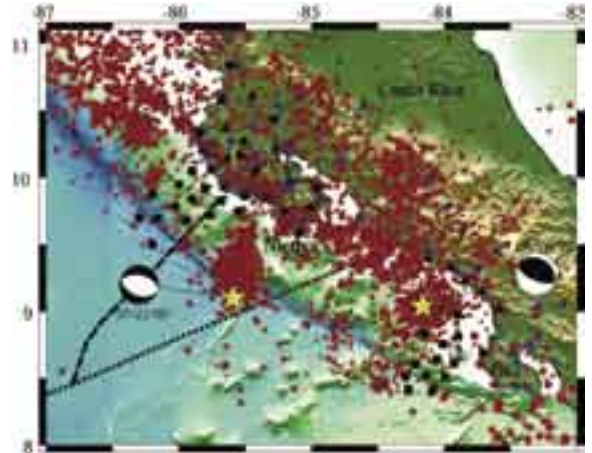


Figure 1. CRSEIZE consisted of 43 campaign GPS stations (blue diamonds) and two passive on/off-shore PASSCAL seismic experiments (black squares and triangles are broadband and short-period sensors) that recorded earthquakes (red circles) along Middle America Trench. Osa Peninsula experiment mainly recorded aftershocks of Mw 6.9, 8/20/99 Quepos earthquake (yellow star; Harvard CMT mechanism). Thick and thin dashed lines mark boundaries of oceanic crust of differing origins.

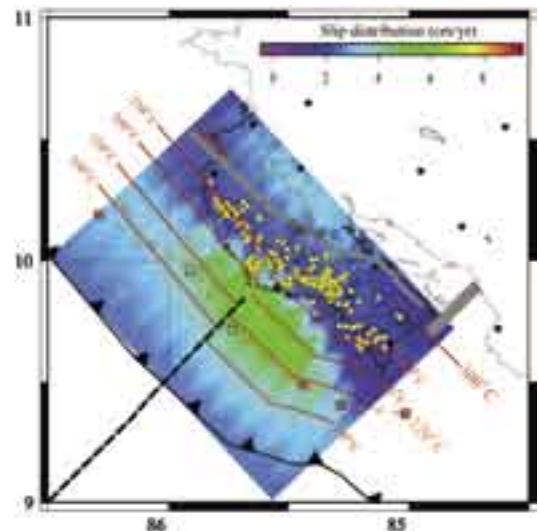


Figure 2. Comparison of well-located earthquakes from CRSEIZE (yellow circles are plate interface events), distribution of locked slip from inversion of the GPS data (Norabuena et al., 2004), modeled isotherms, and Moho from DeShon and Schwartz (2004). Earthquakes reach an up-dip limit where temperatures reach 200-250°C. The up-dip extent of locked slip (~6 cm/yr) occurs coincident with the 100-150°C isotherms that shallows across the East Pacific Rise to Cocos-Nazca Spreading Center generated crustal boundary (dashed line).

Aftershock Study of the Subduction to Strike-Slip Transition of the North American-Caribbean Plate Boundary in the Dominican Republic

Jay Pulliam, Victor Huérfano, Christa von Hillebrandt-Andrade, Denisse Ocasio Campos, Ivelisse Camacho • *Red Sísmica de Puerto Rico, Depto. de Geología, Universidad de Puerto Rico, Mayagüez*

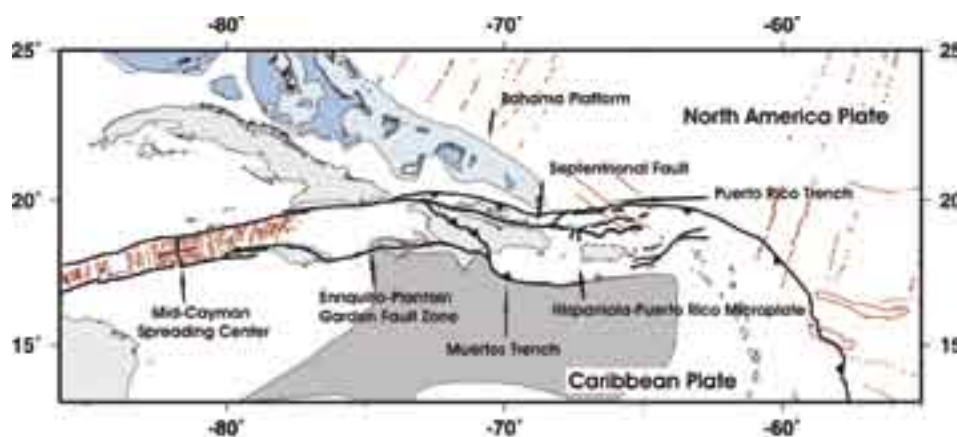
Luis Odonel Gomez • *Instituto Nacional de Recursos Hidráulicos, Santo Domingo, República Dominicana*

Juan Payero • *Instituto Sismológico Universitario de la Universidad Autónoma Santo Domingo, Santo Domingo, República Dominicana*

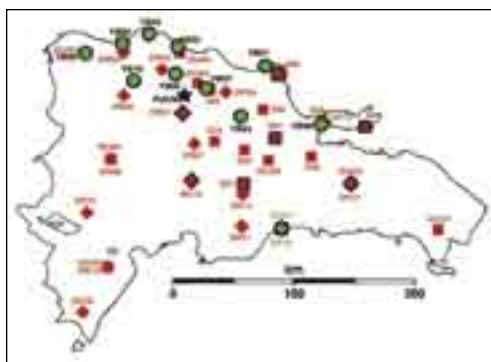
Eugenio Fajardo • *Pontificia Universidad Católica Madre y Maestra, Santiago, República Dominicana*

The Northern Caribbean Plate Boundary Zone is a complex region that has been modified extensively by the relative eastward movement of the Caribbean Plate and the plate's impact with the buoyant Bahama carbonate platform. This movement has produced extensive subduction of oceanic crust belonging to the North American Plate, a broad zone of deformation to accommodate strain, the development of several new transform and normal faults to relieve stress after collisions, the formation and rotation of microplates, and the rearrangement and aggregation of crustal fragments into new islands.

On 22 September 2003, a large ($M_w = 6.5$) earthquake struck the Dominican Republic, causing widespread damage that included partially collapsed buildings and bridges in the cities of Santiago and Puerto Plata and landslides in the mountain-



Schematic of the Northern Caribbean Plate Boundary Zone with the location of the 22 September 2003 main shock (red star).



Map of currently and recently operating seismic stations in the Dominican Republic. The symbol indicates the station's network affiliation: ISU stations are S1-10 and ISU01-10; INDRHI stations are DR01-16; PRSN/UT temporary stations are YB01-10. The star is a broadband station at PUCMM in Santiago. Symbol color indicates the sensor's passband: red = short-period, green = intermediate-period, black = broadband. Black outlines indicate three-component sensors.

ous outlying areas. Aftershocks reaching $M_w = 5.1$ followed for months afterward. This earthquake sequence is the strongest to affect the Dominican Republic since a series of powerful thrust events, which included five earthquakes ranging in magnitude from 7.1 to 8.1, occurred between 1943 and 1953. Prior to 1943, significant earthquakes occurred in 1564 (in which the city of Santiago was destroyed), 1783, 1842, 1887, and 1897.

Following the 2003 Puerto Plata main shock we deployed 10 IRIS PASSCAL broadband seismographs through IRIS's Rapid Aftershock Mobilization Program in and around the aftershock zone for a period of two months and are analyzing the data jointly with data from two permanent seismic networks in the DR. Analyses include producing a new 1D model of earth structure, relocating more than 400 aftershocks, producing a 3D tomographic model of the fault zone from phase arrivals, and computing focal mechanisms. These will help elucidate the strain partitioning between strike-slip and thrust faults and form the basis for a longer-term study of the deep structure and tectonics beneath Hispaniola, which includes a pocket of unusually deep earthquakes, subduction of the Caribbean lithosphere northward—opposing the southwestward subduction of the North American Plate—and a long historical record of devastating, and tsunamigenic, earthquakes.

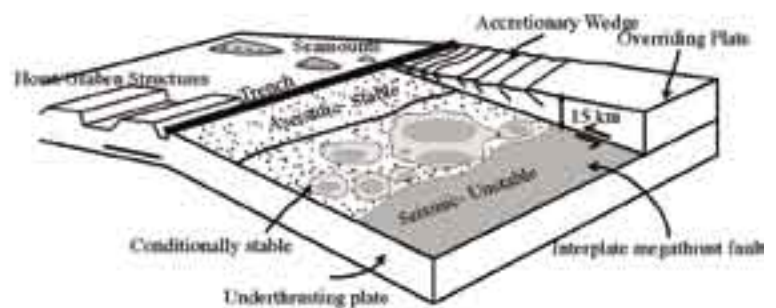
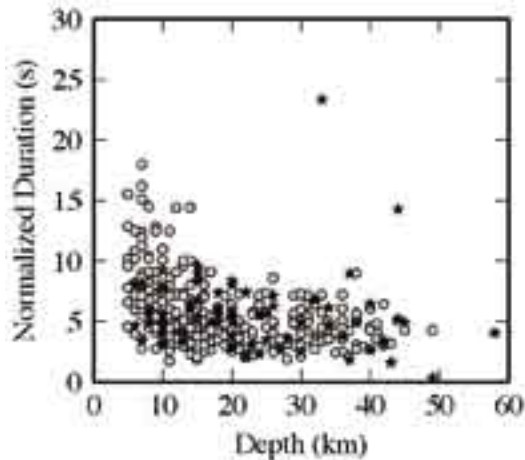
Exploring Subduction Zone Earthquake Rupture

Susan L. Bilek • *New Mexico Institute of Mining and Technology*

Thorne Lay • *University of California, Santa Cruz*

Larry J. Ruff • *University of Michigan*

Subduction zone earthquakes generate significant amounts of moment in great earthquakes, such as the 2004 Mw 9.0 Sumatra-Andaman event. In addition, events such as these can have tragic results, as ground shaking and tsunami can result in large numbers of casualties. We need to increase our understanding of subduction zone earthquake processes and the important tectonic conditions that can lead to the devastating events. Some of our research has explored the rupture characteristics of subduction zone earthquakes, both large and small magnitude, to understand variable rupture and tsunami earthquake occurrence. For example, tsunami earthquakes such as the 1992 Nicaragua event can be very devastating, and models suggest shallow rupture (up to the trench in some cases) though low-rigidity materials can produce the observed tsunami data. Using seismic waveforms obtained through IRIS, we have examined rupture processes of hundreds of earthquakes in 14 global subduction zones to find a depth-dependent behavior of rupture characteristics. These results, summarized below, suggest a depth dependence of frictional properties along the megathrust, which may impact tsunami earthquake generation. Indeed, these results suggest heterogeneous conditions along the megathrust, but that shallow portions of the fault may contain patches of conditionally stable material, as suggested by tsunami models.

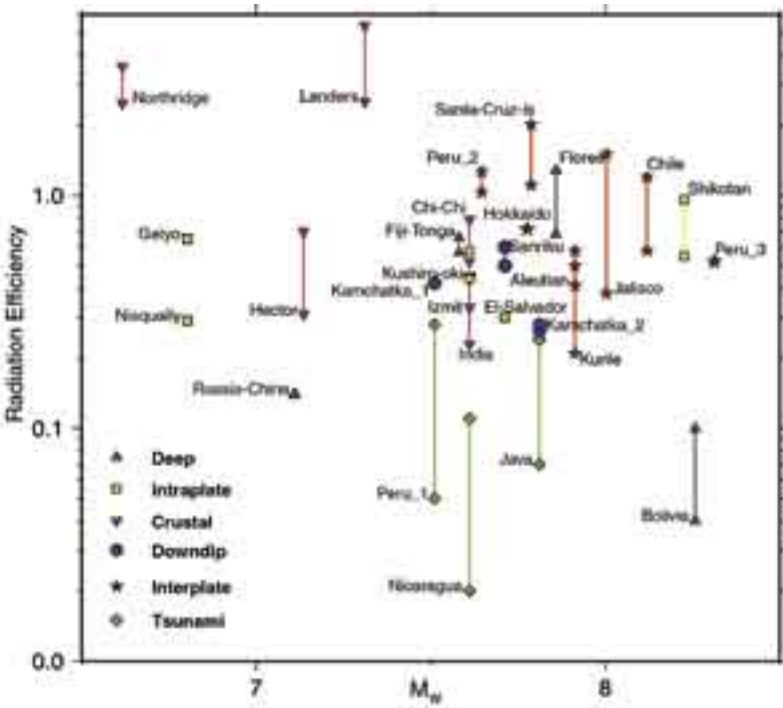


Bilek, S.L., Lay, T., and Ruff, L.J., *J. Geophys. Res.*, 109, B09308, doi:10.1029/2004JB003039, 2004.

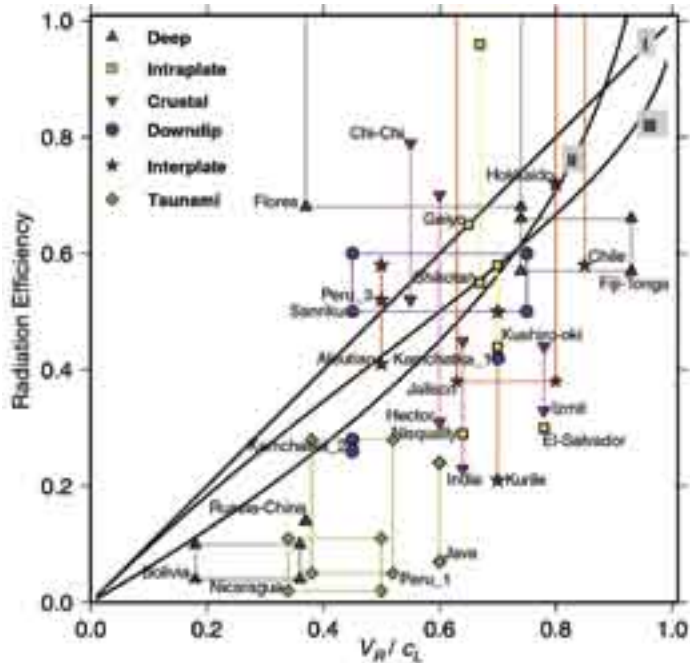
Bilek, S.L. and Lay, T., *Geophys. Res. Lett.* 29, 1673, doi:10.1029/2002GL015215, 2002

Observational Constraints on the Fracture Energy of Subduction Zone Earthquakes

Anupama Venkataraman, Hiroo Kanamori • California Institute of Technology



We computed the radiated energy for 23 large (mostly Mw 7.5) subduction zone earthquakes recorded between 1992 and 2002 and some smaller, well-studied subduction zone and crustal earthquakes. Using estimates of static stress drop and a slip-weakening model we determine the radiation efficiency of these earthquakes. The radiation efficiencies are consistent with the rupture speed estimated for these earthquakes. Most earthquakes have radiation efficiencies between 0.25 and 1 and are hence efficient in generating seismic waves, but tsunami earthquakes and two deep earthquakes, the 1994 Bolivia and the 1999 Russia-China border earthquakes, have very small radiation efficiencies (< 0.25) and hence dissipate a large amount of energy during faulting. We suggest that in these deep events, energy is probably dissipated in thermal processes in the fault zone, while it is possible that the morphology of the trench causes large energy dissipation during the rupture process of tsunami earthquakes.



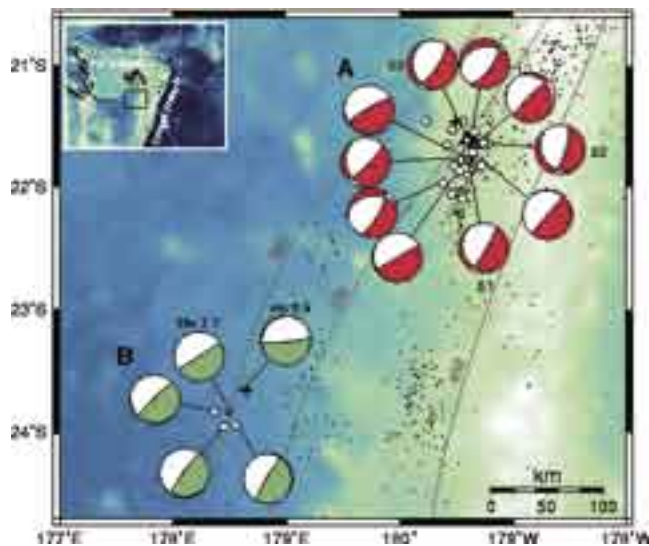
Venkataraman, A., and H. Kanamori, Observational Constraints on the Fracture Energy of Subduction Zone Earthquakes, *J. Geophys. Res.*, 109, No. B5, B05302, 10.1029/2003JB002549, 2004.

Remote Triggering of Deep Earthquakes: Insight from the 2002 Tonga Sequences

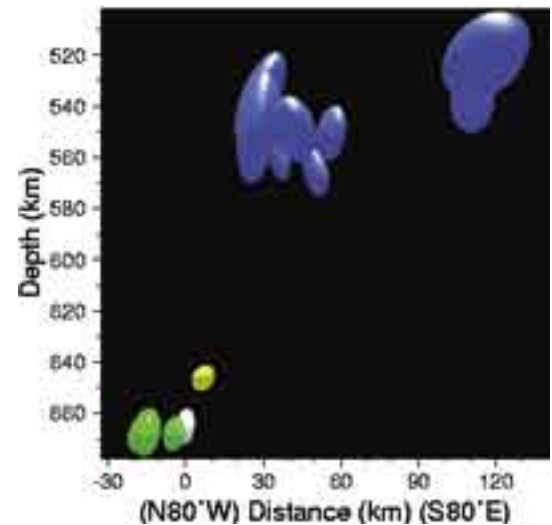
Rigobert Tibi, and Douglas A. Wiens • Washington University

Hiroshi Inoue • National Research Institute, Ibaraki, Japan

It is well established that an earthquake in the Earth's crust can trigger subsequent ruptures, but such triggering has not been documented for deeper earthquakes. Models for shallow fault interactions suggest that static (permanent) stress changes can trigger nearby earthquakes, within a few fault lengths from the causative event, whereas dynamic (transient) stresses carried by seismic waves may trigger earthquakes both nearby and at remote distances. Detailed analysis of the August 19, 2002 Tonga deep earthquake sequences shows evidence for both static and dynamic triggering. Seven minutes after a magnitude 7.6 earthquake occurred at a depth of 598 km, a magnitude 7.7 event (664 km depth) occurred 300 km away, in a previously aseismic region. Nearby aftershocks of the first mainshock are preferentially located in regions where static stresses are predicted to have been enhanced by the mainshock. But the second mainshock and other triggered events are located at larger distances where static stress increases should be negligible, thus suggesting dynamic triggering. The origin times of the triggered events do not correspond to the arrival times of the main seismic waves from the mainshocks and the dynamically-triggered earthquakes frequently occur in aseismic regions below or adjacent to the seismic zone. We propose that these events are triggered by transient effects incorporating nonlinear short-term delay mechanisms in regions where high stress may predominate, but where earthquakes have difficulty nucleating without external influences.



Epicentral locations of the two 2002 Tonga deep earthquake sequences. Dots represent background seismicity. Lines are contours of deep seismicity (Gudmundsson and Sambridge, 1998), with the numbers indicating the depth in km to the seismogenic zone. A) Star indicates the epicenter (S1) of the initial earthquake (Mw 7.6, depth 598 km), triangles its second (S2) and third (S3) episodes of rupture. Cross represents a foreshock that occurred 8 days before the main event. Circles are aftershocks. B) Locations of the triggered earthquake (star) (Mw 7.7, depth 664 km), and its aftershocks (circles). Cross represents a foreshock that occurred about five minutes before the main event.



Vertical cross-section perpendicular to the deep Tonga slab showing the 95% confidence ellipsoid for the location of the triggered 2002 Tonga sequence. White is the main event, yellow its foreshock, green the aftershocks, and blue the relocated background seismicity from the latitude range between -23.25° and -24.25° . Note the lack of seismicity below about 570 km, indicating that the triggered 2002 sequence occurred in a previously aseismic portion of the slab.

Tibi, R., Wiens, D.A. and Inoue, H., Remote triggering of deep earthquakes in the 2002 Tonga sequences, *Nature*, 424, 921-925, 2003.

Coupled Seismic Slip on Adjacent Oceanic Transform Faults

Donald W. Forsyth, Yingjie Yang, Maria-Daphne Mangriotis • Brown University

Yang Shen • University of Rhode Island

In a 4.5 hour period, more than 60 events in an earthquake swarm on the western boundary of the Easter microplate were detected by an array of ocean bottom seismometers and GSN station RPN on Easter Island. The larger events of the swarm were recorded by many GSN stations; the surface wave radiation patterns indicate that these events were strike-slip earthquakes located on two transform faults separated by about 25 km. Slip on the faults was closely coupled, with activity alternating back and forth randomly between the two transforms. Coupled seismic activity is usually attributed to triggering by static stress changes or dynamic stresses in propagating shear waves generated by another earthquake, but these earthquakes are too small for either mechanism to be plausible. The swarm may have been the seismic manifestation of a larger, primarily aseismic, slip event or slow earthquake involving both transforms, perhaps triggered by dike injection on the Easter-Pacific spreading center.

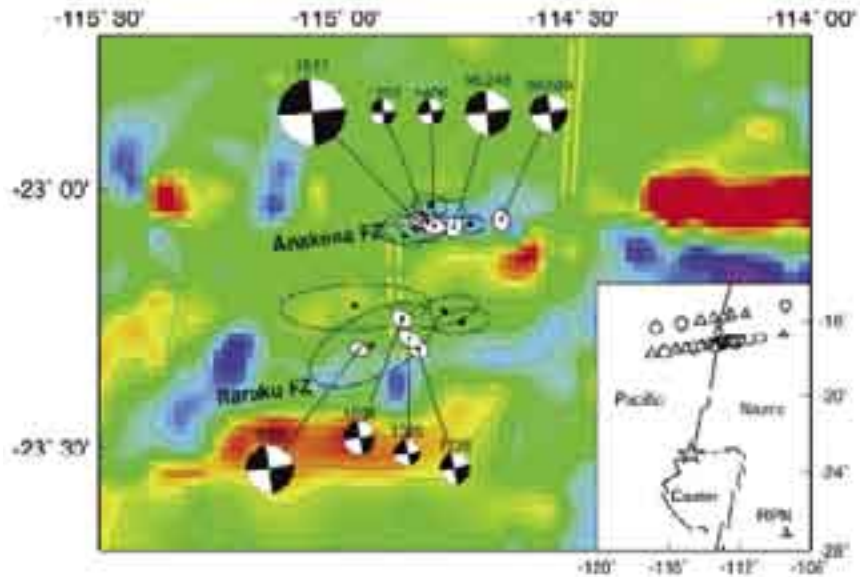


Figure 1. Locations and focal mechanisms of earthquakes in the swarm. Ellipses represent 95% confidence limits of locations relative to reference event (star). Filled ellipses are largest events for which mechanisms have been determined. Area of mechanism diagram is proportional to seismic moment, shaded quadrants represent compressional arrivals, and labels above diagrams indicate origin time or year and Julian day for events not part of the swarm. Colors indicate depth to seafloor, with red shades. Double yellow lines indicate location of spreading centers, dashed where uncertain. Inset shows location of seismometers (triangles) and differential pressure gauges (circles) of the MELT Experiment, Global Seismic Network station RPN, location of swarm (star) and plate boundaries.

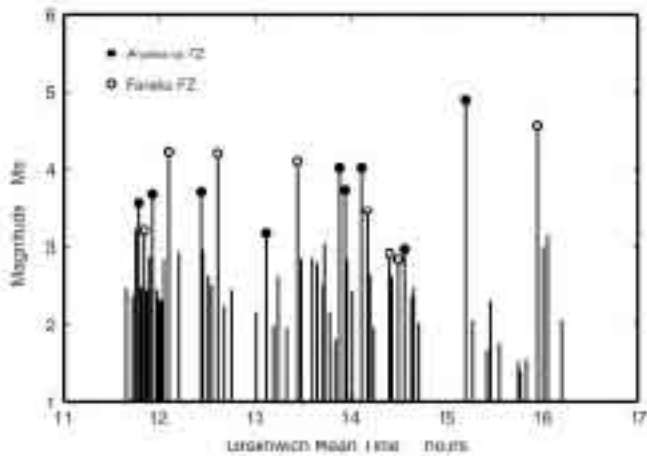


Figure 2. Sequence and magnitude of earthquakes in the swarm. Filled or open circles indicate events large enough to be located with enough precision to distinguish between the groupings on the two different transform faults.

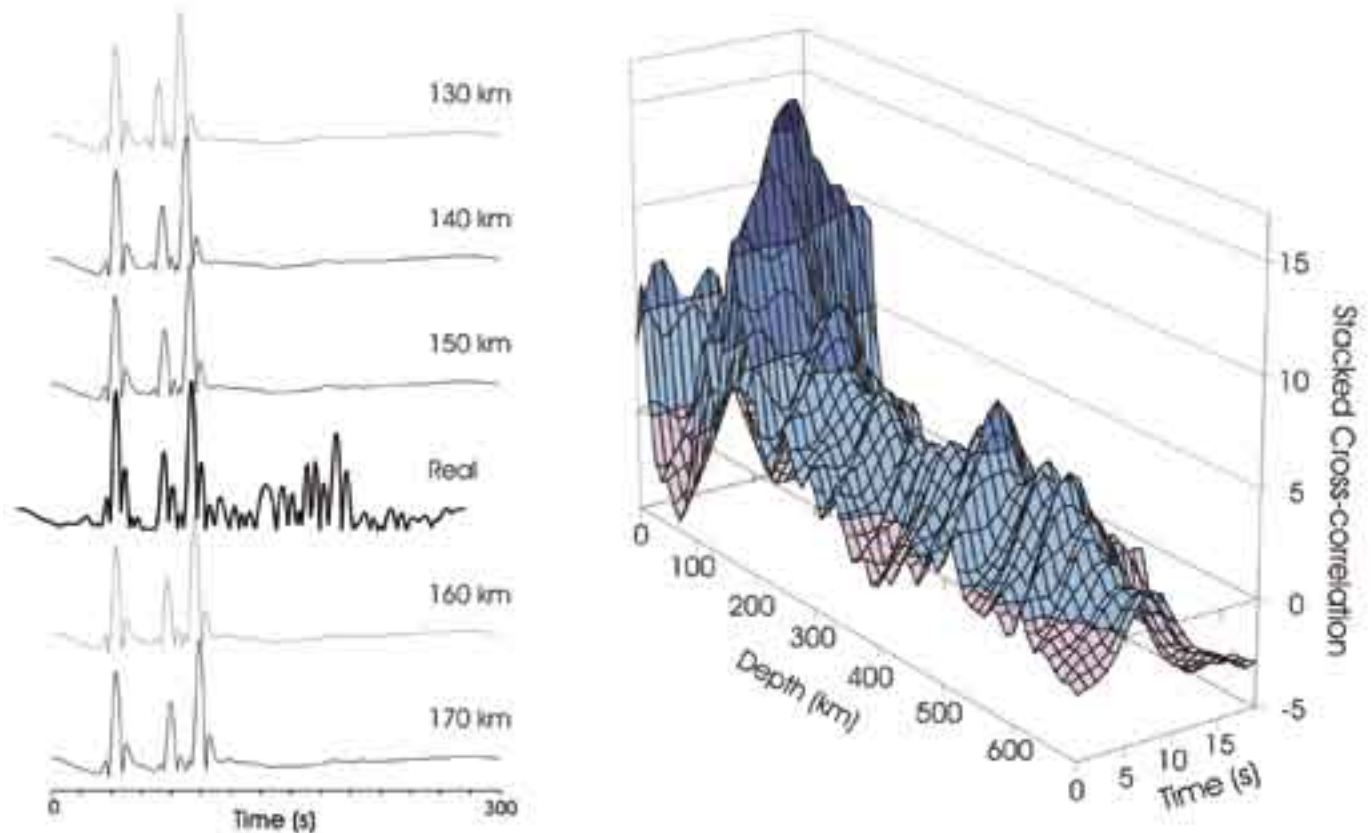
Forsyth, D.W., Y. Yang, M.-D. Mangriotis, and Y. Shen, Coupled seismic slip on adjacent oceanic transform faults, *Geophys. Res. Lett.*, 30(12), 1618, doi:10.1029/2002GL016454, 2003.

This work was supported by National Science Foundation grants OCE-98912208 and CE-9896393.

The Use of Waveform Shapes to Automatically Determine Earthquake Focal Depth

Stuart A. Sipkin • U.S. Geological Survey

Earthquake focal depth is an important parameter for rapidly determining probable damage caused by a large earthquake. In addition, it is significant both for discriminating between natural events and explosions and for discriminating between tsunamigenic and non-tsunamigenic earthquakes. For the purpose of notifying emergency management and disaster relief organizations, as well as issuing tsunami warnings, potential time delays in determining source parameters are particularly detrimental. We present a method for determining earthquake focal depth that is well-suited for implementation in an automated system that utilizes the wealth of broadband teleseismic data that is now available in real-time from the global seismograph networks. This method uses waveform shapes to determine focal depth and is demonstrated to be valid for events with magnitudes down to approximately 5.5.



Example using a magnitude 6.1, intermediate depth (150 km), earthquake that occurred on 15 November 1997, in the Hokkaido, Japan region. (Left) Absolute values of synthetic seismograms computed for an epicentral distance of 40.6° and focal depths ranging from 130 to 170 km, and the corresponding seismogram recorded at station WMQ. (Right) Stacked cross-correlation, using 17 GSN stations, as a function of lag time and assumed depth.

Sipkin, S.A., The use of waveform shapes to automatically determine earthquake focal depth, *Bull. Seismol. Soc. Amer.*, 90, 248-254, 2000.

Broadband Recording of the First Historical Eruption of Anatahan Volcano, Mariana Islands

Sara H. Pozgay, Douglas A. Wiens • Washington University in St. Louis

On May 10, 2003, the first historical eruption of Anatahan volcano in the western Pacific Mariana Islands was recorded by an IRIS/PASSCAL broadband seismograph installed seven kilometers from the crater only four days earlier. The fortuitous timing of the deployment offered the opportunity to study the initial eruption of a dormant volcano with a broadband seismograph. Almost no precursory events were recorded until about 5 hrs before the eruption onset. Approximately one hour before the eruption, the number of volcano-tectonic (VT) earthquakes dramatically increased and a large tilt signal commenced. The tilt signal was constructed from the horizontal components of the seismograph, and indicates substantial inflation of the volcanic center. The magnitude of the tilt is consistent with the inflation of a magmatic chamber at depth of somewhat smaller size than the total volume of material output by the eruption. Subsequent deflation coincided with a reduction in the number of VT events and the onset of volcanic tremor as well as long-period and very long-period volcanic events. After about 36 hours of intense earthquake activity, the number of VT events declined and was replaced by nearly continuous volcanic tremor for the next six weeks. The Anatahan records show that portable broadband seismographs can accurately record a wide variety of volcanic signals including very long-period earthquakes and tilt, even when the instruments are deployed in typical temporary field settings. Such records may contribute considerable additional information about eruption mechanics.

Pozgay, S.H., R.A. White, D.A. Wiens, P.J. Shore, A.W. Sauter, and J.L. Kaipat, Seismicity and Tilt Associated with the 2003 Anatahan Eruption Sequence, *J. Vol. Geothermal Res.*, in press, 2005.

Wiens, D.A., P.J. Shore, S.H. Pozgay, A.W. Sauter, and R.A. White, Tilt Recorded by a Portable Broadband Seismograph: The 2003 Eruption of Anatahan Volcano, Mariana Islands, *Geophys. Res. Lett.*, subm. 2005.



Figure 1. The eruption of Anatahan as observed at dawn on May 10, 2003, from a small ship installing PASSCAL seismographs in the Northern Mariana Islands (photo by A. Sauter).

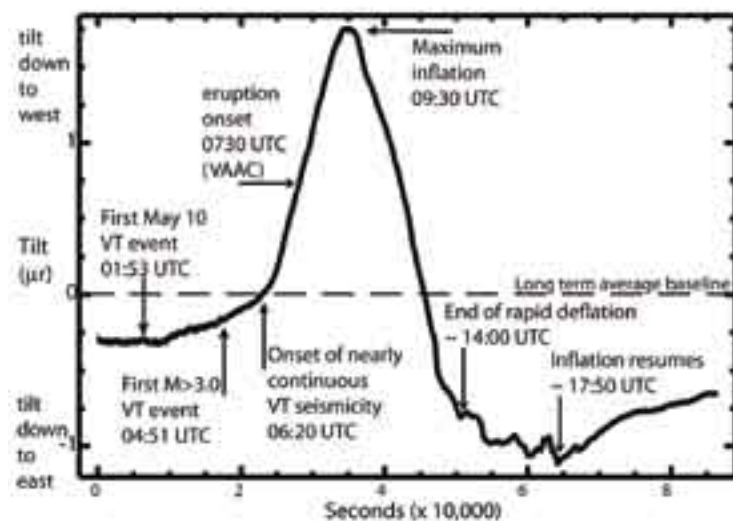


Figure 2. Ground tilt record for May 10, 2003, reconstructed from the horizontal component of the PASSCAL broadband seismograph on Anatahan Island.

Use of Multiple Small Aperture Arrays to Study Deep Subduction-Related Tremor in Cascadia

Wendy McCausland • University of Washington

Steve Malone • Pacific Northwest Seismograph Network

Mario La Rocca • Istituto nazionale di Geofisica e Vulcanologica

Three small aperture (~600 m) seismic arrays were deployed between April and July, 2004, in the northern Puget Sound to observe tremor during an episodic tremor and slip event (ETS). Tremor has been recognized in real-time using stations of the Pacific Northwest Seismograph Network (PNSN) since mid-February, 2003. Approximate epicenters of tremor bursts have been determined using band-passed, rectified and smoothed versions of the signals. Using small aperture arrays of 6 to 7, 3-component short-period seismometers spaced at approximately 200 m we can correlate phases in the dominant frequency band (2-6 Hz) across individual arrays. Array processing techniques (beam forming and zero-lag cross-correlation) are used to determine the slowness and back-azimuth of tremor bursts. Tremor bursts lasting a few seconds can be identified across the stations of each array. Individual bursts from different back-azimuths often occur within five seconds of

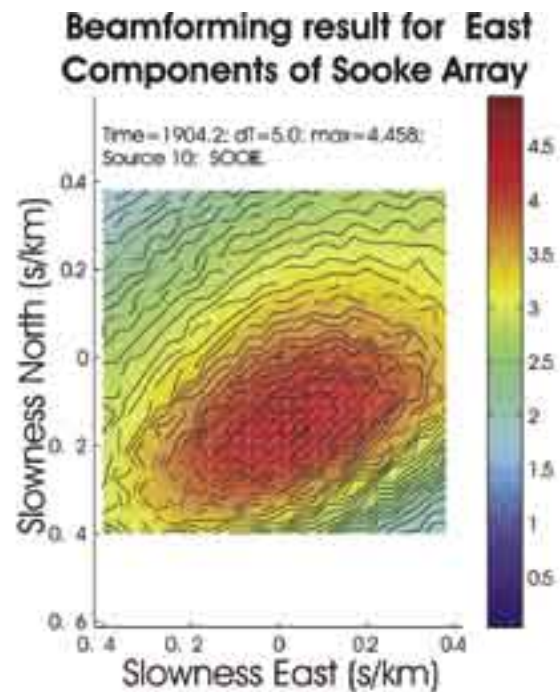


Figure 2. The beam-formed relative amplitude (color shading) is shown on an east-west/north-south plot of slowness for a five second period of tremor shown in Figure 1. The center of the pattern indicates that energy is arriving from the south-south-east with a slowness of about 0.18 sec/km.

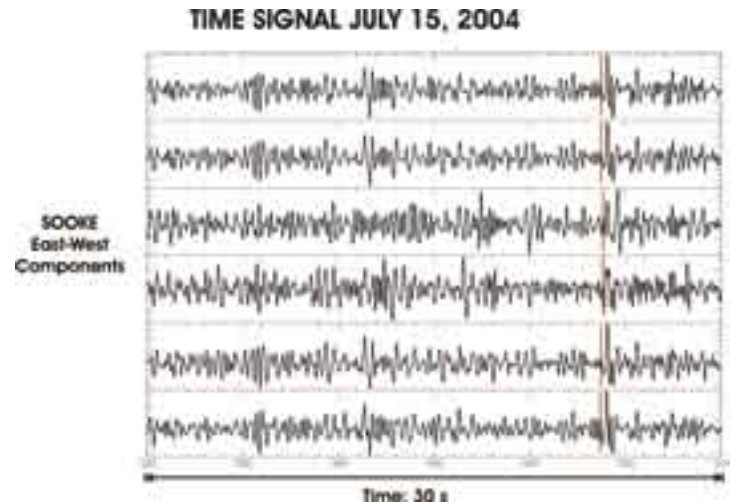


Figure 1. Sample waveforms from six horizontal components of the Sooke array for a 30 second time window during a strong period of tremor. Note the coherence of much of the waveform across the array. A strong burst near the end is marked showing the start of a five second window used for the beam-forming analysis shown in Figure 2.

one another, indicating the presence of spatially distributed but near simultaneous tremor. Earthquake signals have been used to determine the resolution capabilities of the arrays: 0.01 and 0.02 s/km in slowness and 5-10 degrees in back-azimuth. Polarization analyses indicate that the signals are predominantly SH waves, with minor contributions from P and SV waves. Further analyses are ongoing to determine the hypocentral locations of the tremor bursts, and to track their spatial and temporal progression.

La Rocca, M., S. Malone, G. Soccorotti, W. McCausland, D. Galluzzo, and E. Del Pezzo (2004), Small Aperture Array Resolution Capabilities for Use in Locating Deep Tremor, *Eos Trans. AGU*, 85(47), Fall Meet. Suppl., Abstract S53A-0190.

McCausland, W., S. Malone, K. Creager, R. Crosson, M. La Rocca, and G. Saccorotti (2004), Array observations and analyses of Cascadia deep tremor, *Eos Trans. AGU*, 85(47), Fall Meet. Suppl., Abstract S42B-05.

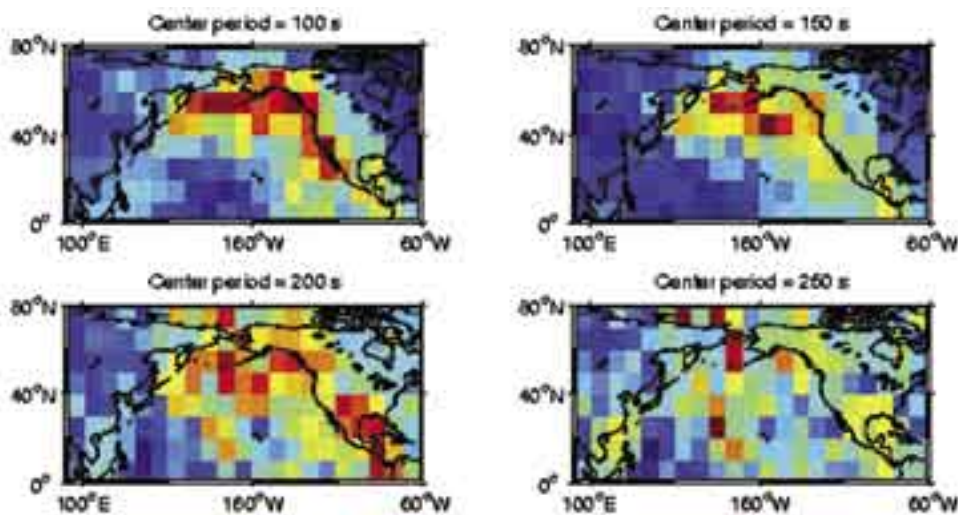
Research funding for this project is provided by NSF grant, EAR-0337144X; instruments for two arrays were provided by Istituto Nazionale di geofisica e vulcanologia, Italy and instruments for the third one, located near Sooke, BC, were supplied by the IRIS-PASSCAL instrument center.

Excitation of Earth's Incessant Free Oscillations by Atmosphere-Ocean-Seaflor Coupling

Junkee Rhie, Barbara Romanowicz • University of California, Berkeley

The observation on long period seismograms of continuously excited free oscillations of the Earth was first made by Japanese scientists in 1998, during intervals free of significant earthquakes. Since then, attention has focused on elucidating the physical mechanism responsible for them. The sum of all small earthquakes remaining in the records cannot explain the observed level of excitation. The mechanism must be shallow, as fundamental modes appear to be preferentially excited. It shows seasonal variability, with peaks in the northern and southern hemisphere winters. Stochastic mechanisms involving turbulent motion in the atmosphere have been proposed as well as random distribution of sources around the world. An

algorithm for the computation of spectra or correlations of signals across long time series, do not have the spacial and temporal resolution to locate these sources.



Results of application of a grid search method to locate the source of the low frequency hum using 6 hours of data from the BDSN array, F-NET and 10 additional quiet GSN stations, on a day without earthquakes (January 31, 2000). In each panel, the data have been narrow bandpass filtered with a different center period. Dark red areas indicate 5 x 5 degrees areas which yield maximum amplitudes of the corresponding network stacks. Resolution is lost at periods greater than 200 sec.

We have developed an array-based method to detect and locate sources of very long period surface wave energy, utilizing the dispersive properties of Rayleigh waves. Our basic approach uses data from two large aperture arrays of very long period seismometers (BDSN in California and F-NET in Japan). We stack the data after projection to the center of each array, and look for directions of arrival of maximum amplitude in the stacks as a function of back-azimuth, taking into account the array response. We show that, for each array, there is a well defined preferential direction, which is stable over one season but changes significantly from winter to summer. The fluctuation as a function of time of the maximum stack amplitudes are correlated across the two arrays and point to the northern Pacific ocean in the northern hemisphere winter and the southern Oceans in the summer, correlating with changes in the global distribution of maximum wave height. The addition of other stations equipped with STS-1 seismometers (GSN and GEOSCOPE) allows us to apply a grid search method to more precisely determine the loci of the multiple sources during a particularly stormy day in the north Pacific ocean.

We infer that the background oscillations originate primarily in the oceans, and are caused by a non-linear coupling mechanism involving the atmosphere (winds), the oceans (transfer of energy from ocean waves to infragravity waves) and the seafloor (transfer of energy to elastic waves).

Rhie, J. and B. Romanowicz, Excitation of earth's incessant free oscillations by Atmosphere-Ocean-Seaflor coupling, *Nature*, 431, 552-556, 2004.

Kinematic Modeling and Complete Moment Tensor Analysis of the Anomalous, Vertical CLVD Bardarbunga, Iceland, Event

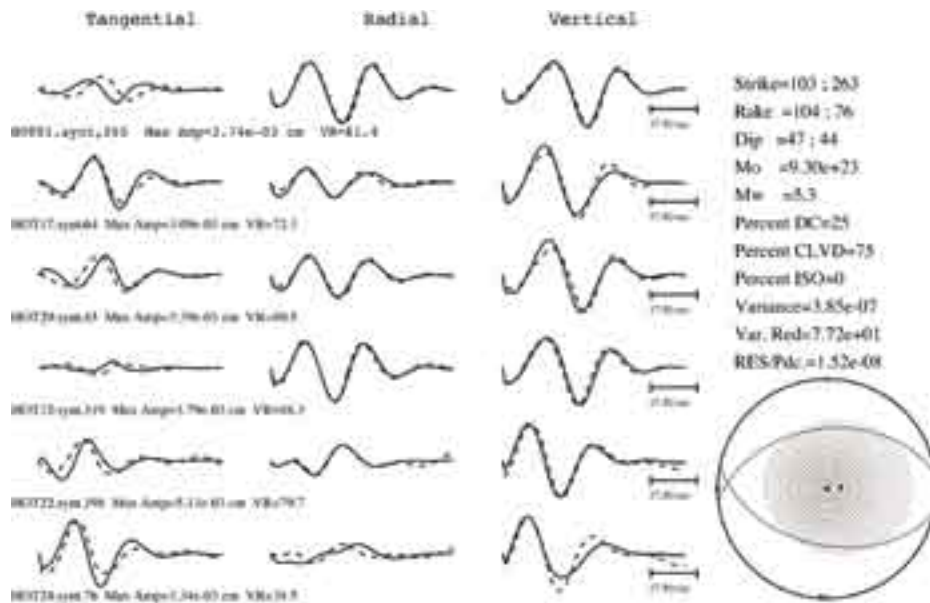
Hrvoje Tkalčić • Lawrence Livermore National Laboratory

Douglas S. Dreger • University of California, Berkeley

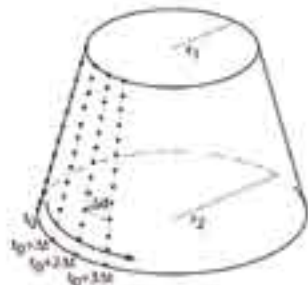
Gillian R. Foulger • University of Durham, United Kingdom

Bruce R. Julian • U.S. Geological Survey, Menlo Park

Using a complete moment tensor inversion method and the seismic data from the HOTSPOT PASSCAL experiment acquired from the IRIS data center, we investigated the September 29, 1996, volcanic event of $M_w = 5.6$ originated beneath the Bardarbunga caldera in Iceland. The corresponding moment tensor is characterized by a significant non-double-couple component (NDC) previously reported in the Harvard centroid moment tensor catalog (CMT) and confirmed by analysis of long-period and intermediate surface wave data. The deviatoric inversion performed by using Iceland HOTSPOT Project stations, yields a NDC solution with a 67% vertically oriented compensated linear vector dipole (CLVD) component, while the full moment tensor solution shows a similar, 66% CLVD component, 32% of double-couple component (DC) and a small volumetric contraction (ISO) of 2%. Statistical tests confirm that CLVD is a stable component of the moment tensor, while ISO is statistically insignificant. Using an elastic finite difference code with a large number of equidistantly distributed point sources, we simulated various rupture scenarios on the walls of a conical surface of the Bardarbunga caldera in order to compare them with the observations. Suites of seismograms for each independent run were produced at locations corresponding to HOTSPOT stations. We then inverted these synthetic data to investigate what portion of the original source information can be recovered by the moment tensor inversion (Figure 1). We were able to identify physical characteristics of a rupture scenario that produces synthetics resembling the observed data to a quite high level of detail. For example, we obtained the



best results for the ruptures extending along one-half perimeter of the caldera, while one-quarter or full-length perimeter ruptures were unlikely scenarios. We found that the rupture velocity, which took place at Bardarbunga, could have been a super-shear one, and we hypothesize that it could have been triggered by a compressional wave field that spread throughout the volume of the caldera.



Full-waveform moment tensor inversion for a half-cone rupture scenario. The observed waveforms are shown by solid lines while the synthetic data are shown by dashed lines. The resulting mechanism is dominated by a vertically oriented strong compensated linear vector dipole. The caldera in finite source modeling is assumed to be a part of a conical surface, dipping at 45 degrees outward, and the rupture is assumed to take place along a segment between 3 and 5 km of depth. A finite source is described with a number of point sources and the rupture is simulated by initiating increment displacements at multiple locations on the caldera walls.

Ambient Earth Noise: A Survey of the Global Seismographic Network

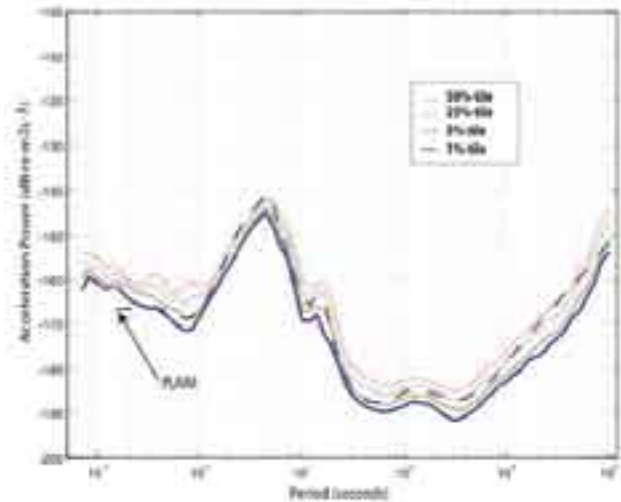
Jonathan Berger, Peter Davis • *University of California, San Diego*

Göran Ekström • *Harvard University*

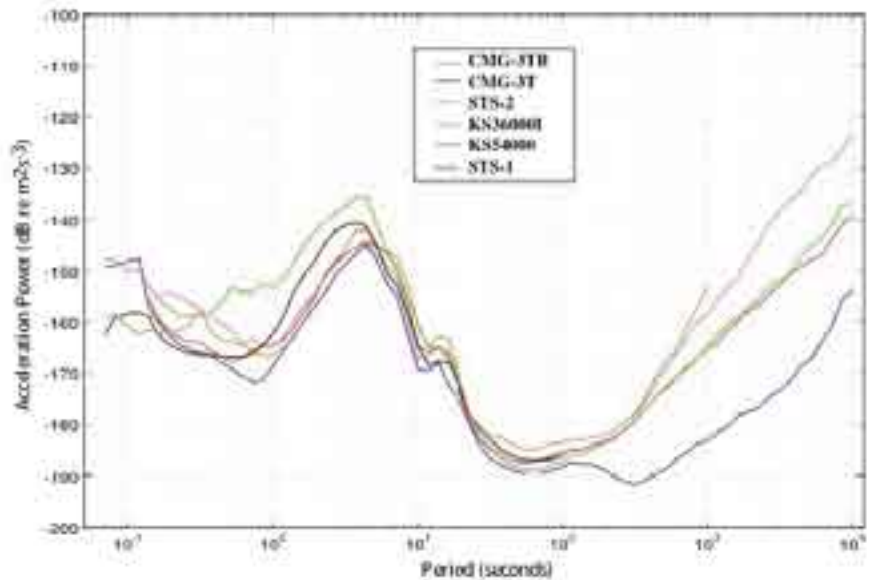
In the decade since the last comprehensive model of ambient earth noise was published (Peterson Low Noise Model, Peterson, 1993), observations of ambient earth noise from the IRIS Global Seismographic Network of widely distributed, similarly equipped, and well-calibrated stations have become available. We have analyzed data from the 118 GSN stations operating during the year July, 2001, through June, 2002. Based upon over 738,000 hourly spectral estimates computed from these stations' data, we have developed a robust noise model that exhibits significant differences from previous models both in the normal mode and body-wave bands.

The figure at the right shows our results for the various percentile distributions of the spectral estimates of GSN noise levels. Over most of the bandwidth covered by the GSN, the 1st percentile spectral values are significantly lower than those of the Peterson Low Noise Mode (PLNM). The exception to this is for periods less than about 0.4 seconds. Here the minimum spectral values of the GSN Noise Model are significantly higher than those for the PLNM. As Peterson (1993) noted in his analysis, there was inadequate data to determine the noise for periods shorter than 0.5 seconds - the data set from the latter two stations consisted of a single 4096-sample section.

The minimum horizontal component noise levels are less than the vertical component noise levels through the microseism band but considerably higher for periods longer than about 30 seconds. There is no systematic bias between the levels of the two directions of horizontal noise. At long periods, some of the horizontal component noise may be caused by local atmospheric pressure fluctuations but a more likely source is thermally induced tilt. The lowest horizontal-component noise levels are observed at stations where the seismometers (all STS-1) are located in tunnels or very well-insulated vaults. All minimum noise levels, both horizontal and vertical, are observed on STS-1 seismometers for periods longer than 1.4 seconds. At periods longer than about 120 seconds, the observed vertical component minimum noise levels are lower than the theoretical KS54000 seismometer instrument noise. At periods longer than about 300 seconds, the observed vertical component noise levels are close to the theoretical STS-1 seismometer noise. These results point to the need for improved seismometers at many of the stations.



The GSN minimum noise levels at the 1st, 5th, 25th, and 50th percentiles for all station and channels with the Peterson low noise model for comparison.



The GSN 1st-percentile noise plotted by sensor.

A Real-time Seismic Noise Analysis System for Monitoring Data Quality and Station Performance

Dan E. McNamara, Ray Buland, Harley Benz • U.S. Geological Survey, Golden

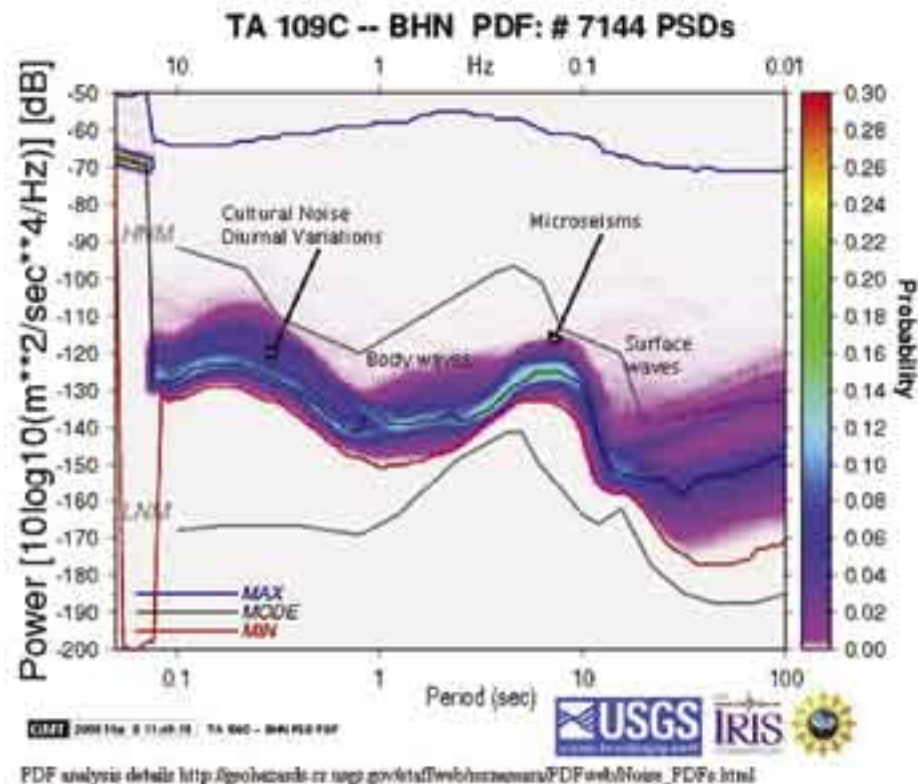
Tim Ahern, Bruce Weertman • IRIS DMC

A new system for analyzing data quality is now available to the seismology community allowing users to evaluate the long-term seismic noise levels for any broadband seismic data channel streaming into the buffer of uniform data (BUD) within the Incorporated Research Institutions for Seismology (IRIS) data management system (DMS). BUD is the IRIS DMS's acronym for the online data cache from which the DMC collects and distributes near-real time miniSEED data holdings prior to formal archiving. The new noise processing software uses a probability density function (PDF) to display the distribution of seismic power spectral density (PSD) and has been implemented against most of the continuous data-stream available within the BUD utilizing the QUACK framework. QUACK is the system at the IRIS DMC responsible for managing the quality control (QC) of the real-time seismic data flowing into the BUD (see <http://www.iris.washington.edu/servlet/quack-query/>). This noise processing system is unique in that there is no need to screen the data for earthquakes, system glitches or general data artifacts, as is commonly done in seismic noise analysis. Instead, with this new analysis system transients map into a low-level background probability while ambient noise conditions reveal themselves as high probability occurrences. In

fa

ti

performance of existing broadband sensors, for detecting operational problems within the recording system, and for evaluating the overall quality of data for a particular station. The advantages of this new approach include: 1) provides an analytical view representing the true ambient noise levels rather than a simple absolute minimum; 2) provides an assessment of the overall health of the instrument/station; and, 3) provides an assessment of the health of recording and telemetry systems. The figure shows a PDF example, with some artifacts and signals identified for the transportable array station TA 109C in southern California. Cultural noise due to automobile traffic, machinery and other human activity generates a strong signal that can vary by 10 dB between day and night time and is observable in the PDFs at high frequencies (1-10 Hz, 0.1-1s). Body waves from earthquakes occur as low probability signal in the 1sec range while surface waves are generally higher power at longer periods. The broad signal >10 s is due to thermal instability of the portable vault design.



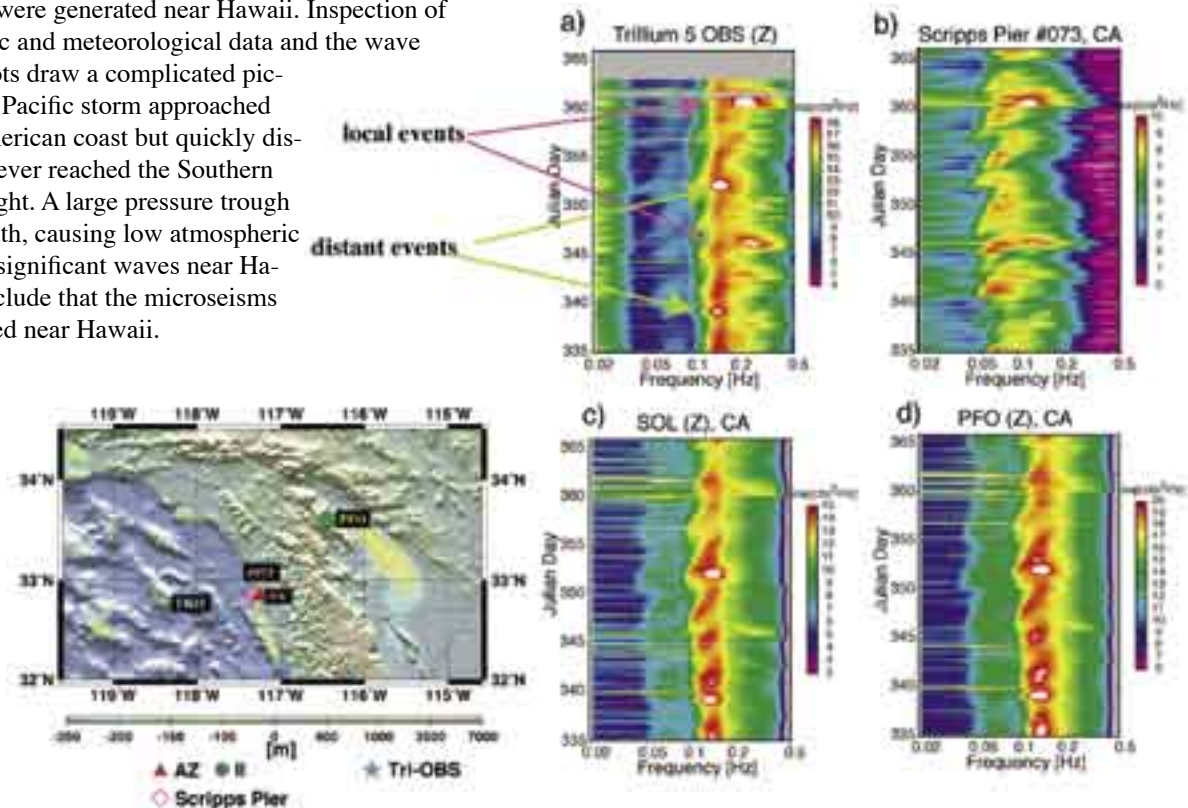
Four Anomalous Episodes in the Late 2003 Microseism Band Offshore Southern California

Bettina Allmann, Gabi Laske • IGPP, Scripps Inst. of Oceanography

The Scripps Ocean Bottom Seismometer (OBS) group has recently test-deployed their new passive seismic instruments. Five Nanometrics Trillium 40 3-component seismometers and Cox-Webb differential pressure gauges were deployed between November 8th, 2003 and January 8th, 2004, operating at a water depth of about 1000 m, 40 km offshore La Jolla, CA. Data were recorded continuously, at a sampling rate of 31.25 Hz.

In the OBS sonograms, we can identify four time periods of high microseismic activity that occurred in December 2003, around Julian days 339, 346, 352 and 360. We can classify these events into two categories. The spectral energy of the events on days 346 and 360 is extended to significantly higher frequencies than the other two events. Zoom-ins of these events exhibit Pierson-Moskowitz dispersion that is characteristic of ocean swell formation under increasing wind speeds. Their signals are much weaker on land station SOL, that is only 2 km from the beach, and on PFO that is 100 km inland. Comparisons with oceanographic (Scripps Pier and buoy records) and meteorological data confirm that these events are associated with North Pacific winter storms that approached the coast further north and then propagated south, generating significant waves within the Southern California Bight.

The two other events distinguish themselves by band-limited energy near the low-frequency end of the double-frequency microseism band. No dispersion is discernible in zoom-ins. Event 339 is clearly visible in the record of seismic station FFC in Canada and station KIP in Hawaii. Inspection of global wave amplitude plots published by the Fleet Numerical Meteorology and Oceanography Center reveals that a large storm approached the North American coast that day. Significant energy must have coupled into the solid earth by non-linear interaction of waves refracted by the coast. This energy then traveled as Rayleigh waves across the Pacific ocean and into the North American continent. The other event is very prominent on the KIP record but not discernible at FFC. The KIP record also exhibits the Pierson-Moskowitz dispersion suggesting that the microseisms were generated near Hawaii. Inspection of oceanographic and meteorological data and the wave amplitude plots draw a complicated picture. A North Pacific storm approached the North American coast but quickly dissipated and never reached the Southern California Bight. A large pressure trough expanded south, causing low atmospheric pressure and significant waves near Hawaii. We conclude that the microseisms were generated near Hawaii.



Left: Location map of the Scripps OBS test deployment in 2003. Also shown are nearby land seismic stations and the Scripps Pier that collects oceanographic and meteorological data. a), c), d) sonograms for December 2003. b) Wave height measured at Scripps Pier. Most of the microseism signal at the seismometers can be found at twice the frequency of waves measured nearby (double-frequency peak).

Ambient Seismic Noise Monitoring in North-Central Illinois

Philip J. Carpenter • Northern Illinois University

Seismic noise monitoring and analysis were conducted as part of a study to evaluate the feasibility of building a new linear collider in northern Illinois, in close proximity to the Fermi National Accelerator Laboratory, just west of Chicago. The Seismic Analysis Code 2000 (SAC2000), free to IRIS members, was used to process data recorded at the Northern Illinois University seismic station, earthquake records downloaded from the IRIS Data Management Center via WILBERII, and data recorded by an engineering seismograph with high-frequency geophones. Power-spectral density estimates were computed from an autocorrelation series in most cases. Using the power density spectra routine of SAC2000, selecting autocorrelation windows of 20 s for the low-frequency data and 2 s for the high-frequency data, we have found distinctive seismic noise peaks among the different sites, regardless of the background noise level (e.g., Figure 1). Low-frequency waveform data typically shows microseism peaks at a frequency of 0.05-0.2 Hz for stations located in the Midwestern U.S. Microseism peak frequency did not decrease with increasing distance from Lake Michigan, suggesting the lake is not the primary source of the microseisms, which may be generated in ocean basins. To investigate local ground motion in more detail, noise from trains, traffic, air-conditioning units and water pumping equipment were recorded with an engineering seismograph in DeKalb, Illinois, using both vertical and horizontal geophones. These data were also analyzed using SAC2000. Train noise exhibits strong peaks in the 3-10 Hz range, both for the vertical and horizontal geophones. Spectra of recordings made near a water treatment plant in DeKalb showed peaks near 10, 30, 90, and 110 Hz, probably related to pumping and mechanical equipment (Figure 2). Seismic noise collected about 100 m from a municipal swimming pool with vertical geophones showed spectral peaks at about 10-30 Hz and 180 Hz. Horizontal geophones at the same location exhibited peaks at 5-15 Hz and 140 Hz. Pool activities, pumping equipment and traffic may contribute to this noise. Delineating particle motion at the recording sites will determine whether dominant motion is due to Rayleigh, Love or body waves. Two-dimensional geophone arrays will also be deployed in the future to determine the origin direction and velocity of each seismic noise component.

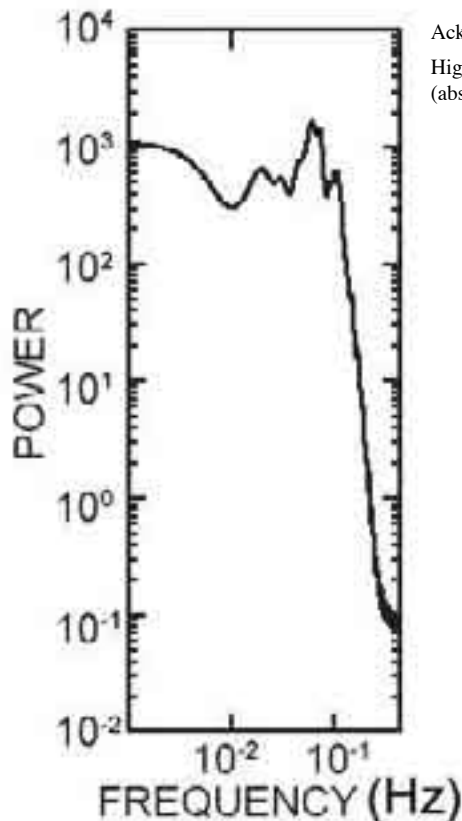


Figure 1. Power spectrum of seismic background noise recorded at the NIU seismic station in DeKalb, IL, showing energy peaks due to microseisms.

Acknowledgement: Support for this work was provided by the Fermi National Accelerator Laboratory.

Higuera-Diaz, I.C. and Carpenter, P.J. Frequency content of ambient seismic noise in north-central Illinois (abstract), *EOS: Trans. Amer. Geophys. Un.*, 25, no. 47, S13C-1074, 2004.

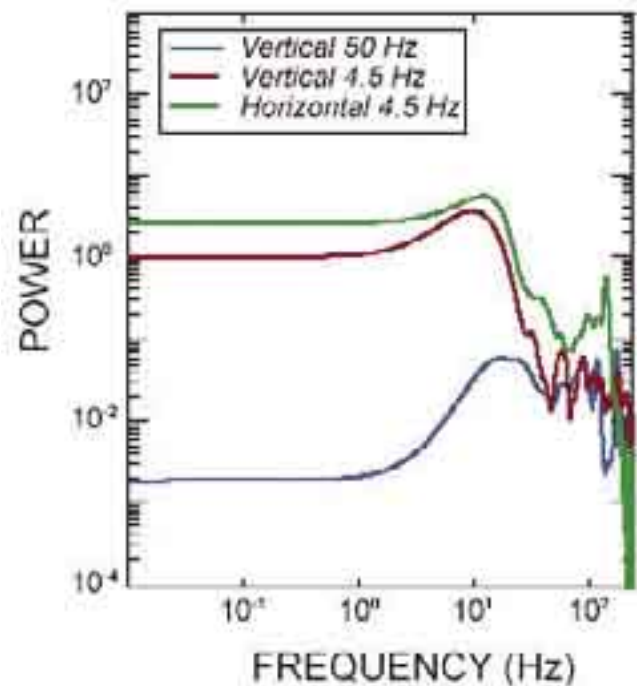


Figure 2. Power spectrum of noise recorded with different geophones near pumps at a water treatment plant.

Strong Directivity of Ocean-Generated Seismic Noise

Vera Schulte-Pelkum • University of Colorado, Boulder

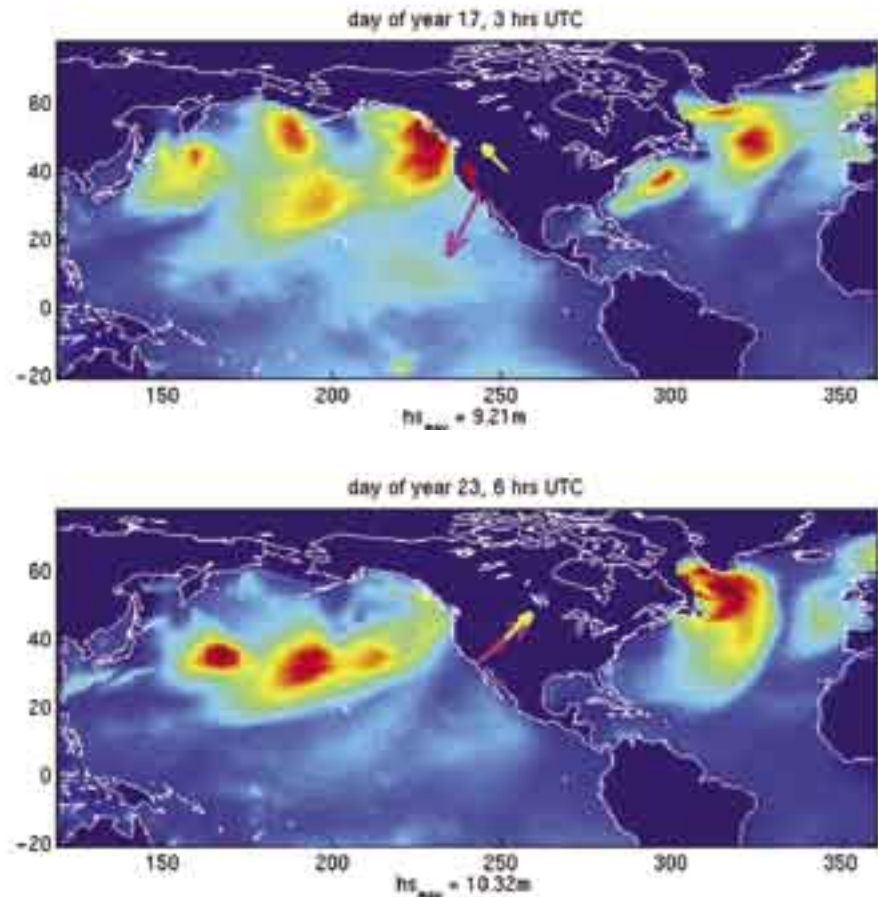
Paul Earle • U.S. Geological Survey, Golden

Frank Vernon • Scripps Institution of Oceanography

We measure direction and amplitude of ocean-generated continuous seismic noise in the western US. Slowness direction of the noise is determined using array beamforming, and particle motion direction from individual three-component stations. We find two surprising results. First, the noise is highly monodirectional at all sites, regardless of coastal distance. A single narrow generation area dominates for most of the time period, interrupted by a second well-defined direction during ocean swell events. Second, we find that a storm off the Labrador coast with not unusual wave heights generates coherent noise across the entire continent. We show the causal relationship between swells arriving at different North American coastal areas and the triggered microseisms in time-lapse movies of ocean swells and concurrent microseisms.

Our results have a number of implications for different fields of research. A useful by-product of our finding that microseisms are a strongly directional noise source is the possibility of using automated processing of the continuous noise as a near real-time check on station polarity and calibration problems, which would be a simply implemented indicator for the state of health of a seismic network. Consistent monodirectional noise may have an influence on seismic azimuthal measurements such as shear wave splitting. Most importantly, our findings should be taken into account in proposed studies which will use seismic noise as a proxy for ocean wave height in investigations of interdecadal climate change.

Schulte-Pelkum, V., P. S. Earle and F. L. Vernon, Strong directivity of ocean-generated seismic noise, *Geochem. Geophys. Geosys.*, 5, doi:10.1029/2003GC000520, 2004.



The figure shows two instances of ocean wave height and corresponding seismic noise directions on land in January 1998. Direction of 2-10 s period noise at the Lodore array in Wyoming plotted as yellow arrow; noise directions at Anza array, California are shown in pink (2-10s period) and red (10-20 s period). Note the excitation of seismic noise from storms hitting distant coasts in Labrador and British Columbia.

Glacial and Climate Controls on Tide-Water Glacier Calving Dynamics: A PASSCAL Seismic Experiment on the Columbia Glacier, Southeast Alaska

Dan E. McNamara • *U.S. Geological Survey, Golden*

Tad Pfeffer, Shad O'Neel • *INSTAAR, University of Colorado*

Columbia Glacier is a large tidewater glacier, ending at an iceberg-calving terminus in Prince William Sound, 35 km west of Valdez, in south-central Alaska. It is presently one of the world's fastest glaciers with an annual average speed at the terminus of approximately 11 km/yr (30 m/day). The glacier is discharging ice into Prince William Sound at rates in excess of 10 km³/yr (O'Neel et al., in press). The retreat is driven by iceberg calving that exceeds incoming ice flux at an average rate of 0.74 km/yr (Pfeffer et al., 2002). This value does not include rapid dynamic thinning that exceeds 7.4 m/yr averaged over the entire glacier area, and 20 m/yr at the present terminus (O'Neel et al., in press; Arendt et al. 2002). Such retreats are irreversible until the terminus reaches a location where the bed rises above sea level, and may be analogous to the rapid breakup of historical ice sheets such as the Laurentide.

In June 2004, we deployed an array of 10 high-frequency and 1 broadband digital seismometers around the lower 10 km of the glacier channel. Seismic sensors, power systems and recording equipment were obtained through the IRIS consortium PASSCAL program. The goal of the one-year study is to characterize small seismic events (icequakes) due to iceberg calving, fracturing and crevassing within the glacier and basal sliding. Our main interest is understanding the temporal and spatial distribution characteristics of icequakes and their relation to the retreat of Columbia Glacier. The type of passive-source seismic field experiment proposed here is relatively rare in glaciology, especially for temperate glaciers. In June of 2005, we will also deploy several high-frequency seismic sensors on the glacier itself and record a minimum of two active-source explosions with the goal of better defining ice velocity and thickness as well as the local rock velocity.

The main objective of the proposed project is to gain a better understanding of the interactions between tidewater calving mechanics and fracture mechanics, and the mechanisms that may force retreats such as climate change and buoyancy instabilities. Since Columbia Glacier is the last of the Alaskan tidewater glaciers to begin rapid retreat, and has a 30+ year □ vatory disappears.

We anticipate that results from this proposed project will be highly pertinent to the glacier/climate interaction debate. In addition to increasing our understanding of fundamental ice-processes, results from the proposed project have implications for important societal issues such as global climate change and hazards related to calving icebergs in shipping seaways and should be addressed by rigorous scientific study. Also, given the rapid changes in Greenland and Antarctica, this study will help our understanding of potential ice sheet instability.

It is evident that the relevant processes cannot be studied with our Columbia Glacier seismology field experiment alone. For this reason an integrated approach involving additional studies in global climate change, geology, and glaciology, are planned. The proposed studies include continued photogrammetric observations to monitor the retreat of the terminus of the Columbia Glacier (Pfeffer et al., 2002), co-located GPS stations to monitor active ice flow and additional sensors to monitor tide levels, barometric pressure, temperature and precipitation.

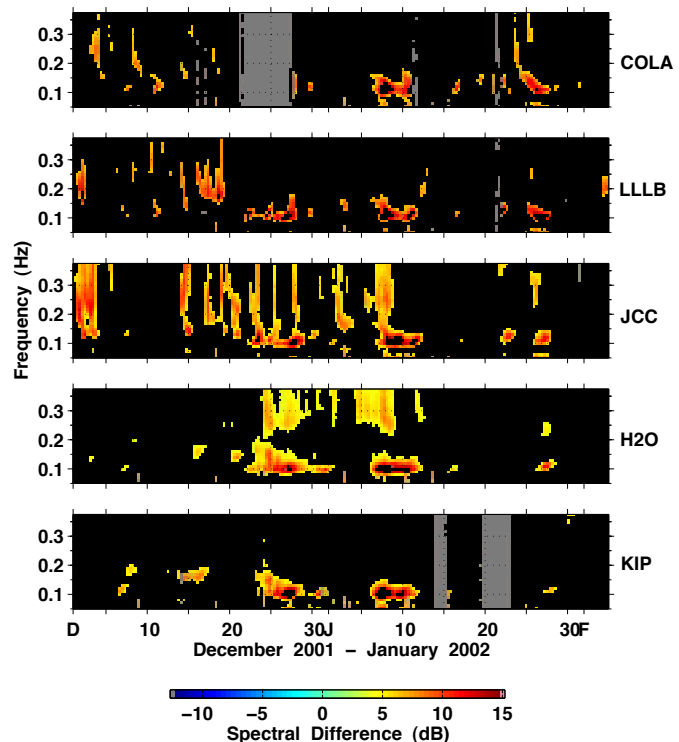
Mid-Ocean-Bottom and Land-based Microseism Correlations

Peter D. Bromirski • Scripps Institution of Oceanography, UCSD

Fred K. Duennebieer • University of Hawaii, Honolulu

Ralph A. Stephen • Woods Hole Oceanographic Institution

Inversion of the double-frequency (DF) microseism band for ocean wave heights from archived seismic data can provide an important diagnostic of climate change (Bromirski et al., 1999; Bromirski et al., 2005a). The usefulness of such inversions requires knowledge of the source areas and propagation attributes of microseisms. The Hawaii-2 Observatory (H2O) is an excellent site for studying microseism characteristics since it is located far from shorelines and shallow water. The DF microseism band can be divided into short period and long period bands, SPDF and LPDF, respectively. A strong correlation of seismic amplitude with wind speed and direction is observed at H2O in the SPDF band from about 0.20 to 0.45 Hz (Bromirski et al., 2005b), implying that the energy reaching the ocean floor is generated locally by ocean gravity waves. Near-shore land seismic stations see similar SPDF spectra, also generated locally by wind seas. Correlation of swell height above H2O with the LPDF band from 0.085 to 0.20 Hz is often poor, implying that a significant portion of this energy originates at distant locations. The LPDF microseism signals recorded at the H2O correlate with signals at other seismic stations around the North Pacific, clearly shown by comparing difference spectrograms (Figure 1). Comparison of relative amplitudes gives an indication of the source region, e.g. higher relative amplitudes at COLA and LLLB compared with JCC, H2O, and KIP implies a Pacific Northwest coastal source region. The times of low relative microseism energy correlate across the stations, indicating that there is little energy being coupled into LPDF microseisms anywhere in the North Pacific during these times. Most of the LPDF energy at H2O appears to be generated by high amplitude storm waves impacting long stretches of coastline nearly simultaneously, and the Hawaiian Islands appear to be a significant source of LPDF energy in the North Pacific when waves arrive from particular directions. The highest DF levels observed at mid-ocean site H2O occur in the SPDF band when two coincident nearby storm systems develop. This extreme event at H2O is not observed at continental sites, indicating high attenuation of these signals. At near-coastal seismic land stations, both SPDF and LPDF microseism levels are generally dominated by local generation at nearby shorelines (Bromirski and Duennebieer, 2002). High relative SPDF levels are generally not observed concurrently at JCC and H2O (Figure 1), indicating that DF microseisms generated near H2O do not propagate well, consistent with low effective Q, and also indicating that open-ocean generated DF microseisms will not significantly affect the statistics of ocean wave parameters determined from inversion of land microseismic spectra.



Difference spectrograms of vertical component data from eastern North Pacific seismic stations located in Hawaii (KIP), central Alaska (COLA), southwestern Canada (LLLB), northwestern California (JCC, NCEDC), and mid-ocean H2O during December 2001 and January, 2002, showing the similarity of energy in the LPDF microseism band. Dark vertical strips indicate times when data are missing.

Bromirski, P.D., R.E. Flick, and N. Graham, Ocean wave height determined from inland seismometer data: Implications for investigating wave climate changes in the NE Pacific, *J. Geophys. Res.*, 104 (C9), 20,753-20,766, 1999.

Bromirski, P.D., Vibrations from the "Perfect Storm", *Geochem. Geophys. Geosys.*, 2(7), doi:10.1029/2000GC000119, 2001.

Bromirski, P.D., and F.K. Duennebieer, The near-coastal microseism spectrum: Spatial and temporal wave climate relationships, *J. Geophys. Res.*, 107 (B8), 2166, 10.1029/2001JB000265, 2002.

Bromirski, P.D., D.R. Cayan, and R.E. Flick, Wave spectral energy variability in the northeast Pacific, *J. Geophys. Res.*, 110(C3), C03005 10.1029/2004JC002398, 2005a.

Bromirski, P.D., F.K. Duennebieer, and R.A. Stephen, Mid-ocean microseisms, *Geochem. Geophys. Geosys.*, 6, doi:10.1029/2004GC000768, 2005b.

Stephen, R.A., F.N. Spiess, J.A. Collins, J.A. Hildebrand, J.A. Orcutt, K.R. Peal, F.L. Vernon, and F.B. Wooding, 4 (10), 1092, Ocean seismic network pilot experiment, *Geochem. Geophys. Geosys.*, 4 (10), 1092, doi:10.1029/2002GC000485, 2003.

Ocean Drilling at the Hawaii-2 Observatory (H2O)

Ralph A. Stephen • Woods Hole Oceanographic Institution

Peter D. Bromirski • Scripps Institution of Oceanography, UCSD

Fred K. Duennebieer • University of Hawaii

On ODP Leg 200 a borehole was drilled at the Hawaii-2 Observatory in preparation for the installation of a high quality broadband borehole seismometer similar to the system deployed on the Ocean Seismic Network Pilot Experiment (OSNPE) (Stephen et al, 2003). The drilling at H2O provided a unique opportunity to observe drilling-related noise from the JOIDES Resolution on a seafloor seismometer in the frequency band from 0.001 to 60Hz. H2O, located on the seafloor midway between Hawaii and California, uses a retired trans-oceanic telephone cable to provide continuous, real-time data transmission to the Makaha cable station on Oahu. At H2O, the University of Hawaii operates a shallow-buried ocean bottom seismometer composed of a Guralp CMG-3T three-component broadband seafloor seismometer and a conventional 4.5-Hz three-axis geophone (Duennebieer et al., 2000, 2002). Data are acquired continuously and are made available to scientists worldwide through the IRIS Data Management System in Seattle.

The figure shows a broadband horizontal component spectrogram for the duration of ODP Leg 200. Seismic signal levels can be associated with wind speed, sea state, shear resonance effects in the sediments, whales, water gun shooting, earthquakes, passing ships, and drilling-related activities such as bit noise and running pipe.

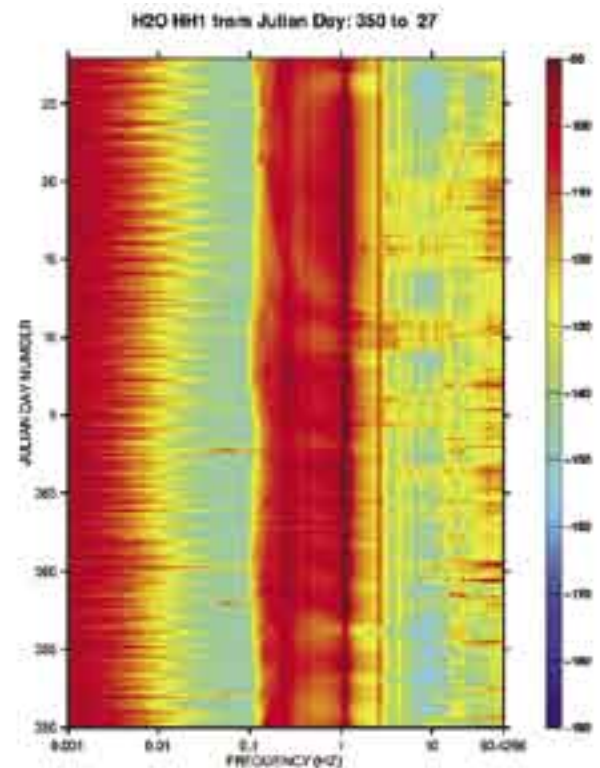
Bromirski, P. D., F. K. Duennebieer, and R.A. Stephen. "Mid-ocean microseisms." *Geochemistry, Geophysics, Geosystems*, 6: doi:10.1029/2004GC000768, 2005.

Duennebieer, F. K., D. W. Harris, J. Jolly, J. Babinec, D. Copson, and K. Stiffel. "The Hawaii-2 observatory seismic system." *IEEE Journal of Oceanic Engineering*, 27: 212-217, 2002.

Stephen, R.A., F.K. Duennebieer, D. Harris, J. Jolly, S.T. Bolmer, and P.D. Bromirski. Data Report: Broadband seismic observations at the Hawaii-2 Observatory during ODP Leg 200. In Kasahara, J., R.A. Stephen, G.D. Acton, and F. Frey (Eds.), Proc. ODP, Sci. Results, 200 (CD-ROM). Available from: Ocean Drilling Program, Texas A&M University, College Station, TX 77845-9547, USA, inpress.

Stephen, R.A., J. Kasahara, G.D. Acton, et al., Proc.ODP. Init. Repts., 200 (CD-ROM). Available from: Ocean Drilling Program, Texas A&M University, College Station, TX 77845-9547, USA, 2003.

Stephen, R.A., F.N. Spiess, J.A. Collins, J.A. Hildebrand, J.A. Orcutt, K.R. Peal, F.L. Vernon, and F.B. Wooding, 4 (10), 1092, Ocean seismic network pilot experiment, *Geochem. Geophys. Geosyst.*, 4 (10), 1092, doi:10.1029/2002GC000485, 2003.



Horizontal component spectrogram for the broadband Guralp sensor (HH1) at the Hawaii-2 Observatory (H2O) during drilling operations from JD 350/2001 to 27/2002 (16 December, 2001 to 27 January, 2002). Large earthquakes are indicated as horizontal red lines in the band 0.01 to 0.1Hz. Variations in the magnitude of the microseisms from 0.1 to 0.3Hz correlate with sea state in the North Pacific (Bromirski et al, 2005). Sediment resonances at 1.1 and 2 Hz dominate even the microseism peak. The red blotches in the frequency band from 2 to 60 Hz correspond primarily to drilling activities. Color, as defined in the bar on the right, indicates energy content in decibels relative to m^2/s^2Hz .

Nanoearthquakes at H2O

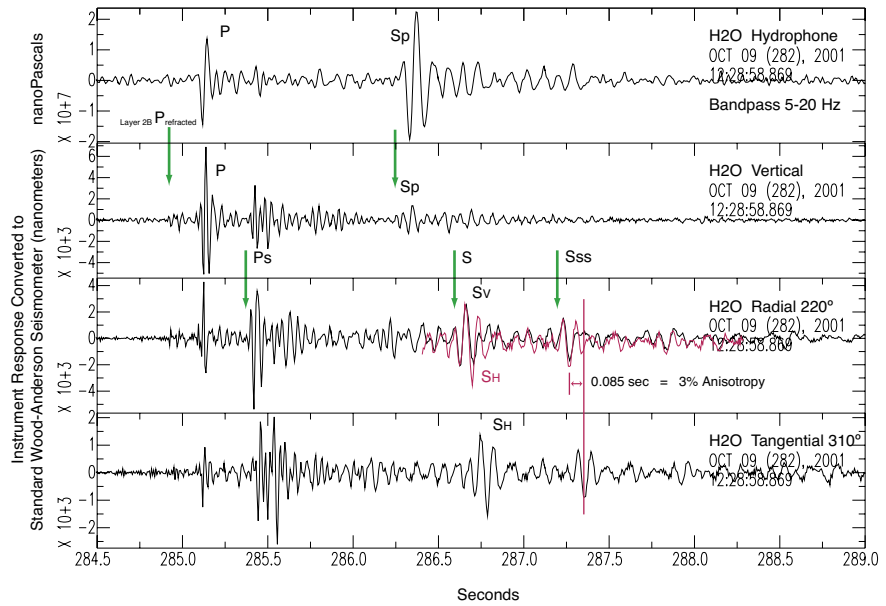
Rhett Butler • *The IRIS Consortium*

Nanoearthquakes ($M_L < 0$) have been observed seismoacoustically at the Hawaii-2 Observatory GSN station, H2O, on the seafloor midway between Hawaii and California (Butler, 2003). Out of a larger data set, the analysis of a sequence of 5 events ($M_L -0.7$ to -2) within an hour yields a number of interesting scientific insights for the uppermost oceanic crust and sediments at the H2O site. The events are consistent with fluid-saturated cracks/faults with very low stress drops (< 1 bar) and fault dimension < 150 m. Using P, and successive water reverberations, PwP & PwwP, the distance can be constrained to about 3.7 km from H2O. The polarization of P waves for the two main events and largest foreshock are all at the same azimuthal bearing of $220^\circ \pm 180^\circ$. The extremely short durations (< 0.1 s) of the nanoearthquakes illuminate the uppermost oceanic crust internally like a “seismic strobe light” that creates distinct seismic arrivals that can be used to investigate the seafloor structure at the H2O site. The observed shear wave reverberations coupled with an ODP determination of layer thickness of 29 m near H2O constrains the average shear wave velocity of the sediments

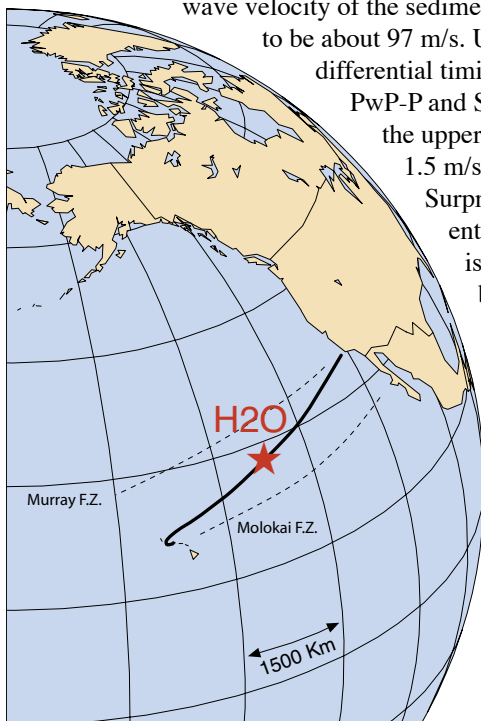
to be about 97 m/s. Using differential timing of PwP-P and S-P,

the uppermost crust has a compressional velocity of about 3.0 km/s and shear velocity of 1.5 m/s, consistent with Layer 2A pillow-like basalts observed by ODP drilling nearby.

Surprisingly, a clear shear wave birefringence is evident for the radial/transverse orientation determined solely from the P-wave polarization. The radial SV component is 0.085 seconds faster than the transverse SH, indicating 3% anisotropy in the basalt, which is consistent with vertically oriented cracks in the basalt. The fidelity of the signals, particularly on the horizontal components, is so good that one can use the particle motion to identify phases at high frequencies, which is only possible with well-coupled, buried sensors.



Hydrophone and seismic observations of the first nanoearthquake are shown from the compressional arrivals through the shear wave reverberations in the sediments. The seismic channels are converted to a Wood-Anderson response for calculation of M_L magnitude ~ -0.7 . The hydrophone channel is dominated by converted compressional wave energy, and effectively filters out shear waves. A small precursor is consistent with a refracted head wave from a Layer 2B basalt velocity, assuming a Layer 2A thickness of about 700 m. Strong conversion of P-to-S and S-to-P is evident at the sediment-basalt interface. Horizontal components are oriented into radial and transverse polarizations, as determined from the polarization of the compressional waves. Note that Ps is substantially larger on the radial component. Multiple reverberations in the sediment layer and shear wave birefringence constrains the shear velocity structure. Arrows indicate predicted arrival times from a simple 3-layered velocity model. The other nanoearthquakes show essentially the same pattern of arrivals.



Butler, R., The Hawaii-2 Observatory: Observation of Nanoearthquakes, *Seismol. Res. Lett.*, 74(10), 290-297, 2003.

Butler, R., The littlest earthquakes in the GSN?, *Seismol. Res. Lett.*, 73, 273, 2002.

Supported by NSF Cooperative Agreement EAR-0004370

The May 18, 1998, Indian Nuclear Test Seismograms at Station NIL

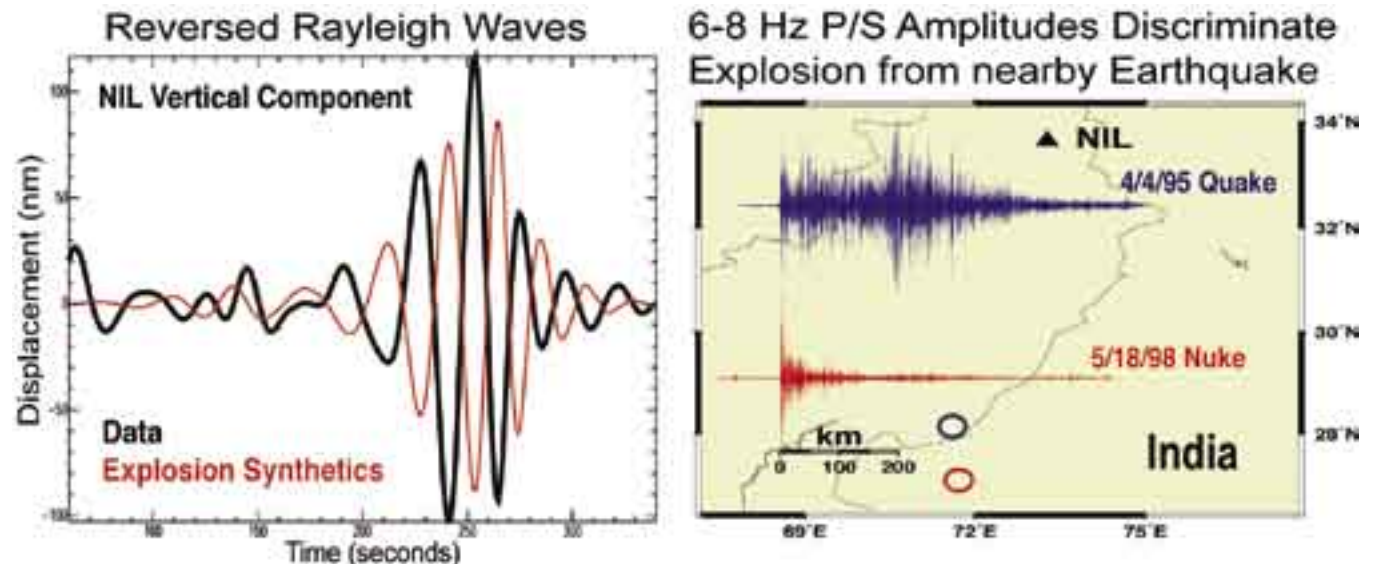
William R. Walter, Arthur J. Rodgers • Lawrence Livermore National Laboratory

David Bowers, Neil Selby • Blacknest, United Kingdom

The last underground nuclear tests were conducted by India and Pakistan in May, 1998. Although the Comprehensive Test Ban Treaty has not entered force, an International Monitoring System (IMS) established by the treaty is nearing completion. This system includes 170 seismic stations, a number of them originally established by IRIS. The IRIS station NIL (Nilore, Pakistan) is close to a planned IMS primary station and recorded some very interesting seismograms from the May 18, 1998, Indian test. We carefully calibrated the path to NIL using a prior Mw 4.4 earthquake that occurred on April 4, 1995, about 110 km north of the Indian test site. We used joint epicentral location techniques along with teleseismic P waves and regional surface waves to fix the epicenter, depth, mechanism and moment of this event. From these we obtained a velocity model for the path to NIL and created explosion synthetic seismograms to compare with the data. Interestingly, the observed Rayleigh waves are reversed, consistent with an implosion rather than an explosion source. The preferred explanation is that the explosion released tectonic stress near the source region, which can be modeled as a thrust earthquake of approximate Mw 4.0 earthquake plus a pure explosion. This tectonic release is sufficient to completely dominate the Rayleigh waves and produce the observed signal (Walter et al., 2005). We also examined the explosion at high frequencies of 6-8 Hz where many studies have shown that relative P/S amplitudes can discriminate explosions from a background of earthquakes (Rodgers and Walter, 2002). Comparing with the April 4 1995 earthquake we see the classic difference of relatively large P/S values for the explosion compared to the earthquakes despite the complication of the large tectonic release during the explosion. (This is LLNL report UCRL-TR-211315).

Rodgers, A. J. and W. R. Walter, Seismic discrimination of the May 11, 1998 Indian nuclear test with short-period regional data from station NIL (Nilore, Pakistan), *Pure Appl. Geophys.*, 159, 679-700, 2002.

Walter, W. R., D. Bowers, N. Selby, A. Rodgers and D. Porter, Tectonic Release from the May 11, 1998 Indian Nuclear Tests, LLNL report UCRL-JRNL-202983-DRAFT (to be submitted in 2005).



Transfer Functions and Seismic Discrimination: a KNET Case Study

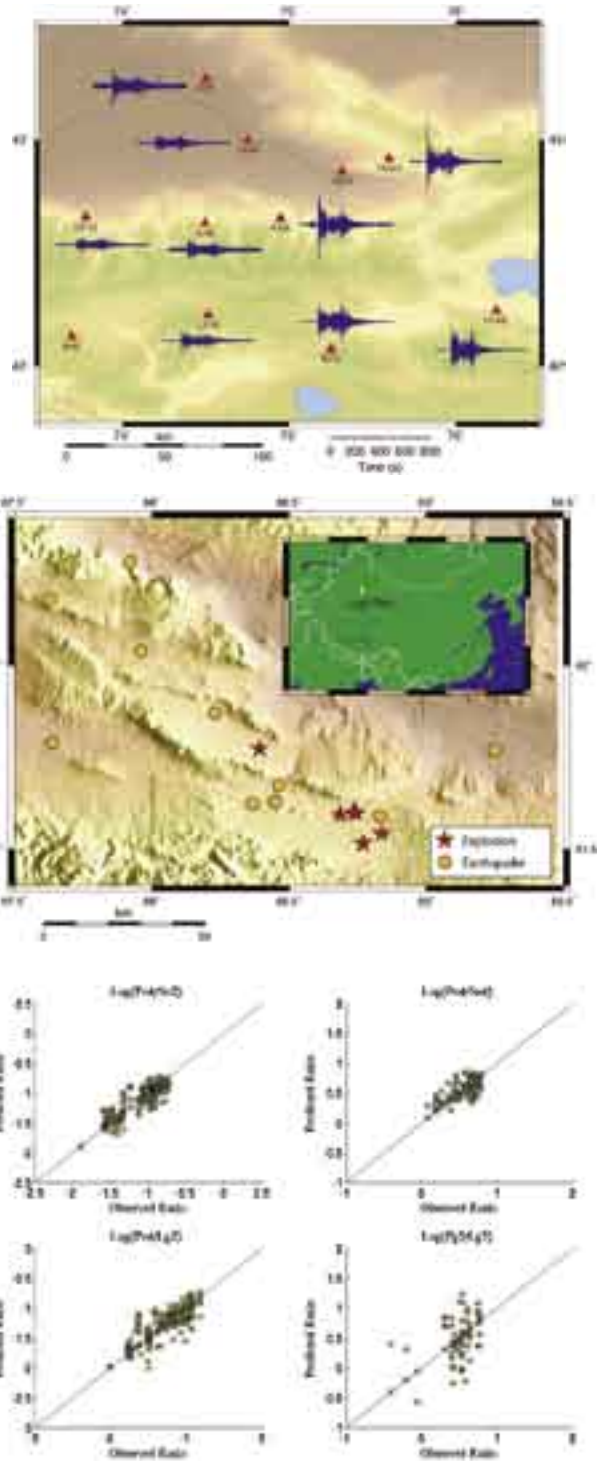
Marie Renwald • Southern Methodist University

Steven R. Taylor, Terry C. Wallace • Los Alamos National Laboratory

The basic challenge of nuclear test monitoring lies in quantitatively identifying earthquakes from explosions. At regional distances (<1500 km from the source), small-yield explosions are generally best detected from natural seismicity. However, regional seismograms can show both great complexity due to the crust-mantle waveguide and great variability for different source-station paths (Figure 1 illustrates an explosion detonated at Lop Nor recorded at the KNET network, which is approximately 1000 km away). To effectively develop regional discriminants at any given station requires a ground-truth database consisting of waveforms from both earthquakes and explosions. Newly-installed stations lack such a database, which severely affects confidence in successfully discriminating between different types of events. To address this problem, we have developed a procedure to predict a discriminant at a newly installed seismic station using the actual discriminant at a long operating station and a transfer function for that specific station pair.

The dataset consists of six explosions and nine earthquakes at or within 100 km of the Lop Nor Chinese nuclear test site (Figure 2) and recorded at the ten-station, very broadband KNET network in Kyrgyzstan. The KNET network is supported by IRIS; data were obtained from the IRIS DMC. We have predicted four discriminants (two phase ratio and two cross spectral ratio) using transfer functions for all possible station combinations. Initial results show good correlation (for three of four discriminants) between the discriminant predicted with a transfer function and the actual discriminant recorded at each station (Figure 3). We also investigated what role interstation distance plays in the success of the prediction; F-statistics suggest that interstation distance does not affect the prediction, implying that historical stations need not be in close proximity. However, placing bounds on this parameter will be important when applying the technique to other regions.

This work was performed under the auspices of the U.S. Department of Energy by Los Alamos National Laboratory under contract W-7405-ENG-36.

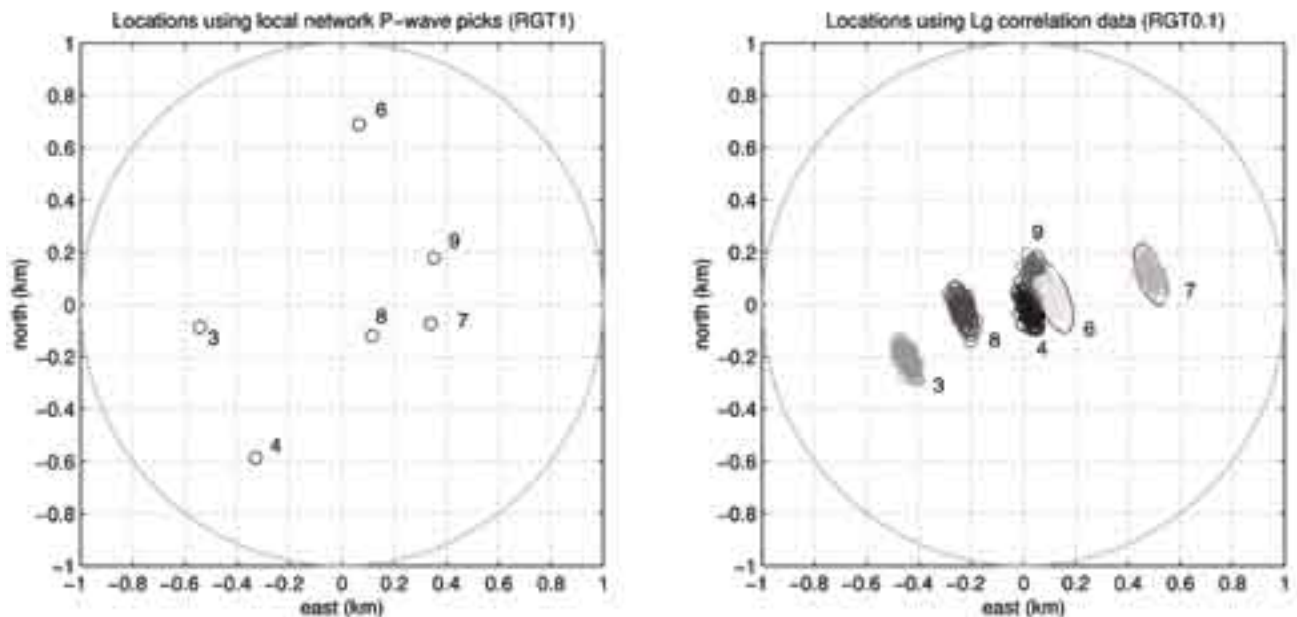


Lg-Wave Cross Correlation and Double-Difference Location

David P. Schaff, Paul G. Richards • *Lamont-Doherty Earth Observatory*

A surprising discovery has been made that in some cases the complex, highly-scattered Lg wave is found to be similar for clusters of events. We analyze in detail a subset of 28 events out of 90 from the 1999 Xiuyan sequence. Cross correlations provide highly accurate differential travel-time measurements. The error estimated from the internal consistency is about 7 ms. These travel time differences are then inverted by the double-difference technique to obtain epicenter estimates that have location precision on the order of 150 meters. The locations are computed with data observed by four to five regional stations 500 to 1000 km away. The epicenter estimates are not substantially affected by the sparseness of stations or large azimuthal gaps. Comparison with a surface trace a few km away and location estimates based on much more dense networks

□ a small number of phases and stations due to weak signal-to-noise ratios and sparse station coverage. This is especially true for monitoring work that seeks to locate smaller magnitude seismic events with a handful of regional stations. Two primary advantages of using Lg for detection and location are that it is commonly the largest amplitude regional wave (enabling detection of smaller events) and it propagates more slowly than P or Sn (resulting in smaller uncertainty in distance for a given uncertainty in travel time).



Comparison of double-difference relative locations for a subset of events in the sequence for a local/regional network (left) using only P-wave phase picks recorded at several hundred stations and for a sparse regional network (archived at IRIS) using Lg cross-correlation measurements (right). The rms travel time residuals are about 1 sec for the P waves and 0.02 sec for Lg. 95% confidence formal error ellipses and bootstrap errors (shaded small circles) are in good agreement (right). Origin in each case is taken as the centroid of the cluster.

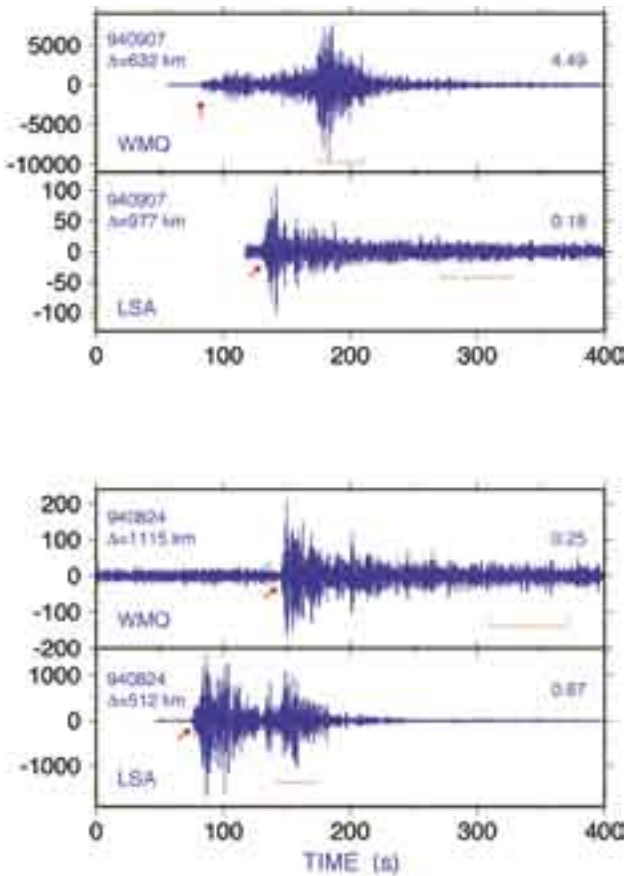
Schaff, D.P., and P.G. Richards, Lg-wave cross correlation and double-difference location: application to the 1999 Xiuyan, China, sequence, *Bull. Seismol. Soc. Am.*, 94, 867-879, 2004.

Strong LG Attenuation in Tibet

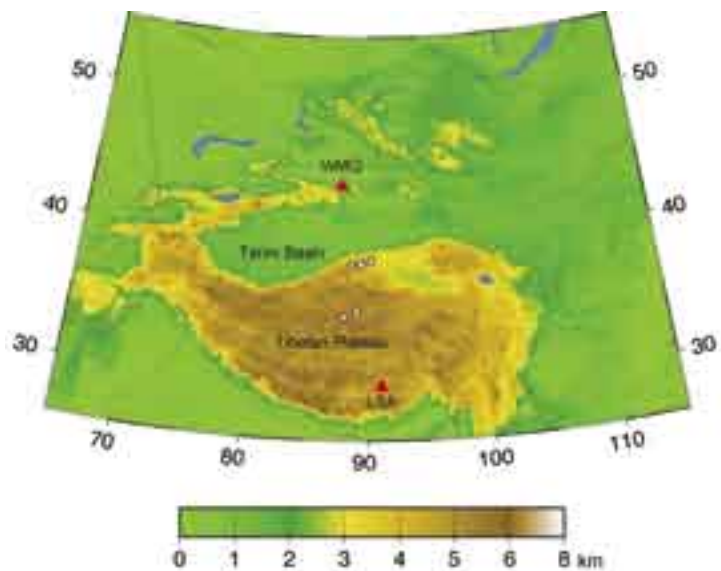
Guang-Wei Fan, Thorne Lay • University of California, Santa Cruz

One of the challenging regions for monitoring nuclear testing treaties is the high plateau of Tibet. In this region earthquake signals have a tendency to look explosion-like due to strong attenuation or blockage of high frequency S-wave energy. Using GSN observations from stations WMQ, LSA, and KMI, we constrain the attenuation of Lg, a reverberating shear wave in the crust, finding very strong attenuation in northern Tibet, and quite strong attenuation in eastern Tibet, consistent with local determinations made for data from InDEPTH deployments. To obtain robust estimates of attenuation, we use data involving two sources and two receivers all along (close-to) a given great circle path. This enables isolation of the attenuation properties on the path segment between the sources using a double spectral ratio method. Systematic analysis of data from CDSN stations near Tibet reveal that the strong amplitude and frequency content variations of Lg signals are most consistent

with progressive attenuation effects rather than blockage on the margins of the Plateau. Mapping out the attenuation behavior may allow more robust seismic identification in this region of the world.



Seismograms from WMQ and LSA for two events at different distances from the stations along the same great-circle path. Note that there must be very acute attenuation of high frequency signal for the path segment between the two events.



Topography map of Tibet, indicating the locations of stations WMQ and LSA, which are used to study attenuation on the path segments between clusters of events (white dots) in northern Tibet. The northern portion of Tibet has very strong attenuation of Lg, with 1 Hz Lg attenuation coefficients of about 79.

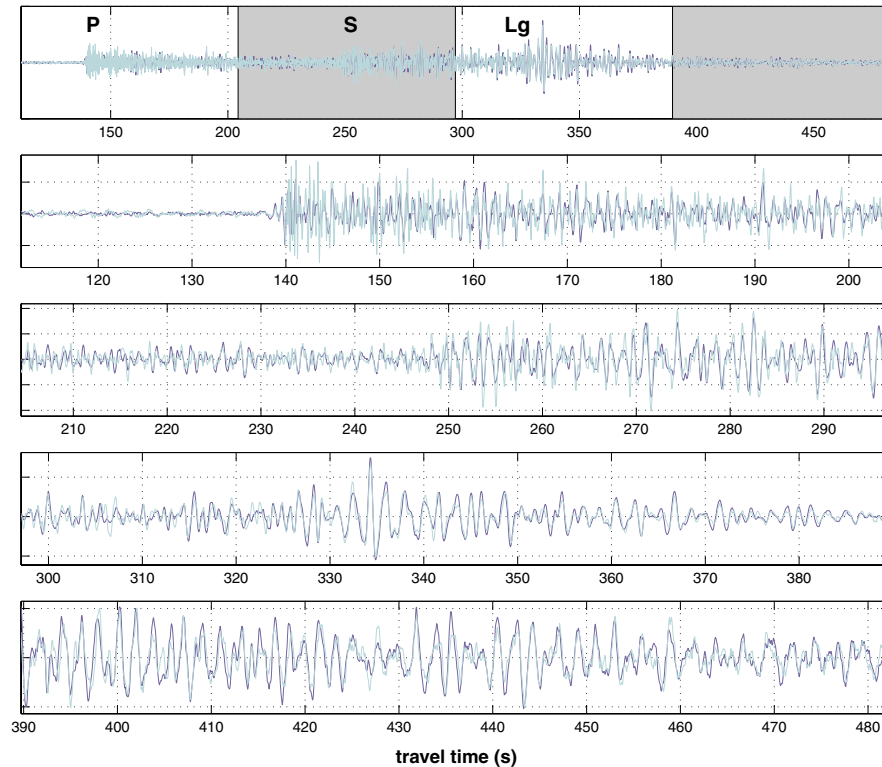
Fan, G.-W., and T. Lay, Strong Lg wave attenuation in the Northern and Eastern Tibetan Plateau measured by a two-station/two-event stacking method, *Geophys. Res. Lett.*, 30, No. 10, 1530, doi:10.1029/2002GL016211, 2003.

Supported by DTRA contract DTRA01-00-C-0211.

Repeating Seismic Events in China

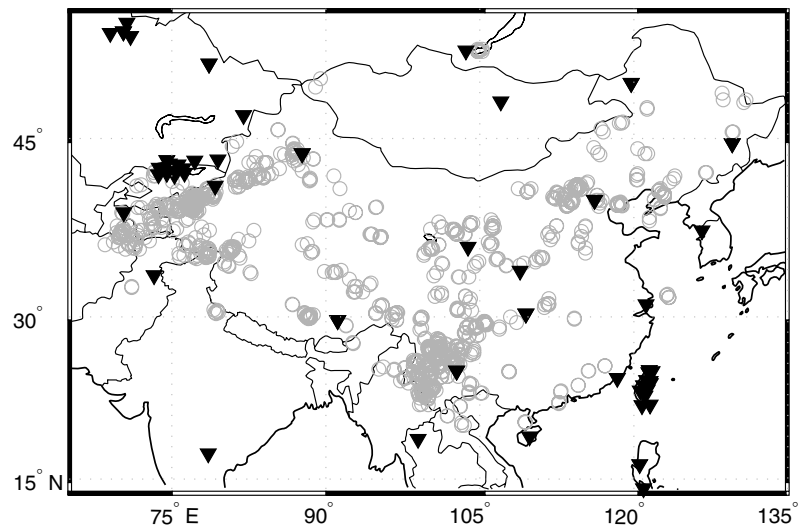
David P. Schaff, Paul G. Richards • *Lamont-Doherty Earth Observatory*

About 10% of seismic events in and near China, from 1985 to 2000, were repeating events not more than about 1 kilometer from each other. We cross correlate seismograms from ~14,000 earthquakes and explosions and measure relative arrival times to ~0.01 seconds, enabling lateral location precision of about 100-300 meters. This is important for studies of seismic hazard, understanding earthquake physics, and nuclear test ban verification. Recognition and measurement of repeating signals in archived data and the resulting improved locations quantifies the inaccuracy of current procedures for picking onset times and locating events.



A pair of similar events in China filtered from 0.5 to 5 Hz. X-axes are travel time in seconds. Y-axes are normalized to unit amplitude. Lower subpanels are enlargements of the white and gray segments. The predicted P wave arrives at 143 s, the S wave arrives at 256 s, and the Lg wave arrives at 315 s.

1301 events (9% of the Annual Bulletin of Chinese Earthquakes – ABCE), 950 doublets satisfying the criteria of cross-correlation coefficients greater than or equal to 0.8 for long windows from 5 seconds before the P wave to 40 sec after the Lg wave on waveforms that are filtered from 0.5 to 5 Hz. Recording stations archived at IRIS are denoted with filled triangles. Events are plotted at their ABCE absolute locations.

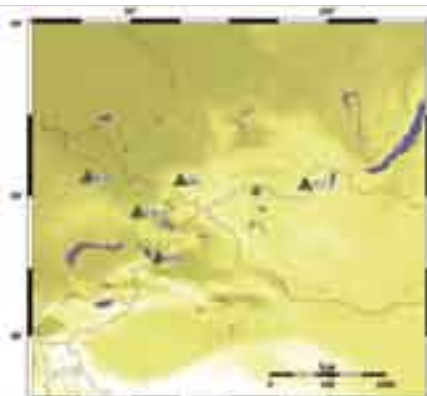
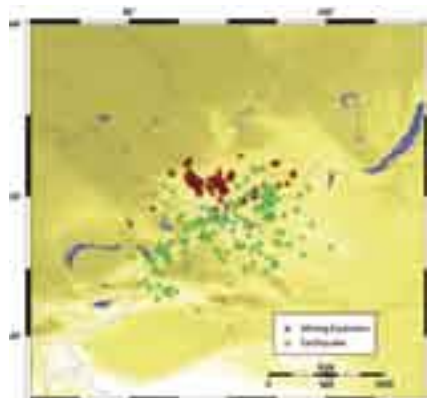


Schaff, D.P., and P. Richards, Repeating seismic events in China, *Science*, 303, 1176-1178, 2004.

A Comprehensive Database for Mining Explosion Discrimination

Marie Renwald, Brian Stump • Southern Methodist University

Stephen Arrowsmith, Michael Hedlin • University of California, San Diego



Historically, event identification for explosion monitoring has focused on the task of separating earthquakes and explosions. This approach was adequate for large events observed at teleseismic distances since there are few other types of manmade sources large enough to be observed. However, with the availability of high-quality regional data, smaller events (m_b 3.5 and below) that include many manmade sources are observed. The present challenge of seismic event identification now includes the task of classifying not only earthquakes and single-fired explosions (nuclear or chemical), but also mining explosions, underground mining collapses, and rock bursts.

In order to investigate smaller, mining-related events, we have assembled a comprehensive database of earthquakes and mining events. This database consists of events in both Russia and the United States and includes ground-truth data for several different kinds of mines (iron, copper, and coal). The Russian portion of the database includes approximately 25,000 waveforms from five stations (which include 4 IRIS stations and one IMS station) for 850 mining events and 250 earthquakes (Figures 1 and 2). The US portion of the database comprises 132 stations (which include IRIS stations and the IMS Pinedale Array) that provide regional coverage of three mines (Figure 3). Nearly 100,000 waveforms were collected for 900 mining events and 450 earthquakes (Figure 4). All of the data, with the exception of data from 2 IMS stations, were recovered from the IRIS DMC.

This database will be used to develop discrimination tools that specifically consider the physical processes that accompany mining explosions and what makes them unique from earthquakes and other types of explosions for classification purposes. The discrimination tools we are presently investigating are described in Stump et al. (2002) and include amplitude ratios, time-varying spectral estimation, waveform correlation, and $M_s:mb$.

Stump, B. W., M. A. H. Hedlin, D. C. Pearson, and V. Hsu, Characterization of mining explosions at regional distances: Implications with the International Monitoring System, *Rev. Geophys.*, 40(4), 1011, 2002.

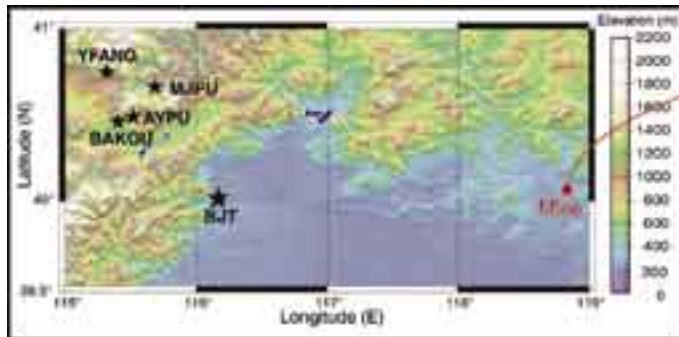
This work sponsored by the National Nuclear Security Administration, Office of Nonproliferation, Office of Defense Nuclear Proliferation.

Intermediate Period Surface Waves from Mining Explosions

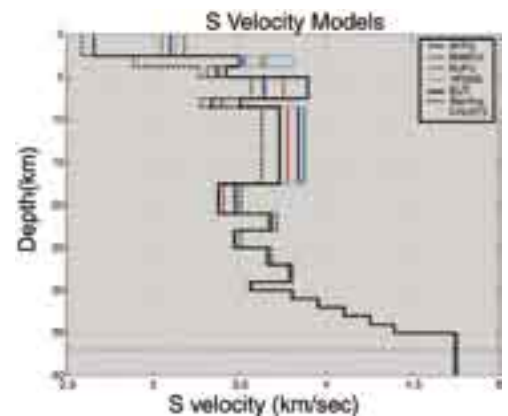
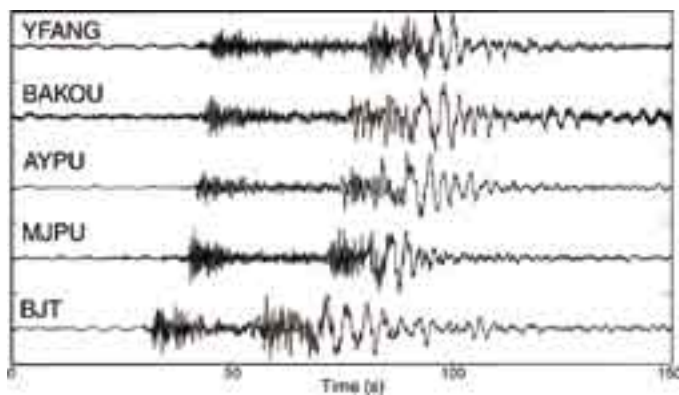
Rong-Mao Zhou, Brian W. Stump, Chris T. Hayward • Southern Methodist University

Yun-Tai Chen, Zhi-Xian Yang • Institute of Geophysics, China Earthquake Administration

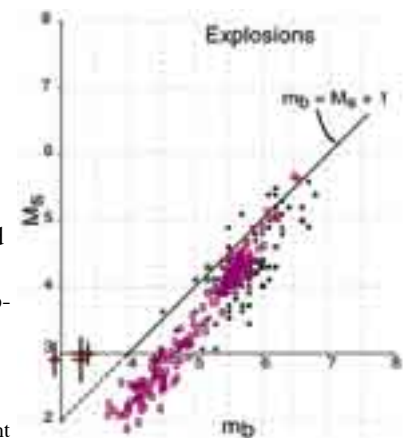
Intermediate period surface waves (2-20 s) are generated by long-source-duration mining explosions. Data from a PASSCAL broadband network in China and a similar deployment in Wyoming are used in a comparative study to understand sources and shallow crustal structure in the two regions.



Typical broadband regional seismograms from long-time-duration mining explosions are illustrated in the panel below. Group velocities of fundamental mode Rayleigh waves were estimated using the Multiple Filter Analysis technique and refined with Phase Matched Filtering. These data were then used to assess the path effects in China and Wyoming. The crustal structure inverted from the fundamental mode Rayleigh wave for China is reproduced below. The paths in this example reflect the importance of the Yanshan uplift to all the paths except BJT.



The velocity models developed from intermediate period surface wave dispersion allow surface wave magnitude estimates to be made from intermediate period surface waves. Such estimates allow the investigation of m_b/M_s ratios as an earthquake-explosion discriminate for smaller industrial explosions. m_b and M_s values for the US and China large mining explosions (red x-marks) are superimposed on explosion measures published by Stevens and Day (1985, black dots) and Bonner et al. (2003, purple rectangles). This comparison suggests that large, long-delay mining explosions that are normally detonated may fall away from the earthquake populations. One event occurred on Aug. 1, 1996, plots in the explosion population. In-mine observations of this event indicate that it did not detonate as planned. A large portion of the blast accidentally detonated simultaneously.

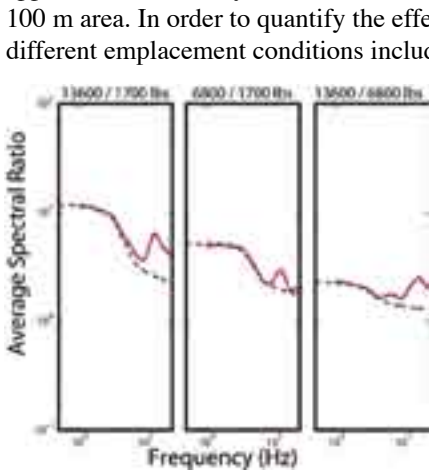
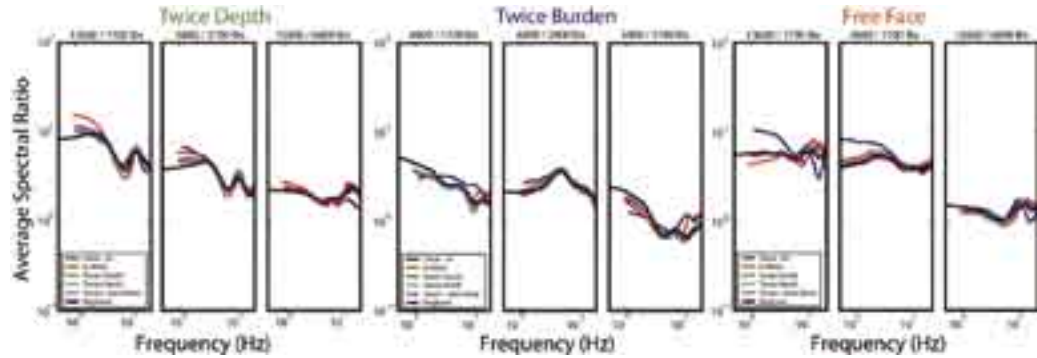


This work was supported by Defense Threat Reduction Agency contract DSWA01-98-C-0176, the Air Force Research Laboratory under contract DTRA01-02-C-0003, and DOE/NNSA under cooperative agreement DF-FC52-03NA99510/A000.

Source Scaling of Single Fired Mining Explosions with Different Confinement and Explosive Size at a Copper Mine in Arizona

Rong-Mao Zhou, Brian W Stump • Southern Methodist University

A series of single-fired (simultaneously detonated) explosions were conducted in an Arizona copper mine as part of the Source Phenomenology Experiment (SPE) using IRIS PASS-CAL seismometers. The explosions spanned yields from 773 to 6181 kg and were all detonated in an approximate 100 m by

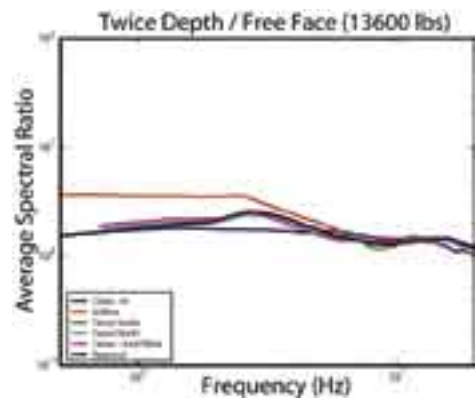


100 m area. In order to quantify the effect of the mine free-face, the individual explosions were also detonated under three different emplacement conditions including at the free-face of the mine under normal burden, twice normal burden and fully contained. The purposes of these experiments were to investigate the generation of regional phases such as Pg, Pn, and Lg from mining explosions, quantify the relationship between yield and seismic amplitudes, quantify the effect of confinement and contrast single-fired waveforms with those from delay-fired explosions. Instrumentation was deployed in the near-source region (100-500 m), local (1-33km) and regional distances. Empirical scaling relations for the different shots in this test series were developed in order to quantify the effects of yield and confinement.

Empirical source scaling relations using the close-in (100-500 m), in mine (1-3 km), local (1-33 km) and regional data are compared for the three confinements. In all cases data at each range document similar scaling. The fully contained scaling (twice depth) quantifies the change in individual source corner as well as absolute source size.

The Mueller-Murphy source model has been used to quantify effects of explosion depth and material in which the explosion is detonated. Material properties were measured for the porphyry granite at the mine and used in forward models for the yield scaling of the fully contained explosions. The forward model of the source scaling is compared to the empirical scaling in the figure to the right illustrating the ability to appropriately account for source order and relative sizes of the absolute energy coupled into the ground.

Typical mining explosions are detonated at a free face or boundary to the pit in order to fail the rock and possibly cast material. Explosions were conducted at the free face in order to quantify energy lost relative to a fully contained explosion. The empirical scaling relations suggest that the free face explosion can experience a factor of 2-4 reduction in amplitude.



Work at SMU on this project was sponsored by the National Nuclear Security Administration Office of Nonproliferation Research and Engineering Office of Defense Nuclear Nonproliferation. Equipment for the study was supplied by the PASSCAL Instrumentation Center.

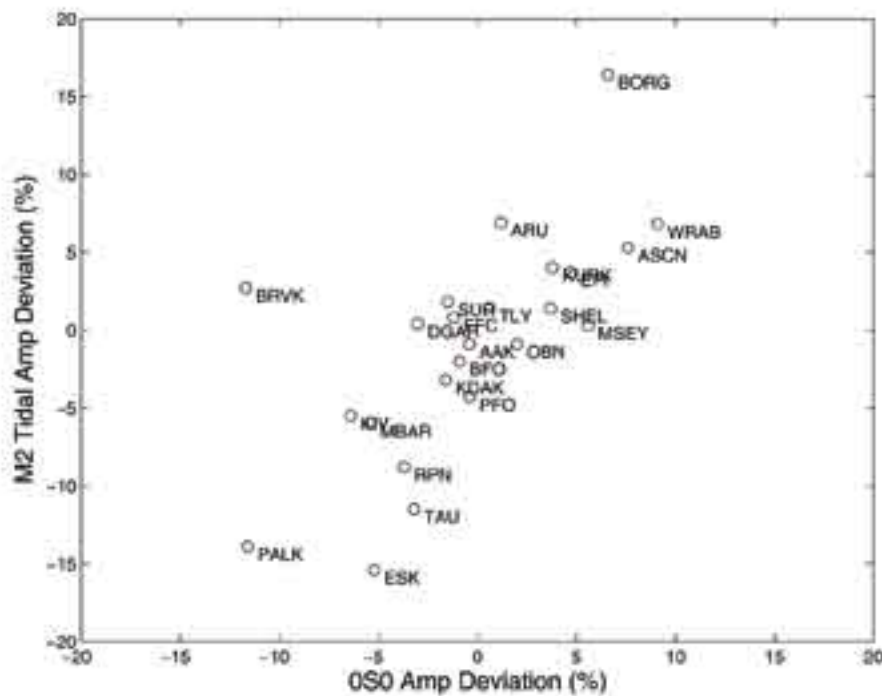
Quality Control of GSN Sensor Response Information

Peter Davis • University of California, San Diego

The Mw 9.0 Sumatran earthquake provides a special opportunity to validate the accuracy of sensor responses. We are in the process of comparing the consistency of free oscillation amplitudes measurements against observations of lunar tides to investigate how accurate are the GSN instrument responses IDA reports to the community.

Shown in the figure are observations of the M2 lunar tide and the mode ${}_0S_0$ each normed to their respective expected values. For the tides, the observed tide at each station was compared to that of a synthetic based upon current models of ocean loading. For the mode, the data are expressed as deviation from the mean for the set. The consistency between the two sets suggests that there is a problem with the published amplitude response. This is quite possible: the accepted GSN practice is to

□
 sor manufacturer's value for the generator constant.



Scatter plot of the M2 tidal amplitude deviations vs observed ${}_0S_0$ amplitudes at IRIS/IDA stations during January 2005 following the Mw 9.0 Sumbawan quake. The network scatter for each period is higher than expected from instrument calibrations for reasons we are investigating.

GSN Station Operator Training

Peter Davis • *University of California, San Diego*

Training of local station operators continues to play an important role in the success of the GSN. During November 2001, UCSD hosted a training session for IRIS/IDA station operators whose stations also function as part of the UN's International Monitoring System (IMS). The program, which was sponsored by the United Nations CTBTO, brought together operators from Chile, Fiji, Iceland, Indonesia, Kyrgyzstan, Peru, Russia, South Africa, Sri Lanka, and Uganda to learn more about the GSN data acquisition system. Operators were given a thorough orientation to the proper operation of all hardware, taught basic equipment troubleshooting procedures, and coached in the usage of software for data acquisition and review.

We expect that training will become an increasingly important issue to GSN hosts in the future. There is a scarcity of trained seismologists in many developing countries, yet the information demands placed by host governments upon nascent national seismic networks are as great as those in technologically advanced nations. As new emergency response infrastructure develops following the Sumatra-Andaman earthquake and tsunami, GSN station host institutions will need personnel fam□

groups to integrate GSN data into their own network data flow and to improve their data analysis capabilities, the GSN will garner tremendous good will among its foreign affiliates throughout the world.



Participants in the UN IMS Technical Training Program for IRIS/IDA station operators held at the Cecil H. and Ida M. Green Institute for Geophysics and Planetary Physics, San Diego, California from 5-9 November 2001.

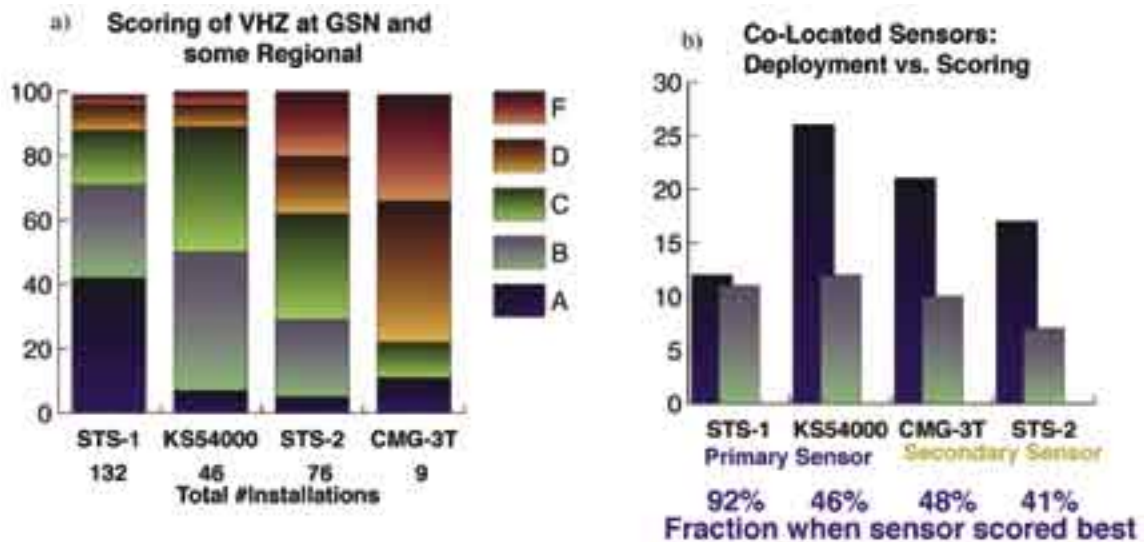
Data Requirements from Low-Frequency Seismology and the Death of STS-1 Sensors

Gabi Laske • IGPP, Scripps Inst. of Oceanography

Free-oscillation seismology has exceptionally high demands on data quality. We need long, gap-free records, with consistently high signal-to-noise performance. The data harvest for a typical very large earthquake (scalar seismic moment $M_0 \geq 5.0 \times 10^{20}$ Nm) is rather sobering. Only 75% of the records downloaded from the IRIS DMC can be used for study.

For the 2004 IRIS Broadband Instrumentation workshop I summarized the experience I gathered from analyzing over 20 large earthquakes in the last 10 years. I inspected each vertical component spectrum visually and assigned grades A-F. A little less than 50% of the records of Wielandt-Streckeisen STS-1 vault sensors (132) meet the highest quality requirements, while the 46 Teledyne-Geotech KS5400 borehole installations (and its predecessor KS36000) yield less than 10% high-quality records. Surprisingly, the fraction of such records at 85 STS-2 and Guralp CMG3 (CMG-3t and CMG-3b) installations is almost as large. Overall, I find that 70% STS-1 records are “acceptable” for analysis, 50% KS54000 records, but less than 30% STS-2/CMG3 records which clearly stresses the importance of observatory-quality very-broadband installations. It is often argued that KS54000s are typically deployed in noisy environments so that my comparison should not be used directly to judge the value of a KS54000. I have also inspected the data from co-located sensors for the 3 largest earthquakes in 2003. Typically, the primary sensor is either an STS-1 or KS54000 and the secondary sensor a STS-2 or CMG-3. In 92% of the cases when an STS-1 is involved, it provides the best records. The same is true for only 46% of the KS54000 records, which implies that in more than half of the cases the secondary sensor (STS-2 or CMG3) provides the better record. The new station at the South Pole, QSPA, hosts all four sensors. For two of the three largest earthquakes in 2003, the STS-1 delivered the best record, while the STS-2 delivered the best for one event. The quality of the CMG-3 is not far behind and, occasionally better, while the KS54000 delivers grade C data. For the Sumatra-Andaman earthquake, the CMG-3 delivered the best data at very low frequencies, while the STS-1 performed relatively poorly, the reason for which is not understood.

Clearly, the STS-1 is the ultimate workhorse of low-frequency seismology. After the 2004 Sumatra earthquake, low-frequency modes could be seen on STS-2 records of many networks, not just the GEOFON network that has consistently been delivering good STS-2 records. The Sumatra earthquake and its March 2005 aftershock were extremely large and it is probably not a good idea to include its data to adjust GSN design goals. Rather, we need to find an adequate successor for the STS-1. This perhaps necessitates the co-deployment of several sensors rather than one very-broadband sensor that can do it all.



a) Grading of available GSN and equivalent vertical recordings. A grade E record has some surface wave trains but no obvious spectral lines. An ‘F’ grade record has no seismic signal or large data gaps. b) Scoring for co-located sensors. Number of records (dark blue) and instances when the sensor provided the best seismogram (light blue).

Development of a New Broadband Optical Seismometer

Mark Zumberge and Jonathan Berger • Scripps Institution of Oceanography

Erhard Wielandt • Stuttgart University

The mainstay observatory-class seismometers used by global networks for the past two decades are no longer manufactured and there is no other commercially available product of sufficient quality on the market today. For such quality instruments, the development risk is high, the development time long, and the market small and apparently not sufficient to provide commercial viability.

To meet the instrumentation requirements of global seismology, we have designed and built a prototype sensor that uses optical fiber interferometry to record the motion of an inertial mass. The use of optical fiber interferometry rather than traditional electronic displacement transducers affords significant advantages. Features of this broadband optical seismometer include:

- A linear, high-resolution displacement sensor;
- Displacement measurement referenced to the wavelength of light, providing continuous calibration;
- Increased dynamic range;
- Increased bandwidth;
- No electronics in the sensor — only optical fiber connection to the seismometer — eliminating heat from electronics in the sensor package and noise pickup from connecting electrical cables;
- Smaller package — our design will be applicable to both vault and borehole installations and should be relatively easy to manufacture.

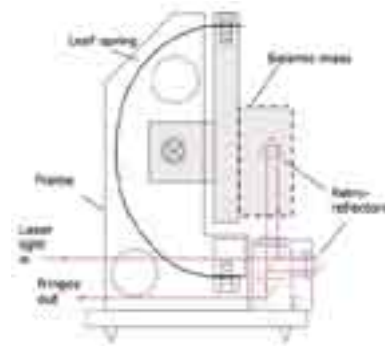


Figure 1. Schematic of vertical-component optical seismometer. The two fringe signals are input to a fast A/D converter (105 sps). An algorithm on the digital signal processor (DSP) continually updates the parameters of an ellipse that characterizes the fringe pattern while instantaneously computing the optical phase (i.e., the mass displacement), yielding a real-time, high-precision fringe resolver. The DSP circumvents the need for an analog data recorder, providing digital data logging with an equivalent dynamic range of about 30 bits.

We have developed an optical displacement transducer that promises to lead to a greatly improved seismometer. The use of optical fiber interferometry in place of electronics adds other important benefits, including immunity to noise pickup, simplification of remote deployment (in a borehole, for example), the elimination of a heat source in the seismometer—an important cause of noise in the best existing systems, and the elimination of components that can be damaged in electrical storms (a problem in many field settings).



Figure 2. Prototype Vertical Optical Seismometer. This unit has a mass of 360 grams and a free period of a few seconds. The spring is a single strip of "NiSpan-C", a trade name for a particular alloy of iron-nickel with small amounts of chromium and titanium.

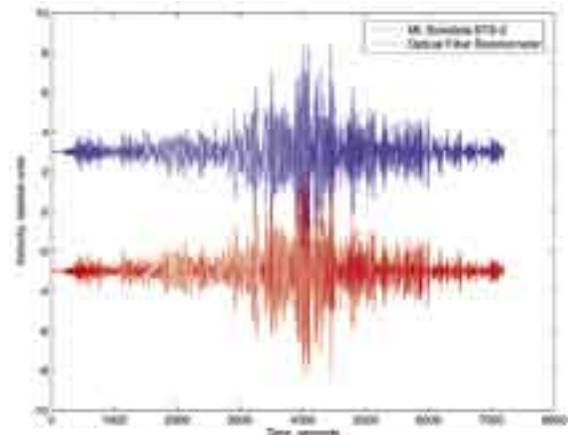


Figure 3. The 2004 Sumatra earthquake provided an opportunity to test our algorithm for converting mass displacement to ground displacement based on the spring-mass mechanical characteristics. This is a challenge because the new sensor does not rely on force-feedback as do conventional sensors. The good agreement between the record from the prototype optical sensor (red) and a conventional sensor (blue) indicates that the processing is correct (although much further work is needed).

Earthquake and Ambient Vibration Monitoring of the 17-Story Steel Frame UCLA Factor Building

Monica Kohler, Paul Davis • University of California, Los Angeles

A unique structural health monitoring program using a 17-story moment-resisting steel frame building with an embedded 72-channel accelerometer array has been implemented on the UCLA campus (Figure 1). The array serves as a prototype for data that can be used in predictive modeling of structures for damage assessment and building code modification. The array records waveforms at 100 and 500 sps. The IRIS Data Management Center is archiving the continuous, 100 sps data for the scientific and engineering community. Nine new digitizers were installed as part of UCLA's NSF Science and Technology Center for Embedded Networked Sensing (CENS) to test embedded network technologies and algorithms with the array.

We have used the data to compute time-varying displacements in 2D (Figure 2, left), the building's finite impulse response, and angles of horizontal rotation associated with torsions, and to identify the higher modes of vibration (Figure 2, right). The observations are being compared with finite element modeling in order to refine the structural model and to perform predictive motion simulations for scenario earthquakes and nonlinear behavior. Our observations show that measurable softening effects are occurring for small earthquakes due to changes in the stiffness of the building or soil when amplitudes get larger (Kohler et al., 2005). For example, the frequency of the first mode of deformation decreases by about 10% but increases to previous pre-earthquake levels within seconds of the earthquake. Our real-time monitoring program illustrates how changes in building characteristics can be continuously monitored to detect significant damage or breakage in a structure.



Figure 1. (left) Photo of Factor building and (right) diagram of sensor locations. Arrows show polarities of sensors on each floor. The 72 channels of building data can presently be viewed on the web at teren.ess.ucla.edu:5813 (password: seismo) in real time.

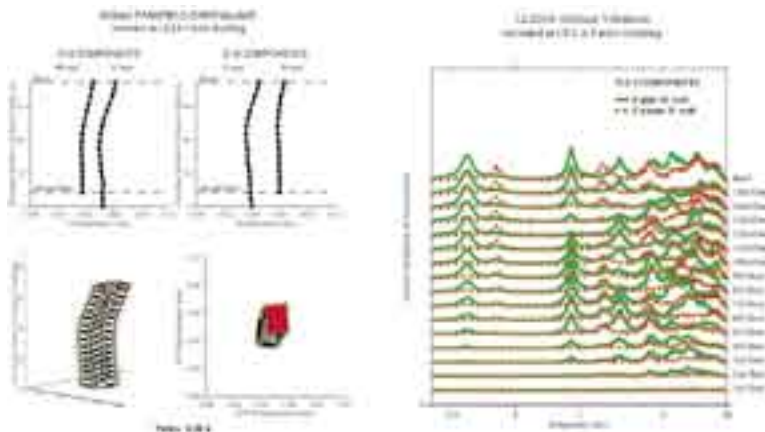


Figure 2. (left) Observed horizontal displacements (filled circles) from the 9/28/04 Parkfield earthquake; frame is from a 24-sec animation, (right) spectra of ambient vibrations summed and stacked to distinguish translational (solid) from torsional (dashed) frequencies.

Kohler, M. D., P. M. Davis, and E. Safak, Earthquake and ambient vibration monitoring of the steel frame UCLA Factor building, *Earthquake Spectra*, accepted, 2005.

Passive Crustal Refraction Experiments Using IRIS/PASSCAL Facilities: New Surveys Show Variable Crustal Thickness in the Western Great Basin

John N. Louie and Michelle Heimgartner • University of Nevada

Utilizing commercial mine blasts and local earthquakes, as well as a dense array of portable seismographs, we have achieved long-range crustal refraction profiles across northern Nevada and the Sierra Nevada Mountains. In our most recent refraction experiment, the Idaho- Nevada-California (INC) transect, we used a dense spacing of 411 portable seismographs and 4.5-Hz geophones. The instruments were able to record events ranging from large mine blasts to small local earthquakes. Our instruments sensed blast first arrivals out to a distance of approximately 400 km. We have obtained 99% data recovery and clear refractions across the central Sierra Nevada and the northern Great Basin. The Northern Walker Lane refraction experiment, completed in 2002, confirms the presence of a thin crust ranging from 19-23 km thick in a 100 km region in the vicinity of Battle Mountain, Nevada. Pn crossover distances of less than 95 km from both the INC and Northern Walker Lane experiments support this observation. We also observe an unexpectedly deep crustal root under the northern Sierra Nevada, over 50 km in thickness and centered west of the topographic crest. In addition, we have created contoured crustal thickness maps based literature cited from previous compilations. These maps integrate our current experiments with past geophysical assessments of the Great Basin. Our seismic-refraction reconnaissance of the western Great Basin will contribute to the assessment of geothermal potential in poorly constrained areas.



(left) Map indicating the location of the Idaho-Nevada-California (INC) Northern Walker Lane refraction experiments (Louie et al., 2004) across the western Great Basin. (right) Record section from the Barrick GoldStrike 100,000-lb mining blast on August 19, 2004: 100 sec long and beginning 8 sec after the blast. The “Texan” recorder transect extends from Fresno, CA (SW), to the Idaho Nevada border (NE), approximately 600 km.

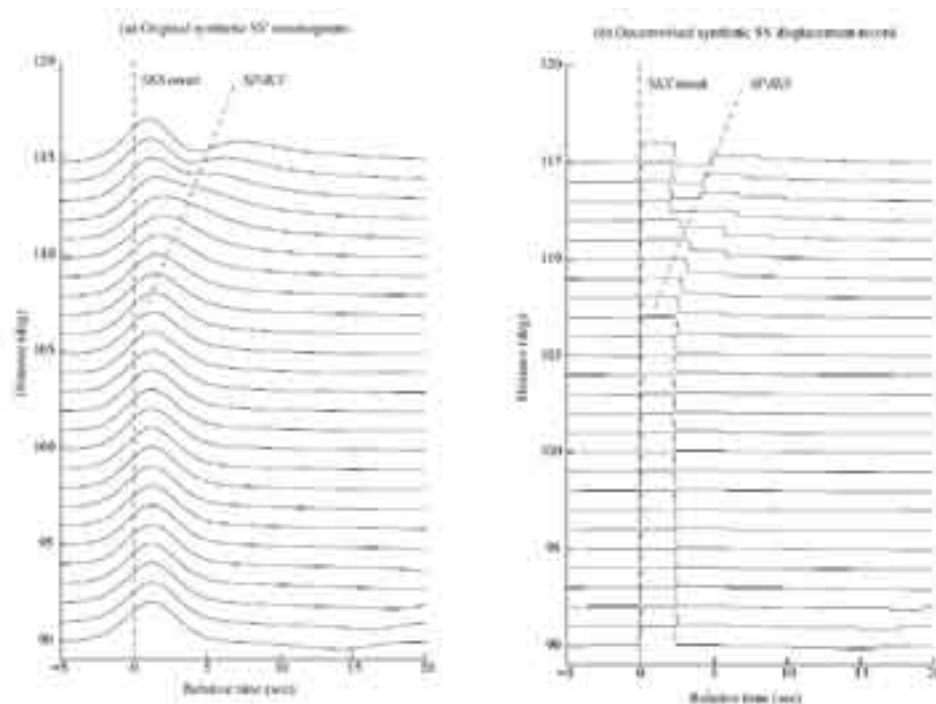
Louie, John N., Weston Thelen, Shane B. Smith, Jim B. Scott, Matthew Clark, and Satish Pullammanappallil, The northern Walker Lane refraction experiment: Pn arrivals and the northern Sierra Nevada root, *Tectonophysics*, 388, no. 1-4, 253-269, 2004.

This material is based upon work supported by the U.S. Department of Energy under instruments numbered DE-FG07-02ID14311 and DE-FG36-02ID14311, managed through the DOE Golden Field Office. Reftek RT-125 “Texan” recorders and field support provided by the NSF-funded IRIS/PASSCAL Instrument Center at New Mexico Tech.

Signal Restoration Through Deconvolution Applied to Deep Mantle Seismic Probes

Wolfgang Stefan, Ed Garnero, Rosemary Renaut • Arizona State University

In this study we present a method of signal restoration to improve the signal-to-noise ratio, sharpen seismic arrival onset, and act as an empirical source deconvolution of specific seismic arrivals. Observed time series are modeled as a convolution of a simpler time series, and an invariant point spread function (PSF) that attempts to account for the earthquake source process. The method is used on the shear wave time window containing SKS and S, whereby using a Gaussian PSF produces more impulsive, narrower, signals in the wave train. The resulting restored time series facilitates more accurate and objective relative travel time estimation of the individual seismic arrivals. We demonstrate the accuracy of the reconstruction method on reflectivity synthetic seismograms. Clean and sharp reconstructions are obtained with real data, even for signals with relatively high noise content. Reconstructed signals are simpler, more impulsive, and narrower, which allows highlighting of some details of arrivals that are not readily apparent in raw waveforms. In particular, phases nearly coincident in time are separately identified after processing. This is demonstrated for broadband observations as well: two seismic wave pairs used to probe deep mantle and core-mantle boundary structure: (1) the Sab and Scd arrivals, which travel above and within, respectively, a 200-300 km thick higher than average shear wave velocity layer at the base of the mantle, observable in the $88^\circ - 92^\circ$ epicentral distance range; and (2) SKS and SPdiffKS (shown), which are core waves with the latter having short arcs of P wave diffraction, and are nearly identical in timing near $108^\circ - 110^\circ$ in distance. A Java/Matlab algorithm was developed for the signal restoration, which can be downloaded from the authors webpage (<http://mathpost.la.asu.edu/~stefan>), along with example broadband data and synthetic seismograms. This method holds promise for facilitating waveform characterization and travel time measurements in large data sets.



(a) SV component reflectivity synthetics, for a source depth of 500 km. Receiver distances are from 90 to 115 degrees, in one degree increments. (b) Deconvolved synthetics. Traces in both panels are aligned at the SKS onset detected in the deconvolved traces of panel (b) using an edge detection method. At a distance of 108 deg, the formation and subsequent move out of SPdiffKS can be seen in both plots, though it is first visible in the deconvolved traces: SKS remains rectangular until the formation of SPdiffKS initiates, which first broadens SKS, and then emerges as an additional rectangle.

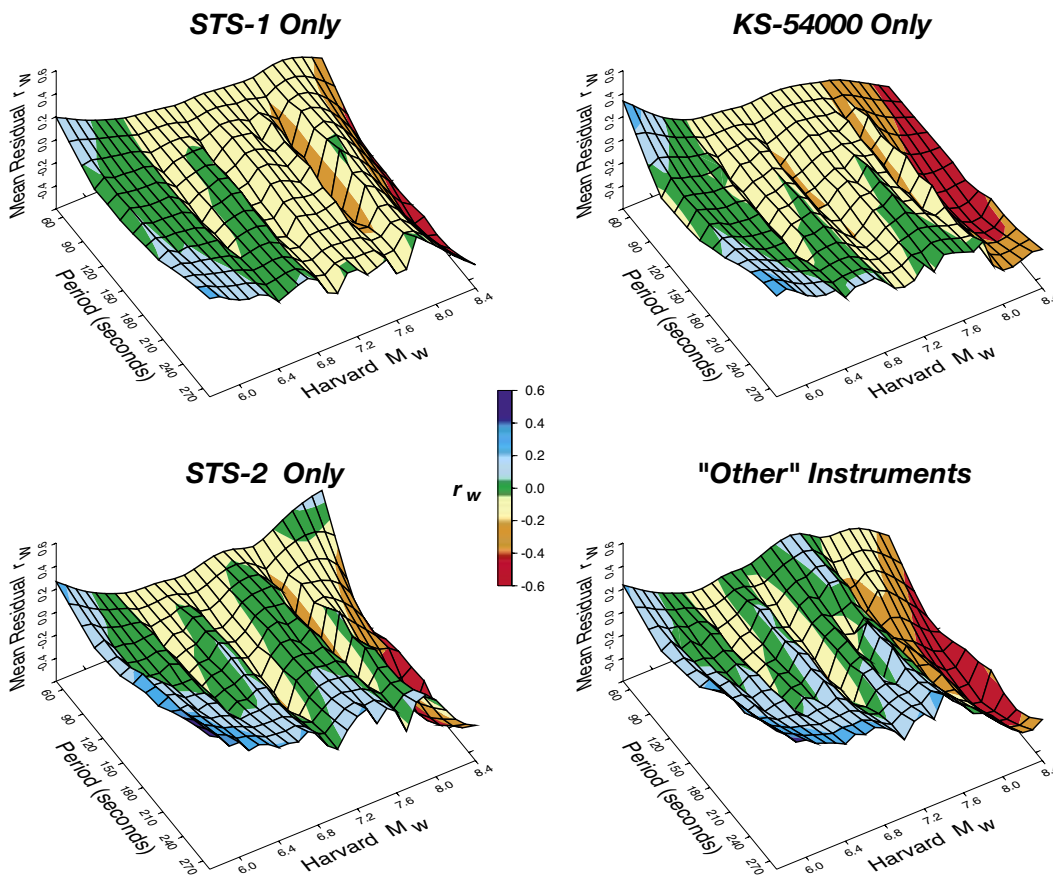
Stefan, W., Garnero, E. and Renaut, R. A., Signal restoration through deconvolution applied to deep mantle seismic probes, *Geophys. J. Int.*, in review, 2005. NSF CMG-02223

The Mantle Magnitude M_m and the Slowness Parameter Θ : Five Years of Real-time Use in the Context of Tsunami Warning

Stuart A. Weinstein • Pacific Tsunami Warning Center, NOAA

Emile A. Okal • Northwestern University

We study a database of more than 115,000 measurements of the mantle magnitude M_m introduced by *Okal and Talandier* (1989), obtained since 1999 as part of the operational procedures at the Pacific Tsunami Warning Center. The performance of this method is significantly affected by the seismic instrumentation at the recording station, with the very broad-band STS-1 and KS54000 systems offering the lowest residuals between measured values of M_m and those predicted from the Harvard CMT catalog, and also by the period at which spectral amplitudes are measured, with the best results between 70 and 250 s. With such mild restrictions, estimates of seismic moments can be obtained in real time by retaining either the maximum value of M_m measured on each record, or its average over the various mantle frequencies, with the resulting residuals on the order of 0.1 ± 0.2 moment magnitude units. M_m deficiencies in the case of the two large earthquakes of Peru (2001) and Hokkaido (2003) are attributed to azimuthal bias from an excess of stations (principally in North America) in directions nodal for the focal mechanism and directivity patterns. We further study a group of more than 3000 measurements of the energy-tomoment ratio Θ introduced by *Newman and Okal* (1998), which allows the real-time identification of teleseismic sources violating scaling laws, and in particular of so-called “tsunami earthquakes”. The use of a sliding window of analysis in the computation of Θ allows the separation of “late earthquakes”, characterized by a delayed, but fast, moment release from truly slow earthquakes. A number of such events are recognized, notably on major oceanic and continental strike-slip faults.



Three-dimensional plots of the residuals r_w as a function of period and seismic moment (expressed as M_w published in the Harvard Catalogue). For each of the standard frequencies, values of r_w are regrouped in magnitude bins of width 0.1 M_w -unit, and an average value computed in each bin. The resulting function is then plotted in three dimensions and color-coded. Separate plots are made for the various types of instruments.

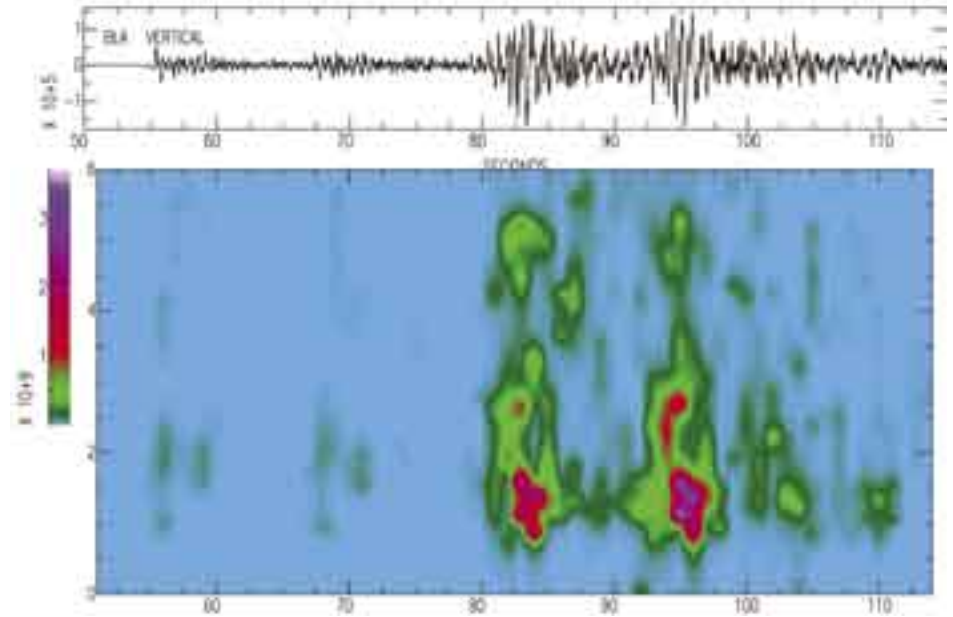
SAC Availability for the IRIS Community

Peter Goldstein • Lawrence Livermore National Laboratory

Arthur Snoke • Virginia Polytechnic Institute

SAC (also known as SAC2000) is a signal processing and analysis code that has been developed by Lawrence Livermore National Laboratory (LLNL) over the past 20+ years for a variety of seismic and geophysical research projects. SAC has evolved into a general purpose interactive program designed for the study of sequential signals, especially time-series data. Emphasis has been placed on analysis tools used by research seismologists in the detailed study of seismic events. Analysis capabilities include general arithmetic operations, Fourier transforms, three spectral estimation techniques, IIR and FIR filtering, signal stacking, decimation, interpolation, correlation, and seismic phase picking. SAC also contains an extensive graphics capability.

SAC is used extensively by the seismic community because: 1) it has a broad range of well-tested, efficient data analysis capabilities (examples include: data inspection, phase picking, signal correction, quality control, unary and binary data operations, traveltimes analysis, spectral analysis including high-resolution spectral estimation, spectrograms and binary sonograms, and array and three-component analysis); 2) it is easy to use and reliable; 3) it has a macro programming language that allows users to develop innovative new analysis techniques; 4) it has interfaces to the Unix operating system, Matlab <www.mathworks.com>, and the Generic Mapping Tools (GMT) software <<http://gmt.soest.hawaii.edu/>> that make it very flexible, allowing researchers to solve many research problems innovatively with minimal programming effort; and 5) the suite of analysis capabilities are integrated so that innovative processing schemes are easily implemented. SAC is also widely used because of its user-oriented development philosophy, which has led to consistent, easy to use capabilities that are backward compatible.



IRIS and LLNL have recently signed a contract to provide IRIS with a license for SAC that would allow the sharing of the SAC/SAC2000 source code with the IRIS community, and provide limited support to facilitate a community development effort.

The first of the above objectives has been met: as of March 1, 2005, the source code can now be downloaded for members of IRIS from Web site <<http://www.iris.edu/manuals/sac/index.htm>>. SAC, and its auxiliary graphics conversion program *sgftops*, have been built successfully on three operating systems: Sun Solaris (2.9), Mac OS X (10.3), and Linux (Redhat 8.0 and Debian). Pre-built binary executables for those operating systems can be downloaded from the same site. Links are also given to a SAC tutorial and users' manual. (Much of the contents of the users' manual can be accessed from within SAC using the help utility.)

Goldstein, P., D. Dodge, M. Firpo, and Lee Minner, SAC2000: Signal processing and analysis tools for seismologists and engineers, Invited contribution to *The IASPEI International Handbook of Earthquake and Engineering Seismology*, Edited by WHK Lee, H. Kanamori, P.C. Jennings, and C. Kisslinger, Academic Press, London, 2003.

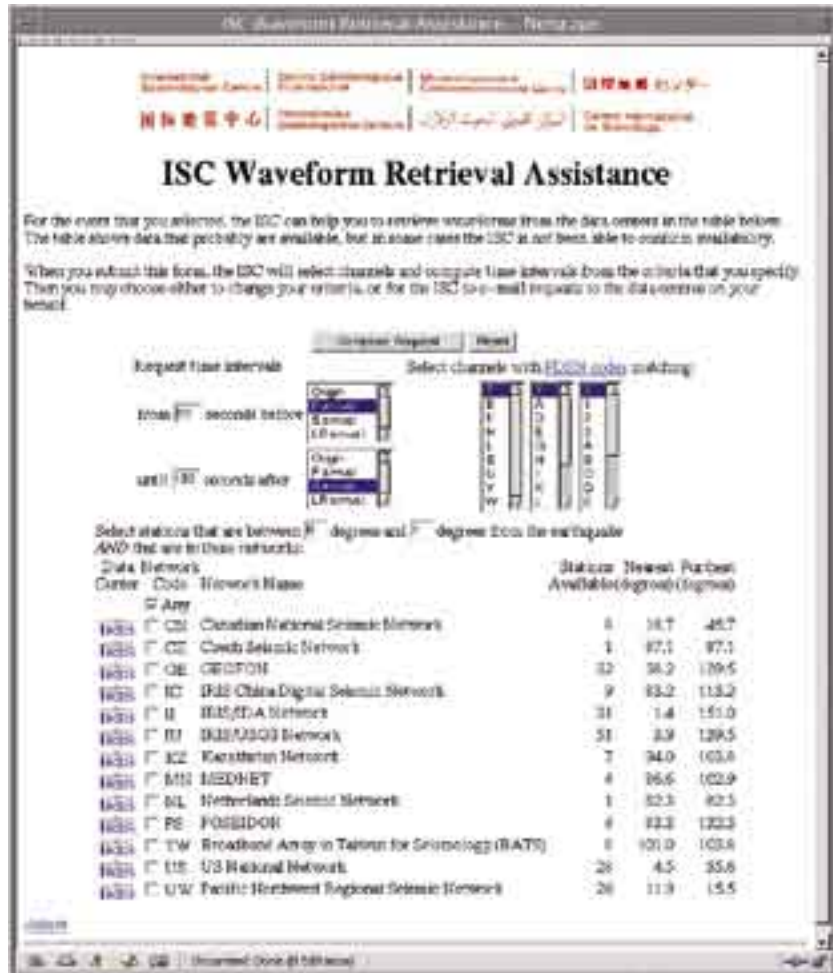
Goldstein, P. and A. Snoke, SAC Availability for the IRIS Community, *DMS Electronic Newsletter*, Vol. VII, No. 1 <<http://www.iris.edu/news/newsletter/vol7no1/page1.htm>>, 2005.

ISC On-line Bulletin and IRIS DMC Waveform Retrieval

Ray Willemann, James Harris • *International Seismological Centre*

After finding events in the ISC Bulletin relevant to their work, the next step many seismologists follow is to obtain waveforms for further study. The ISC began offering systems to assist on-line bulletin users retrieve waveform data for specific events in early 2002. Most of these systems were agency and event specific. However, with the co-operation of the IRIS DMC a system was developed to create a request for the event of interest for data from the continuous waveform archive at IRIS. SeismiQuery was modified by IRIS to produce an inventory for a requested time period and tied to the stations used to locate the event by the ISC. The user could then select the data of interest before a request was submitted after this point contact would be between the user and IRIS directly. It was in operation for just one year during which period waveforms for over 300 events were requested.

From early 2003, a new ISC system has been operating that integrates all available data centre waveform archive/retrieval systems into a single request for each event. This incorporated the work done with IRIS to ensure that an up-to-date inventory was used to create the data request. The system has proven popular with ~700 event requests made in each year of operation.



Web Services at the IRIS DMC

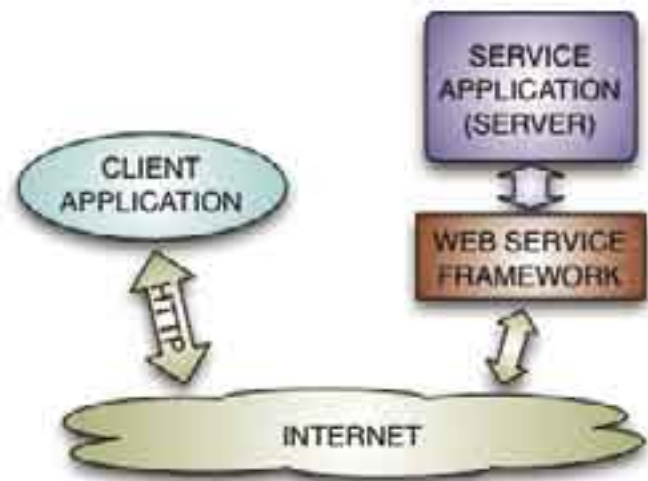
Tim Ahern, Linus Kamb, Joanna Muench • IRIS Data Management Center

IRIS has always been a leader in advancing the use of enabling technologies within the seismological community, including the development and adoption of a comprehensive data file format and tools, web browser-based access mechanisms, distributed archive access, and CORBA-based programmatic interfaces into the archive. The IRIS Data Management Center continues in that role with the development of web services-based interfaces and services.

The adoption of web services answers two important demands in the current scientific research environment. While the Internet has made numerous positive changes in the ways in which scientific efforts are carried out, the prevalence of malicious software threatens to dampen this expansion by limiting many types of Internet access in the form of firewalls. Web services play an important role in by enabling programmatic interfaces over the typically less-restricted http protocol. In addition, web service clients can be built in a wide variety of computer languages and don't require advanced programming skills to successfully implement. Due to these factors, we feel that web services are the components on which a broader community-oriented service framework can be built.

Current efforts at the DMC include a web service front-end to the CORBA-based Data Handling Interface (DHI-WS), a framework to support time-series processing (seismoproc), and the Uniform Product Distribution System (UPDS). The DHI-WS service provides a subset of the DHI interface to provide the commonly accessed

DHI functionality to clients behind firewalls. Seismoproc enables the publishing of seismic data processing algorithm implementations for use by external client applications. UPDS will provide a coherent web services-based system to manage the submission, searching, and access of USArray XML-based Data and Informational Products.



Simplified Access to Services: A client invokes the services of a remote web services-based server using standard http calls across the Internet.

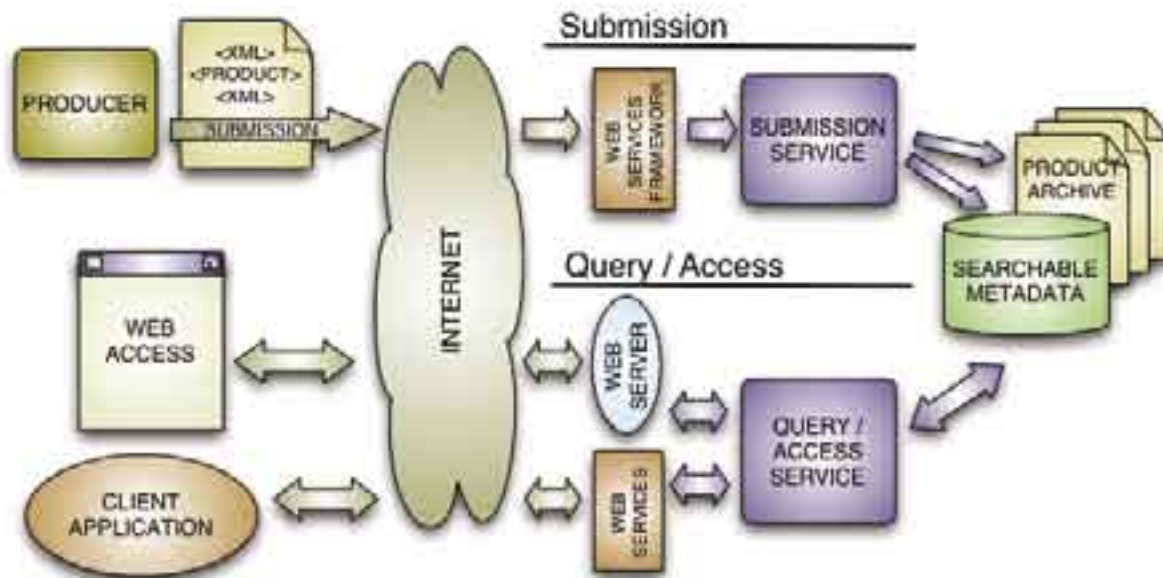
The Uniform Product Distribution System

Linus Kamb, Tim Ahern • IRIS Data Management Center

The IRIS DMC is currently developing the Uniform Product Distribution System (UPDS) for the USArray. The UPDS will provide a coherent Web Services-based system to manage the submission, searching, and access of USArray XML-based Data and Informational Products. A Data Product is any information that is routinely derived from or calculated from raw seismic (or other) data. At another level, a Data Product can be essentially anything, including derived information, images, station information, etc., and even raw data. While targeting USArray products, the UPDS will be able to manage products from other components of EarthScope.

Producers will create and submit XML-encoded products to a UPDS archive, which will extract searchable metadata from the product. Users of the system will then be able to query for available products based on the extracted metadata and download their selections. The UPDS will be structured such that new and as-yet unforeseen product types can be added to the Archive with minimal effort. Different producers will be able to extend the standard product definitions by adding any additional information in their products.

UPDS will have both a web browser-based interface as well as a Web Services-based programmatic interface (API) that will allow client programs to be written that can access the UPDS system. The programmatic interface will support the development of stand-alone GUI applications, command-line clients suitable for use in scripted environments, and background monitoring processes such as Standing Order –type applications. The web interface will provide an interactive method for searching and accessing the archived products. Web forms customized for each product type will be presented that will allow users to browse and query the archived products by their associated metadata.



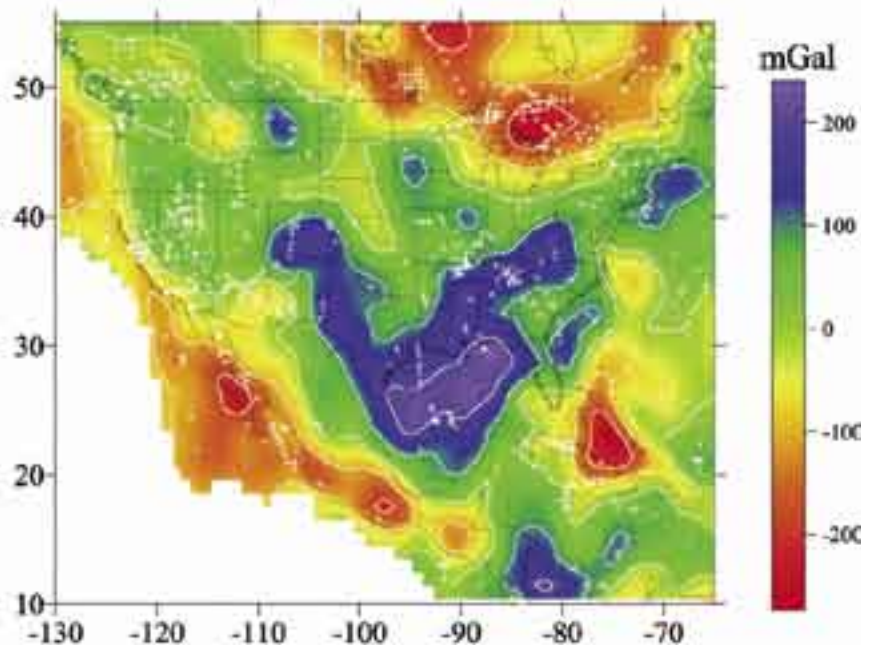
The Uniform Product Distribution System will provide Web Services-based submission and query/access servers to support the archiving, discovery, and access of XML-based data products.

The North American Upper Mantle: Density, Composition, and Evolution

Walter D. Mooney • *U.S. Geological Survey, Menlo Park*

Misha Kaban • *GeoForschungsZentrum (GFZ), Potsdam, Germany*

The upper mantle of North America (NA) has been well studied using various seismic methods. Here we investigate the density structure of the NA upper mantle based on the Bouguer gravity anomaly map. The basis of our study is the removal of the gravitational effect of the crust to determine the mantle gravity field. The effect of the crust is removed in three steps by subtracting the gravitational contributions of: (1) topography; (2) low-density sedimentary accumulations; and (3) the 3D density structure of the crystalline crust. Topographic data are taken from a standard data base; information regarding sedimentary accumulations, including thickness and density, are taken from published maps and summaries of borehole measurements of densities; the structure of the crust is from a recent compilation, with layer densities estimated from compressional wave velocities. The resultant mantle gravity anomaly map shows a negative anomaly (-50 to -400 mgal) beneath western NA and the adjacent oceanic region, and positive anomalies (+50 to +350 mgal) to the east of the NA Cordillera. This pattern reflects the well-known division of NA into the stable eastern portion and the tectonically active western portion. In order to separate the contributions of thermal expansion from mantle composition, we apply an additional correction for the thermal structure of the uppermost mantle. The thermally-corrected map reveals mantle density anomalies that are solely due to compositional variations. These anomalies have a magnitude of +250 to -250 mgal. The upper mantle beneath the Canadian shield exhibits a negative anomaly (-50 to -200 mgal) that is consistent with chemical depletion that results in a mantle composition with lower density, also referred to as the mantle tectosphere. The strongest positive anomaly is co-incident with the Gulf of Mexico, and indicates a positive density anomaly in the upper mantle. Two linear positive anomalies are also seen: one with a NE-SW trend in the eastern USA roughly coincident with the Appalachians, and a second with a NW-SE trend beneath the states of Texas, New Mexico, and Colorado. These anomalies are interpreted as due either to: (1) the presence of the Farallon slab at a depth below 300 km; or (2) mantle density anomalies associated with the accretion of 1.8-0.8 Ga Proterozoic terrains along the southern margin of Laurentia. Based on these results, the evolution of the NA upper mantle is depicted in a series of cartoons that display the primary processes that have formed and modified the crust and lithospheric upper mantle.

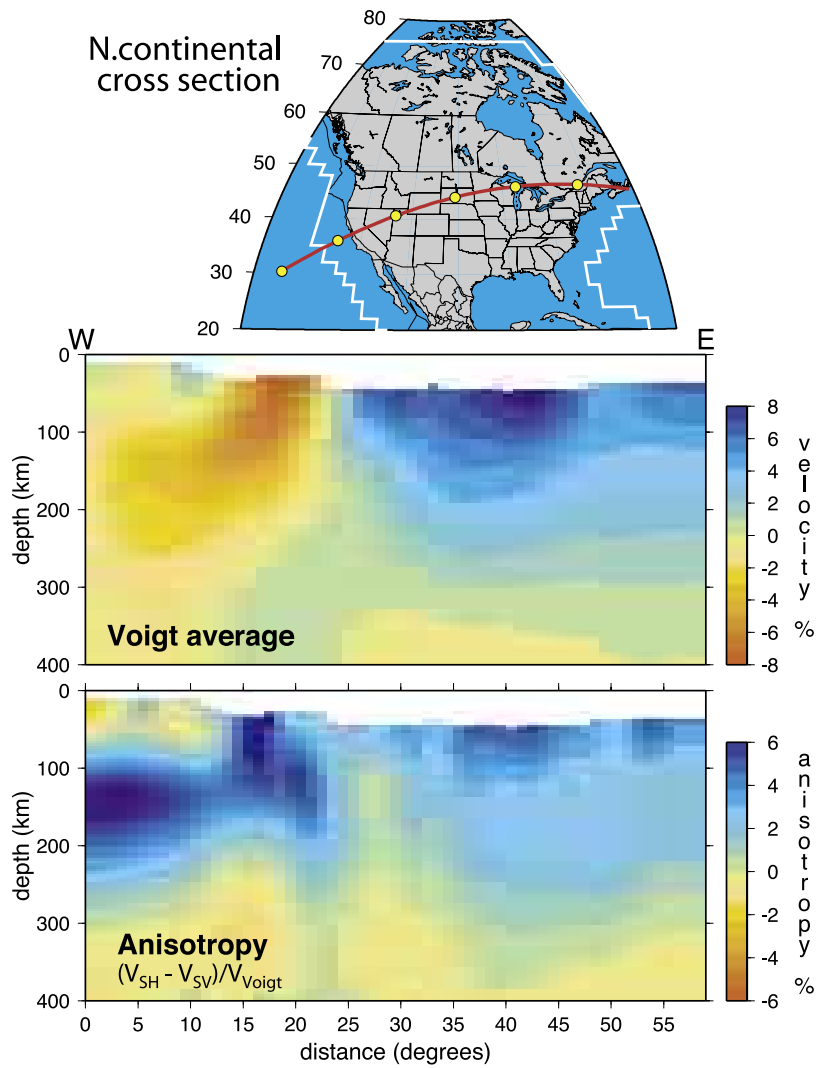


Mantle gravity anomaly after removing the effect of lateral variations in mantle temperature. We calculated the gravity expression of that portion of the Farallon slab below 660 km assuming a positive density contrast of 0.025 g/cc. The resultant anomaly is in excellent geographic agreement with our anomaly located in the Gulf of Mexico.

Tomography of the North American Upper Mantle Using Global and Regional Datasets

Meredith Nettles, Adam M. Dziewonski • Harvard University

We use a hybrid global-regional approach to combine currently available regional and global datasets for tomography of the North American upper mantle, incorporating data from the IRIS GSN with data from the U.S. National Seismograph Network (USNSN), the Canadian National Seismograph Network (CNSN), and several IRIS PASSCAL deployments, including the MOMA, BEAAR, RISTRA, and FLED arrays. We use a large dataset of surface-wave phase-delay measurements at periods of 35-350 s to determine a regional model of the three-dimensional radially anisotropic shear velocity structure under North America that is consistent with long-wavelength, global models of the upper mantle. The model we retrieve resolves structure on a wavelength of a few hundred kilometers throughout most of the continent. The correspondence between major geological features and those imaged in our mantle model is generally good. Radial anisotropy is observed to vary regionally, with systematic differences in anisotropy between oceanic and cratonic provinces. Radial anisotropy is observed to be strong under the Basin and Range, where the amplitude of the anisotropy reaches 4-6%.

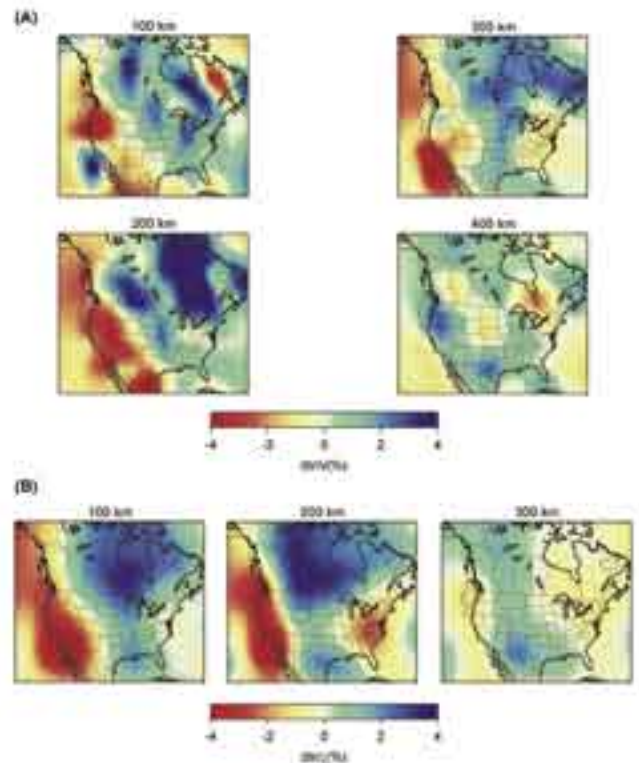


The figure shows cross-sections through the isotropic (top) and anisotropic (bottom) velocity structure of the upper mantle under North America. Note the rapid transition between slow and fast wavespeed in the isotropic structure, and the difference in anisotropic structure under the Pacific plate and the Canadian craton. Yellow dots in the map mark 10-degree intervals along the cross section (red line).

High-Resolution 3D Anisotropic Structure of the North American Upper Mantle from Inversion of Body and Surface Waveform Data

Federica Marone, Barbara Romanowicz • *University of California, Berkeley*

Seismic anisotropy provides insight into paleo and recent deformation processes and therefore mantle dynamics. To date, our knowledge of the North American anisotropic structure arises mainly from global tomographic models or SKS splitting studies which lack horizontal and vertical resolution, respectively, and are limited to either radial or azimuthal anisotropy. Our goal is a high-resolution model for the North American upper mantle incorporating both radial and azimuthal anisotropy. We hope to achieve unprecedented lateral and depth resolution by improving both current methodology and data coverage. In a first step, we inverted long period waveform data simultaneously for perturbations in the isotropic S-velocity structure, the anisotropic parameter $\xi = V_{SH}^2/V_{SV}^2$ and the depth to the Moho, in the framework of normal mode asymptotic theory (NACT) (Li and Romanowicz, 1995). The resulting 2D broad-band sensitivity kernels allow us to exploit the information contained in long-period seismograms for body, fundamental and higher-mode surface waves at the same time. This approach has previously only been applied at the global scale, with a lateral parametrization in terms of spherical harmonics. We have adapted the NACT algorithm for the regional case by implementing a lateral parametrization in terms of spherical splines on an inhomogeneous triangular grid of nodes, with the finest mesh for North America. The inverted dataset consists of more than 100,000 high quality 3-component body, fundamental and overtone surface waveforms, recorded at broad-band seismic stations in North America from teleseismic events and provides a fairly homogeneous path and azimuthal coverage. Our 3D radial anisotropic model shares the large scale features of previous regional studies for North America. We confirm the pronounced difference in the isotropic velocity structure between the western active tectonic region and the central/eastern stable shield, as well as the presence of subducted material (Juan de Fuca and Farallon plate) at transition zone depths. Concerning the anisotropic signature, we observe a positive ξ anomaly in correspondence of the cratonic areas, within the lithosphere, while a negative ξ anomaly beneath the Basin and Range province suggests possible mantle upwelling. In the future, we expect to further improve the data coverage, in particular by taking advantage of the broad-band dataset that will be collected under the USArray effort within EarthScope. The combination of this exceptional set of data with our methodology will allow us to invert for a more complete model of anisotropy that will also include azimuthal information. Hence we will be able to gain 3D detailed insight into mantle dynamics and address unresolved geophysical questions such as the nature and strength of lithosphere/asthenosphere coupling, the depth extent of continental sub-regions and the relation of imaged seismic anisotropy to present-day asthenospheric flow and/or past tectonic events recorded in the lithosphere.



Horizontal slices at different depths through our 3D radial anisotropic model. Anomalies are relative to PREM, (a) Perturbations in the isotropic S-velocity structure, (b) Perturbations in the anisotropic parameter ξ .

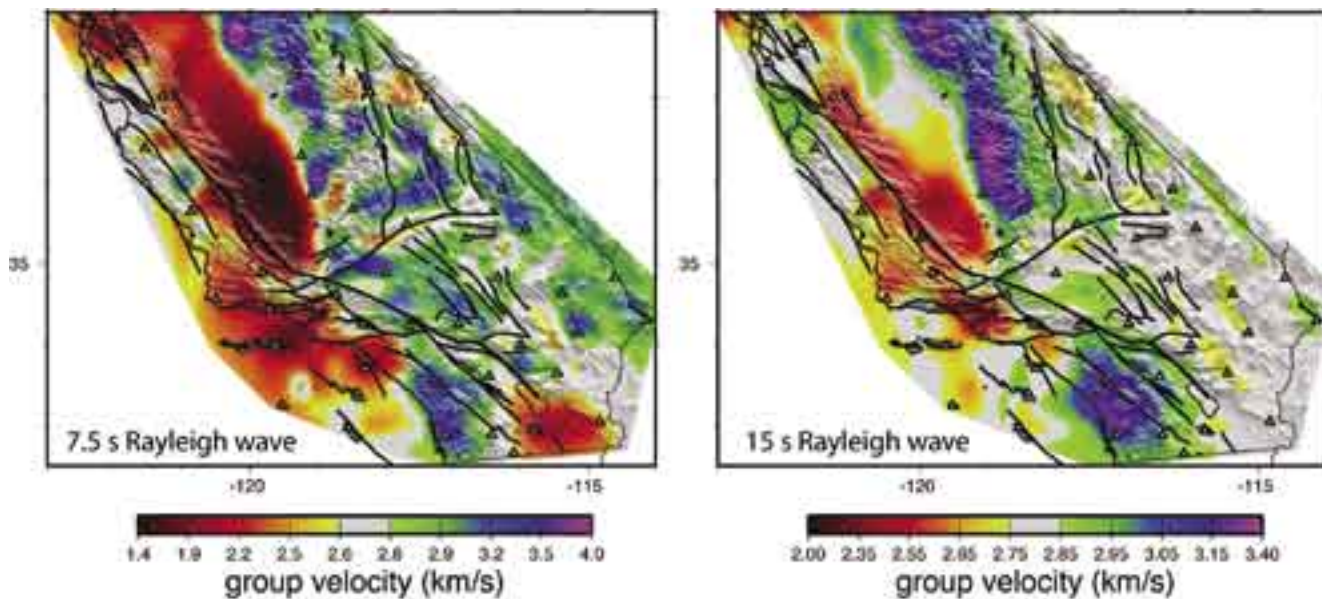
This work has been supported by the NSF grant NSF/EAR-0345481.

High-Resolution Surface Wave Tomography From Ambient Seismic Noise

Nikolai M. Shapiro, Michael H. Ritzwoller • *University of Colorado at Boulder*

Michel Campillo, Laurent Stehly • *Laboratoire de Géophysique Interne et de Tectonophysique Université Joseph Fourier, Grenoble, France*

Rayleigh wave Green functions, extracted by cross-correlating long sequences of ambient seismic noise (Shapiro and Campillo, 2004) normally discarded as part of traditional seismic data processing, contain information about the structure of the shallow and middle crust. Cross-correlating one month of ambient seismic noise recorded at USArray stations in California yields hundreds of short period (6 – 20 s) surface-wave group-speed measurements on inter-station paths. These measurements are used to construct dispersion maps of the principal geological units of California, with low-speed anomalies corresponding to the main sedimentary basins and high-speed anomalies corresponding to the igneous cores of the major mountain ranges (Shapiro et al., 2005). The use of ambient seismic noise as the source for seismic observations addresses several shortcomings of traditional surface wave methods. The method is particularly advantageous in the context of temporary seismic arrays such as the Transportable Array component of USArray or PASSCAL experiments because it can return useful information without earthquakes. The short-period dispersion maps provide homogeneous information about shear wave speeds in the crust which are hard to acquire with traditional methods. The new method enhances resolution because measurements are made between regularly spaced receivers, which may lie much closer to one another than to earthquakes.



Group velocity maps constructed by cross-correlating 30 days of ambient noise between USArray stations in California. Black solid lines show known active faults. White triangles show the locations of USArray stations used in this study.

Shapiro, N.M. and M. Campillo, Emergence of broadband Rayleigh waves from correlations of the ambient seismic noise, *Geophys. Res. Lett.*, 31, L07614, doi:10.1029/2004GL019491, 2004.

Shapiro, N.M., M. Campillo, L. Stehly, and M.H. Ritzwoller, High-Resolution surface wave tomography from ambient seismic noise, *Science*, 307, 1615-1618, 2005.

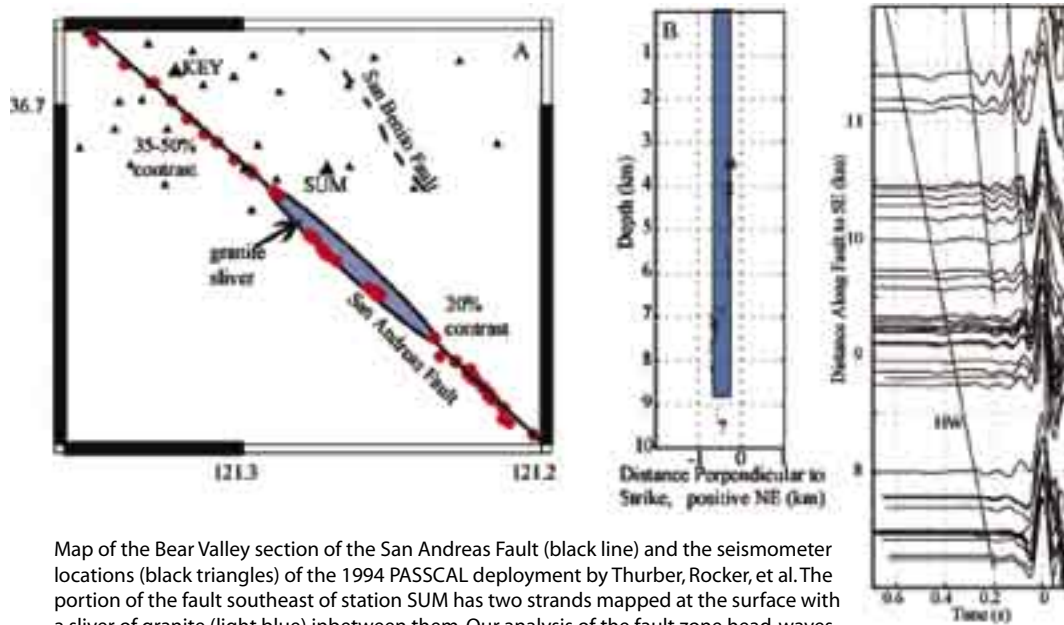
Imaging the Fine Structure of the San Andreas Fault at Seismogenic Depths Using an Archived PASSCAL Dataset

Jeff McGuire • Woods Hole Oceanographic Institution

Yehuda Ben-Zion • University of Southern California

Detailed imaging of fault-zone material properties at seismogenic depths is a difficult seismological problem owing to the short length scales of the structural features. Seismic energy trapped within a low-velocity damage zone has been utilized to image the fault core at shallow depths, but these phases appear to lack sensitivity to structure in the depth range where earthquakes nucleate. Major faults that juxtapose rocks of significantly different elastic properties generate a related phase termed a fault-zone head wave that spends the majority of its path refracting along the fault. We utilize data from a dense temporary PASSCAL array of seismometers in the Bear Valley region of the San Andreas Fault to demonstrate that head waves have sensitivity to fault-zone structure throughout the seismogenic zone. Measured differential arrival times between the head waves and direct P arrivals and waveform modeling of these phases provide high-resolution information on the velocity contrast across the fault. The obtained values document along-strike, fault-normal, and downdip variations in the strength of the velocity contrast, ranging from 20 to 50% depending on the regions being averaged by the ray paths. The complexity of the fault-zone waveforms increases dramatically in a region of the fault that has two active strands producing two separate bands of seismicity. Synthetic waveform calculations indicate that geological observations of the thickness and rock-type (granite) of the layer between the two strands are valid also for the subsurface structure of the fault. The results show that joint analysis of fault zone head waves and direct P arrivals can resolve important small scale elements of the fault zone

ruptures is necessary for evaluating theoretical predictions of the effects that these structures have on rupture propagation.



Map of the Bear Valley section of the San Andreas Fault (black line) and the seismometer locations (black triangles) of the 1994 PASSCAL deployment by Thurber, Rocker, et al. The portion of the fault southeast of station SUM has two strands mapped at the surface with a sliver of granite (light blue) inbetween them. Our analysis of the fault zone head-waves indicates that this granite sliver extends throughout the seismogenic zone (middle panel with black dots for earthquake locations). The right panel shows the headwaves recorded at station SUM, aligned on the direct P arrival (0 time). The headwave (HW) moves out with distance. The reverberations between the HW and the direct wave result from the presence of the intermediate velocity granite sliver (blue region in map).

A Multi-Institutional, Multi-Disciplinary, Multi-Facility Experiment in Garner Valley, CA

Joan Gomberg • U.S. Geological Survey, Memphis

Jamie Steidl • University of California, Santa Barbara

David Simpson • IRIS

Ken Stokoe • Network for Earthquake Engineering Simulation

Paul Bodin • University of Memphis

Frank Vernon • University of California, San Diego

In April, 2004, IRIS, together with the US Geological Survey (USGS) and the Network for Earthquake Engineering Simulation (NEES), launched a new era in collaborative science and engineering. IRIS sponsored a workshop to explore ideas using resources from multiple earthquake science and engineering facilities to tackle challenging and even intractable problems. This led to a follow-up pilot field experiment, which in addition to IRIS, USGS, and NEES, included participants from the Los Alamos National Lab and other NSF-sponsored consortia; the MAEC, SCEC, CENS, and HPWREN. The experiment piggybacked on an earlier planned inaugural demonstration of NEES facilities, held at the NEES Garner Valley Digital Array (GVDA) site in southern California. We recorded ground motions generated by the 'TRex' shaker truck at the GVDA and surrounding Garner Valley during August 18-22, 2004, and collected earthquake

data. Our first study tests the potential for measuring nonlinear sediment response by recording TRex strong shaking on a temporary surface accelerometer micro-array and permanent GVDA down-hole accelerometers. Our second study focuses on ground motion site and basin effects by recording TRex and earthquake signals at 20 temporary real-time, telemetered seismic stations deployed throughout the basin. Our third study focuses on imaging, using basin array data to constrain broad-scale tomographic images. To constrain a higher-resolution image along a profile across the basin, we collected reflection data generated by TRex recorded on densely spaced geophone strings, and conducted a sledge-hammer survey to confirm the location of a suspected buried fault. Finally, we assess the potential for shakers like TRex to do broad-scale, deep imaging as we stack TRex signals emitted repeatedly for nearly an hour, recorded on stations of the regional ANZA and statewide California Integrated Seismic Networks.



Bodin, P., T. Brackman, Z. Lawrence, J. Gomberg, J. Steidl, F-Y. Meng, K. Stokoe, P. Johnson, and F. Pearce, Monitoring non-linear wave propagation in the 2004 Garner Valley Demonstration Project: *EOS, Trans., Amer. Geophys. Union Ann. Mtg.*, 2004.

Gomberg, J., and the Participants in the IRIS/NEES/USGS Workshop and Garner Valley Experiment, Multifacility, Multidisciplinary Earthquake Science and Engineering, *EOS, Trans., Amer. Geophys. Union*, 85, 404, 2004.

Pearce, F., Bodin, P., T. Brackman, Z. Lawrence, P. Johnson, J. Gomberg, J. Steidl, F-Y. Meng, K. Stokoe, R. Guyer and F. Pearce, Non-linear soil response induced in situ by an active source at Garner Valley: *EOS, Trans., Amer. Geophys. Union Ann. Mtg.*, 2004.

The 2004 Garner Valley Experiment Working Group, A Pilot Experiment in Collaborative Science and Engineering: *EOS, Trans., Amer. Geophys. Union Ann. Mtg.*, 2004.

Pearce, F., P. Bodin, T. Brackman, Z. Lawrence, J. Gomberg, J. Steidl F-Y. Meng, R. Guyer, K. Stokoe and P. Johnson, Site-Specific, Nonlinear Soil Response using an Active Source: *Eur. Geosci. Union Gen. Ass., Vienna Austria*, 2005.

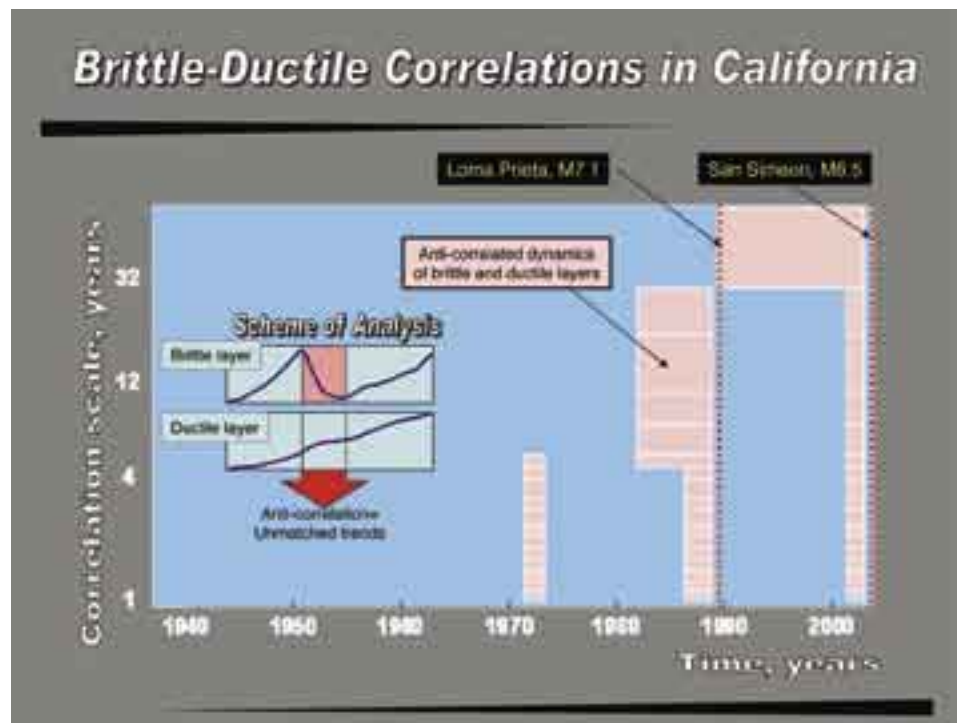
Brittle-Ductile Interactions in California

K. Aki • *La Plaine des Cafres, France*

A. Jin • *National Research Institute for Earth Sciences and Disaster Prevention, Tsukuba, Ibaraki, Japan*

V. Keilis-Borok, Z. Liu, I. Zaliapin • *University of California, Los Angeles*

This paper introduces a statistical technique, based on the recently developed Multiscale Trend Analysis (MTA), for quantifying correlations between non-stationary processes observed at irregular non-coincident time grids. We apply this technique to studying the temporal correlation between the dynamics of the ductile and brittle layers in the lithosphere using seismicity of California during 1940-2003. Our results confirm the previously reported strong positive correlation between the coda Q-1 and seismicity and its drop before major earthquakes observed in California. The proposed technique has significant advantages over the conventional correlation analysis: (1) MTA allows one to work directly with non-coincident time series without preliminary resampling the data; (2) The correlation is defined via the stable objects --- trends --- rather than noisy individual observations, hence it is highly robust; (3) The correlations are quantified at different time scales. The suggested technique seems promising for the wide range of applied problems dealing with coupled time series.



The figure illustrates the brittle-ductile correlation analysis in California, 1940-2003. Horizontal axis represents time, vertical axis represents scale of correlation. Blue area depicts scale-time where the brittle and ductile layers were correlated; pink areas where they were uncorrelated. As suggested by Aki's Brittle-Ductile Interaction Hypothesis, the correlation is destroyed at progressively larger scales as a large regional earthquake approaches. The destruction of correlation at scales larger than 6 years is only observed a couple of years prior to the Loma Prieta and San Simeon earthquakes.

Jin A., Aki K., Liu Z., Keilis-Borok V. I., Seismological evidence for the brittle-ductile interaction hypothesis on earthquake loading, *Earth Planets and Space*, 56 (8), 823-830, 2004.

Zaliapin, I., Jin, A., Liu, Z., Aki, K., and Keilis-Borok V., Temporal (un)correlations between coda Q-1 and seismicity – Multiscale Trend Analysis, *Pure. Appl. Geophys.*, 162, 827-841, 2005.

Steep-Dip Seismic Imaging of the Shallow San Andreas Fault Near Parkfield

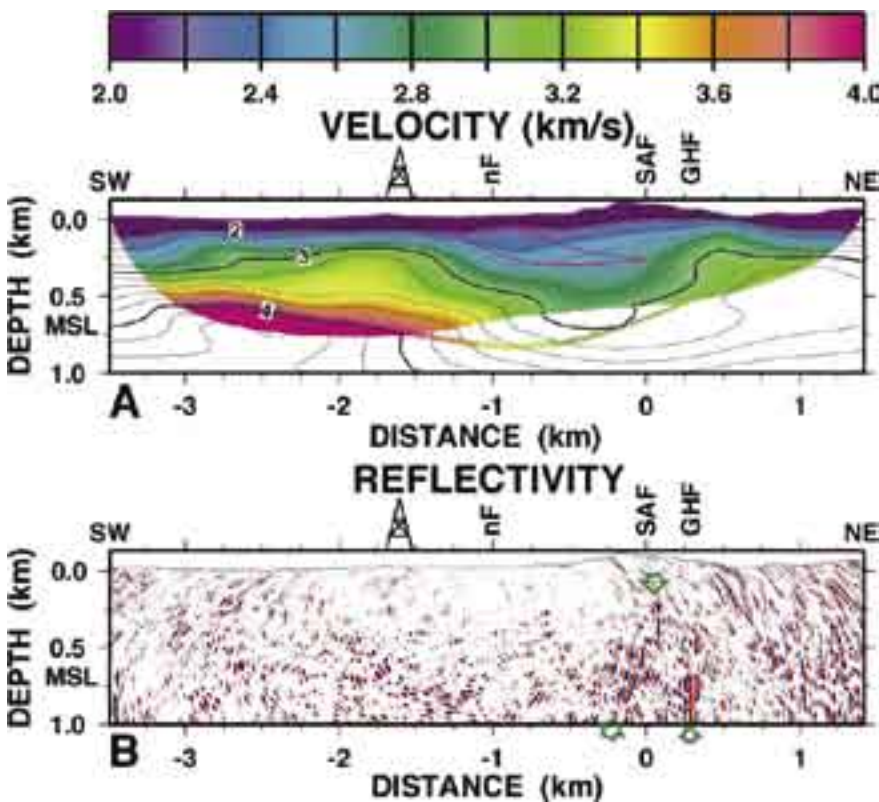
John A. Hole, K C. St. Clair, B J. Carney • Virginia Polytechnic Institute

Rufus D. Catchings, Michael J. Rymer • U.S. Geological Survey, Menlo Park

David A. Okaya • University of Southern California

Seismic reflection and refraction images illuminate the San Andreas Fault to a depth of 1 kilometer at the location of the proposed SAFOD drill site. The prestack depth-migrated reflection image contains near-vertical reflections aligned with the active fault trace. The fault is vertical in the upper 0.5 kilometer, then dips about 70° to the southwest to at least 1 kilometer subsurface. This dip reconciles the difference between the computed locations of earthquakes and the surface fault trace. The □

conductivity, and low density indicate a 1-kilometer-wide vertical wedge of porous sediment and fractured rock immediately southwest of the active fault trace.



Seismic cross sections across the San Andreas Fault (SAF). Surface locations of the Gold Hill Fault (GHF), Buzzard Canyon Fault (BF), and drill site are indicated. The reference datum is 700 m above mean sea level (MSL). (A) Seismic velocity model derived from first-arrival travel times. Contours every 0.2 km/s are labeled in km/s. Areas without rays are white. The magenta line indicates a sample ray path reflected from a vertical plane beneath the surface trace of the SAF. (B) Prestack depth-migrated reflection image. Red and blue indicate positive and negative peaks of a reflected wavelet. Green arrows indicate interpreted reflections from the SAF and GHF fault planes. Migration artifacts create a circular smile pattern across the image, particularly at the ends of the image. Pre-processing to emphasize steep reflectors eliminated energy from shallowly dipping reflectors.

Hole, J. A., Catchings, R. D., St. Clair, K. C., Rymer, M. J., Okaya, D. A., and Carney, B. J., Steep-dip seismic imaging of the shallow San Andreas Fault near Parkfield. *Science*, 294, 1513-1515, 2001.

Foundering Lithosphere Imaged Beneath the Southern Sierra Nevada, California, USA

Oliver S. Boyd, Craig H. Jones, Anne F. Sheehan • University of Colorado at Boulder

We produced seismic velocity and attenuation tomographic models using IRIS supported seismic equipment and infrastructure to reveal garnet-rich crust and mantle lithosphere descending into the upper mantle beneath the southeastern Sierra Nevada. The descending lithosphere consists of two layers: an iron-rich eclogite above a magnesium-rich garnet peridotite. These results place descending eclogite above and east of high P wavespeed material previously imaged beneath the southern Great Valley, suggesting a coherence in the lithospheric removal process previously unsuspected. Utilizing perpendicular orientations of shear waves, we produced a depth-dependent model of seismic anisotropy. This model is consistent with estimates of anisotropy from SKS splitting and allows us to further study the processes producing seismic anisotropy.

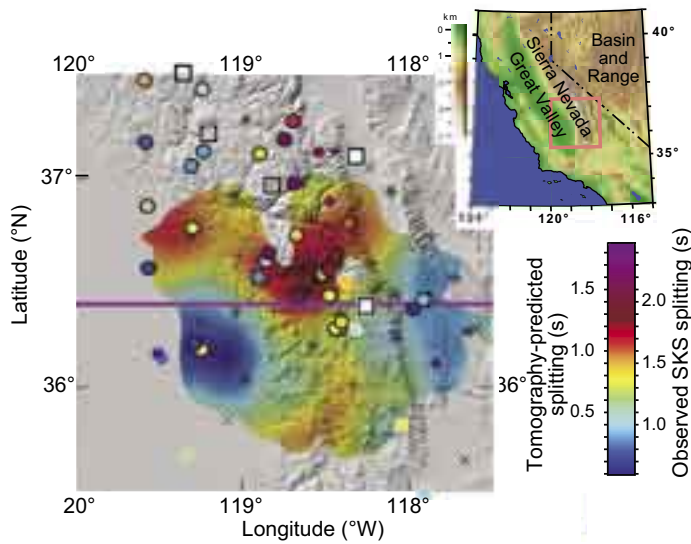
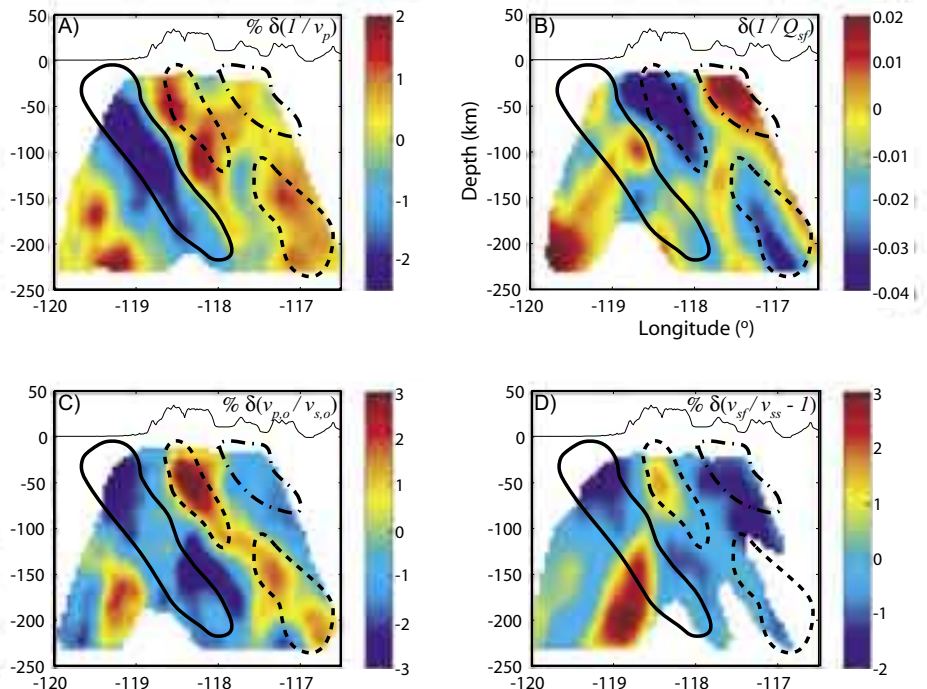


Figure 1. Topographic map of the southern Sierra Nevada overlain with tomographically determined shear wave splitting and independently determined SKS splitting measurements (circles). Open boxes are depleted garnet peridotite xenoliths localities; solid boxes are spinel peridotite xenolith localities.

Figure 2. Tomographic slices along the purple line in Figure 1. Panel A) is the percent change in P-wave slowness; Panel B) change in shear wave attenuation; Panel C) percent change in the ratio of P-wave to S-wave velocity; Panel D) percent change in shear wave anisotropy. Outlines are interpreted positions of bodies of varying composition, solid - depleted garnet peridotite, dashed - eclogite, dashed-dot - fertile spinel peridotite.

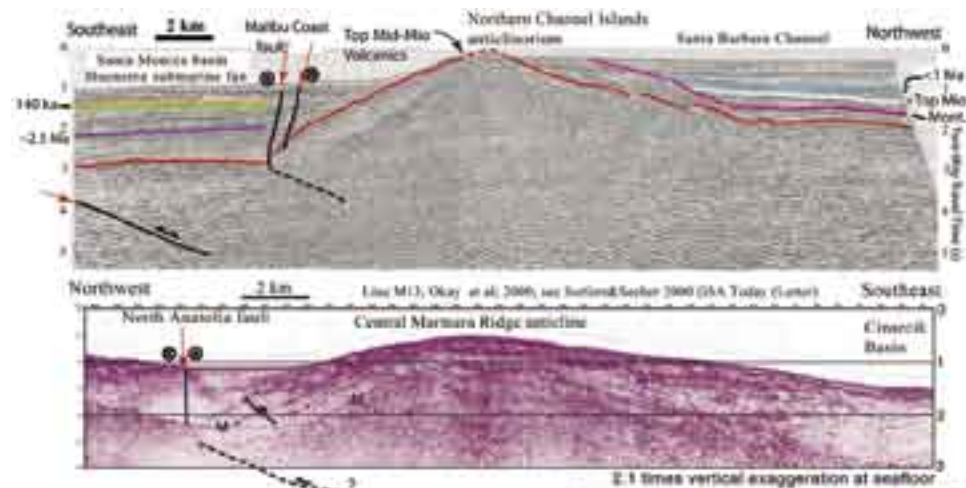


Using Marine Seismic Data to Investigate Active Plate Boundary Deformation: The California Continental Borderland and the Marmara Sea

Christopher C. Sorlien, Craig Nicholson • University of California, Santa Barbara

Significant plate boundary deformation occurs offshore of California and Turkey associated with the San Andreas and North Anatolian fault systems, respectively. In both cases, combinations of low-angle faults beneath long-wavelength folds and adjacent high-angle faults appear to accommodate distributed oblique plate motion and inferred clockwise block rotation. In southern California, predominantly E-W-trending left-lateral faults and associated blind faults and folds of the western Transverse Ranges continue east through the northern margin of Los Angeles basin. Active segments of the North Anatolia fault system in the Marmara Sea are not far from Istanbul. Understanding the nature, geometry, and hazards of this deformation may be best studied where these structures can be well imaged in

the subsurface using marine seismic reflection data. The Marmara Sea has been the subject of intensive marine geological and geophysical studies since the devastating and deadly 1999 earthquakes. Similarly, much of the offshore California Borderland was been previously surveyed by industry for its hydrocarbon potential. The strong similarity of the observed deformation in these two areas and the recent availability of some of these offshore data sets suggest that comparative studies of these two areas offers a wealth of potential insights into the fundamental nature and development of active crustal deformation. This includes a better understanding of the relation between faults and fault-related folding, the partitioning of oblique plate boundary strain on low- and high-angle faults, and the accommodation of distributed plate motion through crustal block rotation. Through the efforts of many colleagues at USGS, IRIS, SCEC, and AGI, together with major industry representatives, several important marine seismic data sets along the western margin of United States from California to Alaska are now becoming available through the National Archive of Marine Seismic Surveys (<http://walrus.wr.usgs.gov/NAMSS/>); and efforts to use these data to investigate the active structures of the California Borderland have already begun.



Comparison of two multichannel marine seismic reflection profiles that show remarkably similar structure at the same scale adjacent to: (above) a left-lateral high-angle fault offshore southern California just east of Anacapa Island, and (below) the right-lateral North Anatolia continental transform fault in the Marmara Sea (inset). Neither high-angle fault can explain the adjacent broad, long-wavelength fold. Low-angle (oblique) thrust faults are likely present beneath these adjacent, active folds.



Childs, J.R and P.E. Hart, National archive of marine seismic surveys (NAMSS): U.S. Geological Survey program to provide new access to proprietary data, *Eos (Trans. AGU)*, 85, n.47, NG43A-0441, 2004.

Nicholson, C., C.C. Sorlien and J.R Childs, Southern California Imaging Project (SCIP): Archiving and using industry data to evaluate plate boundary deformation, *Seismological Research Letters*, 75, n.2, p.258, 2004a.

Nicholson, C., C.C. Sorlien and J.R Childs, GENII: A developing consortium to archive and use industry data to evaluate plate boundary structure, deformation and evolution, 16th Annual IRIS Workshop Program and Abstracts, Tucson, AZ, 2004b.

Polonia, A., et al., Holocene slip rate of the North Anatolian Fault beneath the Sea of Marmara, *Earth and Planetary Science Letters*, 227, pp. 411-426, 2004.

Seeber, L., et al., Uplift and Subsidence from Oblique Slip: The Ganos-Marmara Bend of the North Anatolian Transform, Western Turkey, *Tectonophysics*, 391, pp. 239-258, 2004.

Sorlien, C. C., and L. Seeber, Comment on "Anatomy of the North Anatolian Fault Zone in the Marmara Sea, western Turkey: Extensional basins above a continental transform" by Aksu et al., *GSA Today*, 10, p. 41, 2000.

Work supported in part by NSF award OCE-0327273 (CS) and SCEC awards 075639 (CS) and 083262 (CN).

CANOE: A Broadband Array in Northwestern Canada

Michael Bostock, A. Langlois, I. Al-Khoubbi, Adam Baig, Jean-Philippe Mercier, T. Nicholson, Jounada Oueity • *University of British Columbia*

James Gaherty, Charles Wilson • *Lamont Doherty Earth Observatory of Columbia University*

Edward Garnero, Sean Ford, Nicholas Schmerr, Michael Thorne, Jesse Yoburn • *Arizona State University*

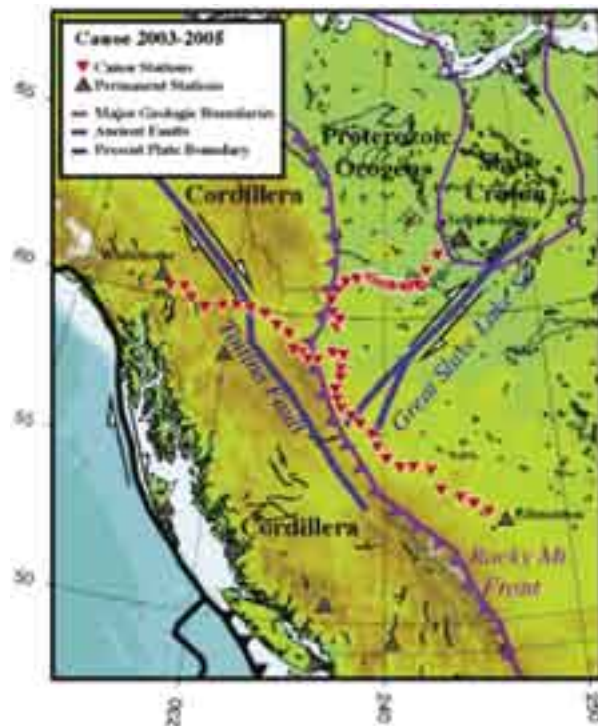
Jason Revenaugh, Anna Courtier • *University of Minnesota*

Megan Avants • *University of California, Santa Cruz*

Noel Barstow • *IRIS-PASSCAL Instrument Center, New Mexico Tech*

The Canadian Northwest Experiment (CANOE) is a nearly sixty broadband-instrument array extending from the Slave Craton in the Canadian NWT, across the Canadian Rockies in northern British Columbia and Yukon and south to Edmonton Alberta where the FLED (Florida to Edmonton) PASSCAL array terminated (Figure 1). The array crosses 4 Ga of geologic time and a series of compressive orogens undisrupted by later periods of extension or extensive hotspot volcanism. Coupled with excellent shallow structural control from Lithoprobe active-source transects, CANOE offers an unparalleled window into deep continental lithosphere structural expression and history. The array also offers excellent deep-mantle sampling of the central Pacific and Hawaii.

A subset of the array was installed in May, 2003. The remaining two-thirds of the array were deployed in May and June of 2004 and will remain until October, 2005. Array endpoints are anchored by permanent stations of the CNSN that are available through the IRIS DMC; typical station spacing within the array is less than 50 km. Data are recorded continuously at 20 samples per second on a mixture of Guralp 3T, 3ESP and 40T instruments. Instruments for CANOE were provided by PASSCAL/IRIS. The members of CANOE wish to thank the PASSCAL Team for training, extensive field assistance and critical logistical support.



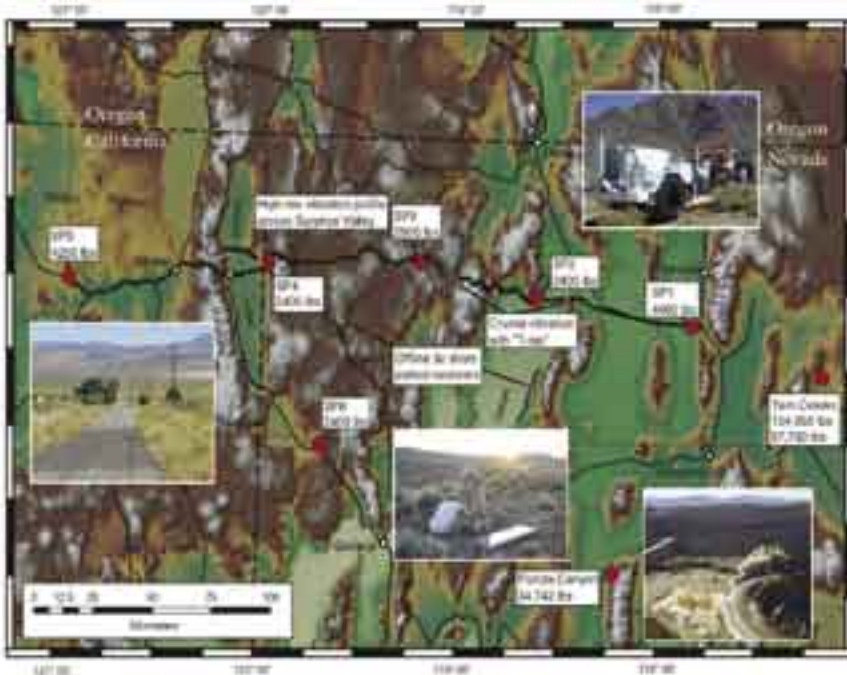
Topographic map of northwestern Canada, showing the CANOE deployment (red triangles) and its relationship to major geologic structures in the region. The array is laid out in three arms, two trending SE-NW that follow the Alaska Highway, and one trending N-NE that follows the Liard and McKenzie Highways. The array is anchored by 3 permanent stations of the CNSN (grey triangles). This geometry will allow us to image the lithospheric expression of the cordillera-to-craton transition, as well as probe the deep signature of the large lithospheric faults and shear zones. It also will provide unprecedented sampling of the core mantle boundary region beneath the central Pacific near Hawaii.

A Refraction/Reflection/Teleseismic Survey of the Northwestern Basin and Range Transition Zone

Simon L. Klemperer, Elizabeth L. Miller, Derek L. Lerch, Ewenet M. Gashawbeza, Joseph P. Colgan • *Stanford University*
 Charles K. Wilson • *Stanford University, now at Lamont-Doherty Earth Observatory*

Active collaboration between the tectonics, crustal seismology, and geochronology research groups at Stanford University provides new constraints on the structure and evolution of the lithosphere. In particular, recent projects in the northwestern Basin and Range Province have utilized active- and passive-source seismology, low-temperature thermochronology, Ar-Ar geochronology, and geologic mapping to characterize the tectonic history and crustal structure of the region.

Northwestern Nevada and northeastern California are characterized by some of the lowest mean elevations, highest heat flow (>100 mW/m², e.g. Blackwell, 2004), and thinnest crust (~ 30 km, e.g. Catchings and Mooney, 1991) in the northern Basin and Range Province. Recent geologic and geo/thermochronologic studies have demonstrated that extensional faulting in this area is both more recent and of considerably lower magnitude than faulting in adjacent parts of the Basin and Range to the south and east (beginning ca. 11-12 Ma and not exceeding 15% in northwestern Nevada, compared to 50-100% or greater extension since Eocene time in central Nevada).



Experiment configuration, showing the refraction, reflection, and teleseismic components. Insets show (top to bottom): NEES vibrator at work in the Black Rock Range, NV; 2D profile line across Surprise Valley, CA; deploying PASCAL instruments for teleseismic recording; mine blast at Twin Creeks Mine, NV.

operated by the Network for Earthquake Engineering Seismology (NEES) and the University of Texas at Austin. (3) 100 short-period 3-component receivers embedded in the active-source phase. (4) A 20 km, 2D high-resolution (40-m receiver, 10-m source spacing) Vibroseis reflection profile across Surprise Valley, CA. (5) A 70 km linear array of short-period teleseismic deployed in the central portion of the experiment for 6 months following the active-source phase.

If northwestern Nevada is relatively little and recently extended, why is it one of the thinnest parts of the northern Basin and Range? Was the pre-extensional thickness significantly less than surrounding regions, or was the area part of the Cretaceous northern Sierra Nevada and characterized by 40-45 km thick crust? How was the crust thinned and when did this occur? Our work is an attempt to answer these questions through a careful reconstruction of the timing and magnitude of extension coupled with seismically determined crustal structure.

Our seismic experiment collected information on the crustal thickness, velocity structure, anisotropy, and reflectivity of this area, and consisted of five parts: (1) A 300 km shot-source crustal refraction profile, with ~ 1100 receivers spaced 100-300 m apart. (2) During the deployment for the refraction experiment, we collected crustal reflection data from both P and S-wave sweeps with the tri-axial "T-Rex" vibrator

American Chemical Society □

NSF-EAR-EARTHSOPE 0346245 "USArray FlexArray augmentation of a seismic study of the extension paradox at the NW margin of the Basin-&-Range Province"

NSF-ENG-CMS-GHS 0444696 "Field demonstration of utility of NEES Vibrator to meet EARTHSOPE science objectives for earthquake-hazard and crustal-structure studies"

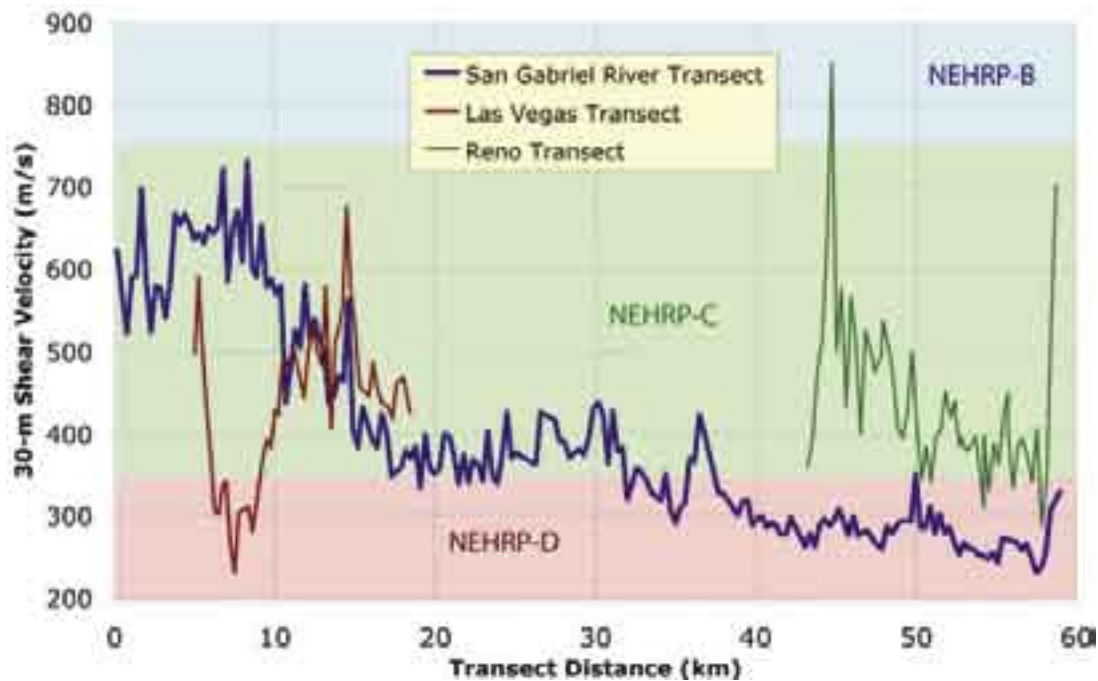
Stanford University Vice-Provost for Undergraduate Education and School of Earth Sciences

Passive Shallow Seismic Experiments Using IRIS/PASSCAL Facilities: Shear-Velocity Assessments at Over 300 Urban Sites

John N. Louie and James B. Scott • University of Nevada

Surveys of shallow shear velocity in the Reno, Los Angeles and Las Vegas urban areas give us information assisting in the mitigation of earthquake hazards, and in preparing for future damaging earthquakes. Three transects (16, 60, and 15 km long respectively) were completed quickly and economically using the refraction microtremor method, providing 100-m-deep shear-velocity profiles of over 300 separate sites. Shear-wave velocity averaged over 30 m depth (V_{s30}) is unexpectedly

□ at 0.3 km distances between measurements, to only 18% at 1.0 km distances. V_{s100} values for the three transects, averaging over the 100 m depth to which most of our measurements are valid, show trends mimicking the V_{s30} trends. Across all three cities our measurements correlate poorly against available USDA soil maps and geologic mapping, and often poorly against hazard mapping when prepared from general maps. Standard maps do not predict the conditions of any individual site with accuracy sufficient for engineering application; special-purpose mapping for shear velocities provides better predictions. A detailed stratigraphic model derived from deep water-well logs in Las Vegas predicts V_{s30} better than maps, but only in thoroughly sampled areas.



Shear velocity averaged to 30 m depth (V_{s30}) for each of >300 sites, plotted as three transects of Los Angeles (blue), Las Vegas (red), and Reno (green). (Transects are placed on the same distance scale for visual convenience only.) IRIS-PASSCAL "Texan" arrays recorded urban microtremor surface waves at each site.

Scott, J. B., M. Clark, T. Rennie, A. Pancha, H. Park and J. N. Louie, A shallow shear-wave velocity transect across the Reno, Nevada area basin, *Bull. Seismol. Soc. Amer.*, 94, 2222-2228, 2004.

This study was funded by the USGS NEHRP Southern California Panel under contract #03HQGR006D, and by Lawrence Livermore Lab, U.S. Dept. of Energy. Reftek RT-125 "Texan" recorders and field support provided by the NSF-funded IRIS/PASSCAL Instrument Center at New Mexico Tech.

Lithospheric Structure of the Rio Grande Rift

The RISTRA Group

The seismic structure of the crust and upper mantle of the southwestern United States has been examined using teleseismic arrivals recorded by IRIS PASSCAL Instruments in LA RISTRA (Colorado PLAteau Rio Grande Rift-Great Plains Seismic TRAnsect). Receiver function estimation and filtering methods developed by Wilson and Aster (2005) produce receiver functions with decreased sensitivity to noise. Crustal thickness and V_p/V_s are estimated using both direct and reverberated P-to-S receiver function modes. Regularized receiver function migration methods produce a multiple-suppressed image of the velocity discontinuity structure of the subsurface. Crustal thickness averages 44.1 +/- 2.3 km beneath the Great Plains (GP) and 45.6 +/- 1.1 km beneath the Colorado plateau (CP). Crustal thinning beneath the RGR is broadly symmetric about the

□ beneath the RGR (figure 2). We observe a prominent northwest-dipping discontinuity, ranging from 65-85 km deep beneath the CP, and possible subcrustal discontinuities beneath the GP. These discontinuities, along with recent xenolith data, are consistent with preserved ancient lithospheric structures such as relict suture zones associated with Proterozoic subduction. An upper mantle discontinuity at 220-300 km depth may correlate with similar structure observed beneath eastern North America. Flat discontinuities at 410 and 660 km depth suggest that there is not a large-scale thermal anomaly beneath the RGR at these depths (Wilson *et al.*, 2005b). Research supported by the NSF Geophysics program and Los Alamos IGPP; instruments and field support provided by IRIS PASSCAL.

Figure 2. Moho modeling for specific lower-crust:upper-crust extension ratios, with the best fit being LC:UC=2.0:1. Note extensive widening of the rift structure at depth. Background colors depict S-wave variations from joint body/surface wave inversion (3.6-4.7 km/s; West *et al.*, 2004). Both after Wilson *et al.* (2005a).

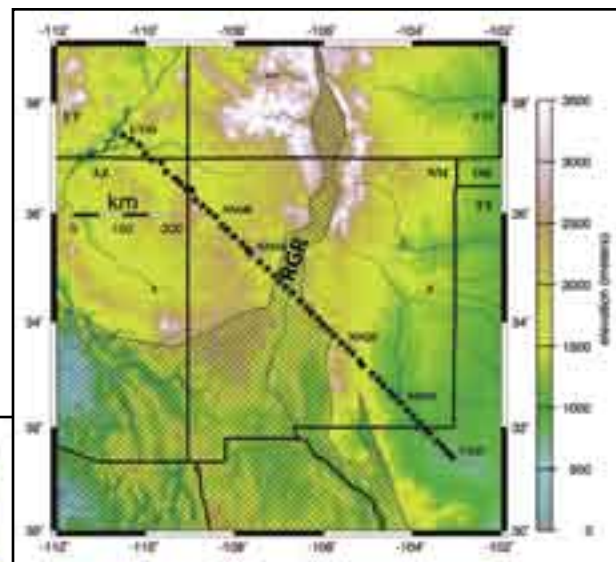
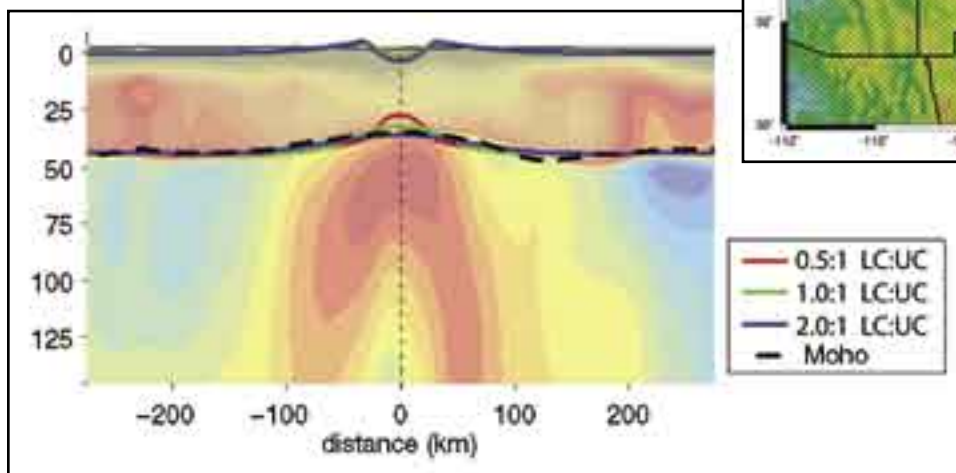


Figure 1. The 960-km RISTRA transect across the Rio Grande rift (RGR) region. Areas of Cenozoic extension are hatched.

West, M., J. Ni, W.S. Baldrige, D. Wilson, R. Aster, W. Gao, and S. Grand, crust and upper mantle shear wave structure of the southwest of the southwest United States: Implications for rifting and support for high elevation. *J. Geophys. Res.* 109, doi: 10.1029/2003JB002575, 2004.

Wilson, D., Aster, R., Alter, and multimode Kirchhoff migration, *J. Geophys. Res.*, in press, 2005.

Wilson, D., Aster, R., West, M., Ni, J., Grand, S., Gao, W., Baldrige, W.S., Semken, S., Lithospheric Structure of the Rio Grande Rift, *Nature*, 433, doi: 10.1038/nature03297, 2005a.

Wilson, D., Aster, R., Ni, J., Grand, S., West, M., Gao, W., Baldrige, W.S., Semken, S., Imaging the seismic structure of the crust and upper mantle beneath the Great Plains, Rio Grande Rift, and Colorado Plateau, *J. Geophys. Res.*, in press, 2005b.

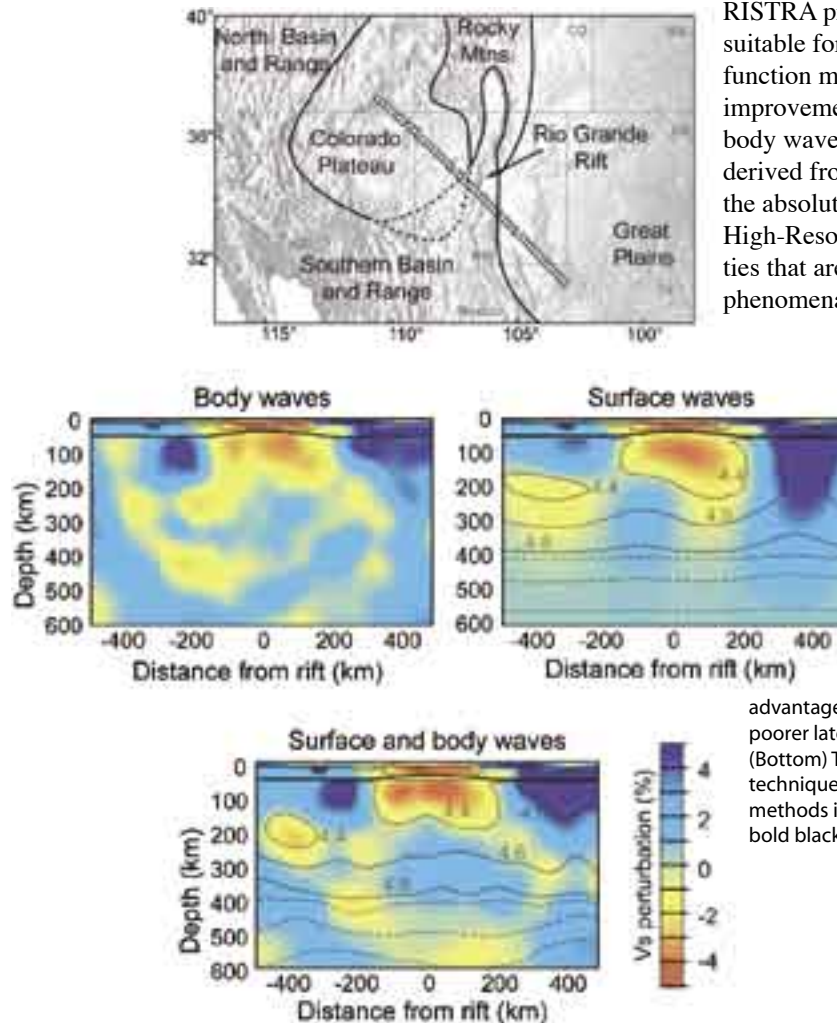
A Simple Approach for the Joint Tomographic Inversion of Seismic Body and Surface Waves.

Michael West • University of Alaska, Fairbanks

Wei Gao, Stephen Grand • University of Texas, Austin

Body and surface wave tomography have complementary strengths when applied to regional-scale studies of the upper mantle. We have derived a straight-forward technique for their joint inversion which hinges on treating surface waves as horizontally-propagating rays with deep sensitivity kernels. This formulation allows surface wave measurements to be integrated directly into existing body wave tomography inversions with modest effort. To demonstrate the method, we use data from an IRIS/PASSCAL seismic array crossing 950 km of the Southwest U.S. The dense station spacing and linear array design of the

RISTRA project provide a uniquely high-quality dataset suitable for both types of tomography, as well as receiver function migration. For large arrays, this method offers an improvement over the standard approach of augmenting body wave tomography with a one-dimensional model derived from surface waves. The joint inversion combines the absolute velocity of a surface wave model with the High-Resolution afforded by body waves—both qualities that are required to understand regional-scale mantle phenomena.



Velocity models using body and surface wave tomographic techniques. (Top) Map of the IRIS/PASSCAL-supported RISTRA deployment. Lower figures are cross sections of the Earth beneath this array. (Middle left) Image derived from traditional teleseismic body wave tomography. Color shades represent velocity perturbations relative to 1-D. This approach yields High-Resolution, but is unable to retrieve actual seismic velocities which are necessary for advanced interpretation. (Middle right) Image derived from surface wave tomography. This approach has the advantage of measuring true seismic velocities but has significantly poorer lateral resolution. True velocity contours are marked in gray. (Bottom) This image was derived using the new joint inversion technique presented in this study. It combines the benefits of both methods illustrated above. The bottom of the crust is marked in bold black.

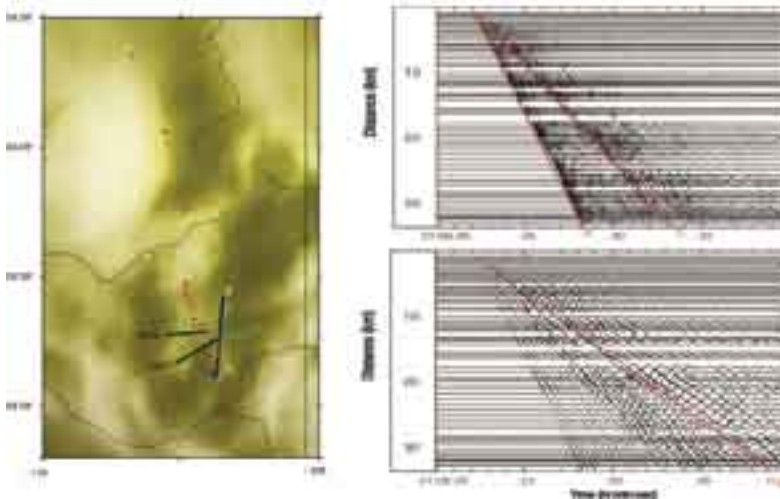
West, M., W. Gao, and S. Grand, A simple approach to the joint inversion of seismic body and surface waves applied to the Southwest U.S., *Geophys. Res. Lett.*, 31, L15615, doi:10.1029/2004GL020373, 2004.

This work was supported by National Science Foundation grants EAR 9614616, 9706094 and 9707188.

Upper-Crustal Structure in SE Arizona from P and Rg Phases Generated by Explosions

Tae Sung Kim, Brian W. Stump • Southern Methodist University

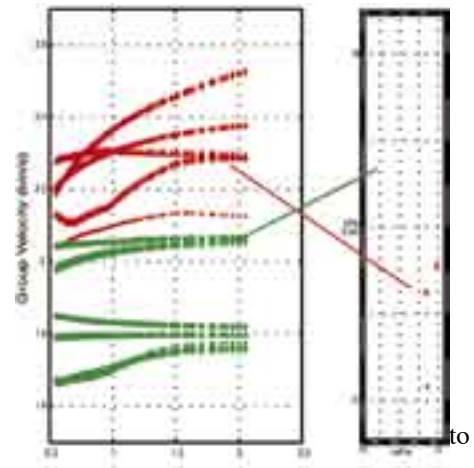
The goal of this study is to constrain upper crust P and S velocity structure around a mine in SE Arizona in order to separate the propagation path effects from explosion signals. This separation will provide the opportunity to quantify the explosion source mechanism of Rg and the relationship between Rg and S phases at near-source and regional distances. As indicated in the map below, a mixed deployment of PASSCAL supplied Texans and broadband CMG-40Ts were located along profiles moving away from the mine. This instrumentation documented the P and S phases from single-fired explosions detonated at the mine.



The locations of the Texan (green), CMG-40T (red) and source (blue) are mapped to the far left. The Texan record section documents the body waves in the upper panel (0.7-20 Hz) and Rg in the lower panel (0.5-3 Hz). The arrival times of the body waves are used as a first estimate of the velocity model along the path. The dispersion of the Rg is then used to refine the model.

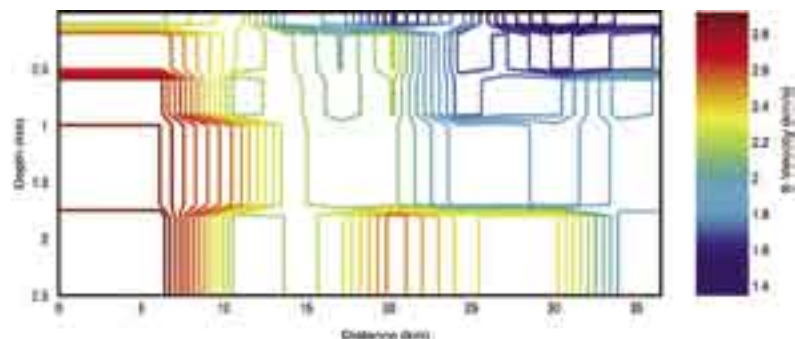
The dispersion curves of the Rg phase recorded on the broadband and Texan data are extracted using the MFA (Multiple Filter Analysis; Dziewonski et al., 1969) and refined by PMF (Phase Match Filter Analysis; Herrin and Go-forth, 1977). Texan and CMG-40T group velocity

dispersion curves in the 0.5-3 Hz band produced similar results after correcting the Texan data for the nominal instrument response. The dispersion curves for the broadband data are displayed to the right. Group velocities along the south section of the array are higher than those along the north section. These results imply a strong lateral variation in shallow crustal velocity structure.



The observed dispersion curves were inverted to constrain the shear wave velocity structure between pairs of stations along the path using the differential inversion method (Jin and Herrin, 1980; Bonner and Herrin, 1999). The shear wave velocity at each mid-point pair is used to produce a 2-D shear wave velocity structure (right). The mapped variation in shear wave velocity is coincident with granite intrusions around the mine as reflected in high velocities over the first 5-10 km and unconsolidated Tertiary and Quarternary pyroclastic and sedimentary rocks from 15 to 35 km. These results will be used assess the relationship between Rg generated by explosions and the regional Lg phase.

Work at SMU on this project was sponsored by the National Nuclear Security Administration Office of Nonproliferation Research and Engineering Office of Defense Nuclear Nonproliferation. Equipment for the study was supplied by the PASSCAL Instrumentation Center.



Probing the Structure and Evolution of the Rocky Mountains

Karl E. Karlstrom • University of New Mexico
Kenneth Dueker, Scott Smithson • University of Wyoming
Eugene Humphreys • University of Oregon
G. Randy Keller, Kate Miller • University of Texas at El Paso
Alan Levander • Rice University
Claus Prodehl • University of Karlsruhe, Germany
Catherine Snelson • University of Nevada at Las Vegas

In spite of strong scientific interest in the region of the Southern Rocky Mountains, our knowledge of the lithospheric structure of this region was modest until a series of seismic experiments began in the mid 1990s. The Continental Dynamics of the Rocky Mountains project (CD-ROM) is the most integrated and ambitious of these projects, and its ultimate goal is to constrain and unravel aspects of Proterozoic, Laramide, and Neogene tectonism and their interactions, and the processes that have shaped the region during the past 2.0 Ga.

The CD-ROM experiment, a coordinated set of passive and controlled source seismic experiments (Figure 1), has produced a new 4-D understanding of the structure and evolution of the lithosphere of the southern Rocky Mountain region. We identify relicts of at least four

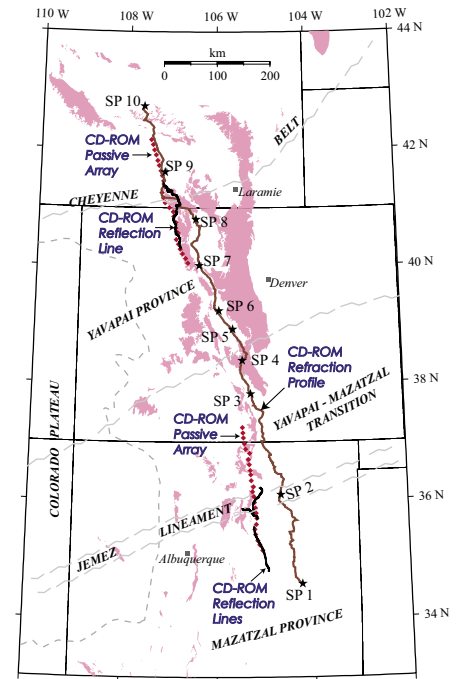


Figure 1. Index map of the integrated CD-ROM seismic experiments. Pink areas are outcrops of Precambrian basement.

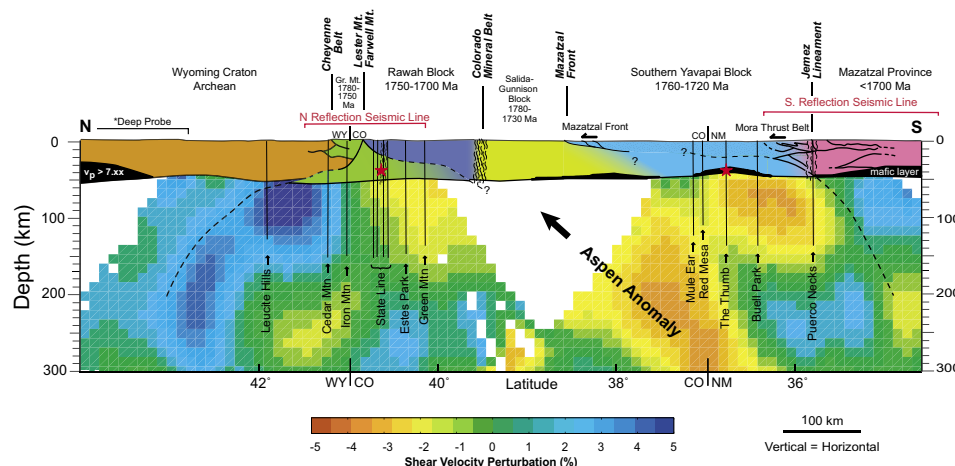


Figure 2. Cross-sectional synthesis of the CD-ROM transect. Generalized geologic cross section merged with S-wave tomographic image. Regional crustal structure is derived from the CD-ROM refraction experiment. More detailed crustal structure in the Cheyenne belt and Jemez lineament areas are generalized from seismic reflection data, with solid black lines in the crust representing well-defined reflections. Locations of xenolith pipes are shown as vertical lines and red stars show samples studied. Dipping elements in the tomographic image, combined with overlying crustal structures are interpreted to be Proterozoic subduction scars, and North American lithosphere is interpreted to extend to > 200 km depth.

subduction zones that were formed during assembly of dominantly oceanic terranes in the Paleoproterozoic (Figure 2). Crustal provinces with different geologic histories correspond to distinct mantle velocity domains, with profound mantle velocity contrasts associated with the ancient sutures. Typically, the transitions between the velocity domains are tabular, dipping, extend from the base of the crust to depths of 150–200 km, and some contain dipping mantle anisotropy. The present day heterogeneous mantle structure, although strongly influenced by ancient compositional variations, has undergone different degrees of partial melting due to Cenozoic heating and/or hydration caused by transient plumes or asthenospheric convection within the wide western U.S. active plate margin. A high-velocity mafic

lower crust is present throughout the Rocky Mountains, and there is ~10-km-scale Moho topography. Both are interpreted to record progressive and ongoing differentiation of lithosphere, and a Moho that has changed position due to flux of basalt from the mantle to the crust.

Continental Dynamics of the Rocky Mountains Working Group, Structure and evolution of the lithosphere beneath the Rocky Mountains: Initial results from the CD-ROM experiment, *GSA Today*, 12, 4-10, 2002.

Dueker, K., H. Yuan, and B. Zurek, Thick-structured Proterozoic lithosphere of the Rocky Mountain region, *GSA Today*, 11, 4-9, 2001.

Karlstrom, K. E. and G. R. Keller, The Rocky Mountain Region -- An Evolving Lithosphere: Tectonics, Geochemistry, and Geophysics: American Geophysical Union, Geophysical Monograph 154, 441p., 2005.

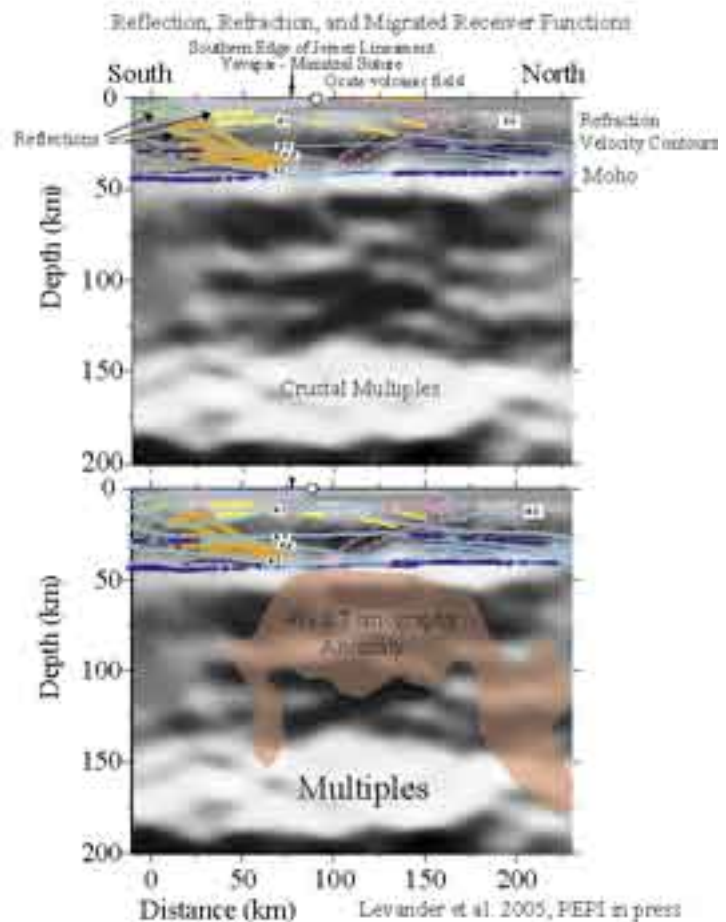
Modern Basalt Extraction Structures in the Southern Rocky Mountains: Multi-band Images from the Jemez Lineament

Alan Levander, Colin A. Zelt, Maria B. Magnani • Rice University

Ken Dueker, Huaiyu Yuan • University of Wyoming

The CD-ROM seismic experiments targeted Paleoproterozoic suture zones in the western U.S. in a north-south study corridor from central New Mexico to central Wyoming. Seismic reflection, refraction, and teleseismic measurements were made across the Jemez Lineament in northern New Mexico, a linear trend of modern volcanics extending SW from southern Colorado to Arizona. The Jemez Lineament spatially coincides with the southern edge of the suture between the Yavapai and Mazatzal island arc terranes thought to be one of the Paleoproterozoic assembly boundaries remaining from initial continental accretion. Karlstrom and Humphreys (1998) have speculated that the assembly boundaries have profoundly influenced Cenozoic tectonism in the western U.S., noting the correlation of NE-SW upper mantle tomography anomalies with geochemical boundaries and mapped suture zones in the Southern Rocky Mountains.

The reflection data image a Paleoproterozoic bivergent orogen occupying more than half the crust marking the Yavapai-Mazatzal orogeny, and bright upper crustal reflections that we interpret as Quaternary basaltic sills (Magnani et al., 2004). Refraction velocities in the upper mantle under a slightly thinned crust suggest that the upper mantle contains 1% partial melt (Hammond and Humphreys, 2000; Levander et al., 2005). In the same upper mantle region the P and S teleseismic tomography models show large-magnitude low-velocity anomalies (Yuan and Dueker, 2005). A pre-stack depth-migrated receiver function image shows a series of subhorizontal, very bright, negative-polarity upper mantle conversions extending from the Moho to depths of ~125 km, roughly corresponding to the tomography low velocity region (Levander et al., 2005). We interpret this complex series of converters in the upper mantle as the source zone for the Quaternary basaltic magmas found at the Jemez Lineament. We speculate that the paleo-suture zone left from continental accretion acts as a crustal conduit for basaltic magmas to pass from the mantle into the crust, form sills, and erupt.



Levander, A., C. A. Zelt, and M.B. Magnani, Crust and upper mantle velocity structure of the Southern Rocky Mountains from the Jemez Lineament to the Cheyenne Belt. *Lithospheric Structure and Evolution of the Rocky Mountain Region*. K. E. Karlstrom and G. R. Keller. Washington, D.C., American Geophysical Union, 2005.

Levander, A., F. Niu, C.-T. A. Lee, and X. Cheng, *Imag(in)ing the Continental Lithosphere*, *Physics of the Earth and Planetary Interiors*, accepted, 2005.

Magnani, M.B., K.M., Miller, A. Levander, and K. Karlstrom, The Yavapai-Mazatzal boundary: A long-lived tectonic element in the lithosphere of southwestern North America, *Geol. Soc. Am. Bull.*, 116, 1137-1142, 2004.

Yuan, H., and K. Dueker, Upper mantle tomographic Vp and Vs images of the middle Rocky Mountains in Wyoming, Colorado, and New Mexico: Evidence for a thick heterogeneous chemical lithosphere, in *Lithospheric Structure and Evolution of the Rocky Mountain Region*, edited by K. E. Karlstrom and G. R. Keller, Washington, D.C., American Geophysical Union, 2005.

Crustal Structure of the Basin and Range, Colorado Plateau, Rocky Mountains, and Great Plains

Hersh Gilbert • University of Arizona

Anne Sheehan • University of Colorado at Boulder

By combining seismic data from multiple past PASSCAL arrays we have created a map of crustal thickness traversing the intermountain-west from the western edge of the Basin and Range to the Great Plains (Figure 1). This map illustrates the variations in crustal structure across the region with the thickest crust (~50 km) found beneath the Rocky Mountains and Great Plains. Thinner crust (30 km) is present beneath the Basin and Range, possibly as a result of thinning that occurred while that region experienced extension. The Colorado Plateau appears as a transitional region between the thicker crust to

□ us to observe variations in the character of the Moho (boundary between the crust and mantle noted in Figure 2). We find that the Moho exhibits diminished amplitudes within the Colorado Plateau, possibly as a result of seismically fast lower crust within the plateau due to underplating of mantle material.

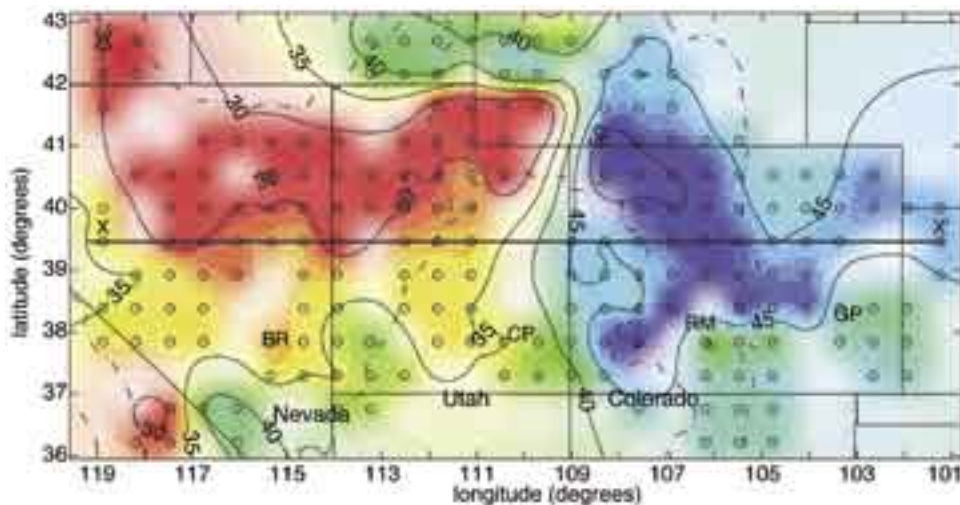
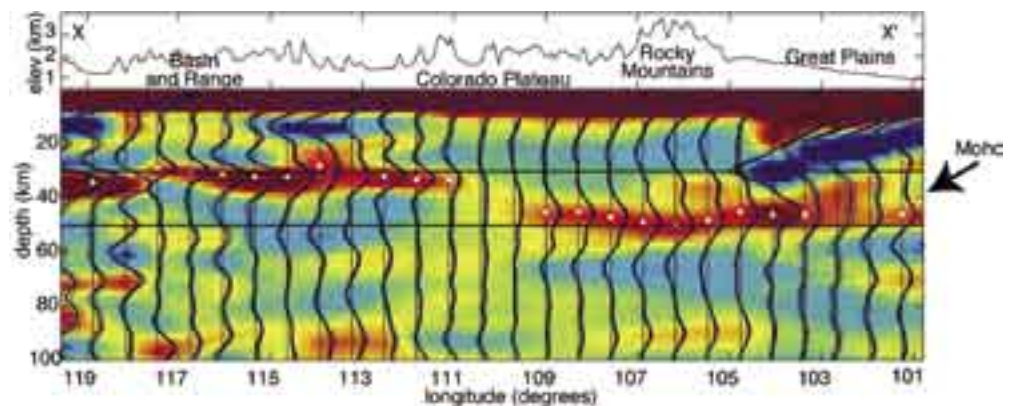


Figure 1. Color contour map of crustal thickness for the intermountain west. Areas of thicker crust are shown as blue colors while red colors show thinner crust. Thicknesses range between 30 and 50 km. Color saturation is scaled by the uncertainty of our observations. Also shown are boundaries (dashed line) between the Great Plains (GP), Rocky Mountains (RM), Colorado Plateau (CP), and Basin and Range (BR) provinces.

Figure 2. West to east cross-sections of geographically stacked receiver functions. Location of this cross-section is indicated on Figure A (line X-X'). Stacked receiver functions and their error are shown in black and thinner blue lines respectively. White circles and error bars show picked depths used to make crustal thickness map (Figure A). Lines are drawn at 30 and 50 km depth for reference.



Gilbert, H. J., and A. F. Sheehan, Images of crustal variations in the intermountain west, *J. Geophys. Res.*, 109, B03306, 2004.

Investigating Crust and Mantle Structure with the Florida-to-Edmonton Broadband Array

Karen Fischer, Stephane Rondenay, Ellen Syracuse, Christine McCarthy, Catherine A. Rychert, Lindsey Doermann, Mariela Salas, Margaret Welsh • *Brown University*

Michael Wyssession, Ghassan Aleqabi, Patrick Shore, Jesse Fisher Lawrence, Brian Shiro, Moira Pyle, Garrett Euler, Tara Mayeau • *Washington University*

During the Florida to Edmonton Broadband Seismometer Experiment (FLED), 28 broadband IRIS/PASSCAL STS-2 seismometers were deployed (May, 2001 to October, 2002) from central Florida to Alberta, Canada (Figure 1). Together with adjacent permanent stations from the IRIS/GSN, USNSN, CNSN, and New Madrid Seismic Network, the roughly linear array crossed diverse tectonic provinces and features, including the rifted continental margin, the Appalachian orogen, the Proterozoic and Archaean provinces of the continental interior, the Mid-Centroid Rift and the Williston Basin. Data quality was in general very good. One project involved constraining crustal structure beneath the array using Ps phases scattered from the Moho and crustal reverberations (Figure 2). Significant features include zones of thickened crust beneath the southern Appalachian mountains, the late-Proterozoic Mid-Centroid Rift in Iowa, and the Williston Basin. Beneath FLED in the southern Appalachians, the ratio of surface topography to excess crustal thickness matches the value found in the northern Appalachians beneath the Missouri-to-Massachusetts Broadband Seismometer Array (MOMA). However, both Appalachian ratios are small when compared to topography/crustal root ratios in young orogens. These results are consistent with global trends in orogenic crustal thickness, mountain topography and gravity anomalies that suggest a systematic decrease with age in the buoyancy of crustal roots relative to the mantle. Such an increase in crustal root density can be explained by gradual metamorphic reactions over hundreds of millions of years.

Other projects completed or underway involve examining the shear-wave splitting in SKS and related phases and their constraints on mantle anisotropy, transition zone discontinuity topography with scattered wave migration, lateral variations in upper mantle heterogeneity and anisotropy using Rayleigh and Love waves, ultra-low velocity zones at the core-mantle boundary using SPdKS phases, mantle attenuation structure beneath North America, lateral variations in the lowermost mantle using ScS-S waves, mantle discontinuities using SS precursors, and D'' thermal boundary layer structure (see later).

NSF Grant #: EAR-9903385, EAR-9903260



Figure 1. The station locations of the Florida-to-Edmonton (FLED) broadband seismic array.

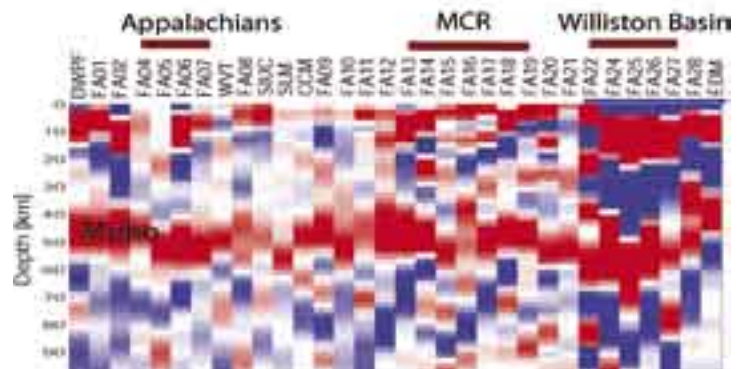


Figure 2. Image of the Moho beneath the FLED array from Ps phases (red or positive arrivals). Waveforms at each station were corrected with an inverse free surface transform, simultaneously deconvolved, and migrated to depth in 1D using a uniform velocity model. True crustal thicknesses (not shown) were modeled allowing for lateral variations in crustal velocities.

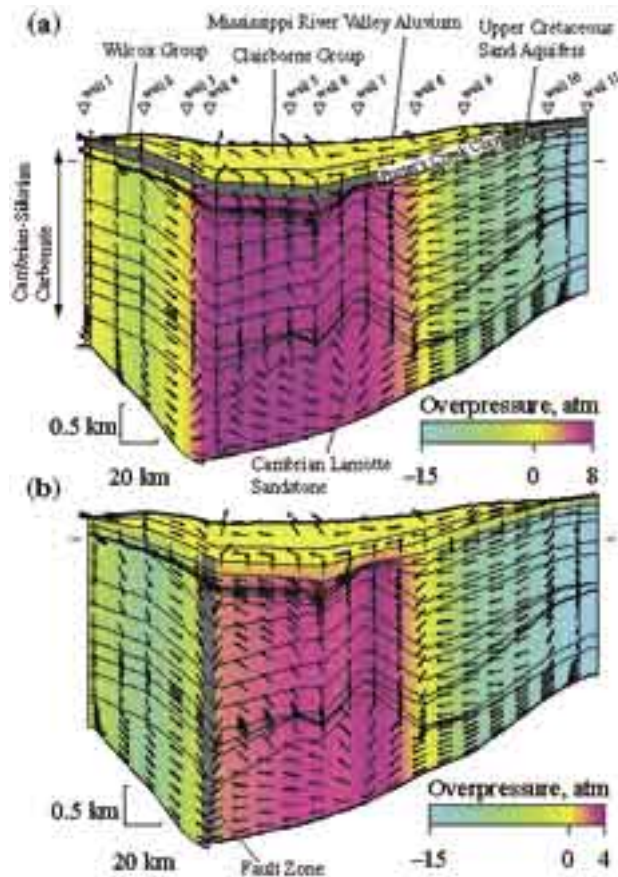
Numerical Analysis of Overpressure Development in the New Madrid Seismic Zone

Lorraine W. Wolf, Ming-Kuo Lee • Auburn University

Sharon Browning • University of Memphis

Martitia P. Tuttle • M.P. Tuttle and Associates

We use mathematical and numerical modeling techniques to evaluate the mechanism of overpressure development in the Mississippi Embayment and discuss potential implications for seismic hazards in the New Madrid seismic zone (NMSZ). The mathematical model explores how the magnitude of excess pore pressure in the basin's discharge area may be explained by the geometry and hydraulic conductivity of basin strata. Our modeling results demonstrate how excess pore pressures of up to 4 atm could be sustained in a wide discharge area of the NMSZ by regional gravity flow. The predicted magnitude of excess pressure is generally consistent with observed elevation heads (10-30 m) of artesian wells that penetrate the Upper Cretaceous and Paleozoic aquifers in the basin. The modeling results demonstrate that overpressures developed at depth in the Mississippi Embayment could be communicated to shallower layers if basin-wide confining units are breached by faults. The model shows that the greatest overpressures develop in Early Paleozoic carbonate rocks and overlying Upper Cretaceous sand aquifers that are capped by regionally extensive confining units (e.g., Porter's Creek Clay). Other researchers note geophysical anomalies, such as low P-wave velocities and low resistivity, in the Paleozoic strata and speculate that the anomalies may reflect elevated pore pressures at shallow depths (< 5 km). The study emphasizes the importance of permeability distributions in overpressure development and suggests that the conditions favoring elevated pore pressures in areas of the NMSZ may significantly influence the hydrologic response of the basin during large earthquake events and possibly reduce the stress required for deformation.



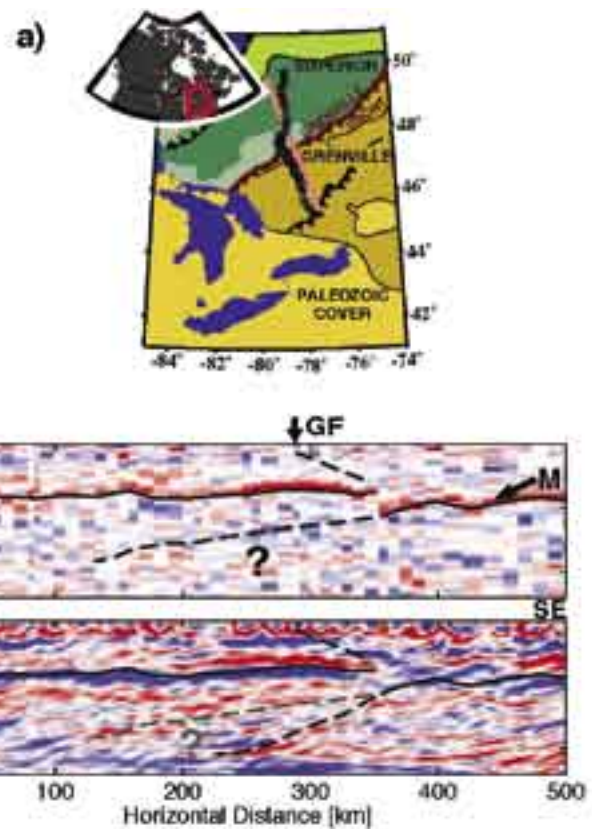
Calculated groundwater flow and overpressure distribution in the Mississippi Embayment in response to regional topography without (a) and with (b) a vertical fault zone. Arrows show predicted flow directions. Colors map abnormal pore pressures from underpressure in the recharge area to overpressure in the discharge area. Gray color maps a permeable fault zone and Upper Cretaceous aquifer. The permeability of non-faulted portion of confining units was held constant as 10-5 darcy for both simulations. Vertical fault in (b) (permeability = 1 darcy) extends from Cambrian strata through the Porter's Creek Clay near well 3. The predicted magnitude of overpressure (< 4 atm) in fault model agrees better with field data of artesian well heads, suggesting that confining units may be breached by faults. Major confining units (Porter's Creek Clay and Clairborne group) inhibit upward groundwater flow, allowing overpressures to develop in underlying Cretaceous sands and Cambrian-Silurian carbonate rocks.

Imaging the Earth With Dense Arrays of Broadband Seismometers

Stéphane Rondenay • *Massachusetts Institute of Technology*

One of the current challenges faced by solid-earth seismologists is the development of new tools for high-resolution imaging of the lithosphere and underlying mantle. While tomographic methods using transmitted body waves and surface waves have proven to be powerful tools for volumetric imaging of seismic anomalies, a wealth of complementary information on internal discontinuities can be obtained from secondary scattered waves in the coda of body waves. The relative arrival time and amplitude of these secondary waves are indicative of the position and magnitude of discontinuities in elastic parameters of the subsurface. The teleseismic P wavefield is of particular interest as it benefits from generally higher signal-to-noise ratio than other (later arriving) primary phases. Scattered waves, notably P-to-S conversions, recorded at single stations have thus been utilized for over two decades as a basis for 1-D modelling of planar discontinuities in the lithosphere. In recent years, a substantial increase in availability and fidelity of broadband seismometers has led to new opportunities for multichannel processing of scattered teleseismic body waves recorded at dense recording arrays, allowing for 2D/3D imaging of subsurface structure. Many of these approaches are similar to industry-oriented (e.g., migration) techniques and generate analogous high-resolution depth sections of the subsurface, down to the mantle transition zone.

Recently developed methods form a continuum with respect to the level of complexity adopted in the treatment of the scattering problem. On one end of the spectrum, images may be produced by simple stacking of normalized P-to-S conversion records (i.e., receiver functions), which are binned according to common conversion points (CCP) and mapped to depth. Finer resolution can be achieved through the stacking of singly scattered wavefields along diffraction hyperbolae to recover relative scattering intensity/potential at individual points through a 2D or 3D model space (Revenaugh, 1995; Ryberg and Weber, 2000; Sheehan et al., 2000). Moving to higher levels of complexity, methods involving inversion/backprojection operators (e.g., Bostock and Rondenay, 1999; Bostock et al., 2001; Rondenay et al., 2005) and full 3D waveform inversion of scattered teleseismic body waves recover either the scattering potential or estimates of localized material property perturbations with respect to an a priori background model.



High-resolution, teleseismic imaging of the lithosphere beneath the Abitibi 1996 broadband array (IRIS-PASSCAL, Lithoprobe). a) Map of study area. b) CCP receiver function profile. Red and blue pulses denote discontinuities with positive and negative downward velocity gradients, respectively. Black lines show interpretation. Abbreviations: GF = Grenville Front, M = Moho. c) S-velocity perturbation profile obtained by 2D Generalized Radon Transform inversion (Rondenay et al., 2005), with red to blue colour scale representing negative (slower) to positive (faster) velocity perturbations.

Bostock, M. G., and S. Rondenay, Migration of scattered teleseismic body waves, *Geophys. J. Int.*, 137, 732-746, 1999.

Bostock, M. G., S. Rondenay, and J. Shragge, Multiparameter two-dimensional inversion of scattered teleseismic body waves, 1, Theory for oblique incidence, *J. Geophys. Res.*, 106, 30,771-30,782, 2001.

Rondenay, S., M. G. Bostock, and J. Shragge, Multiparameter two-dimensional inversion of scattered teleseismic body waves, 3, Application to the Cascadia 1993 data set, *J. Geophys. Res.*, 106, 30,795-30,808, 2001.

Rondenay, S., M. G. Bostock, and K. M. Fischer, Multichannel inversion of scattered teleseismic body waves: practical considerations and applicability, in *Seismic Earth: Array Analysis of Broadband Seismograms*, edited by A. Levander and G. Nolet, Geophysical Monograph Series, AGU, in press, 2005.

Shragge, J., M. G. Bostock, and S. Rondenay, Multiparameter two-dimensional inversion of scattered teleseismic body waves, 2, Numerical examples, *J. Geophys. Res.*, 106, 30,783-30,794, 2001.

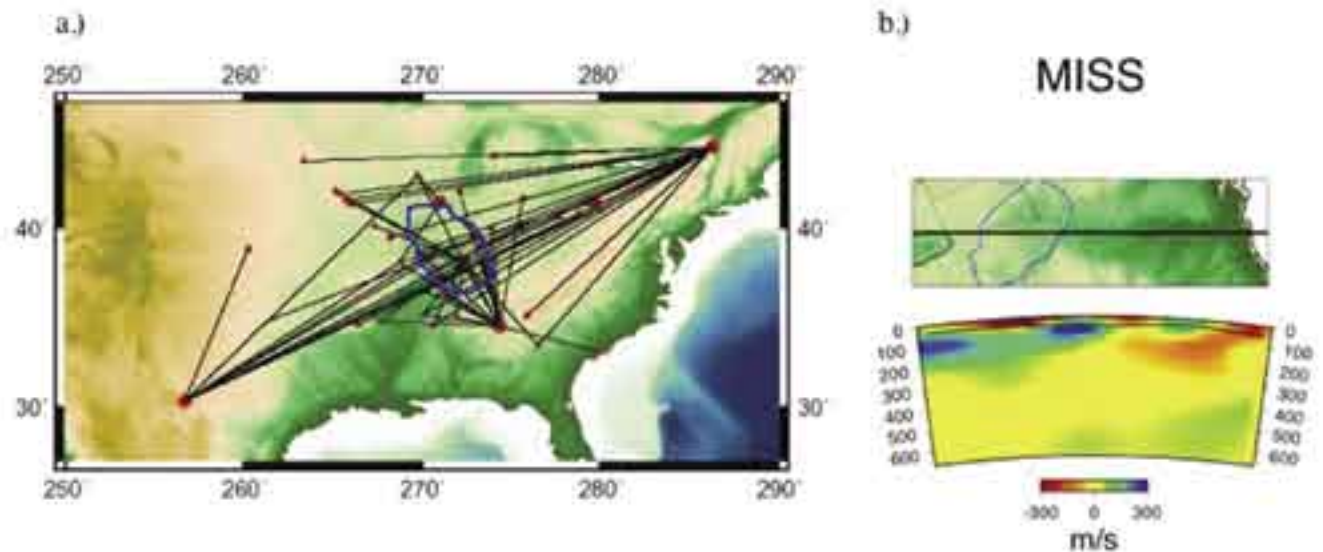
Imaging Upper Mantle Structure Beneath the Illinois Basin

Heather Bedle, Suzan van der Lee • Northwestern University

The Illinois Basin is an oval-shaped cratonic basin which covers parts of southern Illinois and Indiana, western Kentucky, Tennessee, and Missouri. The shallow structure of the Illinois Basin is well-defined and provides constraints which may allow the effects of crustal structure to be removed from seismic waveforms during tomographic inversions. We used IRIS data to test if better constraints of crustal heterogeneities will allow better resolution of the upper mantle S-velocity structure beneath the Illinois Basin. This improved imaging of the crust and the upper mantle S-velocities provides insights into the development of the basin, and addresses the issue of whether it is possible to improve seismic waveform tomography on a regional scale by incorporating crustal constraints.

Fundamental and higher mode waveforms from regional events were obtained from the IRIS DMC and were then inverted to image the three-dimensional upper mantle S-velocity structure under the Illinois basin. The method of partitioned waveform inversion, PWI, (Nolet, 1990; van der Lee and Nolet, 1997) was applied to the waveforms. Utilizing six mid-continent events, a total of 60 seismograms from the IRIS/IDA Network, the IRIS/USGS Network, the Cooperative New Madrid Seismic Network, the PEPP-Indiana network and PASSCAL experiments were fitted in this study (Figure 1a), incorporating external crustal constraints. These constraints were then inverted along with the constraints from S-velocity model NA00 (van der Lee, 2002).

The linear inversions resulted in S-velocity model IL05. Figure 1b represents the deviation of calculated S-velocities for IL05 from the standard one-dimensional Earth model, MC35, for a profile across the Illinois Basin. Both NA00 and IL05 image a slightly thinner seismic lithosphere beneath the Illinois Basin. A thinner seismic lithosphere is also observed in both models south of the Illinois Basin, which may be related to the original upwelling of the mantle during the formation of the Reelfoot Rift.



a.) Event to station ray paths used for the waveform fitting. The Illinois Basin is outlined in blue. Events are red circles and stations are red triangles. b.) Profile across the Illinois Basin shows IL05 S-velocity differences with 1D earth model MC35.

Nolet
8499-8512, 1990.

J. Geophys. Res., 95,

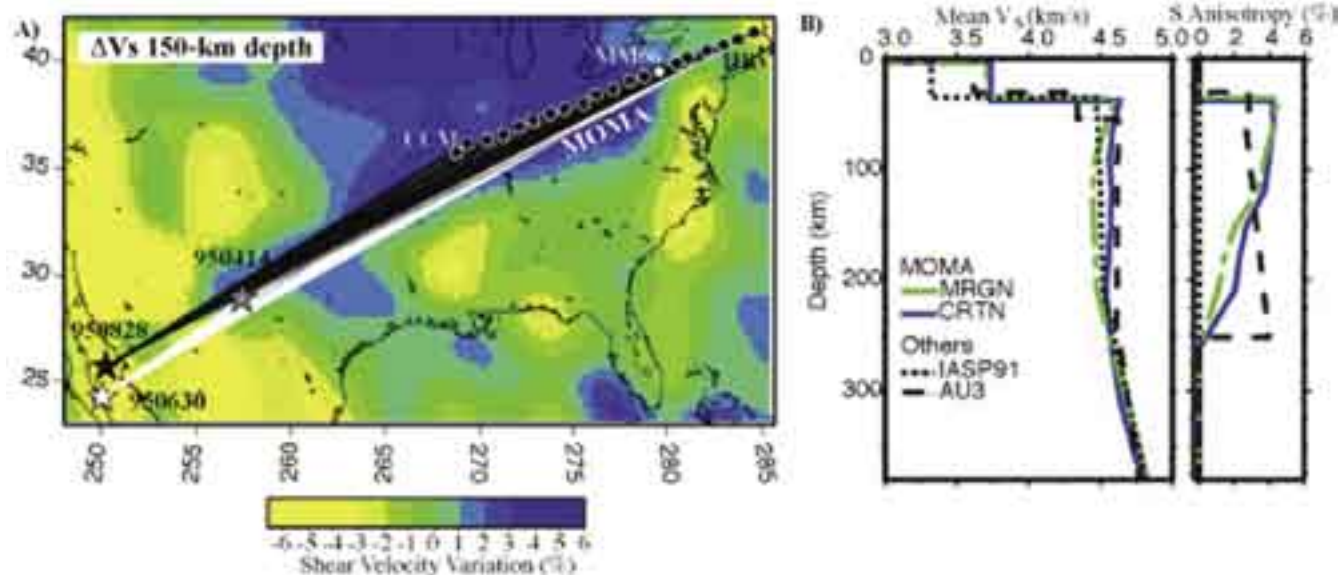
van der Lee, S., High-resolution estimates of lithospheric thickness from Missouri to Massachusetts, USA, *Earth Planet. Sci. Lett.*, 203, 15-23, 2002.

van der Lee, S. and G. Nolet, Upper mantle S velocity structure of North America, *J. Geophys. Res.*, 102, 22815-22838, 1997.

A Surface-Wave Analysis of Seismic Anisotropy Beneath Eastern North America

James B. Gaherty • Lamont-Doherty Earth Observatory of Columbia University

The nature of upper mantle seismic anisotropy beneath central and eastern North America has been evaluated using the phase velocities of surface waves traversing the length of the Missouri-to-Massachusetts (MOMA) PASSCAL broad-band array. Frequency-dependent phase delays of fundamental-mode Love and Rayleigh waves, measured across the array using a cross-correlation procedure, require the presence of anisotropy in the upper mantle. Two-dimensional radially anisotropic structures obtained via linearized inversion of these data contain shear anisotropy with a magnitude of $\sim 3\%$ between the Moho and at least 180 km depth. This anisotropy is approximately constant across the tectonic transition from the craton to the Atlantic margin (Figure 1). Forward models consisting of a shallow, lithospheric layer of azimuthal anisotropy derived from previous shear-wave splitting observations (Fouch et al., 2000) fail to satisfy the surface-wave delay times. The combined surface-wave and splitting results suggest the presence of two layers of anisotropy: a lithospheric layer that produces the phase-delay differences observed in Love and Rayleigh waves but is transparent to vertically propagating shear body waves, and a deeper (presumably asthenospheric) layer that generates the shear-wave splitting. One plausible model is that the lithosphere is characterized by vertically heterogeneous anisotropic fabric, which would produce minimal splitting in vertical shear waves. Such fabric has been hypothesized for regions of weak and complex splitting such as South Africa and Australia; the results here imply that it may be appropriate for North America as well.



(a) Surface-wave raypaths used in this analysis, which propagate along the MOMA array from three earthquakes in western North America. Background shows shear-velocity perturbations at 150 km depth from van der Lee (2002). (b) Radially anisotropic shear-velocity models of the upper-mantle beneath MOMA, derived from inversion of surface-wave delays. Left panel displays mean shear speed ($v_S = (v_{SH} + v_{SV})/2$), while right panel displays shear anisotropy ($v_S = (v_{SH} - v_{SV})/v_S$) in percent. Blue solid curves (CRTN) correspond to the average structure beneath the craton (the region between GSN station CCM and MM06), while green dash-dot curves (MRGN) represent the structure beneath the margin, from MM06 to GSN station HRV. Shown for comparison are isotropic reference model IASP91 (dotted), and radially anisotropic model AU3 (dashed) (Gaherty and Jordan, 1995).

Fouch, M.J., K.M. Fischer, E.M. Parmentier, M.E. Wyssession, and T.J. Clarke, Shear-wave splitting, continental keels, and patterns of mantle flow, *J. Geophys. Res.*, 105, 6255-6276, 2000.

Gaherty, J.B. and T.H. Jordan, Lehmann discontinuity as the base of an anisotropic layer beneath continents, *Science*, 268, 1468-1471, 1995.

Gaherty, J.B., A surface-wave analysis of seismic anisotropy beneath eastern North America, *Geophys. J. Int.*, 158, 1053-1066, 2004.

van der Lee, S., High-resolution estimates of lithospheric thickness from Missouri to Massachusetts, USA, *Earth Planet Sci. Lett.*, 203, 15-23, 2002.

Scattered Wave Imaging of a Sharp Lithosphere-Asthenosphere Boundary Beneath Eastern North America

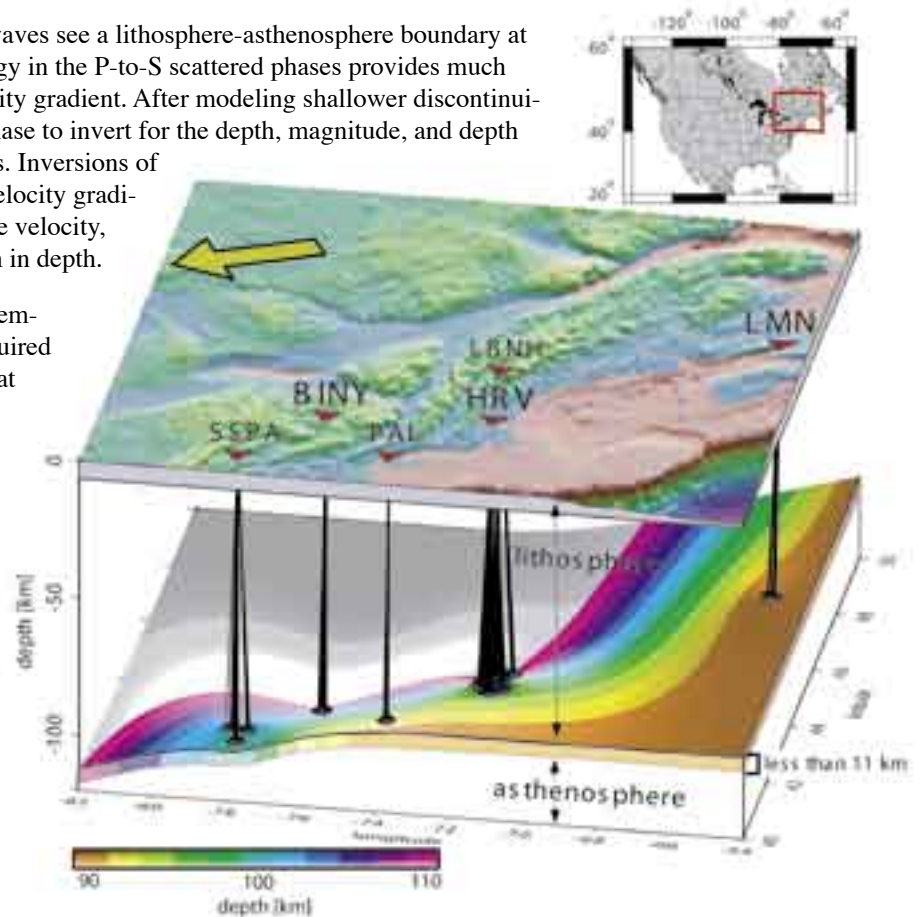
Catherine A. Rychert, Karen M. Fischer • Brown University

Stephane Rondenay • Massachusetts Institute of Technology

Plate tectonic theory hinges on the concept of a relatively rigid lithosphere moving over a weaker asthenosphere; yet, the nature of the lithosphere-asthenosphere boundary has remained ambiguous. To better understand the properties that define the lithosphere and the asthenosphere beneath continents, we have analyzed P-to-S phases produced by scattering beneath permanent broadband stations in eastern North America. We image a negative velocity discontinuity (velocity decrease with depth) at 90-110 km depth, increasing in depth toward the west. The depth of this discontinuity is consistent with the westward dipping lithosphere-asthenosphere boundary imaged by surface-wave tomography (Li et al., 2003; van der Lee, 2002). The existence and depth of the discontinuity are independently confirmed by S-to-P scattered phases at HRV.

Although the scattered and surface waves see a lithosphere-asthenosphere boundary at similar depths, the higher frequency energy in the P-to-S scattered phases provides much sharper resolution of the associated velocity gradient. After modeling shallower discontinuities, we use the shape of the converted phase to invert for the depth, magnitude, and depth range over which the discontinuity occurs. Inversions of data at LMN and HRV require that this velocity gradient be strong, a 3-11% drop in shear-wave velocity, and sharp, occurring over less than 11 km in depth.

Experimental studies suggest that a temperature increase of at least 200° C is required to explain the velocity contrast observed at LMN. However, mantle flow models in which viscosity depends only on temperature and pressure do not produce thermal gradients at the base of the lithosphere large enough to explain the observed velocity contrast, so the lithosphere-asthenosphere boundary requires an additional mechanism such as dehydration, depletion, or melt. The combination of a depleted lithosphere with a hydrated asthenosphere can explain most of the observed velocity gradient. Alternatively, a small amount of partial melt in the asthenosphere can easily explain the observed strong, sharp velocity contrast.



Li, A., D.W. Forsyth, and K.M. Fischer, Shear velocity structure and azimuthal anisotropy beneath eastern North America from Rayleigh wave inversion, *J. Geophys. Res.*, 108 (B8), doi:10.1029/2002JB02259, 2003.

Rychert, C.A., K.M. Fischer, and S. Rondenay, A sharp lithosphere-asthenosphere boundary imaged beneath eastern North America, *Nature* (submitted), 2005.

Three-dimensional view of the lithosphere-asthenosphere boundary and surface topography. Red box in the inset map highlights the location of the study region. Shading on the top plate indicates topography. Yellow arrow points in the direction of absolute plate motion; plate velocity is 2.5 cm/yr. Red triangles denote station locations. The larger text corresponds to the stations (HRV, LMN, BINY) where this phase is most clearly observed. The lower surface represents the location of the base of the lithosphere interpolated from migrated Ps waveform images at the 6 labeled stations. The surface ranges from 90 km (orange) to 110 km (pink). Each color band covers 2 km in depth. Blue circles on the discontinuity surface indicate the conversion points of the Ps phases. Black lines connect piercing points to the station at which the conversion is observed.

Subduction Potential at the Eastern Margin of North America

Suzan van der Lee • *Northwestern University*

Klaus Regenauer-Lieb • *ETH, Switzerland*

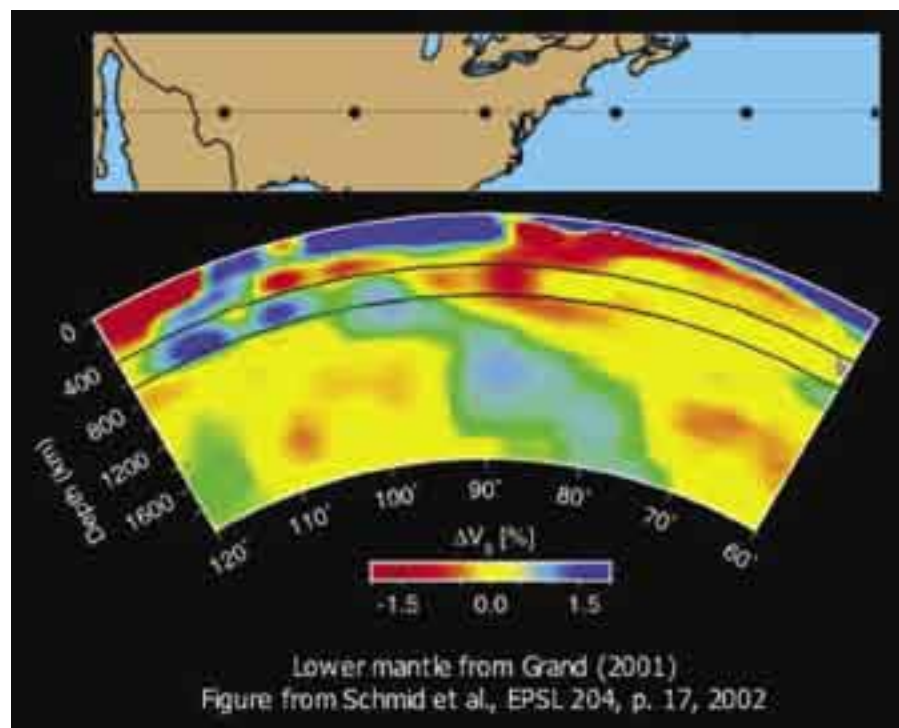
Dave Yuen, S. Mark Wang • *University of Minnesota*

Inferring the processes in and dynamics and evolution of Earth's interior is crucial for predicting how earthquake and volcanic activity will change in time and space. Three-dimensional models of S velocity beneath North America combined with numerical simulations of forming lithospheric shear zones lead us to believe that a subduction zone on the US East coast could be incipient.

S-velocity models for the North American upper mantle show a giant dike of S velocities about 0.1 km/s slower than the average upper mantle. Of temperature or relative content of iron, silicon, carbon dioxide, and water, we deem the latter the most likely explanation for the unusual S-velocity anomaly. Resolution tests, based on a recent set of over a thousand wave trains of continent-wide S and surface waves, show that the shape of the anomaly is resolved. However, S-velocities in the transition zone are underestimated. The low velocity dike connects to a weak low-velocity zone at the top of the upper mantle in Grand's model (2001). The giant dike is east of and parallel to the Appalachians and to the strike of the Farallon slab in the top of the lower mantle (Grand, 2000). The dike most likely represents an upwelling. Past dehydration of subducted Iapetus lithosphere or more recent dehydration of the subducted Farallon plate are potential sources for the inferred wet rock in the low-velocity dike.

Geodynamic modeling shows that large-scale lithospheric faulting associated with subduction zones can develop when the lithosphere is wet. Dry lithosphere such as that of the Atlantic Ocean thus needs to be hydrated to allow a new subduction zone to form on the US East coast. However, numerical modeling shows that a supra-lithospheric ocean cannot sufficiently hydrate the lithosphere and hence the source of hydration must come from below. The hydrous dike-shaped upwelling discussed above is the perfect candidate for such hydration and subsequent initiation of subduction. Under the sediment load off the US east coast the hydrated lithosphere will yield and can form a shear zone that cuts across the entire thickness of lithosphere. A new subduction zone is so initiated, up to half a billion years after a former subduction process provided the necessary ingredient, water.

In the context of this abstract and many others, we are excited about the enormous amounts of new data that will be forthcoming in the next dozen years from the USArray. This data will both revolutionize the resolution with which we can image upper mantle structure at the eastern continental margin, and allow for potentially associated seismic activity to be monitored more closely. Arriving at the east coast, USArray might show us the driving mechanism for the Wilson Cycle.

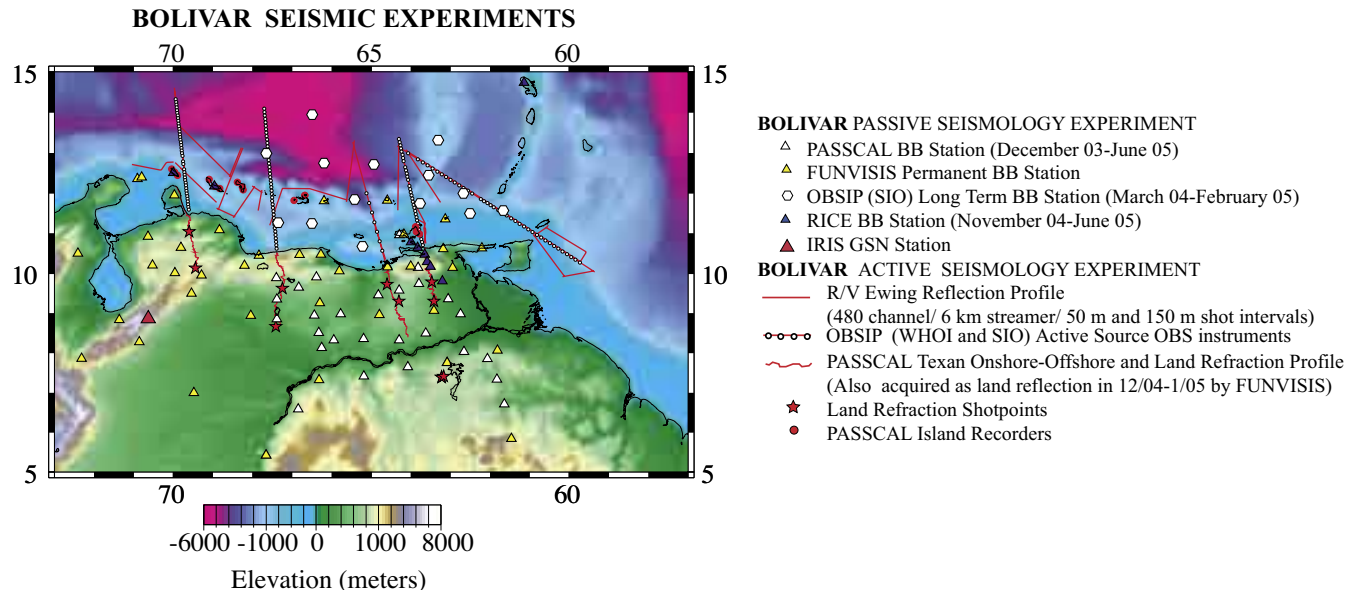


Anomalous S velocity in the North American upper mantle from seismic-tomographic imaging (upper mantle from van der Lee, 2002, and lower mantle from Grand, 2001) using S, multiple S, and surface waves. The upper-mantle column of low-velocity anomalies beneath the eastern continental margin presents a side view of the giant low-velocity dike.

BOLIVAR & GEODINOS: The SE Caribbean Continental Dynamics Project

BOLIVAR & GEODINOS Working Groups

The NSF Continental Dynamics BOLIVAR project (“Broadband Ocean-Land Investigations of Venezuela and the Antilles arc Region”) is investigating accretion of arc-related terranes to the northern SA continent. GEODINOS (GEODINÁMICA RECIENTE DEL LÍMITE NORTE DE LA PLACA SUDAMERICANA) is the Venezuelan government companion project to BOLIVAR. The projects include geological, geochemical, and geophysical investigations involving more than 40 scientists and students at 12 institutions in the U.S. and Venezuela. The study area extends from the Atlantic Ocean to the 71°W meridian, and from the Guyana Shield (6°N) into the Caribbean Sea basin (14°N). This area (>0.7 M km²) is comparable in size to California and its continental margin, and rivals the San Andreas plate boundary zone in geologic complexity.



Geologic studies have included mapping and age dating of igneous rocks of the Leeward Antilles from Aruba to Los Testigos, mapping of brittle deformation structures on the ABC islands, mapping in the coastal high-grade metamorphic belts in Venezuela, basin analysis and analysis of uplift and subsidence patterns in the onshore and offshore region, and 3-D reconstruction of paleogeographic evolution.

The BOLIVAR passive seismology group has now completed a year long experiment recording local, regional, and teleseismic data with a network of 35 PASSCAL, 8 Rice, and 14 OBSIP temporarily installed broadband recorders which complement the 35 satellite-telemetered BB stations operated by FUNVISIS (Fundación Venezolana de Investigaciones Sísmológicas). The 8 Rice BB recorders are currently installed in eastern Venezuela and on the Leeward Antilles Arc.

In June, 2004, the BOLIVAR active seismology group completed marine reflection profiling, and joint land refraction, onshore-offshore, and OBS recording. We acquired ~6000 km of reflection data, including 5 principal reflection/wide-angle transects. Four of these, along meridians, extend from the Caribbean basin across the South Caribbean deformed belt, the Oca-El Pilar fault system, and most of the fold-thrust belt onland in Venezuela. The fifth profile was oriented northwest extending from the Atlantic Ocean east of Trinidad and Tobago across the Antilles arc to the eastern Caribbean Sea. The R/V Ewing provided the sound source for onshore-offshore, OBS, and reflection recording. Dense wide-angle data were recorded using 49 OBSIP instruments deployed 169 times from the R/V Seward Johnson II, and 550 Reftek Texans deployed along each profile on the SA mainland. We also recorded reflection and wide-angle profiles along the length of the Leeward Antilles arc using 15 Reftek 135s. Complementary land reflection seismic profiles along three of the four meridional transects in Venezuela were recently completed by FUNVISIS using 800 Texan recorders. Preliminary playbacks indicate that the airguns were also well recorded by the broadband seismograph array.

The Reflections Under the Scottish Highlands (RUSH) EXPERIMENT: Mapping Fine-Scale Heterogeneities within the Continental Mantle Lithosphere Beneath Scotland, Combining Active- and Passive-Source Seismology

Eugenio Asencio • University of Puerto Rico

James H. Knapp, Thomas J. Owens • University of South Carolina

George Helffrich • University of Bristol

The structure and evolution of the continental mantle lithosphere constitute a fundamental frontier of continental tectonics. Developments in the field of seismology over the last decade in recording technology, data volume, and analysis techniques have led to a potentially powerful capability to integrate active- and passive-source seismology to image upper mantle structure across a spectrum of observational scales. Northern Scotland offers the opportunity to explore this integrated seismological approach due to the variety of observations suggesting fine-scale upper mantle layering. Toward this end, we tapped the BIRPS database of upper mantle reflections identified on near-vertical deep seismic reflection profiles and we deployed 24-broadband PASSCAL seismographs during the summer of 2001 (Asencio et. al., 2001, 2003) across the Scottish Highlands (Figure 1).

We analyze new observational evidence for seismic velocity discontinuities in teleseismic receiver functions in comparison to well-documented discontinuities observed in marine reflection profiles and wide-angle reflection-refraction profiles in northern Scotland. Our study establishes the viability of mapping small amplitude P-to-S (Ps) converted phase arrivals from the upper mantle generated in the P-wave coda of teleseismic earthquakes using well-known receiver function methods (Figure 2).

This investigation (Asencio, 2003) represents the joint use of two different approaches to seismic mapping of lithospheric structures and addresses the utility of correlating active- and passive-source seismology for understanding the tectonic significance and evolution of upper mantle structures. Application of this combined analysis provides some insight into the origin and lateral extent of upper mantle velocity discontinuities beneath Scotland.

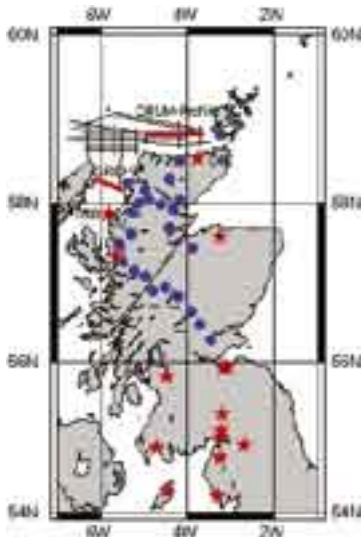


Figure 1. The Reflections Under the Scottish Highland (RUSH) Experiment, showing: (1) PASSCAL broadband stations (blue circles); (2) location of deep seismic reflection profiles (the DRUM and GRID-9 profiles shown in bold red); and, (3) permanent BGS 3-comp. stations (red stars).

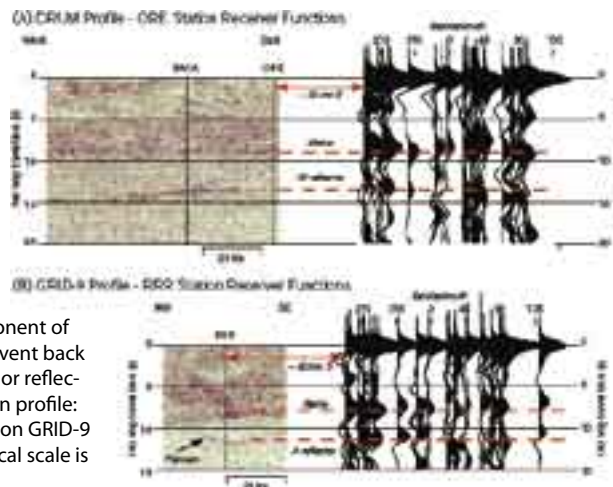


Figure 2. Correlation of radial component of receiver functions (as a function of event back azimuth) at: (A) ORE station with major reflectors on DRUM deep seismic reflection profile; (B) RRR station with major reflectors on GRID-9 deep seismic reflection profile. Vertical scale is two-way travel time in seconds.

Asencio, E., Imaging Lithospheric Structure in Northern Scotland and the South Caspian basin, Ph.D. Dissertation, University of South Carolina, Columbia, U.S., 2003.

Asencio, E., Knapp, J.H., Owens, T.J., and Helffrich, G., Mapping fine-scale heterogeneities within the continental mantle lithosphere beneath Scotland: Combining active and passive-source seismology, *Geology*, 31, pp. 447-480, 2003.

Asencio, E., Knapp, J.H., Owens, T.J., and Helffrich, G., The Reflection Under the Scottish Highlands (RUSH-II) Experiment: Broadband definition of upper mantle structures: *Eos Trans. AGU*, 82, Fall Meet. Suppl., Abstract S12D-0644, 2001.

This work was funded in part by grant EAR0074002 from the US National Science Foundation, grant GR9/04304 from the UK Natural Environment Research Council. We would like to thank the NERC Geophysical Equipment Pool and PASSCAL for providing the equipment and logistical support in the field and the IRIS Data Management Center and the British Geological Survey for making available the data through their automatic data server.

(quasi)-Love Found in Tuscany: US-European Seismic Array in Italy Catches the Big Wave

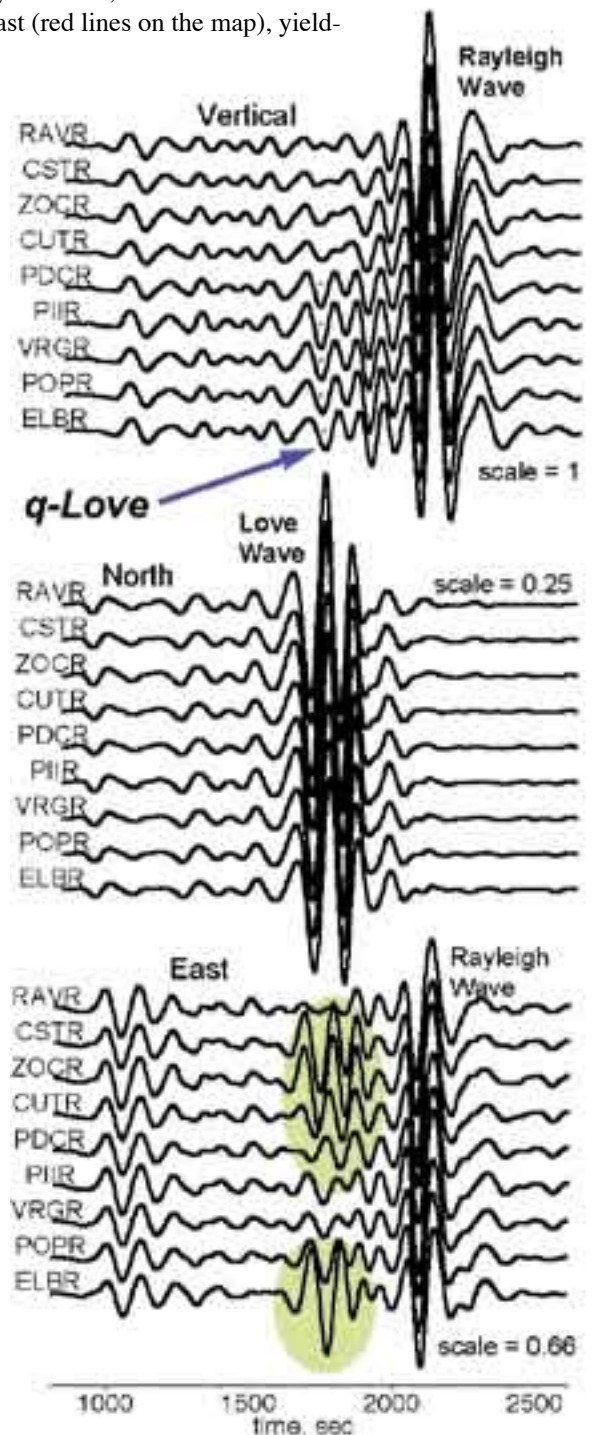
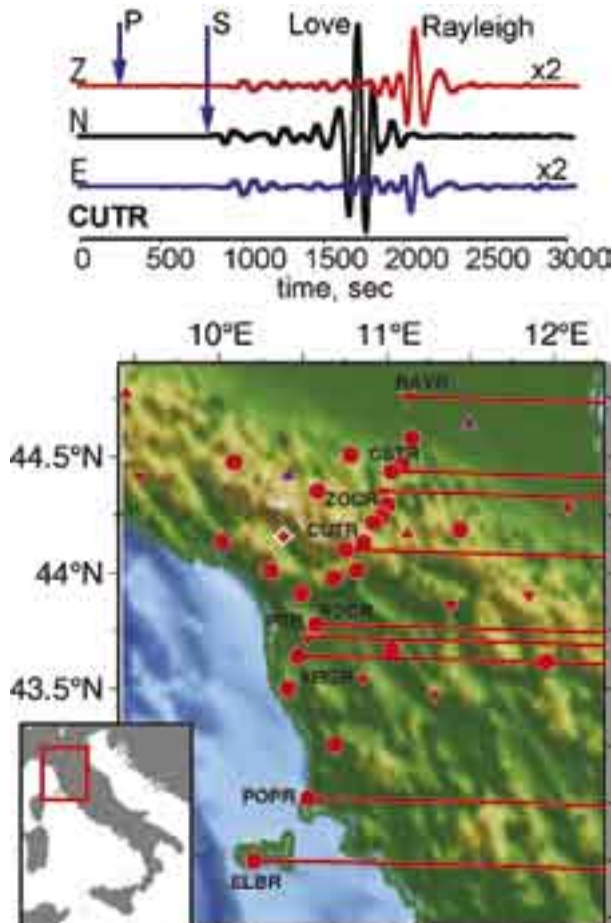
V. Levin • Rutgers University

J. Park • Yale University

RETREAT team

A linear PASSCAL array across the northern Apennines was deployed in Fall, 2004. Waveforms from the Sumatra-Andaman earthquake arrived at the array from due East (red lines on the map), yielding naturally polarized records (below are data from the crest of the Apennines). Record sections along the array show clear distortions of the Love wavefield. In the time window of the Love wave a vertically polarized phase (purple dots, upper right plot) appears on records from all sites in Tuscany, west of the Apennines. This phase is likely a Love-to-Rayleigh converted wave, or quasi-Love wave. It originates most readily from lateral gradients in seismic anisotropy structure. Given raypaths' geometry, its appearance in only Tuscany suggests an association of the anisotropic gradient with descent of Adriatic lithosphere beneath the Apennines. Love wave deflection onto the east component, both within the Apennines, and on the island of Elba (green ovals, lower right plot), is likely associated with complexity in upper mantle structure in Tuscany.

All time series are low-pass filtered at 100 seconds.



PASSCAL Experiments in Central Europe Target Lithospheric Structure

G. Randy Keller, Kate C. Miller • University of Texas at El Paso

Marek Grad • University of Warsaw, Poland

Alexander Guterch • Polish Academy of Science

Central Europe has experienced a complex tectonic history that dominated by the accretion of terranes to the rifted margin of Baltica that extends through central Poland (TESZ – Trans European Suture Zone) and formation of the Alps, Carpathians, and Pannonian basin (Figure 1). Beginning in 1997, Central Europe has been covered by an unprecedented network of seismic refraction experiments (Figure 2). These experiments (POLONAISE’97, CELEBRATION 2002, ALP2002, and SUDETES 2003) have only been possible due a massive international cooperative effort. They along with the BOHEMA and ALPASS teleseismic experiments are providing

exciting new insights into the structure and evolution of the lithosphere in this complex region.

The CELEBRATION 2000 experiment was the most ambitious of these projects and included 147 shots recorded by 1230

seismic stations forming, during three deployments that resulted in an array of profiles whose total length is about 5400 km. The velocity model derived for the longest profile CEL05 (1420 km; Figure 1) is shown in Figure 3 and displays large variations in structure. In the Pannonian part of the profile, crustal structure is relatively simple. The Moho lies at a depth of only 24-25 km. The most complicated structure is observed in the transition from the Pannonian basin, through the Carpathians, and across the TESZ and margin of the EEC (East European Carton or Baltica). In this area, the sedimentary cover with low velocities ($V_p < 5.5$ km/s) reaches a depth of about 20 km, and the Moho deepens to about 50 km.



Figure 2. Index map showing the locations of major seismic refraction experiments in Central Europe.

Guterch, A., M. Grad, H. Thybo and G. R. Keller, POLONAISE '97 – an international seismic experiment between Precambrian and Variscan Europe in Poland: *Tectonophysics*, 314, p. 101-121, 1999.

Keller, G. R., and R. D. Hatcher, Jr., Some comparisons of the structure and evolution of the southern Appalachian-Ouachita orogen and portions of the Trans-European suture zone region: *Tectonophysics*, 314, p. 43-68, 1999.

Grad, M., S. L. Jensen, G. R. Keller, A. Guterch, H. Thybo, T. Janik, T. Tiira, J. Yliniemi, U. Luosto, G. Motuza, V. Nasedkin, W. Czuba, E. Gaczynski, P. Sroda, K. C. Miller, M. Wilde-Piorko, K. Komminaho, J. Jacyna, and L. Korablíova, Crustal structure of the Trans-European suture zone region along POLONAISE'97 seismic profile P4: *Journal of Geophysical Research*, 108, doi:10.1029/2003JB002426, 2003.

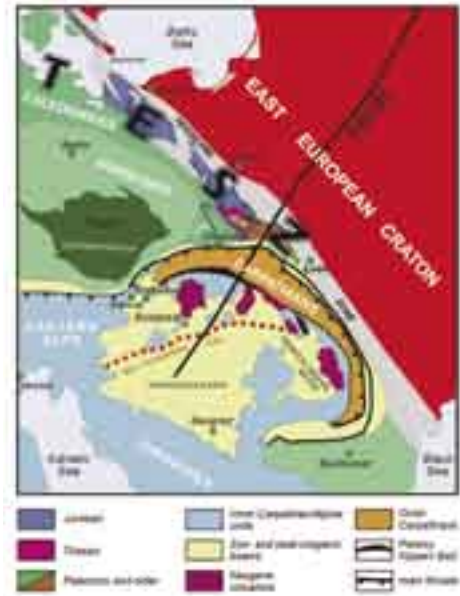


Figure 1. Tectonic map of Central Europe. USB – Upper Silesian block; HCM – Holy Cross Mountains; TESZ – Trans-European Suture Zone.

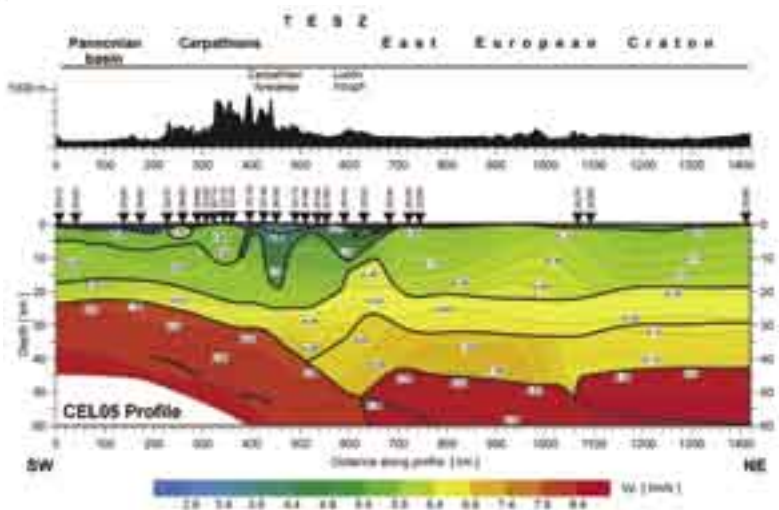


Figure 3. Two-dimensional P-wave velocity model for CELEBRATION 2000 profile CEL05 obtained by forward ray tracing. The thick solid lines are layer boundaries and thin lines are isovelocity contours in km/s; numbered triangles refer to shot points.

Origin and Tectonic Evolution of Active Continental Lithospheric Delamination in the Vrancea Zone, Romania: Project DRACULA

James H. Knapp, Camelia C. Knapp • University of South Carolina, Columbia

Laurentiu Munteanu, Victor Raileanu • National Institute for Earth Physics, Bucharest-Magurele, Romania

Victor Mocanu • University of Bucharest, Romania

The Vrancea seismic zone (VSZ) of Romania (Figure 1) constitutes one of the most active seismic zones in Europe, where intermediate-depth (70-200 km) earthquakes of magnitude in excess of $M_w = 7.0$ occur with relative frequency in a geographically restricted area within the 110° bend region of the southeastern Carpathian orogen (Knapp et al., in press). Project DRACULA (Deep Reflection Acquisition Constraining Unusual Lithospheric Activity), focused on the geodynamic origin of intermediate-depth seismicity of VSZ and utilized a new, comparatively low-cost approach for acquisition of low-fold deep



Figure 2. Digital Elevation Model of Romania, emphasizing the highly arcuate nature of the Carpathian orogen, and showing focal mechanisms for major intermediate-depth earthquakes in the Vrancea seismic zone (VSZ). Crustal earthquakes are shown as small black dots. Note the elevated topography of the hinterland (Transylvanian) and foreland basins of the Eastern Carpathians. Topography from USGS GTOPO 30 (Smith and Sandwell, 1997); maximum elevation is 2544 m. Focal mechanisms from ISC catalogue.

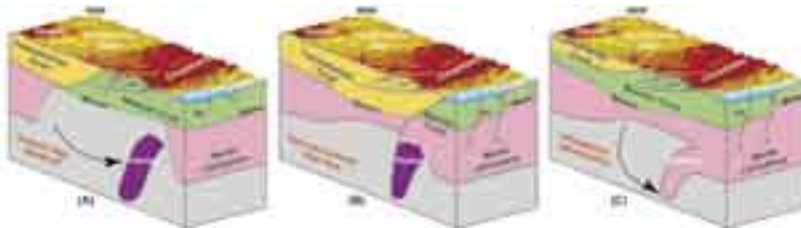


Figure 3. 3-D perspective lithosphere-scale block models, illustrating contrasting scenarios for geodynamic setting of the Vrancea zone. (A) Oceanic slab subduction and break-off (B) Oceanic slab subduction and progressive lateral tear within the Carpathian foreland (C) Continental lithospheric delamination. Green = Moesian/East European crust; Yellow = Transylvanian crust; Pink = Continental mantle lithosphere; Purple = Oceanic lithosphere; Grey = Asthenosphere. VSZ is located in lower front corner of models.

seismic reflection data. Funded by NSF Tectonics, Project DRACULA was carried out during the summer of 2004 and resulted in the acquisition of 320 km of high-quality deep reflection data in three separate profiles (DRACULA I, II, and III) concentric about the VSZ in order to discriminate among three contrasting geodynamic models (Figure 2). The deep (60 s TWT) High-Resolution (4 ms sampling interval) seismic reflection data were recorded with the full complement of 800 stand-alone Reftek-125 (Texan) seismometers and 4.5 Hz geophones from the combined PASSCAL/UTEP instrument pool. A 50 m station spacing provided industry-standard spatial resolution, while the 1 km shot spacing economized on cost. The source effort consisted of 10 kg in each of two holes drilled to 12 m, for a total of 20 kg per shotpoint.

Preliminary results of Project DRACULA show exceptional reflectivity on many single-fold shot gathers. In particular, coherent laterally extensive, sub-horizontal reflections are evident throughout the crust and upper mantle beneath the Carpathian hinterland, in some cases down to 30 s TWT. Beneath the Carpathian foreland, coherent reflectivity is evident to 36 s TWT. Integration of these data with crustal seismicity, surface geology, and topography shows little if any evidence for subduction of a relic oceanic slab, and implies other viable geodynamic mechanisms, such as active continental lithosphere delamination (e.g., Nelson, 1991; Seber et al., 1996; Figure 2), to explain the Vrancea zone seismicity.

Knapp, J. H. Knapp, C. C., Raileanu, V., Matenco, L., Mocanu, V., and Dinu, C., Crustal Constraints on the Origin of Mantle Seismicity in the Vrancea Zone, Romania: The Case for Active Continental Lithospheric Delamination, *Tectonophysics* (in press).

The Eastern Turkey Seismic Experiment: The Study of a Young Continent-Continent Collision

Eric Sandvol • *University of Missouri*

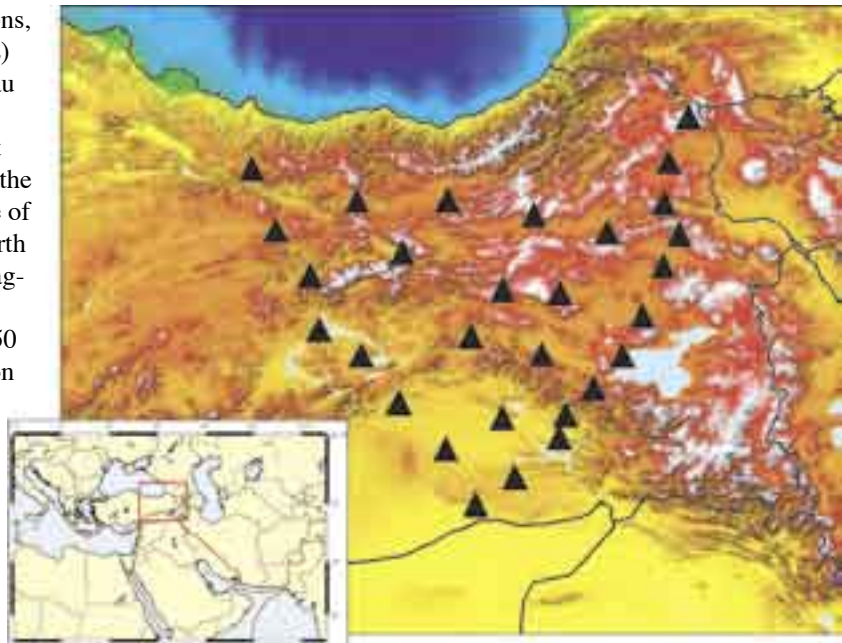
Niyazi Turkelli • *Bogazici University, Istanbul, Turkey*

Muawia Barazangi • *Cornell University*

During the last 10-20 million years the tectonics of Turkey and the Anatolian plateau can be described as the convergence of three continental plates: the Anatolian, Arabian, and Eurasian plates form a diverse suite of tectonic boundaries. This tectonic environment makes the East Anatolian plateau and Bitlis suture an excellent natural laboratory to study the early stages of continental collision and its consequences. Until now, the only well-studied example for active continental collision has been that of India colliding with Eurasia and the subsequent uplift of the Tibetan plateau.

In order to address these important questions, the Eastern Turkey Seismic Experiment (ETSE) was conducted across the East Anatolian plateau and the northernmost Arabian plate. ETSE was a 29 broadband station PASSCAL network that was designed to improve our understanding of the Bitlis/Zagros thrust zones, as well as the nature of continental escape along the EAFZ and the North Anatolian Fault Zone (NAFZ), through the imaging of upper mantle and crustal structure. The average station separation was approximately 50 km. The ETSE western traverse crosses a region where it has been well documented that the Anatolian block is escaping westward, while the ETSE eastern traverse crosses a region where the deformational regime is far more complex.

The East Anatolian High Plateau is a region of average ~2 km elevation exhibiting active diffuse N-S shortening and widespread Pliocene to recent volcanism. Its elevation was hitherto thought to result from a presumed crustal thickness of about 55 km. Seismic data collected by ETSE have shown, however, that its maximum crustal thickness is only some 45-48 km (Zor et al., 2003). Combined with tomographic models of regional seismic velocity and attenuation, this shows that most of the East Anatolian High Plateau is devoid of mantle lithosphere (Al-Lazki et al., 2003; Gok et al., 2003). The absence of mantle lithosphere is ascribed to break-off of northward subducted slab beneath the prism and the widespread volcanism to melting its lower levels because of direct contact with hot asthenosphere. The East Anatolian High Plateau is thus supported not by thick crust, but by hot mantle. The ETSE results offer a multi-disciplinary investigation of one of the earth's best examples of ongoing continent-continent collision.



Al-Lazki, A., Sandvol, E., Seber, D., Turkelli, N., Mohamad, R., and Barazangi, M., Tomographic Pn velocity and anisotropy structure beneath the Anatolian plateau (eastern Turkey) and the surrounding regions, *Geophys. Res. Lett.*, 30, 8040, doi:10.1029/2003GL018912, 2003.

Gok, R., Sandvol, E., Turkelli, N., Seber, D., and Barazangi, M., Sn Attenuation in the Anatolian and Iranian Plateaus and Surrounding Regions, *Geophys. Res. Lett.*, 30, 8042, doi:10.1029/2003GL018912, 2003.

Orgulu, G., Ahktar, M., Sandvol, E., and Barazangi, M., The Seismotectonics of the Eastern Anatolian Plateau, *Geophys. Res. Lett.*, 30, 8040, doi:10.1029/2003GL018912, 2003.

Zor, E., Sandvol, E., Gurbuz, C., Turkelli, N., Seber, D., and Barazangi, M., The Crustal Structure of the East Anatolian Plateau from Receiver Functions, *Geophys. Res. Lett.*, 30, 8044, doi:10.1029/2003GL018912, 2003.

Systematic High-Resolution Imaging of the Karadere-Düzce Branch of the North Anatolian Fault

Zhigang Peng • University of Southern California, now at University of California, Los Angeles

Yehuda Ben-Zion • University of Southern California

The spatial extent and material properties of the damaged fault zone rock have important implications for many aspects of earthquake behavior. Fault zone structures with material discontinuity interfaces and low-velocity layers of damaged fault zone rock can produce several indicative wave propagation signals, including scattering, anisotropy, non-linearity, and guided head and trapped waves. We perform a systematic analysis of such signals from seismic data recorded by a PASSCAL seismic network deployed along and around the Karadere-Düzce branch of the north Anatolian fault during the 1999 Mw 7.4 İzmit and Mw 7.1 Düzce earthquake sequences. Our results can be summarized as follows: The observed fault zone trapped waves are generated by relatively shallow structures that extend generally only over the top ~3-4 km of the crust. The shallow trapping structure is ~100 m wide and is surrounded by broader (~1 km) anisotropic and scattering zones that are also confined primarily to the top 3 km. The average delay times for ray paths that propagate along the rupture zone are larger than for the other paths. The apparent crack density in the damaged shallow fault zone rock is about 7%. Systematic analyses of anisotropy and scattering measured from waveforms generated from repeating earthquakes do not show precursory temporal evolution of properties before the Düzce mainshock. The anisotropy results show small co-seismic changes. However, the scattering results show clear co-seismic changes and post-seismic logarithmic recovery after the Düzce mainshock. A strong correlation between the co-seismic delays and intensities of the strong ground motion generated by the Düzce mainshock implies that the radiated seismic waves produce the velocity reductions in the top portion of the shallow crust.

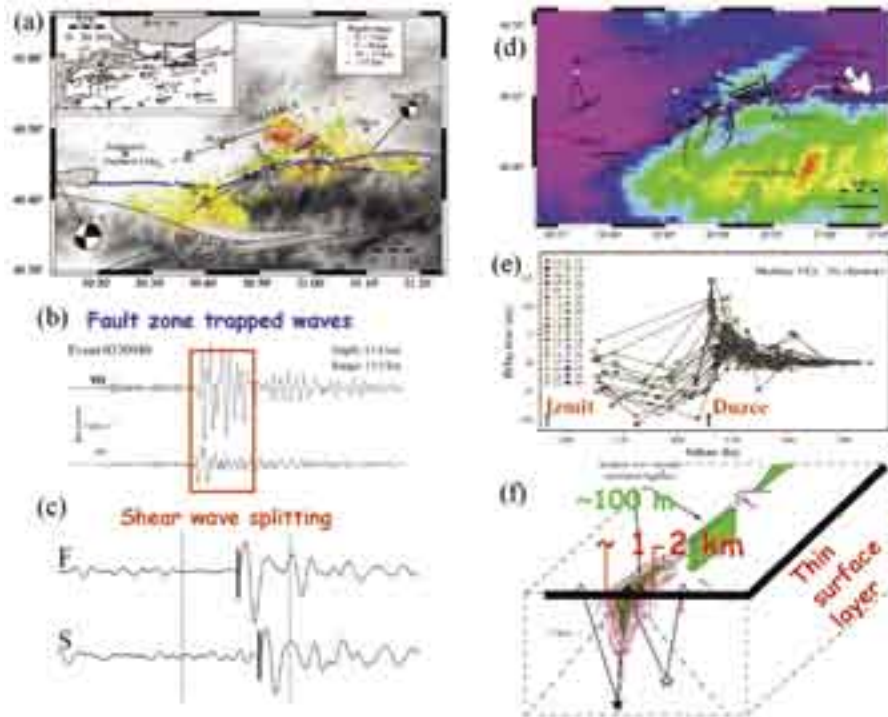


Figure 1. (a) Hypocentral distribution of ~18000 earthquakes recorded by the PASSCAL seismic experiment along the Karadere-Düzce branch of the north Anatolian fault. (b) An example of fault zone waveforms recorded by stations on (VO) and off (FP) the fault. (c) An example of rotated horizontal seismograms showing splitted shear waves. (d) A summary plot of average splitting parameters (bars) in our study area. The bars are oriented parallel to the average fast direction and scaled by the average delay time. (e) Median delay times for the early S-coda waves plotted against the earthquake occurrence times for the vertical-component seismograms generated by 36 repeating clusters and recorded at station VO. (f) A schematic summary of the proposed fault zone model around the study area. See the text and references for more information.

Ben-Zion, Y., Z. Peng, D. Okaya, L. Seeber, J.G. Armbruster, N. Ozer, A.J. Michael, S. Baris and M. Aktar. A shallow fault zone structure illuminated by trapped waves in the Karadere-Düzce branch of the north Anatolian fault, western Turkey, *Geophys. J. Int.*, 152, 699-717, 2003.

Peng, Z. and Y. Ben-Zion. Systematic analysis of crustal anisotropy along the Karadere-Düzce branch of the north Anatolian fault, *Geophys. J. Int.*, 159, 253-274, 2004.

Peng, Z. and Y. Ben-Zion. Turkey, earthquake sequences, *Geophys. J. Int.*, 160, 1027-1043, 2005.

Peng, Z., and Y. Ben-Zion. Temporal changes of shallow seismic velocity around the Karadere-Düzce branch of the north Anatolian fault and strong ground motion, submitted to *Pure Appl. Geophys.*, 2005.

Tectonic Structure and Surface Wave Dispersion in Eurasia and North Africa

Michael E. Pasyanos • Lawrence Livermore National Laboratory

LLNL has performed a large-scale study of surface wave dispersion across Eurasia and North Africa. The spatial resolution of the inversion has been improved by increasing path density and adopting a variable smoothness conjugate gradient method for the group velocity tomography (Pasyanos, 2005). This technique allows us to achieve higher resolution where the data allow without producing artifacts. The current results include both Love and Rayleigh wave inversions across the region for periods from 7 to 100 s at 1° resolution. While short-period group velocities are sensitive to slow velocities associated with large sedimentary features, and intermediate periods to differences in crustal thickness, at longer periods the group velocities are sensitive to structures in the upper mantle. One would expect hot, upwelling material to have slow group velocities at these periods, while cold material should be fast. Figure 1 shows a map of 80 s group velocities with plate boundaries (solid lines), hot spots (crosses and triangles), and the boundaries of stable platforms and Achaean cratons (single and double hatched lines, respectively). At this period, there are indications that the slow velocities associated with rift zones are deeper-seated than in convergence zones, where the slow velocities are confined to the wedge. A significant correspondence can also be found between fast velocities and older crust. For example, while it appears that orogenic zones like the Tethys Belt are slow, stable continental areas are fast. These older areas are underlain by thick, cold, fast lithospheric material. Two exceptions seem to be the Sino-Korean Paraplatform, which has had its lithospheric mantle more recently affected by nearby subduction, and the Benue Trough in Cameroon, which is the remnant of a failed rift system. Figure 2 shows the correlation between lithospheric thickness and 80 s Rayleigh wave group velocities. The thicknesses of the continents are derived from the 1300° C isocontour from Artemieva and Mooney (2001), whereas the thicknesses of the oceanic lithosphere are derived from the oceanic age. The correlations here are quite significant, with older, thicker lithosphere about 0.35 km/s faster than a younger, thinner one.

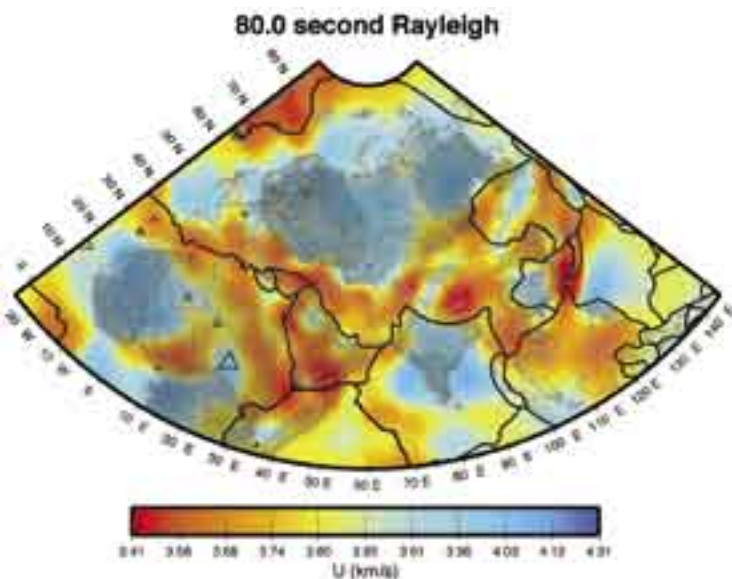


Figure 1. Map of 80 s Rayleigh wave group velocities shown with plate boundaries (thick lines), hot spots (triangles and crosses), and boundaries of platforms and cratons (hatched lines).

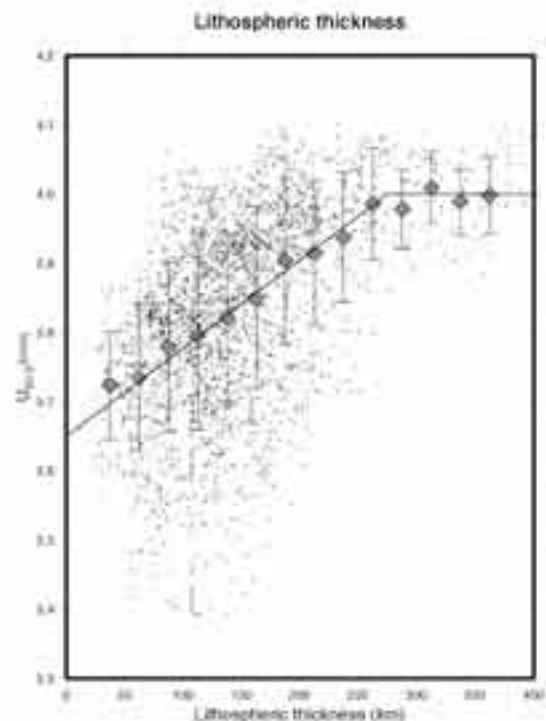


Figure 2. Correlation between 80 s Rayleigh wave group velocities (in km/s) and lithospheric thickness (in km). Diamonds and bars indicate the mean and standard deviation of group velocity values in that thickness range.

Artemieva, I.M., and W.D. Mooney, Thermal structure and evolution of Precambrian lithosphere, *J. Geophys. Res.*, 106, 16387-16414, 2001.

Pasyanos, M.E., A Variable-resolution surface wave dispersion study of Eurasia, North Africa and surrounding regions, *J. Geophys. Res.*, in review, 2005.

Upper Mantle Q and Thermal Structure Beneath Tanzania, East Africa from Teleseismic P Wave Spectra

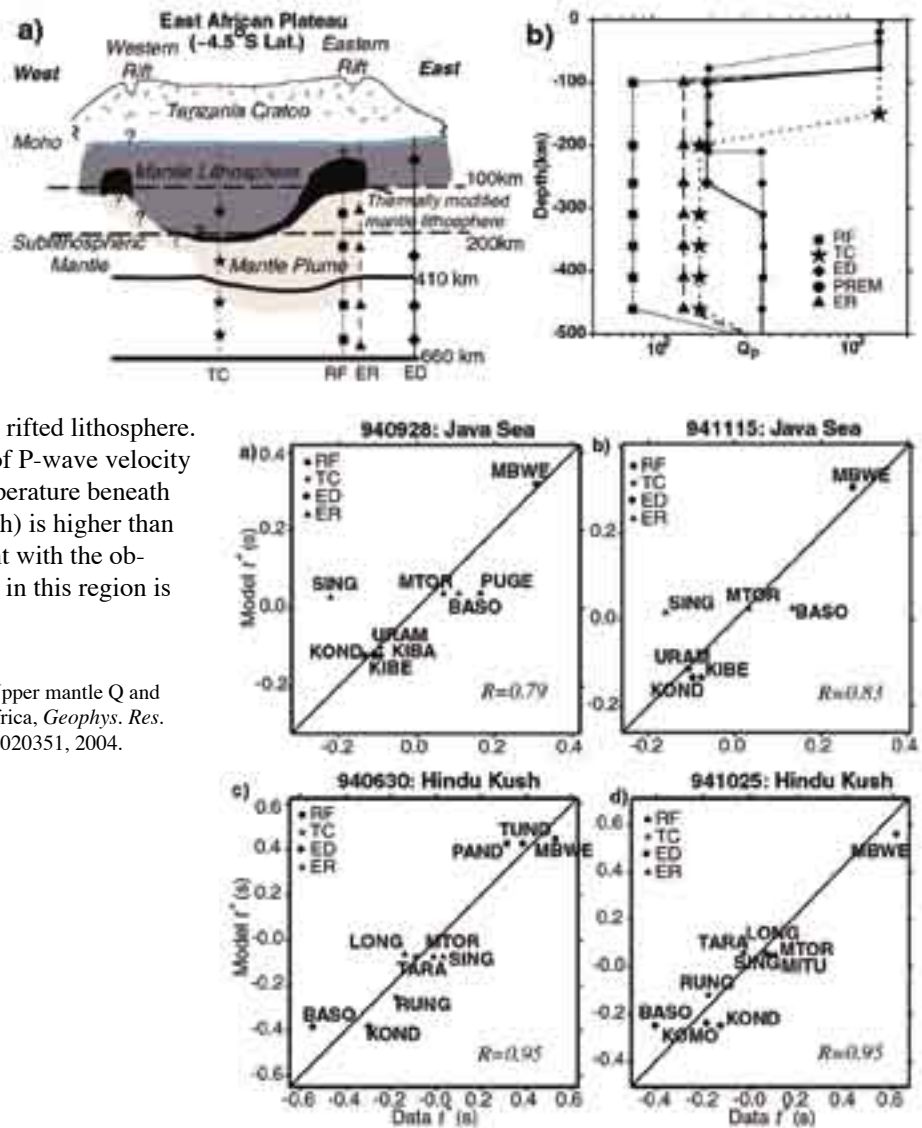
Anupama Venkataraman • Stanford University

Andrew A. Nyblade • Pennsylvania State University

Jeroen Ritsema • Institut de Physique du Globe, Paris, France

We measure P-wave spectral amplitude ratios from deep-focus earthquakes recorded at broadband seismic stations of the Tanzania network to estimate regional variation of sublithospheric mantle attenuation beneath the Tanzania craton and the eastern branch of the East African Rift. One-dimensional profiles adequately explain the systematic variation of P-wave attenuation in the sublithospheric upper mantle: beneath the cratonic lithosphere, while it is ~ 80 beneath the rifted lithosphere. By combining the values and a model of P-wave velocity perturbations, we estimate that the temperature beneath the rifted lithosphere (100-400 km depth) is higher than ambient mantle temperatures, consistent with the observation that the 410-km discontinuity in this region is depressed by 30-40 km.

Venkataraman, A., A. Nyblade, and J. Ritsema, Upper mantle Q and thermal structure beneath Tanzania, East Africa, *Geophys. Res. Lett.*, 31, No. 15, L15611, 10.1029/2004GL020351, 2004.



Structure and Evolution of the Main Ethiopian Rift

Simon Klemperer • Stanford University

G. Randy Keller • University of Texas at El Paso

Kevin Mickus • Southwest Missouri State University

Tanya Furman • Pennsylvania State University

The Ethiopia Afar Geoscientific Lithospheric Experiment (EAGLE) was undertaken in 2003 by an international team composed primarily of U. S., British, and Ethiopian scientists and students to provide a snapshot of lithospheric break-up at the transition between continental and oceanic rifting. Our focus is the Main Ethiopian Rift (MER) that extends from central Ethiopia into Afar towards the Gulf of Aden and Red Sea oceanic rifts. The MER cuts across the uplifted Ethiopian plateau, which is a major Oligocene flood basalt province associated with the impact of the Afar mantle plume. In addition to a large passive seismology effort led by the British group, EAGLE included a large controlled-source seismic experiment incorporating two ~400 km refraction lines along and across the rift and a two-dimensional array ~100 km in diameter spanning the rift at the intersection of the two profiles (Figure 1). A total of 23 explosive sources were recorded by approximately 1000 “Texan” seismographs and ~100 broadband seismometers, requiring mobilization of the national seismic pools of the UK and Denmark as well as IRIS-PASSCAL. Our resulting crustal and sub-Moho P-wave seismic velocity model provides insight into the magmatic and structural processes occurring beneath the MER. The most significant results relate to: (1) the variation in velocity within the mid and upper crust along the axis of the rift, from an average of ~6.2 km/s beneath the flanks to ~6.6 km/s beneath the axial magmatic segments (Figure 2); (2) the emplacement of a high-velocity body (V_p ~7.4 km/s) in the lower crust beneath the northwestern margin of the rift; (3) the dramatic variation in crustal thickness along the axis of the rift; and (4) the presence of a possibly continuous mantle horizon beneath both linear profiles. These are interpreted respectively in terms of: (1) the presence of cooled gabbroic bodies separated and laterally offset from one another and lying beneath the overlying Quaternary volcanic centers along the axis of the rift; (2) a ~10 km thick mafic underplated layer emplaced at the base of the crust and associated with Oligocene flood basalt magmatism over the now uplifted northwestern Ethiopian

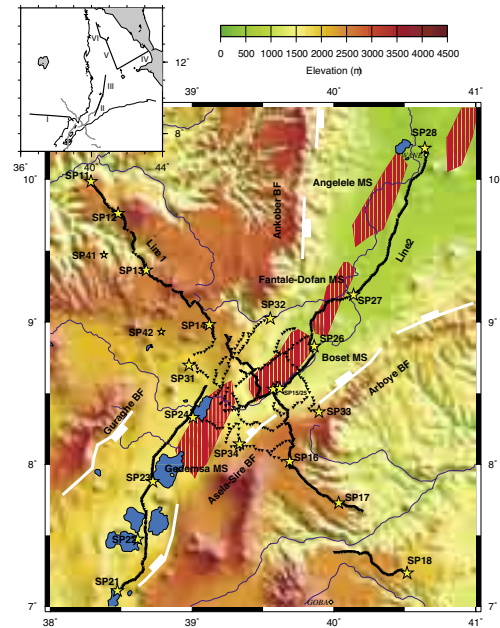
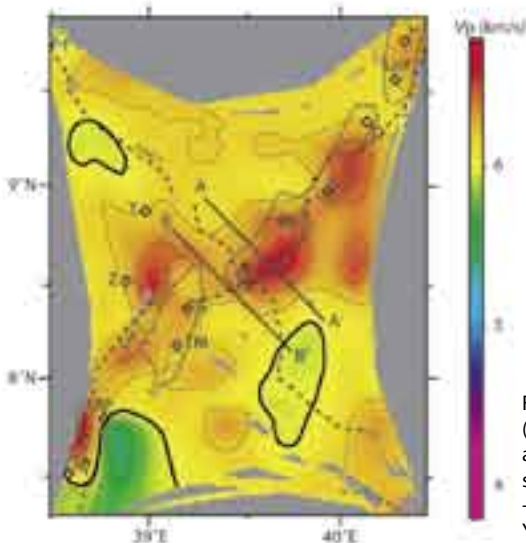


Figure 1. Index map of the EAGLE controlled source experiment. Line 1 crossing the rift valley; Line 2 follows the rift valley; and Line 3 is the array deployed in the region where Lines 1 and 2 cross. Yellow stars are shotpoints. Elongate areas shaded in red are magmatic segments that were targeted in this study. The inset shows the locations of previous studies in the region.



plateau; (3) thinning of the crust from ~40 km beneath the southwestern MER to ~26 km in the northeast beneath Afar; and (4) the possible identification of a boundary in the mantle at a depth of ~60 km caused by shearing due to stresses caused by lateral ‘spreading’ of the upwelling anomalous mantle beneath the rift and its surroundings.

Keranen, K., Klemperer, S.L., Gloaguen, R. & the EAGLE Working Group, Imaging a proto-rift axis in the Main Ethiopian Rift, *Geology*, 32(11), 949 – 952, 2004.

Maguire, P., Ebinger, C., Stuart, G., Mackenzie, G., Whaler, K., Kendall, J.-M., Khan, M., Fowler, C., Klemperer, S., Keller, G., Harder, S., Furman, T., Mickus, K., Asfaw, L., Ayele, A., & Abebe, B., Geophysics project in Ethiopia studies continental breakup. *EOS (Transactions American Geophysical Union)*, 84(35), 342-343, 2003.

Figure 2. Horizontal slice through the 3-D tomographic model at 10 km below the surface (after Keranen et al., 2004). EAGLE Lines 1 & 2 dashed. High-velocity bodies (red) interpreted as solidified magmatic intrusions beneath the rift floor. Sections AA' and BB' are vertical slices shown in Keranen et al. (2004). Diamonds identify volcanoes: Al - Aluto, B - Boset, D - Dofan, F - Fantale, G - Gademsa, H - Hertale, K - Kone, LHF - Liado Hayk Field, TM - Tullu Moje, Sh - Shala, Y - Yerer, Z - Zikwala

The Upper Mantle P Wave Structure Beneath Ethiopia and Kenya

Yongcehol Park, Margaret H. Benoit, Andrew A. Nybalde • *Pennsylvania State University*

Charles A. Langston • *University of Memphis*

The origin of uplift and rifting and volcanism in East Africa is controversial, and has been commonly attributed to one or more mantle plumes. To examine upper mantle structure beneath Ethiopia and the Kenya rift, we have modeled the P- wave velocity variations by inverting travel time residuals from teleseismic earthquakes recorded by the 2000-2002 Ethiopia Broadband Seismic Experiment, the 2001-2002 Kenya Broadband Seismic Experiment, the KRISP85 and KRISP90 experiment, and permanent stations ATD, FURI, and KMBO. The P model for Ethiopia shows strong velocity variations between 150 and 400 km depth. At 150 km depth, the low velocity region is centered beneath the Afar Depression, Main Ethiopian rift, and slightly west of the rift under the western portion of the Ethiopia Plateau. Deeper in the models (200 – 400 km depth), the center of the low-velocity structure appears to shift westward across the Western Ethiopian Plateau, offset from the strike of the Main Ethiopian rift. Additionally, the model reveals faster-than-average velocities beneath the Eastern Ethiopia Plateau and the northwest section of Western Ethiopian Plateau. The model obtained for Kenya shows a strong low-velocity region beneath the Kenya rift that shifts to the west with depth. In spite of the limited resolution, it is apparent that the thermally-perturbed upper mantle structure extends to depths in excess of 300 km, and dips to the west beneath the Tanzania Craton.

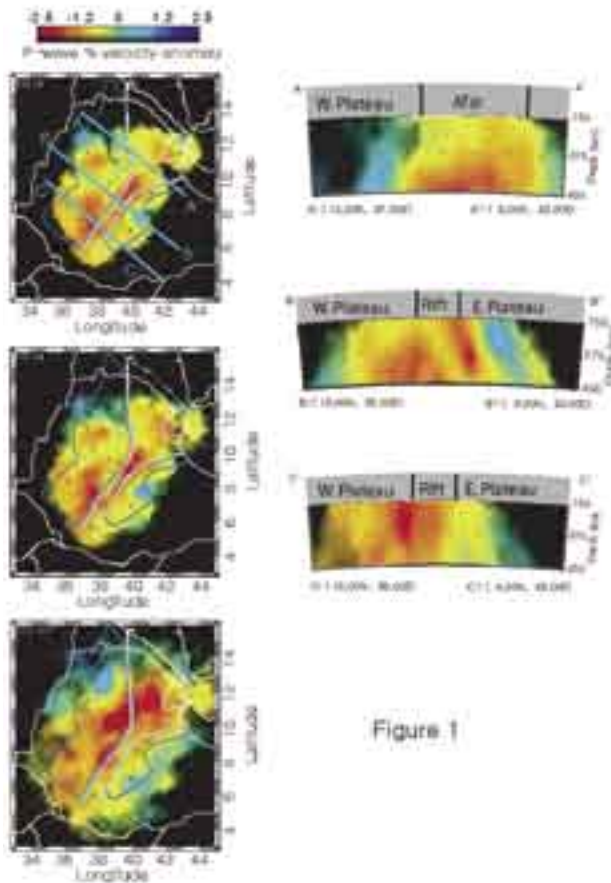


Figure 1

Horizontal cross sections sliced through P-wave velocity models from travel time tomography for Ethiopia. Horizontal cross sections through the model are shown for depths of 150, 200, and 400 km. Political boundaries are shown in white and approximate rift boundaries are outlined in grey. The 2,000 m elevation contour line is shown in blue. Station locations are depicted as small white squares.

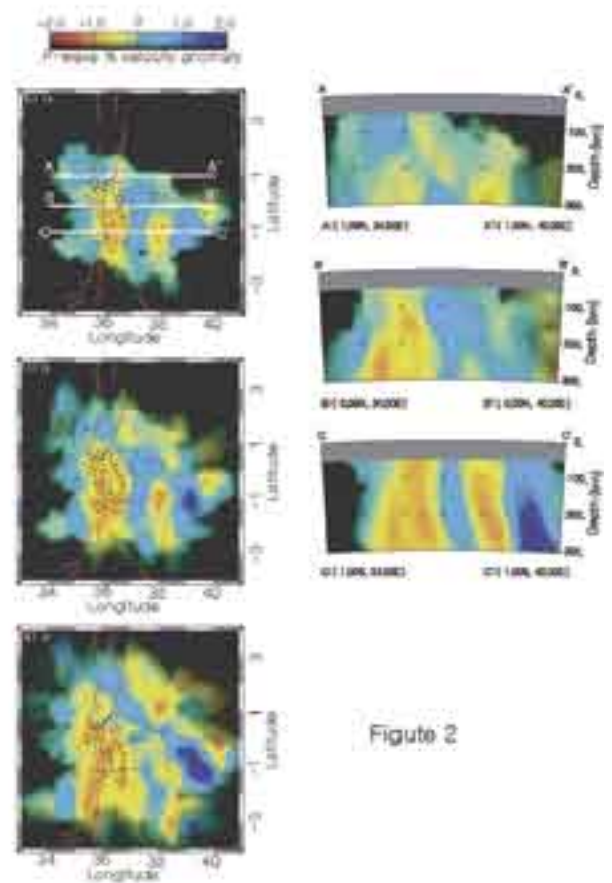


Figure 2

Horizontal cross sections sliced through P-wave velocity models from travel time tomography for Kenya. Horizontal cross sections through the model are shown for depths of 150, 200, and 400 km. The Kenya rift is shown in red, and station locations are depicted as small white squares.

Crustal Structure Beneath Ethiopia and Kenya: Implications for Rift Development in Eastern Africa

Mulugeta T. Dugda, Andrew A. Nyblade, Charles Ammon • *Pennsylvania State University*

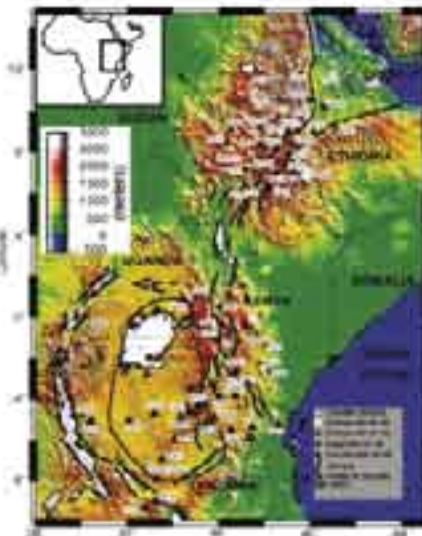
Jordi Julia • *Duke University*

Charles A. Langston • *University of Memphis*

Silas Simiyu • *Kenya Power Generating Company*

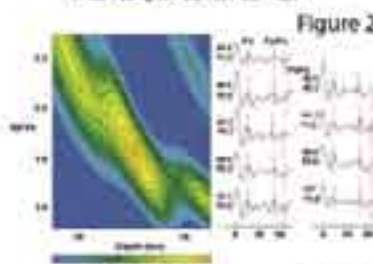
The East African Rift System (EARS) is one of the largest continental rift systems on Earth, extending from the Afar region of Ethiopia southward to beyond the Zambezi River (Figure 1). Crustal structure was investigated within and surrounding the Eastern Branch of the EARS in Ethiopia and Kenya to determine the extent to which the Precambrian crustal structure has been modified by the Cenozoic tectonism found there. Two methods of receiver function analysis, the H-k method (Figure 2), and direct stacks of the waveforms, were used to analyze broadband seismic data that came from two IRIS/PASSCAL broadband seismic experiments conducted in Ethiopia between 2000 and 2002 and in Kenya between 2001 and 2002 (Figure 1). Crustal thickness to the east of the Kenya rift varies between 39 to 42 km and Poisson's ratios for the crust vary between 0.24 and 0.27 (Figure 3). To the west of the Kenya rift, Moho depths vary between 37 and 38 km and Poisson's ratios vary between 0.24 and 0.27. These findings support previous studies showing that crust away from the Kenya rift has not been modified extensively by the Cenozoic rifting and magmatism. Beneath the Ethiopian Plateau on either side of the Main Ethiopian Rift, crustal thickness ranges from 33 to 44 km, and Poisson's ratios vary from 0.23 to 0.28. Within the Main Ethiopian Rift, Moho depths vary from 27 to 38 km, and Poisson's ratios range from 0.27 to 0.35 (Figure 3). A crustal thickness of 25 km and a Poisson's ratio of 0.36 were obtained for a single station in the Afar Depression. When compared to the Mozambique Belt crust in Tanzania and Kenya, as well as global averages, these results indicate that the crust beneath the Ethiopian Plateau has not been modified significantly by the Cenozoic rifting and magmatism.

Figure 1



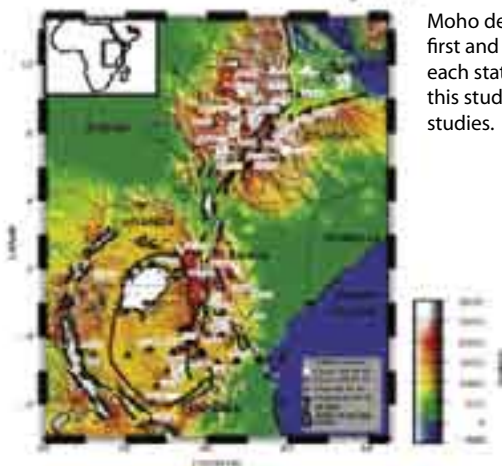
Location map of the study region showing topography, Precambrian terrains, the outline of the Cenozoic East African rift system, and the distribution of broadband seismic stations in Ethiopia, Kenya and Tanzania.

Figure 2



H-k stack of receiver functions for a V_p value of 6.5 km/s for station DMRK. To the left of each receiver function, the top number gives the event azimuth and the bottom number gives the event distance in degrees. Contours map out percentage values of the objective function.

Figure 3



Moho depths and Poisson's ratios (the first and the second numbers next to each station, respectively) obtained in this study and for Tanzania by previous studies.

Small-Scale Variations in Seismic Anisotropy Near Kimberley, South Africa

Matthew J. Fouch, David R. Bell • Arizona State University

Paul G. Silver • Carnegie Institution of Washington

Jean N. Lee • Harvard University

Using broadband seismic data from the IRIS PASSCAL broadband telemetered array installed near Kimberley, South Africa, we place new constraints on seismic anisotropy in an area of extensive mantle modification within an Archean cratonic setting (Fouch et al., 2004). The array was installed as part of the multidisciplinary Kaapvaal Project, which extensively studied the region via petrologic, geochemical, and seismic means, and provided a unique opportunity to meld the results of a broad range of datasets to examine processes of cratonic evolution.

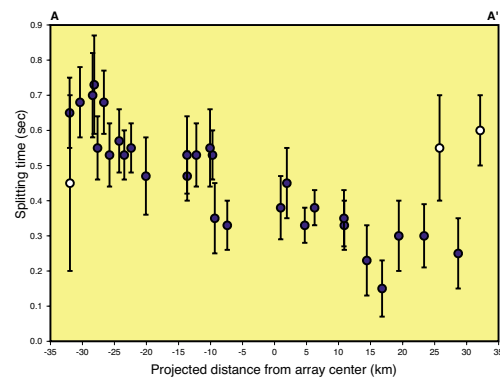


Figure 2. Stacked shear wave splitting time versus distance along projection of array midline from Figure 1a. Thin lines denote 95% confidence limits for each station. Splitting times show a linear decrease from NW to SE (A to A'), with the exception of stations Kaapvaal stations SA18 and SA19 and IRIS/GSN station BOSA (white circles).

ences in relative arrival times across the array (Figure 1d). The combined relative arrival time and splitting analyses indicate that a significant change in the strength of anisotropic structure is required across the region. Our results are most consistent with a model in which variations in seismic anisotropy near the Kimberley region are constrained to the lithosphere with an average anisotropic strength of $\sim 1.8\%$, extend to depths no greater than 150 km, and are primarily controlled by a significant change in the strength of anisotropy within the lateral bounds of the seismic array.

We hypothesize that the observed seismic anisotropy is due to strain induced lattice preferred orientation of olivine caused by the amalgamation and deformation of the eastern and western blocks of the Kaapvaal craton. This collisional process mechanically weakened the region to generate the observed mantle fabric, which was exploited by significant rifting events that may have subsequently enhanced the regional fabric. Our results support the notion that seismic anisotropy beneath Archean continental regions is not created (or alternatively not preserved) during initial continental formation, but instead is generated during subsequent significant mantle deforming events.

Fouch, M.J., P.G. Silver, D.R. Bell, and J.N. Lee, Small-scale variations in seismic anisotropy near Kimberley, South Africa, *Geophys. J. Int.*, 157, 764-774, doi: 10.1111/j.1365-246X.2004.02234.x, 2004.

Silver, P.G., S.S. Gao, K.H. Liu, and the Kaapvaal Seismic Group, Mantle deformation beneath southern Africa. *Geophys. Res. Lett.*, 28, 2493-2496, 2001.

We analyze the shear wave splitting of SKS phases recorded near Kimberley. These phases exhibited consistent fast polarization directions of \sim NE SW (Figure 1a) and splitting times that ranged from 0.15 s in the SE to nearly 0.75 s in the NW regions of the array (Figures 1a, 2). Multi-channel cross correlation of relative arrival times of teleseismic SKS phases across the array revealed clear azimuthal variations and a relative arrival time range comparable to the shear wave splitting delay time range (Figures 1b, 1c). A like analysis of teleseismic PKP phases did not exhibit significant differ-

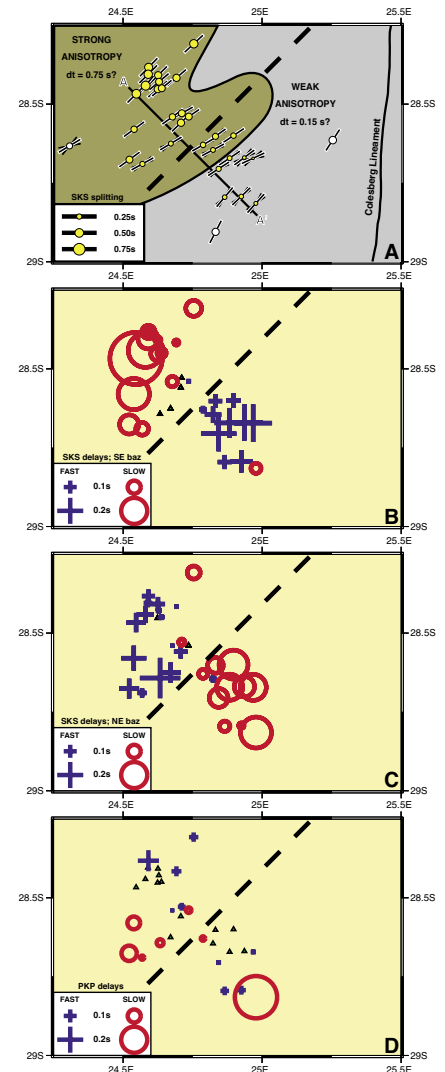


Figure 1. Results from shear wave splitting and relative delay time analysis of SKS and PKP phases recorded at the Kimberley telemetered array. Proposed boundary of strong/weak anisotropic domain is delineated by dashed line. a) Stacked shear wave splitting results. Azimuth of black bars denote fast polarization direction; thin black bars denote 95% confidence limits for fast polarization directions; size of circles is scaled to splitting time. For figures 1b-1d, crosses (faster than average arrivals) and circles (slower than average arrivals) are scaled to magnitude of relative arrival time. Triangles denote relative arrival times of ± 0.025 s.

Xenolith Constraints on Seismic Velocities in the Upper Mantle Beneath Southern Africa

David E. James, F. R. Boyd, Richard W. Carlson • *Carnegie Institution of Washington*

Derek Schutt • *Carnegie Institution of Washington, University of Wyoming*

David R. Bell • *Arizona State University*

Seismic velocities and rock densities are calculated for approximately 120 geothermobarometrically calibrated Cretaceous age mantle xenoliths from the Archean Kaapvaal craton and adjacent Proterozoic mobile belts (Figure 1) (James et al., 2004). Velocity and density estimates are based on the elastic and thermal moduli of constituent minerals under equilibrium P-T conditions at the mantle source. Results are consistent with tomographic evidence that cratonic mantle is higher in velocity by 0.5-1.5% and lower in density by about 1% relative to off-craton Proterozoic samples at comparable depths. Seismic velocity variations between cratonic and non-cratonic xenoliths are controlled dominantly by differences in geotherm, with compositional effects secondary. Differing geotherms between cratonic and non-cratonic regions have a relatively minor influence on density, where composition remains the dominant control.

Figure 2 shows computed velocities for low-T (equilibrium) cratonic xenoliths. The P-wave velocity-depth curve is positive over the depth range 50-180 km, whereas S-wave velocities decrease slightly over the same depth interval, consistent with recent surface wave studies (Larson et al., 2005). Seismic velocities and densities for the highly depleted cratonic xenoliths differ significantly from values predicted for both primitive mantle peridotite and mantle eclogite: Dense and more fertile primitive mantle peridotite, even for a cratonic geotherm, is characterized by velocities about 1% lower for P and about 1.5% lower for S relative to low-T garnet lherzolite at 150-km depth. For a cratonic geotherm, the calculated density of primitive garnet peridotite at 150-km depth is 2-3% greater than that for the Kaapvaal xenoliths.

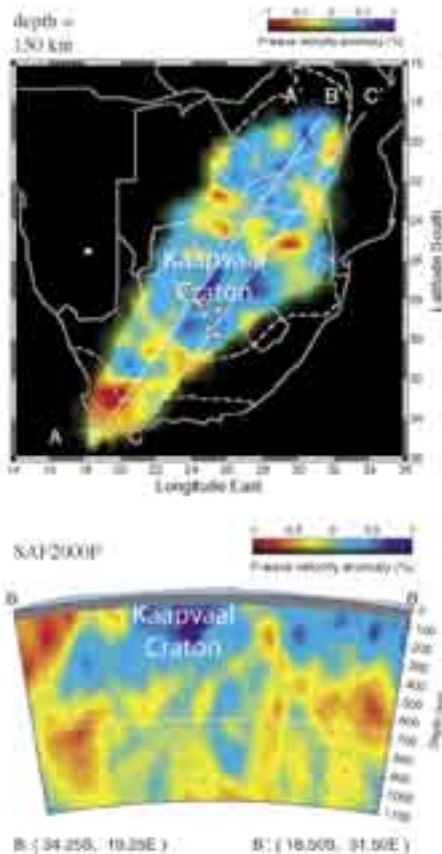


Figure 1. Relative P-wave velocity perturbations from inversion of seismic delay times (James and Fouch, 2002). Blues are positive velocity anomalies, red are negative. (Top) Horizontal section of velocity perturbations at 150 km depth with overlaid geologic provinces. (Bottom) Vertical cross-section along line B-B' of the horizontal section. Topography, scaled by a factor of 20, is shown in light green.

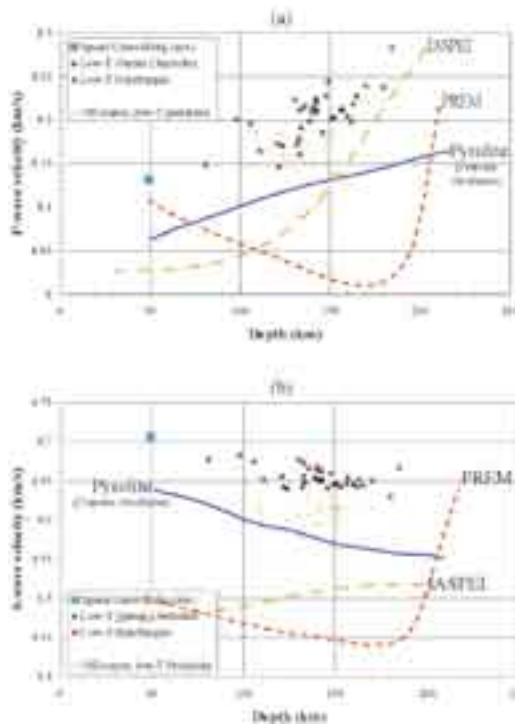


Figure 2. P and S velocities vs. depth for low-T (equilibrium) cratonic xenoliths (large symbols). Small orange symbols are for low-T off-craton xenoliths. The solid blue lines (pyrolite) are calculated velocities for primitive mantle peridotite based on a cratonic geotherm. The computed seismic velocities for cratonic xenoliths are substantially higher than are those for fertile mantle or for earth models IASPEI or PREM.

James, D.E., F.R. Boyd, D. Schutt, D.R. Bell, and R.W. Carlson, Xenolith constraints on seismic velocities in the upper mantle beneath southern Africa, *G-cubed*, 5, doi:10.1029/2003GC000551 (Q01002), 1-32, 2004.

James, D.E., and M.J. Fouch, Formation and Evolution of Archean Cratons: Insights from Southern Africa, in *The Early Earth: Physical, Chemical and Biological Development*, edited by C. Ebinger, C.M.R. Fowler, and C.J. Hawkesworth, pp. 1-26, Geological Society, London, 2002.

Larson, A.M., J.A. Snoko, and D.E. James, S-wave velocity structure beneath the Kaapvaal Craton from surface-wave inversions compared with estimates from mantle xenoliths, *Geophys. J. Int.*, submitted, 2005.

S-Wave Velocity Structure Beneath the KAAPVAAL Craton

Angela Marie Larson, J. Arthur Snoke • Virginia Polytechnic Institute

David E. James • Carnegie Institution of Washington

Two-station Rayleigh-wave inversions for pure paths across the Kaapvaal craton of southern Africa yield velocity-depth profiles consistent with seismic estimates obtained from approximately 100 mantle xenoliths brought to the surface in kimberlite pipes. The cratonic xenoliths, all from the undisturbed region of the southern Kaapvaal craton and all less than 100 Ma in age, had been previously analyzed thermobarometrically to obtain an equilibrium P-T profile of the cratonic mantle to about 180 km depth. We use the seismic velocity-depth and density-depth profiles calculated on the basis of these P-T data and the mineral modes and compositions of the xenoliths (James et al., 2004) to generate starting models for the inversion. The seismic velocity and density-depth profiles from xenolith data are merged via smooth joins with those of the PREM global model for depths of 220 km and greater. The inversion is based on a composite of 16 pure-path fundamental-mode Rayleigh-wave dispersion curves from five events (Figure 1) across the southern Kaapvaal craton as shown in Figure 2A (Larson et al., 2005). The S-wave velocity-depth models differ only slightly from the velocity-depth models estimated from mantle xenoliths (see Figure 2 and caption for further explanation). S-wave velocities beneath the craton decrease slowly with depth to about 4.6 km/s at 200 km, but never approach values that could be considered asthenospheric (i.e. 4.3–4.4 km/s). These results are consistent with other studies of cratonic areas showing that low velocity zones tend to be very weak. Moreover, the fact that the surface wave results are consistent with predictions from the xenolith data is a strong indication that the velocity structure (i.e. thermal structure) of the upper 180 km of the mantle beneath the Kaapvaal craton has not significantly changed over the past 100 million years.

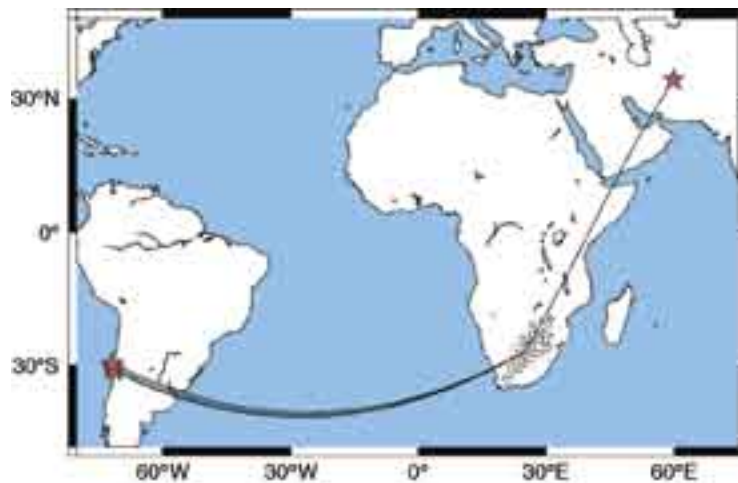


Figure 1. Epicenters of five events (stars) with great circle paths to Kaapvaal array. Fundamental mode Rayleigh wave inversion was based on a composite of sixteen pure-path two-station phase velocity dispersion curves with distant station backazimuths within two degrees of the near station backazimuth to the event (Figure 2).

James, D.E., F.R. Boyd, D. Schutt, D.R. Bell, and R.W. Carlson, Xenolith constraints on seismic velocities in the upper mantle beneath southern Africa, *G-cubed*, 5, doi:10.1029/2003GC000551 (Q01002), 1-32, 2004.

Larson, A.M., J.A. Snoke, and D.E. James, S-wave velocity structure beneath the Kaapvaal Craton from surface-wave inversions compared with estimates from mantle xenoliths, *Geophys. J. Int.* (submitted), 2005.

Snoke, J.A., and M. Sambridge, Constraints on the S-wave velocity structure in a continental shield from surface wave data: comparing linearized least squares inversion and the direct-search neighborhood algorithm, *J. Geophys. Res.*, 107 (10.1029/2001JB000498 (8 pp.)), 2002.

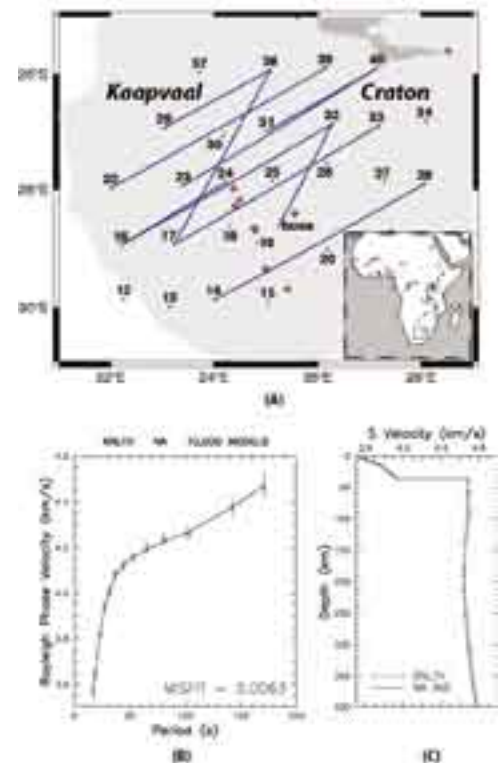


Figure 2. (A) Map of southern Kaapvaal craton indicating two-station Rayleigh-wave paths (blue lines) and xenolith localities (colored diamonds). (B) Neighborhooth Algorithm (NA) fit to the composite of 16 pure-path surface wave dispersion curves (Snoke and Sambridge, 2002); (Larson et al., 2005). (C) S-wave velocity-depth profile from NA inversion of pure-path Rayleigh wave data. Dashed line labeled XNLTH is the velocity-depth profile obtained from Kaapvaal craton xenolith data, merged with the global PREM model for depths > 220 km as a starting model. The maximum S-wave velocity around 4.75 km/s in the uppermost mantle decreases to a minimum of about 4.6 km/s at 200 km depth.

Kyrgyz Seismic Network KNET: Application of KNET Data in Scientific Researches

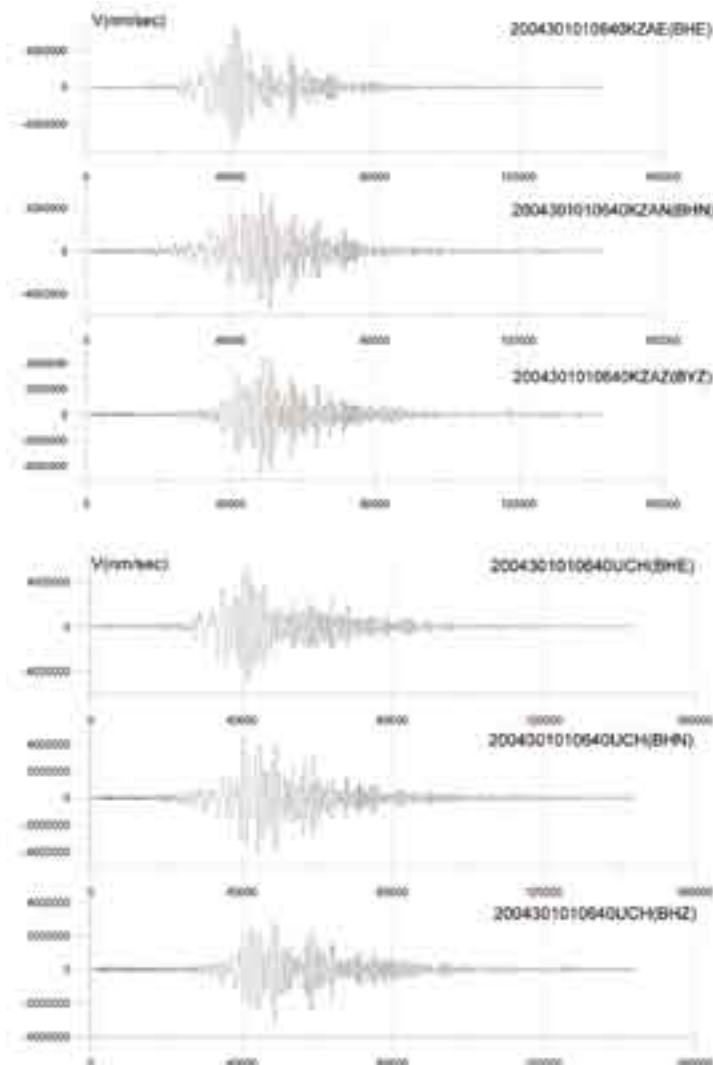
Seismic data from KNET are widely used by researches from many countries.

Research branches include the following topics:

- seismic velocity distribution and structure of Tien Shan and Central Asia;
- calibrated records for the study of seismic wave propagation;
- studies related to monitoring of nuclear explosions and their detection threshold;
- study of deep structures of the Earth,
- investigation of focal mechanisms and seismotectonic strains and many others.

KNET data are used by the national Institutes of Seismology of Kyrgyzstan and Kazakhstan, National Nuclear Center of Kazakhstan, Research Station of the Russian Academy of Sciences and different emergency departments. In recent years, different institutes of the Russian Academy of Sciences have started to use KNET data in their research. The following tasks are now being solved: on-line monitoring of regional seismic conditions, application of KNET data for routine report services, tracking of changes in regional geodynamic conditions for seismic risk assessment, studies of deep structures of investigated areas. The National Nuclear Center of Kazakhstan together with the Lamont laboratory (USA) uses KNET data to conduct verification research.

Due to the convenient territorial location of KNET, the Center monitors nuclear



explosions in China, India and Pakistan. In progress is the creation of a united digital catalogue of Central Asia that would include data from seismic networks of KNET, Kyrgyzstan, Kazakhstan and Uzbekistan. KNET data attracts the interest of scientists from China. They are interested in integration of KNET and digital networks located in the Tarim Platform. Due to the absence of good communication channels, at present these tasks remain unsolved. KNET data are also used during interpretation of results of electromagnetic monitoring, measurements of earth surface movements by the method of space geodesy, and analysis of geoelectric structure based on magnetotelluric sounding in relevance to problems of modern geodynamics.

There are enormous lists of publications based on KNET results (Appendix to reports on KNET exploitation, 2002, 2003, etc.), including three PhD theses:

1. Robert John Mellors (University of California, USA, 1995) – “Two studies in Central Asian seismology: a teleseismic study of the Pamir/Hindu Kush seismic zone and analysis of data from the Kyrgyzstan broadband seismic network.”
2. Albina Adamova (Institute of Seismology, NAS KR, 2004) – “Three-dimensional velocity model of Tien Shan earth’s crust by seismotomographic studies.”
3. N.A.Sycheva (Research Station RAS, 2005) – “Studies of focal focus mechanisms and seismotectonic deformations of the Northern Tien Shan by the data from digital seismic network KNET.”

Characterizing Crustal Deformation in the North Tien Shan Using Geodetic and KNET Seismic Data

Robert J. Mellors • San Diego State University

Alexander Zubovich • Scientific Station of Institute for High Temperatures, RAS, Bishkek, Kyrgyzstan

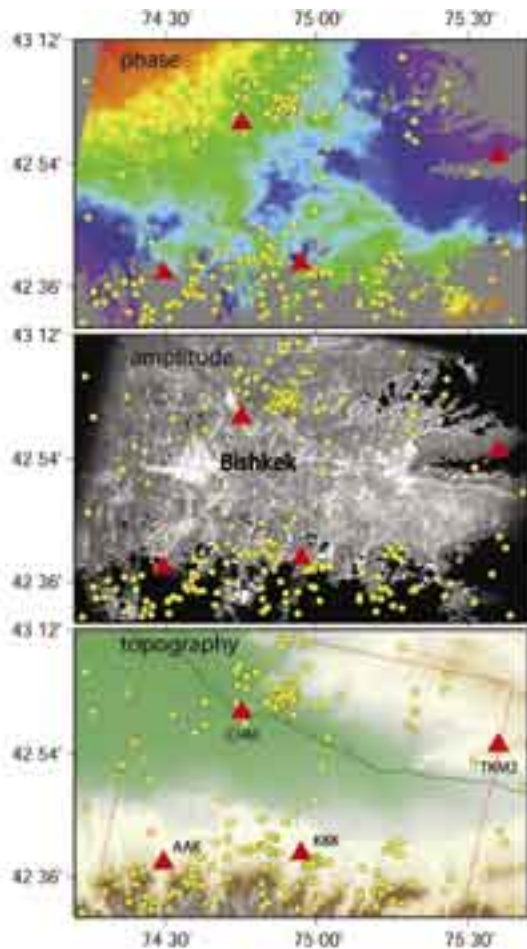


Figure 1. Images of the interferometric phase (top), radar amplitude (middle), and topography (bottom) centered on the city of Bishkek, Kyrgyzstan (bright area on amplitude image). The yellow dots are earthquakes and quarry blasts recorded by the KNET seismic network from 1992 to 1998. Red triangles denote KNET stations and the red line on the bottom (topography) image represents the radar scene boundaries. Color changes on the phase image represent variations in line-of-sight phase change as measured between two radar images taken in 1999. Due to the short time span, much of the visible phase change may be due to atmospheric effects in this specific image.

In an ongoing collaborative effort between San Diego State University and the Institute of High temperature Physics in Bishkek, Kyrgyzstan (IFTRAN), we investigate ground deformation in the North Tien Shan Mountains of Central Asia using a combination of interferometric synthetic aperture radar (InSAR), Global Positioning System (GPS), and seismic data from the Kyrgyzstan seismic network (KNET). The goals are to measure a range of deformation including continuous tectonic crustal deformation, episodic events associated with earthquakes, and ongoing slope failure events. By combining this data with seismicity maps from the KNET seismic catalog we identify areas of high strain with high spatial and temporal resolution. Identification of areas of high strain will be important for both scientific study of thrust movements and earthquake hazard mitigation. We are also working on identifying and modeling specific earthquakes with both InSAR data and KNET waveform data using method developed on Southern California data (e.g. Mellors et al., 2004).

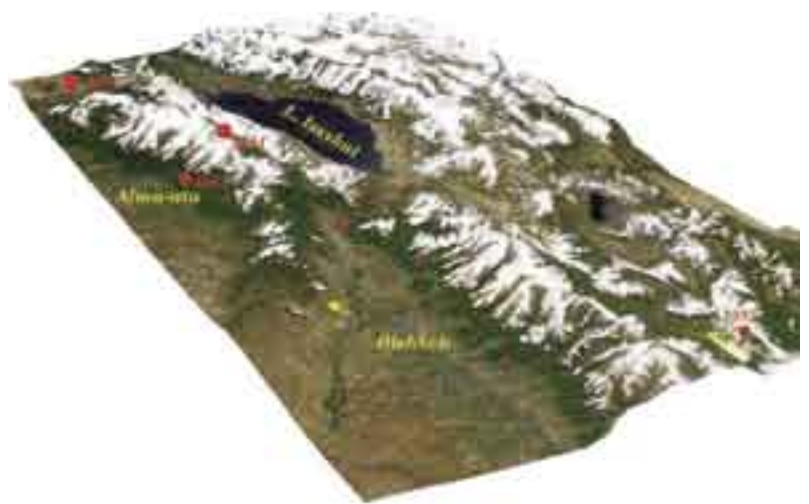


Figure 2. Optical satellite image of Northern Tien Shan draped over digital elevation model with background seismicity as recorded by KNET marked by yellow dots and historical large earthquake marked by red dots.

Mellors, R. J., H. Magistrale, P. Earle, and A. Cogbill, Comparison of moderate earthquakes in Southern California using InSAR and seismology, *Bull. Seismo. Soc. of Amer.*, 94, (6), 2004-20014, 2004.

The work is funded by the U.S. Civilian Research & Development Foundation.

High-Resolution Surface Wave Slowness Tomography in Central Asia

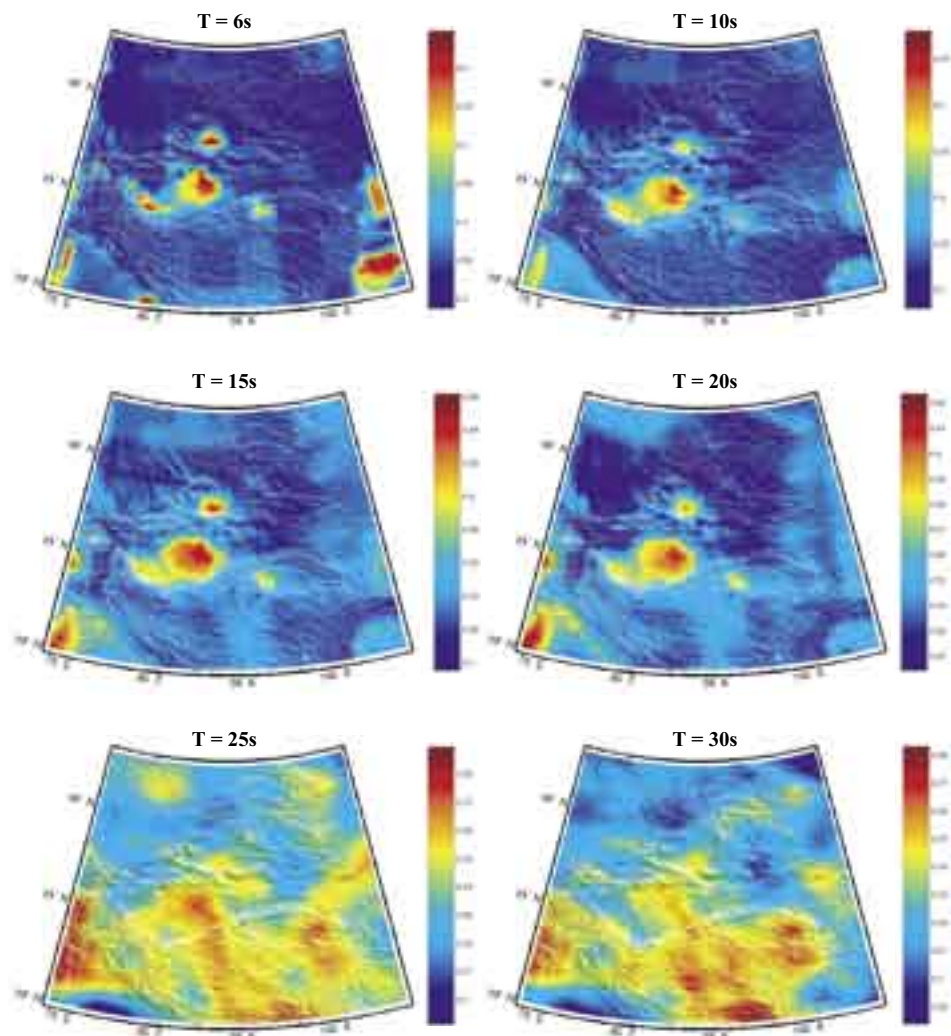
Monica Maceira, Steven R. Taylor, X. Yang • Los Alamos National Laboratory

Charles J. Ammon • Pennsylvania State University

Aaron A. Velasco • University of Texas at El Paso

We compute short-period, high-resolution surface-wave slowness maps for central Asia using Bayesian tomography. We focus on the region between 69° and 108°E and 29° and 54°N and used seismograms from more than 1100 events. Using multiple-filter and phase-matched filter techniques, we measured the dispersion characteristics of the signals between 6 and 30 seconds period. These Rayleigh-wave group velocity dispersion curves were used to compute high-resolution, half-degree cell size, slowness tomographic maps. Because short periods are primarily sensitive to upper crustal structures, the images display low velocities associated with the Tarim, Junggar, and Qaidam basins. Relatively high velocities are associated with mountainous tectonic features such as the Tian Shan. We validated our maps using dispersion curves from 640 events that were not used to construct the tomographic model. The model predictions show a significant variance reduction at short and intermediate periods (6 to 15 s) with respect to the prior model. Our model also shows 15% improvement in surface-wave detection capability with respect to previous 1D models. These high-resolution, short-period tomography maps can help improve regional magnitude estimations for construction of mb: Ms discriminants. Moreover, the short-period surface-wave tomographic results show unprecedented resolution that reveals greater geologic detail than has previously been achieved using surface waves, and which give us insight into the shear-velocity structure of the crust underlying this part of Asia.

Maciera, M., S.R. Taylor, C.J. Ammon, X. Yang, and A.A. Velasco, High-resolution Rayleigh wave slowness tomography for central Asia, *J. Geophys. Res.*, 110, No. B6, B06304, doi:10.1029/2004JB003429, 2005.



Rayleigh wave slowness maps for different periods. The slowness values are expressed in s/km. Note that the color scale is different for each map.

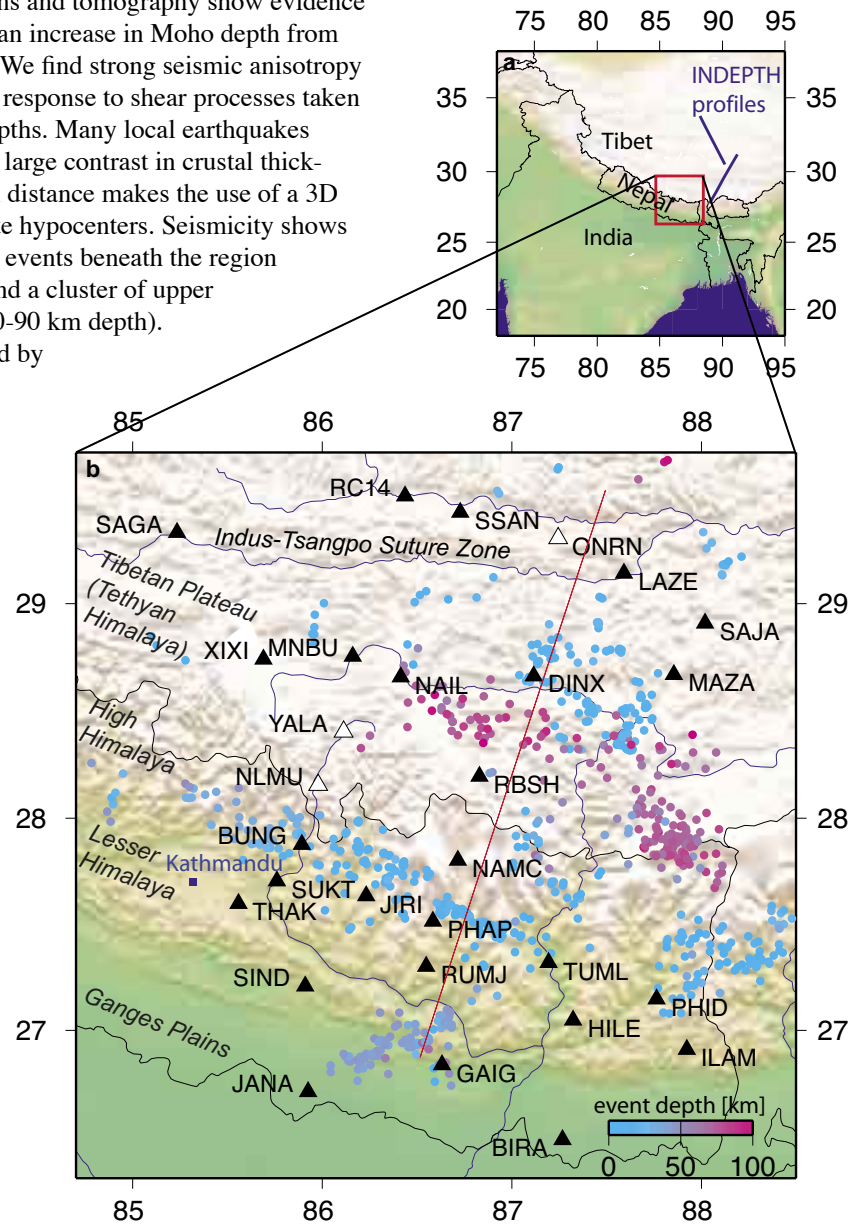
Seismic Imaging of the Himalayan Collision Zone

Sheehan, Anne F., Vera Schulte-Pelkum, Gaspar Monsalve, Tom de la Torre • University of Colorado at Boulder

Francis Wu • SUNY Binghamton

The Himalayan Nepal Tibet PASSCAL Seismic Experiment (HIMNT) included the deployment of 28 broadband seismometers throughout eastern Nepal and southern Tibet in order to better understand the mountain building processes of this region. Our new images from receiver functions and tomography show evidence of the basal decollement of the Himalaya and an increase in Moho depth from 45 km beneath Nepal to 75 km beneath Tibet. We find strong seismic anisotropy above the decollement, which may develop in response to shear processes taken up as slip in great earthquakes at shallower depths. Many local earthquakes were recorded during the deployment, and the large contrast in crustal thickness and velocity structure over a small lateral distance makes the use of a 3D velocity model important to determine accurate hypocenters. Seismicity shows strong alignment of shallow (15-25 km depth) events beneath the region of highest relief along the Himalayan Front, and a cluster of upper mantle earthquakes beneath southern Tibet (70-90 km depth).

The upper mantle earthquakes are not expected by weak-mantle models. Focal mechanisms of these upper mantle earthquakes are almost all strike-slip, markedly different from the normal faulting mechanisms observed for earthquakes in the mid and upper crust beneath Tibet. This change in the orientation of the major horizontal compression axis from vertical in the upper crust to horizontal in the upper mantle suggests a transition from deformation driven by body forces in the crust to plate boundary forces in the upper mantle. Several lines of evidence point to a decoupling zone in the Tibetan mid or lower crust, which may be related to the presence of a previously suggested flow channel in the Tibetan mid crust. Surface wave tomography results reveal a strong east-west lithospheric thickness variation across the Himalayan arc, with thicker lithosphere to the west of Kathmandu and thinner to the east. This lithospheric thickness variation seems to affect the nature of subduction across the Himalayan arc, and likely has implications for seismogenesis and the strength of the lithosphere. Our preliminary results indicate that upper mantle depth Tibetan earthquakes are only found in the regions with thinner lithosphere.



(Top) Overview map with topography. Study area outlined in red. Location of INDEPTH profiles shown in blue. (bottom) Topography map showing HIMNT seismic stations (black diamonds). Hypocenters located within our network are color coded by depth.

Receiver Function Imaging of the Eastern Syntaxis of Tibet

Brian Zurek, Anne Meltzer, Stephane Sol • *Lehigh University*

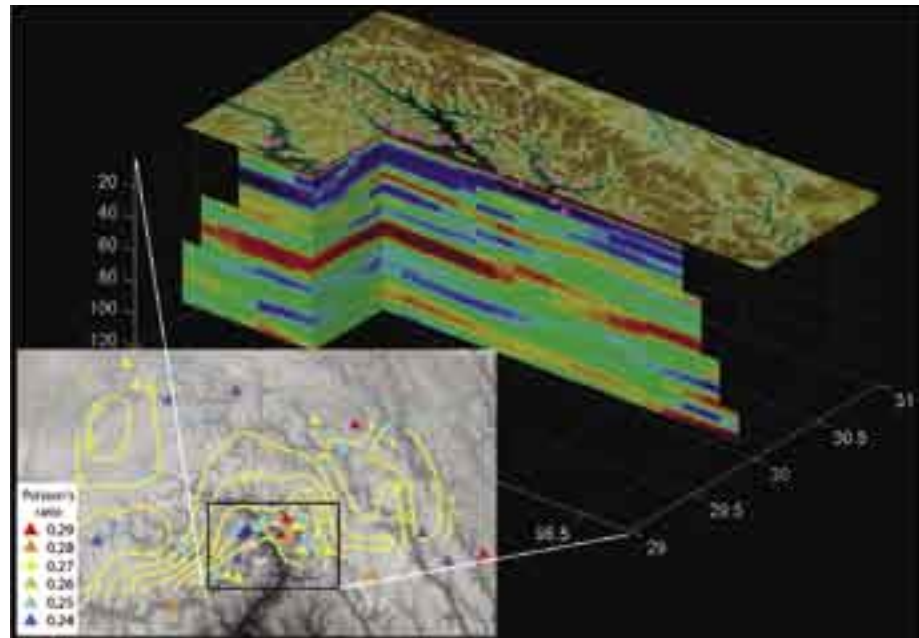
Xuanyang Zhang, Jianlong Zhang • *Chengdu Institute of Geology and Mineral Resources, China*

In July of 2003, as part of the larger Continental Dynamics study, a temporary PASSCAL seismic network (Eastern Syntaxis Seismic Experiment) was installed throughout the eastern syntaxis of Tibet. The network consisted of a 50-element regional, ~50 km spaced, broadband array that provides coverage across the eastern syntaxis and a dense, ~15 km spaced, array of 20 short-period seismometers, installed in the vicinity of the Namche Barwa Massif. The array extends the observations made from previous PASSCAL experiments in central Tibet across the syntaxis toward the eastern margin of the plateau.

A unique characteristic to the syntaxis is that shortening can be accommodated by mechanisms that either compress along strike of the collision or extruded laterally off to the side. This lateral motion is evident at the eastern syntaxis from Global Positioning data (GPS), which shows a clockwise rotation of material around the syntaxis. □

strike-slip faults from the central plateau across to the eastern margin. While a general picture of the architecture and kinematics can be observed on the surface, little was known about the internal processes that occur within the lithosphere when a collision comes to an end. This work is therefore part of a greater Continental Dynamics project concerning the geodynamics of indenter corners whose aim is to study: 1) how orogens and their plateaus come to an end, 2) how deformation is partitioned throughout the lithosphere and 3) the manifestation of the interaction between surface processes and tectonics.

Preliminary receiver function results have shown that the crustal thickness correlates reasonably well ($r = 0.52$) to filtered topography (200 km) with the thinnest crust occurring in the vicinity of the highly exhumed Namche Barwa Massif. The average Poisson's value throughout the syntaxis is reasonably low (0.25), which would indicate a fairly felsic crust, and the lack of extensive partial melt. These results would indicate that within the eastern syntaxis deformation appears to be coupled throughout the crust and that there is a connection between surface processes and tectonics.



Receiver function common conversion point stack of lithospheric structure for stations around the Namche Barwa massif, imbedded is a map of topography with depth to Moho superimposed as yellow contour lines, stations are color coded to crustal average Poisson's ratio.

Zeitler, P.K., A.S. Meltzer, P.O. Koons, D. Craw, B. Hallet, C.P. Chamberlain, W.S.F. Kidd, S.K. Park, L. Seeber, M. Bishop, and J. Shroder, Erosion, Himalayan geodynamics, and the geomorphology of metamorphism, *GSA Today*, 11 (1), 4-9, 2001.

Shear-Wave Splitting Beneath the Eastern Syntaxis Tibetan Experiment

Stéphane Sol, Anne Meltzer, Brian Zurek, Peter Zeitler • *Lehigh University*

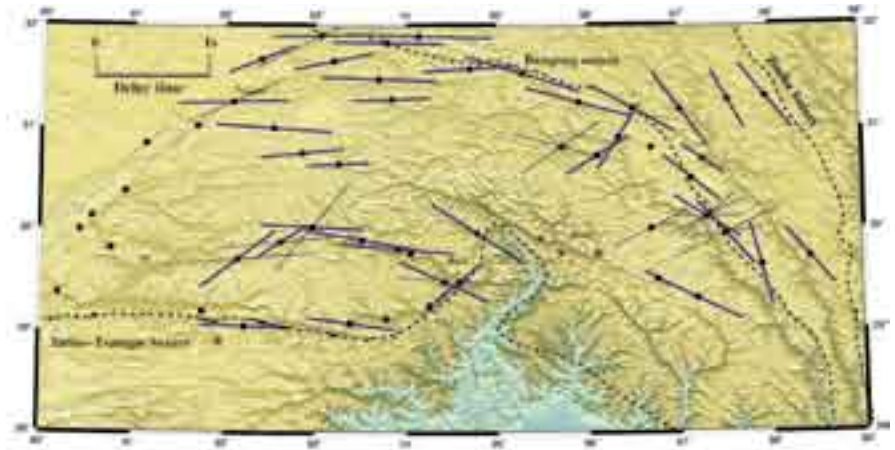
Xuang Zhang, Jianlong Zhang • *Institute of Geology and Mineral Resources, China*

A dense IRIS-PASSCAL passive seismic experiment of 48 broadband and 19 short-period stations was deployed in south-eastern Tibet from July, 2003, to November, 2004. The array is roughly bounded in the south by the Gangdese Thrust system that runs along the Indus-Yalu suture, and in its north and east margins by the Bangong-Nujiang suture. This experiment has been designed to answer crucial questions regarding to the geodynamics of the active Indian-Asian collision. One of these key questions is whether a decoupling zone exists separating the upper crust from the deeper lithosphere. To elucidate this crust-mantle relationship, we performed the SKS and SKKS splitting analysis at all the broadband stations from this array.

While earlier splitting studies have been done in the central part of the plateau using primarily a linear N-S configuration (McNamara et al., 1994; Sandvol et al., 1997; Huang et al., 2000), our rectangular array should not only confirm changes when crossing major tectonic boundaries, but also probe the potential lateral (E-W) variations in lithospheric structure. This E-W station coverage is important because this direction coincides with the direction of the main faults and should permit a better understanding of the interaction of lateral extrusion with lithospheric deformation.

At a regional scale, the observed splitting pattern does not exhibit a consistent widespread fast direction, ruling out the presence of anisotropy associated with asthenospheric flow at least as the main component. The most striking feature in this

□ of the suture not only when this one is roughly orogen-parallel, but also when the suture undergoes a perceptible change to S-E around the Eastern syntaxis. This remarkable southeastward clockwise rotation of strain around the Himalayan syntaxis has been previously recognized at crustal scale from multidisciplinary studies such as GPS or structural geology. Another observation is the N-E fast orientation at the western stations that appears to be consistent with the direction of the strike-slip fault that runs along the eastward Gulu rift. The observed bulk of anisotropy is contained in the lithospheric mantle as suggested by the fair amount of splitting as well as the Fresnel zone approach. The correlation between the surface deformation with the mantle strain directions suggests that the lower crust should be strong to allow an effective crust-mantle coupling in contradiction with some studies in the central plateau that implied the presence of a weak lower crust.



Topographic map summarizing the preliminary average fast shear-wave polarization direction and delay time at few INDEPTH stations (west) and at all the broadband stations of the Eastern Syntaxis experiment. The blue lines represent well-constrained fast directions while black lines indicate fast directions measured along a singular backazimuth. The red circles indicate null anisotropy from a wide range of backazimuths, the black circles alone represent null anisotropy associated with either a limited number of measurements or a poor azimuthal coverage, and the green circle depicts the Lhasa station (LSA) that exhibits a complex anisotropic pattern as a function of backazimuths (not shown here). The brown lines show splitting parameters from few INDEPTH stations (McNamara et al., 1994; Sandvol et al., 1997). The suture zones are represented by black dotted lines.

Structure and Deformation of the Tibetan Lithosphere

Nikolai M. Shapiro, Michael H. Ritzwoller • University of Colorado at Boulder

Intermediate-period Rayleigh and Love waves propagating across Tibet are affected by strong radial anisotropy within the mid-to-lower crust, consistent with a thinning of the middle crust by about 30% (Shapiro et al., 2004). The anisotropy is largest in the western part of the plateau (Figure 1) where moment tensors of earthquakes indicate active crustal thinning. The preferred orientation of mica crystals resulting from crustal thinning can account for the observed anisotropy. The mid-to-lower crust of Tibet appears to have thinned more than the upper crust, consistent with deformation of a mechanically weak layer in the mid-to-lower Tibetan crust that flows as if confined to a channel.

Inversion of broadband surface-wave dispersion data (Ritzwoller et al., 2002; Shapiro and Ritzwoller, 2002) reveals a coherent pattern of high-velocities in the mantle underlying the Tibetan plateau, as shown in Figure 2. The high velocities in western Tibet appear to be derived from underthrust Indian lithosphere and a more speculative underthrusting of Asian lithosphere is apparent in eastern Tibet. In central Tibet, however, the high-speed zone appears to be detached from both the Indian and Asian lithosphere. Overlying this feature is a low-speed anomaly coincident with high attenuation and the blockage of regional phases.

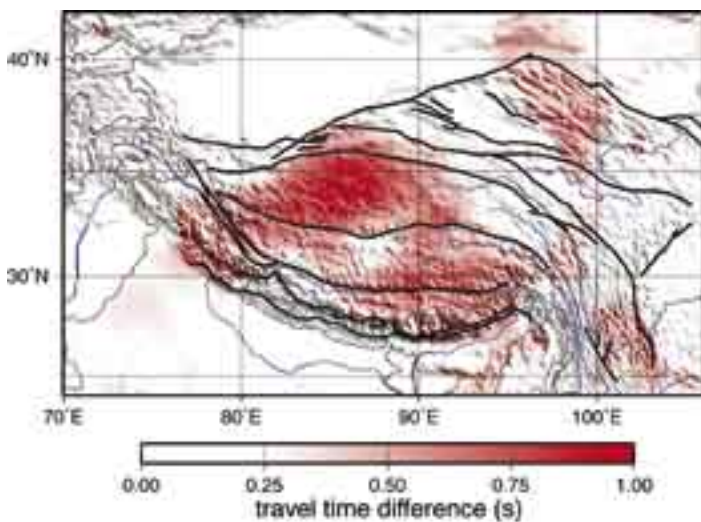
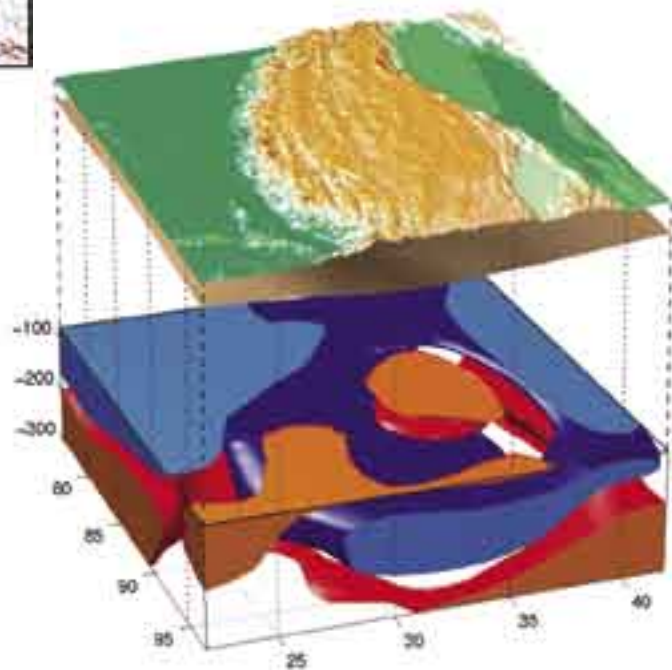


Figure 1. Strength of radial anisotropy in the middle crust from the best-fitting radially anisotropic model, represented as the idealized travel time difference between SV and SH waves propagating vertically through the middle crust. Solid lines show selected major active faults, and dashed lines are approximate locations of sutures.

Figure 2. Smoothed isosurface representation of shear wave speeds beneath the Tibetan Plateau. The blue and red surfaces are the +2% and the -1% perturbations, respectively, relative to a regional average at each depth. Topography on the surface and the Moho is vertically exaggerated. (Moho topography is estimated along with crust and mantle velocities.)



Ritzwoller, M.H., N.M. Shapiro, M.P. Barmin, and A.L. Levshin, Global surface wave diffraction tomography, *J. Geophys. Res.*, 107(B12), 2335, doi:10.1029/2002JB001777, 2002.

Shapiro, N.M. and M.H. Ritzwoller, Monte-Carlo inversion for a global shear velocity model of the crust and upper mantle, *Geophys. J. Int.*, 151, 88-105, 2002.

Shapiro, N.M., M.H. Ritzwoller, P. Molnar, and V. Levin, Thinning and flow of tibetan crust constrained by seismic anisotropy, *Science*, 305, 233-236, 2004.

Lithospheric Deformation within a Continental Strike-Slip Fault Zone: Marlborough Fault System, South Island, New Zealand

Charles K. Wilson • *University of Colorado at Boulder, now at Lamont-Doherty Earth Observatory*

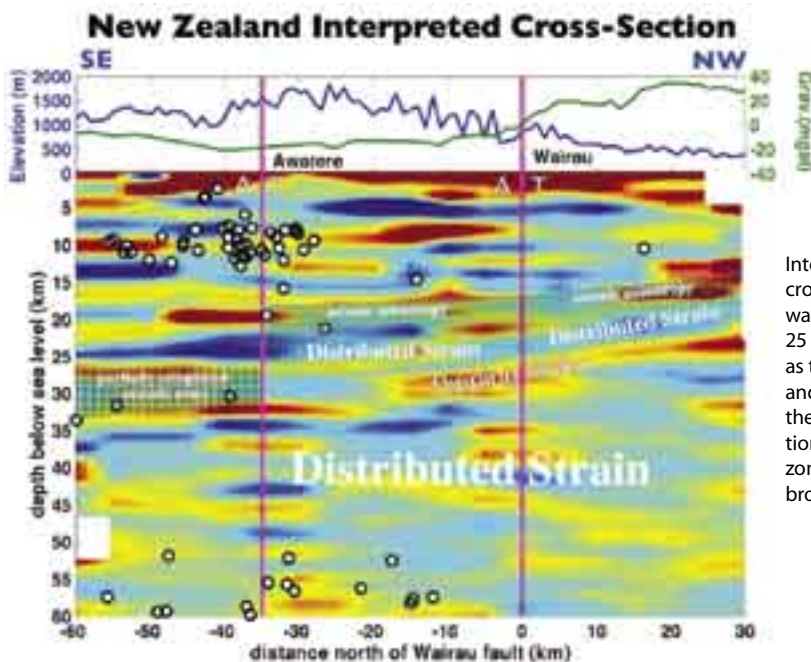
Craig H. Jones, Peter Molnar, Anne Sheehan • *University of Colorado at Boulder*

Oliver S. Boyd • *University of Colorado at Boulder, now at U.S. Geological Survey, Golden*

Near-surface deformation associated with major continental strike-slip faults is easy to recognize simply by walking the surface trace of the fault system. Less clear are the mechanisms that accommodate slip between continental plates in the lower crust and upper mantle. Do strike-slip faults continue as narrow near-vertical shear zones into the mantle? Is strain in the lower crust distributed over a broad region with flow in the lower crust accommodating relative motion between the upper crust, lower crust, and mantle lithosphere? Answering these questions would help us to understand the depth and location of earthquakes and the coupling between the crust and mantle along strike-slip boundaries, as well as the strength of the continents as a function of depth.

The South Island of New Zealand straddles a major strike-slip fault system that delineates the boundary between the Pacific and Australian plates. The system is well developed with several hundred kilometers of right lateral offset. At the northern end of the South Island, present day relative motion is almost entirely strike-slip and is distributed across the 4 major faults of the Marlborough fault system with most of the total offset being absorbed along the northernmost strand, the Wairau fault.

From December, 2000, to June of 2002, we occupied over 100 sites across the Marlborough Fault System with short-period and broad-band three component instruments provided by IRIS-PASSCAL. Our scientific goals were to create crustal images of the fault system using teleseismic converted waves and to identify the presence or absence of seismic anisotropy in the crust and upper mantle beneath the fault system. Seismic images produced by the experiment showed a nearly 10-kilometer difference in crustal thickness from north to south beneath the Wairau fault that was connected by a Moho ramp. Azimuthal variations in the amplitude of the converted phases supported the ramp interpretation as well as the presence of crustal anisotropy at a mid-crustal interface. These observations indicate that strike-slip deformation associated with the relative motion between the Pacific and Australian plates becoming distributed over a broader region (~60 km) in the lower crust and upper mantle beneath the Wairau fault (Wilson et al., 2003).



Interpreted Common-Conversion-Point Stacked cross-section of depth-migrated teleseismic converted waves. We interpret the strong conversion from near 25 km depth that dips to the south beneath the Wairau as the Moho. The smooth transition in Moho depth and the presence of mid-crustal anisotropy beneath the Wairau fault support the conclusion that deformation is not confined to a narrow near-vertical shear zone in the lower crust but instead is distributed over a broad region.

Wilson, C.K., Jones, C.H., Molnar, P., Sheehan, A.F. and O.S. Boyd, Distributed deformation in the lower crust and upper mantle beneath a continental strike-slip fault zone: Marlborough Fault System, South Island, New Zealand, *Geology*, 32, 837-840, 2004.

Seismically Imaging the East Antarctica/West Antarctica Boundary with TAMSEIS

Jesse Lawrence, Douglas Wiens, Patrick Shore • Washington University

Andrew Nyblade, Sridhar Anandkrishnan, Donald Voight • Pennsylvania State University

The Transantarctic Mountain Seismic Experiment (TAMSEIS) provided (data to calculate) receiver functions, surface wave phase velocities, and differential S-wave attenuation measurements for parts of the West Antarctica Rift System (WARS), the Transantarctic Mountains (TAMs), and East Antarctica (EA). The 41 broadband seismometers deployed as part of TAMSEIS provided new insight into the differences between the WARS, the TAMs, and EA crust and mantle. Combined receiver function and phase velocity inversion with niching genetic algorithms produced accurate crustal and upper-most mantle seismic velocity models (Figure 1). The crustal thickness increases from 20 ± 2 km in the WARS to a maximum of 40 ± 2 km beneath the crest of the TAMs at 110 ± 10 km inland. Farther inland, the crust of EA is uniformly 35 ± 3 km thick over a lateral distance greater than 1300 km. A temperature increase of $\sim 300^\circ\text{C}$ and density decrease of $\sim 1\%$ beneath WA are indicated by high phase velocities and low attenuation beneath EA and low velocities with high attenuation beneath. The transition between East and West Antarctica occurs 100 ± 50 km inland from the Ross Sea.

The seismically inferred density profile agrees remarkably well with observed gravity and topography anomalies measured by airborne geophysical surveys. The positively buoyant thermal and erosional loads found in the TAMs are sufficient to cause the observed pattern of asymmetric slump blocks through flexural uplift (Figure 2).

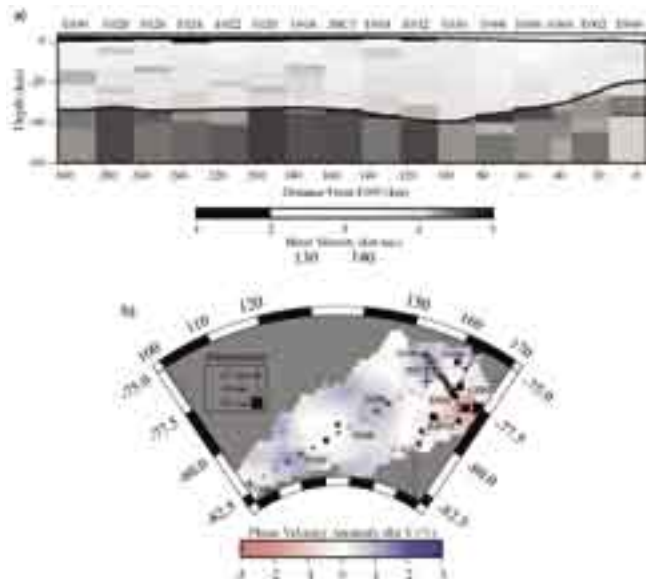


Figure 1: a) This composite 2D profile of shear velocity follows the (roughly) E-W linear sub-array across the TAMs. b) The average differential attenuation measurement for each station correlates remarkably well with 120-second phase velocities.

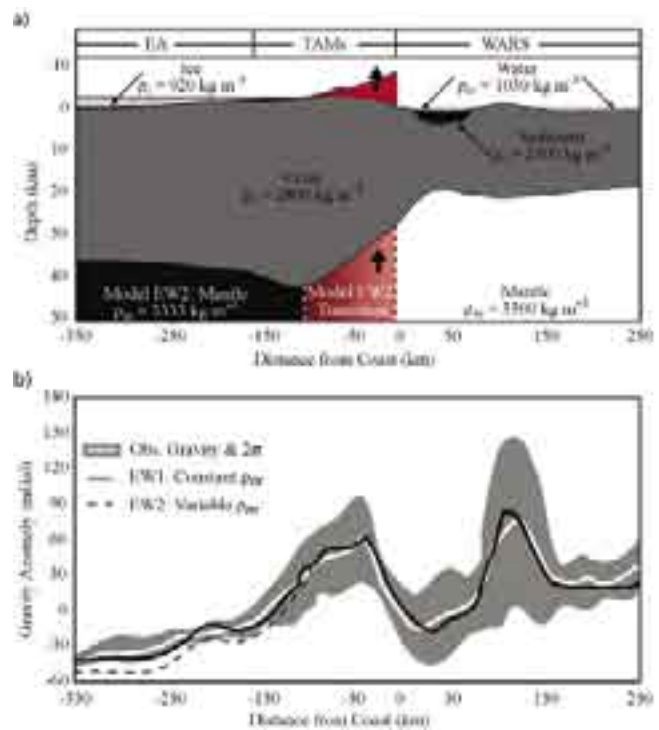


Figure 2: The a) 2D density models used for calculation of b) theoretical free-air gravity. The gravity data are clearly better fit by model EW2, in which the mantle density increases from West to East Antarctica.

Upper Mantle Velocity Structure Beneath the TAMSEIS Network, Antarctica

Timothy Watson, Andrew Nyblade, Sridhar Anandkrishnan, Donald Voight • *Pennsylvania State University*

Douglas Wiens, Patrick Shore • *Washington University*

The Transantarctic Mountains (TAM), extending more than 3500 km in length and reaching heights of 4500m, are characterized by gently tilted fault blocks resulting from vertical crustal movement in the Cenozoic. Paralleling much of the West Antarctic Rift System (WARS), the TAM is considered by many to be a classic example of rift flank uplift, however evidence supporting a clear uplift mechanism has yet to be provided. Thus the PASS-CAL Transantarctic Mountain Seismic Experiment (TAMSEIS) was conducted to investigate the crustal and upper mantle structure beneath the TAM as well as the adjacent East Antarctic craton and WARS in the vicinity of Ross Island. TAMSEIS consisted of 41 temporary broadband seismometers deployed between December, 2000, and December, 2003, in three arrays (Figure 1a).

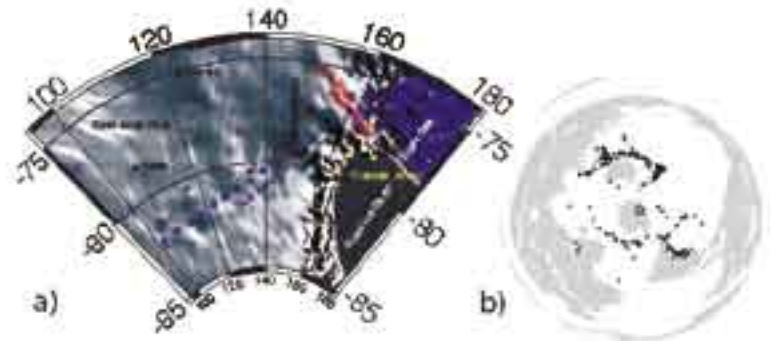


Figure 1. a) An elevation map of the TAM in the Ross Sea region displaying the TAMSEIS network. The blue circles mark the N-S Array stations (80 km station spacing), the red triangles mark the E-W array stations (20 km station spacing), the yellow squares mark the Coastal Array stations (variable distances), and the black triangles mark the GSN station locations. b) An earthquake distribution map displaying the locations of the 324 events used in the P-wave tomography study.

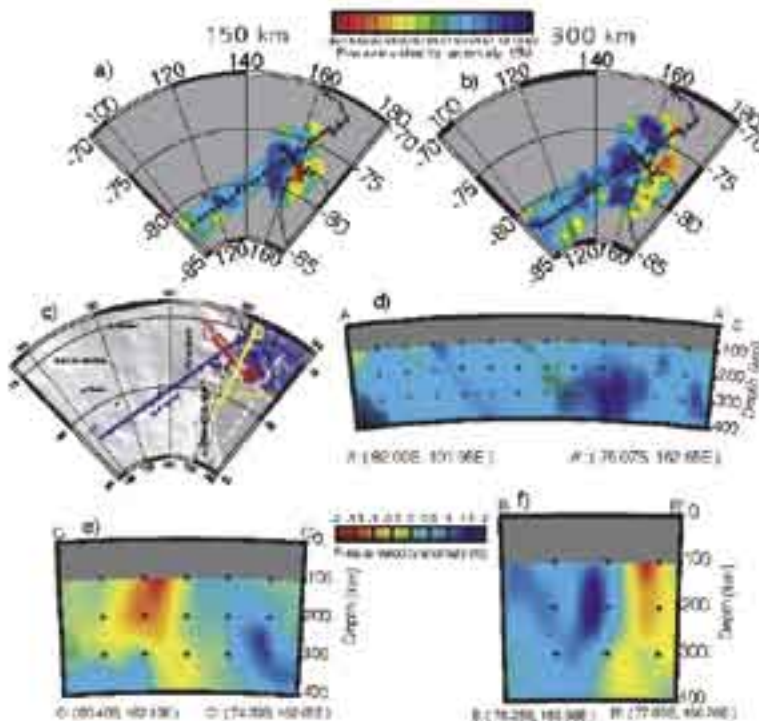


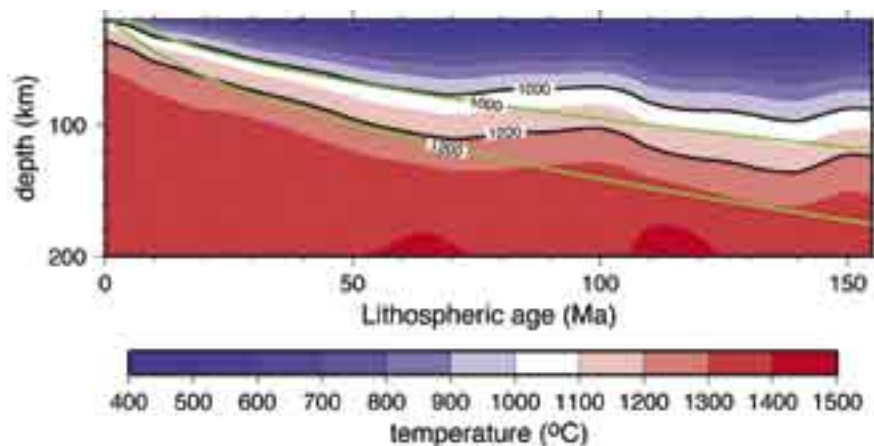
Figure 2. a) 150 km depth slice through the P-wave model b) 300 km depth slice through the P-wave model. c) Transect key d-f) Cross sections A-A', B-B' & C-C' respectively, through the P-wave model from 100 - 400 km depth.

Utilizing the TAMSEIS data as well as data from 3 Global Seismic Network stations (SBA, VNDA, & TNV), body-wave tomography was conducted to estimate the upper mantle velocity structure beneath the stations. In total, 3934 P-waves were picked from 324 events (Figure 1b) and 2244 S-waves were picked from 174 events. Both P and S wave tomography results reveal a low-velocity anomaly in the upper mantle extending 200 km beneath the TAM in the vicinity of McMurdo Sound. The low-velocity anomaly extends NNE with depth beneath the Ross Sea. At its western boundary, the low-velocity anomaly makes a sharp contact with the faster velocities that accompany the upper mantle beneath the East Antarctic Craton (Figure 2d,f).

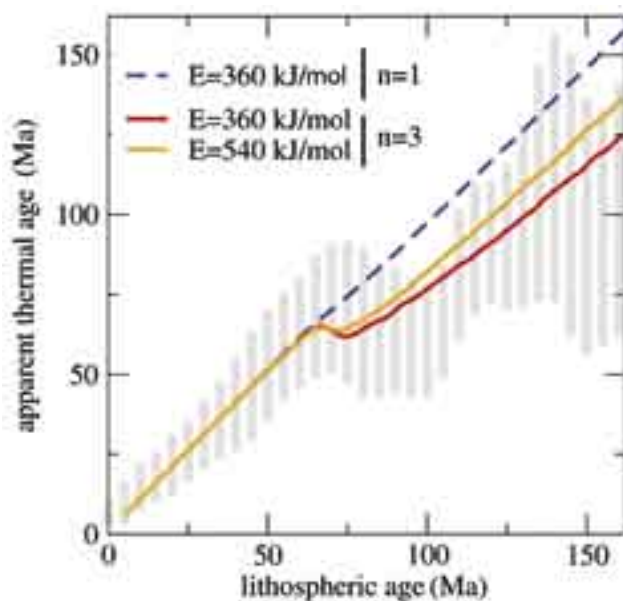
Cooling History of the Pacific Lithosphere: Evidence for Thermal Boundary Layer Instabilities and Dislocation Creep

Michael H. Ritzwoller, Nikolai M. Shapiro, Shijie Zhong • University of Colorado at Boulder

Numerous studies based mostly on surface observables (e.g., topography, heat flux) have established that the oceanic lithosphere, particularly across the Pacific, does not cool continuously as it ages. Observations of surface wave dispersion used to construct a model of shear wave speeds and temperatures in the upper mantle establish that the Pacific lithosphere has experienced a punctuated cooling history (Figure 1), cooling diffusively at ages younger than ~70 Ma and then reheating in the central Pacific between ages of about 70 and 100 Ma. At ages from 100 Ma to about 135 Ma, the processes of reheating are substantially weaker than in the Central Pacific. Uppermost mantle temperatures can also be summarized in terms of the “apparent thermal age” of the lithosphere (Figure 2). Using numerical simulations of mantle convection with realistic plate motions and various rheologies, thermal boundary layer instabilities (TBI) are shown to develop naturally as the plate cools. The average thermal structure of the Pacific upper mantle can be matched if the mantle deformation mechanism is dislocation creep ($n = 3$) with an activation energy of about 360 kJ/mol, consistent with that for dislocation creep for olivine determined from laboratory studies.



Average temperature profile of the Pacific upper mantle versus lithospheric age. The green lines are isotherms from a diffusively cooling half-space. An average temperature perturbation relative to the half-space cooling model develops in the Central Pacific due to processes of reheating that occur between 70 and 100 Ma, revealing the punctuated cooling history of the Pacific lithosphere.



Apparent thermal age plotted versus lithospheric age across the Pacific. Apparent thermal age is defined as the lithospheric age at which a purely diffusively cooling temperature profile would most closely resemble the observed thermal structure. For a Newtonian mantle rheology governed by diffusion creep ($n = 1$), realistic activation energies do not reproduce the observed average thermal structure of the Pacific. But for a non-Newtonian rheology governed by dislocation creep ($n = 3$), realistic activation energies can reproduce the punctuated cooling history of the Pacific.

Ritzwoller, M.H., N.M. Shapiro, and S. Zhong, Cooling history of the Pacific lithosphere, *Earth Planet. Sci. Lett.*, 226, 69-84, 2004.

Van Hunen, J., S. Zhong, N.M. Shapiro, and M.H. Ritzwoller, New evidence for dislocation creep from 3-D geodynamic modeling of the Pacific upper mantle, submitted 2005.

Advances in Active-Source Seismic Imaging Using Traveltime and Waveform Tomography

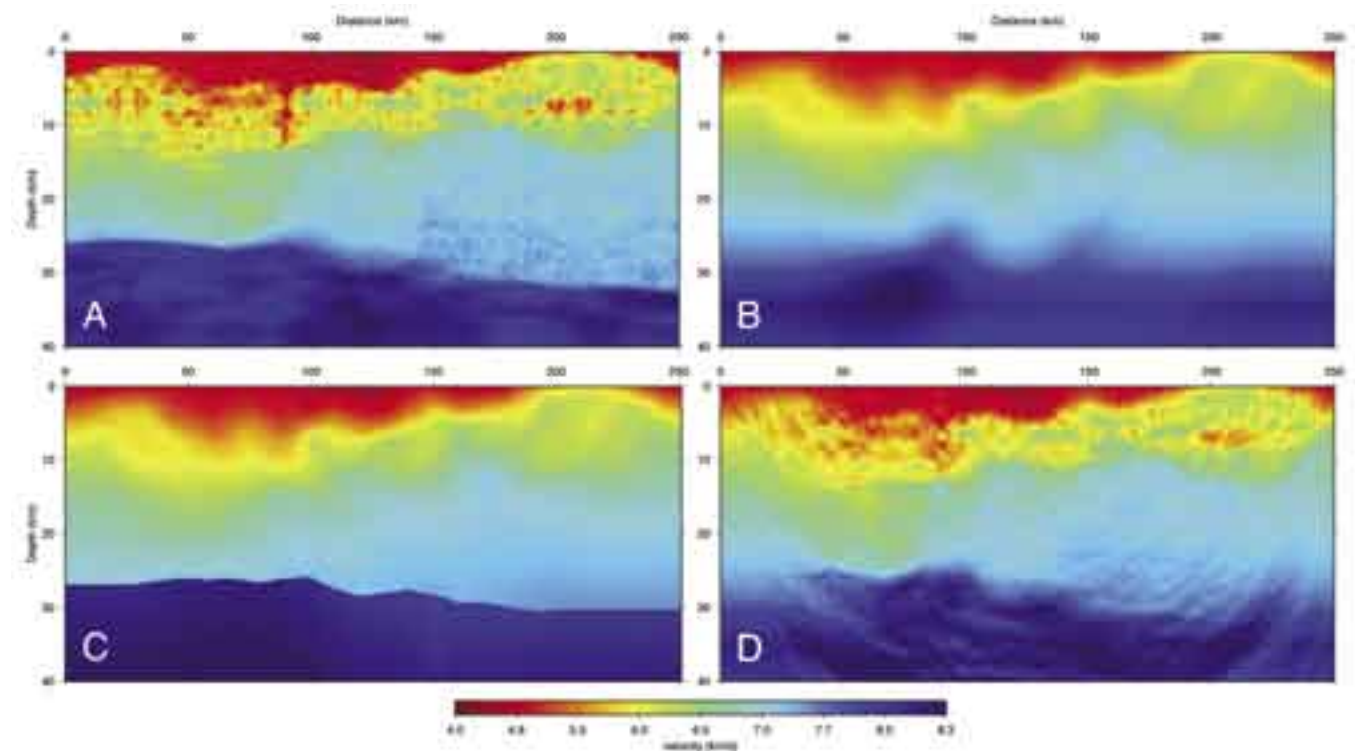
Colin A. Zelt • *Rice University*

John A. Hole • *Virginia Polytechnic Institute*

R. Gerhard Pratt • *Queen's University, Canada*

In 2003, as part of a workshop funded by IASPEI, NSF, IRIS and Virginia Tech, a realistic active-source synthetic dataset was made available to the community for the purpose of testing inversion and imaging algorithms by workers who, at the time, did not know what the true model was. The synthetic wide-angle dataset, consisting of 51 shots and 2779 receivers, was calc

hole/ccss/. The survey design is consistent with experiments that could be supported by the IRIS-PASSCAL Instrument Center in about three years. The true model contains large-scale features such as a low-velocity zone and regions where the crust-mantle boundary is sharp and smooth, as well as intermediate to wavelength-scale stochastic features. Both first arrival and simultaneous PmP/Pn traveltimes were applied to obtain smooth velocity models that compare favorably with the large-scale features of the true model. The model obtained from first-arrival traveltimes was used as a starting model for 2-D acoustic, frequency-domain waveform tomography. The final model from waveform tomography matches the large and intermediate-scale (down to ~ 1 km) features of the true model, including the low-velocity zone and the structure of the crust-mantle transition zone. The combined results from traveltimes and waveform tomography show the complementary nature of these approaches and the potential for the analysis of real active-source crustal data in the future.



True velocity model and inversion results. A) True model. B) Model derived from traveltimes tomography using first arrivals. C) Model derived from traveltimes inversion using first arrivals and wide-angle reflections from the Moho. D) Model derived from waveform tomography using (B) as the starting model.

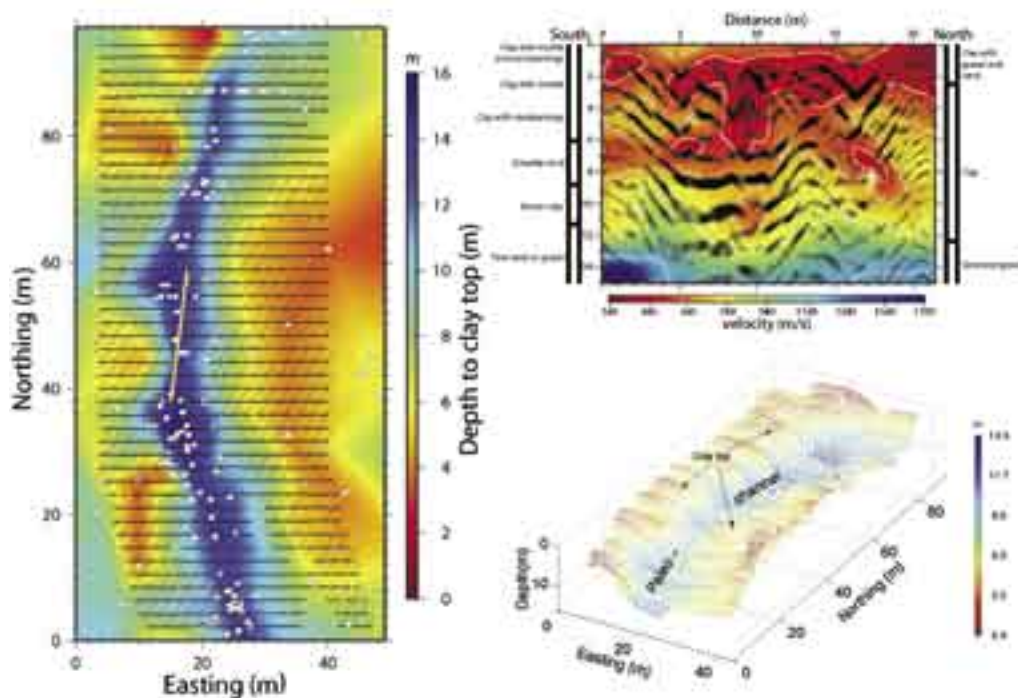
Hole, J.A., C. A. Zelt and R. G. Pratt, *Advances in Controlled-Source Seismic Imaging*, *EOS*, 86, No. 18, p. 177, 181, 2005.

High-Resolution Waveform Tomography at a Ground Water Contamination Site

Fuchun Gao, Gian Luigi Fradelizio, Alan Levander, Colin Zelt • Rice University

Shallow (< 20 m) High-Resolution seismic compressional velocity models have been constructed at a ground water contamination site at Hill Air Force Base (HAFB) to identify the base of a paleo-channel in a clay aquitard buried beneath alluvium, using data recorded by 630 PASSCAL instruments. The dataset has useful energy between ~10 Hz and ~250-350 Hz. Waveform tomography has been applied to a VSP-2D surface dataset and a 3D surface reflection dataset (Figure, left). The velocity model from the former application (Gao et al., 2005) reveals surprisingly large vertical and lateral velocity heterogeneities, which may compromise some conventional seismic imaging tools (Figure, top right). The vertical velocity gradient is ~80m/s/m in the paleo-channel. Lateral heterogeneities in velocity as large as 200 m/s occurring over ~1.5 m are recovered in the model. The structural details in the model correlate well with two lithologic logs and a post-stack depth-migrated image, using the 2D data recorded at the surface between the two VSP boreholes.

Waveform tomography applied to the 3D surface reflection dataset yields 45 2D velocity models for profiles sorted out from the 3D dataset. The locations of the 45 2D seismic profiles are the 45 geophone lines shown as black lines in (Figure, left). From each of the 45 waveform tomography models, the cross-sectional geometry of the buried paleo-channel can be identified by following the velocity contour of 800m/s. The combination of the 45 cross-sectional images gives the 3D geometry of the paleo-channel bottom (Figure, bottom right). The 3D geometry reconstructs the structural host for the polluted ground water. Since the pollutant DNAPLs are heavier than water, they are believed to pond at the deepest points of the paleo-channel. The reconstructed geometry can be used for placement of extraction wells at the site to aid remediation efforts.



Location of the experiment site in UTM coordinates (left plot), the correlation of the waveform tomography velocity model with two lithologic logs and a depth migrated reflection image (top right), and the reconstructed 3D geometry of the paleo-channel (bottom right). In the left plot, parallel black lines are geophone lines, red dots are source locations in the 3D reflection experiment and the light yellow line is the location of surface spread of the VSP experiment. The color map shows the depths to top of clay based on boreholes. White circles are borehole locations. A velocity model from travel time tomography is used in the depth migration. The origin point (0,0) of the site map (left) is at (570127.22 m, 89219.48 m) in UTM coordinates.

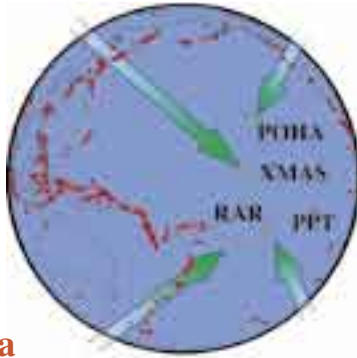
Gao, F., A. Levander, R. G. Pratt, C. Zelt and G. Fradelizio, Waveform tomography at a ground water contamination site: VSP-surface dataset, *Geophysics* (in press), 2005.

Hunting for Ocean Island Moho: The Snipe Bites Back

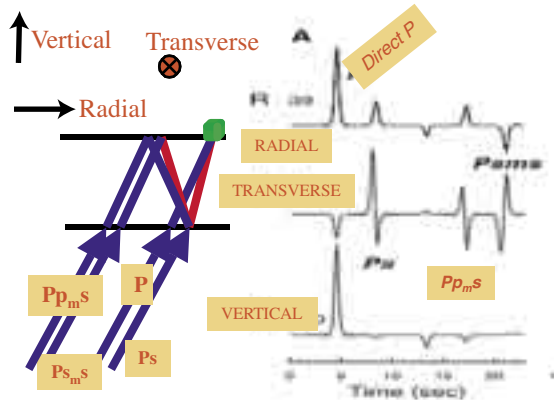
Garrett Leahy & Jeffrey Park • Yale University

Vadim Levin • Rutgers University

Number of events per station
 POHA -- 76
 RAR -- 166
 XMAS -- 67
 PPT -- 187



Idealized Data

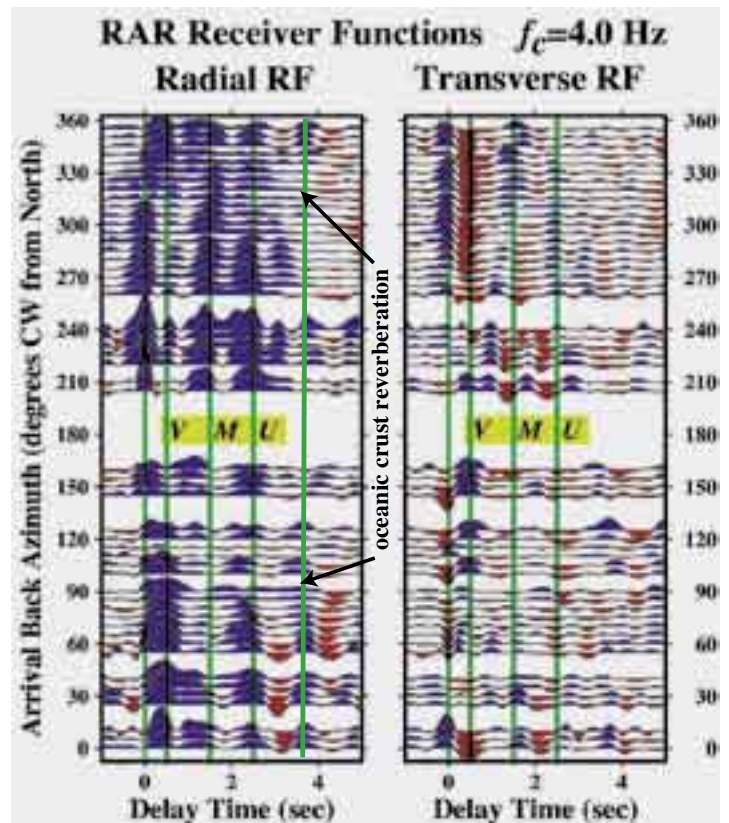
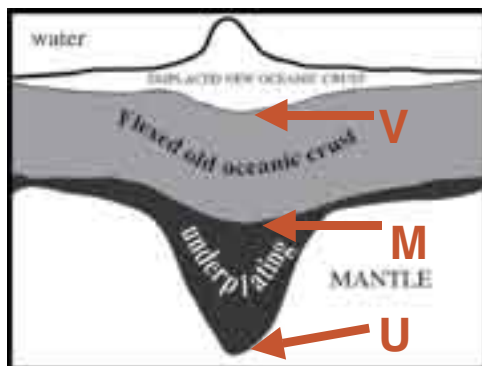


The structure of oceanic crust conforms in general to a very simple model. However, fine scale variations of this structure in anomalous regions (such as beneath ocean islands) remain poorly resolved. We estimated teleseismic receiver functions (RFs) at three GSN stations (RAR, POHA, XMAS) and one Geoscope station (PPT) on islands in the Pacific region. The RF method is ideal for examining fine structure of the crust because it is sensitive to the interfaces between layers, though less sensitive to average wavespeed. RFs at these ocean island stations display a train of Ps conversions from shallow depths, rather than the isolated Moho conversion typically seen at continental stations. We find that a simple three-layer structure explains the main features of the RFs, with old oceanic crust sandwiched between an extruded volcanic layer and an underplated layer. GSN data indicate that ocean islands share a common structure, a principal feature of which is crustal underplating, with a total crustal thickness of 11-20 km.

Because new receiver function estimators resolve higher frequencies, more detail emerges...

- V – bottom of the volcano
- M – original oceanic Moho
- U – underplated Moho

Matched amplitude variation for radial/trans RF on the V interface indicates interface dip or anisotropy



G. Leahy and J. Park, Hunting for Oceanic Island Moho, *Geophys. J. Int.*, 160, 1020-1027, 2005.

Seismic Hazards Investigations in Puget Sound (SHIPS): I

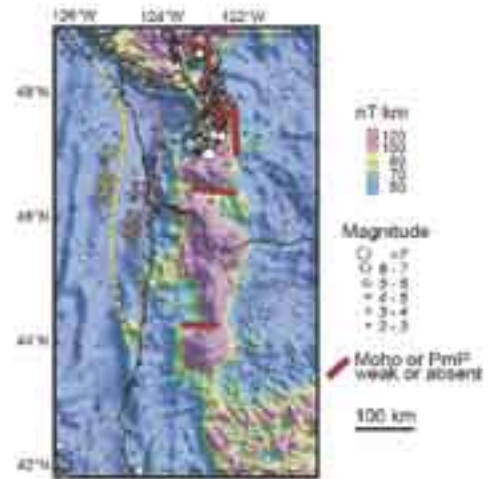
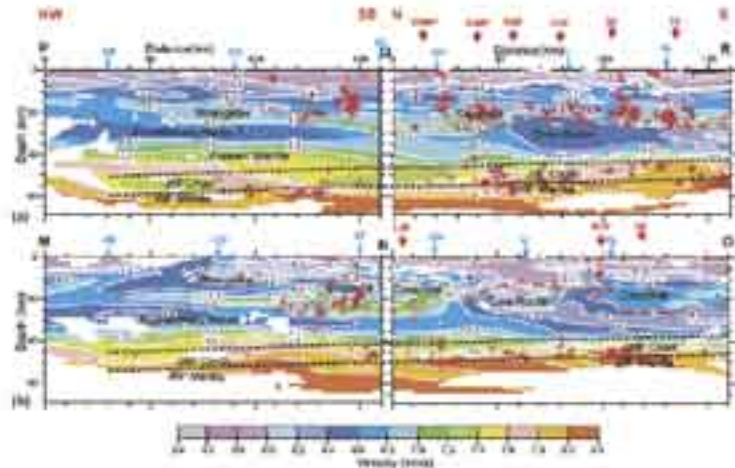
Tom Brocher • U.S. Geological Survey, Seattle

The SHIPS Working Group

In 1998, 1999, 2000, and 2002, the U.S. Geological Survey, the Geological Survey of Canada, and academic collaborators conducted a series of seismic reflection and refraction studies of crustal and upper mantle structure, as well as site response studies in western Washington and southwestern British Columbia. These experiments have been conducted under the umbrella of Seismic Hazards Investigations in Puget Sound (SHIPS), and each has involved the use of a large (generally between 200 and 670) number of IRIS/PASSCAL short period recording systems and sensors. A variety of controlled sources, including airguns, explosions, and even the implosion of the Kingdome, were used in these studies and a number of local earthquakes and teleseisms, including the 1999 Chi-Chi earthquake, were recorded.

SHIPS provided an exceptionally detailed view of the forearc of the Cascadia subduction zone. Perhaps the most important new result is the mapping in three dimensions of a low velocity zone at the base of the crust (Figure 1) that is electrically conductive, seismically reflective, and aseismic, and which appears to connect updip with the Olympic Core Complex of accretionary sedimentary rocks (Ramachandran et al., 2005). This layer lies at the same depth as preliminary determinations of the depths of non-volcanic tremor events that occur during the Episodic Tremor and Slip (ETS) events every 14 months or so. The strong indication is that these ETS events are occurring within the partially subducted accretionary sediments beneath the forearc.

Another important result of SHIPS is the mapping of a large region of hydrated forearc upper mantle along the Cascadia margin (Brocher et al., 2003). Metamorphic reactions in subducting slabs release water to the overlying forearc upper mantle: this water serpentinizes the upper mantle and reduces the P- and S-wave velocities of the upper mantle. We have mapped locations along the Cascadia margin where PmP arrivals are either very faint or entirely absent. We find that these regions correlate closely with regions of the upper mantle that appear to be strongly magnetic (Figure 2). Our interpretation is that when the mantle is serpentinized, magnetite is formed: thermal calculations indicate that this magnetic wedge of serpentinite lies below the Curie temperature. Thus, low-frequency magnetic anomalies in subduction zones appear to define regions where the forearc upper mantle has been serpentinized as a result of metamorphic reactions in the subducting slab (Blakely et al., 2005).



Blakely, R.J., T.M. Brocher, and R.E. Wells, 2005, Subduction zone magnetic anomalies and implications for hydrated forearc mantle, *Geology*, in press.
 Brocher, T.M., T. Parsons, A.M. Tréhu, C.M. Snelson, and M.A. Fisher, 2003, Seismic evidence for widespread serpentinized forearc upper mantle along the Cascadia margin, *Geology*, 31, 3, 267-270.
 Ramachandran, K., R.D. Hyndman, and T.M. Brocher, 2005a, Northern Cascadia subduction zone: Tomographic 3D P-wave velocity structure, *Geophys. J. Int.*, submitted.

Seismic Hazards Investigations in Puget Sound (SHIPS): II

Tom Brocher • U.S. Geological Survey, on behalf of the SHIPS Working Group

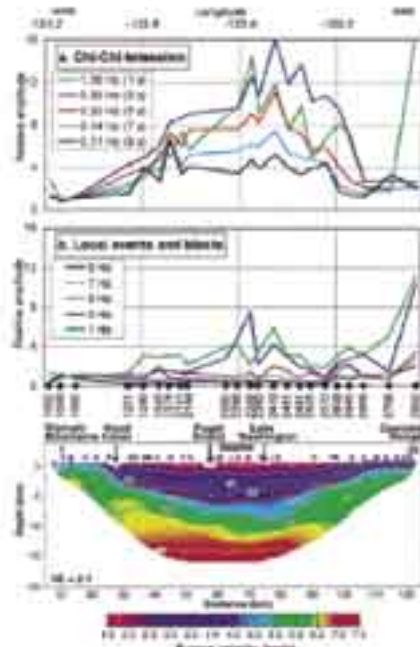


Figure 1. Profiles across the Seattle basin showing spectral amplitudes at frequencies relative to bedrock sites (a, b) and a profile showing the P-wave velocity structure of the Seattle basin derived from tomographic analysis of the 1999 SHIPS data (bottom). The numbers in parentheses in the legend on the rtop graph are the wave periods in seconds. The red contour on the velocity model (4.5 km/sec) is interpreted to be near the top of basement rocks below the basin. Note the large amplification of 1.0- to 0.2- Hz waves (1- to 5-sec periods) over the basin (a). Stations contributing to the upper plots are listed, as are the locations of the Olympic Mountains, the Cascade Range, the city of Seattle, and our blasts (stars).

Results obtained from SHIPS experiments permit a much more sophisticated characterization of the geometry of plate convergence along the northern Cascadia subduction zone as well as earthquake hazards posed by this subduction zone. Examples of these new results range from (1) characterization of crustal fault geometry and its variation along strike in the Puget Lowland from high-resolution seismic tomography studies (e.g., Brocher et al., 2001; Van Wagoner et al., 2002; Ramachandran et al., 2004), (2) determining the velocity and intrinsic attenuation structure within the Seattle basin (Li et al., 2005; Pratt and Brocher, 2005), (3) documenting the amplification of low frequency (3-7 second period) weak ground motions and the attenuation of higher frequency (above 7 Hz) weak ground motions by the Seattle basin (Pratt et al., 2003; Li et al., 2005; Figure 1), (4) using high-resolution 3D tomography models to calculate synthetic ground motions for scenario earthquakes in Puget Sound (Pitarka et al., 2004), and (5) imaging the subducting Juan de Fuca slab beneath the forearc and determining whether the in-slab seismicity lies within the crust or the upper mantle of the subducting slab (Trehu et al., 2002; Preston et al., 2003; Figure 2).

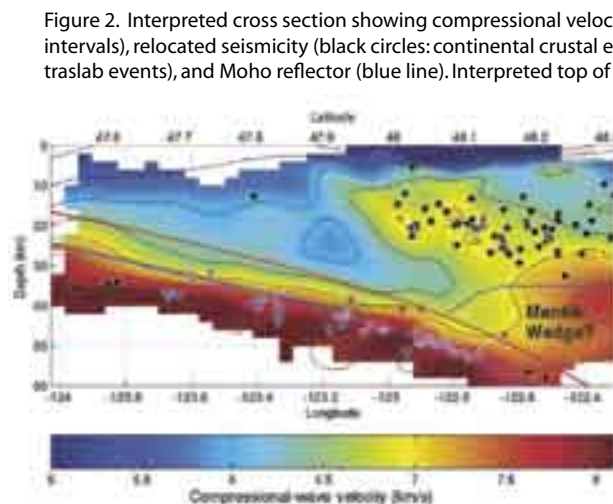


Figure 2. Interpreted cross section showing compressional velocities (contoured at 0.5-km/s intervals), relocated seismicity (black circles: continental crustal events; colored symbols: intraslab events), and Moho reflector (blue line). Interpreted top of subducting plate (red line) is drawn 7 km above reflector. The region between these lines is interpreted to be the subducting oceanic crust, composed of basalt above 40-km depth (horizontal green line) and beginning to transform to eclogite below. Subducting mantle is below the blue line. Low velocities in the mantle wedge imply the presence of serpentinite. There is no vertical exaggeration.

- Brocher, T.M., T. Parsons, R.A. Blakely, N.I. Christensen, M.A. Fisher, R.E. Wells, and the SHIPS Working Group, Upper crustal structure in Puget Lowland, Washington: Results from the 1998 Seismic Hazards Investigation in Puget Sound, *J. Geophys. Res.*, *106*, 13,541-13,564, 2001.
- Li, Q., W. Wilcock, T.L. Pratt, C.M. Snelson, and T.M. Brocher, Seismic attenuation structure of the Seattle basin using Dry SHIPS Experiment data, *Bull. Seism. Soc. Am.*, in press, 2005.
- Pitarka, A., R. Graves, and P. Somerville, Validation of a 3D velocity model of the Puget Sound region based on modeling ground motion from the February 28, 2001 Nisqually earthquake, *Bull. Seism. Soc. Am.*, *94*, 1670-1689, 2004.
- Pratt, T.L., T.M. Brocher, C.S. Weaver, K.C. Creager, C.M. Snelson, R.S. Crosson, K.C. Miller, and A.M. Tréhu, Amplification of seismic waves by the Seattle basin, *Bull. Seism. Soc. Am.*, *93*, 533-545, 2003.
- Preston, L.A., K.C. Creager, R.S. Crosson, T.M. Brocher, and A.M. Tréhu, Intraslab earthquakes: Dehydration of the Cascadia slab, *Science*, *302*, no. 5648, p. 1197-1200, 2003.
- Ramachandran, K., S.E. Dosso, C.A. Zelt, G.D. Spence, R.D. Hyndman, and T.M. Brocher, Upper crustal structure of southwestern British Columbia from the 1998 Seismic Hazards Investigation in Puget Sound, *J. Geophys. Res.*, *109*, B9, B09303, doi: 10.1029/2004JB003092, 2004.
- Tréhu, A.M., T.M. Brocher, K. Creager, M. Fisher, L. Preston, G. Spence, and the SHIPS98 Working Group, Geometry of the subducting Juan de Fuca plate: New constrain□
<http://geopubs.wr.usgs.gov/open-file/of02-328/>
- Van Wagoner, T.M., R.S. Crosson, K.C. Creager, G.F. Medema, L.A. Preston, N.P. Symons, and T.M. Brocher, Crustal structure and relocated earthquakes in the Puget Lowland, Washington from high resolution seismic tomography, *J. Geophys. Res.*, *107*(B12), 2381, doi:10.10129/2001JB000710, 2002.

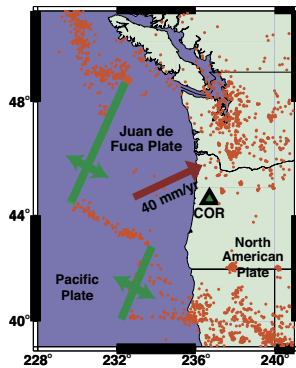
Subduction-Zone Anisotropy Beneath Corvallis, Oregon: A Serpentine Skidmark of Trench-Parallel Terrane Migration?

Jeffrey Park • Yale University

Huaiyu Yuan • University of Wyoming

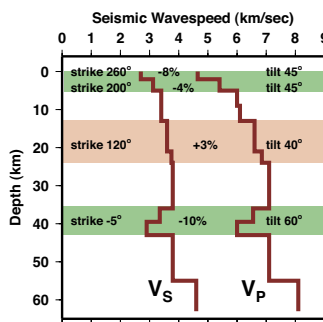
Vadim Levin • Rutgers University

We studied the back-azimuth dependence of Ps converted phases at GSN station COR (Corvallis, Oregon) using broadband P receiver functions computed from 602 earthquakes. The amplitudes and polarities of the transverse Ps phases are largely two-lobed, which indicates anisotropy with a tilted symmetry axis. A double-peaked Ps conversion at 4.5–6.5-s delay has the moveout of a dipping slab, but is not consistent with simple deflection of the Ps phase by the dipping interface. A polarity flip on the transverse RF near north-south back azimuth indicates an anisotropic symmetry axis aligned north-south, far from plate convergence (N68°E). The Ps phase is modeled using reflectivity synthetics with a highly anisotropic layer of depressed wavespeed (VP~6.0 km/s) near 40 km depth, at the slab interface with the overriding N. American plate. 1-D modeling suggests 10% anisotropy in the supraslab layer, with a slow symmetry axis oriented N5°E at a 60° tilt from the vertical. Adjustments for the effect of slab-interface dip on Ps amplitude suggest a somewhat lower 7% anisotropy. We infer a thin (7 km) anisotropic detachment zone for the northward slippage of the Siletz forearc terrane along the top of the slab, a motion consistent with GPS measurements and models of regional lithospheric dynamics. Serpentine is a likely constituent for the deep anisotropic layer, owing to its reduced Vp and high Poisson ratio. The ductile rheology and hydrated composition of serpentine make it a plausible lithology for a detachment zone.

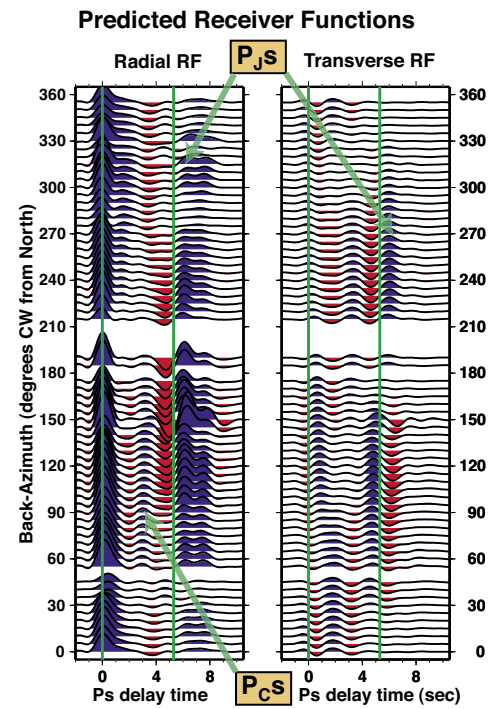
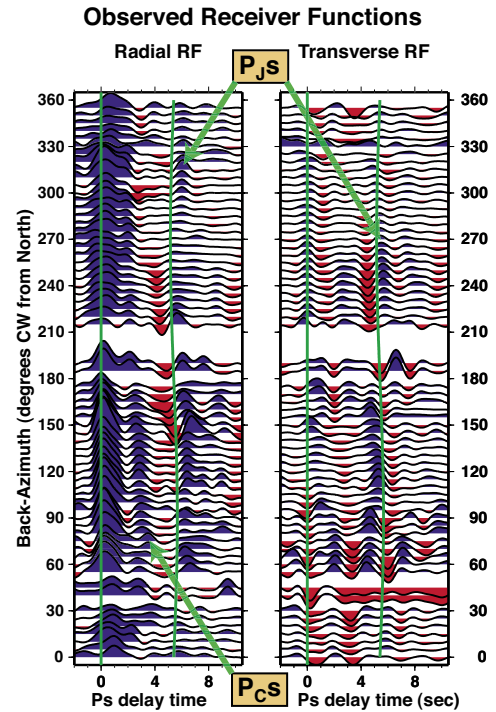


P_{CS} - midcrustal conversion
P_{JS} - slab conversion

The polarity flips of the Ps phases in back-azimuth align with the apparent anisotropic symmetry axis. The negative-positive doublet on the radial RFs indicates a low-velocity layer above the Juan de Fuca slab.



Preferred Model for COR



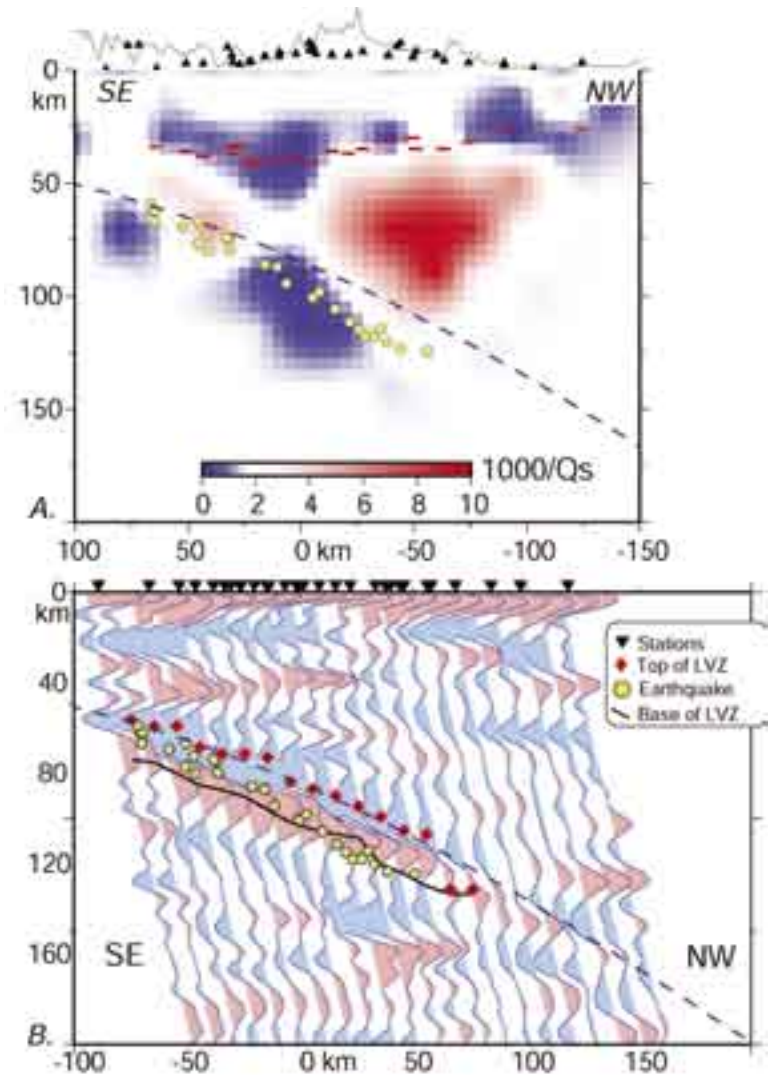
Park, J., H. Yuan, and V. Levin, Subduction zone anisotropy beneath Corvallis, Oregon: A serpentine skidmark of trench-parallel terrane migration?, *J. Geophys. Res.*, 109, B10306, 10.1029/2003JB002718, 2004.

Imaging Subduction Beneath Alaska: Results From BEAR

Geoffrey A. Abers, Aaron Ferris • Boston University

Douglas H. Christensen, Joshua C. Stachnik • University of Alaska, Fairbanks

Subduction beneath Alaska differs strongly from elsewhere in the North Pacific: North America's largest mountains have arisen, and arc magmatism is absent. To better understand the relationship between subduction, magmatism, and orogenesis, we conducted in 1999-2001 the Broadband Experiment Across the Alaska Range (BEAR), 36 PASSCAL broadband seismographs at 10-15 km spacing across the Alaska Range. These data have provided some of the best resolved images of subduction anywhere; we show two examples here. (A) Attenuation tomography (Stachnik et al., 2004) shows a high-attenuation, presumably hot mantle wedge underlying the Alaska Range. However, attenuation is small to the SE, above where the slab is less than 75 km depth, indicating that part of the mantle remains cold and isolated from large-scale flow. The Q values and their measured frequency dependence suggest subsolidus conditions, 50-150 K cooler than temperatures inferred beneath active arcs elsewhere from similar measurements. (B) Prominent P-S conversions from the downgoing slab, in receiver functions (Ferris et al., 2003), show that the top of the slab is a low-velocity channel at depths less than 130 km, indicating that subducting crust has not converted to eclogites until this depth. Strong conversions are absent below 130 km depth, as are intraslab earthquakes. Subducted crust is seismically slow probably because hydrous minerals or free fluids are present, and it is the release of these fluids which embrittles the surrounding material, allowing earthquakes to occur. Deeper, the absence of fluids precludes seismogenesis. The images also show that subducting crust here is 2-3 times thicker than typical oceanic crust, and may indicate exotic terrane subduction to at least 130 km depth. Subduction of this buoyant crust could explain the shallow dip of the thrust zone beneath Alaska and the Neogene rise of the Alaska range.



Results from BEAR transect, in cross section, in the Denali region of the Alaska subduction zone. (A) S-wave attenuation, from Stachnik et al. (2004). Yellow circles: Earthquakes; red lines: Moho depths from receiver functions. Topography, top, exaggerated 12 times. (B) Receiver function image, corrected from Ferris et al. (2003). Receiver functions are projected to P-to-S conversion point in a 1D velocity model. Diamonds and solid line show top and bottom of low-velocity crust, from waveform inversion, accounting for ray bending by dipping slab. In both, yellow circles show earthquakes, located in same model as receiver functions, and dashed line shows inferred top of slab.

Ferris, A., G.A. Abers, D.H. Christensen, and E. Veenstra, High-Resolution image of the subducted Pacific (?) plate beneath central Alaska, 50-150 km depth, *Earth Planet. Sci. Lett.*, 214, 575-588, 2003.

Stachnik, J.C., G.A. Abers, and D. Christensen, Seismic attenuation and mantle wedge temperatures in the Alaska subduction zone, *J. Geophys. Res.*, 109, B10304, doi:10.1029/2004JB003018, 2004.

The TUCAN Broadband Seismic Experiment: Imaging the Central America Subduction Factory

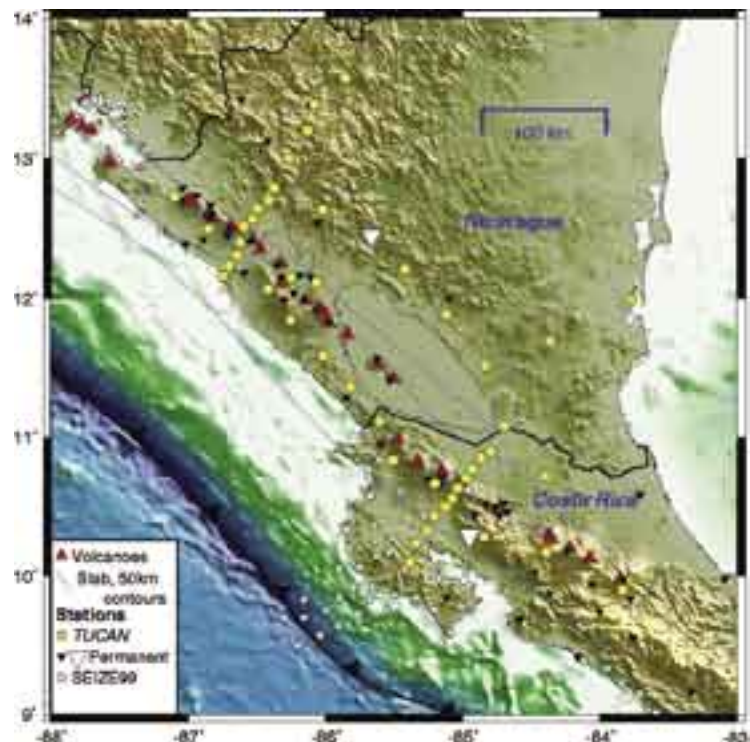
Geoffrey A. Abers, Laura Auger, Ellen Syracuse, Gustavo Reyes • *Boston University*

Karen M. Fischer, Catherine Rychert, David Abt, Alexis Walker • *Brown University*

J. Marino Protti, Victor Gonzalez Salas • *OVSICORI, Costa Rica*

Wilfried Strauch, Pedro Perez • *INETER, Nicaragua*

The “Subduction Factory” processes the solids and volatiles entering oceanic trenches and produces volcanic arcs, deep earthquakes, and long-term modifications to the deep earth. Central America exhibits some of the global extremes in the factory operation: in the Nicaragua volcanic arc, fluxes of geochemical tracers associated with subducting sediment are among the highest on the planet, while in the adjacent Costa Rica arc, many of the same tracers are weak to absent. For this reason, the MARGINS Program has selected Central America as one of two focus areas for its Subduction Factory initiative. In advancing understanding of the Subduction Factory, seismic imaging of the downgoing plate, mantle wedge and upper-plate crust form a primary data set for understanding the cycling of volatiles and production of melt. To accomplish this, we deployed in July-August of 2004 the TUCAN seismic array (Tomography and other things Under Costa Rica And Nicaragua) of 48 broadband PASSCAL seismographs, operating until early 2006. The array includes two dense transects across the arc at 10 km spacing, in both Costa Rica and in Nicaragua, accompanied by distributed stations sampling arc and backarc along strike over 450 km. From the array data, we have begun applying a wide variety of imaging strategies to constrain structure from both teleseismic signals and signals from earthquakes within the downgoing slab. Overall, the data recovery and quality has been outstanding, with recovery of 90-95%. Analysis of these data and integration with parallel geochemical studies of arc lavas appear sufficient to characterize subduction here as well as any place on the planet.



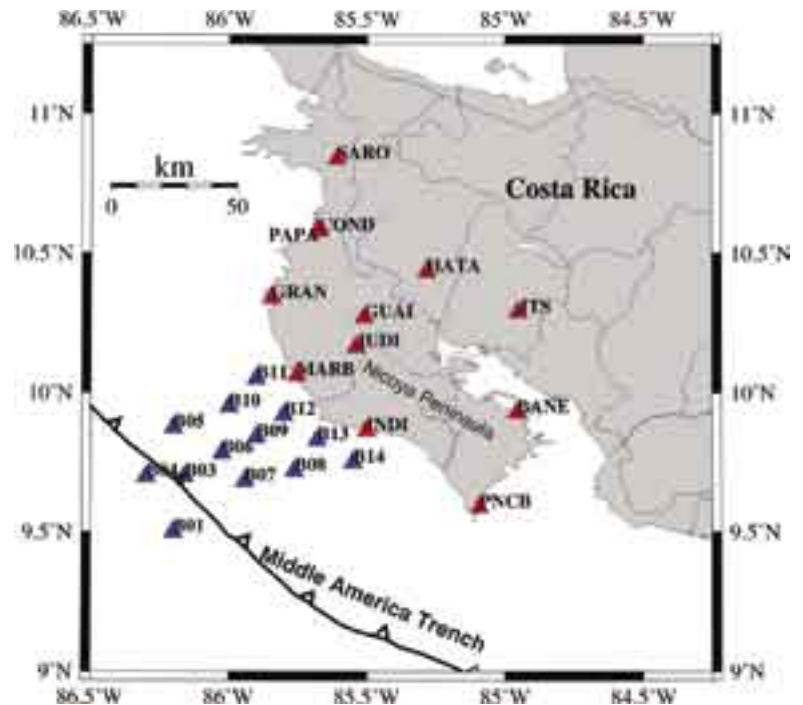
The TUCAN broadband experiment in Costa Rica and Nicaragua. Yellow circles show TUCAN broadband stations, July 2004 – March 2006. Other seismic stations in the region include permanent broadband (open triangles), short-period (black triangles) and the 1999 SEIZE PASSCAL experiment (gray circles). Red triangles show the active arc front, and thin blue lines show 50 km contours to Wadati-Benioff zone. Here, the 20-25 Ma Cocos plate subducts beneath the Caribbean, producing earthquakes to a depth of 300 km.

Receiver Function Analysis of the Nicoya Peninsula, Costa Rica

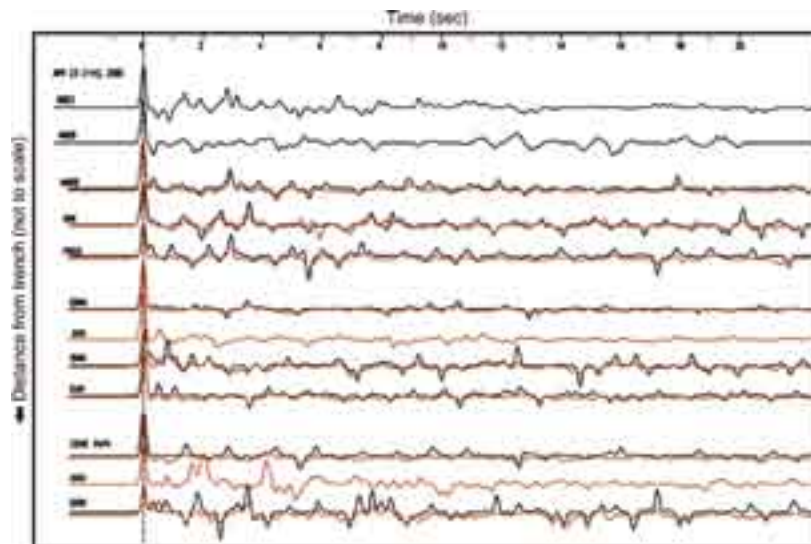
Claudia Flores, Susan Schwartz • University of California, Santa Cruz

CRSEIZE (Costa Rica Seismogenic Zone Experiment) was a collaborative effort to identify and describe subduction zone processes occurring on the southern section of the Middle American Trench. This experiment consisted of deployed standard IRIS/PASSCAL three-component broadband and short period instruments on land as well as three-component broadband ocean bottom seismometers and hydrophones, and geodetic surveying throughout Costa Rica.

Receiver function analysis using time-domain deconvolution techniques (Ammon, 1991; Ligorria and Ammon, 1999) is applied to broadband data collected during CRSEIZE to constrain the depths to major boundaries such as the top of the subducting slab, the oceanic crust-mantle interface of the slab, and the base of continental crust in the overlying plate. Previous tomography studies using CRSEIZE data (Deshon, 2004; Deshon and Schwartz, 2004) suggest the existence of a serpentinized forearc mantle wedge and a change in the location and depth of the seismogenic zone from north to south beneath Nicoya Peninsula. With receiver function analysis, we hope to verify the depth and range of this mantle wedge and find other characteristics of the slab-plate interface where interplate earthquakes occur. Current work suggests that the velocity contrast resulting from the slab-continental crust interface seems to be reduced as you move away from the trench. Other



Map of CRSEIZE broadband stations located on land (red triangles) and ocean bottom (blue triangles) on and offshore Nicoya Peninsula, Costa Rica.



Plot of receiver functions with respective distance from trench increasing going down. Receiver functions are shown in black for one event at recording stations and red for stacked receiver functions at respective stations (note: stations COND and PAPA are combined).

arrival phases, such as PKP(AB), and statistical analysis of all receiver functions will be used to improve the quality and reduce the uncertainty of our final results.

Ammon, C. J., The isolation of receiver effects from teleseismic P waveforms, *Bull. Seismol. Soc. Am.*, *81*, 2504-2510, 1991.

Deshon, H. R., Seismogenic zone structure along the Middle America subduction zone, Costa Rica, Ph.D. thesis, 356, pp., Univ. of Calif. Santa Cruz, 2004.

Deshon, H. R., and S. Y. Schwartz, Evidence for serpentinization of the forearc mantle wedge along the Nicoya Peninsula, Costa Rica, *Geophys. Res. Lett.*, *31*, doi:10.1029/2004GL021179, 2004.

Ligorria, J. P. and Ammon, Iterative deconvolution and receiver-function estimation, *Bull. Seismol. Soc. Am.*, *89*, 1395-1400, 1999.

Crustal and Upper Mantle Structure in the Flat Slab Region of Central Chile and Argentina

Hersh Gilbert, Susan Beck, George Zandt, CHARGE working group • University of Arizona

The shallow dips of the subducting Nazca plate appear to significantly influence the tectonics of central Chile and Argentina where magmatism and deformation are present nearly 1000 km away from the plate boundary. We calculate receiver functions from data recorded by the recent PASSCAL CHARGE array (Figure 1), which transected the Andes and Sierras Pampeanas in this region, to constrain the crustal structure of this region. Beneath the northern transect of the CHARGE array, where the Nazca slab flattens near 100 km, we find the crust is over 60 km thick beneath the Andes and that it thins to the east (Figure 2). The thick crust, however, extends ~200 km to the east of the high elevations. Estimates of Poisson's ratio, which can be used to make inferences about crustal composition, vary along ancient terrane boundaries exhibiting higher values to the west. Interestingly, we observe that the amplitude of the phase corresponding to the Moho on receiver functions diminishes to the west, complicating our images of crustal structure. These observations of thickened crust within a region of low elevations, diminished receiver function arrivals, and reports of high shear-wave speeds atop of the mantle wedge overlying the shallowly subducted Nazca slab, suggest to us that a portion of a lower crust beneath the western Sierras Pampeanas has been eclogitized. Receiver function arrivals marking the location of the Nazca slab remain more elusive, suggestive of a small impedance contrast between the slab and overlying mantle.

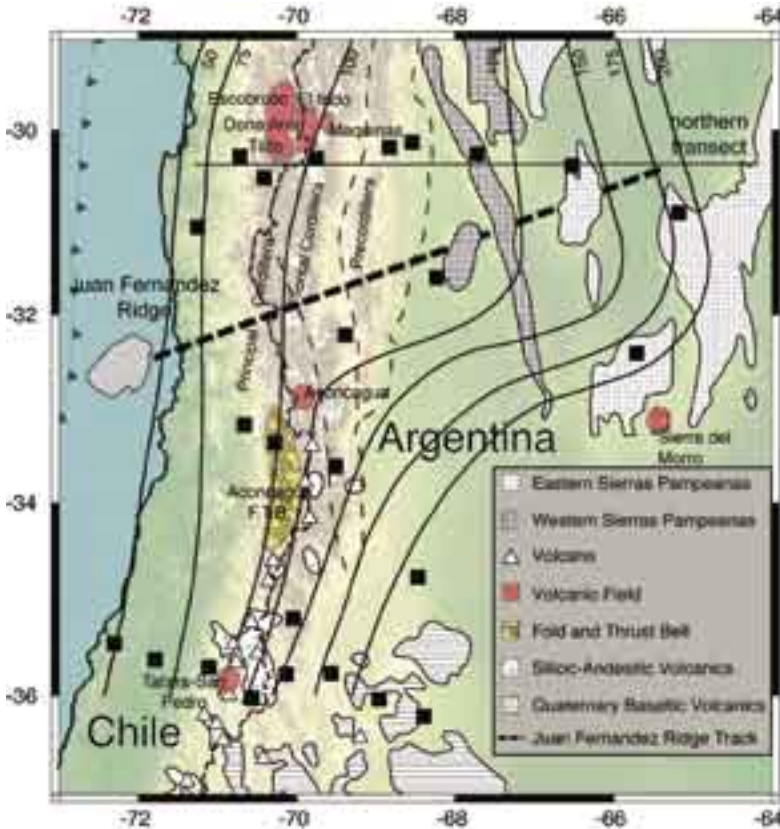


Figure 1. Locations of CHARGE stations shown as black squares plotted on a map of volcanism in central Chile and Argentina including the Sierra del Morra, Dona Ana, and Maquinas areas as well as other important landmarks such as the Aconcagua region. The track of the Juan Fernandez Ridge is shown as a heavy dashed line and solid lines mark the depth contours of the Nazca slab (Cahill and Isacks, 1992). Thin dashed lines mark the boundaries between the Principal Cordillera, Frontal Cordillera, and Precordillera. Locations of various volcanic fields are shown for reference.

Gilbert, H., S Beck, and G. Zandt, Lithospheric and Upper Mantle Structure of Central Chile and Argentina, *Geophys. J. Int.*, in review, 2005.

Wagner, L. S., S. L. Beck, and G. Zandt, Upper mantle structure in the south central Chilean subduction zone (30 to 36S), *J. Geophys. Res.*, doi:10.1029/2004JB003238, 2005.

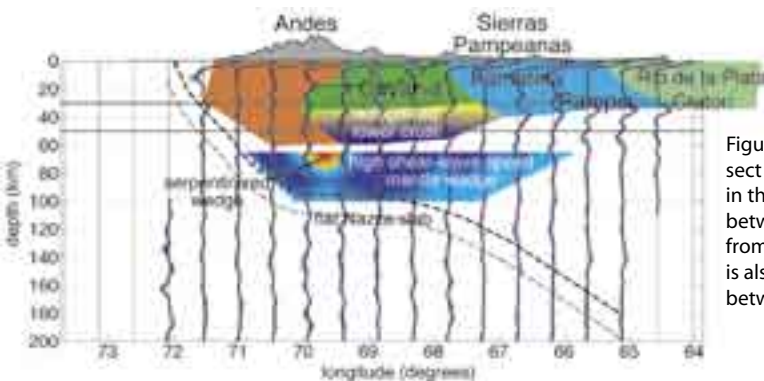


Figure 2. Summary cartoon of results from the northern CHARGE transect presenting major observations. Variations in the Moho signature in the northern transect correlate well with locations of the boundary between the Cuyania and Famatina terranes. A nearby cross-section from a local shear-wave tomographic model (Wagner et al., 2005) is also presented (high (blue) and low (red) speed anomalies range between +4% blue to -4%).

Imaging Shallow Subduction Zones With Surface Waves

Michael H. Ritzwoller, Nikolai M. Shapiro • University of Colorado at Boulder

Intermediate and long period surface waves can image relatively old (>40 Ma) subducting lithosphere above ~250 km. These images are complementary to teleseismic body wave images, which are best below ~200 km depth. Examples are shown here of the upper mantle beneath the Aleutian and Sumatra-Andaman subduction zones. These are interesting regions to contrast as the incoming plate transitions from convergence to oblique incidence. The Pacific Plate moves obliquely to the western Aleutians west of about 173°E and the Indian Plate moves similarly compared to the Andaman Sea. Beneath the western Aleutians (Figure 1) there is a “slab portal” in the region of oblique incidence. The lateral termination of the high shear wave speeds, which are diagnostic of the slab, coincides with a gap in deep seismicity. In contrast, high speed shallow subducting lithosphere is imaged along the entire Sunda Arc (Figure 2), from the Andaman Sea, where oblique incidence occurs, to Sumatra and Java. The age of the subducting lithosphere varies appreciably along the arc, being youngest (~40 Ma) off northern Sumatra near the initiation of the great Sumatra-Andaman Islands earthquake of Dec 26, 2004, and its largest aftershock that occurred on Mar 28, 2005. Very high temperatures are observed in the supra-slab mantle wedge in the Andaman back-arc. The thermal structure of the mantle from the Andaman Sea to Java may have contributed to the location of the initiation of rupture of the great earthquake, the strength of seismic coupling, and the differential rupture speed between the northern and southern segments of the earthquake.

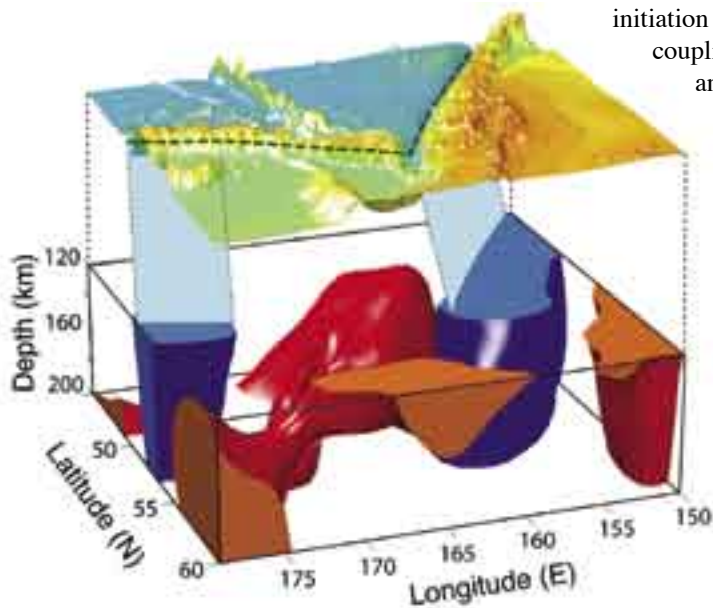
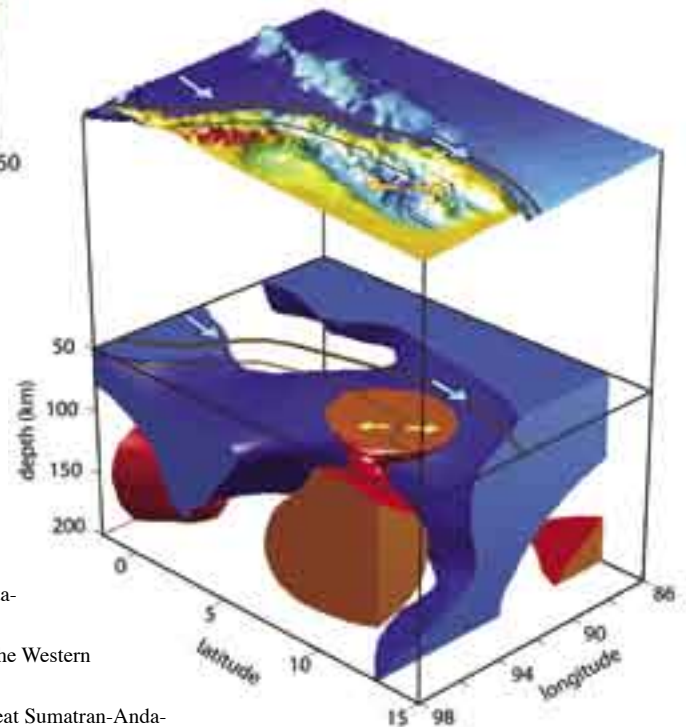


Figure 1. Shear wave speeds beneath the western Aleutians. The blue surface (+1.2%) represents oceanic lithosphere subducted beneath the Aleutians east of 173°E and beneath southern Kamchatka and the red surface (-1.2%) reflects low velocities of material that penetrates through the slab portal beneath the western Aleutians. The dark green lines mark the locations of the Aleutian and Kamchatka Trenches and the light blue surfaces show projections of the subducted oceanic lithosphere on the trenches.

Figure 2. Similar to Figure 1, but for northern Sumatra and the Andaman Sea. The blue surface (+1.2%) is oceanic lithosphere subducted at the Sunda and Andaman trenches and the red surface (-1.5%) reflects low velocities beneath the Andaman spreading center, relative to a regional average at each depth. Brown lines show the active plate boundaries, blue arrows are relative plate motion, and yellow arrows indicate extension in the Andaman Basin.



Levin, V., N.M. Shapiro, J. Park, and M.H. Ritzwoller, Seismic evidence for catastrophic slab loss beneath Kamchatka, *Nature*, 418, 763-767, 2002.

Levin, V., N.M. Shapiro, J. Park, and M.H. Ritzwoller, The slab portal beneath the Western Aleutians, *Geology*, 33(4), 253-256, 2005.

Ritzwoller, M.H., N.M. Shapiro, and E.R. Engdahl, Structural context of the great Sumatran-Andaman Islands earthquake, submitted 2005.

Detailed Structure and Sharpness of Upper Mantle Discontinuities in The Tonga Subduction Zone

Rigobert Tibi, Douglas A. Wiens • Washington University

The Seismic Arrays in Fiji and Tonga (SAFT) experiment, which consisted of two arrays of broadband seismic stations in the Fiji and Tonga islands operating from July, 2001, to August, 2002, provides an ideal opportunity to perform a detailed local investigation of upper mantle discontinuities near one of the Earth's coldest subduction zones. Recordings of deep Tonga earthquakes from the arrays are stacked and searched for reflections and conversions from upper mantle discontinuities in the Tonga subduction zone. In comparison with the commonly used teleseismic approaches, the short path lengths for the local data provide smaller Fresnel zones and high frequency content for precise mapping of discontinuity structure. This is particularly important for a subduction zone, where variations in temperature and water content are expected to cause small-scale changes in topography and sharpness of the discontinuities. To enhance the low-amplitude discontinuity phases s410p, P660p and S660p, deconvolved seismograms from each event/array pair are aligned on the maximum amplitude of the direct P wave and subsequently slant-stacked. For the 410-km discontinuity, the results show no systematic variations in depth with distance to the cold slab. The 660-km discontinuity varies between 656 and 714 km in depth. For the southern and central parts of the subduction zone, the largest depths occur in the core of the Tonga slab. For the northern part, two separate depressions

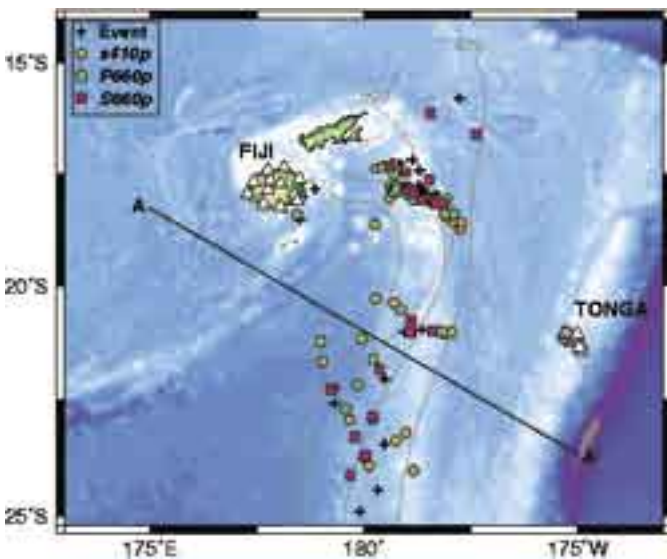


Figure 1. Map showing the locations (white triangles) for the Fiji and Tonga arrays. Crosses indicate the epicentral locations of the 25 earthquakes used. The locations of the bounce and piercing points at the upper mantle discontinuities for the different seismic phases investigated are shown. Pink hexagons are for s410p, green circles for P660p and red squares for S660p. Gray lines are contours of deep seismicity (Gudmundsson and Sambridge, 1998), with the numbers indicating the depth in km to the seismogenic zone. Line AA' shows the location of the vertical cross section in Figure 2.

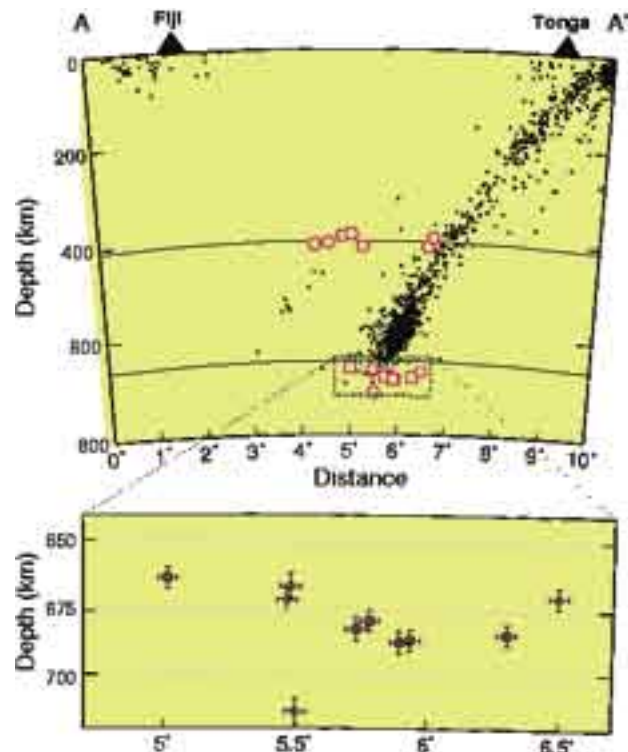


Figure 2. (top) Vertical cross section along line A-A' in Figure 1 showing the bounce and piercing point locations for s410p (hexagons), P660p (circles) and S660p (squares). Thin lines indicate the nominal depths of 410 and 660 km for the discontinuities. Seismicity (dots) is from Engdahl et al. (1998). Width of the cross section is 240 km. (bottom) Enlargement showing the detailed topography of the 660-km discontinuity.

of the 660 are observed. These anomalies are interpreted as being induced by the active, steeply subducting Tonga deep zone and a subhorizontally lying remnant of subducted lithosphere from the fossil Vityaz trench, respectively (Chen and Brudzinski, 2001). Interpreting the deflections of the 660 in terms of local temperatures implies a thermal anomaly of -800K to -1200K at 660 km depth. Except for the southern region where it may thicken, the width of the depressed 660 region implies that the Tonga slab seems to penetrate the 660 with little deformation. Waveform modeling suggests that both the 410 and 660 discontinuities are sharp. The 660 km discontinuity is at most 2 km thick in many parts of the region, and a first-order discontinuity cannot be precluded. The 410 thickness shows somewhat more variability and ranges from 2 km to 10 km outside the slab, and is at most 10 km thick within the slab. This suggests that the subduction process does not produce dramatic effects on the sharpness of the discontinuities.

Tibi, R., and Wiens, D.A., Detailed structure and sharpness of upper mantle discontinuities in the Tonga subduction zone from regional broadband arrays, *J. Geophys. Res.* 110, B060313.

Evidence of Mid-Mantle Deformation From Shear-Wave Splitting

James Wookey, J-Michael Kendall • *University of Leeds, United Kingdom*

Guilhem Barruol • *CNRS, Universite Montpellier, France*

Until recently, the mid-mantle region of the Earth (the transition zone and the uppermost-lower mantle) has been considered isotropic. In this study we present evidence of anisotropy in the mid-mantle region near the Tonga-Kermadec subduction zone, inferred from shear-wave splitting in teleseismic S phases recorded at Australian seismic stations. We analyse the seismograms after applying a wavefield decomposition method to remove the effects of shear-coupled P waves. Lag times of between 0.7-6.2 s are observed, and given the absence of splitting in SKS phases at the Australian stations, we infer the presence of significant anisotropy in the mid-mantle. Forward modeling suggests that the uppermost 100 km or so of the lower mantle is the most likely location for this anisotropy, and we propose several scenarios that might account for this (Figure 2). These involve the lattice-preferred orientation of anisotropic lower-mantle minerals such as MgSiO_3 perovskite, or the shape-preferred orientation of inclusions of a subducted phase such as basaltic melt.

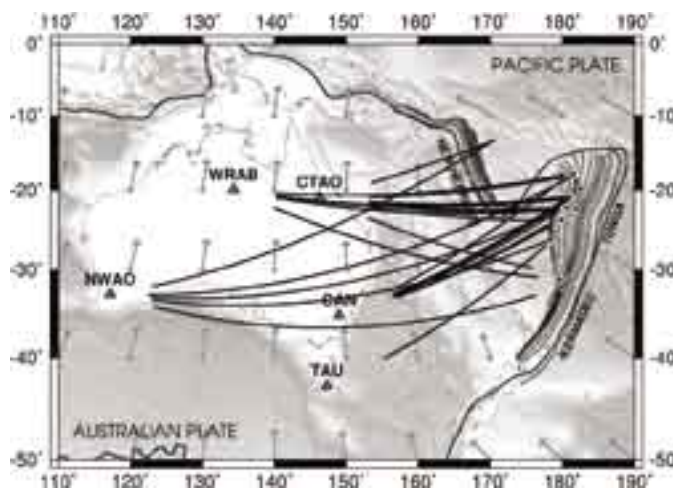


Figure 1. Map showing locations of events (circles), stations (triangles) and predicted raypaths in the lower mantle. Also shown are plate motions in the hotspot reference frame (arrows) and depth of seismicity of the Tonga, Kermadec and New Hebrides subduction zones.

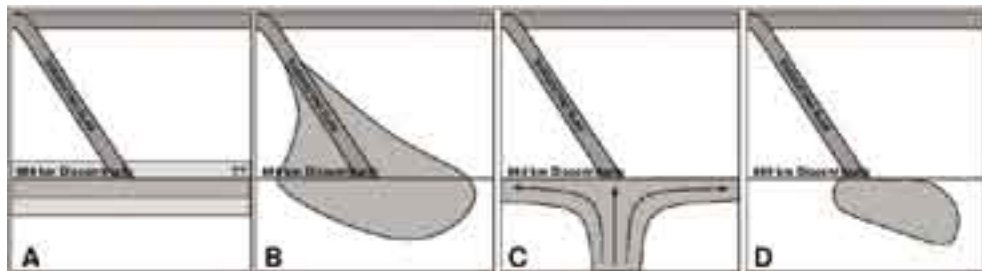


Figure 2. Possible scenarios of mid-mantle anisotropy. Three postulate the lattice-preferred orientation (LPO) of mid-mantle minerals, in a global boundary layer (Panel A), by stress-fields associated with subduction (Panel B) or by an upwelling in the lower mantle (C). The final scenario is the shape-preferred orientation (SPO) of subducted material (for example, basaltic melt) in a 'megalith' in the uppermost lower mantle.

Wookey, J., Kendall, J-M. and Barruol, G., Mid-mantle deformation inferred from seismic anisotropy, *Nature*, 415, 777-780, 2002.

Wookey, J., and Kendall, J-M., Evidence of mid-mantle anisotropy from shear wave splitting and the influence of shear-coupled P waves, *J. Geophys. Res.*, 109, doi:10.1029/2003JB002871, 2004.

Seismic Anisotropy in the Izu-Bonin Subduction System

Matthew J. Fouch, D. Karen Anglin • Arizona State University

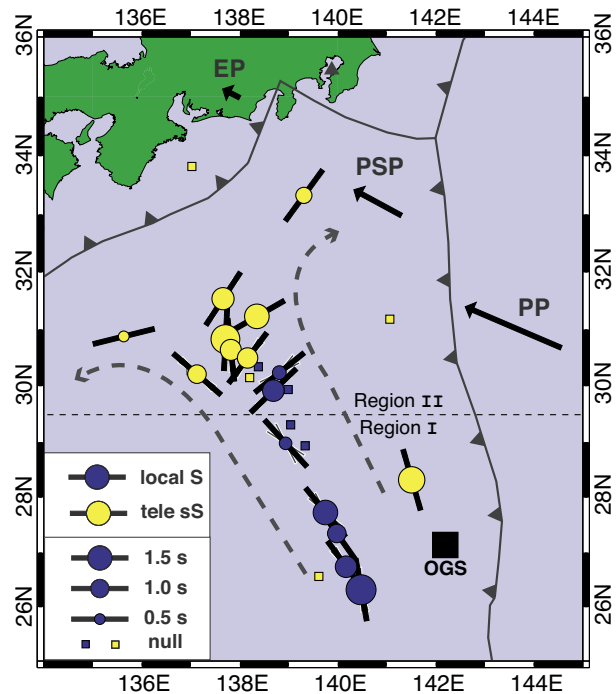
Using broadband seismic data from 12 IRIS Global Seismic Network (GSN) stations, we evaluated shear wave splitting in local S and teleseismic sS phases from earthquakes that sample the Izu-Bonin subduction system backarc to examine the dynamics of slab deformation and mantle flow (Anglin and Fouch, 2005).

We utilized the particle motion analysis method of Silver and Chan (1991) to measure the best fitting splitting parameters, fast polarization direction (ϕ) and splitting time (δt), on all waveforms. For teleseismic sS splitting analyses, we first corrected the waveform for station-side anisotropic effects by rotating and time-shifting the waveform according to either splitting derived from teleseismic S on the same waveform (Fischer and Yang, 1994) or published SKS splitting parameters from IRIS GSN stations. SKS corrections generally produced simpler waveforms and clearer splitting results; we therefore applied published SKS corrections to sS waveforms.

Splitting times for local S phases range from 0.6 to 1.7 s and 0.9 to 3.2 s for teleseismic sS phases. Fast polarization directions range from \sim NW-SE to \sim ENE-WSW and suggest complex mantle deformation across the region. Shear wave splitting parameters from this study demonstrate more complexity than earlier work by Fouch and Fischer (1996), who found relatively simple, convergence-parallel fast polarization directions across the region.

Our preferred interpretation of the dataset is that splitting variations reflect a rapid change in mantle flow direction across the Izu Bonin region. To the south (region I), variations are likely caused by a combination of convergence parallel mantle flow, trench parallel shear along the plate boundary, and inherent slab fabric. In region II to the north, δt values from local events are smaller and ϕ values exhibit more complexity. Here, phases sample a larger volume of mantle wedge and exhibit a first-order rotation in ϕ values, suggesting that mantle flow in this region is diverted from NW flow to NE-SW flow. This diversion is likely due to trench parallel subslab mantle flow behind the oceanward side of the Philippine Sea plate south of the Philippine Eurasian trench.

We propose that several yet uninvestigated subduction systems may also exhibit signatures of trench parallel subslab mantle flow, indicating that subslab mantle near some subduction zones is either partially or fully decoupled beneath subducting slabs. An analysis of waveforms from IRIS GSN stations will enable more a comprehensive documentation of this component of the subduction system. If confirmed for other regions, this constraint must be incorporated in future dynamic models of subduction.



Map view of shear wave splitting results for the Izu Bonin subduction system. Plate motions of the Eurasian plate (EP), Philippine Sea plate (PSP), and Pacific plate (PP) denoted by black arrows scaled to local velocities. In this region, the PP subducts beneath the PSP at \sim 55 mm/yr and the PSP subducts beneath the EP at \sim 40 mm/yr. Gray lines delineate plate boundaries approximated by bathymetric oceanic trench locations; overriding plate marked with teeth.

Blue and yellow symbols denote local S and teleseismic sS observations, respectively; circles scaled to denote splitting times (δt); black bars represent fast polarization direction (ϕ); small gray bars represent 95% confidence region in ϕ ; small squares denote null values. Local S measurements are plotted at the earthquake epicenter; teleseismic sS measurements are plotted at the free surface bounce point along the raypath. sS δt values are shown as 50% of total measured value as these phases have roughly double the path length in the wedge compared to local S paths. ϕ values rotate from \sim NNW-SSE in the south (region I) to a more complex pattern in the north (region II) with an average ϕ of \sim NNE-SSW. δt values are smallest and most null measurements exist near the transition between regions. Gray dashed arrows show inferred flow direction based on the splitting measurements.

Finite Difference Synthetic Test for Kirchhoff Migration of Receiver Function on Subducting Slab

Sangwon Ham, Alan Levander, Fenglin Niu • Rice University

Receiver function imaging enables higher resolution imaging than traveltimes tomography, and dense and portable seismic array deployments permitting the migration techniques are possible with the Japanese seismic networks and IRIS PASS-CAL deployments. We conducted Kirchhoff migration for the synthetic data generated from two-dimensional elastic wave finite-difference modeling to verify the imaging quality of the migration code and to understand the relationship between the physical parameters of the subsurface and the migrated image (Levander, 1988; Levander 2005). The slab geometry from High-Resolution tomography in Japan (Zhao et al., 1994) was used to construct a synthetic model. We set up the parameters for the synthetic modeling, receiver function generation, and migration to simulate the geometry of the earthquake on February 26, 2001, in India.

We can verify that migration with a smoothed 2D version of the velocity distribution gives an improved image of the slab geometry than that with a 1D velocity model (Figure 1). We simulated the effect of various model parameters like epicentral distances (i.e. incidence angle of the incoming wave) on the migrated image. We found that the conversion coefficient in the migrated image is strongly dependent on the P-wave incidence angle, hence the epicentral distance (Figure 2). We will get more quantitative results for the effect of the subsurface parameters on the migrated image that are the subject of a forthcoming publication.

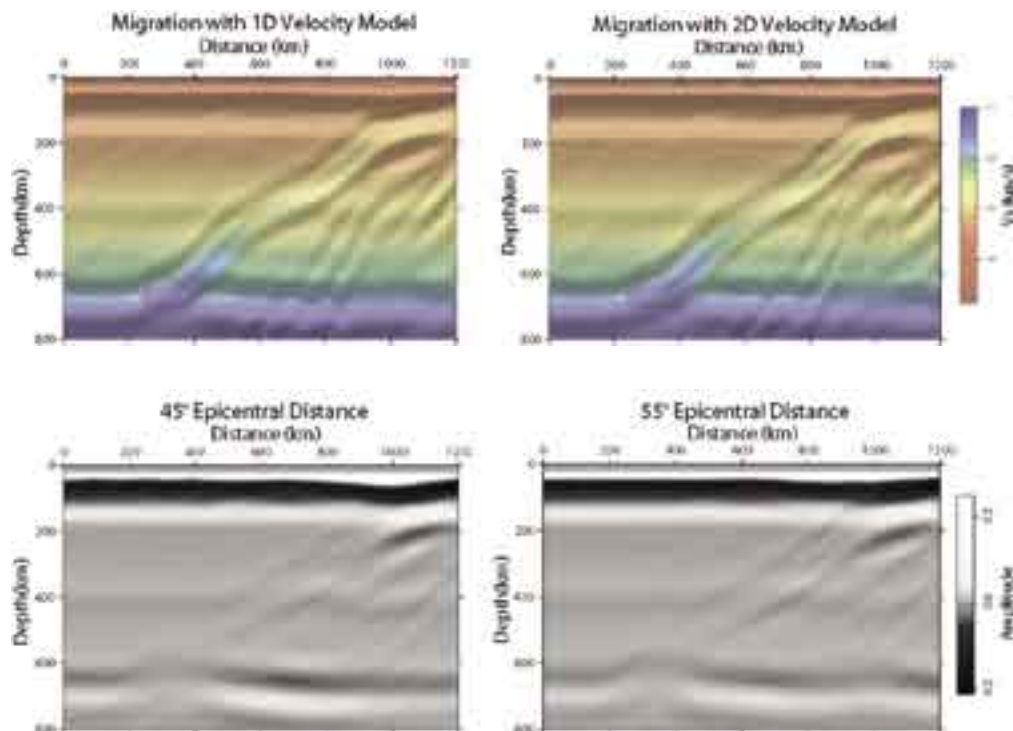


Figure 1. Effect of velocity model on the migrated image. Migration with 2D velocity model (right) shows better top boundary constraint of the slab geometry than that with 1D velocity model (left).

Figure 2. Effect of epicentral distance on the migrated image. Migration with 55° epicentral distance (right) shows stronger boundary constraint of the slab geometry than that with 45° epicentral distance (left).

Zhao, D., A. Hasegawa, and H. Kanamori, Deep structure of Japan subduction zone as derived from local, regional, and teleseismic events, *J. Geophys. Res.*, 99, 22,313-22,329, 1994.

Levander, A., F. Niu, C.-T.A. Lee, and X. Cheng, Imag(in)ing the Continental Lithosphere, *Physics of the Earth and Planetary Interiors*, accepted, 2005.

This research is supported by NSF CMG 0222270

Observations of Shear Wave Birefringence in Subduction Zones: A Guide to Mantle Flow?

Vadim Levin • *Rutgers University*

Valerie Peyton • *U.S. Geological Survey, Albuquerque*

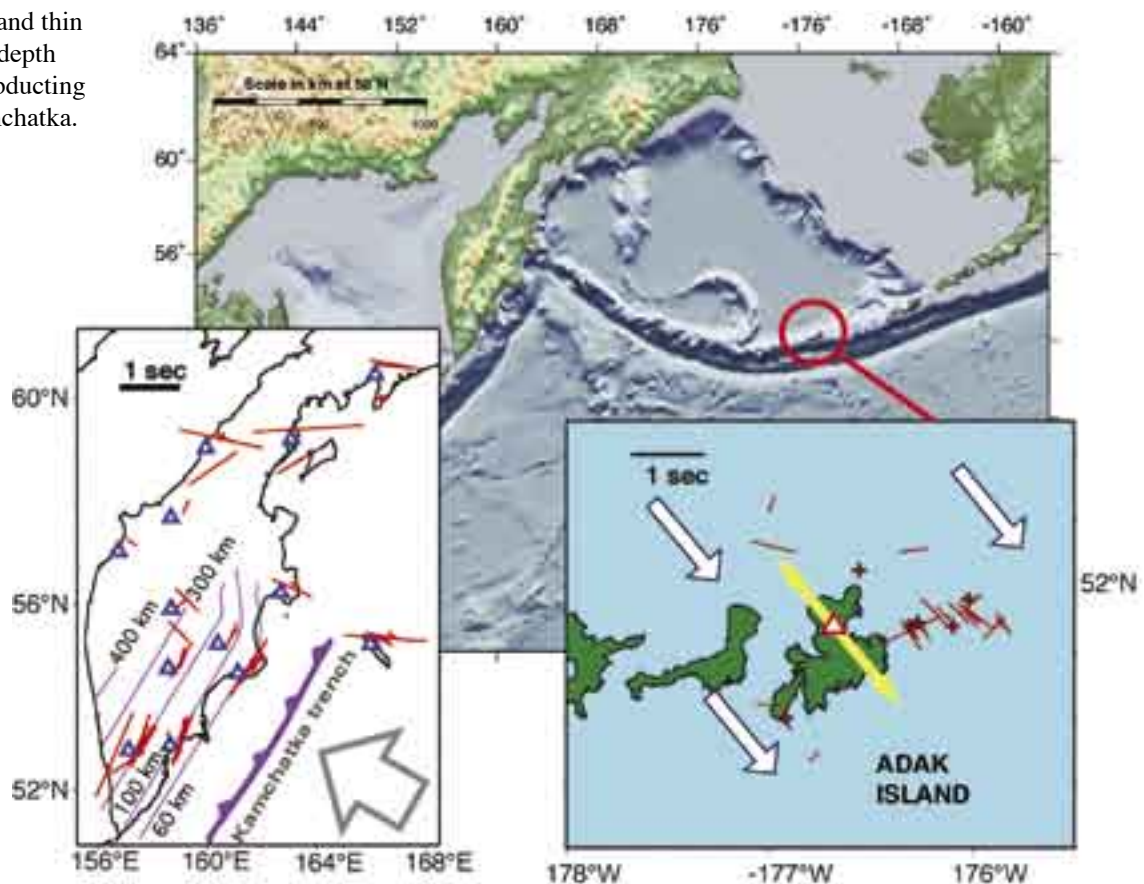
Jeffrey Park • *Yale University*

Holly Bender, William Menke • *LDEO*

In Earth's upper mantle the deformation of olivine crystals should lead to directional dependence of seismic wave speed, offering a way to map patterns of mantle flow through the study of anisotropy indicators in seismic waves. For example, the birefringence in core-refracted teleseismic shear waves (SKS) in two regions of the northwestern Pacific were studied using data from GSN stations ADK and PET, and a PASSCAL deployment on Kamchatka (1998-1999 SEKS campaign).

At Adak island in the central Aleutians the fast polarization of shear waves is closely aligned with oblique convergence between Pacific and North American plates (right plot). In Kamchatka, areas underlain by the subducting Pacific plate show fast polarization direction orthogonal to the near-normal convergence between North America and Pacific plates. In both cases the anisotropic signal is strong enough to require upper mantle involvement. The dramatic difference in the relationship between the geodynamic regime and the pattern of anisotropy indicators suggests that the "mapping" of the latter into the former involves extra complexity that we do not fully understand at the moment.

On the plots below red bars denote individual estimates of shear wave birefringence parameters, plotted at map positions of 200 km piercing points for corresponding rays. In the right plot red crosses show measurement with delays < 0.1 s, white arrows show relative North America - Pacific plate motion, and the yellow arrow shows fast shear wave polarization in the best-fitting one-layer anisotropic model found by matching synthetic seismograms to observed waveforms. In the left plot the open arrow shows relative plate motion, and thin purple lines show depth contours of the subducting plate beneath Kamchatka.

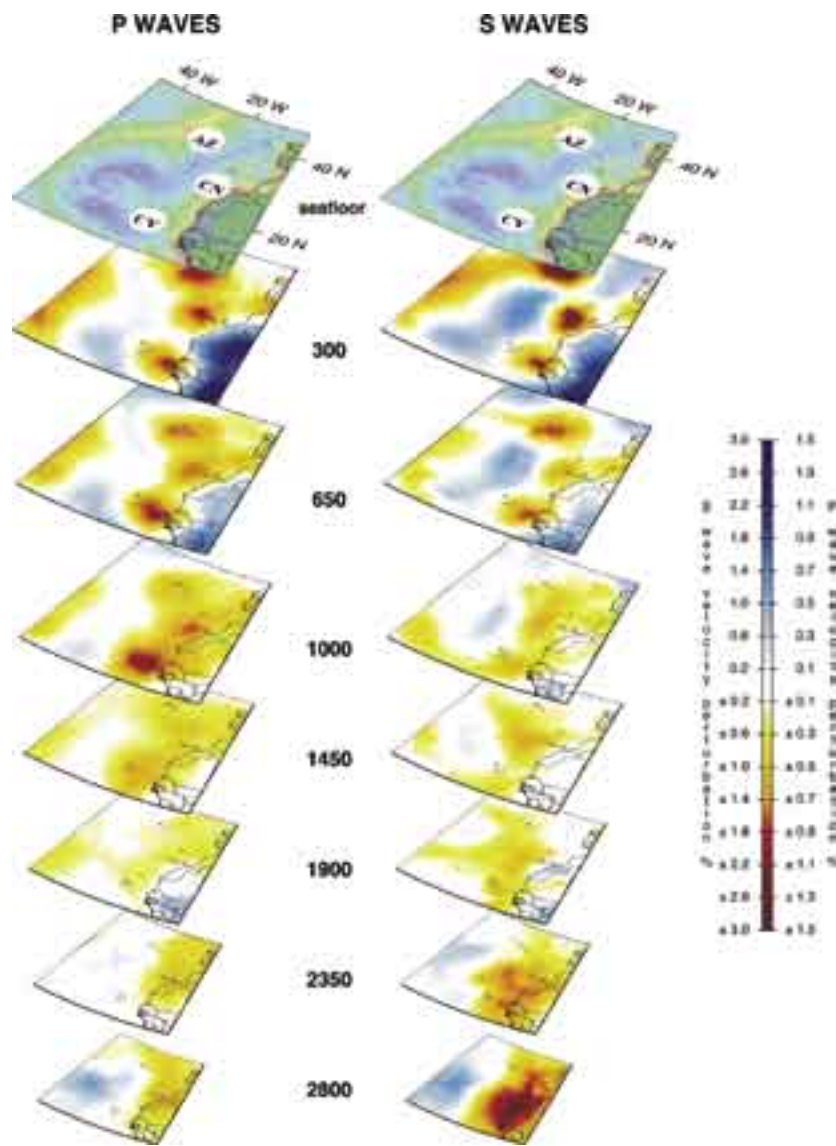


Deep Plumes in the Earth's Mantle

Raffaella Montelli, Guust Nolet, F. Anthony Dahlen • *Princeton University*

Guy Masters • *IGPP, University of California, San Diego*

In the past few years, incorporation of wave-diffraction effects in seismic tomography has led to significant improvements in the imaging of small-scale structure in the earth's mantle. The new tomographic images clearly show the source region of many hotspots. The majority of hotspots cap plumes originating deep into the lower mantle. This figure shows an example of a family of plumes beneath three well known hotspots: Azores, Canary and Cape Verde. They have been obtained by inverting GSN data measured by cross-correlation. The left image has been obtained by jointly inverting the long period data with a selection of short-period P waves from the International Seismological Centre (ISC) data base. The image on the right has been obtained by inverting long-period S waves only. These are 40 by 40 degree cross-sections centered around Canary. Vertical scale has been exaggerated to avoid overlapping of the horizontal sections. Colors indicate the percentage P- and S-wave velocity perturbations with respect to a 1D background reference model.

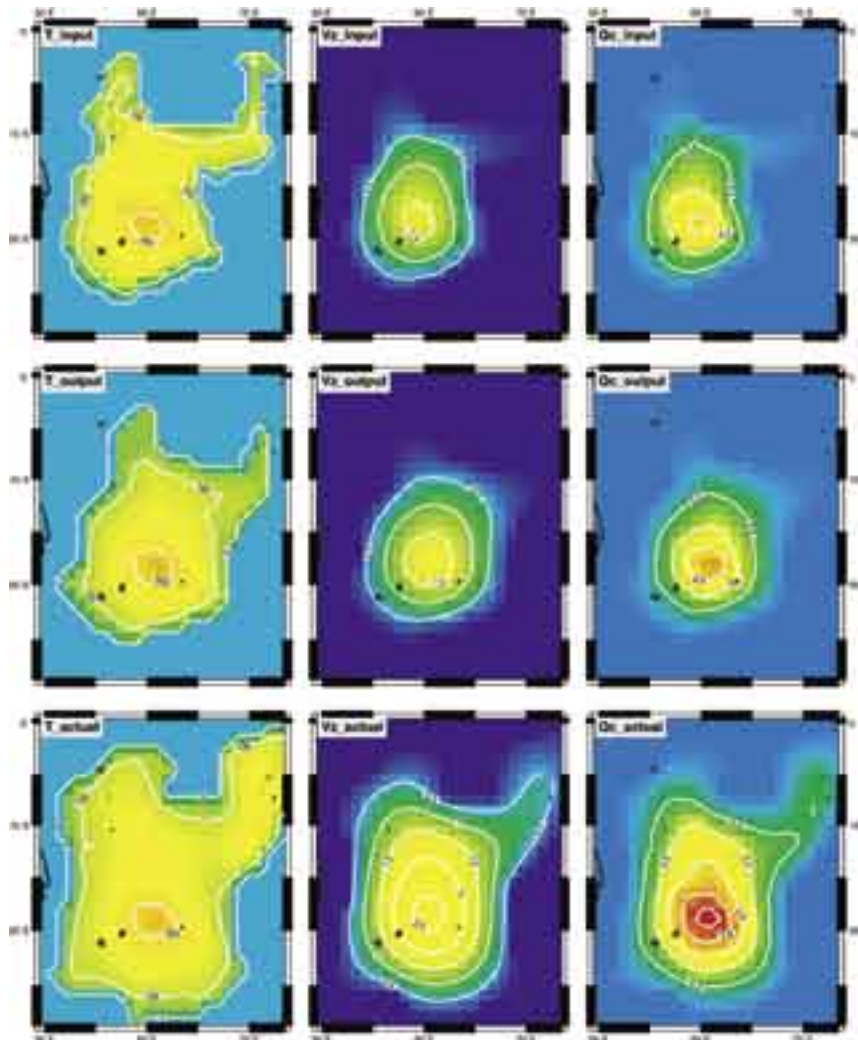


Plume Heat Flux Estimates

Guust Nolet, Raffaella Montelli • Princeton University

Shun Karato • Yale University

The global coverage with broad-band seismic stations is now such that our resolving power in selected locations is good enough to make quantitative estimates of plume flux. This figure shows an example of a resolution test for a cross-section through the Reunion plume at a depth of 1100 km. The left image shows the temperature anomaly (degrees K), the center column the rise velocity in cm/yr computed for a viscosity at background temperature of 1.6×10^{23} Pa-s and an iron enrichment ΔX_{Fe} of 0.3%. On the right we show the associated heat flux in W/m^2 . These quantities were computed for three different models, from top to bottom: the model that was input to generate data for the resolution test, the model resulting from the tomographic inversion of these synthetic data, and the model resulting from the tomographic inversion of the actual data. In this case the heat flux (0.12 TW) calculated from the tomographic image of the synthetic model was slightly higher than the input heat flux of 0.10 TW. The 'observed' heat flux calculated for the same values of viscosity and iron enrichment is 0.29 TW (biased) or 0.24 TW (corrected for bias). These estimates become lower when the effect of anelasticity is taken into account. The units are K (left), cm/yr (center) and W/m^2 (right).



Detection of Upper Mantle Flow Associated with the African Superplume

Mark D. Behn • Woods Hole Oceanographic Institute

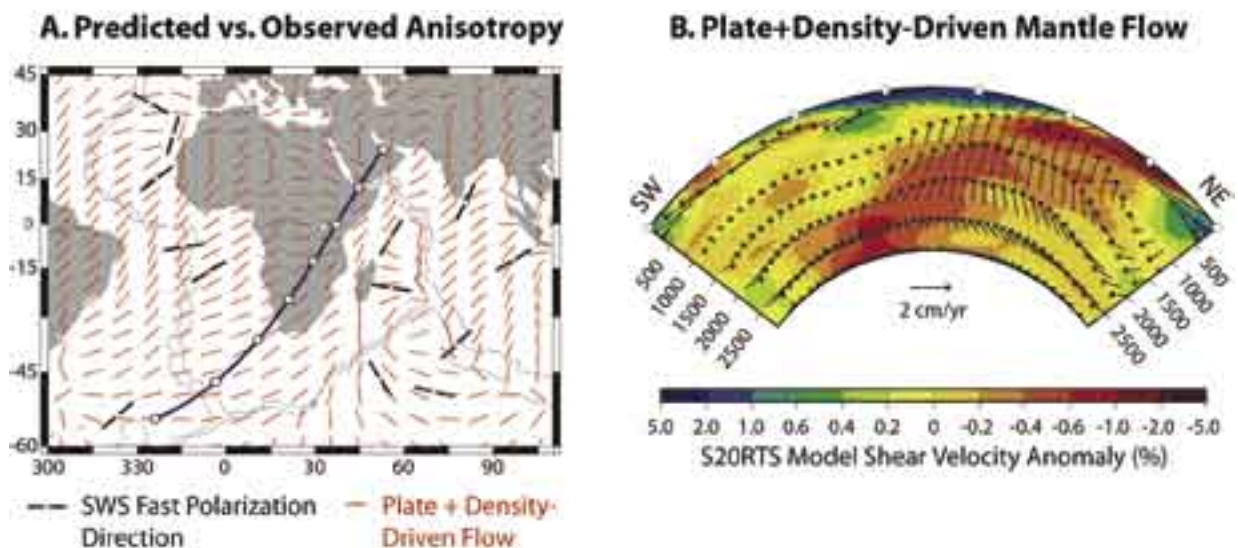
Clinton P. Conrad • University of Michigan

Paul G. Silver • Carnegie Institution of Washington

A continental-scale, low seismic velocity anomaly in the mid-to-lower mantle beneath Africa is a robust feature of global tomographic models. Assuming the low velocities are associated with warm, less-dense material, the African seismic anomaly has been ascribed to a long-lived thermal upwelling from the lower mantle. Such a large-scale upwelling is predicted to affect the regional horizontal flow field in the upper mantle. To test this model we compared seismic anisotropy inferred from shear wave splitting measurements with instantaneous flow calculations that incorporate mantle density structure determined from seismic tomography. We calculated splitting parameters at 13 ocean-island GSN and Geoscope stations surrounding Africa. Splitting measurements from island stations are ideal for interpreting anisotropy induced by asthenospheric flow because they lack a thick overlying lithosphere that may also contribute to the observed anisotropy. We tested for a possible lithospheric contribution by comparing the splitting measurements with the fossil spreading directions. We found that although the fossil

□ poor fit to the data at stations located farther off-axis. Thus, we conclude that far from a ridge axis the observed anisotropy is dominated by asthenospheric flow. To test for an active component of mantle upwelling, we considered several models with □

net-rotation (NNR) or hotspot reference frames, 2) driven by plate motions at the Earth's surface, or 3) driven by a combination of plate-motion and mantle density heterogeneity inferred from either seismic tomography or the history of subduction. We found that the best-fitting flow field is one generated by plate motions and density heterogeneity associated with large-scale upwelling originating in the lower-mantle beneath southern Africa and is manifest as a radial pattern of flow at the base of the asthenosphere. This model provides a significantly better fit to the observed anisotropy than a model in which mantle flow is driven through a passive response to subduction.



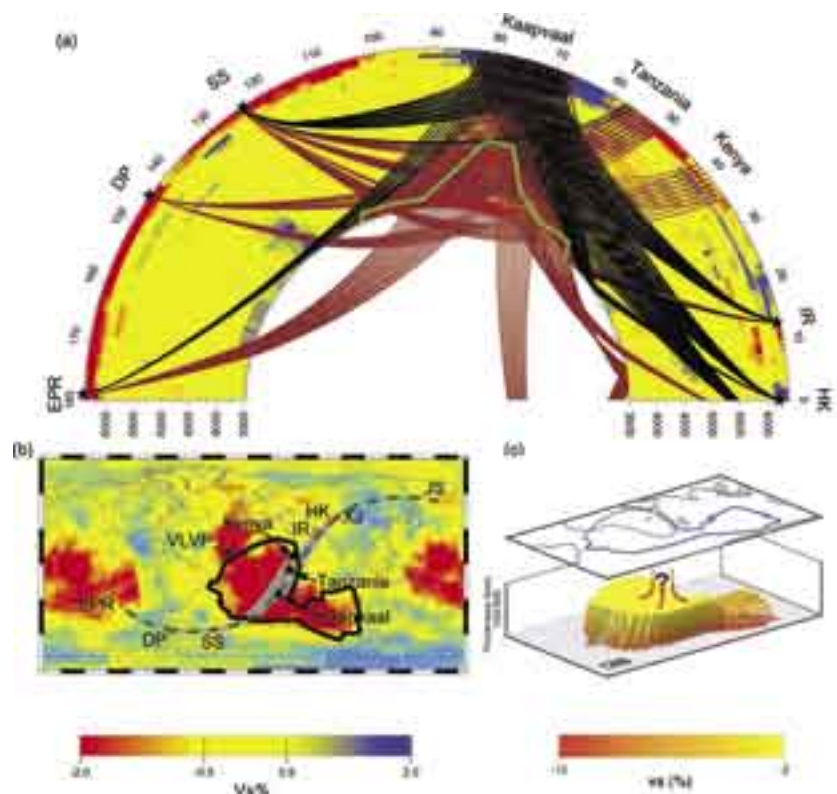
A.) Comparison of splitting observations to anisotropy predicted from global mantle flow. Black symbols indicate the orientation of the fast polarization direction from shear-wave splitting measurements at GSN and Geoscope stations. Red bars show horizontal projection of maximum shear calculated at the center of the asthenosphere for plate+density-driven mantle flow. Flow is calculated using the S20RTS tomography model (Ritsema et al., 1999) and the NUVEL-1A plate motions (DeMets et al., 1994). B.) Predicted flow field illustrating upwelling from lower mantle beneath southern Africa.

Behn, M.D., C.P. Conrad, and P.G. Silver, Detection of upper mantle flow associated with the African Superplume, *Earth Planet. Sci. Lett.*, 224, 259–274, 2004.

Structural Features and Velocity Structures of the “African Anomaly”

Yi Wang, Lianxing Wen • SUNY at Stony Brook

The IRIS PASSCAL experiments have supplied the seismology community with high-quality, freely available and spatially dense datasets. The high-quality broadband seismic data recorded in three PASSCAL experiments in Africa (the Tanzania, the Kaapvaal, and the Kenya/Ethiopia experiments) revealed a very-low velocity province occupying from the South Atlantic Ocean to the Indian Ocean in the lowermost mantle and locally extending 1300 km above the core-mantle boundary beneath southern Africa (we term it the “African anomaly”). The base of the “African anomaly” exhibits an L-shaped form changing from a north-south orientation in the South Atlantic Ocean to an east-west orientation in the Indian Ocean and occupies an area of about $1.8 \times 10^7 \text{ km}^2$ and a volume of about $4.9 \times 10^9 \text{ km}^3$. The dense seismic data and the development of hybrid method also revealed detailed structural features of the “African anomaly”. The base of the “African anomaly” has rapidly varying thicknesses from 300 km to 0 km, steeply dipping edges and a linear gradient of shear velocity reduction from -2% (top) to -9% to -12% (bottom) relative to the Preliminary Reference Earth Model (Wen et al., 2001; Wen, 2001; Wen, 2002; Wang and Wen, 2004). Its extension into the mid-lower mantle beneath southern Africa exhibits a “cusp-like” geometry with both flanks dipping toward its apex and its lateral dimension increasing with depth. The average shear velocity decreases are -5% in the base and -2% to -3% in the portion in the mid-lower mantle, and an S- to P- velocity perturbation ratio ($\delta \ln V_s / \delta \ln V_p$) is 3:1 for the entire “African anomaly” (Wang and Wen, 2005). Our ability to constrain both the geometry and velocity structures of the “African anomaly” brought significant progress in understanding the origin and dynamics of the anomaly (Wen et al., 2001). The structural features and velocity structures of the “African anomaly” unambiguously indicate that the “African anomaly” is compositionally distinct and geologically stable. It has also been suggested that the velocity structure in the lowermost mantle can best be explained by partial melt driven by a compositional change produced in the early Earth’s history (Wen et al., 2001).



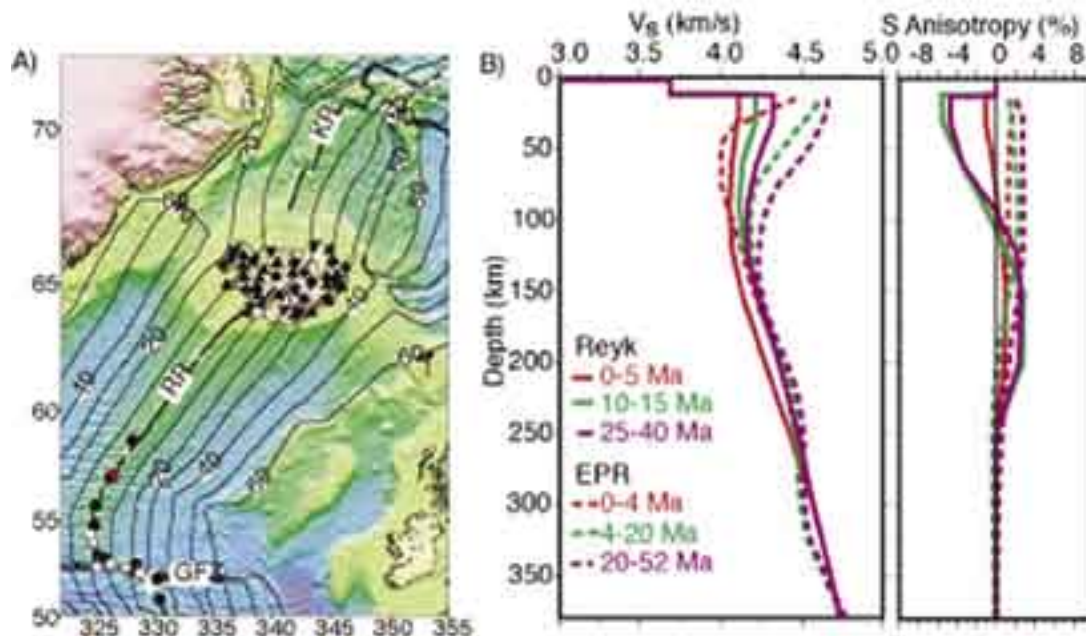
(a) Geometry (green contour) and ray paths of the seismic phases used to constrain the geometry and S-velocity structure of the “African anomaly” in a 2-D cross section along the East Pacific Rise (EPR), Drake Passage (DP), South Sandwich Islands (SS), Iran (IR), and Hindu Kush (HK). Black and red traces represent propagation paths without and with observed travel time delays that can be attributed to the “African anomaly”, respectively. Black stars represent seismic events. Seismic arrays and earthquake locations are denoted at the top of the Earth’s surface. (b) Map view of great-circle paths (gray traces), locations of earthquakes (red stars) and seismic arrays (black triangles). The thick green dashed curve represents the 2-D cross section shown in (a) and the thick black contour is the geographic boundary of the base of the “African anomaly” shown in (c). (c) Three-dimensional views of structure features and velocity structure of the base of the “African anomaly” (vertical exaggeration: 5.55, viewed from N).

- Wen, L., Seismic evidence for a rapidly varying compositional anomaly at the base of the Earth’s mantle beneath the Indian Ocean, *Earth Planet. Sci. Lett.*, 194, 83 – 95, 2001.
- Wen, L., P. Silver, D. James, and R. Kuehnel, Seismic evidence for a thermo-chemical boundary layer at the base of the Earth’s mantle, *Earth Planet. Sci. Lett.*, 189, 141 – 153, 2001.
- Wen, L., An SH hybrid method and shear velocity structures in the lowermost mantle beneath the central Pacific and South Atlantic oceans, *J. Geophys. Res.*, 103, doi:10.1029/2001JB004999, 2002.
- Wang, Y., and L. Wen, Mapping the geometry and geographic distribution of a very low velocity province at the base of the Earth’s mantle, *J. Geophys. Res.*, 109, doi:10.1029/2003JB002674, 2004.
- Wang, Y., and L. Wen, Geometry and P- and S- velocity structures of the “African anomaly”, submitted to *J. Geophys. Res.*, 2005.

Seismic Evidence for Hotspot-Induced Buoyant Flow Beneath the Reykjanes Ridge

James B. Gaherty • Lamont-Doherty Earth Observatory of Columbia University

Volcanic hotspots and mid-ocean ridge spreading centers are the surface expressions of upwelling in Earth's mantle convection system, and their interaction provides unique information on upwelling dynamics. I investigated the influence of the Iceland hotspot on the adjacent mid-Atlantic spreading center (the Reykjanes Ridge, RR) using seismic surface waves from mid-Atlantic ridge earthquakes recorded at the Global Seismic Network station BORG and stations of the ICEMELT and HOTSPOT PASSCAL deployments (left). The surface waves from these events travel along and adjacent to the RR, and the travel times of these waves are sensitive to the average crust and upper-mantle velocity along each path. These delay times were inverted for age-dependent models of radial anisotropy (right). The models show a distinct pattern of shear anisotropy (ΔV_S), with negative values ($V_{SV} > V_{SH}$) above about 100 km depth, and positive values between about 100-200 km depth. This pattern of anisotropy is unlike that in comparable oceanic models, which display $\Delta V_S > 0$ throughout the upper 200 km of the mantle. This anisotropy suggests that the hotspot induces buoyancy-driven upwelling in the mantle beneath the ridge. In this model, the melt-zone upwelling is driven by buoyancy associated with retained melt, melt residuum, and/or locally hot



(left) Bathymetric map of the North Atlantic study region. Surface waves of earthquakes (open circles) from the Reykjanes Ridge (RR) and the Gibbs Fracture Zone (GFZ) were recorded on Iceland at BORG and the ICEMELT and HOTSPOT stations (inverted and upright triangles, respectively). Seafloor age is contoured at 20 Ma intervals. (right) Upper-mantle shear-velocity models of the Reykjanes region. Left panel displays mean shear speed ($v_S = (v_{SH} + v_{SV})/2$), while right panel displays shear anisotropy ($v_S = (v_{SH} - v_{SV})/v_S$) in percent. Three age regions are shown: 0-5 Ma (short dash), 10-15 Ma (long dash), and 25-40 Ma (solid). Also shown (dash-dot lines) are shear-velocity models for Pacific upper-mantle (Nishimura and Forsyth, 1989).

mantle. Such models produce a tight circulation within the melting zone, and as the mantle material moves out of the spreading center, a near-vertical fabric associated with the downgoing limb of the circulation is retained in the off-axis lithosphere to a depth of ~60-100 km. This result suggests that buoyancy-driven upwelling is an important component of ridge dynamics, especially in environments where passive sea-floor spreading is too slow to accommodate melt production. It also implies that the anisotropic structure of oceanic lithosphere may not be as simple as inferred through studies from the fast-spreading Pacific ridges, and that this structure holds important clues to ridge and plume dynamics.

Gaherty, J.B., Seismic evidence for hotspot-induced buoyant flow beneath the Reykjanes Ridge, *Science*, 293, 1645-1647, 2001.

Imaging Seismic Velocity Structure Beneath the Iceland Hotspot – A Finite-Frequency Approach

Shu-Huei Hung, Ling-Yun Chiao • National Taiwan University

Yang Shen • University of Rhode Island

Tomographic models based on hypothetically infinite-frequency ray interpretation of teleseismic travel-time shifts have revealed a region of relatively low P and S wavespeeds extending from shallow mantle to 400 km depth beneath Iceland. In reality, seismic waves have finite-frequency bandwidths and undergo diffractive wavefront healing. The limitation in ray theory leaves large uncertainties in the determinations of the magnitude and shape of the velocity anomaly beneath Iceland and its geodynamic implications. We developed a tomographic method that utilizes the banana-shaped sensitivity of finite-frequency relative travel times from the paraxial kernel theory. Using available seismic data from the ICEMELT and HOTSPOT PASSCAL Experiments (Figure 1), we applied the new method

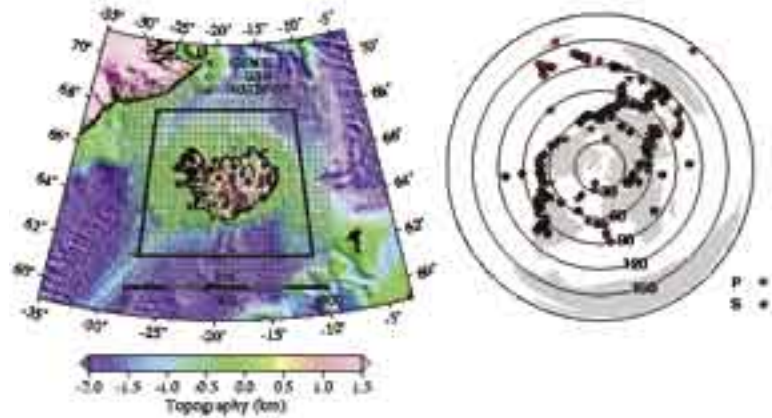


Figure 1. (Left) Location of study area and seismic stations in Iceland. The data in this study are from two temporary broadband seismic arrays of the ICEMELT and HOTSPOT Experiments and one GSN station, BORG. The outer box spans ~1000 km in both latitude and longitude directions and is divided into equally-spaced grids for model parameterization in travel time tomography. (Right) Azimuthal coverage of the earthquakes with useful P- and S-wave arrivals.

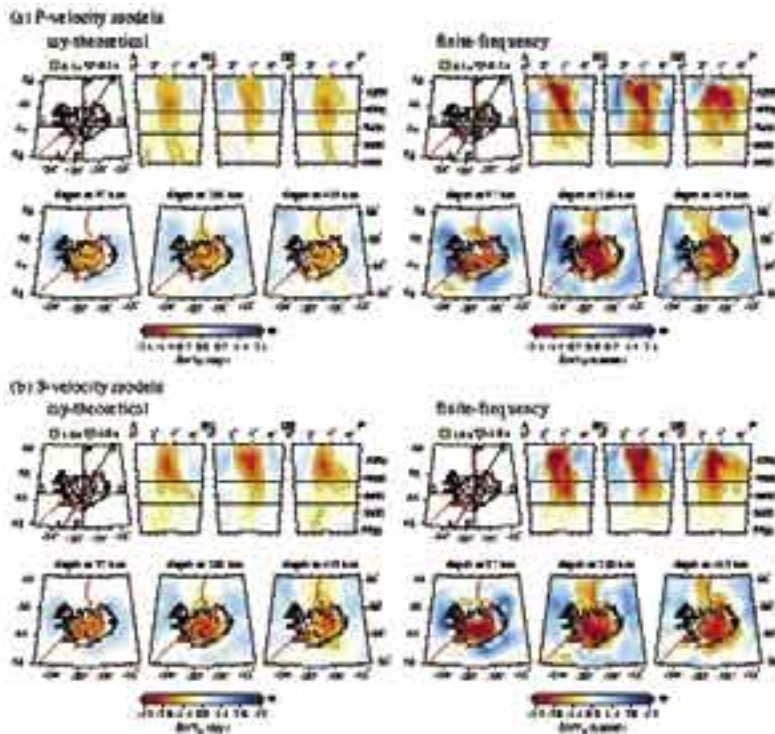


Figure 2. Comparison of the tomographic images of (a) P- and (b) S-wavespeed perturbations in the ray-theoretical (left) and finite-frequency kernel (right) models. The contours shape the region in which the P and S velocities are at least 0.5% and 1.0% lower than those in the surrounding mantle. All the models reveal a columnar zone of low-velocity anomaly of ~250-300 km in diameter beneath central Iceland. In the finite-frequency models this low-velocity feature extends to the base of the upper mantle, while the maximum resolvable depth for the ray-based models is ~400 km. Both P- and S-velocity perturbations in the kernel-based models are significantly larger than those in the ray-theoretical models. The station corrections are indicated by squares for the positive or relatively-slow and triangles for the negative or relatively-fast velocity anomaly.

to image subsurface velocity structure beneath Iceland. Given similar fit to data, the kernel-based models yield the root-mean-square amplitudes of P- and S-wavespeed perturbations about 2-2.8 times those from ray tomography in the depths of 150-400 km. The kernel-based images show that a columnar low-velocity region having a lateral dimension of ~250-300 km extends to the base of the upper mantle beneath central Iceland, deeper than that resolved by the ray-based studies (Figure 2). The improved resolution in the upper-mantle transition zone is attributed to the deeper crossing of broad off-path sensitivity of travel-time kernels than in ray approximation and frequency-dependent wavefront healing as an intrinsic measure of the distance from velocity heterogeneity to receivers.

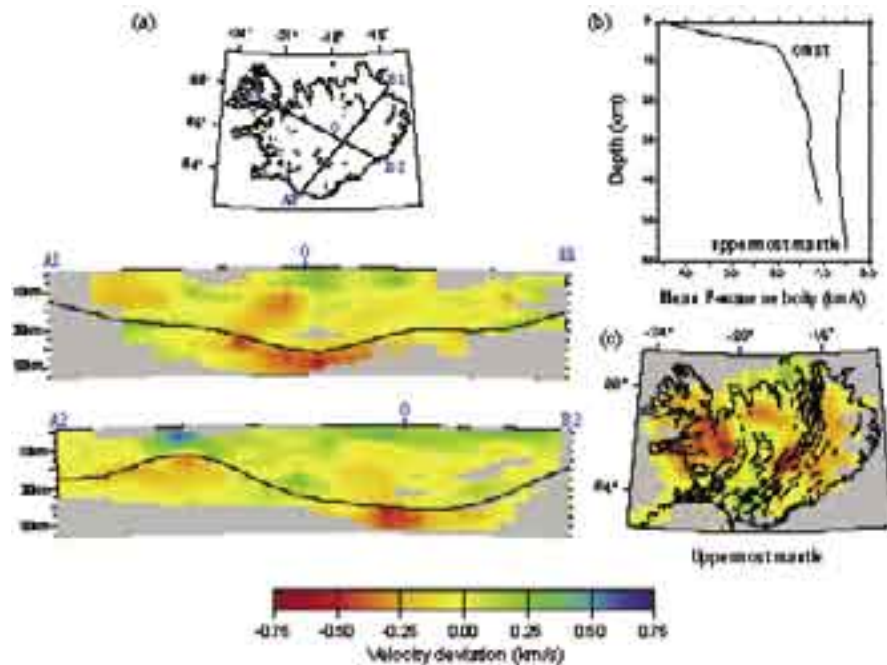
Hung, S.-H., Y. Shen, L.-Y. Chiao, Imaging seismic velocity structure beneath the Iceland hot spot: a finite frequency approach, *J. Geophys. Res.*, 109, 8305, doi: 10.1029/2003JB002889, 2004.

Research was supported by NSC of Taiwan (SHH and LYC) and NSF (SHH and YS) and instruments of the HOTSPOT Experiment provided by IRIS PASSCAL.

Crustal and Uppermost Mantle Structure Beneath Iceland from Local Earthquake Tomography

Ting Yang, Yang Shen • University of Rhode Island

The structure of the crust and uppermost mantle beneath Iceland, the keys to understanding the magma plumbing system of the hotspot and hotspot-ridge interaction, was poorly constrained in previous seismological investigations. We developed a three-dimensional P-wave velocity model of the Icelandic crust and uppermost mantle from tomographic inversion of over 3500 first-arrivals from local earthquakes recorded in Iceland. The model shows a broad low-velocity anomaly in the middle and lower crust underlying a high-velocity body in the shallow crust in central Iceland. With seismic rays traversing below the crust, the inversion also reveals a pronounced P-wave velocity reduction, about 5% or 1.4 - 2 times that in the 100-400 km depth range imaged by teleseismic tomography, in the uppermost mantle beneath central Iceland. The large velocity reduction requires an excess temperature of up to 500 degrees or, more likely, a combination of excess temperature and partial melt. The localized nature of the region of low velocity beneath central Iceland and the lack of comparable velocity reduction along the volcanic zones suggest a relatively focused melt supply of the hotspot.



The P-wave velocity model from local earthquake tomography. Values in the cross-sections are deviations in wave speed (km/s) from the average velocity for the crust or the uppermost mantle at each depth, which is shown in (b). (a) Vertical cross-sections of the P-wave velocity model through central Iceland; Black lines indicate the Moho in Allen et al. (2002). (c) Map view of the velocity anomaly beneath the Moho.

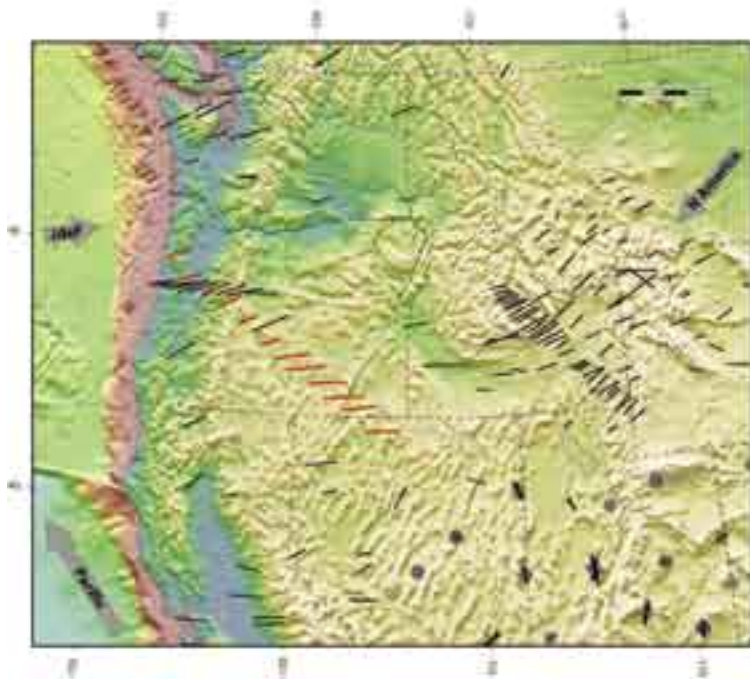
Yang, T., and Y. Shen, P-wave velocity structure of the crust and uppermost mantle beneath Iceland from local earthquake tomography, *Earth Planet. Sci. Lett.*, in press.

Allen, R.M. et al., Plume driven plumbing and crustal formation in Iceland, *J. Geophys. Res.* 107, (2002), doi:10.1029/2001JB000584, 2002.

The Origin of Hotspot Volcanism in the Pacific Northwest

Richard M. Allen, Mei Xue • *University of California, Berkeley*

In the northwestern United States there are two hotspot tracks: the Newberry track and the Yellowstone track. Both are located on the North American Plate with the Yellowstone track parallel to plate motion and the Newberry track oblique to it. While a mantle plume is often cited as the cause of the Yellowstone track, the Newberry track cannot be the product of plate motion over a stationary mantle source. Instead,



Variation in shear-wave splitting fast directions across the Pacific Northwest. Our shear wave splitting results are shown in red along with those from other studies (Fabritius, 1995; Ozalaybey and Savage, 1995; Barruol et al., 1997; Polet and Kanamori, 1997; Schutt et al., 1998; Savage and Sheehan, 2000; Schutt and Humphreys, 2001; Savage, 2002; Currie et al., 2004; Waite et al., submitted) in black with sticks indicating the fast direction. Our results show a WNW-ESE fast direction adjacent to the coast which is consistent with all splitting observations in the Cascadian forearc and parallel to absolute plate motion of the Juan de Fuca plate. The fast direction rotates to E-W inland along the OATS array consistent with observations in the western Snake River Plain.

proposed causal mechanisms for the Newberry track include upper mantle processes where melt buoyancy-driven convection is directed west-northwest, parallel to the hotspot track, by subduction-driven corner flow, or alternatively by topography of the base of the lithosphere. Alternatively, lithospheric processes such as fracture propagation have been proposed as the cause of the volcanism.

In this SKS splitting study, we collected data from the OATS (Oregon Array for Teleseismic Study) array deployed along the Newberry track from NW to SE Oregon. Measurements were made for 23 events at 12 OATS stations and show a gradual rotation of the fast polarization direction from NE-SW at the northwest end of the array to E-W to the southeast, consistent with regional observations (see figure). Most stations also exhibit null results when the event back azimuth was parallel or perpendicular to the fast direction determined from other events, strongly indicating a single layer of anisotropy. The first order observation is that the SKS splits are not aligned with the Newberry hotspot track. This suggests there is little or no mantle flow oriented along the track implying that the hotspot is not the product of asthenospheric flow. It therefore seems likely that the Newberry hotspot track is the product of lithospheric processes.

Shear Wave Splitting in the Great Basin Solves the Elevation Problem: It Was a Simple Plume-like Upwelling All Along

Kris Walker • University of California, San Diego

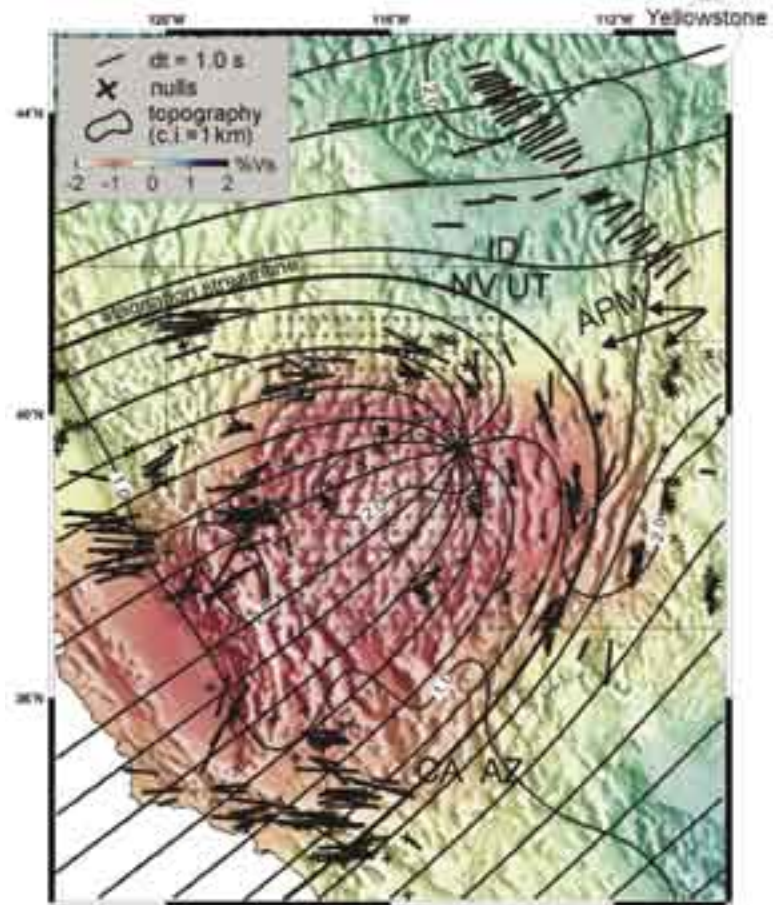
Simon Klemperer • Stanford University

Goetz Bokelmann • University of Montpellier, France

The Great Basin has an average elevation of 2 km. The average crustal thickness of 32 km does not explain this high elevation, hence the mantle appears to be anomalously buoyant. Around 16-17 Ma, an outpouring of flood basalts erupted throughout the northern Basin and Range, including a linear progression of felsic volcanism from McDermitt volcano in northern Nevada toward the northeast and northwest to the current locations of Yellowstone and Newberry, respectively. Published tomographic images show a low-velocity zone beneath Nevada at ~350 km depth, although the images do not reveal fine structure. Receiver functions suggest a low-velocity zone atop the 410 km discontinuity in northern Nevada that pinches out beneath eastern Nevada.

In Walker et al. (2005) we present new teleseismic shear-wave splitting data from six IRIS broadband seismic stations deployed along the axis of the SRP from 6/2000-9/2001. We show the first-order anisotropy signal is explained by a single layer of anisotropy with a horizontal fast axis. Considering the lithosphere is quite thin in the Great Basin and the lack of correlation between fast directions and geologic fabrics at the surface, it is likely that the anisotropy is located in the asthenosphere. We quantitatively modeled our station fast directions, as well as splitting fast directions from numerous other stations throughout the Basin and Range. We find that they are best explained by a lattice preferred orientation of olivine due to horizontal shear along the base of the plate associated with the gravitational spreading of buoyant

plume-like upwelling material beneath eastern Nevada into a southwestward flowing asthenosphere (with respect to a fixed hotspot reference frame). This parabolic asthenospheric flow (PAF) model for the Great Basin easily explains the observed high elevations, high mantle buoyancy, low-velocity anomaly beneath eastern Nevada, high heat flow, and depleted geochemistry of some erupted basalts. An upwelling model may also be consistent with the results of turning-ray waveform and receiver-function modeling, which suggests the low-velocity zone atop the 410-km discontinuity beneath the northern Basin and Range does not exist beneath eastern Nevada. The lack of Pliocene-Recent major volcanism in eastern Nevada suggests that a significant amount of the buoyancy flux is due to compositional buoyancy. This model also implies that existing upwellings beneath Yellowstone and Newberry are not responsible for the high elevations we observe in the Basin and Range today.



Walker, K.T., Bokelmann, G.H.R., and Klemperer, S.L., Shear-wave splitting beneath the Snake River Plain suggests a mantle upwelling beneath eastern Nevada, USA, *Earth Planet. Sci. Lett.*, 222, 529-542, 2004.

Walker, K.T., Bokelmann, G.H.R., Klemperer, S.L., and Nyblade, A., Shear-wave splitting around hotspots: Evidence for upwelling-related mantle flow?, *Proceedings, Plume IV; Beyond the Plume Hypothesis; Tests of the plume paradigm and alternatives*, G. Foulger, J.H. Natland, D.C. Presnall, and D.L. Anderson (Eds.), (in press), 2005.

Collaborative Research: Geodynamics of the Yellowstone Hotspot Constrained by Seismic and GPS Imaging

Robert B. Smith • *University of Utah*

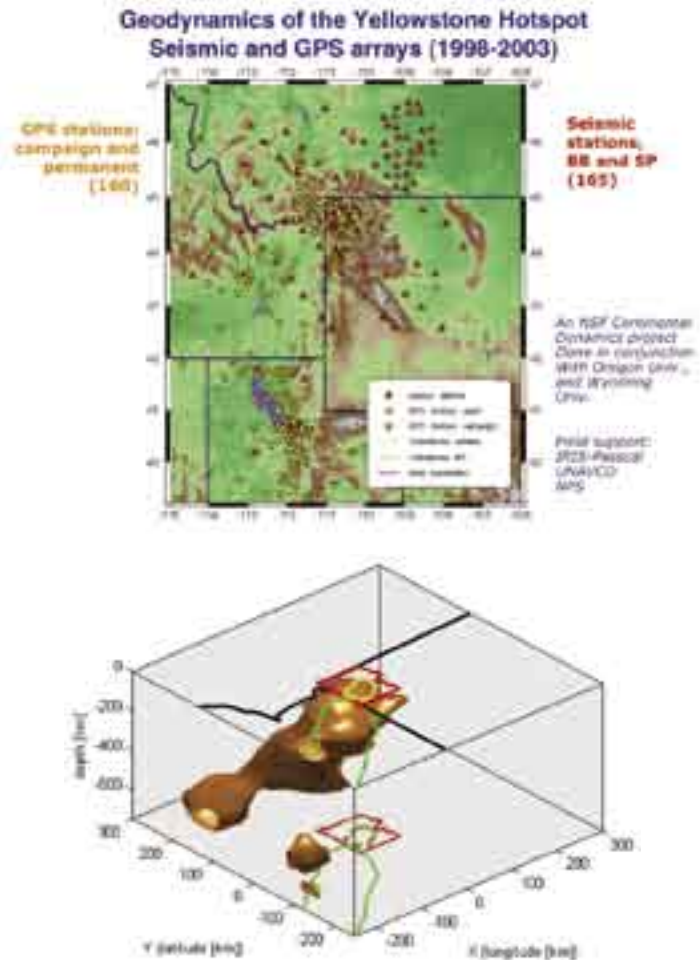
Eugene Humphreys • *University of Oregon*

Paul Tackley • *University of California, Los Angeles*

Ken Dueker • *University of Wyoming*

A collaborative research project funded by the NSF Geodynamics Program with seismic monitoring supported by the IRIS PASSCAL Instrument Center and GPS instrumentation supported by UNAVCO Facility.

The goal of this study is to evaluate the underlying source of the Yellowstone Hotspot and to geodynamically model its effect on the tectonics and topography of the western U.S. Yellowstone is characterized by 2 Ma caldera-forming volcanism at the NE end of a 800-km long 16 Ma track of volcanism across the Snake River Plain. This system is modeled by SW motion of the N. American plate across a mantle hotspot source hypothesized to be a plume. To evaluate the causative mechanism, two major field experiments were conducted. An 80-station 600 km x 500 km array of portable seismographs were deployed over two years, 2000-2002. Teleseismic data from this array provided high-resolution 3D Vp and Vs tomographic images that revealed a narrow low-velocity anomaly tilted west and extending from Yellowstone to 650 km depth. GPS data were acquired by 160 temporary deployed stations and 16 permanent stations that were used to assess caldera motions and regional kinematics. Together these data along with constraints from mantle return flow models have been employed to develop kinematic and geodynamical models of the system.



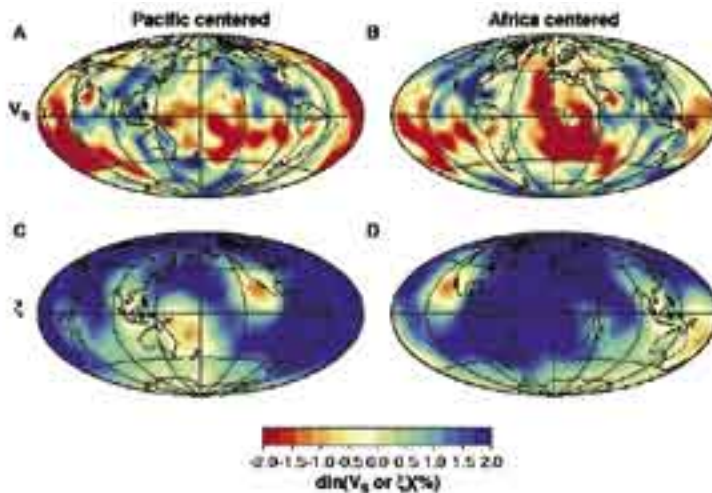
(Top) Map of seismic and GPS station location deployed for the Yellowstone hotspot experiment. (Bottom) 3D isosurface image from tomographic reconstruction outlining a tilted low-velocity body, i.e. a mantle plume, extending WNS beneath the Yellowstone to resolved depths of 650 km, the bottom of the mantle transition zone.

A Three-Dimensional Radially-Anisotropic Model of Shear Velocity in the Whole Mantle

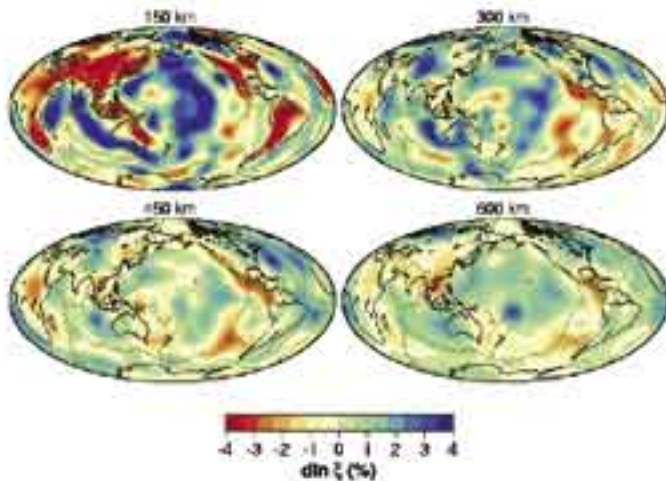
Mark Panning, Barbara Romanowicz • Berkeley Seismological Laboratory

We have developed a 3D radially anisotropic shear velocity model of the whole mantle using a large three-component surface and body waveform dataset, derived primarily from IRIS GSN as well as Geoscope stations, using an iterative inversion for structure and source parameters based on Nonlinear Asymptotic Coupling Theory (NACT) (Li and Romanowicz, 1995). The model is parameterized in terms of isotropic V_S and an anisotropic parameter, ξ , which is defined by $\xi = V_{SH}^2/V_{SV}^2$.

The model shows a link between mantle flow and anisotropy in a variety of depth ranges.



Isotropic V_S (top) and ξ (bottom) structure at 2800 km depth, centered under the Pacific (left) and Africa (right).



ξ structure at four depths in the upper mantle and transition zone.

The isotropic V_S model matches the common features of S tomographic models. The uppermost 200 km shows tectonic features, with fast velocities in the continental interiors and slower oceans and tectonically active regions. In the transition zone, the most prominent features are the fast subducted slabs. Mid-mantle velocity anomalies are low in amplitude, and white in spectrum. In the lowermost 500 km, the amplitudes of heterogeneity increase, and show a degree 2 pattern with rings of higher velocities surrounding two lower velocity regions under the central Pacific and Africa.

In the ξ model of the upper mantle, we observe positive anomalies ($V_{SH} > V_{SV}$) starting at ~ 80 km under oceanic regions and ~ 250 km under old continents, suggesting horizontal flow beneath the lithosphere (Gung et al., 2003). We also observe a $V_{SV} > V_{SH}$ signature at ~ 200 -300 km depth beneath major ridge systems with amplitude correlated with spreading rate. In the transition zone (400-700 km), regions of subducted slab material are associated with negative ξ anomalies ($V_{SV} > V_{SH}$), while the ridge signal decreases except under the East Pacific Rise.

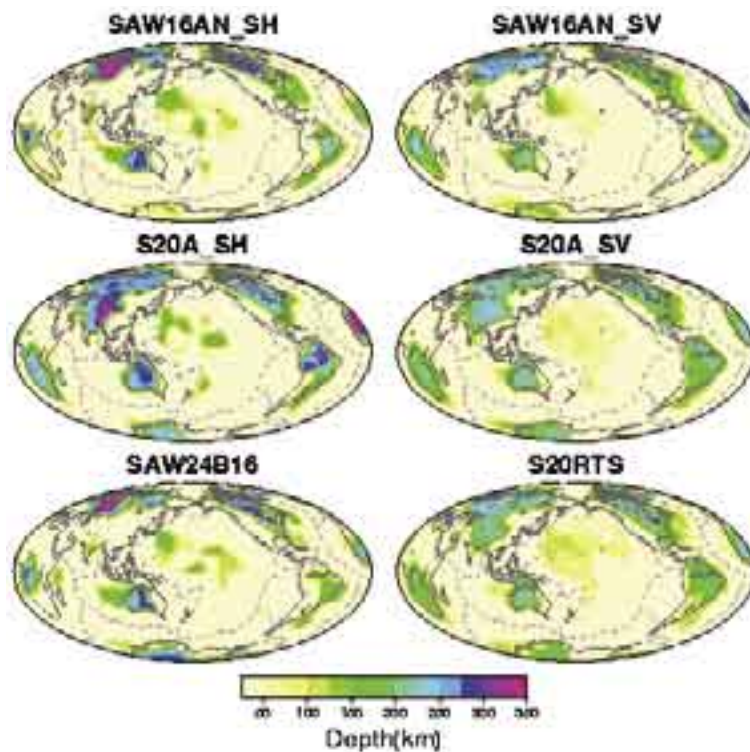
We also observe strong radially symmetric $V_{SH} > V_{SV}$ in the lowermost 300 km (Panning and Romanowicz, 2004). The 3D deviations from this degree 0 signature are associated with the transition to the large-scale superplumes under the central Pacific and Africa, suggesting that $V_{SH} > V_{SV}$ is generated in the predominant horizontal flow of a mechanical boundary layer, with a change in signature related to transition to upwelling at the superplumes.

Gung, Y., M. Panning, and B. Romanowicz, Global anisotropy and the thickness of continents, *Nature*, 422, 707-711, 2003.

Panning, M.P. and B. Romanowicz, Inferences on flow at the base of Earth's mantle based on seismic anisotropy, *Science*, 303, 351-353, 2004.

Global Anisotropy and the Thickness of Continents

Yuancheng Gung, Mark Panning, Barbara Romanowicz • Berkeley Seismological Laboratory



Maximum depth for which the velocity anomaly with respect to the reference model PREM (Dziewonski and Anderson, 1981) is greater than 2%, for different S-velocity models. Left: "SH" type models; right: "SV" type models. Bottom: V_{SH} model SAW24B16 (Mégnin and Romanowicz, 2000) compared to V_{SV} model S20RTS (Ritsema et al., 1999); middle: SH and SV parts of model S20A (Ekström and Dziewonski, 1998) obtained by inverting T component data and Z,L component data separately; top: SH and SV parts of anisotropic model SAW16AN discussed here. While the roots of continents generally extend to depths greater than 300-350 km in SH models, they do not exceed 200-250 km in SV models.

Since the concept of "tectosphere" was first proposed, there have been vigorous debates about the depth extent of continental roots. The analysis of heat flow, mantle xenoliths, gravity and glacial rebound data indicate that the coherent, conductive part of continental roots is not much thicker than 200-250 km. Some global seismic tomographic models agree with this estimate but others indicate much thicker lithosphere under old continents, reaching at least 400 km in depth.

Although global Vs models differ from each other significantly in the depth range 200-400 km under the main continental shields, these differences are consistent when they are classified into three categories, depending on the type of data used to derive them: 'SV' (mostly vertical or longitudinal component data, dominated by Rayleigh waves in the upper mantle), 'SH' (mostly transverse component data, dominated by Love waves), and 'hybrid' (3 component data). 'SH' and 'hybrid' models are better correlated with each other than with 'SV' models, and this difference is accentuated when the correlation is computed only across continental areas. Also, 'SH' (and 'hybrid') models exhibit continental roots that exceed those of 'SV' models by 100 km or more. These disagreements can be reconciled when taking into account anisotropy.

We have developed a radially anisotropic model of the upper mantle, based on the inversion of waveforms of fundamental and higher mode surface waves, in the framework of Non-Linear Asymptotic Coupling Theory (Li and Romanowicz, 1995), and including truly anisotropic kernels. Significant radial anisotropy with

$V_{SH} > V_{SV}$ is present under most cratons in the depth range 250-400 km, similar to that reported earlier at shallower depths (80-250 km) under ocean basins. We propose that in both cases, this anisotropy is related to shear in the asthenospheric channel, located at different depths under continents and oceans. The seismically defined lithosphere is then at most 200-250 km thick under continents. The Lehmann discontinuity, observed mostly under continents around 200-240 km, and the Gutenberg discontinuity, observed under oceans at shallower depths (~ 60-80 km), may both be associated with the bottom of the lithosphere, marking a transition to flow-induced asthenospheric anisotropy (Gung et al., 2003).

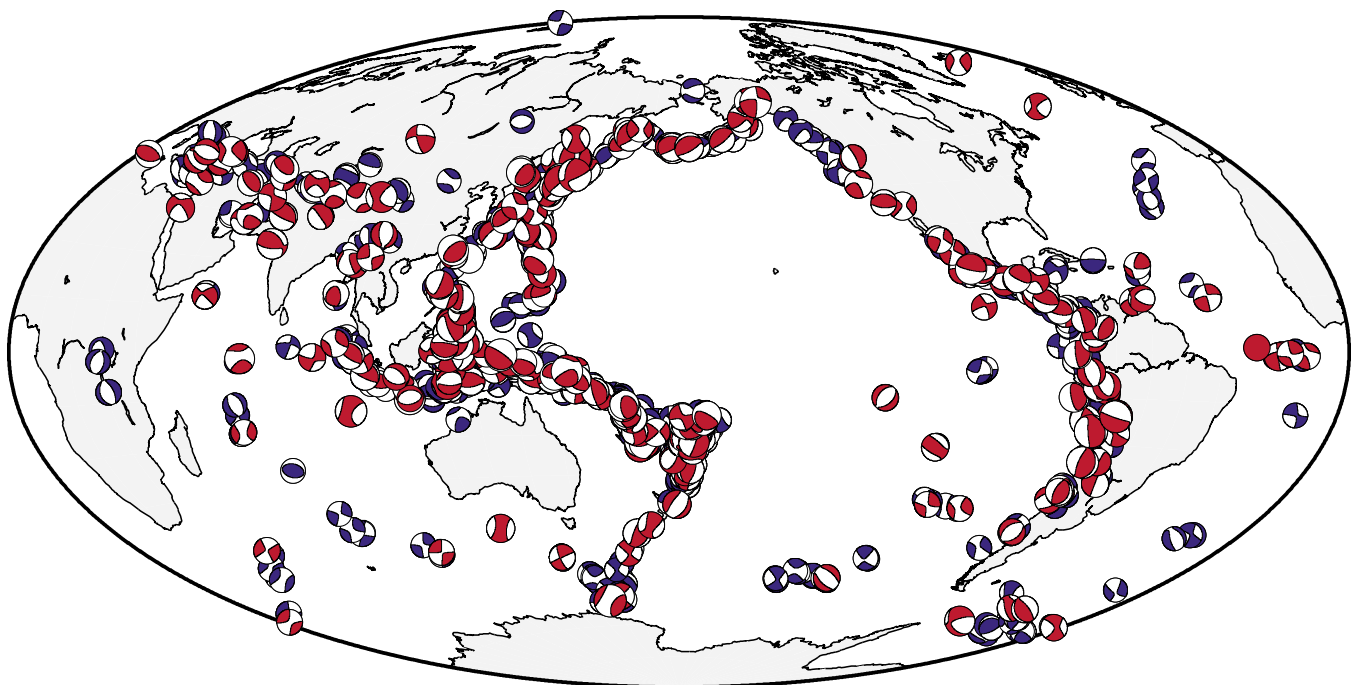
Gung, Y., M. Panning and B. Romanowicz, Global anisotropy and the thickness of continents, *Nature*, 422, 707-710, 2003.

NSF grant which supported this work: EAR- 9902777

Imaging the Anisotropic Shear-wave Velocity Structure of the Earth's Mantle

Bogdan Kustowski, Adam M. Dziewónski, Göran Ekström • *Harvard University*

Over the last 10 years, dozens of new stations of the Global Seismographic Network have been deployed in remote and previously uninstrumented regions. The seismograms recorded at these sites provide new constraints on the structure of the Earth's mantle. We use seismograms from the years 1994-2003 to build a new set of waveform data to constrain the transversely isotropic shear-wave velocity structure of the mantle. The waveforms are iteratively inverted for earthquake source mechanisms and for the earth structure using the technique of Woodhouse and Dziewónski (1984). Our new data set consists of 219 well-recorded earthquakes and 10 great ($M_w \geq 8$) earthquakes. The Harvard CMT solutions of these events are shown in red. Several tens of magnitude 6 earthquakes, which we are also planning to include in the inversion, are shown in blue. All the events distributed throughout the earth recorded by the expanding Global Seismographic Network provide unprecedented global ray-path coverage. The number of seismograms used in the waveform inversion exceeds 120,000 and represents a 60-fold increase compared with the work of Woodhouse and Dziewónski (1984). To further improve resolution in the uppermost and lowermost parts of the mantle, we complement the waveform data set with measurements of surface-wave phase velocities (Ekström et al., 1997) and body-wave travel times (Liu, 1997), respectively. In addition to the anisotropic shear-wave velocity structure, we map the topography of the transition zone discontinuities using measurements of long-period SS precursors (Gu et al., 2003). The new model will improve our knowledge about the structure and dynamics of the Earth's mantle and will allow for more accurate determination of the earthquake hypocenters and source mechanisms.



Gu, Y.G., A. M. □
J. Int., 154, 559-583, 2003.

Geophys.

Global Analysis of Upper Mantle Anisotropy Using Automated SKS Splitting Measurements

Matthews S. Evans • *University of Leeds, International Seismological Centre, United Kingdom*

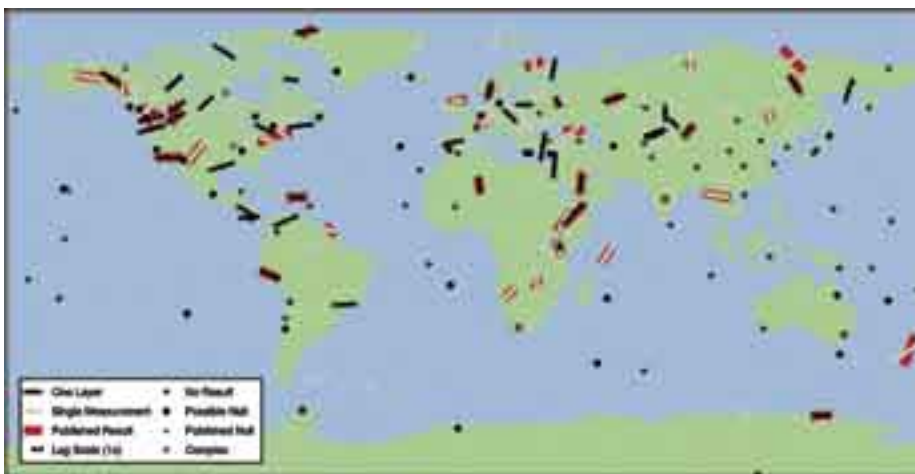
J. Michael Kendall • *University of Leeds, now at University of Bristol, United Kingdom*

Raymond J. Willemann • *International Seismological Centre, now at IRIS*

We have developed an automated method to measure shear-wave splitting and applied it to SKS phases archived by various data centers. Using an automated system we are able to process data in a quantity and with a consistency not possible with manual measurements. To date we have processed over 100,000 station/event combinations from over 200 stations distributed globally, although our stringent quality control measures mean that only approximately 2 percent produce reliable estimates of splitting.

When a polarized shear wave passes through an anisotropic medium, it is split into two perpendicular S waves that are separated in time. In measuring splitting, we seek a polarization angle and time shift that removes the effect of the anisotropy, minimizing either the energy on the transverse component or the smaller of the two eigenvalues calculated from the covariance matrix. We report results from both methods, to allow consistency in comparisons with the results of other researchers and because we find consistent differences in results at some stations. Error estimates are calculated using both the methods of Silver and Chan (1991) and Sandvol and Hearn (1994).

Where it is possible to compare, we find that our automated results agree well with manual measurements. The quality of results at individual stations is variable, being influenced both by the volume of available data (determined by station deployment date and the distribution of natural seismicity), and the performance of the STA/LTA picker used to define the start of the SKS window. When we have reliable results from a range of back azimuths, we compare the distribution of results with those predicted from single and multiple layers of anisotropy. Where this is not possible we report the polarization angle and lag time for the most convincing splitting measurement. Where even this is not possible and where a sufficient number of events have been processed, a station is interpreted as a null, which may mean that it is underlain by an isotropic or transversely isotropic mantle. For stations suggesting either single-layer anisotropy or where an individual splitting measurement has been used, we find an average lag value of 1.15 seconds. There seems to be some relation between splitting parameters and tectonic environment.



Stars represent complex anisotropy, (dipping or multiple layers), characterized by splitting parameters varying with back azimuth. Single layer solutions are shown with thick black lines, with fast polarization direction and magnitude of splitting represented by the orientation and length respectively. A grey line is from a single measurement. An open line is for 'no result'. A closed circle is a reliable null value. The STA/LTA picker often does poorly at ocean stations. Map includes results from other authors, (red symbols), which show good correlation with our results.

Funding for this project was provided by NERC grant NER/A/S/2001/00524.

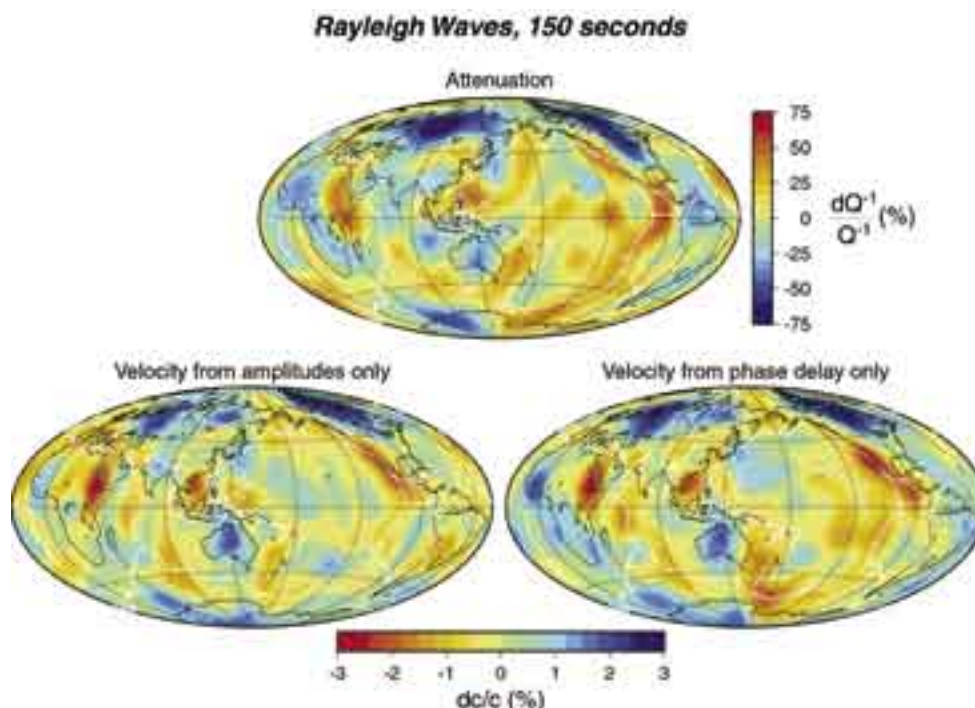
Investigating Attenuation and Velocity Structure from Surface-Wave Amplitudes

Colleen Dalton, Göran Ekström • *Harvard University*

We have investigated upper-mantle attenuation ($1/Q$) structure using a large data set of fundamental-mode Rayleigh-wave amplitudes measured from seismograms recorded by the stations of the IRIS/USGS GSN and other global networks. Historically, the development of Q models has lagged behind that of velocity models in large part because of the difficulties involved in measuring and interpreting seismic-wave amplitudes. Specifically, effects on the amplitude due to source excitation, focusing and defocusing by lateral velocity heterogeneity, and instrument response must be accounted for before the data can be interpreted in terms of anelastic structure. Despite these complications, improving models of seismic-wave attenuation in the mantle is an important objective of seismology, as Q is highly sensitive to temperature and can provide an independent set of constraints on the Earth's internal structure that is complementary to the results of elastic-velocity tomography. Additionally, large lateral variations in attenuation will cause significant dispersion of waves traveling at different periods and must be considered when constructing and comparing velocity models derived from seismic observations from different portions of the seismic frequency band.

Our inversion solves for spherical-harmonic maps of attenuation and phase velocity (for periods spanning 50 - 250 seconds) in addition to scalar amplitude correction factors for each source and receiver that provided data for the inversion. The effect of focusing on the wave amplitude is related to the second derivative of phase velocity perpendicular to the ray path; we correct for it using the linear approximation of Woodhouse and Wong (1986). The degree-12 attenuation maps that result

□ longest periods (i.e., for waves sampling the transition zone). The top figure shows the retrieved lateral variations in attenuation for 150-second Rayleigh waves, which are primarily sensitive to structure between 150 - 300-km depth. The East-Pacific Rise, western United States, and Red Sea region are highly-attenuating features, while old continental shields such as the Baltic region, Canada, Antarctica, and the cratons of Africa appear as areas of low attenuation. When attenuation and source and receiver uncertainty are adequately treated, the amplitude data can also provide strong constraints on global phase velocities. The bottom figure shows phase-velocity maps for 150-second Rayleigh waves determined from the amplitude data alone (no travel times) (left) and from phase-delay measurements alone (right). The correlation between the two is quite striking (correlation coefficient = 0.76). It appears that when the extraneous effects on wave amplitude are properly accounted for, an improved image of 3-D anelastic structure can be achieved.

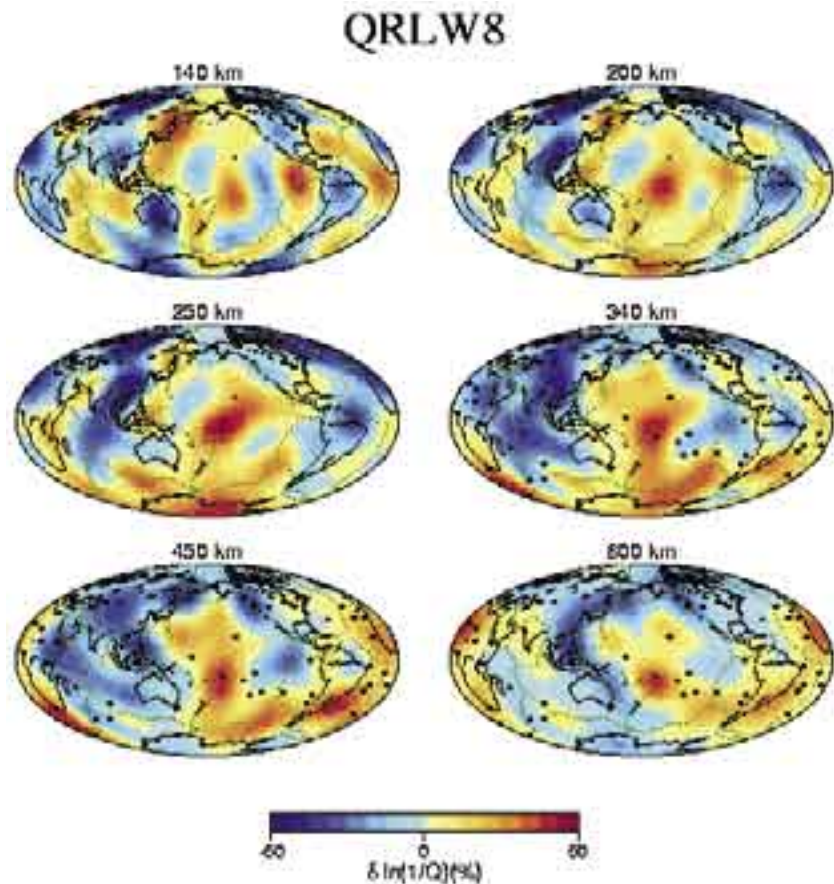


Global Tomographic Model of Q in the Upper Mantle Obtained Using Long-period Waveform Data

Yuancheng Gung, Barbara Romanowicz • Berkeley Seismological Laboratory

We developed a degree 8 three-dimensional Q model (QRLW8, Gung and Romanowicz, 2004) of the upper mantle, derived from three component surface waveform data in the period range 60-400 sec. These waveform data were collected from stations of the IRIS/GSN and Geoscope networks. The inversion procedure involves two steps. In the first step, 3D whole-mantle velocity models are derived separately for elastic SH (transverse component) and SV (vertical and longitudinal component) velocity models, using both surface and body waveforms and the NACT approach (Non-linear asymptotic coupling theory, Li and Romanowicz, 1995). In the second step, the surface waveforms thus aligned in phase are inverted to obtain a 3-D Q model in the depth range 80-670 km.

Various stability tests were performed to assess the quality of the resulting Q model, and in particular to assess possible contamination from focussing effects. We find that the 3D patterns obtained are stable, but the amplitude of the lateral variations in Q is not well constrained, because large damping is necessary to extract the weak Q signal from data. The model obtained agrees with previous results in that a strong correlation of Q with tectonics is observed in the first 250 km of the upper mantle, with high attenuation under oceanic regions and low attenuation under continental shields. It is gradually replaced by a simpler pattern at larger depths. At the depths below 400 km, the Q distribution is generally dominated by two strong minima, one under the southern Pacific and one under Africa, which correlate strongly with the two minima observed in elastic tomographic models in the deep mantle, suggesting continuity into the upper mantle of the upwelling flow originating in these regions at the base of the mantle (Romanowicz and Gung, 2002). Moreover, most hotspots are located above regions of low Q in the transition zone. On the other hand, ridges are shallow features in both velocity and Q models.



Model QRLW8 derived from three component data at different depths in the upper mantle. Blue and red regions are regions of low and high attenuation, respectively. Black dots are hotspots according to the list by Richards et al. (1988).

Gung, Y. and B. Romanowicz, Q tomography of the upper mantle using three-component long period waveforms, *Geophys. J. Int.*, 157, 813-830, 2004.

Romanowicz, B. and Y. Gung, Mega-upwellings from the core mantle boundary to the lithosphere: implications for heat flux, *Science*, 296, 513-516, 2002.

NSF grants which supported this work: EAR- 9902777 and EAR-0308750

Compressional-Wave Studies on the Frequency Dependence of and Lateral Variations in Mantle Attenuation

Linda M. Warren • *Carnegie Institution of Washington*

Peter M. Shearer • *University of California, San Diego*

We study the frequency dependence of and lateral variations in P-wave attenuation in the mantle by analyzing the spectra from >18,000 P and >14,000 PP arrivals. We select seismograms from the IRIS FARM database from large, shallow earthquakes at epicentral distances of 40°-80° for P waves and 80°-160° for PP waves and compute the spectrum for a 12.8-s-long window around each arrival. Each spectrum is the product of source, receiver, and propagation response functions as well as local source- and receiver-side effects, and we use a stacking procedure to isolate the propagation effects. Using separate absorption bands in the upper and lower mantles, we model the average depth and frequency dependence of mantle Q by combining measurements of the amplitude decay of the propagation log spectra between 0.16 and 0.86 Hz with long-period $Q\beta$ values of other workers. We find that the upper mantle is more attenuating than the lower mantle and that this contrast is greater at higher frequencies. At 1 Hz, the top 220 km of the mantle is ~6 times more attenuating than the lower mantle. In addition, our results indicate that the up-

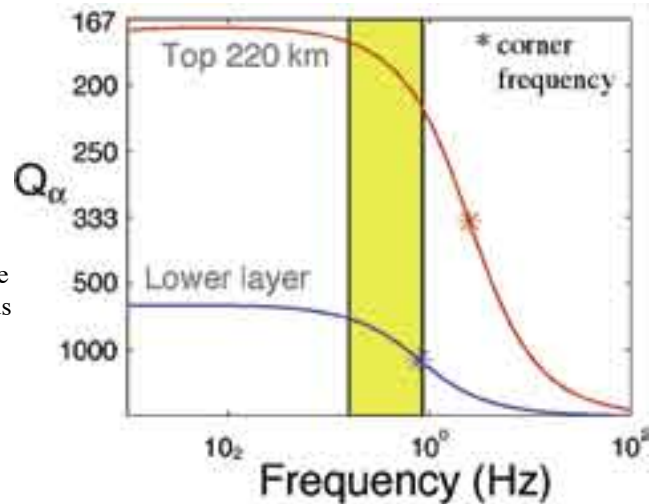


Figure 1. Absorption band Q_α model for the Earth's mantle. The top 220 km of the mantle is more attenuating than the lower mantle, and this contrast increases with frequency. The yellow region indicates the analyzed frequency band.

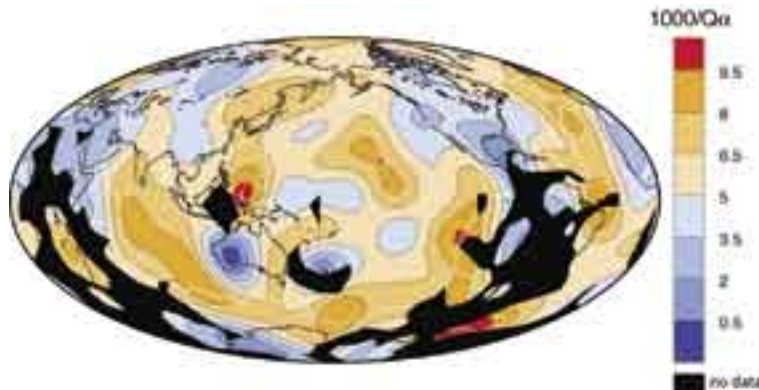


Figure 2. Lateral variations in upper-mantle compressional-wave attenuation generally correlate with surface tectonics.

per corner frequency of the absorption band is higher for the upper mantle than at greater depths; the lower layer is about twice as attenuating at 0.1 Hz than at 1 Hz, whereas upper mantle attenuation is relatively constant across this band. Since lower-mantle attenuation is small, we interpret deviations in spectral decay as lateral variations in upper mantle attenuation. The resulting map of more and less attenuating regions generally correlates with previously-published attenuation models and surface tectonics. Continents are usually less attenuating than the global average, whereas oceanic regions tend to be more attenuating.

Warren, L.M., and P.M. Shearer, Investigating the frequency dependence of mantle Q by stacking P and PP spectra, *J. Geophys. Res.*, 105, 25,391-25,402, 2000.

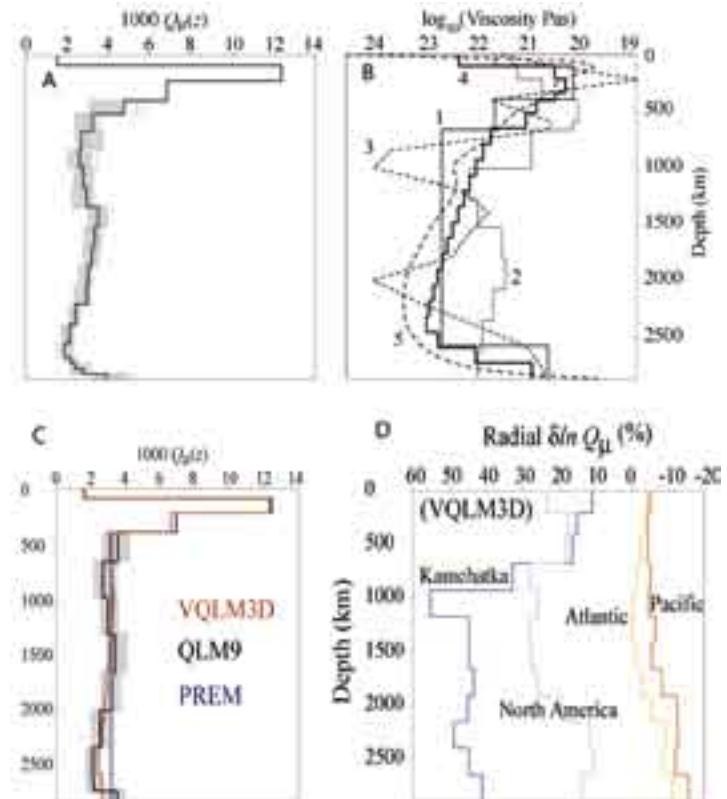
Warren, L.M., and P.M. Shearer, Mapping lateral variations in upper mantle attenuation by stacking P and PP spectra, *J. Geophys. Res.*, 107, 2342, doi:10.1029/2001JB001195, 2002.

Using IRIS Digital Data to Determine the Radial Attenuation Structure of the Lower Mantle

Jesse Fisher Lawrence • Washington University, now at University of California, San Diego

Michael Wyession • Washington University

We employed a niching genetic algorithm to invert ~30,000 differential ScS/S attenuation values for a new spherically-symmetric radial model of shear quality factor ($Q\mu$) with high sensitivity to the lower mantle. The data were obtained from all broadband shear waves available from the IRIS DMC after 1990. The new radial $Q\mu$ model, QLM9, possesses greater sensitivity to $Q\mu$ at large mantle depths than previous studies. Differential ScS-S attenuation as a function of event-to-station distance provides an excellent mechanism for determining lower mantle quality factor structure regardless of upper mantle structure. This model is robust for both shallow and deep event data sets. On average, lower mantle $Q\mu$ increases slightly with depth, which supports models of increasing viscosity with depth. QLM9, when compared to viscosity and temperature (with significant caveats), is in agreement with geodynamic expectations. There are two higher- $Q\mu$ regions at ~1000 and ~2500 km depth, which roughly correspond to high-viscosity regions observed by Forte and Mitrovica. There is a lower- $Q\mu$ layer at the core-mantle boundary, as expected based upon the presence of the lowermost mantle thermal boundary layer. There is also a relatively low- $Q\mu$ region in the mid-lower mantle. However, as three-dimensional tomographic modeling of shear wave attenuation shows, there is tremendous lateral variation in the shear-wave attenuation of the lower mantle, so a radial model of $Q\mu$ may be of some general use for geodynamics applications, but it is important to remember that it is averaging over huge lateral variations. As such, it is interesting how nearly-constant the vertical profile is across the lower mantle. The slight increase in $Q\mu$ in the mid-lower-mantle may be suggesting that descending subducted lithosphere doesn't spend a lot of time in the mid-lower mantle.



A. The lower mantle radial Q model QLM18 of Lawrence and Wyession (2005). Gray shading shows the range of other low-cost models from the genetic algorithm search. B. Mantle viscosity models: 1. Hager and Richards (1989); 2. Forte and Mitrovica (1996); 3. Forte and Mitrovica (2001); 4. Steinberger and Calderwood (2001); 5. McNamara et al. (2003). C. Comparison of the PREM and QLM9 models with the laterally averaged radial model from the 3D mantle model VQLM3D (Lawrence and Wyession, 2004). D. Radial profiles for VQLM3D from 4 different geographic regions.

Lawrence, J. F., and M. E. Wyession, QLM9: A new radial quality factor (Q) model for the mantle, *Earth Planet. Sci. Lett.*, 2005 (in press).

Lawrence, J. F., and M. E. Wyession, 3D Whole-Mantle Velocity and Quality Factor, *Eos Trans. AGU*, 85(17), Jt. Assem. Suppl., Abstract S43A-05, 2004.

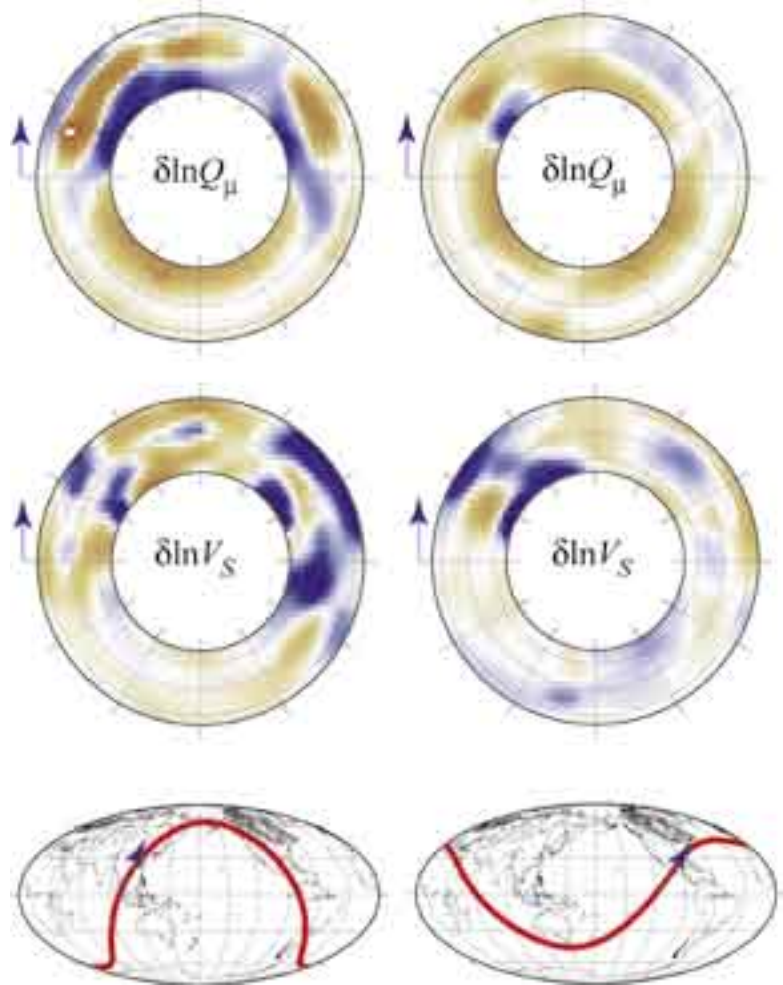
NSF Grant #: NSF-EAR-0207751

Whole-Mantle 3D Seismic Attenuation: Evidence for Global Mass Flux

Jesse Fisher Lawrence • Washington University, now at University of California, San Diego

Michael Wysession • Washington University

By combing through available broadband digital data from the IRIS DMC, we constructed a three-dimensional tomographic model of the seismic shear wave attenuation in the mantle. The model was obtained from all available digital broadband records during 1990-2001. The data consist of over 70,000 high-quality differential attenuation measurements of ScS-S, SS-S, ScS-SS, S-S, sScS-sS, sSS-sS phase pairs. The use of differential measurements removes contaminating source effects, which is the same in both phases, as well as near-source and near-receiver structural anomalies. The result is that our data have the best resolution in the lower mantle, which has previously been largely unexamined with 3D modeling. The differential attenuation measurements (taken as t^* values) are inverted using the LSQR routine over a long-wavelength 5×5 degree grid for a 3D model of shear wave quality factor (Q). These t^* star measurements are also used to generate a whole-mantle 3D shear wave velocity model. While the velocity model does not have resolution equal to other models that incorporate surface wave and normal mode data, because it uses the same paths as went into the Q model, it is of interest in interpreting the attenuation anomalies. There is a very strong suggestion of whole-mantle flow in the attenuation tomography. High- Q sheet-like anomalies extend from the surface to the core-mantle boundary region (CMBR) at subduction zones, dominating the model. The African and Pacific superplumes involve low- Q anomalies that extend from the CMBR to the surface. For the Pacific superplume, the low- Q anomalies extend vertically from core to crust, but with the African superplume, the low- Q anomalies do not extend directly up into the sub-African upper mantle, but rather branch east and west up towards the Atlantic and Indian Ocean spreading centers. While the interpretation of seismic Q in terms of anelasticity is challenging (as there are other factors such as seismic scattering, water content, grain size, and deviatoric strain that can influence it), if we assume that the Q anomalies are influenced to the first order by temperature variations, then this model strongly supports whole-mantle mass flux between the surface and the base of the mantle.



Two global slices through the shear velocity and attenuation models of Lawrence and Wysession (2004), obtained from differential shear wave phases.

Lawrence, J. F., and M. E. Wysession, QLM9: A new radial quality factor (Q) model for the mantle, *Earth Planet. Sci. Lett.*, 2005 (in press).

Lawrence, J. F., and M. E. Wysession, 3D Whole-Mantle Velocity and Quality Factor, *Eos Trans. AGU*, 85(17), Jt. Assem. Suppl., Abstract S43A-05, 2004.

NSF Grant #: NSF-EAR-0207751

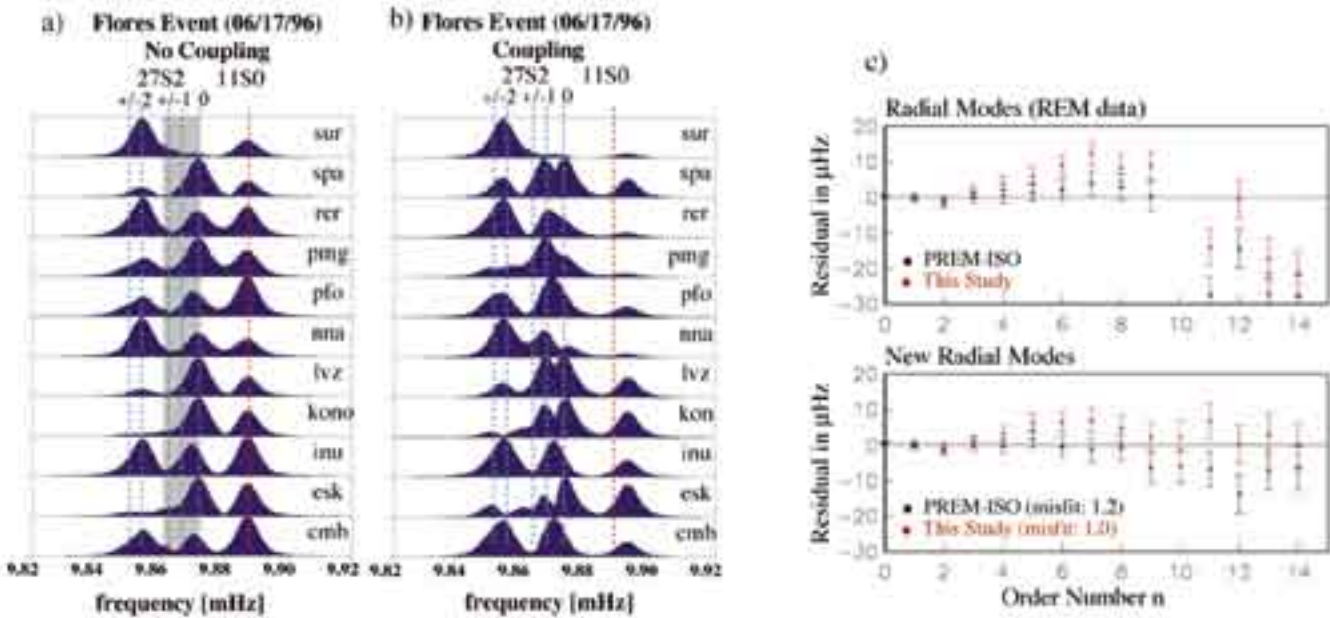
New Measurements of Radial Mode Eigenfrequencies

Gabi Laske • IGPP, Scripps Inst. of Oceanography

Radial mode eigenfrequencies are commonly thought to be measured with great ease and precision. The reason for this is that these modes have no geographic pattern so one should be able to measure frequencies from a spectrum observed at any station in the world. Yet, radial modes often seem inconsistent with spherical Earth models that fit all other mode frequencies.

It turns out that radial modes are sometimes strongly coupled. The strongest coupling is predicted to be with neighboring $l = 2$ modes, sometimes more than 50 mHz away. The coupling is caused by the Earth’s hydrostatic ellipticity and aspherical structure of harmonic degree 2. Mode coupling due to ellipticity alone can cause a frequency shift for the radial modes by more than 4 mHz (e.g. ${}_{11}S_0$ and higher). Given that mode frequencies can be measured to within 0.1 microHz, this shift is significant, and some singlets of $l = 2$ modes have indeed been misidentified as the radial mode in the past. Including the spectra of the June 23, 2001, Southern Peru and the November 14, 2001, China Earthquakes we have reanalyzed radial mode eigenfrequencies and obtained a mode dataset that is internally more consistent than previous ones. Only small perturbations to PREM are needed to fit the new data, together with the current best estimates of “Reference Normal Mode Data” (available on the Reference Earth Model web site: //mahi.ucsd.edu/Gabi/rem.html). The smallest perturbation to isotropic PREM that is consistent with our radial mode data requires no 220 km discontinuity but there exists a trade-off between higher shear velocities and densities in the lid and lower values in the asthenosphere below. Slightly higher velocities are also required above the CMB and the inner core boundary.

The great December 26, 2004, Andaman-Sumatra earthquake still awaits detailed mode analysis. However, new frequency estimates for the gravest radial mode, “breathing mode” ${}_0S_0$ have been reported with error bars smaller than the coupling effects from neighboring modes. This stressed the importance of having a state-of-the-art global seismic network running as well as, investigating possible systematic effects in the measurements very carefully.



a) Spectra obtained for coupled-mode synthetic seismograms when only selfcoupling is considered. Effects that removed singlet degeneracy come from Earth’s rotation and hydrostatic ellipticity, mantle model S16B30 and hypothetical $l = 2$ structure in the upper 200 km of the inner core. Core structure split the mode anomalously (grey bar marks effects from rotation/ellipticity alone). b) When mode coupling between ${}_{27}S_2$ and ${}_{11}S_0$ is considered. Coupling significantly shifts the frequency of ${}_{11}S_0$. Also note that the amplitudes are affected, as observed by Park (1990). c) Old and new radial mode data and residuals with respect to isotropic PREM and our new model.

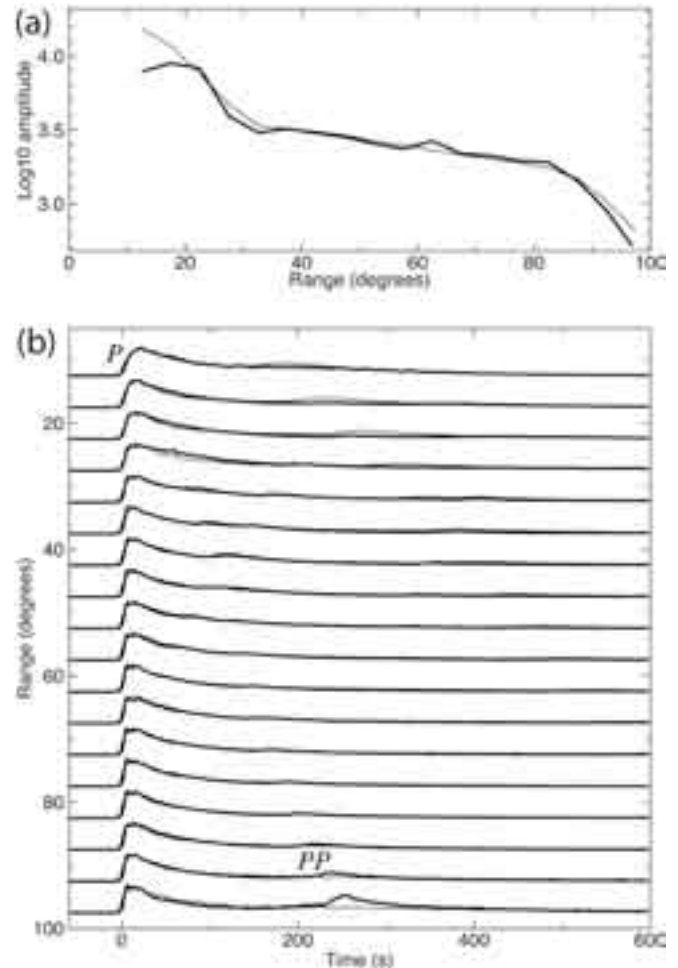
Zurn, W., Laske, G., Widmer-Schmidrig, R. and F. Gilbert. Observation of Coriolis coupled modes below 1mHz, *Geophys. J. Int.*, 143, 113-118, 2000.

The Global Short-Period Wavefield Modeled with a Monte Carlo Seismic Phonon Method

Peter Shearer • University of California, San Diego

Paul Earle • U.S. Geological Survey, Golden

At high frequencies (~ 1 Hz), much of the seismic energy arriving at teleseismic distances is not found in the main phases (e.g., P, PP, S, etc.) but is contained in the extended coda that follows these arrivals. This coda results from scattering off small-scale velocity and density perturbations within the crust and mantle and contains valuable information regarding the depth dependence and strength of this heterogeneity as well as the relative importance of intrinsic versus scattering attenuation. Most analyses of seismic coda to date have concentrated on S-wave coda generated from lithospheric scattering for events recorded at local and regional distances. Here we examine the globally averaged vertical-component, 1-Hz wavefield (>10 degree range) for earthquakes recorded in the IRIS FARM archive from 1990 to 1999. We apply an envelope-function stacking technique to image the average time-distance behavior of the wavefield for both shallow (< 50 km) and deep (> 500 km) earthquakes. Unlike regional records, our images are dominated by P and P-coda owing to the large effect of attenuation on PP and S at high frequencies. Modeling our results is complicated by the need to include a variety of ray paths, the likely contributions of multiple scattering, and the possible importance of P-to-S and S-to-P scattering. We adopt a stochastic, particle-based approach in which millions of seismic “phonons” are randomly sprayed from the source and tracked through the Earth. Each phonon represents an energy packet that travels along the appropriate ray path until it is affected by a discontinuity or a scatterer. Discontinuities are modeled by treating the energy normalized reflection and transmission coefficients as probabilities. Scattering probabilities and scattering angles are computed in a similar fashion, assuming random velocity and density perturbations characterized by an exponential autocorrelation function. Intrinsic attenuation is included by reducing the energy contained in each particle as an appropriate function of travel time. We find that most scattering occurs in the lithosphere and upper mantle, as previous results have indicated, but that some lower mantle scattering is likely also required. A model with 3% to 4% RMS velocity heterogeneity at 4-km scale length in the upper mantle and 0.5% RMS heterogeneity at 8-km scale length in the lower mantle (with intrinsic attenuation of $Q\alpha = 450$ above 200 km depth and $Q\alpha = 2500$ below 200 km) provides a reasonable fit to both the shallow and deep earthquake observations, although many tradeoffs exist between the scale length, depth extent and strength of the heterogeneity.



Comparisons between the envelope stack for shallow event data (heavy line) with the predictions of the phonon method applied to the scattering model (thin line). (a) Peak P-wave amplitude as a function of source-receiver distance. (b) Coda envelopes in 5 degree range bins plotted as a function of time from the direct P arrival. Amplitudes are normalized to the same energy in the first 30 s.

Shearer, P.M. and P.S. Earle, The global short-period wavefield modelled with a Monte Carlo seismic phonon method, *Geophys. J. Int.*, 158, 1103-1117, 2004.

Discovery of Strong Upper Mantle Reflectors From Back-Scattering of Near-Podal PKPPKP Waves Using Data Acquired From IRIS

Hrvoje Tkalčić, Megan P. Flanagan • Lawrence Livermore National Laboratory

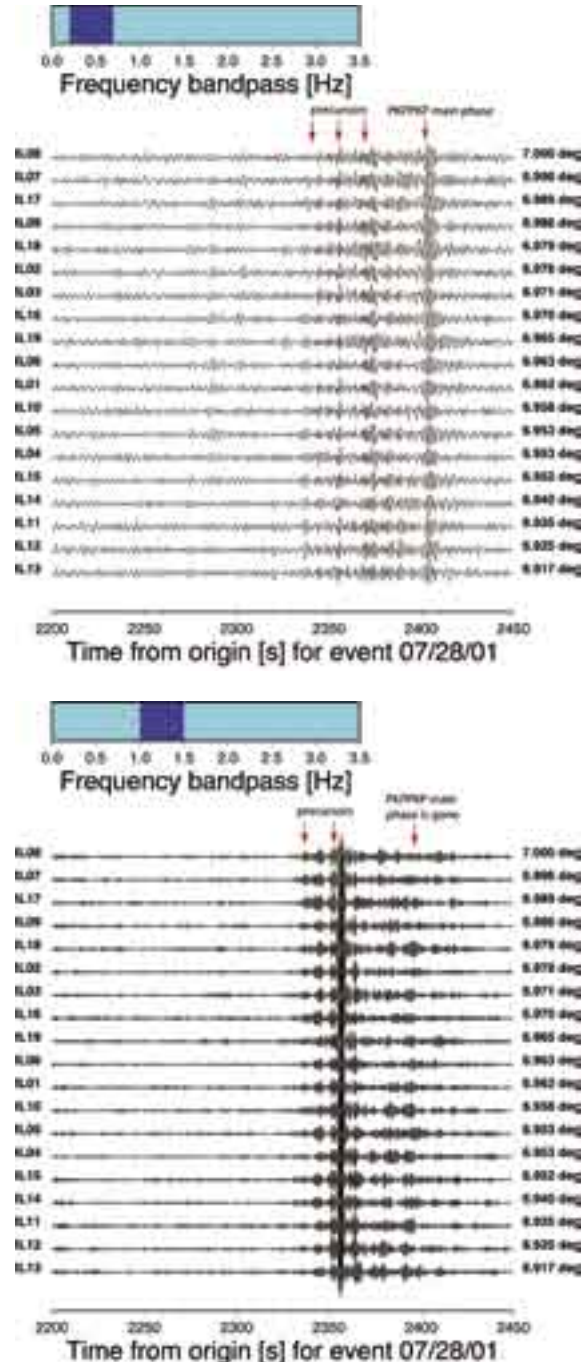
Vernon Cormier • University of Connecticut

Precursors to PKPPKP waves have long been interpreted as PKPPKP waves that did not reach Earth’s opposite surface but were reflected underside from unknown discontinuities in the upper mantle. As the amount of evidence grew, the 410 and 660-km discontinuities were gradually accepted as global features of Earth’s interior.

However, a scattering hypothesis (e.g. work by Cleary, 1981) threw a considerable doubt on underside reflection hypothesis and established a powerful alternative explanation for many observations. Thus, PKPPKP precursors corresponding to inconsistently observed, less-prominent features at, for instance 220 km and other depths in the mantle, were often disputed. A common denominator of these early observations, however, was that they were assembled at epicentral distances of about 50-70 degrees, corresponding to a maximum in the expected amplitudes due to PKP triplication. Here, we report unprecedented observations at near-podal epicentral distances of very clear and energetic PKPPKP precursor arrivals. This is a result of a systematic and thorough search over waveforms available through the IRIS acquisition system, for both individual and array records (Tkalčić and Flanagan, 2004; Tkalčić et al., in preparation).

The figure shows vertical components of short-period ILAR array data for two bandpass filters: a) 0.2-0.7 Hz and b) 1.0-1.5 Hz. The event was located in the southern Alaska, about 7 degrees away from ILAR network. At 0.2-0.7 Hz, the main and precursor arrivals of energy are visible at all ILAR stations, which were sorted with respect to the epicentral distance. At 1.0-1.5 Hz, the energy of the main phase is below noise level, but sharp onsets of the precursors are persistent. We interpret these precursors as back-scattering from upper mantle reflectors. The earliest individual packet of energy corresponds to the underside reflection from about 220 km depth, and the latest one corresponds to the reflection from about 150 km depth in the mantle. Forward-scattered PKPPKP waves at such short epicentral distances would in fact produce a postcursor arrivals to PKPPKP. We explain the high-energy content of the precursors versus the main arrivals by a difference in attenuation experienced by the additional two legs that the main PKPPKP phase spends in the antipodal lithosphere.

Tkalčić, H. and Flanagan, M.P., Structure of the Deep Inner Core From Antipodal PKP-PKP Waves, *Eos Trans. AGU*, 85(47), Fall Meet. Suppl., Abstract T54A-06, 2004.



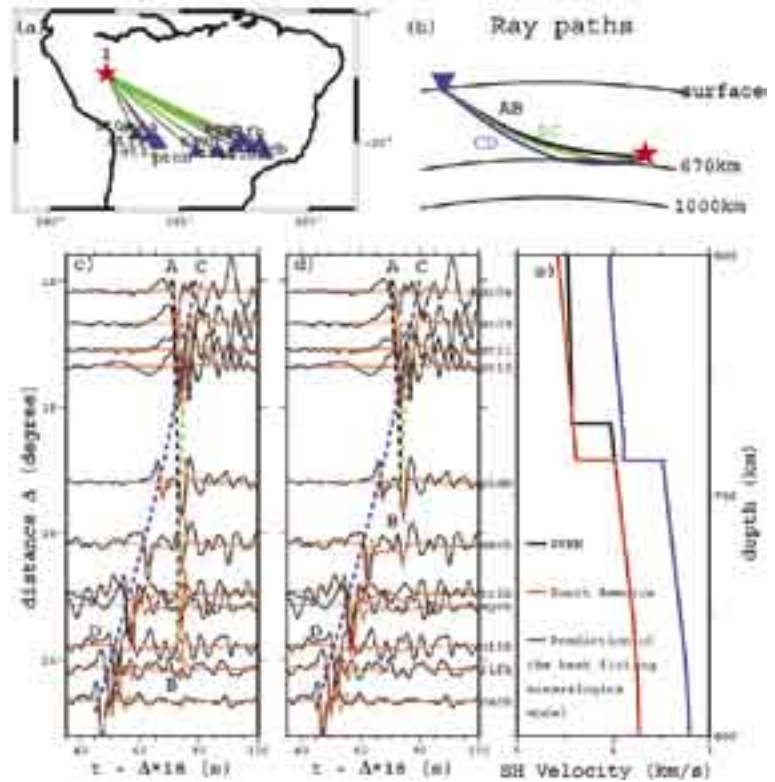
Vertical components of short-period ILAR array waveforms for two bandpass filters: a) 0.2-0.7 Hz and b) 1.0-1.5 Hz. The earthquake was located in the southern Alaska, about 7 degrees away from ILAR network.

SH Velocity and Compositional Models Near the 660-km Discontinuity Beneath South America

Yi Wang, Lianxing Wen, Donald Weidner • SUNY at Stony Brook

The IRIS PASSCAL experiments have supplied the seismology community with high quality, freely available and spatially dense datasets. The high quality broadband seismic data recorded in two PASSCAL experiments in South America (BANJO and BLSP) provide us with an opportunity to investigate the upper mantle seismic structure beneath South America. The dense observations also minimize the effects of lateral seismic heterogeneities on the seismic results. We constrain SH-wave velocity structures near the 660-km discontinuity beneath South America using triplicated phases near the discontinuity recorded in the epicentral distance range of $10^\circ - 30^\circ$ for a deep event. The seismic data suggest that the velocity gradient above the 660-km discontinuity is larger than that of Preliminary Earth Reference Model (PREM), while the velocity jump and the velocity gradient below the 660-km discontinuity across the discontinuity are the same as PREM. The large velocity gradient above the 660-km discontinuity requires existence of the ilmenite phase in the bottom of the transition zone; the velocity jump across the discontinuity can be explained by the presence of more garnet above the discontinuity than in the pyrolite model; and the high velocity gradient in the top of the lower mantle can be explained by the gradual transformation of garnet to prevoakite persisting to a greater depth. Such a mineralogical model may be explained by an aluminum content of 3.4% in the top of the lower mantle and a low temperature and/or low Al content in the bottom of the transition zone beneath South America.

Wang, Y., L. Wen, D. J. Weidner and Y. He, SH velocity and compositional models near the 660-km discontinuity beneath South America and northeast Asia, *J. Geophys. Res.*, (Submitted).



(a) Great circle paths from the seismic event (star, 1994/11/04, $\text{evdp} = 597$ km) to stations (triangles), with the green segments indicating the portions that the CD branch travels below the 660-km discontinuity. (b) Ray paths of the triplications near the 660-km discontinuity for a source depth of 597 km. The AB branch is the direct SH wave propagating above the discontinuity; the BC branch is the reflection off the discontinuity; and the CD branch is the seismic wave traveling below the discontinuity. (c-d) Comparisons of observed tangential displacements for the seismic waves sampling the transition zone beneath South America (event in (a)) (black traces) and synthetic waveforms (gray traces) calculated using (c) PREM and (d) our best fitting model, along with predicted travel time curves of the three branches of the seismic phases (dashed lines). (e) The best fitting SH velocity models based on the seismic data (red) and a mineralogical model (blue), along with PREM (black) as reference. (Since the best fitting SH velocity models based on the seismic data and a mineralogical model are very close, the prediction of the best fitting mineralogical model is shifted a little to make it distinguishable.)

Seismic Evidence for Accumulated Oceanic Crust Above the 660-km Discontinuity Beneath Southern Africa

Yang Shen • University of Rhode Island

John Blum • University of California, San Diego

High-pressure assemblages of subducted oceanic crust are denser than the normal upper mantle but less dense than the uppermost lower mantle (Ringwood, 1991; Hirose et al., 1999). Thus, subducted oceanic crust may accumulate at the base of the upper mantle. Direct observational evidence for this hypothesis, however, remains elusive. We present an analysis of a negative-polarity shear wave converted from a compressional wave at a seismic discontinuity near 570 - 600 km depth beneath southern Africa. The negative polarity of the converted phase indicates a $\sim 2.2 \pm 0.2\%$ S-velocity decrease with depth at the seismic discontinuity. This velocity reduction is associated, however, with a low-velocity contrast at the 660-km discontinuity. The exsolution of Ca-perovskite in former oceanic crust at depths greater than 600 km and the associated small volume fraction of ringwoodite are plausible explanations for the apparent paradox between the negative velocity discontinuity and the low velocity contrast at the 660-km discontinuity.

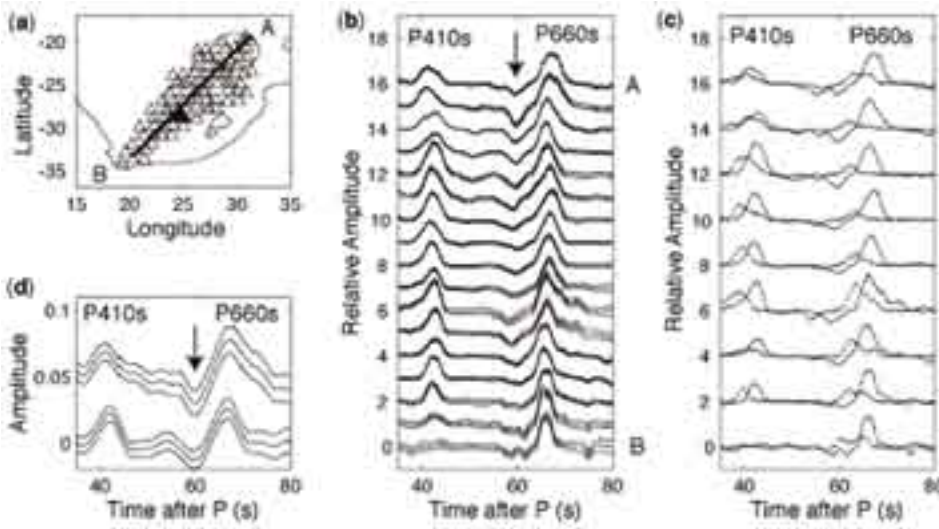


Figure 1. (a) Locations of broadband seismic stations (triangles) and the profile of the receiver function stacks (line). Circles with a radius of 2° outline two of the overlapping patches used in stacking. (b) Waveforms of the stacked receiver functions along the profile in (a) and their 95% confidence limits determined by bootstrapping. Arrow marks the arrival of the negative-polarity phase. An nth root (n=2) stacking process is used to enhance coherent phases and suppress random noise. (c) A comparison of the receiver functions stacked along Pds moveout curves (solid lines) and reverberation moveout curves (dotted lines). Every other trace in (b) is shown for legibility. (d) Waveforms of two linearly stacked receiver functions from the two patches outlined in (a) and their 95% confidence limits. The bottom trace corresponds to the patch near the center of the array. The scale of the vertical axis is relative to the amplitude of the P wave on the vertical component. The top trace has been shifted upwards by 0.05.

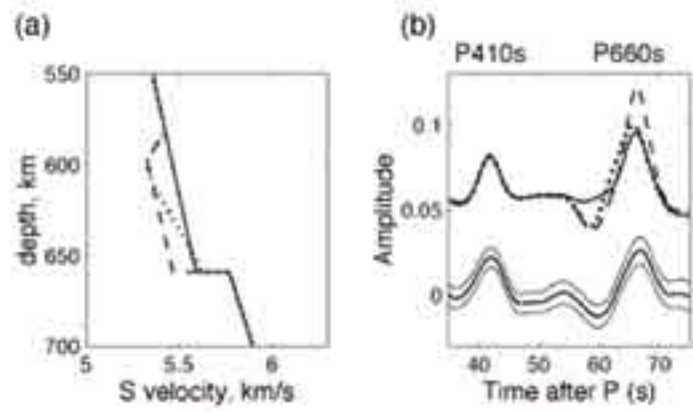


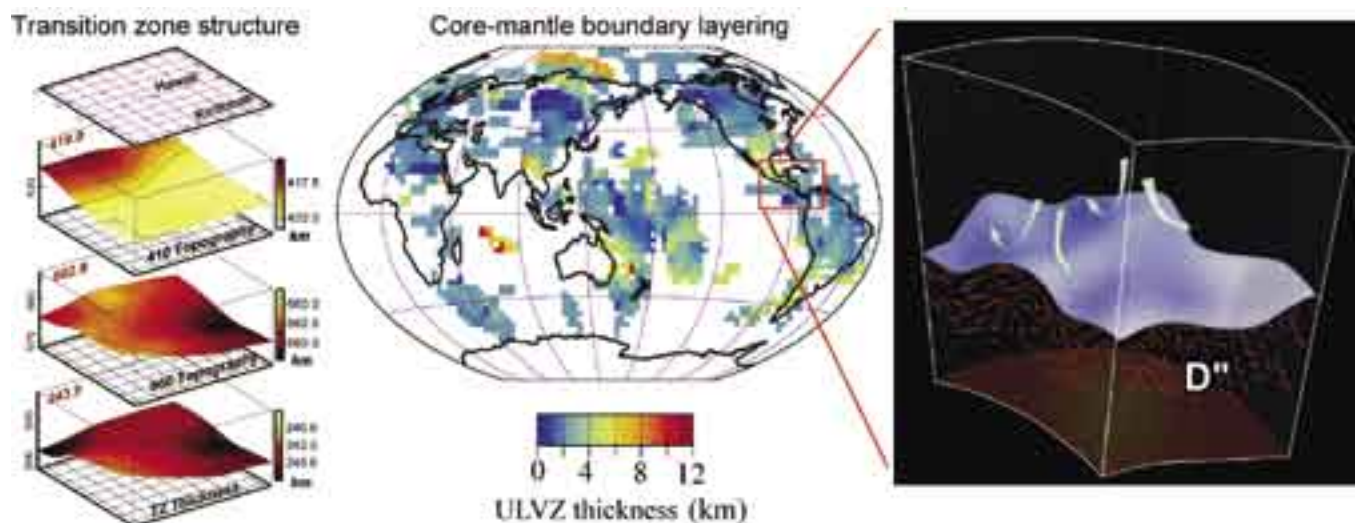
Figure 2. (a) Two possible scenarios may cause a negative-polarity P-to-S conversion near a 590-km depth: a uniform reduction in velocity at the base of the upper mantle (dashed line) and a velocity reduction near 590 km followed by a greater than normal velocity gradient (dotted line). The reference shear velocity structure (solid line) is a modified iasp91 model with a smaller velocity contrast at the 660-km discontinuity to provide a better fit to the observed P660s amplitude. (b) The top traces are the synthetic receiver functions for the three velocity models in (a). Line styles match those in (a). Arrow marks the converted phase from the velocity reduction near 590 km depth. The waveform of a linearly stacked receiver function from the center patch in Figure 1a and its 95% confidence limit are shown for comparison. The top traces are shifted upwards by 0.05.

Shen, Y., and J. Blum, Seismic evidence for accumulated oceanic crust above the 660-km discontinuity beneath southern Africa, *Geophys. Res. Lett.*, 30, 1925, doi:10.1029/2003GL017991, 2003.

Seismic Investigation of Upper and Lower Mantle Boundary Layering

Edward J. Garnero, Nicholas Schmerr, Michael S. Thorne • Arizona State University

Both the upper and lower mantle contain important chemical and dynamical processes that likely govern the evolution and structure of the whole planet. Our work is focused on seismic methods that help to reveal the present day structure in the upper and lower mantle. The upper mantle transition zone (TZ) is predicted to change thickness as a function of temperature and chemistry, thus mapping TZ thickness holds promise as a mantle thermometer (Schmerr and Garnero, 2005). In the deepest mantle, there is evidence for fine-scale layering with ultra-lowered shear and compressional velocities (Thorne and Garnero, 2004; Rost et al., 2005). These velocity reductions are restricted to the lowest 5-50 km of the mantle, and are compatible with a partial melt origin; the ultra-low velocities may relate to deepest mantle plume genesis. At slightly larger vertical scales, the lowermost 200-300 km show evidence for horizontal layering (Thomas et al., 2004) and seismic anisotropy (Garnero et al., 2004). The IRIS the Data Management System has played a fundamental role in our analyses, as these studies would not have been possible without it.



Upper mantle discontinuity structure from stacking of SS precursor data to image structure beneath the mid-Pacific, centered on the Hawaiian hotspot. A) Location of SS precursor stacking bins, each bin is $101/4$ in radius, and records with Fresnel zones falling within the bin are included in the stack for that bin. B&C) Topography on the 410 and 660 km discontinuities of the mantle, color scaled to indicate a hot anomaly (yellows) or cool anomaly (reds). The 410 and 660 are generally anticorrelated in this plot. D) Transition zone thickness beneath the region, scaled in the same manner as the discontinuities.

Garnero, E.J., Maupin, V., Lay, T., and M.J. Fouch, Variable azimuthal anisotropy in Earth's lowermost mantle, *Science*, 306, 5694, 2004.

Rost, S., E.J. Garnero, Q. Williams, and M. Manga, Seismological constraints on a possible plume root at the core-mantle boundary, *Nature*, 435, 2005.

Schmerr, N., and Edward J. Garnero, Probing the nature of 410- and 660-km discontinuities beneath the central Pacific Ocean using SS-precursors, *J. Geophys. Res.*, in review, 2005.

Thomas, C., Garnero, E.J., and Lay, T., High-resolution imaging of lowermost mantle structure under the Cocos Plate, *J. Geophys. Res.*, 109, doi:10.1029/2004JB003013, 2004.

Thorne, M.S., and E.J. Garnero, Inferences on ultralow-velocity zone structure from a global analysis of SPdKS waves, *J. Geophys. Res.*, 109, B08301, doi:10.1029/2004JB003010, 2004.

Study of Earth's Layered Structure on a Global Scale Using Broadband Seismic Datasets

Stephen S. Gao, Kelly H. Liu • Kansas State University

Whether the Earth's lower mantle is layered or has steady velocity gradients has important implications on various models related to the dynamics of the Earth's deep interior. We are being funded by the National Science Foundation to systematically search for discontinuities in the Earth's lower mantle.

Networks/experiments that contributed to the project include GDSN, GEOSCOPE, US Advanced National Seismic Systems, Southern African Seismic Experiment, and Northern and Southern California Seismic Networks and a few smaller-scale portable experiments. About 80% of the seismograms were obtained from the IRIS Data Management Center. We have manually checked all the seismograms and have converted them into P-to-S receiver functions (RFs). About 60,000 high-quality radial receiver functions are moveout-corrected and stacked to image possible sharp velocity discontinuities in the lower mantle. Stacking of ray-piercing points beneath caps of different sizes is being finalized.

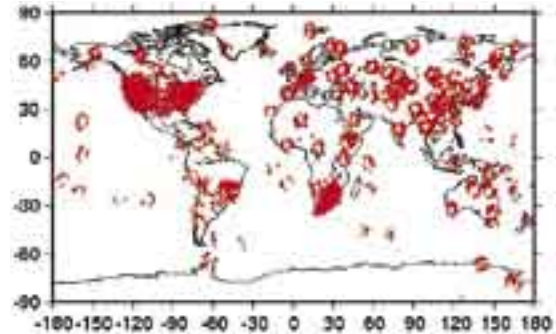


Figure 1. Distribution of ray-piercing points of P-to-S converted phase at 1000 depth.

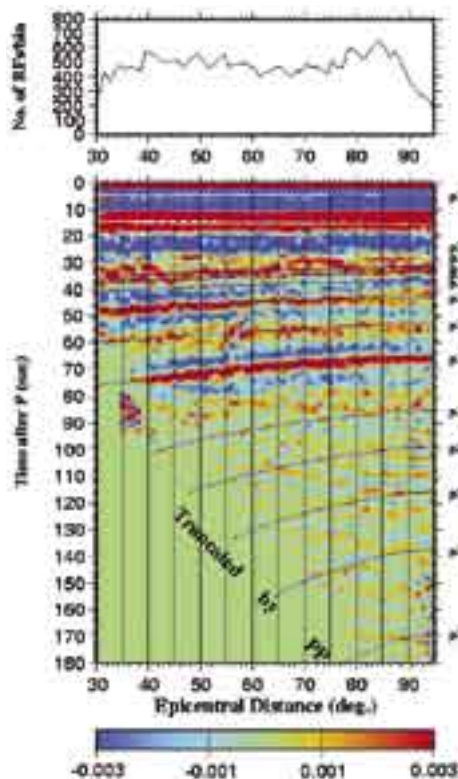


Figure 2. Binned and stacked receiver functions for the 0.02-2.0 Hz band. Receiver functions are binned according to their focal-depth-corrected epicentral distances into 1 deg bins and those in the same bins are then stacked.

Figures 1, 2, and 3 show preliminary results beneath the largest cap (i.e., the whole earth). Possible discontinuities at depths around 850, 900, 1100, 1220, and 1600 km are observable. For each observed seismogram, we are generating a synthetic seismogram using the real focal mechanism and station-event geometry. We will then convert the synthetics into receiver functions and stack them for the purpose of identifying multiples and other non P-to-S phases originated from known discontinuities.

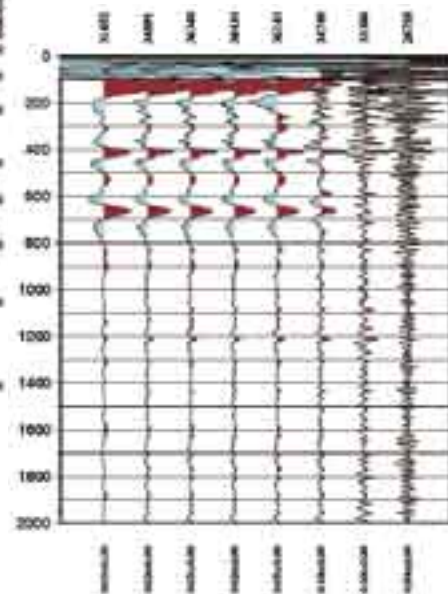


Figure 3. Depth phase images for the entire earth for a sequence of frequency bands.

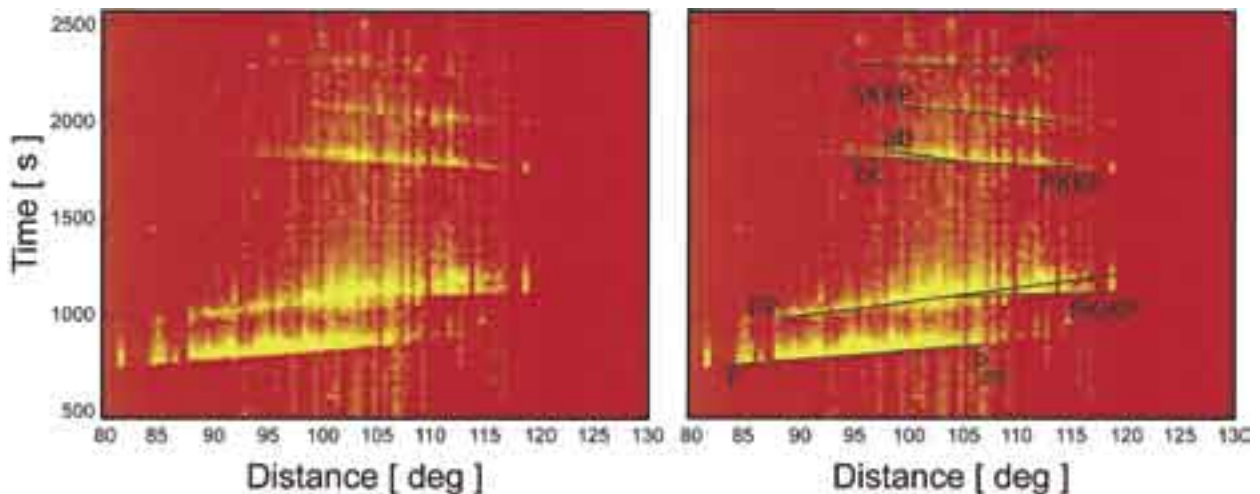
Since early this year, the same data set has also been used to map crustal thickness and V_p/V_s beneath the stations by stacking hundreds of high-quality P-to-S converted phases at the Moho recorded by each of the stations. The main scientific objective of the NSF-funded project is to answer the critical question of whether continental formation processes have been the same over geologic times, or have been changing temporally. This project will also produce a brief description of tectonic history and geologic setting in the vicinity of each of the stations.

Probing the Earth's Interior by Stacking Stacked Short-Period Seismic Array Data

Sebastian Rost, Michael Thorne • *Arizona State University*

The short-period teleseismic wave field contains a great deal of information about the small-scale structure of Earth's interior. Due to the low signal-to-noise ratio of short-period arrivals, it is challenging to use this information in global seismological studies. Seismological arrays and networks can be used to increase the signal-to-noise ratio of seismic arrivals. By stacking seismic traces that are recorded at an array, the coherent part of the seismic wave field can be enhanced while suppressing incoherent noise. One array processing method often used is Nth-root slant-stacking. The result of this stacking method shows seismic energy as slowness (incidence angle) v. time (a vespagram). This enables the identification of coherent arrivals by travel-time and slowness that otherwise might be below the noise level.

We use the information from a large number of vespagrams to map the short-period vertical seismic wave field. Approximately 500 recordings from the small aperture Yellowknife array (YKA) located in northern Canada were used to calculate vespagrams. Data were obtained through the NetDC from IRIS. In order to use the information from the vespagrams we condense the information from slowness-time space into a new, multidimensional time-series, by moving a sliding time window across the vespagrams. The highest stacked energy in the time window (i.e. the stack for the slowness that yields the highest amplitude), is used to construct a new time series. From the vespagram we are able to obtain information about traveltimes, slowness, amplitude, polarity and backazimuth. The figure shows the new time series constructed in this manner, showing stacked energy. Displays containing slowness, polarity, and back-azimuth information can also be plotted. The energy displays allow the detection of several major seismic phases. Future research will focus on subtle coherent arrivals (e.g. the scattered energy arriving before the phase PP in the distance range 95° to 105°) using a larger number of array recordings.



a) Stacked image for ~500 earthquakes recorded at YKA. Each line represents one new time series calculated from vespagrams. Stacked seismic phases are sorted by epicentral distance. Larger stack energy is shown in yellow. Zero energy is red. Several sharp arrivals can be identified. b) Travel-time predictions for major seismic phases in panel a) are labeled.

Finite-Frequency Tomography of D'' Shear Velocity Heterogeneity Beneath the Caribbean

Shu-Huei Hung, Ling-Yun Chiao • National Taiwan University

Edward J. Garnero • Arizona State University

Ban-Yuan Kuo • Academia Sinica, Taiwan

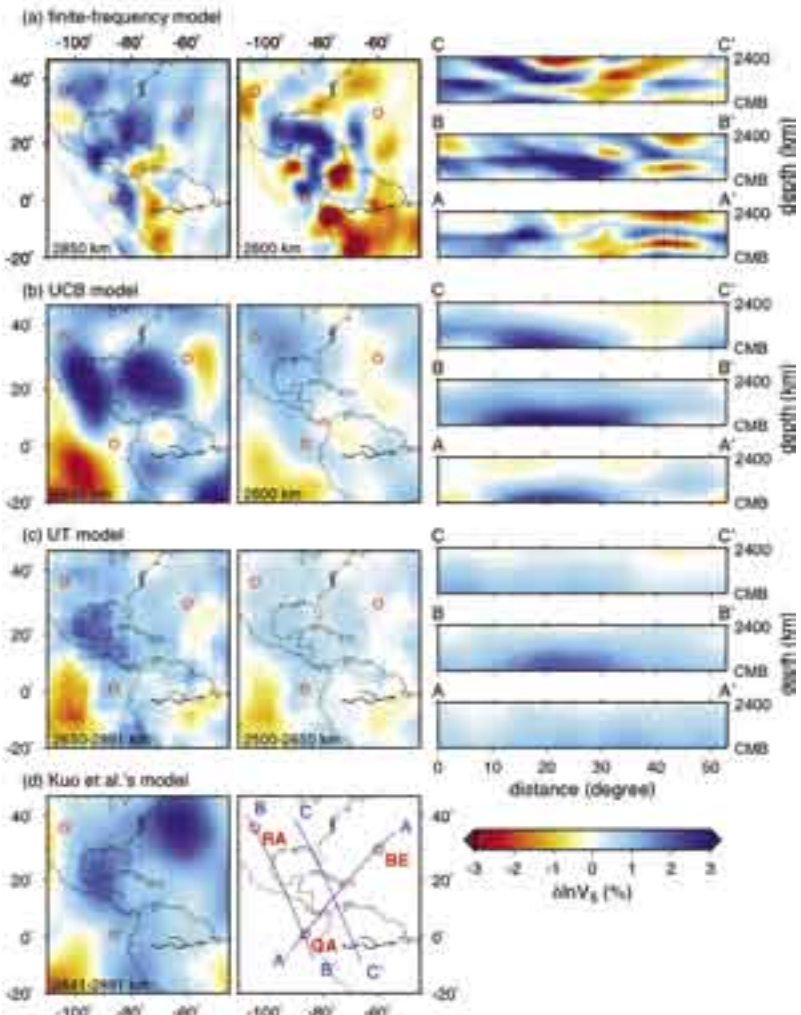
Thorne Lay • University of California, Santa Cruz

The shear velocity structure in the lower-most 500 km of the mantle beneath the Caribbean and surrounding areas is determined by seismic tomography applied to a suite of Sdiff-SKS, ScS-S, Scd-S and ScS-Scd differential times from IRIS, CNSN, WWSSN, TRInet, and BDSN stations across North America.

The inclusion of triplication arrivals in the inversion, a first for a deep mantle tomographic model, is possible because of the widespread presence of a D'' velocity discontinuity in the region. Born-Fréchet kernels are used to characterize how the finite-frequency data sample the structure for all of the differential arrival time combinations. The use of 3-D kernels stabilizes the tomographic inversion relative to a ray-theory parameterization, and a final model with 60 and 50 km correlation lengths in the lateral and radial dimensions, respectively, is retrieved. 3-4% velocity fluctuations are resolved in an area which is characterized as high velocity in larger-scale tomographic inversions. Features that may correspond to small boundary layer thermal instabilities appear to be embedded on the margins of high velocity regions.

Hung, S.-H., Edward J. Garnero, L.-Y. Chiao, B.-Y. Kuo, and T. Lay, Finite-frequency tomography of D'' shear velocity heterogeneity beneath the Caribbean, *J. Geophys. Res.*, in press, 2005.

Research supported by NSF grants EAR-0135119 and 0125595.



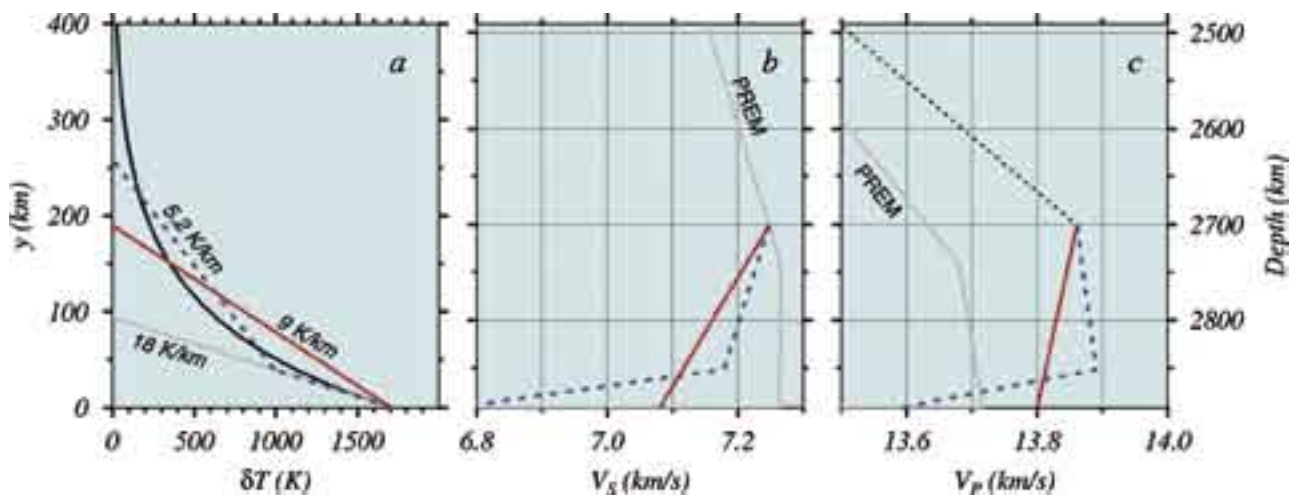
Comparison of shear velocity variations relative to the PREM model from (a) the finite-frequency model, (b) the UC Berkeley model, (c) the U. Texas model, and (d) the Model of Kuo et al. (2000). Except for (d) the corresponding models are shown at two depths, with cross-sections indicated in the lower map being shown on the right. Note the increase in spatial resolution of the regional inversion.

A Seismological Determination of the Temperature Gradient in D'' Beneath the Western Pacific

Ban-Yuan Kuo • Academia Sinica, Taiwan

Chin-Wu Chen • Massachusetts Institute of Technology

We characterize the velocity gradient of D'' for a region in the western Pacific using gradient-sensitive seismological probes: the amplitudes and traveltimes of the diffracted P and S phases. Sorted from many hundreds of waveforms initially requested from the IRIS GSN archive, tens of high-quality measurements each in amplitude ratio and differential time were analyzed to constrain the regional-scale vertical gradients of V_p and V_s . The V_s models were grid-searched using synthetic waveforms over the parameter space of the thickness (H) and the gradient. Solutions show negative deviation from PREM, and a tradeoff between gradient and H from -0.00088 s^{-1} , for 190 km to -0.00049 s^{-1} , for 240 km with a typical error of 0.00015 s^{-1} . For two sets of H values, 190 km and 240 km, the gradients of V_p were determined solely by amplitude to be -0.00032 s^{-1} and 0.00015 s^{-1} , respectively, shrouded in relatively large errors of $0.0002\text{--}0.0003 \text{ s}^{-1}$. We derive the temperature gradient from the resolved velocity gradients using the seismological-thermodynamic equation of Doornbos et al. (1986), and arrive at $9.0 \pm 5.8 \text{ K/km}$ and $5.7 \pm 4.1 \text{ K/km}$ over 190 and 240 km, respectively. The difference in gradient between these two models is statistically significant at high confidence levels, and the combination of the two models is consistent with a non-linear temperature profile that steepens toward the core-mantle boundary.

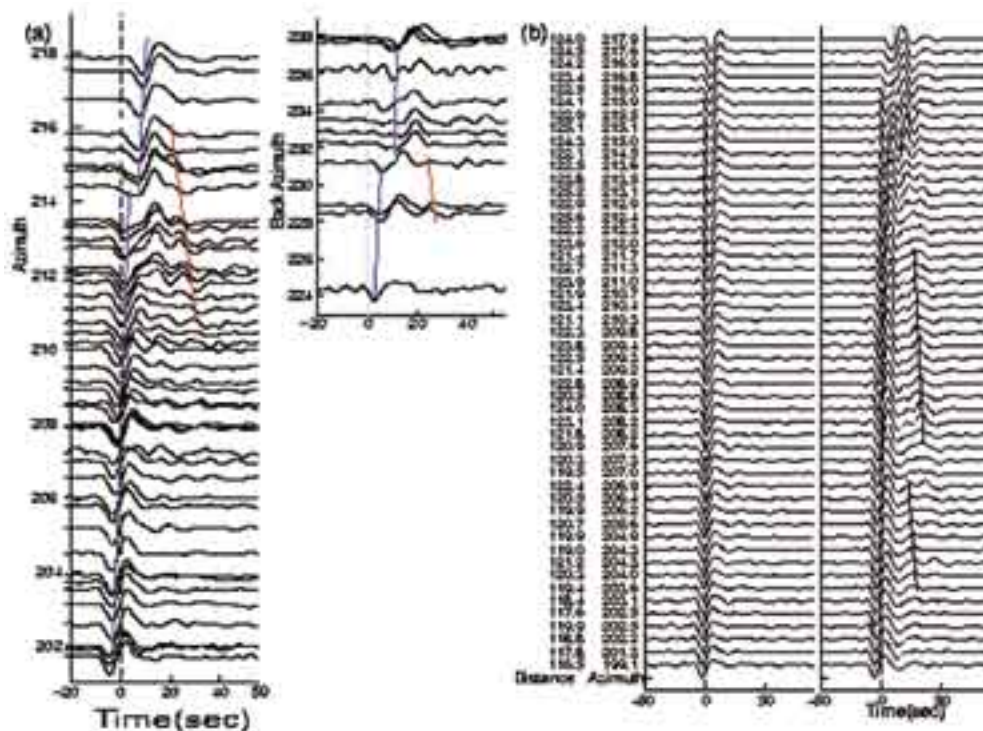


The combination of V_p and V_s models best constrained by amplitudes and times of diffracted phases yields a temperature model of D''. Shown here are a set of single-gradient models for $H = 190 \text{ km}$ (red solid lines) and a set of example two-gradient models (blue dashed lines) that is consistent with the observations. (a) Temperature, (b) V_s , and (c) V_p . The exponential function in (a) (solid curve) is a more realistic temperature profile equivalent to the linear 9K/km model. This profile satisfies the observations, but is non-unique. The gradient right above the CMB for the exponential is 18 K/km (gray line), twice of the value for the single-gradient model.

Sharp Lateral Boundaries in the D'' Region

Akiko To, Barbara Romanowicz, Yann Capdeville • University of California, Berkeley

We report that a sharp lateral boundary exists at the southern edge of the Pacific superplume. The set of SHdiff wave forms, which graze the South Pacific superplume, have similar features to those observed previously at the southeastern edge of the African superplume. The similarity of the two observed SHdiff waveform sets at relatively high frequencies indicates that the low velocity regions in the lower mantle under Pacific and Africa, observed as the strong degree-2 pattern in shear velocity tomographic models, have a similar nature also at finer scales. We used the coupled mode/spectral element method (CSEM)(Capdeville et al, 2003), which can handle strong lateral variations of the velocity in the D'', to construct synthetic waveforms. The middle figure shows that the postcursors are refraction from the lateral boundary in D'' region. The existence of these pulses suggests that modeling heterogeneity outside of the great circle path can help constrain the 3D structure, especially the shape and velocity contrast at the boundary at the base of the mantle.



(a) Observed velocity waveforms. Left; SHdiff Waveforms which sample the southern boundary of the African super plume. Event at 1997 Sep 04 in Fiji-Tonga region recorded at South Africa (PASSCAL experiment SASEK). Right; SHdiff waveforms that sample the southern boundary of the pacific superplume. Events are in Fiji-Tonga region recorded at the station BDFB of Global Telemetered Southern Hemisphere Network in Brazil. All the waveforms are collected through IRIS. Both waveform sets show a rapid shift of the arrival time with respect to the azimuth and are followed by a secondary or multiple pulses.

(b) Synthetic waveforms calculated by CSEM down to 8 seconds. They are calculated for the source and station configuration which samples the southern border of the African super plume. The left panel shows the waveforms from the original tomographic model, which do not show the secondary arrivals nor the broadening of the first arrivals. The right panel shows waveforms constructed from a model whose anomaly is saturated to either -1.75% or 2.75% based on the original tomographic model. The waveforms constructed from the modified model capture the features of observed waveforms (right panel of Figure 1a). The azimuth where the jump of the first arrival is observed matches the data well and they are followed by secondary or multiple arrivals.

To, A., B. Romanowicz, Y. Capdeville and N. Takeuchi, 3D effects of sharp boundaries at the borders of the African and Pacific Superplumes: Observation and modeling. *Earth Planet. Sci. Lett.*, 233,137-153, 2005.

Capdeville, Y., A. To and B. Romanowicz, Coupling spectral elements and modes in a spherical earth: an extension to the "sandwich" case, *Geophys. J. Int.*, 154, 44-57, 2003.

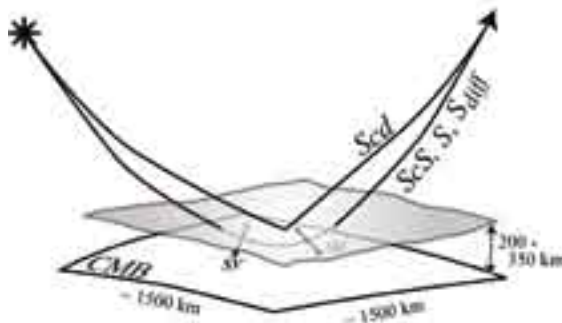
NSF award number EAR-0106000

D'' Shear Velocity Heterogeneity, Anisotropy, and Discontinuity Structure Beneath the Caribbean

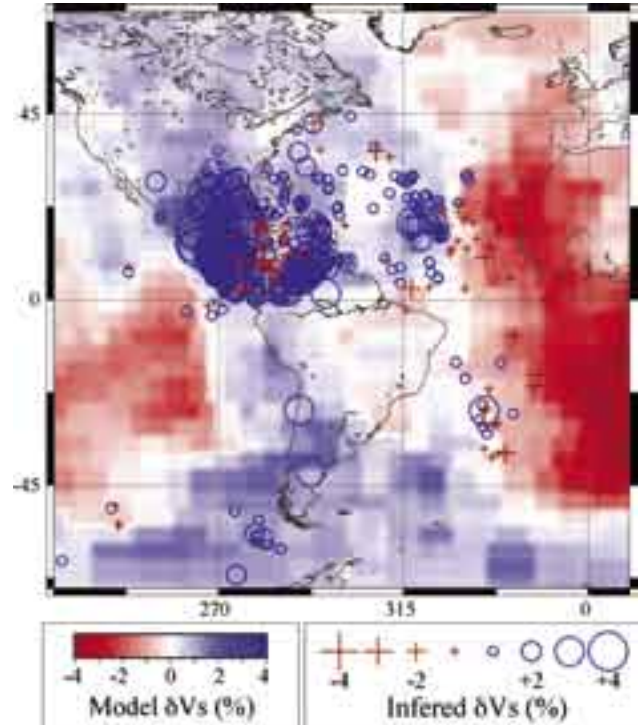
Edward J. Garnero • Arizona State University

Thorne Lay • University of California, Santa Cruz

The D'' region in the lowermost mantle beneath the Caribbean and Central America has been investigated using shear waves from South American earthquakes recorded by GSN, CNSN, BDSN, and TRInet stations in North America. We develop a composite map of volumetric shear velocity heterogeneity, shear wave anisotropy, and lateral extent of the D'' discontinuity in the region, with some extension out into the Atlantic. Corrections for aspherical mantle structure shallower than 250 km above the core-mantle boundary are applied to the differential travel time and shear wave splitting observations. The region below the Caribbean is characterized by having large-scale regions of higher than average shear velocity, but there are localized zones



Cartoon of the general attributes of the lowermost mantle under the Caribbean, which involves a laterally extensive high shear velocity layer beneath an abrupt shear velocity increase. This gives rise to reflections and to splitting of shear waves that penetrate into the layer.



Measured shear wave travel time anomalies plotted at the raypath midpoint for all of our data, superimposed on a large-scale tomographic image for the lowermost mantle from Steve Grand's 2002 model. The anomalies are from differential times of ScS-S and S-SKS, with the velocity anomaly attributed to that portion of the path within a 250-km-thick layer at the base of the mantle.

of reduced velocity beneath northern South America and the Caribbean. There is extensive shear wave splitting in the region, with some variability in character. While much of the region has early SH arrivals, there are some waveforms that appear to involve fast arrivals that are predominantly, but not purely polarized as SH. The reflections from the top of D'' are relatively uniformly observed, but on a local scale we observe waveforms that show no clear reflector. Whether this is due to lateral disruption of the reflector, topographic defocusing of the reflections, attenuation or some other cause is not yet resolved.

Garnero, E. J., and T. Lay, D'' shear velocity heterogeneity, anisotropy and discontinuity structure beneath the Caribbean and Central America, *Phys. Earth Planet. Inter.*, 140, 219-242, 2003.

Supported by NSF grants EAR-9814554, EAR-9996302, and EAR-0125595.

Using Array Methods to Investigate Possible Causes for PKP Deviations

Jenny Black, Christine Thomas • University of Liverpool, United Kingdom

Three branches of the core seismic phase PKP (PKP_{df}, PKP_{bc} and PKP_{ab}) are analysed using array techniques for various global paths. One such path utilizes data from the Tien Shan, available from the IRIS dataset. The stations of KNET and GHENGIS record earthquakes from the central Andes. Backazimuth and slowness deviations from the theoretical ray paths are measured to investigate deep Earth structure. In the resulting data, slowness deviations from ak135 (Kennett et al., 1995) are larger than for other studied paths (e.g. Black and Thomas, 2004) suggesting that somewhere along this path an anomalous region is encountered. This is especially true for PKP_{bc} and PKP_{df}, which suggests that this region is either the core mantle boundary or deeper. Ray tracing is being carried out to further explore the origin and nature of this anomaly in detail.

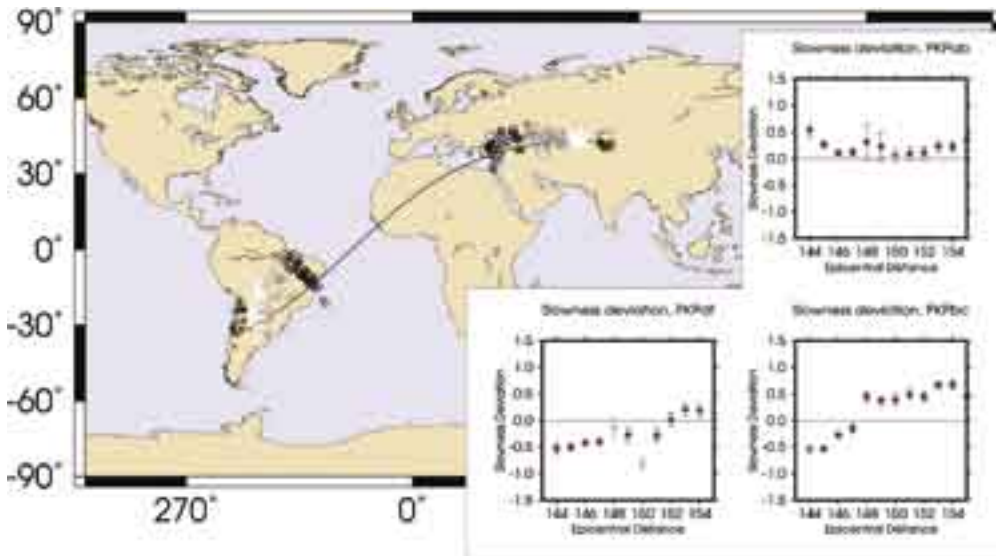


Figure (main) World map showing location of the KNET and GHENGIS stations (black triangles), earthquakes (black stars), and CMB entry and exit locations for the three phases (black circles for PKP_{ab}, grey for PKP_{bc} and white for PKP_{df}). (inset) Graphs of slowness deviation vs. epicentral distance for this data. Data is binned with respect to distance; bins are 2° wide and overlap by 1°. The pale points are from bins containing less than 4 events. Deviations are from ak135.

Black, J.A. and Thomas, C., Using an array approach to investigate possible causes for PKP differential travel time deviations, *Geophys. J. Int.*, submitted 2004.

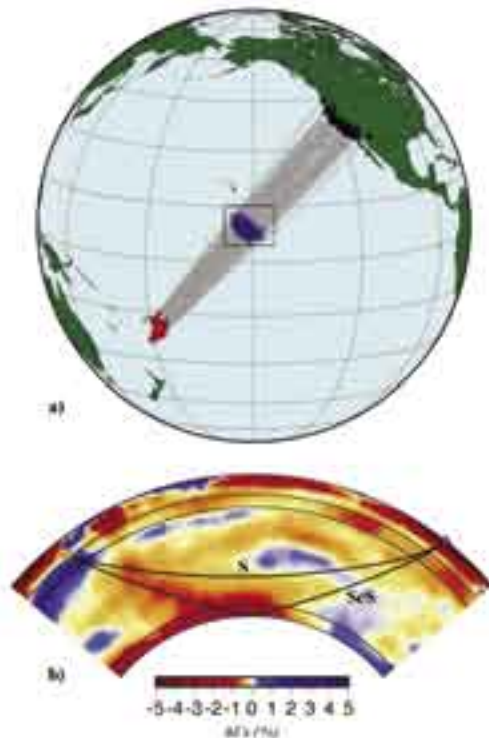
Kennett, B.L.N., Engdahl, E.R. & Buland, R., Constraints on seismic velocities in the Earth from travel times, *Geophys. J. Int.*, 122, 108-124, 1995.

Lateral Variation of the D'' Discontinuity Beneath the Pacific

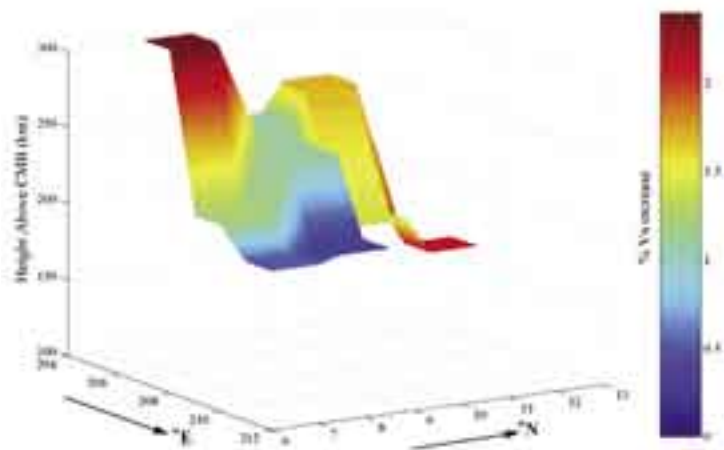
Megan Avants, Thorne Lay • University of California, Santa Cruz

Sara A. Russell • Weston Geophysical

Small-scale variability of the D'' shear velocity discontinuity beneath the central Pacific is being imaged using 363 broadband tangential component S waveforms recorded by GSN, BDSN, and TRInet stations in western North America for 39 deep focus events in the Tonga-Fiji region. Double-array stacking of spatially binned subsets of data demonstrates variations in timing and relative amplitude of reflection from the deep mantle discontinuity on scale lengths of about 130 km across the 6°x8° region of D'' sampled. Waveform modeling using localized one-dimensional structures indicates variations of discontinuity shear velocity increase ranging from 0.3% to 2.4% and discontinuity depths ranging from 2568 to 2730 km. The discontinuity tends to deepen and weaken from southwest to northeast across the study area, a trend that correlates with local spatial gradients in shear velocity anomalies and ScS splitting measurements. The existence of a shear velocity discontinuity in this region is somewhat surprising. While the discontinuity is more variable than in circum-Pacific regions, it has about the same general characteristics, thus it is likely to originate from a similar fundamental cause. It is not reasonable to invoke a slab-related explanation as the region is far removed from subduction, and there is no major depth variation as predicted by a high Clapeyron slope phase transition. Chemical heterogeneity of the D'' layer may provide the answer to the D'' discontinuity after all.



(a) Base map showing the raypath configuration for this study. (b) Cross-section through a global tomographic model showing the basic structure sampled by our geometry. The deep mantle in this region has slow shear velocities, particularly in the D'' region.



Topography on the D'' reflector inferred from localized double-array stacks. The discontinuity is shallower in the region to the southwest.

Avants, M., T. Lay, and S. A. Russell, Lateral variation of the D'' shear velocity discontinuity beneath the central Pacific, *J. Geophys. Res.*, submitted, 2005. Supported by NSF grants EAR-0125595.

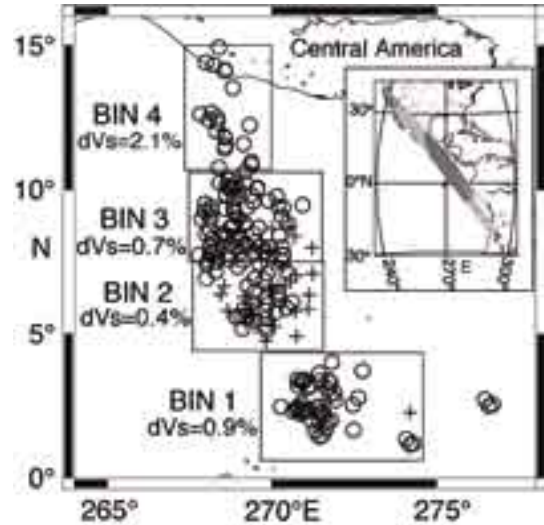
Lateral Variation of the D'' Discontinuity Beneath the COCOS Plate

Thorne Lay • University of California, Santa Cruz

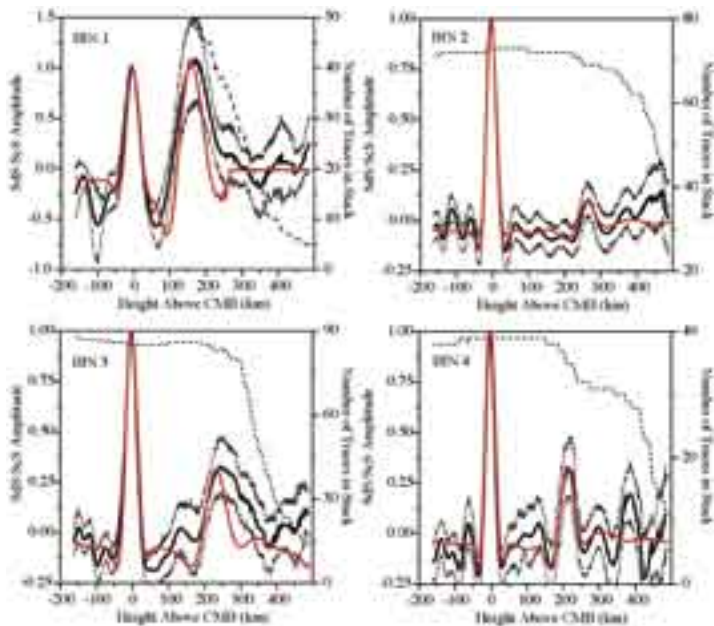
Edward J. Garnero • Arizona State University

S. A. Russell • Weston Geophysical

Broadband shear-wave signals from 15 deep South American earthquakes reveal small-scale variations in the D'' shear-velocity discontinuity beneath the Cocos Plate. The data, from GSN, BDSN and TRInet stations in the western U.S., provide imaging for a preliminary stage of the USArray deployment. This dense distribution of stations is used for double-array stacking procedures, using suites of observations from different sources and receivers that sample common mid-points in spatially localized bins. The data sampling each of 4 bins provide coherent stacks of energy turning at depths above the core-mantle boundary, which is associated with ScS reflections observed in all of the data. When the data are processed using a uniform reference model for stacking, reflections of varying strength are detected at apparent depths that vary by over 100 km. Models that match the amplitudes require lateral variations in the structure above or below the reflector. If all the variations are mapped into the D'' layer, satisfactory models are found for a discontinuity at uniform depth of 264 km above the CMB, with laterally varying velocities of 0.9% to 2.6% within D''. This set of models matches all of the data except in the southernmost region, where differential times suggest a somewhat deeper discontinuity (by 50 to 100 km), with some velocity decrease above the D'' region.



Map indicating the raypath configuration and fine scale bins used for double-array stacking of the recordings in the western U.S. for South American earthquakes. The average velocity anomaly for each bin inferred from ScS travel time anomalies is shown.



Double array stacks of energy relative to ScS (imaged at the core-mantle boundary) as a function of depth relative to the CMB, for each of the 4 bins (dark solid lines, with bootstrap variances in dotted curves). The number of traces contributing to the stack at each depth is shown in dashed lines. The red lines are stacks of synthetics for a uniform discontinuity depth 264 km above the CMB, with laterally varying velocity in the D'' layer.

Lay, T., Edward J. Garnero, S. A. Russell, Lateral variation of the D'' discontinuity beneath the Cocos plate, *Geophys. Res. Lett.*, 31, L15612, doi:10.1029/2004GL020300, 2004.

Supported by NSF grants EAR-0125595 and EAR-0135119.

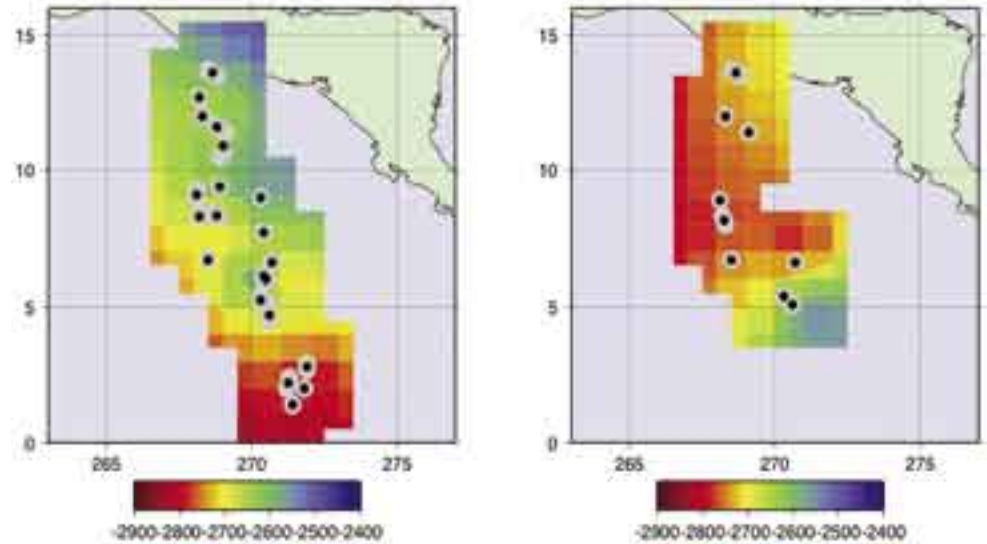
Migration of the Lowermost Mantle Structure Under the COCOS

Christine Thomas • *University of Liverpool, United Kingdom*

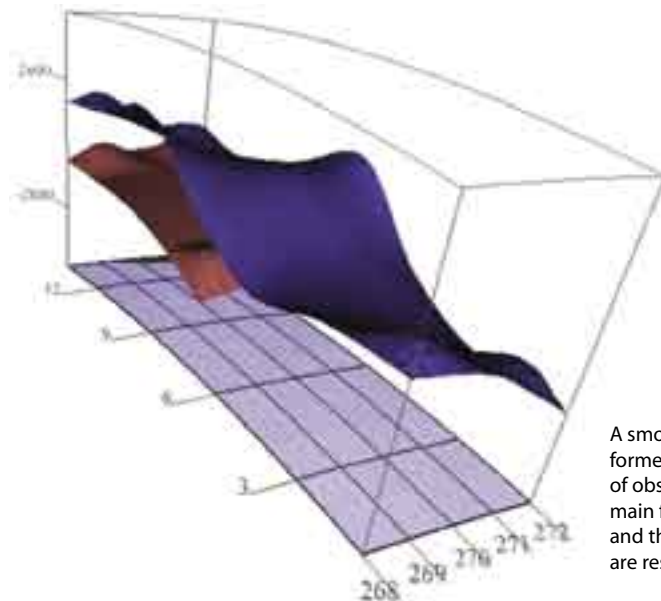
Edward J. Garnero • *Arizona State University*

Thorne Lay • *University of California, Santa Cruz*

A simplified point-scattering migration method is applied to shear-wave observations from GSN, BDSN, and TRInet stations for deep South American earthquakes. The S waves traverse the lowermost mantle beneath the Cocos Plate. Migration allows image development with few a priori assumptions about the structure, in contrast to forward modeling waveforms. In this preliminary application to deep mantle structure, we migrate subsets of data from individual events that sample very localized areas. This allows a detailed mapping of apparent reflector depth across the localized study area to be obtained. It should be recognized that use of a homogeneous background



Maps indicating the depth of a reflector at the top of D'' giving rise to positive (left) and negative (right) arrivals in the waveforms. The migration procedure used seeks very fine-scale resolution of the reflector depth, under the assumption of a homogeneous background model. The apparent topography of the boundary will tradeoff with volumetric velocity heterogeneity within the D'' layer. The positive reflector appears to deepen by about 100 km on average in the southern portion of the study area. The northern portion of the study area has evidence for a negative reflector about 100 km below the positive reflector.



model and very localized data sampling can lead to artificial topography in the image, but significant detail may also be revealed. The image of the D'' reflector that is recovered indicates the presence of a southward increase in depth, rather abruptly at around 5°N . There is clear evidence for an additional reversed-polarity arrival in the northern region, but the migration used here cannot resolve robustly where this energy comes from. It may be from a deeper velocity decrease or, as appears more likely, from out-of-plane scattering.

A smoothed 3D image of the two reflectors imaged in this study. The images are formed from piecing together local reflector images from stacks of small numbers of observations, so some of the undulations may be exaggerated. However, the main features of southward deepening of the shallower reflector at the top of D'' and the presence of some form of scatter of negative arrivals in the northern region are resolved.

Thomas, C., Edward J. Garnero, and T. Lay, High-resolution imaging of lowermost mantle structure under the Cocos Plate, *J. Geophys. Res.*, 109, B08307, doi:10.1029/2004JB003013, 2004.

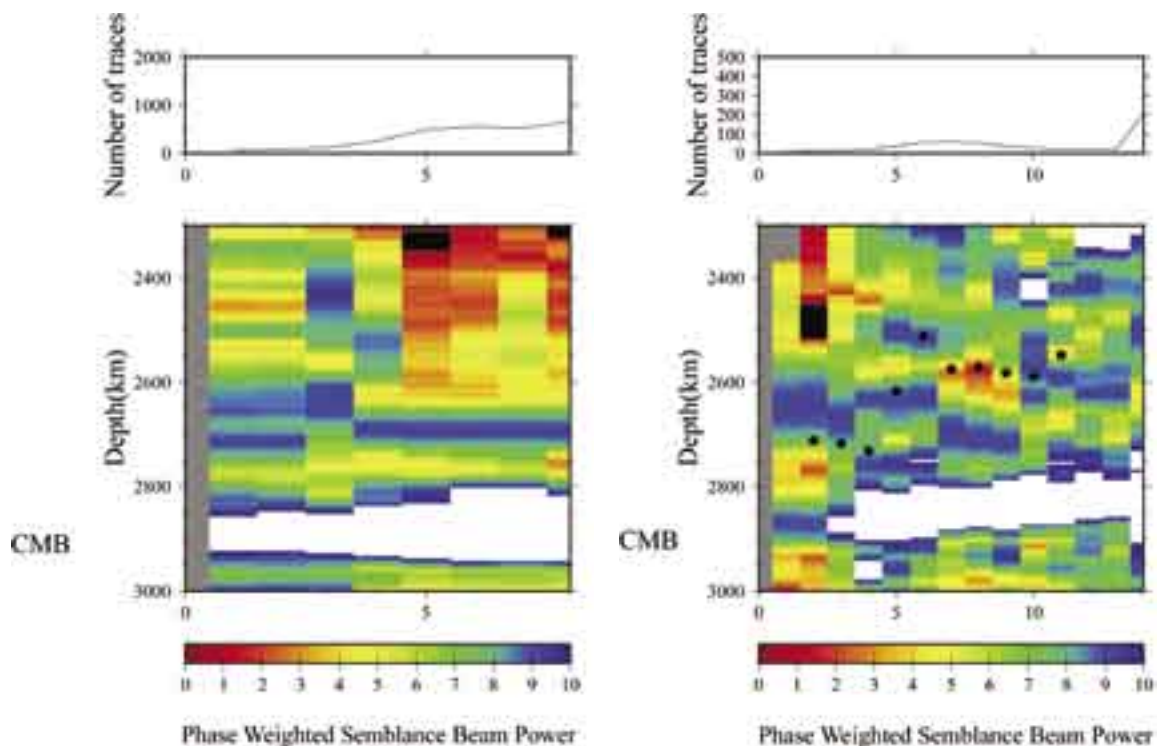
Supported by NSF grants EAR-0125595 and EAR-0135119.

Lateral Variation of P- and S-Wave Velocity Discontinuities in the Lower Mantle Beneath the Cocos Plate

Tadashi Kito, Christine Thomas • University of Liverpool, United Kingdom

Ed Garnero • Arizona State University

A double-beam method (Kito et al., 2004) has been used to image the lateral variation of the D'' discontinuities under the Cocos Plate. We used P and S waves from deep earthquakes in South America recorded at Californian broadband network stations. The data were band-pass filtered between 1 – 10 s for P waves and low-pass filtered at 0.3 Hz for S waves. We set bins to cover the PcP and ScS reflection points and shifted them by 1 degree in the direction of the latitude whose sizes are 4 degrees for P waves and 2 degrees for S waves. Steps of discontinuities were observed both in the P and S waves. The discontinuities in the southern part of our study area tend to be deeper than those in the northern part. This qualitatively agrees with a previous study by Thomas et al. (2004) and Lay et al. (2004), although the exact reflector depth is slightly different (up to ± 100 km difference). It is noted that P waves seem to have less lateral variations than S waves. The depth variation of the CMB is probably due to the velocity structure in the mantle which should be corrected in the future.



The left panel shows the result from P waves and the right one is the result from S waves. The left side corresponds to the south and the right side corresponds to the north in each panel. The white areas are PcP and ScS energy, respectively, which is saturated due to their large amplitude. The black dots in the S panel indicate the average reflector depth taken from Thomas et al. (2004). The blue colour suggests high coherent energy which is indicative of discontinuities.

Kito, T., Krüger, F., and Negishi, H., Seismic heterogeneous structure in the lowermost mantle beneath the southwestern Pacific, *J. Geophysical Res.*, 109, doi:10.1029/2003JB002677, 2004.

Lay, T., E.J.Garnero, and S.A. Russell, Lateral variation of the D'' discontinuity beneath the Cocos plate, *Geophys. Res. Lett.*, L15612, doi:10.1029/2004GL020300, 2004

Thomas, C., Garnero, E. J., and Lay, T., High-resolution imaging of lowermost mantle structure under the Cocos Plate, *J. Geophysical Res.*, 109, doi:10.1029/2004JB003013, 2004.

Observation of P-Wave Velocity Discontinuities in D'' Beneath Southeast Asia Using Migration Techniques

Jeremy Chaloner, Christine Thomas • University of Liverpool, United Kingdom

We utilize a simplified migration technique to image the P-wave velocity structure in D'' beneath southeast Asia using records of earthquakes in the Philippines recorded at the KNET and GHENGIS arrays, obtained through the IRIS DMC. Traces are stacked according to the travel times from event to station via a 3D grid of hypothetical isotropic point scatterers in the lower mantle – if a point in the grid corresponds to a real reflection surface, the traces will sum coherently (Thomas et al., 2004).

We find strong evidence for one reflector at a height of 250 km above the CMB, and weaker evidence for a second reflector approximately 50 km above the CMB, which may correspond to a double crossing of the post-perovskite phase boundary (Hernlund et al., 2005).

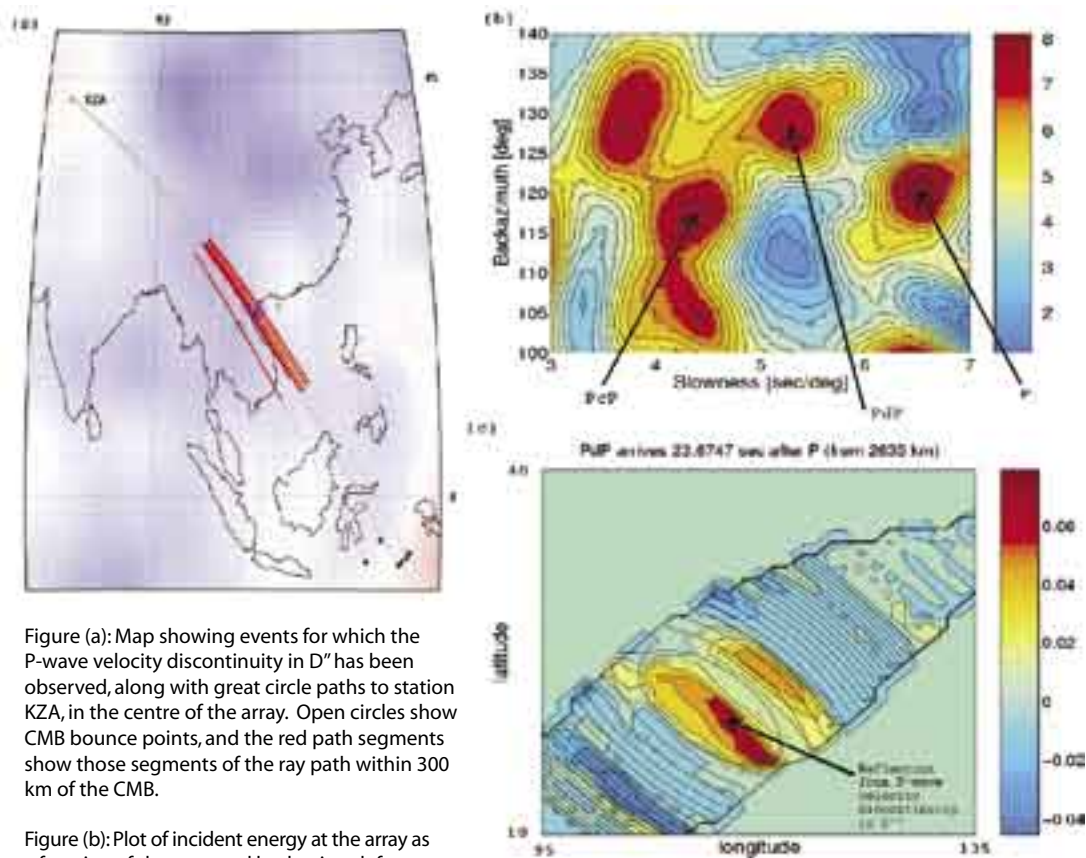


Figure (a): Map showing events for which the P-wave velocity discontinuity in D'' has been observed, along with great circle paths to station KZA, in the centre of the array. Open circles show CMB bounce points, and the red path segments show those segments of the ray path within 300 km of the CMB.

Figure (b): Plot of incident energy at the array as a function of slowness and back azimuth for an event on 17 June 1998. Great circle back-azimuth for this event was 120°; epicentral distance from event to array is 68°. Theoretical slowness for P is 6.22 sec/deg, and 4.20 sec/deg for PcP. The reflection from a velocity discontinuity in D'', denoted PdP, can be recognized by its intermediate slowness between P and the reflection from the CMB. The fact that the majority of the energy in PdP appears ~10° off the great circle path may be an indication of topography in the reflecting surface.

Figure (c): Horizontal section through the grid of potential scattering points at a depth of 2635 km for the same event as figure (a), showing amplitude at the receiver following stacking. The reflection from a velocity discontinuity in D'' can be clearly seen.

C. Thomas, J. M. Kendall and J. Lowman, Lower-mantle seismic discontinuities and the thermal morphology of subducted slabs, *Earth Planet. Sci. Lett.*, 225, 105-113, 2004.

J. W. Hernlund, C. Thomas and P. J. Tackley, A doubling of the post-perovskite phase boundary and structure of the Earth's lowermost mantle, *Nature*, 434, 882-886, 2005.

Funded by the Natural Environment Research Council, reference NER/S/J/2004/13122.

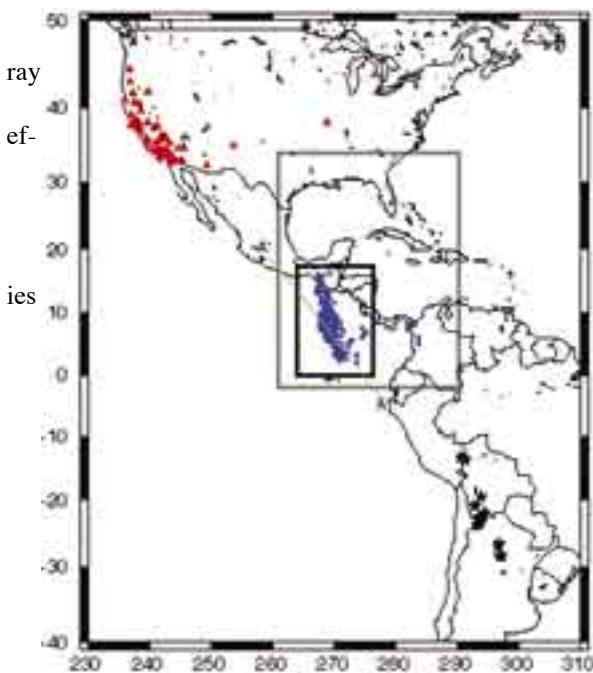
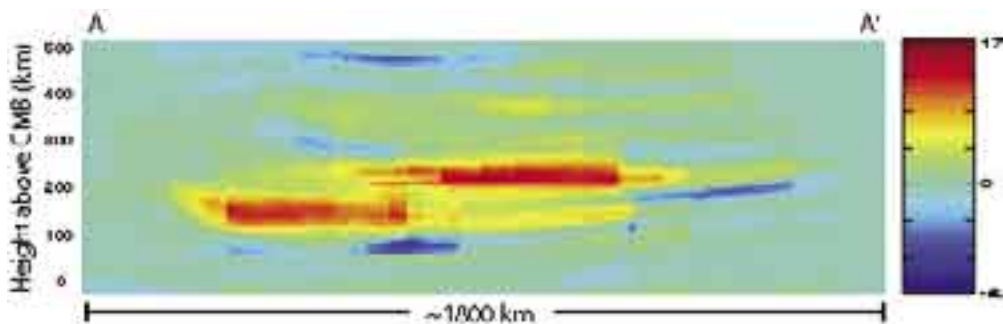
A Step in the D'' Discontinuity Imaged by Kirchoff Migration Through 3D Tomographic Models

Alex Hutko, Thorne Lay • University of California, Santa Cruz

Justin Revenaugh • University of Minnesota

Ed Garnero • Arizona State University

A simple migration scheme is used to image topography of between 50 and 100 km over less than 200 km laterally of the D'' discontinuity. Correcting for first-order travel-time perturbations based on one-dimensional ray tracing through S-wave tomography models does not change our interpretation, but does affect the absolute depth of the reflector. The abrupt change in its height is unlikely to be due to a phase change and temperature differences alone, so chemical heterogeneities are required



to be consistent with the observations. We also observe a low-velocity scatterer that is approximately 2 degrees in diameter. This feature is more model dependant but agrees with finite frequency tomography results from Hung et al. (2004). Though this ray-based method does not account for bending of the ray path due to three-dimensional structure nor does it include scattered energy after the

has reached its turning point, we find it works remarkably well where data density is sufficient, while having significant gains in efficiency over wave equation based methods. In its initial phase, US Array will have an aperture approximately three times greater than currently available to study the lower mantle beneath the Americas. The greater number of crossing rays, which is critical for lower mantle studies, will undoubtedly lead to further exciting discoveries and new constraints for other members of the Earth science community.

Map showing earthquakes (black stars), seismographs (red triangles), ScS bounce points on the CMB (blue dots), and the great circle paths along which the migrated data stack (bottom figure) was made (green lines). Our data set consists of 273 seismograms from 61 receivers recording ground displacement from 15 deep earthquakes. The black rectangle shows the area where our resolution is high enough to map D'' discontinuity topography and detect features as small as 100 km. The grey rectangle shows the approximate area that we will be able to image at High-Resolution with data from US Array. Imaging small features in the lowermost mantle across large scale lengths is key to understanding their relationship with the overlying tectonics.

Hung, S.-H., Garnero, E. J., Chiao, L.-Y., Kuo, B.-Y., Lay, T., Finite-frequency tomography of D'' shear velocity heterogeneity beneath the Caribbean, *J. Geophys. Res.*, in review, 2005.

Lay, T., E.J. Garnero, and S.A. Russell, Lateral Variation of the D'' Discontinuity Beneath the Cocos Plate, *Geophys. Res. Lett.*, 31, doi:10.1029/2004GL020300, 2004.

Thomas, C., Garnero, E.J., and Lay, T., High-resolution imaging of lowermost mantle structure under the Cocos Plate, *J. Geophys. Res.*, 109, doi:10.1029/2004JB003013, 2004.

Lowermost Mantle Anisotropy Beneath the Central Pacific

Juliana M. Rokosky, Thorne Lay • University of California, Santa Cruz

Edward J. Garnero • Arizona State University

Analysis of lowermost mantle anisotropy is a crucial step in fully characterizing the deep mantle. We utilize a large number of Tonga-Fiji events recorded by California stations to assess shear-wave splitting of core reflections (ScS). Shear-wave splits (ScSH-ScSV) and differential travel times ($\text{ScS-S}_{\text{DATA}} - \text{ScS-S}_{\text{PREM}}$) are calculated for over 390 records from 37 events, a

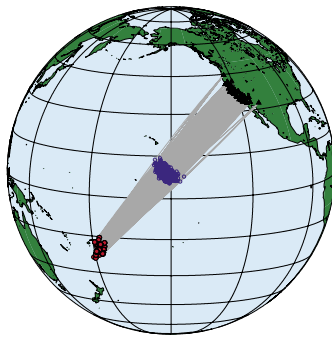


Figure 1. Raypaths for data used in this study. Red circles indicate sources, black triangles indicate receivers, and blue circles are CMB bouncepoints.

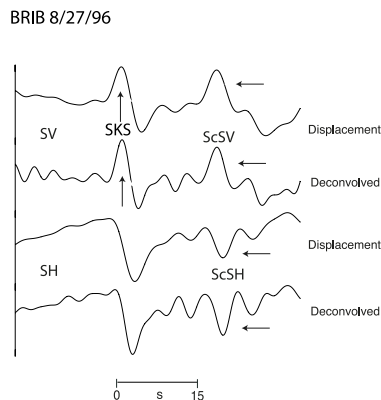


Figure 2. Data example from station BRIB in Briones. Receiver-corrected records are deconvolved using an average source wavelet for event, obtained by stacking transverse component ScS arrivals. Source wavelet deconvolution equalizes signal between events and improves the resolution of peak arrival times.

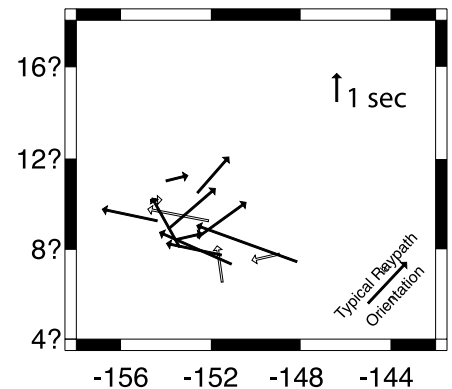


Figure 3. Preliminary results from polarization analyses on approximately 15% of the data. Arrows are oriented in the azimuth of the fast polarization direction and their lengths scaled to splitting magnitude. White arrows indicate B quality results.

nearly five-fold increase in data from previous work in the region. There is a trend of increasing ScS travel-time delays from the southwest to the northeast, suggesting that deep-mantle shear velocity decreases in this direction. While ScS splitting is pervasive, when measured by simple peak-to-peak methods (valid for VTI-like anisotropy) it is not as simply organized as suggested in prior work. To assess whether azimuthal anisotropy can better explain observed shear-wave splitting under the Central Pacific, we perform polarization analyses on suitable data following the methods of Silver and Chan (1991). While preliminary results do suggest a bimodal pattern reported in previous work (Russell et al. 1999), significant remaining scatter hints that other factors may be obscuring our ability to easily characterize deep mantle anisotropy in this region. Work is currently being done to assess the accuracy of receiver corrections applied to the data, as such inaccuracies could contribute to this scatter.

Russell, S. A., T. Lay, Edward

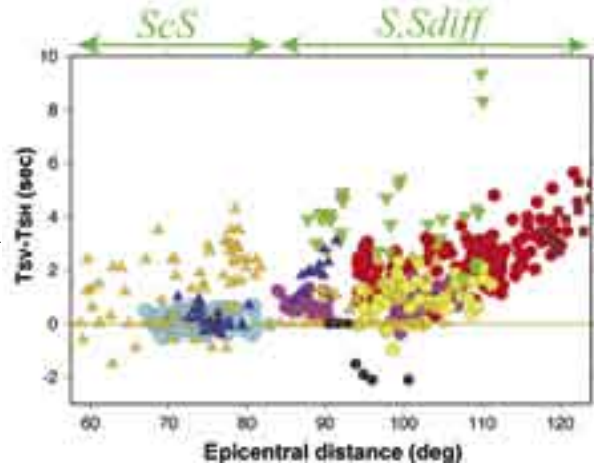
Pacific imaged using broadband ScS waves, *J. Geophys. Res.*, 104, 13183-13200, 1999.

D'' Anisotropy From Lamellae and Transverse Isotropy

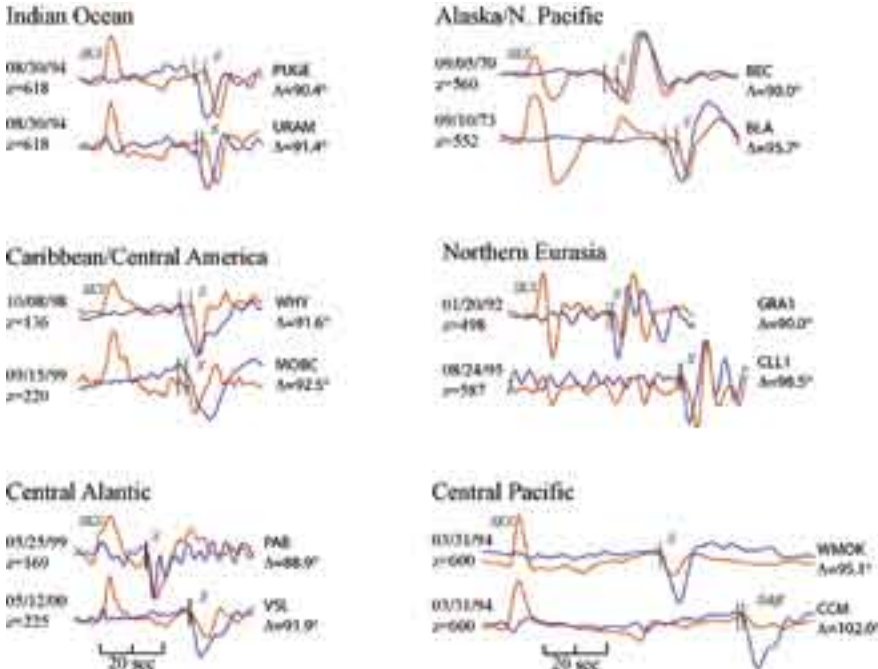
Melissa M. Moore, Edward J. Garnero • Arizona State University

Thorne Lay, Quentin C. Williams • University of California, Santa Cruz

Observations of shear-wave splitting in the lowermost mantle may hold key information for revealing the dynamics of the lower mantle boundary layer. The majority of observations are consistent with horizontally-polarized shear wave components having slightly higher velocity than vertically-polarized shear wave components. This is consistent with radial anisotropy or vertical transverse isotropy in the deep mantle. Such anisotropy could arise due to horizontal shearing of velocity heterogeneities that gives a distribution of lamellae on scales finer than the seismic wavelengths, from distributions of melt aligned in the boundary layer, or from sheared crystalline structure with fast axes randomly oriented in the horizontal plane in the boundary layer. Numerical models are compared with data to assess the magnitude and scale lengths of those models that can be locally approximated with layered isotropic or transversely isotropic models. The lack of azimuthal coverage of most regions leaves open the possibility of azimuthal anisotropy in many regions, but it is established that single, or sparse lamellae models are not likely to be responsible for the observations. It appears that globally there may be regions of lattice-preferred orientation and other regions of shape-preferred orientation responsible for shear-wave splitting in the lowermost mantle.



Composite of global shear wave splitting measurements for the D'' region treated as simple SV-SH differential arrival times. Measurements from various studies are indicated with different colors, and splitting measured from ScS and Sdiff observations are separated in distance.



Shear waveforms from GSN, WWSSN, and other broadband stations for paths traversing different regions of the lowermost mantle. SH waveforms are in blue, and SV waveforms in red. Differences in the onset times of S (Sdiff) are indicated by small vertical picks. Note that the SV arrivals tend to be later than SH when there is significant difference, and the magnitude of the splitting tends to increase with distance.

Moore, M. M., Edward J. Garnero, T. Lay, and Q. Williams, Shear wave splitting and waveform complexity for lowermost mantle structures with low-velocity lamellae and transverse isotropy, *J. Geophys. Res.*, 109, B02319, doi: 10.1029/2003JB002546, 2004.

Supported by NSF grants EAR-0125595 and EAR-0135119.

Azimuthal Anisotropy in the D'' Layer Beneath the Caribbean Sea

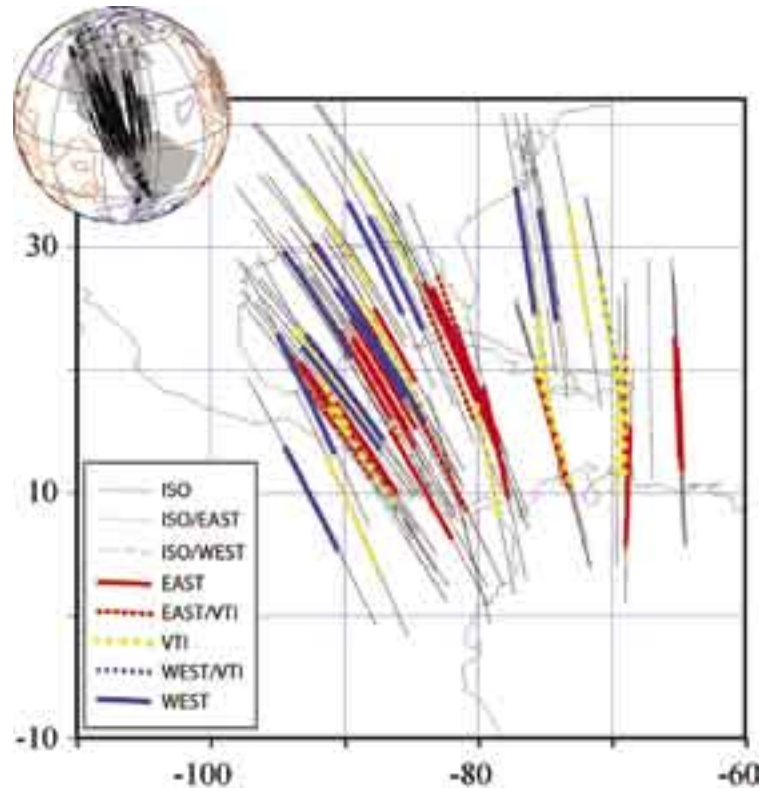
Valérie Maupin • *University of Oslo, Norway*

Edward J. Garnero, Matthew J. Fouch • *Arizona State University*

Thorne Lay • *University of California, Santa Cruz*

The anisotropic structure in the lowermost mantle beneath the Caribbean Sea is modeled in detail. The data require the presence of azimuthal anisotropy, in contrast to prior interpretations, and we model the waveforms in detail to place some bounds on the symmetry orientation for the azimuthal anisotropy. The data used are CNSN and GSN observations of deep focus earthquakes in South America. In the first systematic modeling of a large number of waveforms for models of azimuthal anisotropy in D'', we exploit variations in initial polarization associated with varying focal mechanisms to help to constrain the anisotropy. While there is only limited azimuthal coverage, which precludes determination of the overall symmetry, we find coherent patterns in the distribution of satisfactory models for tilted transverse isotropy (hexagonal symmetry with symmetry axis departing from the vertical (radial) direction). The data are close to being consistent with transverse isotropy because the fast wave is close to being the transverse arrival in all cases. Some data are most consistent with vertical transverse isotropy because the fast wave is purely polarized as SH, but this is the exception in this data set. Mapping out azimuthal anisotropy appears to be viable, and holds the promise of greatly adding to our understanding of processes in the deep mantle boundary layer.

Map showing raypaths of data sampling the deep mantle beneath the Caribbean. For the segment of each raypath within a 250-km-thick layer at the base of the mantle, the preferred geometry of the transverse isotropy symmetry axis is indicated. Note the spatial coherence of paths preferring an east or west-dipping tilt to the symmetry axis.



Garnero, E. J., V. Maupin, T. Lay, and M. J. Fouch, Variable azimuthal anisotropy in Earth's lowermost mantle, *Science*, 306, 259-260, 2004.

V. Maupin, Edward J. Garnero, T. Lay, and M. J. Fouch, Azimuthal anisotropy in the D'' layer beneath the Caribbean, *J. Geophys. Res.*, 110, B08301, 2005.

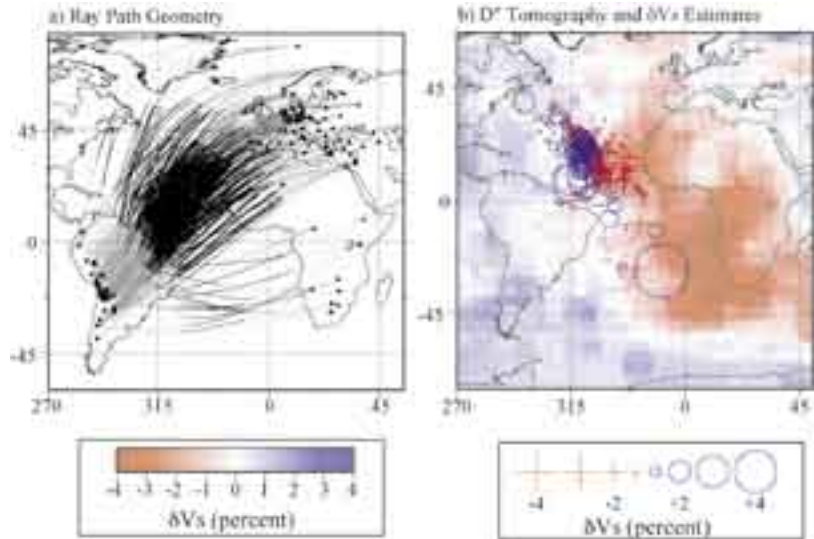
Supported by NSF grants EAR-9996302, and EAR-0125595.

Isotropy or Weak Vertical Transverse Isotropy in D'' Under the Atlantic

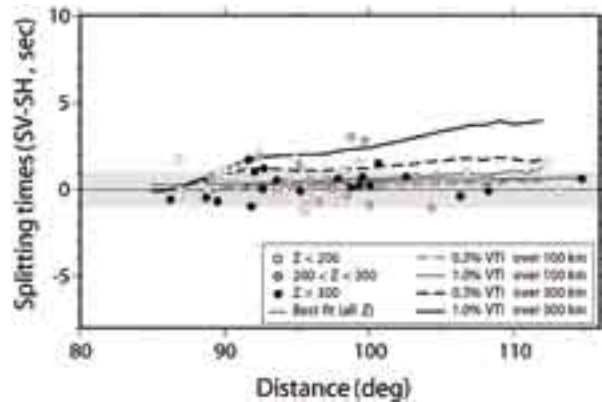
Edward J. Garnero, Melissa M. Moore, Matthew J. Fouch • Arizona State University

Thorne Lay • University of California, Santa Cruz

Shear velocity properties of the D'' region below the central Atlantic are explored using GSN, Geoscope, and GEOPHON recordings from Europe and Africa for intermediate and deep-focus earthquakes in South America. Regional shear velocity heterogeneity near the base of the mantle is mapped by analysis of S-SKS differential times corrected for aspherical mantle structure above D''. There is a lateral gradient from faster to slower velocities moving from west to east across the region, with PREM-like average velocities under the central Atlantic. 105 shear wave splitting times are measured, with corrections being applied for lithospheric anisotropy whenever possible. While some of the larger values have SV delayed relative to SH, the majority of data show little evidence for transverse isotropy or azimuthal anisotropy. Assuming vertical transverse isotropy distributed over a 300-km-thick region, as observed under the Caribbean, the magnitude of anisotropy is found to be less than 0.25%.



Maps of (a) raypaths and (b) shear velocity anomalies within a 250 km thick D'' layer under the Atlantic. Note the strong lateral gradient in shear velocity, which corresponds to the transition from higher velocities in the west to slower velocities offshore of Africa in the large-scale tomographic model of Grand (2002).



Shear wave splitting measures made under the assumption of vertical transverse isotropy (SV-SH differential arrival times) for the data set traversing the deep mantle under the Atlantic. Predictions for models with uniform VTI of 0.5% and 1.0% distributed over a 100 or 300 km thick layers are shown.

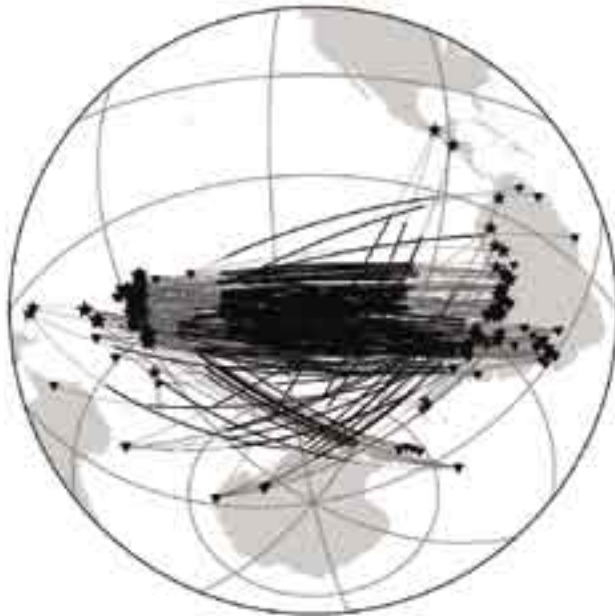
Garnero, E. J., M. M. Moore, T. Lay and M. J. Fouch, Isotropy or weak vertical transverse isotropy in D'' beneath the Atlantic Ocean, *J. Geophys. Res.*, 109, B08308, doi:10.1029/2004JB003004, 2004.

Supported by NSF grants EAR-9996302, and EAR-0125595.

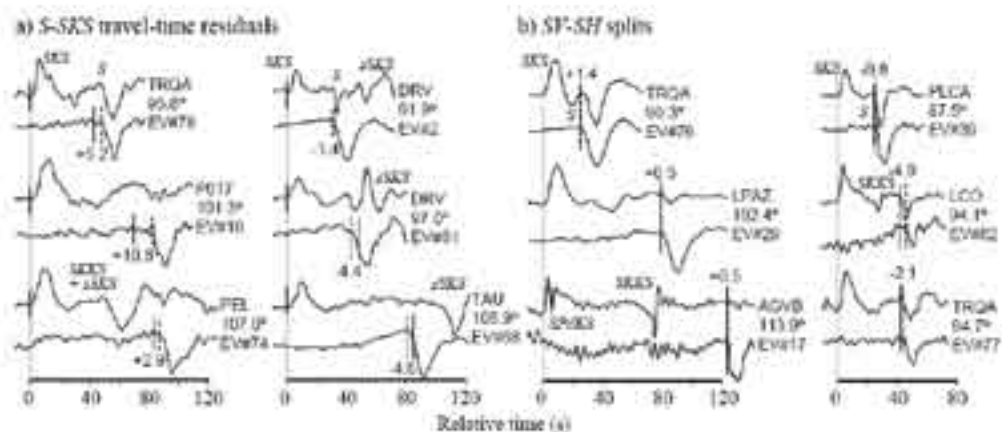
A Strong Lateral Shear Velocity Gradient and Anisotropy Heterogeneity in the Lowermost Mantle Beneath the Southern Pacific

Sean R. Ford, Edward J. Garnero, Allen K. McNamara • Arizona State University

Velocity heterogeneity and seismic anisotropy in the D'' region beneath the southern Pacific Ocean is investigated using broadband shear waves from southwest Pacific and South American earthquakes recorded by permanent and temporary stations in Antarctica, Australia, South America, and on islands in the South Pacific. Shear velocity perturbations (δV_S) are inferred from the differential times between hand-picked horizontally polarized (SH) direct or diffracted S arrivals and vertically polarized (SV) SKS arrivals. Derived patterns in δV_S roughly agree with global shear velocity models, but reveal a stronger shear velocity lateral gradient north of $\sim 50^\circ\text{S}$ where δV_S transitions from approximately $+0.5$ to -1.0% (relative to radially averaged reference models) over less than 600 km along the base of D'' . Waveform analyses provide an even stronger constraint on the transitional region, where there is a change in waveform behavior occurring over length scales less than 300 km. Differential times between SKKS and SKS, calculated by cross-correlating SKS with Hilbert-transformed SKKS, support large δV_S amplitudes and help to constrain the location of the transitional region. Anisotropy in D'' (k_S) is inferred from handpicked differential times between the SV and SH components of direct or diffracted S, and display a slight spatial trend where the SH component precedes the SV in the north and east of the study area, but arrives after SV in the center and southwest of it. However, there is high k_S variability in the center of the study region. There is no apparent correlation between δV_S and k_S . Abrupt changes in the character of velocity and anisotropy in this region of D'' may be related to chemical heterogeneity at the boundary of the Pacific Superswell, as well as small-scale convection in the deep mantle.



Stations (triangles), events (stars), great-circle projections of ray paths (grey lines), and great-circle projections of the PREM-calculated ray paths in a 300 km thick D'' (thicker black lines) used in this study.

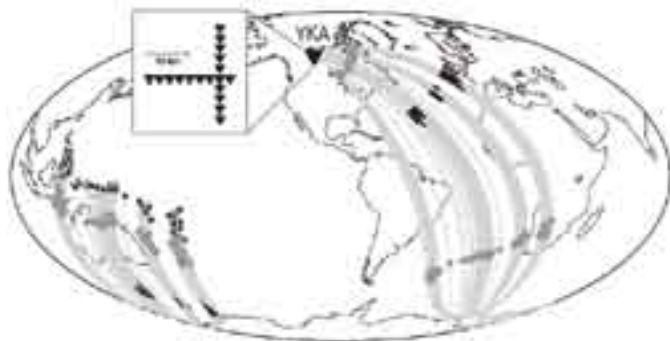


(a) Examples of waveforms used in the S-SKS differential travel-time residual (δT_{S-SKS}) analysis. The dashed lines show handpicked S_{SH} arrivals and the solid lines are the PREM-predicted S arrival time relative to the handpicked SKS arrival (light grey line). Values of δT_{S-SKS} are above S arrivals. (b) Examples of waveforms used in the shear-wave splitting (T_{SV-SH}) analysis. The dashed lines show S_{SH} arrivals, and solid lines mark S_{SV} onsets. Splitting times are above S arrivals. Traces are normalized in time to the SKS arrival, and scaled to the maximum amplitude of each trace. Top trace of each pair is the SV component, bottom trace is SH.

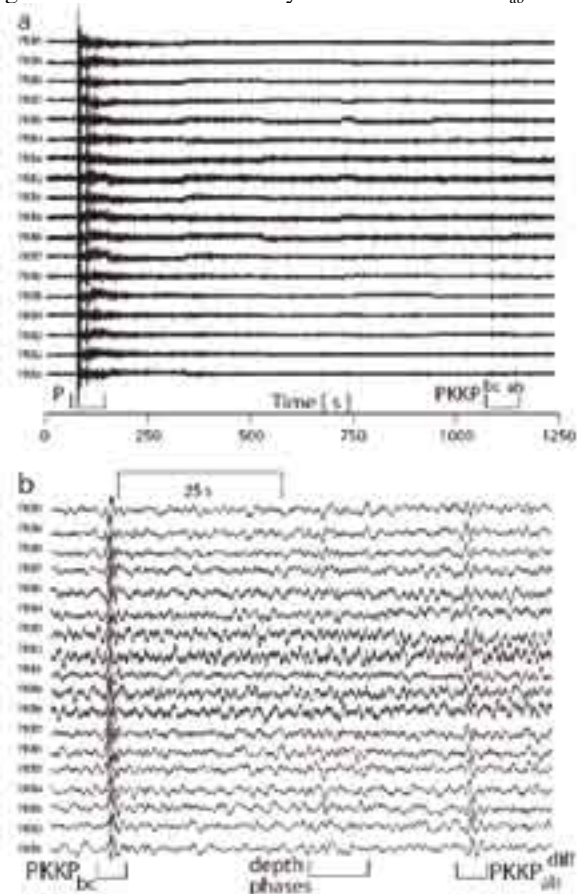
Detection of an Ultralow Velocity Zone at the CMB Using Diffracted PKKP_{ab} Waves

Sebastian Rost, Edward Garnero • Arizona State University

Seismic phases diffracted around Earth’s core contain direct information about lowermost mantle wave speeds. By measuring the slowness or ray parameter of incident diffracted energy from array recordings, seismic velocity along the diffracted path can be estimated. Here we apply this principle to diffraction of the major arc seismic phase PKKP_{ab} recorded at the Canadian Yellowknife array to study P-wave velocity variations along the core-mantle boundary. We observe PKKP_{ab}^{diff} about 7.5 degrees past the ray-theoretical cut-off distance for PKKP_{ab} in array processed seismic data. We utilize 330 western Pacific rim earthquakes which sample the deepest mantle beneath the northern Atlantic or the south Pacific Ocean. Slowness and backazimuth values are measured by applying frequency-wavenumber analysis to the array data. Mapping PKKP_{ab}^{diff} slowness estimates to the lowermost mantle yields 4 to 19% P-wave velocity reductions relative to PREM, in good agreement with the magnitude of velocity reductions commonly mapped in ultra-low velocity zones. The PKKP_{ab}^{diff} slowness and backazimuth variations combined with results from previous studies imply that the lowered velocities solely occur at the base of the mantle beneath the northern Atlantic Ocean, along the receiver sides of raypaths. PKKP_{ab}^{diff} array measurements thus hold important potential for mapping ultra-low velocity zone structure in as-of-yet unprobed regions of the lower mantle, as well as for providing independent information about lower mantle structure to be used in combination with established probes in previously studied regions.



Earthquake (black circles) to receiver (YKA, black triangle) geometries for data analyzed in this study. Also shown are PKKP raypaths along the major arc of the great-circle path (grey lines), and PKKP_{bc} CMB entry, exit, and mid-reflection points (grey diamonds). Diffracted arc lengths PKKP_{ab}^{diff} for earthquakes in Table 1 are also shown (thick black line segments).



a) Raw YKA recordings for the event on April 1st 1991 UTC 05:25 (source depth $h = 90$ km). The time window from P to PKKP for all 18 recording stations of the array are shown. Epicentral distance to YKA is 95.63 deg, with a backazimuth of 270.35 deg. Recordings of the short-period vertical instruments with a dominant period of ~ 1 s are shown. b) Zoom into the PKKP time window for the same event. Amplitudes are normalized to the PKKP_{bc} amplitudes. Note the apparent lower frequency content of PKKP_{ab}^{diff} due to the loss of higher frequencies from diffraction.

NSF # EAR-0125595

Examining the Base of the Mantle Using IRIS FLED PASSCAL Data

Michael Wyession, Ghassan Aleqabi, Patrick Shore, Jesse Fisher Lawrence, Brian Shiro, Moira Pyle, Garrett Euler, Tara Mayeau • Washington University

Karen Fischer, Stephane Rondenay, Ellen Syracuse, Christine McCarthy, Catherine A. Rychert, Lindsey Doermann, Mariela Salas, Margaret Welsh • Brown University

The Florida-to-Edmonton (FLED) PASSCAL array provided a unique opportunity to examine the velocity structure at the base of the mantle. This array (for details, see the previous one-pager “Investigating Crust and Mantle Structure with the Florida-to-Edmonton Broadband Array”) followed upon the success of the MOMA (Missouri-to-Massachusetts) array in being an excellent way to examine both crust/upper mantle structure as well as the structure of the core-mantle boundary region (CMBR). The FLED array data are being used in several different ways to look at CMBR structure because North America is well-situated with respect to the seismicity of the Pacific rim to record large numbers of high-quality core phases. One project underway involves using core-reflected ScS and SdS waves from primarily South American earthquakes to look at the velocity and discontinuity structure of the CMBR beneath Central America. Another project uses the phase SPdiffKS to examine the ultralow velocity layer at the base of the CMBR.

In the example shown in the figures here, the dispersive nature of core-diffracted P waves is used to examine lateral variations in the vertical velocity structure of the lowermost mantle. The ray parameter of core-diffracted waves varies as a function of frequency due to the vertical change in velocity at the base of the mantle. Understanding the vertical velocity structure is important because it can provide constraints on the strength of the thermal boundary layer in the CMBR, and therefore of the amount of heat conducting from the core into the mantle. We generate synthetic dispersion curves for different models of the CMBR and then compare them to data. We find that many regions (most of our coverage is beneath the Pacific) are compatible with a PREM-type velocity model for D', while others require slower velocities. There are no regions of the CMBR beneath the Pacific we have found that display velocities faster than PREM. In certain areas of D', such as beneath the northern Pacific, the data suggest a structure with a discontinuity at the top of D', but most Pacific regions do not require this.

NSF Grant #: EAR-9903385, EAR-9903260

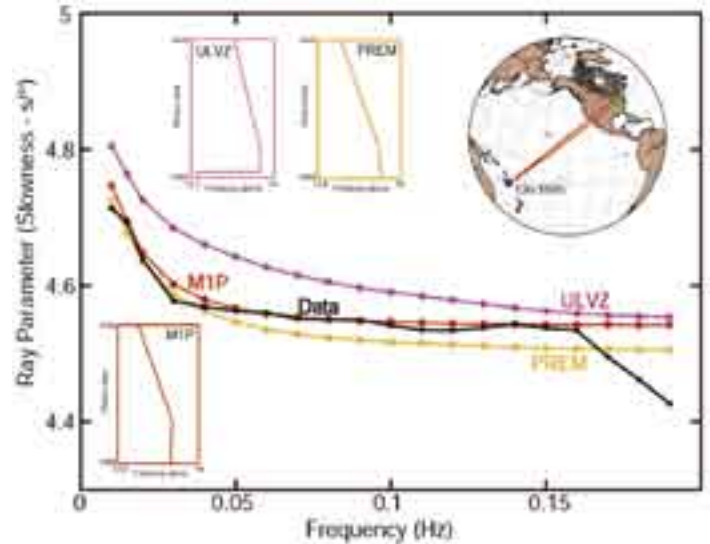


Figure1. An example of using a Pdiffracted wave dispersion curve to constrain CMBR vertical velocity structure, shown for a western Pacific earthquake recorded at the MOMA array. The Pdiffracted dispersion suggests velocities at this region of the lowermost mantle beneath the eastern Pacific that are slower than PREM, fit by the M1P model shown. The dispersion curve cannot be fit by an ultralow velocity zone model, which would have the wrong shape.

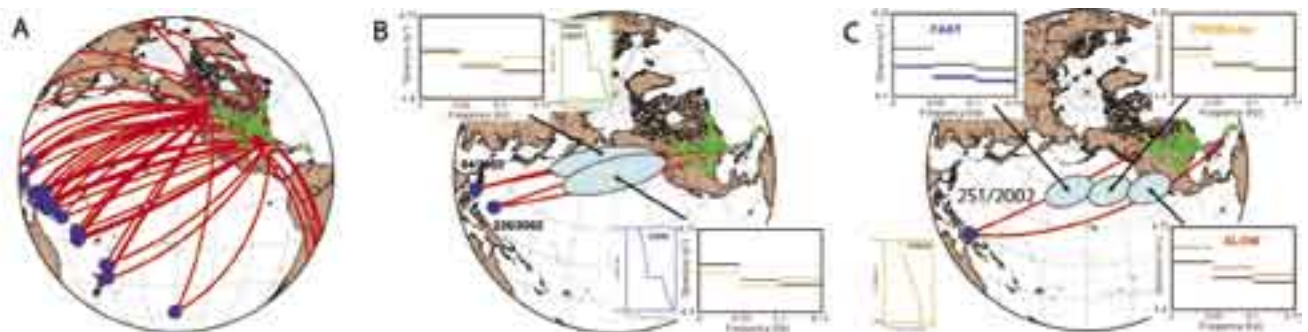


Figure 2. Using Pdiffracted waves recorded at FLED and nearby stations to examine lateral variations in the vertical structure above the CMB. A. Map showing earthquake locations (blue circles) and ray paths. B. Two earthquakes that sample a region of the lowermost mantle well-modeled by a velocity discontinuity at the top of D' in the manner of Solomatov and Moresi. C. Region of the lowermost mantle that shows no evidence of a D' discontinuity, but shows significant lateral variation in D' velocity structure beneath the northern Pacific.

An Observation of PKJKP: Inferences on Inner Core Shear Properties

Aimin Cao, Barbara Romanowicz • University of California, Berkeley

Nozomu Takeuchi • University of Tokyo

The seismic phase PKJKP, which traverses the inner core as a shear wave, and would provide direct evidence for its solidity, has been difficult to detect. Using stacked broadband records from the Grafenberg array in Germany, we document a high signal-to-noise phase, whose arrival time and slowness agree with theoretical predictions for PKJKP. The back-azimuth of this arrival is also consistent with predictions for PKJKP, as is the comparison with a pseudo-liquid inner core model. Envelope modeling of the PKJKP waveform implies a slightly larger shear velocity gradient with depth in the inner core than that of the PREM model.

(A) Observed vespagram for PKIKP+PKiKP and their depth phases (the energy level is amplified 1.6 times). The center of the energy maximum is for a slowness of ~ 1.9 s/deg, which is the average of slownesses of PKIKP (1.85 s/deg) and PKiKP (2.04 s/deg) predicted from PREM. The following weaker energy maximum corresponds to pPKIKP+pPKiKP, and has the same slowness, as predicted from PREM. (B) Stacked waveforms for PKIKP+PKiKP and their depth phases for the energy maximum in (A). (C) Observed vespagram for the potential PKJKP (energy level is amplified 40 times). The slowness of the energy maximum is ~ -1.6 s/deg, close to the PREM prediction of -1.43 s/deg. The arrival time is also compatible with PREM (1695 sec for the maximum energy, compared to a prediction of 1690 sec for the high frequency onset of the pulse). (D) Stacked waveform corresponding to the energy maximum in (C). (E) Vespagram in the back-azimuth and travel time domain. This shows the direction of arrival of the detected energy, which we identify as PKJKP, in the negative slowness range of Figure 2C. The estimated back-azimuth is $\sim 223^\circ$, which shows that the observed energy propagates along the major arc from the source (the expected back-azimuth of PKJKP is 218°). This indicates that the observed phase is not a near-array scattered phase, and provides additional evidence for its identification as PKJKP (Cao et al., *Science*, 2005).

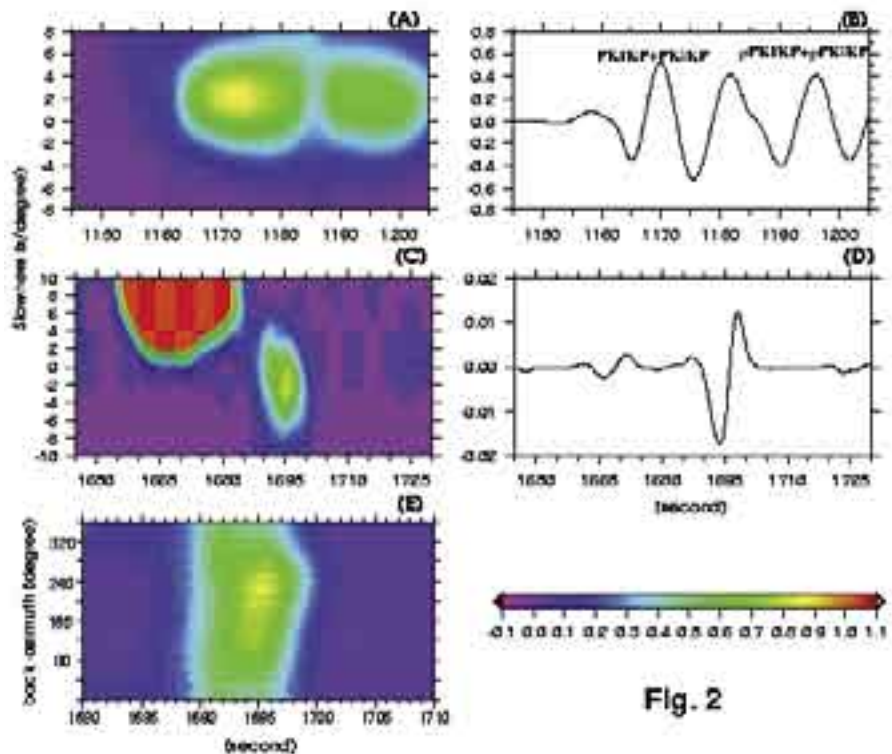


Fig. 2

A. Cao, B. Romanowicz, N. Takeuchi, An observation of PKJKP: Inferences on inner core shear properties, *Science*, (10.1126/science.1109134), 14 April, 2005.

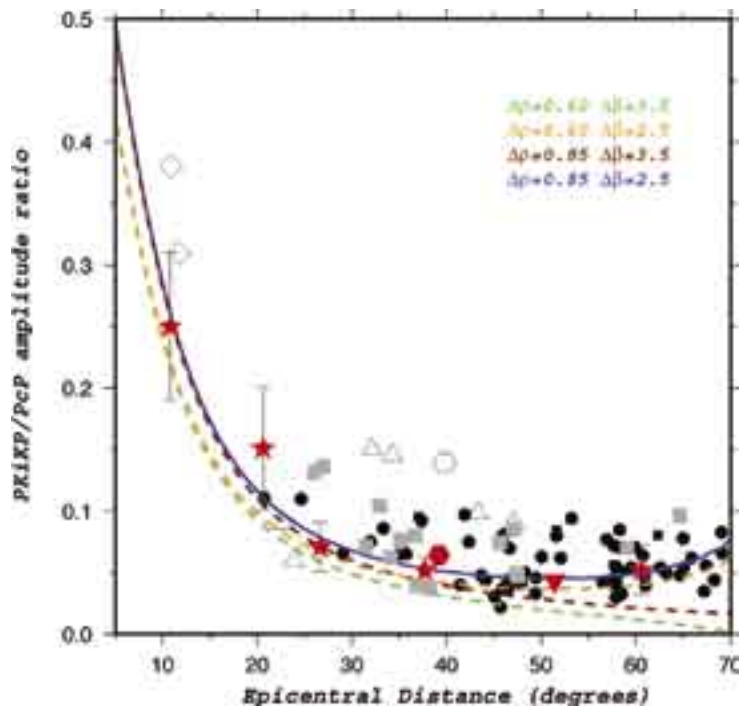
NSF Grant No. EAR-0308750

Constraints on Density and Shear Velocity Contrasts at the Inner Core Boundary

Aimin Cao and Barbara Romanowicz • University of California, Berkeley

The density jump ($\Delta\rho_{ICB}$) at the Inner Core Boundary (ICB) is an important constraint on the dynamics and history of the Earth's core. Two types of seismological data sensitive to $\Delta\rho_{ICB}$ have been studied since the 1970's: free oscillation eigenfrequencies and amplitudes of core reflected phases (PKiKP/PcP). The reference PREM model, based largely on normal mode data, has a relatively low value of $\Delta\rho_{ICB} = 0.60 \text{ g/cm}^3$, whereas most studies based on PKiKP/PcP amplitude ratios find significantly larger values, sometimes in excess of 1.0 g/cm^3 . It has been argued that, because PKiKP is rarely observed in the distance range considered (10° - 70°), the latter type of measurement provides only upper bounds on $\Delta\rho_{ICB}$ (e.g. Shearer and Masters, 1990). We have analyzed 10 years of high quality global broadband data accumulated since the work of Shearer and Masters (1990). We systematically analyzed over 4500 seismograms from intermediate/deep events (depth $> 70 \text{ km}$) and nuclear explosions, in the distance range 10° - 70° . The data were filtered in the band-pass 0.7 - 3 Hz . We performed a rigorous data selection and identified 5 pairs of very clear (Quality A), and 15 possible (Quality A-) PKiKP and PcP arrivals. In addition, 58 records showed no PKiKP but a clear PcP.

These data provide a much less dispersed dataset than previously available, with the quality A data at the lower end of the ensemble of amplitude ratios versus distance. We combine our high-quality measurements with two measurements from the literature that fall within our rigorous selection criteria and obtain estimates of $\Delta\rho_{ICB}$ in the range 0.6 - 0.9 g/cm^3 and $\Delta\beta_{ICB}$ in the range 2 - 3 km/s . Our estimate of $\Delta\rho_{ICB}$ is in agreement with a recent reevaluation of normal mode data (Masters and Gubbins, 2003), thus reconciling results from body wave and mode studies and providing a tighter constraint on $\Delta\rho_{ICB}$ for geodynamicists. Our study also provides evidence for a shear velocity gradient at the top of the inner core.



Measurements of PKiKP/PcP amplitude ratios. The red stars denote the Quality A data, and their error bars are derived from the fractional ratios of the average peak-to-peak amplitudes of background noise to the peak-to-peak amplitude of the identified phase arrivals; the red hexagon is Shearer and Masters' (1990) second measurement with clear PKiKP; the inverted red triangle is a stacking measurement (Schweitzer, 1992) which has been remeasured by the author himself recently; the grey squares denote the Quality A- data; and the black dots are the Quality B data. The curves are the theoretical PKiKP/PcP amplitude ratio calculated with respect to PREM model. For the dashed green curve $\Delta\rho_{ICB} = 0.60 \text{ g/cm}^3$ and $\Delta\beta_{ICB} = 3.5 \text{ km/s}$ (original values in PREM model); for the dashed orange curve $\Delta\rho_{ICB} = 0.60 \text{ g/cm}^3$ and $\Delta\beta_{ICB} = 2.5 \text{ km/s}$; for the dashed red curve $\Delta\rho_{ICB} = 0.85 \text{ g/cm}^3$ and $\Delta\beta_{ICB} = 3.5 \text{ km/s}$; and for the solid blue curve $\Delta\rho_{ICB} = 0.85 \text{ g/cm}^3$ and $\Delta\beta_{ICB} = 2.5 \text{ km/s}$ (our best fitting values using PREM model). The open symbols are other data from previous studies, which were not used in our analysis (triangles: Souriau and Souriau, 1989; hexagon: Shearer and Masters, 1990; diamonds: Engdahl et al., 1970; Bolt and Qamar, 1970) (Cao and Romanowicz, GJI, 2004).

Cao, A., and Romanowicz, B. Constraints on Density and Shear Velocity Contrasts at the Inner Core Boundary, *Geophys. J. Int.*, 157, 1146-1151, 2004.

Masters, G., and Gubbins, D. On the resolution of density within the Earth, *Phys. Earth Planet. Int.*, 140, 159-167, 2003.

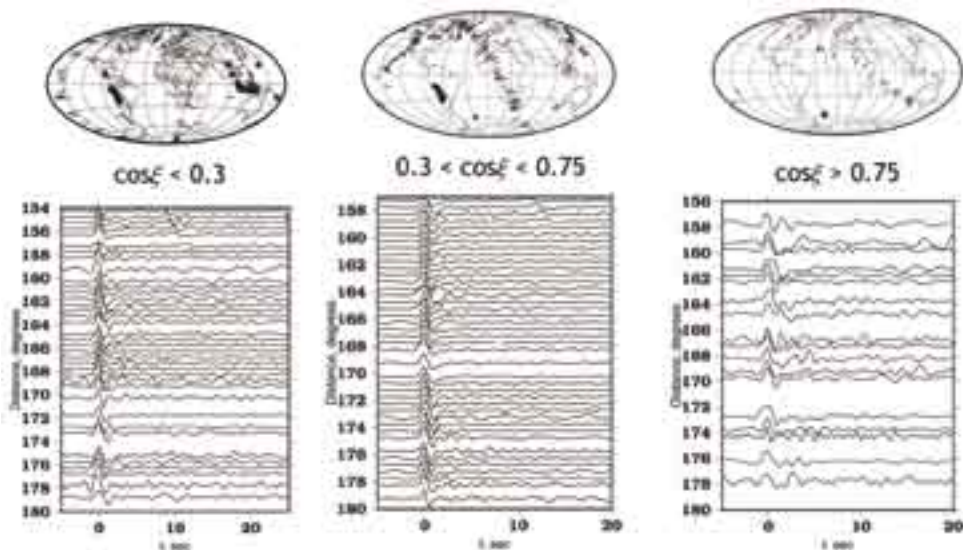
Shearer, P.M., and Masters, G. The density and shear velocity contrast at the inner core boundary, *Geophys. J. Int.*, 102, 491-498, 1990.

NSF Grant No. EAR-0308750

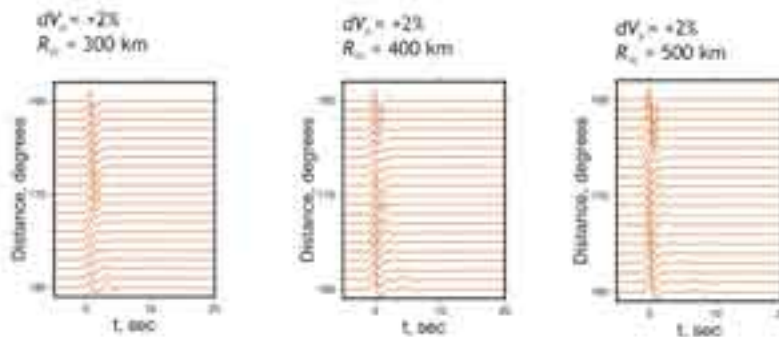
Waveform Search for the Innermost Inner Core

Vernon F. Cormier, Anastasia Stroujkova • *University of Connecticut*

Waveforms of the PKIKP seismic phase in the distance range 150° to 180° are analyzed for evidence of an inner-most inner core of the type proposed by Ishii and Dziewonski having an abrupt change in elastic anisotropy near radius 300 km. Seismograms synthesized in models having a discontinuity at 300 km radius in the inner core exhibit focused diffractions around the innermost sphere at antipodal range that are inconsistent with observed PKIKP waveforms. Successful models have either a transition in elastic properties spread over a depth interval greater than 100 km or an innermost sphere that exceeds 450 km radius. Evidence of a sharp discontinuity in the lower to mid-inner core is sparse in existing global seismic data. Some examples, however, can be found of PKIKP complexity near 161°, consistent with a triplication created by a 475 km radius discontinuity. An abrupt change in either viscoelastic or scattering attenuation at this radius is also observed in PKIKP waveforms, suggesting the existence of an innermost sphere with low, regionally uniform, seismic attenuation. In contrast to the relatively uniform inner-most inner core, a 0 to 100 km thick region at the top of the inner core exhibits strong lateral variations in attenuation and velocity structure, suggesting lateral variations in the processes of solidification, flow and re-crystallization at the inner core/outer core boundary. Analogous to the evidence for an abrupt fabric change in the upper-most inner core, the seismic evidence for an innermost inner core may represent another fabric change near 700 km depth from the inner core/outer core boundary. This last and deepest change may simply signify the end stage of solidification, flow and re-crystallization, resulting in the highest ordering and largest grain sizes of intrinsically anisotropic crystals.



Waveform profiles stacked in 0.5 distance intervals for different orientations of PKIKP rays with respect to the rotational axis (polar $\cos\xi < 0.3$, intermediate $0.3 < \cos\xi < 0.75$ (middle panel), and equatorial $\cos\xi > 0.75$).



Seismograms synthesized in inner core models having a +2% P-velocity discontinuity at radii 300 km (left), 400 km (middle), and 500 km (right).

Cormier, V.F., and A. Stroujkova, Waveform search for the innermost inner core, *Earth Planet. Sci. Lett.*, *submitted*.

Near-Podal Observations of PKPPKP Waves and Implications for Central Inner Core Structure

Hrvoje Tkalčić • Lawrence Livermore National Laboratory

The amplitude and radial dependence of hypothesized inner core anisotropy are not well known. Apart from previously observed complexity in geometry, some recent results suggest changes in anisotropic properties in the regions of the inner core close to the planetary center. With the spatial distribution of large earthquakes and current configuration of seismographic stations worldwide, it is difficult to achieve sampling of the deep interior of the inner core, except for paths nearly parallel to the equatorial plane. Figure 1 demonstrates this property. Even if a large earthquake occurs at extreme latitudes, say at -50° s, although possible to find antipodally positioned locations on the globe, such geometries could not produce angles between the PKP leg and the Earth's rotation axis (ξ) smaller than 35 degrees. This makes interpretation of anisotropic properties near the planet's center, at a minimum, very challenging.

PKPPKP and even more exotic seismic waves are used to examine inner core structure. Breger et al. (2000) reported that the travel times of PKPPKP waves recorded at NORSAR network with polar geometries sampling the top 400 km of the inner core were not anomalously advanced. The near-podal PKPPKPdf waves show much promise for studying inner core structure. Figure 2 illustrates

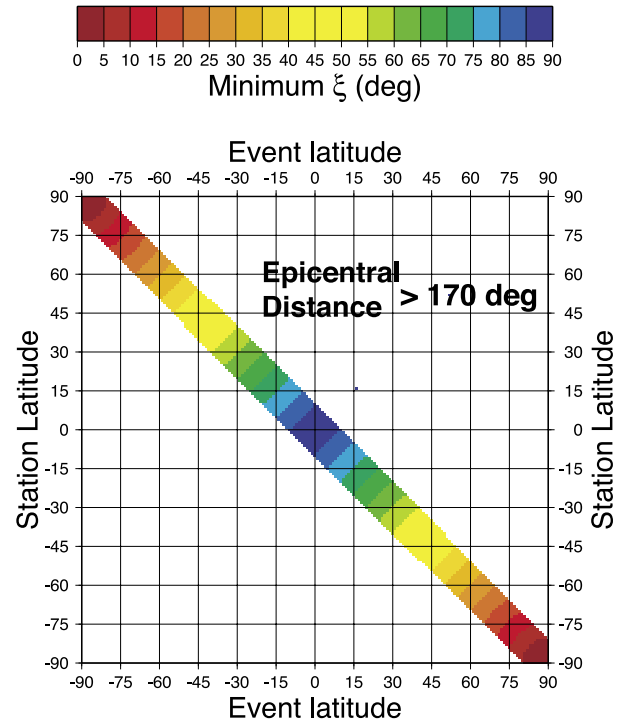


Figure 1. Theoretical space of minimum angle between PKP leg in the inner core and the Earth's rotation axis, that can be achieved for antipodal (epicentral distance larger than 170 degrees) PKP paths.

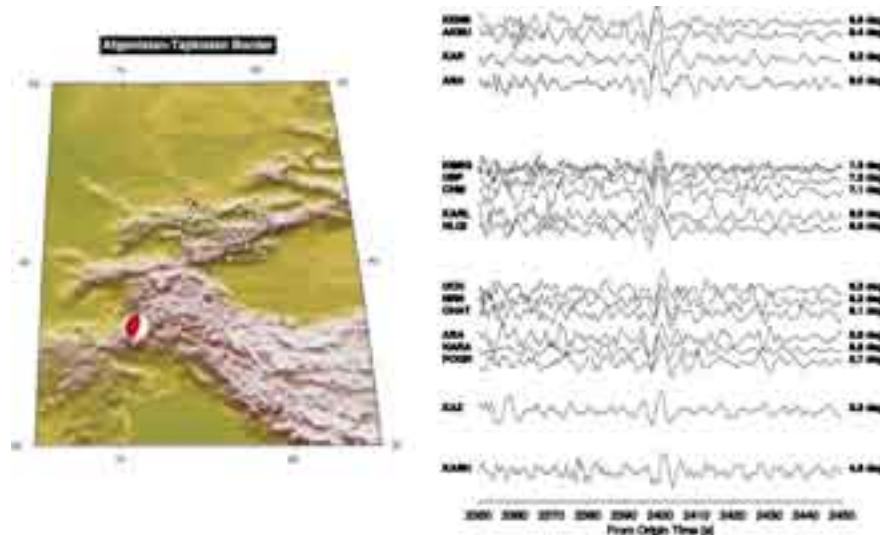


Figure 2. Vertical components of the Kyrgyz Seismic Telemetry Network records bandpassed between 0.2 and 1.0 Hz for an earthquake near the Afganistan-Tajikistan border. PKPPKPdf waves arriving at a steep incidence angle are visible at all records.

an example of one near-podal PKPPKPdf observation, recorded by the Kyrgyz Seismic Telemetry Network for an Afganistan-Tajikistan border earthquake. Preliminary results from analyzing near-podal PKPPKPdf travel times suggest that the central part of the inner core is not fast in the direction parallel to Earth's axis, which is in contradiction with presently hypothesized anisotropy models. Painstakingly collected data points from near-podal PKPPKPdf travel times will thus have very important implications for our understanding of the anisotropy and other properties of the deep inner core.

Breger, L., B. Romanowicz and S. Rousset, New constraints on the structure of the inner core from P'P', *Geophys. Res. Lett.*, 27, 2781-2784, 2000.

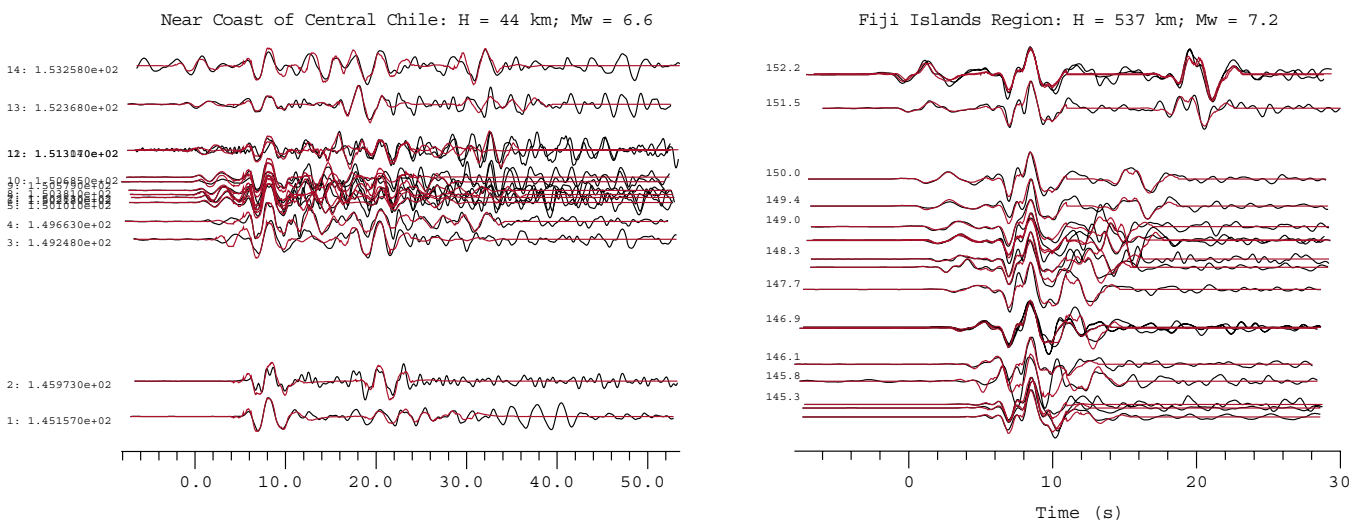
Non-linear Waveform and Delay Time Analysis of Triplicated Core Phases: A New Method to Extract Differential Travel Times From Interfering Data

Raphael Garcia • *Institut de Physique du Globe*

Sebastian Chevrot • *Observatoire Midi Pyrenees, France*

Hrvoje Tkalic • *Lawrence Livermore National Laboratory*

A new method to measure differential travel times and attenuation of seismic body waves has been developed. The problem is formulated as a non-linear inverse problem which is solved by simulated annealing inversion. Following examples demonstrate the potential of the technique, which is able to determine differential traveltimes and waveforms of the core phases, even when they interfere on the seismograms or when additional depth phases are present. This method has been applied to IRIS data in order to recover the structure of the Earth's core. The main interest for such studies is the increase of the data coverage by adding shallow earthquake data usually rejected due to the interference between the direct and depth phases.



Examples of data fit for a shallow earthquake (on the left) and a deep earthquake (on the right). The IRIS data are aligned on the PKPbc core phase arrival, the PKPdf and PKPab core phases are seen respectively before and after this arrival. For the

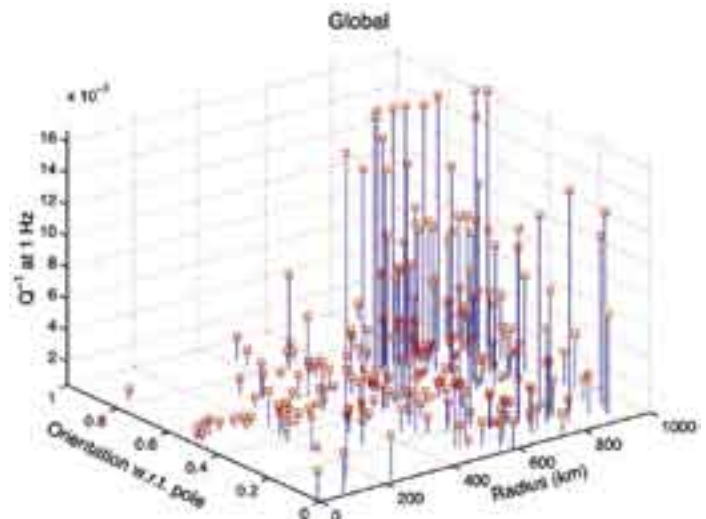
Garcia R., S. Chevrot and M. Weber, 2004 Non linear waveform and delay time analysis of triplicated core phases, *J. Geophys. Res.*, 109, B01306, DOI: 10.1029/2003JB002429

Velocity and Attenuation in the Earth's Inner Core

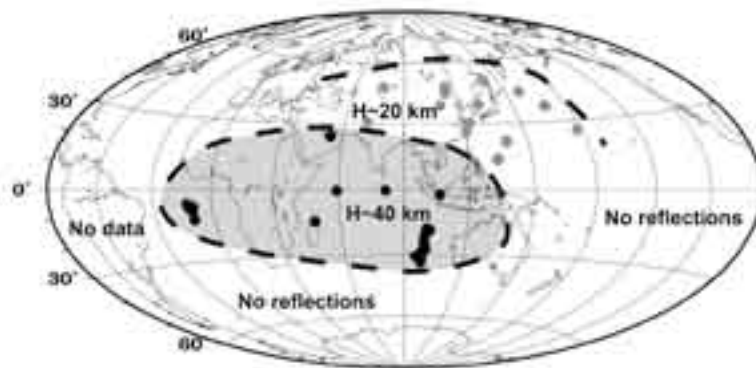
Vernon F. Cormier, Anastasia Stroujkova • University of Connecticut

Xu Li • Massachusetts Institute of Technology

Broadband velocity waveforms of PKIKP in the distance range 150° to 180° are inverted for a model of inner core attenuation due to forward scattering by a three-dimensional heterogeneous fabric. A mean velocity perturbation of $8.4\% \pm 1.8\%$ and a scale length of heterogeneity of 9.8 ± 2.4 km are determined from 262 available PKIKP ray paths. The velocity perturbations are larger for polar than equatorial paths, decrease with depth, and show anisotropy in both global and regional data (Figure at right). For paths beneath North America, the smallest scale lengths (1-5 km) tend to lie in either the upper 200 km of the inner core or along paths close to the rotational axis. The depth dependence of attenuation is roughly similar to that obtained assuming a viscoelastic origin, except a more abrupt transition is seen between higher attenuation in the upper inner core and lower attenuation in the lower inner core. This transition may be sharp enough to produce either a first or second order discontinuity with depth in the long-wavelength (composite) elastic moduli. A fabric that satisfies the observed depth dependence and anisotropy of attenuation requires solidification of iron crystals having high (>10%) intrinsic anisotropy, which are preferentially aligned in time and depth. Since weak velocity dispersion, elastic anisotropy, attenuation anisotropy, and their depth dependence agree with that predicted by such a fabric, we suggest that scattering attenuation is not a small fraction but rather the predominant mechanism of attenuation in the inner core in the 0.02 to 2 Hz frequency band.



Q^{-1} (1 Hz) as a function of radius and ray direction at the turning point of the PKIKP ray path for global data. Note the steep rise in attenuation at the radius of 600 km.



The structure of the uppermost 100 km of the inner core was examined from PKIKP and PKiKP waveforms in the distance range of 118° – 140° . We found evidence of a low-velocity layer in the uppermost inner core in the equatorial region predominantly located between longitude 20° W to 140° E (Figure at left). In the latitudinal direction the anomaly is detectable from 35° S beneath the Indian Ocean to 60° N underneath Asia. The maximum thickness of the low-velocity layer inferred from waveform modeling is 40 km with velocity jump of about 3%. We speculate that this layer may represent newly solidified core in the area where vigorous compositional convection in the outer core coincides with new crystal growth in the inner core.

Cormier, V.F., and X. Li. Frequency dependent attenuation in the inner core: Part II. A scattering and fabric interpretation, *J. Geophys. Res.*, 107, 10.1029/2002JB1796, 2002.

Stroujkova, A., and V.F. Cormier. Regional variations in the uppermost 100 km of the Earth's inner core, *J. Geophys. Res.*, 109, doi: 10.129/2004JB002976, 2004.

Anisotropy of the Inner Core

Miaki Ishii • Scripps Institution of Oceanography

Adam M. Dziewonski • Harvard University

The Earth’s inner core, buried beneath the crust, mantle, and outer core, is a difficult target to study. Nevertheless, large collections of inner-core sensitive data at IRIS and other institutions are allowing for improved imaging of this deepest structure. We have investigated the anisotropic property of the inner core using normal-mode data obtained from seismograms available at the IRIS Data Management Centre, as well as body-wave information from IRIS and elsewhere (Figure 1).

To obtain an inner-core model that is compatible with long-period free oscillations and short-period body-wave data, we invert the normal-mode, absolute and differential travel-time measurements simultaneously for a model of inner-core anisotropy. This model predicts a difference in wave speed of about 0.2 km/s with fast wave propagation along the Earth’s rotation axis and slow wave propagation along the equatorial plane (Figure 2).

Although arrival times of PKP-DF (or PKIKP) from epicentral distances between 120° and 173° are consistent with such anisotropy, PKP-DF observations from nearly antipodal distances (between 173° and 180°) deviate significantly from the predictions based upon the joint inversion. The antipodal data correspond to the central 300 km of the inner core, and they require a

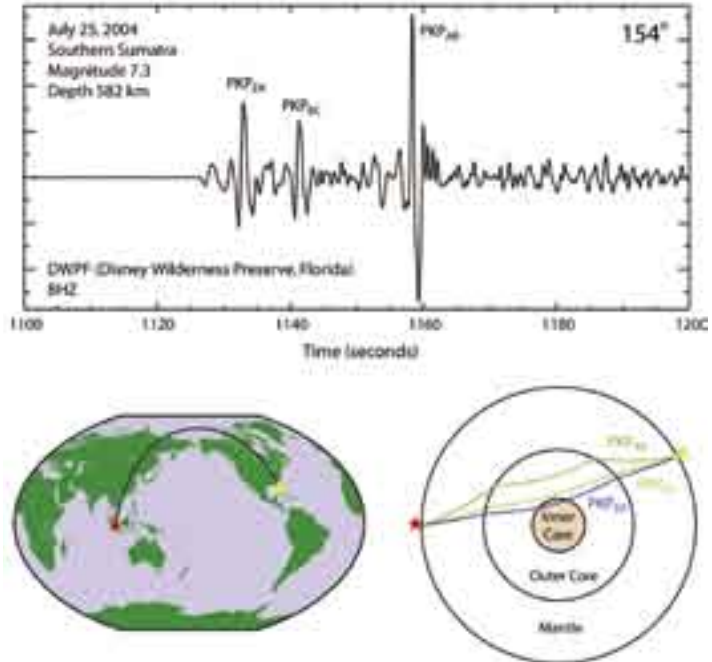


Figure 1. Core Phases: A seismogram showing the three core phases recorded at DWPF station after a magnitude 7.3 event in southern Sumatra. The bottom left figure shows the earthquake (star) and station (triangle) locations as well as the ray path (black curve). The bottom right figure shows the ray path inside the Earth for the three phases.

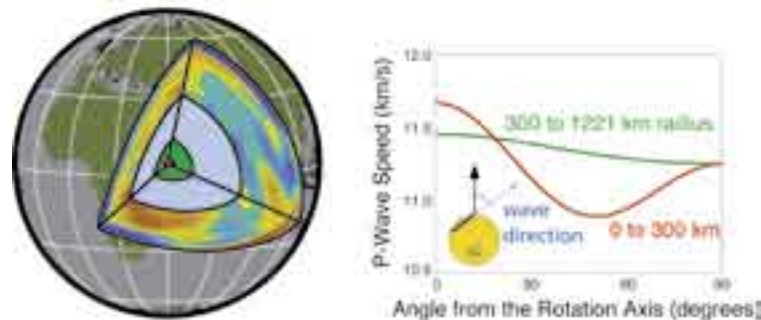


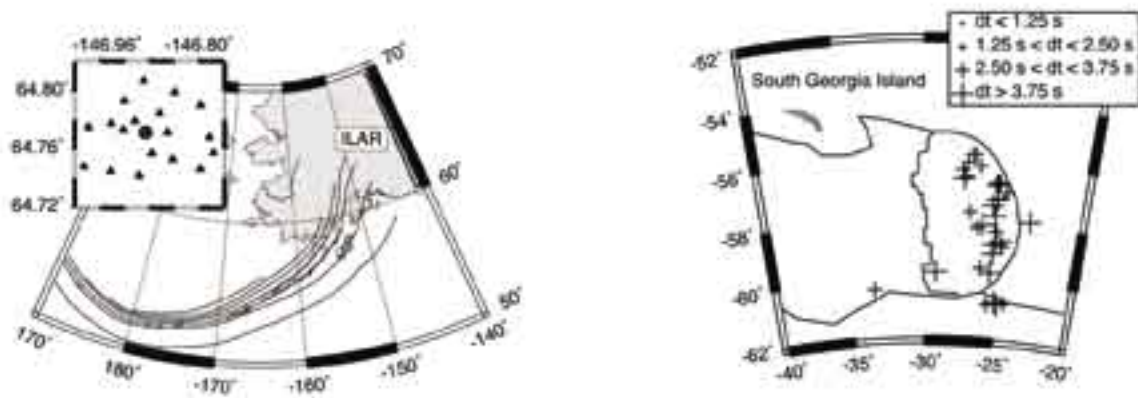
Figure 2. Inner Core Anisotropy: Dependence of the wave speed on the angle the wave makes with the rotation axis (right) for the central 300 km (red curve) and overlying inner core (green curve). The two layers of the inner core correspond to the green and red regions on the left plot. They are quite small in comparison to the outer core (pale blue) and mantle shown with velocity variations.

difference in wave speed of about 0.8 km/s. Furthermore, even though the fast propagation direction is the same as in the overlying layer, the direction of slow propagation is ~45° from the rotation axis. These observations suggest that the inner core consists of at least two layers (Figure 2).

Slowness Anomalies of PKP Phases Recorded in Alaska: Implications for Inner Core Anisotropy

Keith D. Koper, Veronica Parker • Saint Louis University

The Eielson, Alaska seismic array (ILAR) is well situated to record PKP(DF) waves from earthquakes occurring in the South Sandwich Islands (SSI) region. Such ray paths are nearly aligned with Earth's rotation axis and are useful for constraining models of inner core anisotropy. The many previous studies of PKP(DF) waves traversing the SSI-Alaska corridor generally find waves that arrive several seconds fast, with highly attenuated and often complicated shapes. Simple laterally homogeneous models of inner core anisotropy cannot explain these observations, and it may be the case that mantle heterogeneities are biasing the SSI-Alaska PKP(DF) waves. In this study, we take advantage of the small-aperture of ILAR to make independent measurements of differential PKP(DF) -PKP(BC) travel times and differential PKP(DF) -PKP(BC) horizontal slowness vectors for 37 SSI earthquakes that occurred from 1996-2004. Anomalies in slowness (ray parameter and backazimuth) of a phase reflect heterogeneous Earth structure in a manner complementary to travel time anomalies. We find a mean differential travel time residual of 3.3 s, a mean differential ray parameter of 2.0 s/deg, and that PKP(DF) waves arrive from a backazimuth rotated approximately 25 counterclockwise relative to corresponding PKP(BC) waves. We use a niching genetic algorithm to generate a suite of nearly 10,000 radial Earth models that are consistent with both the differential travel times and differential ray parameters. These isotropic models represent a 2D slice through a 3D cylindrically anisotropic model of the inner core, making an angle of approximately 25° with respect to Earth's rotation axis. Our modeling indicates that (1) mantle heterogeneities are not responsible for the properties of PKP(DF) from SSI-ILAR, (2) the lower several hundred kilometers of the outer core has a slightly lower velocity, and/or velocity gradient, than current reference models, and (3) the outer inner core along this path is nearly isotropic with a transition to strong anisotropy (8%) occurring at a radius of 600-900 km.



(Left) The Eielson array (ILAR) consists of 19 short-period, vertical component seismometers deployed with an effective aperture of about 10 km. The reference point for forming array beams is element 14 and is indicated by the circle. The solid lines represent contours (50 km increments) of the surface of the subducting Aleutian slab (Gudmundsson & Sambridge, 1998). (Right) Epicenters for the earthquakes used in this study, with plate boundaries from Bird (2003). The differential travel time residuals are defined as $dt = (PKP(BC) - PKP(DF))_{obs} - (PKP(BC) - PKP(DF))_{theo}$, and AK135 is used to calculate the theoretical times. The earthquakes occurred between 1996 and 2004 and each has a magnitude of at least 5.5 M_w .

Transition From Isotropic Upper Inner Core to Anisotropic Lower Inner Core: The Importance of Anisotropic Ray Tracing

Ken Creager, Ares Ouzounis, Sara DeRosier • University of Washington

Differential travel times of PKiKP - PKIKP indicate that in the western hemisphere the outermost inner core is isotropic, and slightly slower than global models such as PREM. On the other hand, observed travel-time residuals of PKP_{BC} - PKIKP and PKP_{AB} - PKIKP increase systematically from 1 to 6 s as a function of increasing ray turning depths for ray paths that are parallel to Earth's spin axis (Figure 1). Rays perpendicular to the spin axis typically have slightly negative residuals. These observations suggest the outermost inner core is nearly isotropic and that strong anisotropy exists deeper in the inner core. We invert these times for models characterized by an outer isotropic layer and a deeper anisotropic layer separated by a transition zone with thickness varying from 0 to 150 km. Models determined by linear inversions using ray paths calculated from isotropic models can only adequately fit the observations if the isotropic layer is between 50 and 150 km thick (Figure 2). However, the strong gradients imposed by the anisotropic model force large deviations in ray paths, so a non-linear scheme with appropriate ray tracing is needed. Using anisotropic ray tracing we find that models with an isotropic layer ranging from 150 to 300 km thick all adequately fit the travel-time data. However, thick isotropic layers require correspondingly stronger anisotropy below. Finally, models with discontinuities and linear gradients up to 150 km thick cannot be distinguished by travel times alone.

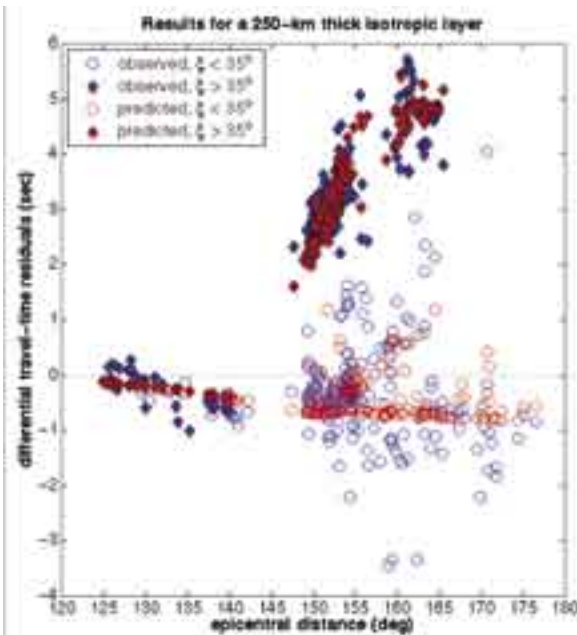


Figure 1. Differential travel times versus epicentral distance for PKiKP-PKIKP (distance < 145°), PKPBC-PKIKP (distance 145° - 155°), and PKPAB-PKIKP (distance 150° - 180°). Observed data (blue) are fit very well by the theoretical times (red) calculated for a model with a 250-km thick upper inner core. Solid symbols correspond to data with ray paths nearly parallel (within 35° degrees) to the spin axis, while open symbols are for rays not parallel to the spin axis.

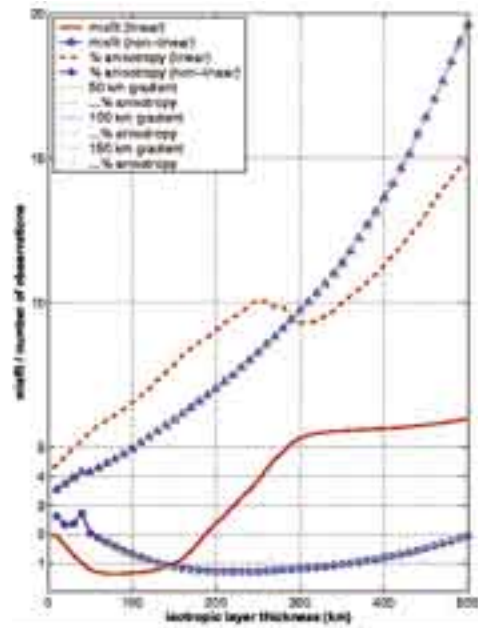


Figure 2. Normalized variance (lower curves) and magnitude of anisotropy (upper curves) versus thickness of upper inner core isotropic layer. A model that fits the data to within the estimated errors would have a normalized variance of 1. Magnitude of anisotropy is defined as the maximum velocity minus the minimum velocity divided by the Voigt average times 100%. Red symbols correspond to linear inversions using ray paths calculated for a reference isotropic earth model; blue symbols represent non-linear inversions using ray paths calculated for the anisotropic model. Nonlinear inversions show that times of first arrivals cannot distinguish among models with discontinuities or gradients up to 200 km wide separating the two layers.

Inner Core Anisotropy From PKP Travel Times at Near Antipodal Distances

Xinlei Sun, Xiaodong Song • University of Illinois at Urbana-Champaign

Observed PKP travel time residuals used in this study

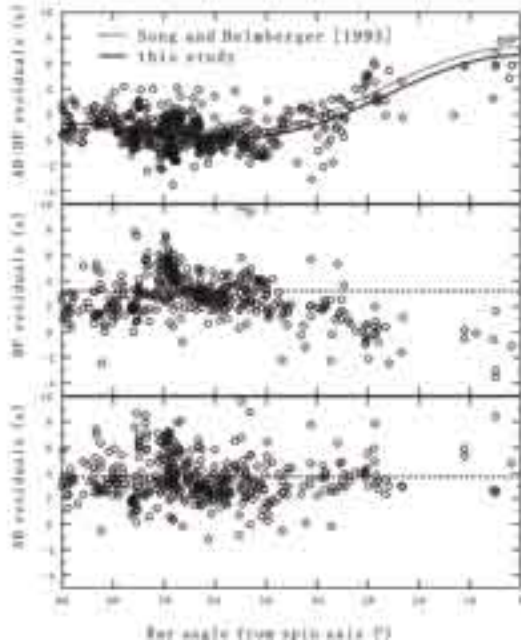


Figure 1. Travel time residuals relative to PREM versus the angle of the DF leg in the inner core from the spin axis. (A) Residuals of AB-DF differential times. Assuming a model of uniform anisotropy in the inner core with symmetry around the spin axis, we obtained a least-squared model with 2.5% anisotropy amplitude (solid line). The dotted line is the anisotropy model from Song and Helmberger (1993) with 3% anisotropy averaged over the top 500 km of the inner core. (B) Residuals of DF absolute times. The dashed line is the average of the DF residuals of the equatorial paths with ray angle from spin axis larger than 60 degrees. Note the DF rays for the polar paths are anomalously fast relative to equatorial paths. (C) The same as (B), but for the AB residuals. Note the AB residuals for the polar paths do not appear anomalous.

The central region of the inner core is difficult to study because of poor sampling of seismic data. Previous studies from PKP(AB-DF) differential travel times at large distances suggest that the central part of the inner core is very anisotropic (Vinnik et al., 1994; Song, 1996). These differential times, however, can be affected greatly by strong heterogeneity in the lowermost mantle (e.g., Breger et al., 2000). We've examined a unique data set of PKP travel times from global digital and analog stations at near antipodal distances (Sun and Song, 2002). Most of the digital data are obtained from the IRIS DMC.

Cross points of all DF and AB rays in this study at CMB

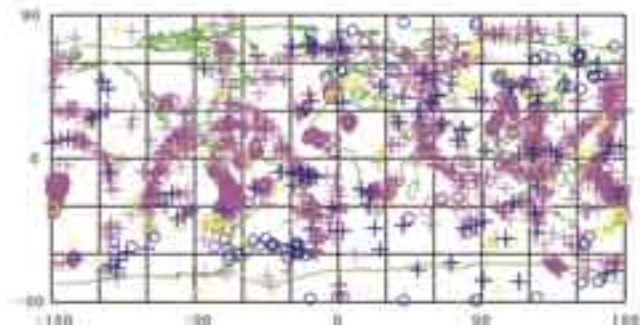


Figure 2. Cross points at the core-mantle boundary (CMB) of all the antipodal PKP rays in this study. Circles and crosses are DF and AB cross points, respectively. The colors of the symbols represent cross points from equatorial (purple), polar (blue), and others paths (yellow), respectively. Note because of DF rays are nearly vertical, DF cross points roughly represent the locations of sources and stations.

We obtained 638 AB-DF differential travel-time measurements and absolute travel-time measurements (470 for DF, 466 for AB) at distances greater than 168 degrees (Figure 1). The observed AB-DF residuals for the polar paths are consistently larger than those of the equatorial paths by over 3-4 standard deviations (Figure 1). Assuming a uniform cylindrical anisotropy model, the average inner core anisotropy amplitude is about 2.5%. We conclude that most of the AB-DF anomalies for the polar paths are likely from the inner core anisotropy and not from mantle heterogeneity.

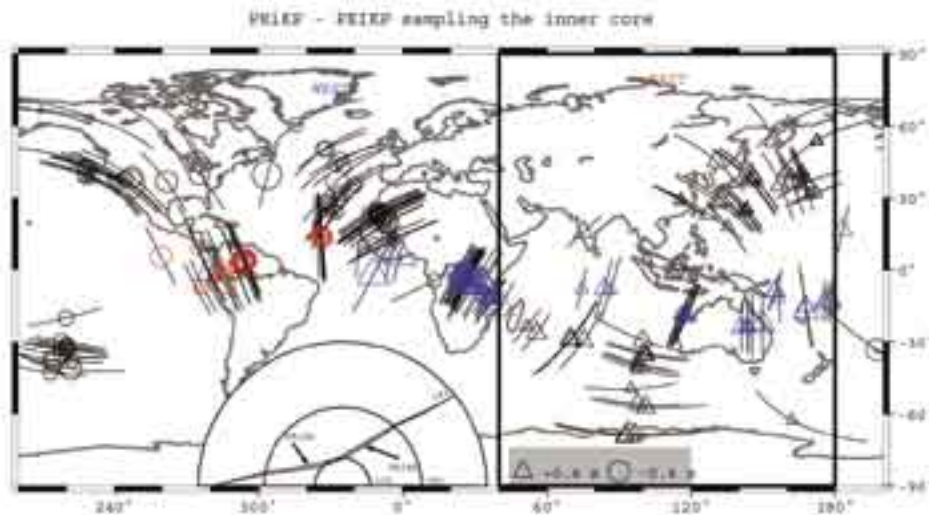
- (1) Although often sparse and not uniform, the ray coverage of the AB rays at the CMB is quite good, with data at all latitudes and longitudes, thus they are affected by both slow and fast mantle anomalies (Figure 2). The regions sampled by the AB rays of the polar paths are well sampled by the AB rays of the equatorial paths.
- (2) The DF residuals are negatively correlated with the AB-DF residuals while the AB residuals have a much weaker correlation with the AB-DF residuals (Figure 1B, C).
- (3) We compare several mantle models with the data. Our results suggest that the mantle structure can explain part of the residuals of the equatorials paths, but cannot explain the polar path anomalies.

Sun, X.L., and X.D. Song, PKP travel times at near antipodal distances: Implications for inner core anisotropy and lowermost mantle structure, *Earth Planet. Sci. Lett.*, 199, 429-445, 2002.

Hemisphericity and Regional Seismic Anisotropy in the Top 80 km of the Earth's Inner Core

Wen-che Yu, Lianxing Wen • SUNY at Stony Brook

The IRIS Consortium has been providing freely available, high-quality broadband seismic data to the scientific community. The IRIS high-quality broadband data have led to many discoveries of unique features of the Earth's inner core. The global coverage of the Global Seismographic Network (GSN) and dense coverage of many regional seismic networks have revealed the hemispherical variations in seismic velocity and attenuation and regional seismic anisotropy in velocity in the top 80 km of the Earth's inner core (Niu and Wen; 2001; Wen and Niu, 2002). Information from seismograms, such as the arrival time and the wave shape of the seismic waves transmitted through the inner core (PKIKP), allows seismologists to study velocity and attenuation structures of the inner core. The observed PKiKP-PKIKP differential travel times exhibit a distinct east-west hemispherical pattern with the PKIKP waves sampling the eastern hemisphere being about 0.7 s larger than the western hemisphere (Niu and Wen, 2001; Wen and Niu, 2002). The above observations indicate that the east-west hemispherical variations in velocity with the eastern hemisphere being about 0.8%-1.3% higher than that in the western hemisphere. The observed amplitude ratios of the PKIKP/PKiKP show a similar pattern, but with those sampling the high-velocity eastern hemisphere having smaller amplitude ratios. The observed amplitude ratios indicate that the eastern hemisphere has higher attenuation. Recently, we also examine the PKiKP-PKIKP phases sampling the inner core globally and along various directions recorded in the GSN and many regional seismic networks (Yu and Wen, 2005). The PKiKP-PKIKP differential travel times do not show polar-equatorial anisotropy in most regions in the top 80 km of the inner core. However, in a localized region beneath Africa, the PKiKP-PKIKP differential travel times exhibit anisotropy in velocity with the velocity along the polar direction being about 1.3%-1.8% higher than that along the equatorial direction. The hemispherical variations in □ core may shed light on the dynamics of the inner core and possible mechanisms on the inner core formation.



Map view of the PKiKP-PKIKP differential travel time residuals relative to PREM displayed as PKIKP ray segments in the inner core and symbols at their turning points. Circles and triangles indicate negative and positive differential travel time residuals. The differential travel time residuals along the polar (equatorial) paths are indicated by color (black) symbols. The size of the symbols is proportional to the magnitude of the differential travel time residuals. It is evident that the differential travel time residuals show a distinct east-west hemispherical variation in velocity and a localized anisotropy in velocity beneath Africa. Ray paths of the PKiKP and PKIKP are shown in the inset.

Niu, F., Wen, L. Hemispherical variations in seismic velocity at the top of the Earth's inner core, *Nature*, 410, 1081-1084, 2001.

Wen, L., Niu, F. Seismic velocity and attenuation structures in the top of the Earth's inner core, *J. Geophys. Res.*, 107, NO. B11 2273 doi:10.1029/2001JB00170, 2002.

Yu, W., Wen, L. Regional variations of seismic anisotropy in the top 80 km of the Earth's inner core, Gordon Research Conference, 06/12-06/17, Mount Holyoke, MA., 2005.

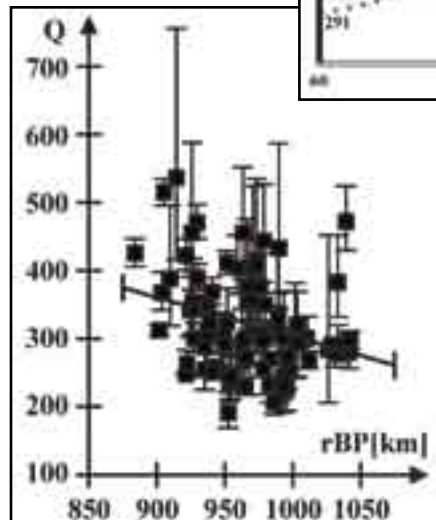
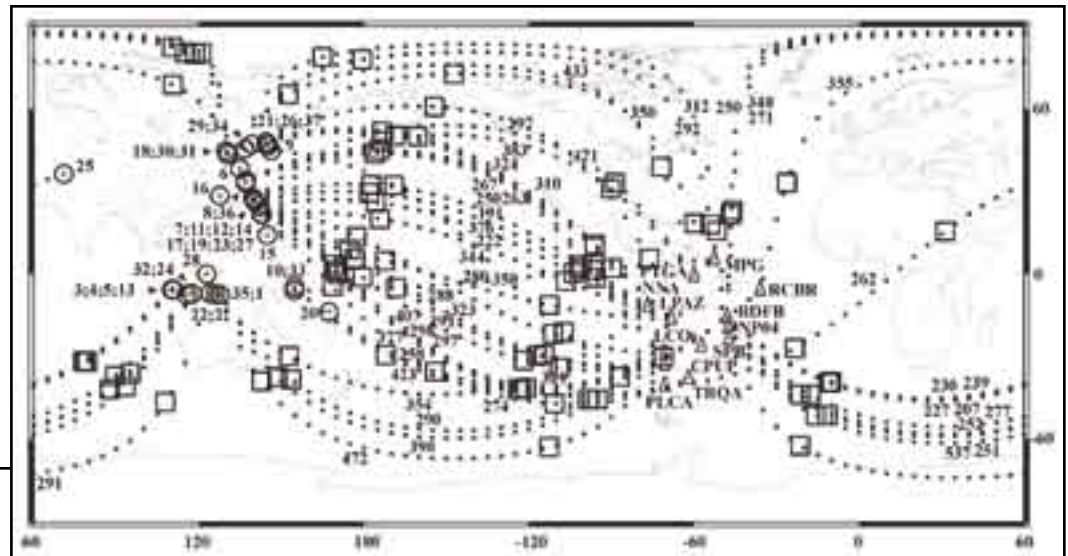
Uppermost Inner Core Attenuation From PKP Data Observed at Some South American Seismological Stations

Marian Ivan • *University of Bucharest, Romania*

Vasile Marza, Daniel de Farias Caixeta, Tassia de Melo Arraes • *University of Brasilia, Brasil*

More than 200 digital recordings from the online archive maintained by the Incorporated Research Institutions for Seismology (IRIS) have been examined for clear PKP phases. Q_p factor at the top of the inner core has been derived using the amplitude spectral ratio (PKPbc versus PKPdc) method (e.g. Cormier, 1981; Bhattacharyya et al., 1993; Souriau & Roudil, 1995; Tseng et al., 2001; Helffrich et al., 2002) applied to the waveforms of suitable, strong (magnitude > 6.0) intermediate depth and deep ($h > 150$ km) earthquakes recorded at some selected South American stations. In most cases, the sampled volume of the inner core is centered beneath the Pacific Ocean, but some Q_p values correspond to volumes under South Africa and under the Northern Atlantic. The obtained average value of Q_p is 323 ± 16 (at 95% confidence level), close to a normal (Gaussian) distribution. The maximum depth of penetration of the PKPdc phase into the inner core is roughly 333 km, suggesting a possible increase of Q_p with depth, but no definite geographical variation.

Location of permanent stations and epicenters. Dotted lines show surface projections of the PKPdc rays. Piercing points to the inner core boundary are indicated by rectangles. Individual Q_p values are displayed in the proximity of the bouncing point surface projection.

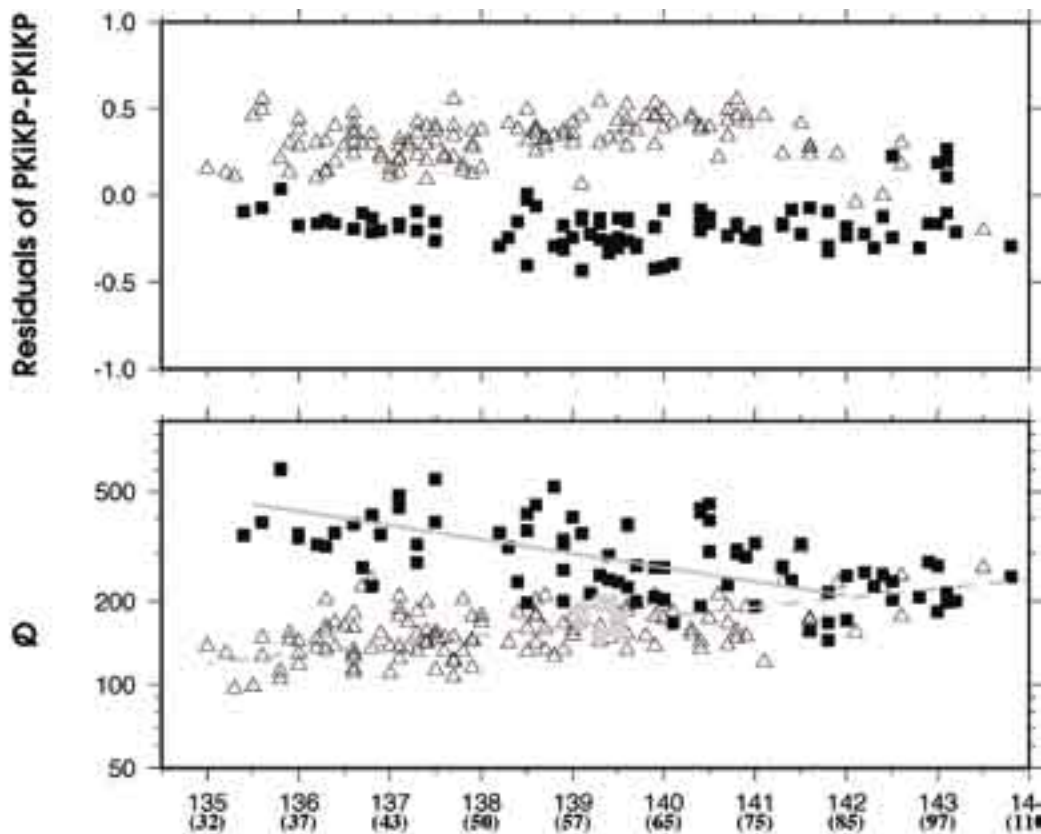


Q_p values versus radius of the bouncing point of the PKPdc wave.

Hemispherical Transition of Seismic Attenuation at the Top of the Earth's Inner Core

Aimin Cao and Barbara Romanowicz • University of California, Berkeley

In contrast to the liquid outer core, the earth's inner core is mostly solid, and its composition is more purely iron. Based on dynamic arguments related to the freezing process of the inner core, and the observation of much lower P-wave quality factor in the inner core ($Q\alpha < 450$) than in the outer core ($Q\alpha > 10,000$), it has been suggested that a mushy layer with liquid inclusions may exist at the top of the inner core. On the other hand, seismic measurements indicate that $Q\alpha$ increases towards the center of the inner core. We here present estimates of $Q\alpha$ in the depth range 32-110 km beneath the Inner Core Boundary (ICB), based on the measurement of PKIKP/PKiKP amplitude ratios after a narrow band-pass filtering (0.7-2.0 Hz). Our measurements indicate that there are pronounced hemispherical differences in the values of $Q\alpha$ (~ 335 and ~ 160 in the western (180° W to 40° E) and eastern (40° E to 180° E) hemispheres, respectively), and in the depth of transition from decreasing to increasing $Q\alpha$ (< 32 km beneath the ICB in the eastern hemisphere and ~ 85 km in the western hemisphere). Below 85 km, the hemispherical pattern disappears. We also confirm the existence of a correlated hemispherical pattern in P velocity down to 85 km. The P velocity and $Q\alpha$ variations are compatible with an interpretation in terms of small hemispherical variations of temperature at the top of the inner core and their influence on the morphology of porosity and connectivity of liquid inclusions in the mushy zone. The disappearance of the differences in $Q\alpha$ beneath 85 km provide constraints on the likely depth extent of the mushy zone.



(top) Differential travel time residuals (referring to PREM). The measurement error is less than ~ 0.1 second. (bottom) Q with respect to the epicentral distance and depth beneath the ICB. The average standard deviations are from ~ 24 , ~ 43 , to ~ 50 . High-lighted green squares show the data sampling offshore northwest of Africa. The event epicentral distances were all calibrated with a reference focal depth of 100 km (Cao and Romanowicz, 2004)

A. Cao, B. Romanowicz, Hemispherical Transition of Seismic Attenuation at the Top of the Earth's Inner Core, *Earth Planet. Sci. Lett.*, 228, 243-253, 2004. NSF Grant No. EAR-0308750

Differential Inner Core Superrotation From Earthquakes in Alaska Recorded at South Pole Station

Xiaodong Song • University of Illinois at Urbana-Champaign

Anyi Li • Lamont-Doherty Earth Observatory of Columbia University

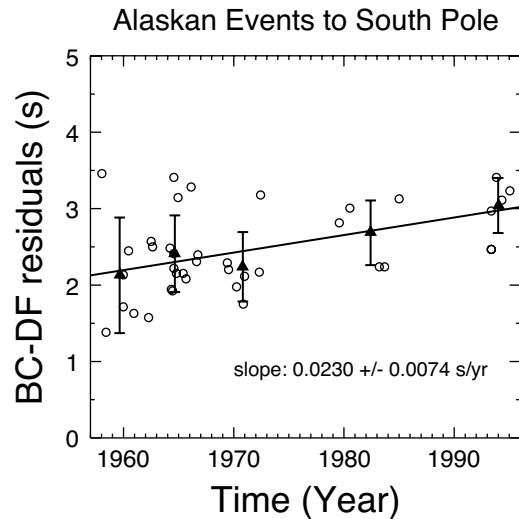


Figure 1. Residuals of PKP (BC-DF) times for earthquakes in Alaska to the station at South Pole (SPA) as a function of earthquake time of occurrence. The residuals are calculated relative to the PREM using the Earthquake Data Report (EDR) location, normalized by the times that the rays travel through the inner core, and multiplied by the average (126.2 s) of the times in the inner core of all the rays. The solid line is the linear regression of the residuals on event occurrence times.

way have increased by about 0.85 s over 37 years with standard error of 0.27 s (Figure 1). Figure 2 plots the observed travel time residuals (normalized by the travel times in the inner core) as a function of longitude and time. Plotted also are equi-residual contours of the residuals and bilinear fits (dashed lines) on longitude and time to the residuals. The temporal trend and the longitudinal gradient are observable directly from both the observed residuals and the equi-residual contours. The temporal gradient (along horizontal direction) and the longitudinal gradient (along vertical direction) from the bilinear fits are 0.01849%/yr and -0.02192%/deg, respectively, giving a rough estimate of the rotation rate of 0.84 deg/yr, if we assume such travel time changes are caused by shifts of a laterally-varying inner core structure due to an inner core rotation around the spin axis (Creager, 1997). Using a technique to invert simultaneously for the inner core structure and the rotation rate (Song, 2000), the rotation rate determined from the new pathway is about 0.6 deg/yr faster than the mantle.

One of the most convincing points of evidence for differential inner core rotation has been the temporal change of differential PKP (BC-DF) times from earthquakes in the South Sandwich Islands recorded at stations in Alaska (Song and Richards, 1996). Song and Li (2000) provided an independent support for a differential inner core rotation from a new ray path from earthquakes in southern Alaska to the South Pole station (SPA). The pathway has several characteristics that help us study the inner core rotation. (1) It is a north-south path with small ray angles from the spin axis, which was previously identified to have large BC-DF anomalies (Song and Helmberger, 1993). The largest anomalies and lateral variations from the inner core have all been identified with north-south paths; thus a north-south path is a good start to detect travel-time changes. Furthermore, if the axis of the inner core rotation is the same or close to the spin axis, the effect of rotation on travel times is expected to be most easily observable along north-south ray paths. (2) The SPA station has a long history of continuous operation. (3) The great circle paths from anywhere in the globe to SPA are along the corresponding longitudes of the sources, making it easy to sample a sweep of inner core longitudes needed to determine the lateral variation of the patch sampled.

We found that the differential PKP (BC-DF) travel times along the path-

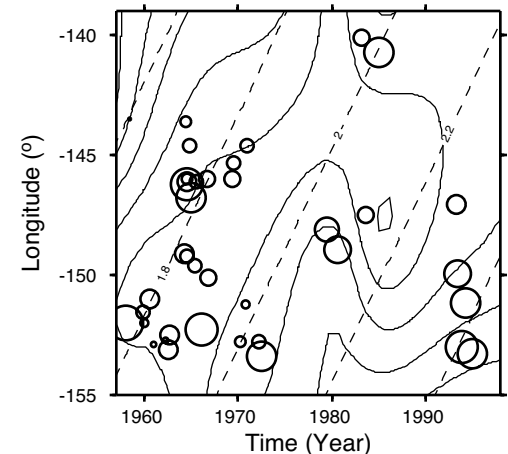


Figure 2. Travel time residuals from the Alaska-SPA paths as a function of event occurrence times and longitudes of the ray paths in the inner core. The residuals (circles) are expressed as percentages of the travel times that the rays travel through the inner core. The circle sizes indicate the relative sizes of the residuals. The equi-residual contours are plotted at every 0.2% interval. The dashed lines show bilinear fits on time and longitude to the normalized residuals at 0.2% intervals.

Song, X.D., Joint inversion for inner core rotation, inner core anisotropy, and mantle heterogeneity, *J. Geophys. Res.*, 105, 7931-7943, 2000.

Song, X.D. and A.Y. Li, Support for differential inner core superrotation from earthquakes in Alaska recorded at South Pole station, *J. Geophys. Res.*, 105, 623-630, 2000.

Support for Inner Core Super-Rotation from High-Quality Waveform Doublets

Xiaodong Song, Yingchun Li, Xinlei Sun • University of Illinois at Urbana-Champaign

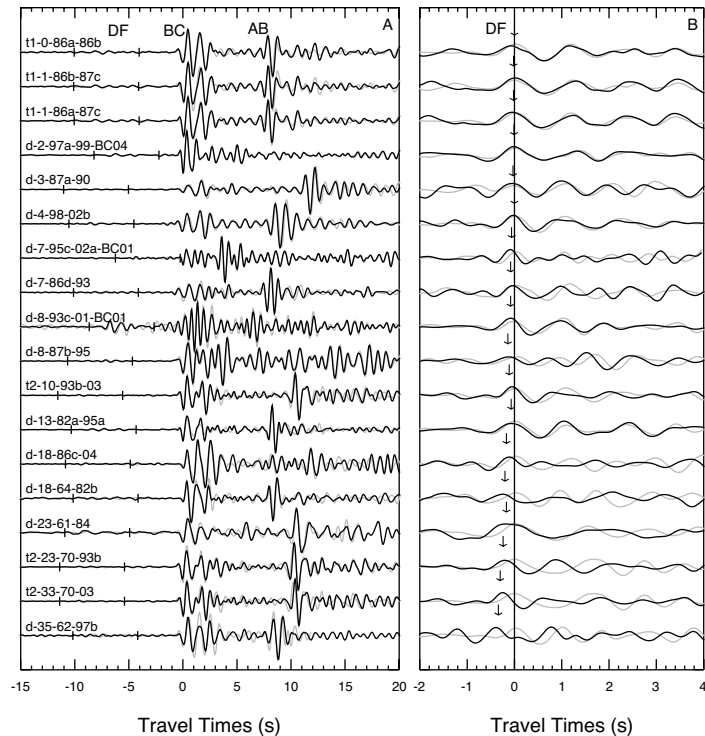
Jian Zhang, Paul G. Richards, Felix Waldhauser • Lamont-Doherty Earth Observatory of Columbia University

Differential inner core rotation was inferred from temporal change of travel times through the inner core (Song and Richards, 1996). However, claims of such a travel-time change have been challenged and reinterpreted as artifacts of systematic event mislocations, mantle heterogeneity, and other causes (e.g., Souriau, 1998). Waveform doublets potentially can provide much stronger proof of temporal change in travel times through the inner core (Li and Richards, 2003). The high similarity of the whole waveforms in a waveform doublet ensures that the two events indeed occur at the same location and sample the same Earth structure. The waveform similarity also allows measurements of relative time shifts with high precision.

We have recently found 18 high-quality waveform doublets with time separation of up to 35 years in the South Sandwich Islands (SSI) region, for which the seismic signals that have traversed the inner core as PKP(DF) show a consistent temporal change of travel times at up to 58 stations in and near Alaska, and a dissimilarity of PKP(DF) coda (Zhang et al., 2005). Using waveform doublets avoids artifacts of earthquake mislocations and the contamination of small-scale heterogeneities. Our new results greatly strengthen the original claim of seismological evidence for inner core super-rotation.

The figure overlays waveforms of the SSI doublets in order of increasing time separation, most of which were recorded at the GSN station at College Alaska (COL/COLA). We see that the waveforms of the PKP branches that do not traverse the inner core, PKP(BC) and PKP(AB) at College station and Beaver Creek array stations (BC01 and BC04), are highly similar. The high similarity of BC and AB signals in our doublets is due to propagation paths outside the inner core that sample the same heterogeneities. Observed differences in DF give information on changes in the inner core.

Our basic observations are that when signals from these high-quality waveform doublets are aligned on the BC phase, the DF phases for event pairs with time separation of less than 4 years overlap with each other rather well; but the DF phase of the later event arrives consistently earlier than that of the earlier event for doublets separated by more than 4 years, and the DF phase is seen to arrive progressively earlier as the time separation increases. The temporal change of the DF travel times is about 0.09 s per decade with standard error of 0.005 s. We also see that the waveforms of the DF coda become dissimilar when the time separation is larger than 7-10 years. The DF coda is presumably caused by scattering within a complex anisotropic heterogeneous structure. Thus, the observed breakdown of waveform similarity provides new and powerful evidence for motion of the inner core.



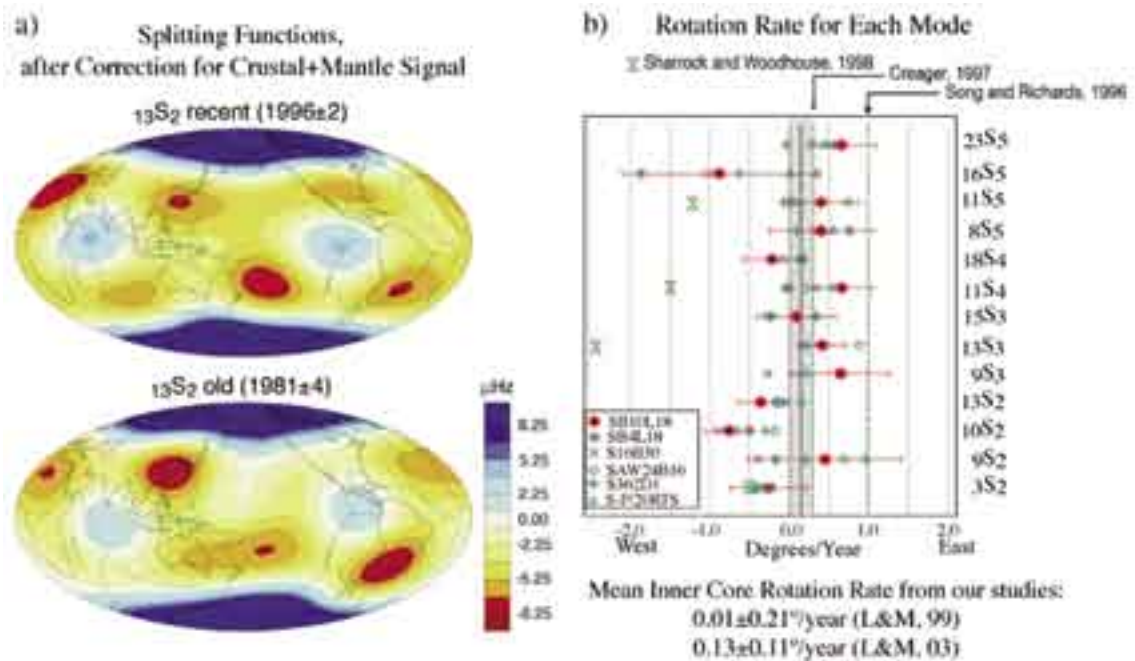
(A) PKP waveforms at College, Alaska station and Beaver Creek array stations BC01 and BC04 of 18 SSI doublets. The traces (grey for the earlier event, dark for the later one) are aligned with the PKP(BC) phase. They are sorted with increasing time separation from top to bottom (the year difference and the years of the two events are indicated in the label). (B) Enlarged view of PKP(DF) segments marked by ticks in (A). The traces have been shifted so that the onset of the DF arrival of the earlier event of each doublet is roughly aligned. The arrow marks the measured difference of BC-DF times.

The Earth's Free Oscillations and the Differential Rotation of the Inner Core

Gabi Laske, Guy Masters • IGPP, Scripps Inst. of Oceanography

Differential rotation of the inner core (IC) was initially inferred by body-wave studies that reported a super-rotation rate of 0 to 3 degrees per year. The wide range of inferred rotation rate is caused by the sensitivity of such studies to local complexities in structure. The analysis of free oscillations is insensitive to local structure and is therefore a better candidate for estimating differential rotation.

In principle, the analysis of the time dependence of "splitting functions" that display local frequency shifts for a mode caused by Earth's internal 3D-structure gives us clues whether structure has changed over the last few decades. Unfortunately, the data volume and quality for earthquakes 20 years ago is insufficient to construct splitting functions with high precision. We have therefore chosen a forward approach in which we optimize the hypothesis of an assumed rotation rate against the fit of older data. We construct the "recent" splitting function using data for recent great earthquakes. We isolate the contribution from the inner core and "correct" the splitting function with an assumed rotation rate and determine the fit to older data. We repeat this procedure for each inner-core sensitive mode and then determine the mean inner core rotation rate. Analyzing 9 modes, our initial results indicated that IC differential rotation has essentially been zero over the last 20 years, though our error bars allowed for a small relative rotation of up to $0.3^\circ/\text{yr}$. A subsequent study with 4 additional modes and 23 additional earthquakes cut our error bars in half and our current estimate is a small super-rotation of $0.13^\circ/\text{yr}$. Since inner-core sensitive modes are also sensitive to mantle structure, we need to make sure that our result does not depend on the model we choose to correct our splitting function. It turns out that results using different models are not significantly different. However, we suspect systematic effects for certain modes that consistently give westward rotation rates. A possible process that is currently investigated is the coupling to other modes.



a) Recent and past splitting functions for mode $13S_2$. The past splitting function is not accurate enough to reliably constrain inner core rotation b) Inner-core rotation rates obtained for 13 inner-core sensitive modes. Grey and symbols mark results when using our own mantle model for corrections, blue symbols mark models from other workers. Our data are most consistent with a small rotation rate of $0.24^\circ/\text{yr}$ or less.

G. Laske, and G. Masters, The Earth's Free Oscillations and the Differential Rotation of the Inner Core, in: V. Dehant, et al. (eds.) "Earth's Core: Dynamics, Structure, Rotation", *Geodynamics Series 31*, AGU, Washington, D.C., 5-21, 2003.

G. Laske, and G. Masters, Limits on differential rotation of the inner core from an analysis of the Earth's free oscillations, *Nature*, 402, 66-68, 1999.

The U.S. Educational Seismology Network

Michael W. Hamburger, Gary L. Pavlis • *Indiana University*

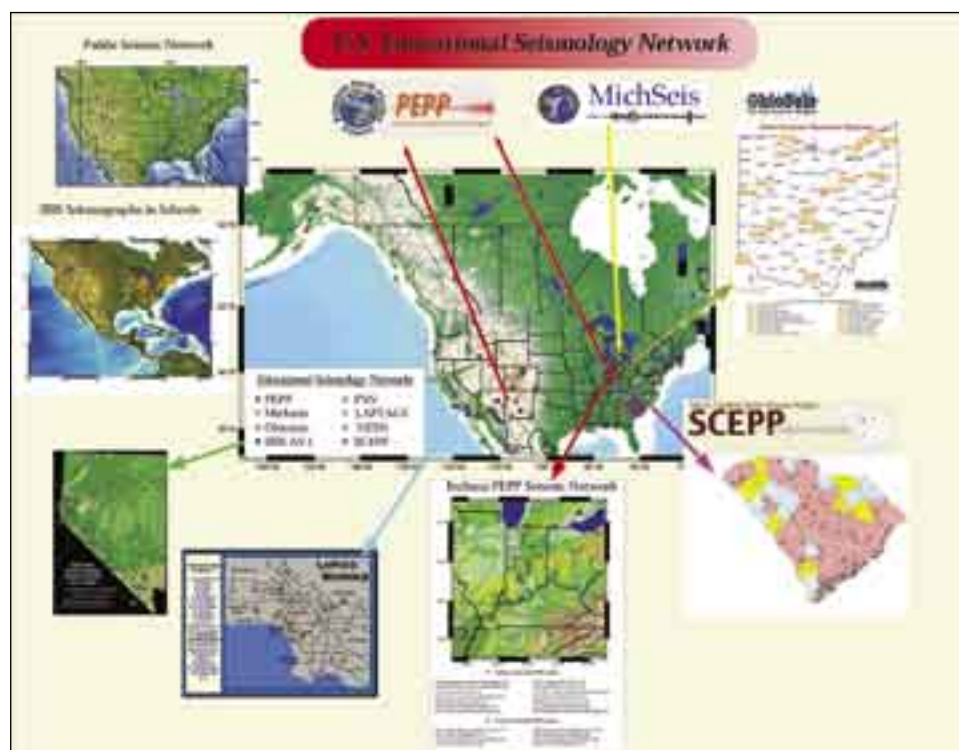
Larry W. Braile • *Purdue University*

Tom Owens • *University of South Carolina*

John Lahr • *U.S. Geological Survey (Emeritus)*

Over the past five years, IRIS and its member institutions have contributed to a growing movement that seeks to introduce students to geophysical study of the Earth through the deployment of seismological sensors in educational settings. These science outreach programs promote the use of seismographs and seismic data to improve scientific literacy, spark student interest in scientific research, increase their understanding of natural hazards, and to actively engage them in real-world scientific research. Following community initiation and involvement, IRIS has taken the lead in organizing and energizing this new approach to earth science education—the U.S. Educational Seismology Network, or USESN.

The mission of the USESN is to promote the use of seismographs and seismic data for science education. This project has emerged out of several independent educational seismology initiatives, whose collective efforts have resulted in the development of a 300+ station national school seismograph network. The USESN effort is envisioned to include support for a full range of educational seismograph options, from display-oriented, stand-alone systems to networked broadband instruments. USESN seeks to provide an organizational structure for the coordination of the numerous educational seismology activities that are developing across the country. The primary goals of the USESN initiative are to: (1) promote the installation and operation of



educational seismographs and effective use of seismic data; (2) disseminate high-quality curricular materials and educational services that promote the use of seismology in science education; and (3) provide an organizational framework for coordination and advocacy of educational seismology across the country. A 2003 national workshop led to a prioritization of efforts in curriculum development, professional development, resolution of technical issues, and organizational structure. Additional information about the USESN initiative can be found at <http://www.indiana.edu/~usesn/> and <http://www.iris.edu/>.

Braile, L.W., M. Hall-Wallace, J. Taber, and R. Aster, The IRIS Education and Outreach Program, *Seis. Res. Lett.*, 74, 503-510, 2003.

Hamburger, M.W., G.L. Pavlis, R. A. Phinney, D. Steinberg, T.J. Owens, M. Hall-Wallace, New Science Education Initiative brings Seismology into the Classroom, *EOS, Trans. Am. Geophys. Un.*, 82, 266-267, 2001.

Hamburger, M.W., and G.L. Pavlis, New midwestern seismic network combines research and education, *CUSEC Journal*, 9, 17-19, 2003.

Hamburger, M.W. and J. Taber, Towards Integration of Educational Seismology Programs: The U.S. Educational Seismology Network, *Seis. Res. Lett.*, 74, 603-604, 2003.

Hamburger, M.W., and J. Taber, Focusing on Seismology Education, *EOS Trans. Am. Geophys. Un.*, 85 (12), 116, 2004.

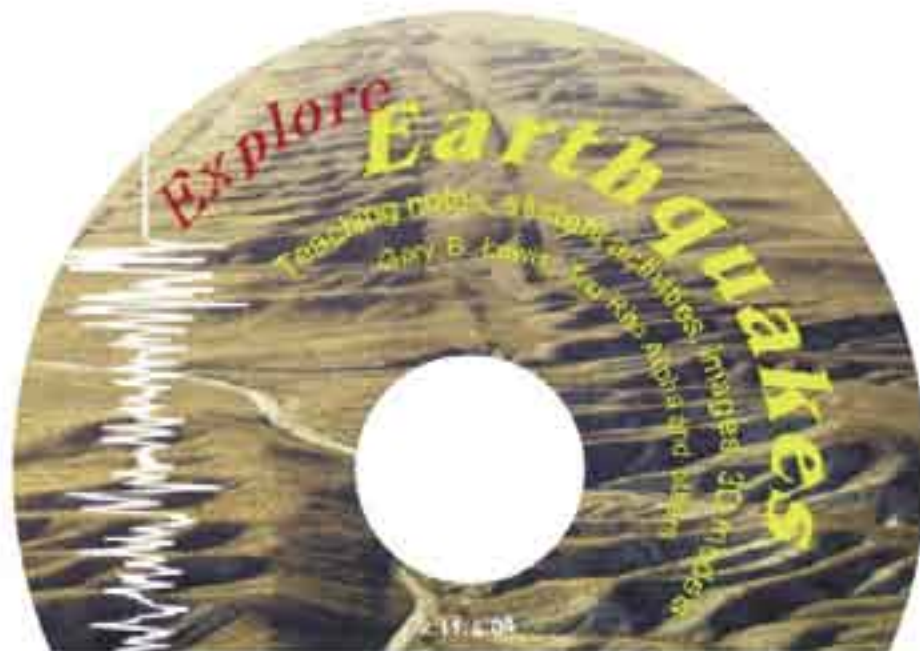
Support for this initiative has been provided through NSF grant REC-99106 and supplement to Cooperative Agreement 0004370.

IRIS and Geological Society of America

Christine McLelland • *Geological Society of America*

The Geological Society of America (GSA) and IRIS have combined efforts and resources to create an Earthquake teacher resource available on CD-ROM, part of GSA's Explore Geoscience Series. The *Explore Earthquakes* CD-ROM is an excellent resource that focuses on education for the teacher by including a detailed teacher background text on earthquakes and a large number of IRIS Earthquake Fact Sheets. Dozens of images and diagrams allow educators to illustrate their earthquake lectures and classes with the latest information. For students, twelve earthquake-related activities from both organizations are included. The CD also contains 3-D models of fault blocks that students can construct, allowing them a concrete model of abstract concepts.

The CDs have been marketed to educators on a national level by GSA. They are available for purchase at \$9.95. A large number of the CDs have also been distributed free of charge by IRIS and GSA at teacher meetings, where popular workshops allow educators to see first hand the content of these resources. A workshop at the National Science Teachers' Association Convention in Anaheim, April, 2006, is scheduled and expected to be well attended (70-100 teachers).



IRIS

THE
GEOLOGICAL
SOCIETY
OF AMERICA



Geological Society of Australia

ISBN 0-8137-7607-4

Global Seismicity Monitor as an Interactive Museum Display

Carolyn Rebbert • *Bruce Museum of Arts and Science*

Louise Palmer • *Independent Curator*

The Bruce Museum of Arts and Science in Greenwich, Connecticut, developed the family-friendly exhibition *Great Women, Great Science* that was on display from August 14, 2004 – April 10, 2005. Interactive displays engaged visitors in learning the science behind the discoveries of four prominent scientists from the first half of the 20th century.

One of the most successful and popular displays was in the section featuring Danish geophysicist Inge Lehman. IRIS designed a website that provided visually attractive displays of global seismic events and is updated every 20 minutes. The site also provided information on past events both globally and locally, and provided a view of the seismic trace recorded by a local station. Visitors accessed the information through a touch screen where they could select the desired view. Within a given screen, touching a particular earthquake event produced a pop-up banner with data on the quake.



The programmers at IRIS adjusted the design to make it fit our visitor's needs, coached us in adjusting the settings on our monitor, and all within our rather tight schedule. They were also available for consultation throughout the run of the exhibition, provided educational materials for our teacher workshop, and listened to our suggestions for some museum-friendly design changes.



During the run of the exhibition, approximately 67,000 visitors came to the museum. The museum led 25 tours of the exhibition for a total of 404 visitors including second-grade girl scouts, other elementary and middle school student groups, and high school, college and adult groups. We plan on incorporating the touch-screen display in our permanent science gallery.

IRIS/USGS Seismology Displays at the American Museum of Natural History, New York

Edmond A. Mathez • *American Museum of Natural History*

IRIS has become an important partner with the American Museum of Natural History in educating students and the public alike about earthquakes. There are two venues in which this education takes place.

The first is in the Hall of Planet Earth, a permanent exhibit that opened in June, 1999. A significant proportion of the approximately 4.0 M people that visit the museum each year see HOPE, which therefore has an important influence on how the public understands our planet. HOPE was conceived as an educational exhibit. This means, for example, that information is presented in layers of differing sophistication, allowing accessibility to a wide audience. Also, the local k-12 earth science curriculum was partially restructured around the exhibit content. As a result, HOPE is used extensively by school groups, including undergraduate university students. HOPE was planned before the IRIS/USGS seismology display was available. Two years ago, with IRIS support, HOPE was retrofitted with the seismology display. Since it is presented in the context of the larger science, we sense that the display has been particularly effective in transmitting its message that earthquakes are part of the larger workings of the Earth. The display has also attracted the attention of the news media, and has served as a backdrop in our attempts to explain current events, such as the Sumatra-Andaman earthquake and accompanying tsunami.

A nearly identical IRIS/USGS seismology display exists in the Discovery Room at AMNH. The Discovery Room is a permanent interactive exhibit that offers families, especially children between the ages of five and twelve, the opportunity to engage in the process of science. Children (accompanied by adults) explore an array of puzzles, games, artifacts, and specimens. These offer scientific challenges but also serve as gateways to the rest of the Museum. The IRIS/USGS display constitutes an important part of Earth science activities in the Room. The drums were installed at the eye level of grade school children, who are fascinated to learn that the pens they see moving are “taking the pulse” of the Earth. Older visitors are drawn to the screen showing the changing map and the color print of the tectonic plates beside it. After they have studied the display or heard an explanation by the Discovery Room staff, single visitors often run off to bring the rest of their party to see. Those visitors then become the explainers for others.

Visitors have been fascinated by the Indian Ocean tsunami data and ongoing disturbances near Sumatra. On the bulletin board beside the drums is a 17 March New York Times article discussing the work of seismologists after the tsunami, including the speculation that another large quake could follow the December one. The drum sheets showing the M8.7 quake that occurred eleven days later are posted below. Other educational additions are a notebook of IRIS information sheets (“one pagers”), such as “Why do earthquakes happen?”; children’s books on earthquakes; a slinky that staff use to illustrate P and S wave motion; and a diagram showing how to find the epicenter of a quake by triangulation. Over 100k visitors have used the Discovery Room each year since it opened in June, 2001.



Experiences with the IRIS E&O Lecture

Michael Wyession • *Washington University*

NOVA programs are great. Interactive high-tech museum displays are very cool. Web-based teaching tools can be very instructive. However, there is still nothing that can take the place of contact with a knowledgeable human being, and that is why classroom teachers will not be replaced with computer screens and why the IRIS E&O Lectureship is so successful.

I have been fortunate to be able to represent the seismological community in a series of about a dozen lectures that I have given at Science Centers and other venues across the country (e.g., Smithsonian Museum, Chicago Field Museum, National Science Teachers Convention, etc.). My talk, nominally titled “Earthquakes, Tsunami, and a Modern Journey to the Center of the Earth,” has been a smattering of varied seismological topics that include plate tectonics, earthquake hazards, our changing perceptions of earthquakes, seismic wave propagation, exploration seismology, attempts to predict earthquakes, nuclear verification, and global dynamics as determined through 3D seismic tomography. The “tsunami” aspect of the talk was not part of my original plan for the lecture, but a strength of earthquake studies has always been its relevance to current activities, and following the events of December 26, 2004, the Sumatra-Andaman earthquake became a significant and well-received part of the presentation.



I tried to draw upon my experiences both teaching high school (long ago!) and currently training high school teachers (on how to teach earth science) to make the talk engaging, and I tried to alternate between the seriousness of earthquake hazards and nuclear monitoring and the humor of giant Namazu and Hollywood’s goofy attempts to portray a journey to the center of the earth. Though my presentation was primarily a PowerPoint lecture, I tried to break it up with some demonstrations of propagating and standing waves using a slinky and a gong, and having kids help me with the demonstrations.

In all cases I had wonderful responses from people attending, who enthusiastically said that they learned a tremendous amount. But I also learned some things as well:

1. People love earthquakes. If you don’t kick them out at some point, people will continue to ask questions about them all night. In one case, the question-and-answer period went on for more than an hour, and nobody left until the janitor had to close up the building!
2. People love slinkies. IRIS provided slinkies for everyone who attended (for use during the wave demonstrations), and kids of all ages loved them.
3. Show a picture of the fault area of the Sumatra-Andaman earthquake superimposed on the Juan de Fuca plate, and even if there are hundreds of people in the audience (more than 400 in the case of the talk at the American Museum of Natural History in NYC), you can hear a pin drop.
4. People think it is very cool that if you take four months of seismic records following the Sumatra-Andaman earthquake and speed it up, it really does sound like a gong.
5. Everyone has an earthquake story of their own.
6. Nearly everyone has an Aunt Bertha in San Francisco whose parakeet acted strangely before the 1989 Loma Prieta earthquake.
7. Put up an email address, and people will write to you. I put my email address at the end and offered to send my PowerPoint lecture to anyone interested. I was flooded with emails after each talk, especially from teachers who wanted to use parts of it in their classes.

Presenting the IRIS E&O Lecture has not only been an honor, but a tremendously rewarding experience. You never know what will be the inspiration that will cause someone to decide upon a field of study or research. And though there was nothing in my talk that someone couldn’t have found with a little work in a library or over the internet, the excitement I felt from people as they participated in a personal exchange with me, as well as the enthusiasm of the email correspondences that followed, demonstrated that these kinds of lectures can be very influential for people of all ages, professions, and interests.

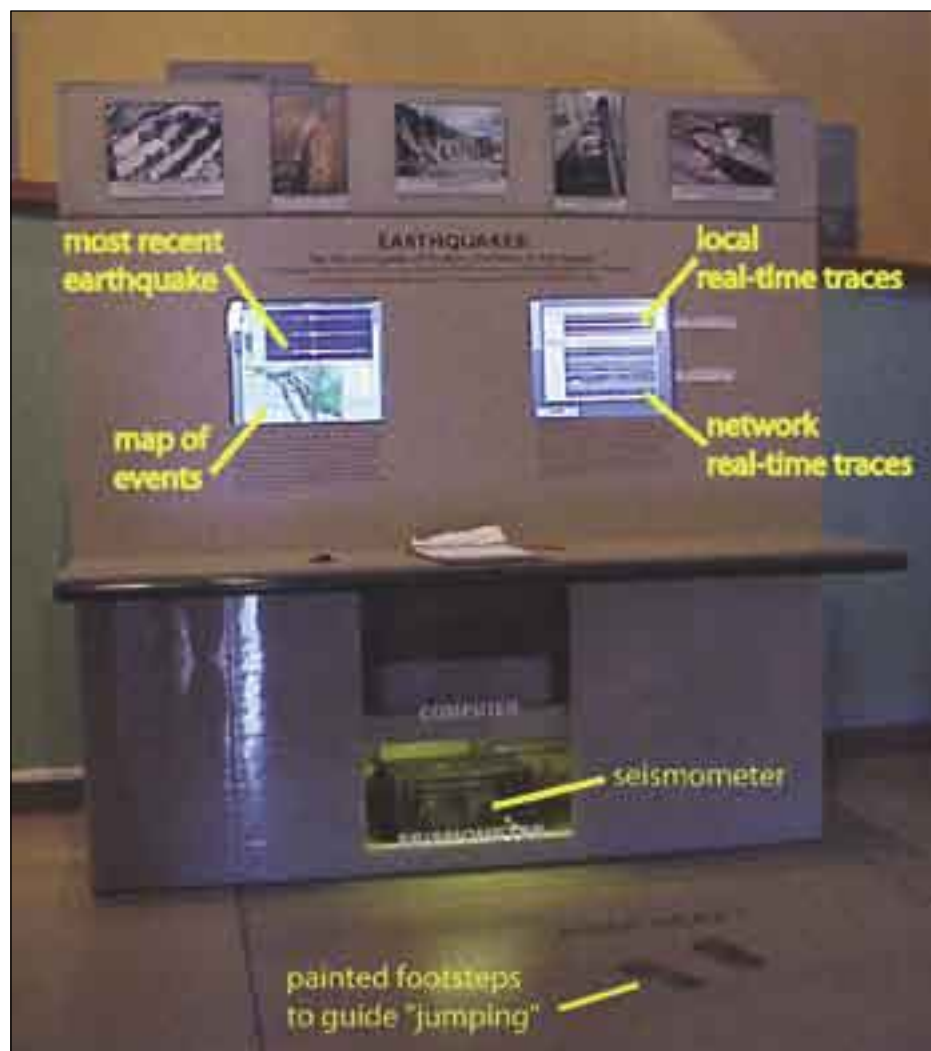
A Real-Time Interactive Educational Seismology Exhibit

Robert J. Mellors, Eric Riggs • *San Diego State University*

Jennifer Eakins, Frank Vernon • *University of California, San Diego*

Paul Kilburg • *Mission Trails Regional Park, San Diego*

A museum display installed at the Mission Trails Interpretative Center in San Diego combines a local seismometer with real-time seismic data from nearby seismic stations accessed through the Internet and shown on dual monitors. The combination simultaneously provides both interactivity and high-quality seismic data from nearby seismic stations, and is displayed on one of the monitors. Simultaneously, maps of associated seismicity ranging from local to worldwide are displayed on the other screen using a browser connected to the Internet. This allows a choice of maps and displays, such as the IRIS seismic monitor. Displaying data from several stations on one screen aids in distinguishing earthquakes from noise and demonstrates clearly how seismic waves travel across the region. Another key feature is that the data from the sensor are available for incorporation into regional seismic networks in real-time without requiring any additional work by staff at the museum, thereby providing data for both the interactive display and to supplement local area networks. The display has been operational for several years and is viewed by approximately 6,000 people per year.



A picture of the operational exhibit. Note footprints to show people where to "jump".

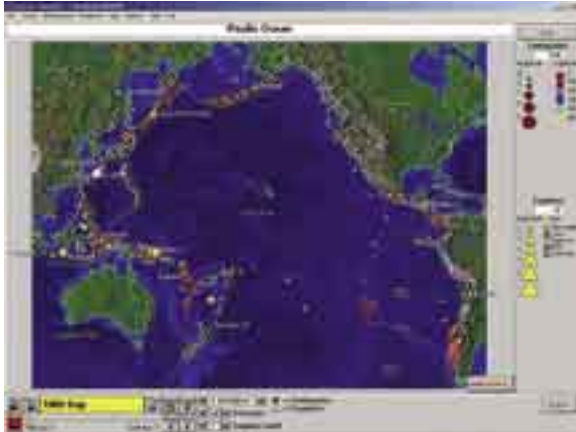
A Suite of Educational Computer Programs for Seismology

Alan L. Jones • State University of New York at Binghamton

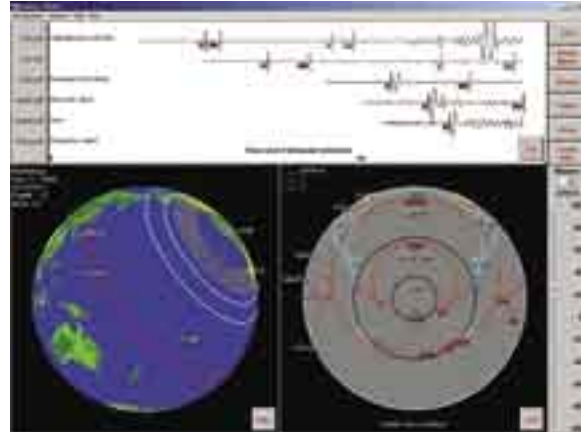
Lawrence W. Braile • Purdue University

Cheryl J. Braile • Happy Hollow School, West Lafayette, Indiana

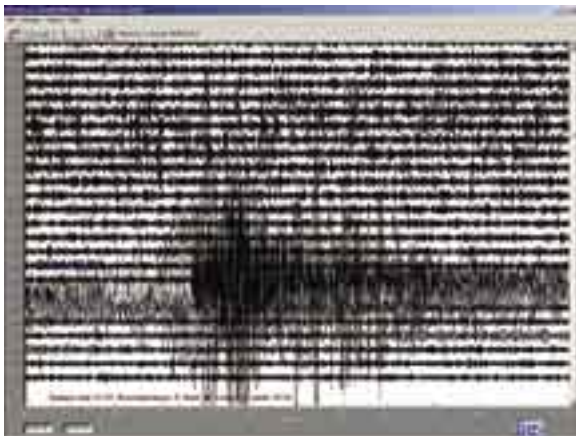
A set of four educational programs have been developed with partial support from IRIS. They all run under Windows.



Seismic/Eruption: shows where and when earthquakes and volcanic eruptions occur in speeded up time. Students can watch as earthquake and eruption activity outlines the earth's plate boundaries.



Seismic Waves: Animates seismic wave propagation through the earth and over the surface of the earth and shows actual seismograms as recorded at seismic stations.



AmaSeis: Displays seismic activity on a helicorder-like display. The figure shows the 2005/12/26 magnitude 9.0 Sumatra-Andaman earthquake. The computer is connected to the educational -1 seismometer. Students can extract seismograms and do analyses on them.



EqSelect: Allows the student to select P-arrivals and use these to locate an earthquake iteratively. Seismograms can be downloaded from the IRIS Wilbur site or from schools which share their seismograms.

Jones, A.L., Braile, L.W., Braile, S.J, A Suite of Educational Computer Programs for Seismology, *Seimol. Res. Lett.*, 74, 605-617, 2003.

Educational Seismograph Teaching Modules

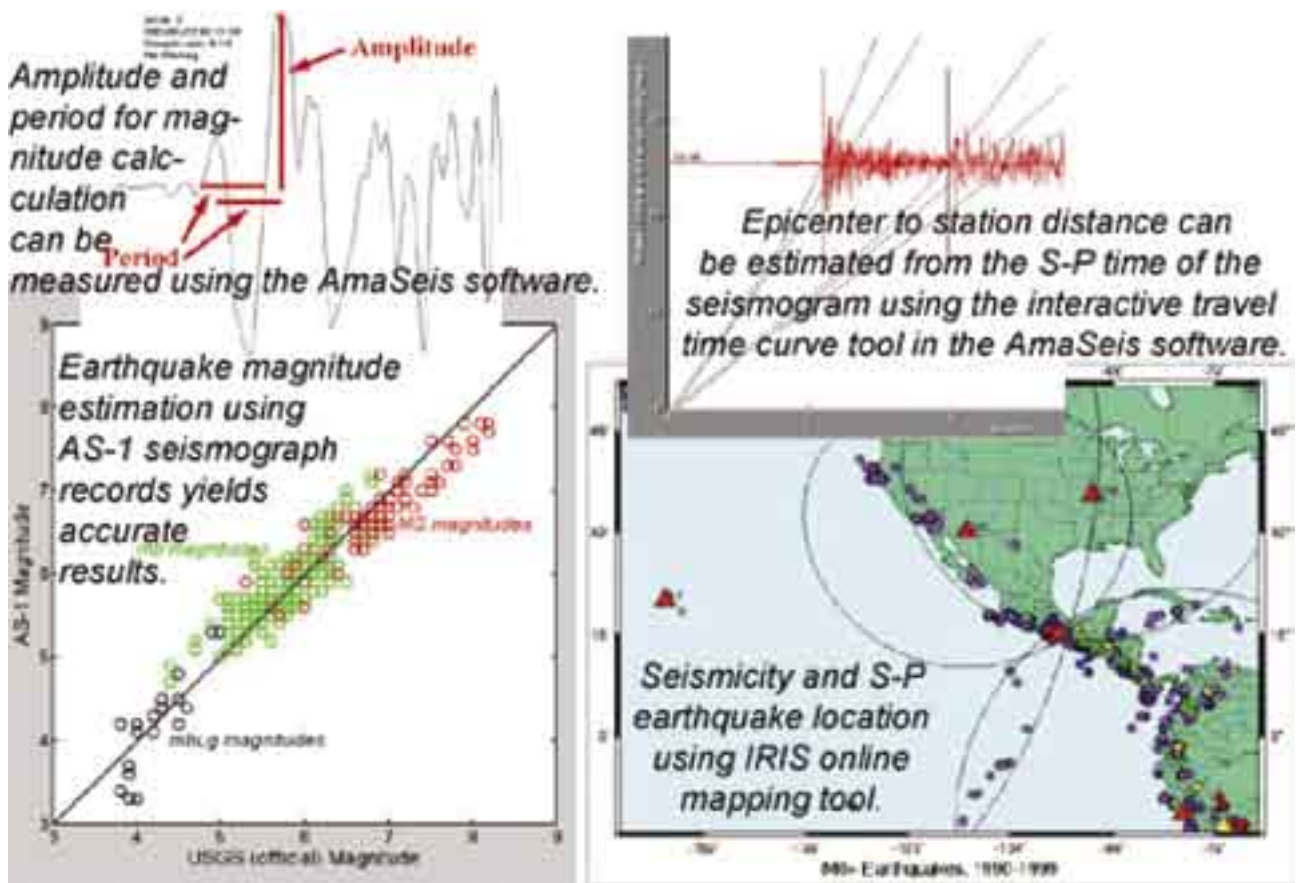
Lawrence W. Braile • *Purdue University*

Several teaching modules and educational resources for use with educational seismographs have been developed and made available on the Internet. The materials are designed for use with the AS-1 seismograph that is part of the IRIS Seismographs in Schools program. However, some of the materials can be used with seismograph data from other instruments, from data downloaded from seismogram archives (the IRIS DMC and the SpiNet website), or from pre-assembled seismograms included with the teaching modules. Most of the materials make use of the AmaSeis software that has been developed by Alan Jones (SUNY-Binghamton) with support from the IRIS E&O program. The materials include: Using AmaSeis (Using the AmaSeis seismogram viewer and downloading seismograms from the Internet – A Tutorial); Accessing Earthquake Informa-

and online S-minus-P location mapping); MagCalc (Earthquake Magnitude Calculator for the AS-1 Seismograph; an online tool (and resource with examples) for calculating magnitudes from AS-1 seismograms); Calculating Magnitudes: (Calculating Magnitudes from AS-1 Seismograms); EQ Location and Magnitude Calculation: (Earthquake location using the S minus P method and magnitude determination); and, How Often? (How often do earthquakes appear on the Seismograph?).

The materials are available at: <http://www.eas.purdue.edu/~braile/edumod/as1lessons/as1lessons.htm>.

Funding for this development provided by IRIS and the National Science Foundation.



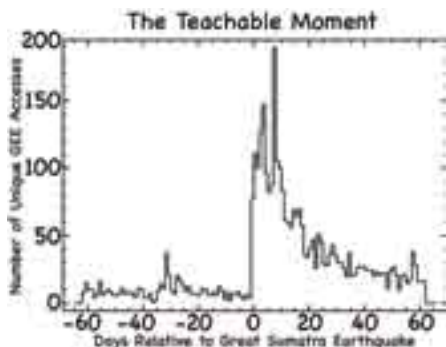
The Global Earthquake Explorer: A Versatile Tool for Science Education

Thomas J. Owens, Philip Crotwell • *University of South Carolina*

Since the observation of the first instrumentally-recorded earthquake in the late 1800's, the discovery and documentation of the mysteries of the Earth's deep interior and the earthquake rupture process have proceeded hand-in-hand with improvements in instrumentation and data exchange. The pioneering discoverers in the first half-century were those scientists fortunate enough to have a seismograph at their institute. The excitement of observing a distant earthquake as its energy was recorded was a powerful catalyst for curiosity-driven scientific investigations. One hundred years later, we have vastly expanded the quantity and availability of high-quality seismological data. We have established the infrastructure to effectively deliver this data to central archives in near-real time. Through these advances, access to data from research observatories around the globe is no longer limited to trained seismologists. This vast archive of data, and



its availability in real-time, is a resource with tremendous potential to educate and inform learners at all levels through both formal and informal learning venues.

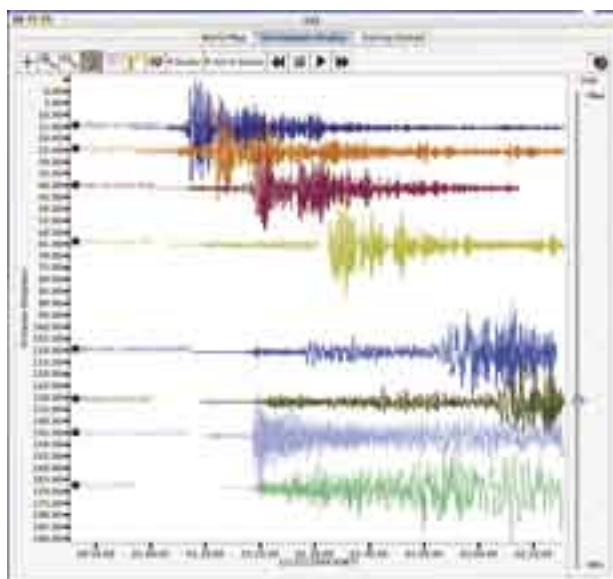


Over this last 5 years, IRIS has invested in developing the capability to ingest data into the IRIS Data Management Center (DMC) in real-time. On average, data from 650-700 seismic stations around the globe flow into the IRIS DMC in real-time. The latency for ~80% of these stations is 30 minutes or less; 95% arrive within 6 hours.

Thus, within literally minutes of a major earthquake, a full suite of seismograms is available for utilization by students and teachers around the globe. The opportunity to provide educators with true “teachable moments” is upon us if we can provide appropriate access to data.



To prepare for this moment, the University of South Carolina and IRIS Education & Outreach began developing the



Global Earthquake Explorer, a versatile software package that streamlines access to seismograms in the IRIS DMC in a manner designed for an education environment. The impact of having such a tool available was dramatically demonstrated after the Great Sumatra Earthquake of December 26th, 2005. The upper left figure is a histogram of unique accesses to GEE in the 60 days before and after this earthquake. GEE usage was increased by a factor of nearly 200 in the days after the earthquake. Although the exact cause of the secondary peak about 10 days later is not certain, it corresponds to the resumption of classes in many areas of the US. Interestingly, GEE usage remained about a factor of 2 higher 60 days after this earthquake!

Using GEE, students, educators, and the general public could access hundreds of seismograph stations and easily create their own view of the earthquake through a simple point-and-click interface (bottom left). In addition to easy access to real-time data, GEE provides structured learning modules and a robust suite of analysis tools for amateur and professional seismologists alike.

The Use of IRIS Instrumentation in Undergraduate Education

Gary L. Pavlis • *Indiana University*

It has been my experience that teaching college undergraduates basic geophysics is more effective when taught in a hands-on fashion. I have taught a senior-level class in elementary geophysics for a number of years. I focus the class around a series of real-data exercises collecting common geophysical data including gravity, magnetics, electrical resistivity, electromagnetic, and one or more seismic methods. IRIS recently acquired several multichannel seismic systems that I have used over the past several years in teaching this course. Figure 1 shows a photo of students using these instruments in the field. Figure 2 shows results by one of the students from our 2005 experiment. This experiment was shot in a karst terrain, which is the reason for the large statics in the (uncorrected) common offset gather shown in Figure 2. The target of that experiment was an underground limestone mine. The survey



Figure 1. Students conducting high-resolution seismic survey.

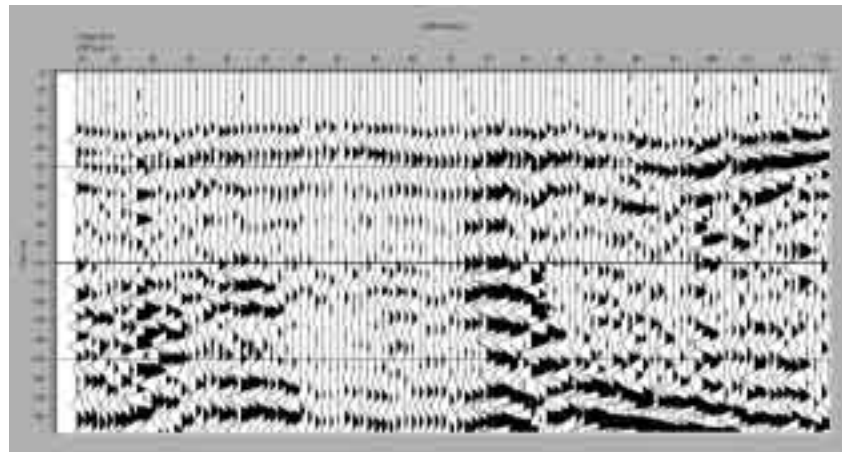


Figure 2. Common-offset gather of data collected during experiment shown in Figure 1. Data were collected in a karst area with an underground mine midway through the survey (at approximately CMP northing of 80 m). Data are plotted at true amplitude.

crossed the edge of property owned by the mining company at around the 80 m mark on the survey. The area north (right side of Figure 2) of 80 m was known to have been mined with the top of the mining cavity located at approximately 20 m below the ground surface. The group's interpretation of these results is that the strong difference in the signals recorded at the two ends of this section is due to strong scattering of both body and surface waves (bottom part of the section) by the mining void. This level of detailed data collection and analysis capability would not have been possible without the availability of the instrumentation and software the class was able to use because of the IRIS facilities.

Seismic Reflection Processing Workshop

Roger A. Young • *University of Oklahoma*

A 2-day workshop was presented to a class of 17 university students, faculty, and staff from IRIS institutions at the University of Portland on 7-8 June 2005. The workshop was arranged by John Taber (IRIS), Bob Butler (UP), and Cathy Snelson (UNLV) and was assisted by Matt Ralston (of the Parallel Geoscience Corp). This was an interactive, computer-based course of instruction in fundamentals of seismic reflection processing. It was designed to extend the understanding of principles taught by lectures in an introductory college course in seismic exploration.



The course objective was to come to an understanding, through a hands-on processing experience, of the consequences of model simplifications and mathematical assumptions imposed on the real earth during the processing of seismic data. Course notes were contained within the book, *A Lab Manual of Seismic Processing* (EAGE, 2004). Each student received his own copy. The book included an attached CD-ROM containing the complete Seismic Processing Workshop (SPW) software package used in the workshop and keyed to the workshop seismic data set, the seismic data set itself, and all intermediate processing results generated in the Lab Manual.

Instruction consisted of a sequence of 12 labs taking students from trace gathering through semblance velocity analysis, NQ correction/velocity analysis iteration, and post-stack time migration. Morning and afternoon computing sessions were supplemented by an evening discussion of the classical understanding of the response of a thin-bed (the Widess model) contrasted with new insights from spectral decomposition methods.

IRIS and PASSCAL INTERN

Aaron Hirsch • *University of Nevada, Las Vegas*

IRIS INTERN

The summer after my junior year, I had the great opportunity to participate in the IRIS summer internship. I worked with Dr. Catherine Snelson at the University of Nevada Las Vegas. I was able to work and learn about seismic studies and instrumentation. Before this internship, I had no experience with anything remotely close to seismology. From that moment, I was hooked. I am now a graduate student at the University of Nevada Las Vegas with Dr. Cathy Snelson as my advisor. Without



this internship, I would not be where I am today and I would not have realized by true passion in geology. I love where my life and career are going and this could not have been accomplished with this IRIS internship.

PASSCAL INTERN

It is ironic that I am the first to be both an IRIS intern as well as a PASSCAL intern. I am currently in Socorro, NM at PASSCAL working with every seismic instrument imaginable. I am learning to trouble-shoot, test, experiment, field-deployment, data-analyze, and program all of the instrumentation as well as the sensors. I have and continue to learn a significant amount about seismology, the instrumentation involved, and all the inner-workings of PASSCAL. I have also developed many friendships here that will continue throughout my career

in seismology. The associated picture is not of me on any experiment because all of my field photos are at UNLV. The photo is of me, extremely happy, and doing what I love and that is what I hope this 1-pager has conveyed. I truly appreciate everything that the IRIS-PASSCAL internship has done for me. I hope that future interns have the same experience that I was able to have. Thank you.



Seismology Education Programs at the University of Portland

Robert Butler • *University of Portland*

Seismology is a cornerstone of three education programs at the University of Portland. IRIS software and teaching resources are used extensively in all these educational programs.

University courses have been developed for non-science majors. Three courses (Earth Systems Science; Natural Hazards of the Pacific Northwest; Introduction to Marine Science) include seismology as a fundamental component. The Earth Systems Science course is required for undergraduate majors in the College of Education and we seek to inform these students about ways to include seismology in their future K-12 teaching. Seismicity and earthquake hazards in the Pacific Northwest are a particular focus in the Natural Hazards of the Pacific Northwest course.

A public seismology display is being constructed in the lobby of the largest classroom building on campus. This display will feature the AS-1 seismometer as well as real-time displays of world and Pacific Northwest seismicity and earthquake information.

Seismology education programs have been constructed for K-12 teachers. A one-day workshop on Earthquakes and Tsunami for teachers in Portland Public Schools was organized for June 20, 2005. This workshop will capitalize on heightened public awareness about earthquakes and tsunamis in the wake of the Indian Ocean tsunami and the tsunami hazard in the Pacific Northwest. "Teachers on the Leading Edge" is an NSF-sponsored field-based teacher professional development program designed by a collaboration of university Earth scientists and science education specialists, USGS scientists, and K-12 science educators. The inaugural August 5 – 20, 2005 program will feature a field-based and problem solving investigation of active continental margin geology to provide a regional geologic sense of place and an understanding of how plate tectonic processes have shaped Pacific Northwest geology. Program themes include: (1) Convergent margin processes from great earthquakes to continent building through volcanism and accretion; (2) Earth System Science using the John Day Fossil Beds to investigate the 30 million year record of faunal and floral succession and paleoclimate changes; (3) Geophysical studies that illuminate the geology beneath the tree-covered landscape and provide an introduction to anticipated EarthScope discoveries of continents in motion; and (4) Geologic hazards as wondrous but not mysterious aspects of living on the leading edge of our continent. Seismology is a critical framework member for three of these four program themes.



Roots of Sitka spruce trees that subsided into the intertidal zone during the 1700 AD Great Cascadia earthquake.



Brian Atwater (USGS Seattle) pointing out tsunami sand deposit from the 1700 AD Great Cascadia earthquake in the banks of the Lewis and Clark River near Ft. Clatsop, Oregon.

Influence of IRIS on the Construction of a College-Level Seismology Course

Michael Wyession • Washington University, St. Louis

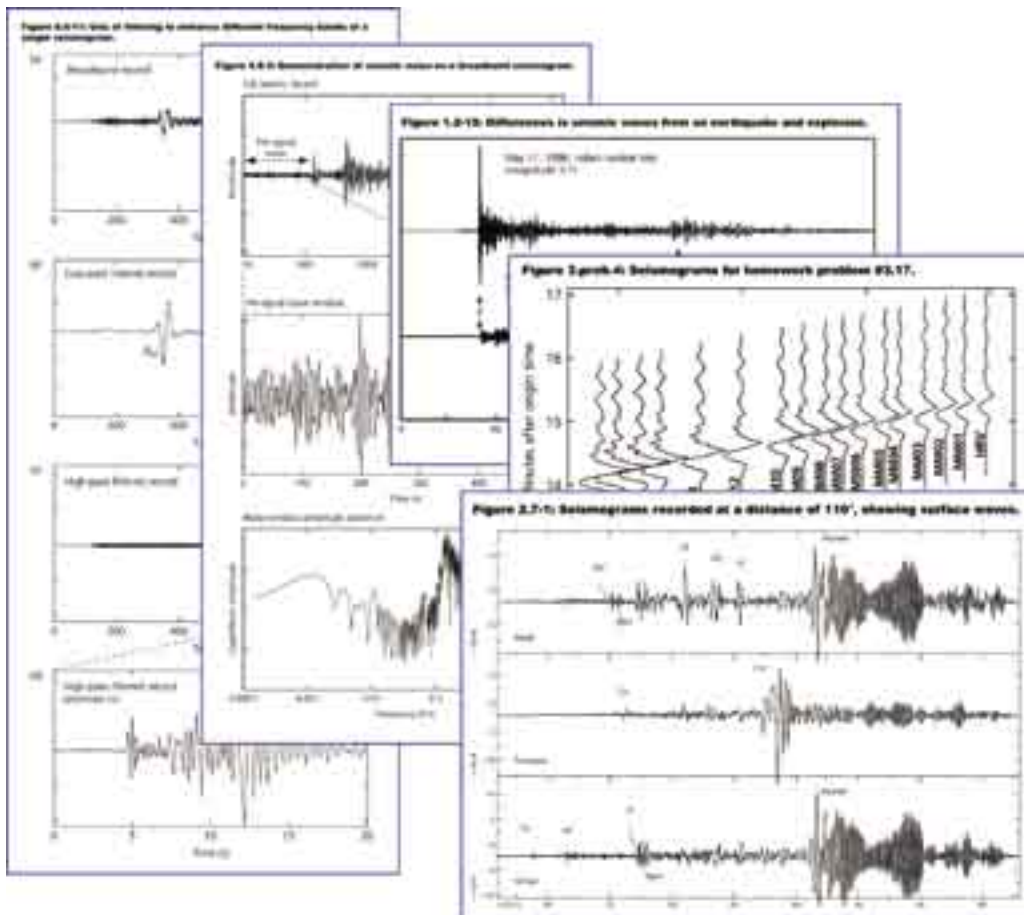
Seth Stein • Northwestern University

IRIS has played an enormous role in the teaching of seismology at an undergraduate and graduate level. In addition to direct E&O efforts, the science that IRIS has facilitated plays a central role in the lexicon of any college course in seismology and geophysics. We have created an undergraduate/graduate course in earthquakes, seismology, and earth structure with an accompanying textbook and web site. Throughout the course, the contributions of IRIS are evident. Of the 600 figures in the book/web site, some are taken directly from IRIS, while many others were created using IRIS data. For instance, a lot of examples drew upon data from the authors' familiarity with the IRIS PASSCAL MOMA experiment (Wyession et al., 1996). Even more figures show research discoveries that were facilitated using IRIS data. There are some parts of a seismology course that deal with the theoretical physical foundations of the science, and these do not have an IRIS influence. However, as soon as data and any applications to the real earth are incorporated, the influence of IRIS becomes immediately obvious. This influence is especially apparent in the areas of seismic rupture, earth structure, seismotectonics, and the societal aspects of seismology. For instance, in most of our examples of seismic waves, digital seismograms were obtained from the IRIS DMC and then incorporated into figures in order to best demonstrate the points at hand.

Stein, S. and M. E. Wyession, *An Introduction to Seismology, Earthquakes, and Earth Structure*, Blackwell Scientific, 498, 2003.

Wyession, M. E., K. M. Fischer, T. J. Clarke, G. I. Al-eqabi, M. J. Fouch, L. A. Salvati, P. J. Shore, R. W. Valenzuela, Slicing into the Earth: Seismic mapping with the Missouri-to-Massachusetts broadband deployment, *EOS*, 77, 477, 480-482, 1996.

<http://epsx.wustl.edu/seismology/book/>



A sample of figures from Stein and Wyession (2003) showing the influence of IRIS. Figure 1.2-19 was adapted from an IRIS E&O image, while the rest were created using IRIS seismic data. In addition to figures made using IRIS data, countless more figures, and much of the book text concerning our understanding of the interior of the earth, owe their existence to data obtained, archived, and distributed through IRIS.

Collaborative Teacher Workshops at the Visualization Center at Scripps Institution of Oceanography (San Diego)

Debi Kilb • *University of California, San Diego*

Within the last two years we have initiated an annual teacher workshop at the Scripps Institution of Oceanography's Visualization Center (SIO VizCenter). These workshops are a collaborative effort that included members from multiple institutions and sub-disciplines including: the U.S. Geological Survey (USGS), the Southern California Earthquake Center (SCEC), the Birch Aquarium at Scripps (BAS), Scripps Institution of Oceanography's (SIO's) Institute of Geophysics and Planetary Physics (IGPP), San Diego Supercomputer Center (SDSC), and San Diego State University (SDSU). The Incorporated Research Institutions for Seismology (IRIS) generously provides curriculum materials, posters, books and many of the supplies for these workshops. Based on responses and surveys, there is clearly a need for Earth science teacher workshops in the San Diego region and a clear measurable benefit to IRIS, SCEC and NSF.



Snapshot from the 3D interactive visualization (<http://siovizcenter.ucsd.edu/library/objects/index.php>) of the magnitude 5.4 earthquake on 16 June 2004 near Rosarito Mexico (red diamond denotes the earthquake hpyocenter).

A common problem is that 3D interactive teaching materials are frequently developed without consulting classroom teachers. As teachers' time becomes more and more valuable and the technology rapidly advances, the gap between development and practicum increases. Our annual teacher workshops help to provide a local link between these two communities. Teachers frequently lack the p□

internalized by students. Teaching tools are typically limited by 2D representations (map or cross sectional views) of difficult concepts like fault plans and Benioff zones--features that are far better illustrated using 3-D data that can be manipulated and viewed □

much needed content knowledge for K-12 Earth Science teachers. These workshops give us the opportunity to introduce teachers, and in turn their students, to freeware 3D technological tools that can be used in their own classrooms.



Photos from Hands-on activities at the SIO teacher workshops. From right to left: Human Seismic Wave, Tectonic Plate Puzzle, Graduation Photos, Hands on Our Earth.

One of the beauties of using the VizCenter for these workshops is that the center's wall sized (~9' x 29') curved screen is easily viewable by up to ~40 people. Using the technology available in the SIO VizCenter allows us

to demonstrate the use of 3D interactive visualizations to improve teaching and learning. These products can be ported directly to the classroom with minimal computer expense. Using the technology at our center, we can export the tools to almost any system (Windows NT, Mac OSX, SGI, Sun, PC Windows2000 and PC Linux). This allows access to high quality 3D interactive teaching tools, yet reduces hardware costs for an in-class visualization system to the cost of a low-end laptop (less than \$1,000).

Throughout the years we have also assessed the needs San Diego teachers have for high-tech teaching tools. In our surveys we fou□

unable to administer their machines to download software. Almost all teachers were comfortable with using computers in teaching. Based on the teachers' feedback we can reassess our goals and continually make updates to meet the needs of the participants.

Project SLAM: A Flexible Field Seismology and Earthquake Studies Teaching Module

Matthew J. Fouch, Steven M. Semken • *Arizona State University*

Jody L. Cecil • *Paseo Hills School, Deer Valley Unified School District, Phoenix, AZ*

Steve Cecil • *C-Level Designs, Glendale, AZ*

A current challenge in science education and outreach is to provide students the vital link between scientific information learned in the classroom and the process of acquiring and evaluating new scientific data. The Earth sciences are uniquely positioned to leverage the allure of fieldwork as a driving force behind discovery that can be translated to the classroom with relatively little effort. More specifically, the advent of portable broadband seismometers has led to significant advances in our understanding of Earth's interior, structure, and dynamics. The primary goal of our efforts is to provide students the link between field seismology studies and the classroom from grade 7 to the introductory college level.

We have therefore constructed a series of field seismology and earthquake studies teaching exercises to provide a first step at bridging this gap. This teaching module, named Project SLAM (Seismology Learning and Analysis Module), is publicly available on a web site (<http://slam.asu.edu>), and includes a interactive teaching component as well as downloadable documents for distribution in classes. An example page from the website is shown in the Figure. The project was funded through the IRIS Education and Outreach program.

The exercises in SLAM combine exciting and educational aspects of three areas of Earth sciences research, including the development of field seismology arrays, exploring earthquake activity, and understanding Earth structure. We utilize a multitude of Internet resources to enable a flexible system that can be used for a broad range of grade levels. For example, students work through the process of evaluating various locations in the U.S. for a hypothetical portable seismometer installation. Students are asked evaluate a site's power, noise, accessibility, and safety using several WWW resources including the U.S. Census Bureau, TerraServer, and MapQuest.



Example of a SLAM interactive activity. In this exercise, students learn about the requirements for good field seismometer locations. For purposes of simplicity, we focus on the four primary parameters of power, noise, safety, and accessibility (list items #1-4 in figure). We utilize a multitude of Internet resources to enable a flexible system that can be used for a broad range of grade levels. Students are asked evaluate site parameters using several WWW resources including the U.S. Census Bureau, TerraServer, and MapQuest. Following this introduction, students are either assigned or choose a site from a list (pictures near bottom of figure). These sites were specifically chosen to represent a breadth of possible seismometer locations, ranging from Central Park in New York City to the Mojave Desert in California to farmlands in Idaho. The purpose of providing this range of sites forces students to realize that there is not a single "correct" site; rather, the variability of locations demonstrates that seismometer sites rarely possess excellent parameters for all site factors.

The recently initiated EarthScope program will produce an enhanced level of public awareness and excitement regarding studies of Earth's interior. Some of the activities in Project SLAM are ideal for integration into a broader-scale Education and Outreach component that can enable students and classrooms to help discover appropriate locations for seismometers as USArray marches across the U.S. over the next 10 years.

Fouch, M.J., J.L. Cecil, S. Cecil, and S. Semken, Project SLAM: A flexible field seismology and earthquake studies teaching module, 16th Annual IRIS Workshop, Tucson, AZ, 2004.

The Boston College Educational Seismology Project: Inviting Students Into the World of Science Research

Alan Kafka, Michael Barnett, John Ebel • *Boston College*

Weston Observatory, a research laboratory of the Department of Geology and Geophysics at Boston College, in partnership with the Boston College Lynch School of Education, offers a unique educational opportunity for students, teachers, and their communities to be directly involved with scientific research. This project uses seismology as a medium for inviting students into the world of science research by inquiry-based learning through investigation of earthquakes recorded by seismographs in K-12 classrooms. Seismology is an interdisciplinary science that requires understanding a wide range of scientific concepts, and seismology also teaches students how the natural environment impacts our everyday lives. Thus, seismology offers numerous possibilities for introducing students to the nature of scientific inquiry and to a wide range of important scientific ideas.

It is truly fascinating that it is possible to record earthquakes at great distances using seismographs. In fact, it does not take a particularly complex seismograph to record earthquakes from across the globe. Seismographs measure the pulse of the Earth, and provide direct information about earthquakes, plate tectonics, and the structure of the Earth's interior. Thus, having their own seismograph in the classroom gives students a way of collecting real-world data and making measurements that provide them with an understanding of the interior structure of the Earth and processes by which the Earth changes. The AS1 seismograph, which serves as the classroom seismograph for this work, is ideal for this purpose because it is affordable, records earthquakes quite well considering its low cost, and is relatively simple to install and operate.

We operate AS1 seismographs in classrooms and provide curriculum resources, as well as research exercises, for students in the K-12 schools. The exercises associated with these in-class seismographs teach students not only about seismology and earthquakes, but also about plate tectonics, earthquakes, volcanoes, and mountain building, as well as about how the forces of nature shape the Earth's surface. Furthermore, our seismology curriculum, based on the in-class seismographs, also teaches students about various aspects of physics, such as energy, mechanics, and waves.



Figure 1. Science teacher Joseph Bergin and his students at Garfield Elementary School in Brighton, MA, viewing the seismogram of the magnitude 9.0 Sumatra earthquake recorded in their classroom.

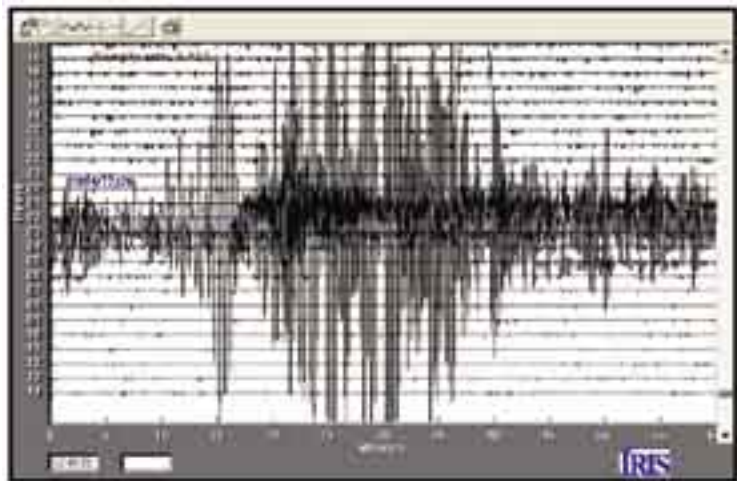


Figure 2. The December 26, 2004, Sumatra earthquake (magnitude 9.0) recorded by an AS1 seismograph operating at Garfield Elementary School.

Seismographs in Schools

John C. Lahr • U.S. Geological Survey Emeritus Scientist



In this picture John is showing Depot Bay, Oregon, Kids Zone students Chyanne Miller and Marcos Garcia (back row) and Javier Jimenez and Harley Seward (front row) how the AS1 seismic system works.

shaking as well as from earthquake-triggered hazards such as landslides and tsunamis.

Due to recent advances in computer technology, today it is not difficult to purchase and operate a seismograph station. Seeing earthquakes recorded on their “own” school instrument, an instrument that they can operate and understand, is far more interesting to students than simply finding a similar seismograph on a web site. This is an effective “hook” to get their attention, especially when a newsworthy event has been recorded

During two vacation trips around the U.S. in 2004, John made stops along the way to help educators operate their seismic stations. John talked with the students and assisted the teachers with their seismometers, as well as helping them with activities associated with the “Seismographs in Schools” program.

USGS Emeritus Scientist Dr. John Lahr continued his affiliation with IRIS and his desire to educate students about earthquakes into his retirement. John worked at the USGS for 32 years and since 1999 he has been active in the IRIS Education and Outreach Program.

The Education and Outreach Program has provided seismographs to more than 100 teachers participating in their Seismographs in Schools program, which is aimed at informing students and the general public about seismology and earthquakes. Seismology provides an exciting and interesting context for many required subjects, including general science, physics, and mathematics. Thus, seismology and earth science can be integrated with concepts that are addressed by the current Education Standards to achieve a better understanding of both. In addition, a basic understanding of seismology is necessary to obtain public support for the mitigation strategies that have been developed to save lives and reduce property damage resulting directly from earthquake



The Magnitude 9.0 Indonesia earthquake of December 26, 2004, was well recorded by many IRIS Seismographs in Schools systems. The record above was recorded at Mattawan High School in Mattawan, Michigan.

Earth and Space Science Professional Development Project

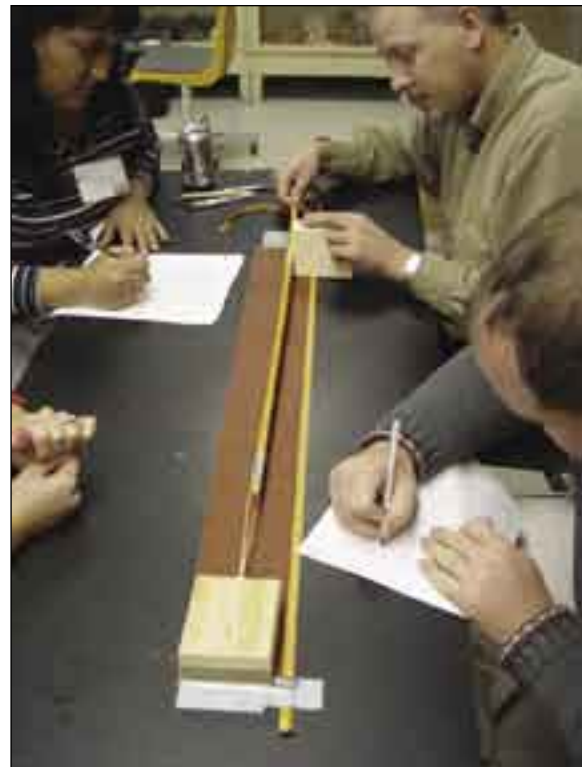
Richard McClure • *Cibola High School, Yuma, Arizona*

As the science department chair at a high school with 2,700 students, staffing highly qualified teachers in all subject areas is a constant and great challenge. This challenge is multiplied by the role of freshmen academies in which teachers are blocked in subject area teams, leaving one period to teach out of the subject area of their expertise. Last year, five teachers, highly qualified to teach biology, were needed to teach seven sections of earth science, effecting over 200 students. Without a major university offering sciences course work in our area these teachers struggle to provide the latest activities for their students. This is where the IRIS Earth and Space Science Professional Development Project has become a cornerstone of teacher development and training in Yuma, AZ.

The concept of the IRIS Earth and Space Science Professional Development Project was developed by Graciela Rendon-Coke, Cibola High School's lead Earth Science Teacher. Mrs. Rendon-Coke has been involved with the IRIS Seismometers in Schools project since 1998. Seeing the need of earth science professional development in our area, Mrs. Rendon-Coke contacted IRIS with the proposal for staff development. Through the efforts of Mrs. Rendon-Coke and Michael Hubenthal of IRIS, the IRIS Earth and Space Science Professional Development Project became a reality in January of 2005.

On January 26-29, 2005, Twenty-four teachers representing seven school districts in Yuma County, Arizona and Imperial County, California met at Cibola High School for training in seismology and plate tectonics. Larry Braile of Purdue University, Aaron Velasco of the University of Texas El Paso, Michael Hubenthal and John Tabor of IRIS provided three days of in services covering over 20 different activities for teachers to bring back to their students. This was followed by a local field trip to Southern California faults, obsidian cliffs and mud volcanoes. The final outcome of the project was the development of a county-wide curriculum which met the Arizona State Science Standards. A compilation of time lines, units and lab activities was provided to all the workshop participants.

From my perspective as a mentor and evaluator of teachers, the effect the IRIS Earth and Space Science Professional Development Project had on students can only be described as dynamic. Teachers who had avoided activities for the first half of the year had their students out of their seats actually doing earth science. Students were being exposed to the latest data available and analyzing this data in the manner of a true scientist. Even the teachers who were highly qualified in the teaching of earth science were renewed and energized, bringing a renewed passion to their students. Most importantly, the students became more motivated to participate in class. This was evident in the decline in the failure rate of earth science students from first semester to second semester.



The IRIS Education Program in Support of the National Earth Science Teachers Association

M. Frank Ireton • NESTA



The IRIS Education Program has assisted the National Earth Science Teachers Association (NESTA) through several efforts, most notably in the cooperative work to develop and publish the Spring 2005 issue of *The Earth Scientist*, NESTA's quarterly journal. With assistance and funding from the IRIS Education Program the Spring 2005 issue featured the first color cover in the journal's history, a number of articles that included IRIS research and classroom activities, and a poster of the 2004 Sumatra earthquake. The issue was completed in time for distribution at the 2005 meeting of the National Science Teachers Association (NSTA) and NESTA Earth and Space Science Resource Day. As a result of this special issue and the high quality, NESTA has seen a growth in membership and in opportunities to work with other professional associations to publish similar themed issues in the future.

The IRIS Education Program has supported the NESTA coordinated Earth and Space Science Resource Day (ESSRD) activities at NSTA national conventions as mentioned above. The ESSRD activities are a cooperative venture led by NESTA and the American Geophysical Union. This event provides a day of focused Earth and space science activities for meeting attendees. Starting with a keynote speaker for breakfast followed by a Share-a-thon—with IRIS participation—and three science lectures. The IRIS Education Program has sponsored one of the science lectures at the last two meetings and is committed for the 2006 meeting in Anaheim, California. The IRIS Education Program has also sponsored speakers at NSTA regional meetings for similar NESTA events.

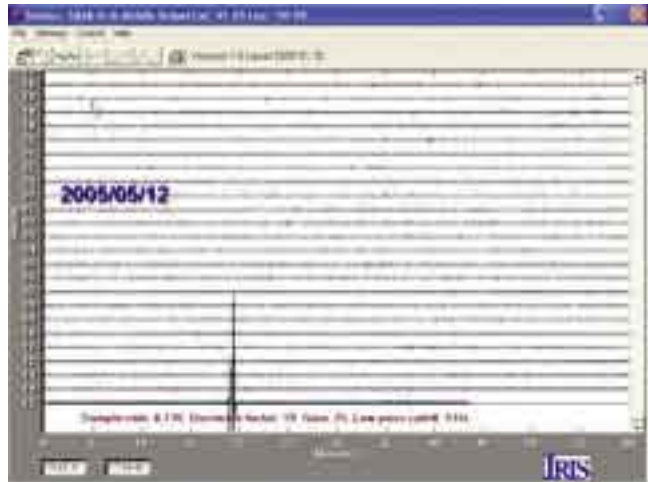
Through out these ventures with NESTA the IRIS Education Program has provided support with a “can do” attitude and enthusiasm. This support has enhanced NESTA programs and provides for a richer experience for NESTA members. NESTA looks for a continued relationship with the IRIS Education Program.



Impact of a School Seismograph on a Rural Illinois Middle School: Bringing Real Time Recordings Into the Classroom

Karen Urick • Erie Middle School, Illinois

As a participant in the IRIS AS-1 Seismographs in Schools' project I have been able to bring earthquake seismographs into the classroom. On several occasions we saw an earthquake occurring on our seismograph before it was reported in our local news. I learned about this project while attending a workshop at a National Science Teachers Association Meeting. I received a free seismograph for my classroom. This seismograph came with technical support that made it possible to use. Teachers are busy people and do not have time to figure out everything for themselves. Mr. John Lahr, a retired seismologist with the USGS, visited my school in the fall of 2004 and assisted me in getting it set up. In November of 2004, IRIS provided financial support for me to attend the regional meeting of the NSTA in Seattle, Washington for additional training. In my 19 years of teaching science I have never had something as hands-on as the seismograph that has impacted my students.



With the e-mail assistance of Mr. Lahr, my building principal and the district computer tech, I was able to connect my seismograph to the district website (<http://www.erie1.net/>). Listed below are two comments I just received today regarding a series of Icelandic earthquakes:

"Way cool!"

"I just wanted to say thanks on all the work you do for this project. I myself really enjoy the info you pass along. It is a neat learning experience also."



The students check the seismograph every day. When seismic waves are detected the first thing students want to know is where it is from and how large it is. We use the seismograph extensively in our earthquake unit. Using a recent seismogram the students measured the Richter magnitude and the distance the earthquake was from our school. We maintain a world map in our classroom with pictures of each seismogram we have recorded posted by each location of the earthquake. In our plate tectonics unit we were to visually determine how scientists determine plate boundaries by looking at our own map. The local paper took an interest after the Sumatra Tsunami on December 26. They printed an article on our seismograph and gave IRIS credit for sponsoring the program.

<http://qconline.com/qcn.com>

Seismographs in Schools: Shaking Things Up in the 5th Grade

Jerry Cook • Phoenix Country Day School in Paradise Valley, AZ.

Our school is part of the IRIS “Seismographs in Schools” program. In the beginning of the school year I explain to the students how the seismometer works and place a large world map on the wall of the classroom. The students quickly start to plot earthquakes on the wall map. We get our information from the USGS Web site to plot events. As we plot earthquakes the kids see right away that they are not located randomly. In addition, I print a seismogram for each earthquake and post them on the wall with the location written on each one. As I post the recordings the students get a good feel for how far away the events are. The students do a good job identifying events as “close”, “across the big puddle”, or “somewhere in between”. Close are those events from Arizona, Nevada, or along the plate boundary from the Sea of Cortez to Parkfield. The kids recognize these seismograms as having a relatively small “P”,

a relatively larger “S”, and no clear surface waves. These quakes are frequent and range in magnitude from 3.9 to 5.5. Those events from “across the big puddle” typically have a relatively large “P” no “S” and fairly obvious surface waves. Then there are all the other recordings that don’t fit neatly into either of these two categories. The “somewhere in between” seismographs are usually from South and Central America although we have recorded some from the Caribbean and near the North Pole also.



Jerry Cook’s fifth grade students showing off the seismograph in their classroom.



Picture of Jerry Cook’s fifth grade classroom. Note all of the seismograms hanging on the wall and a layered Earth model activity next to them.

When there is an earthquake within 600 kilometers of the school, I extract and print out the event and have the students estimate the epicenter using S-P times. I always have a stack of maps in the classroom in case an earthquake occurs. They then draw a circle around Phoenix on a photocopied map and make an educated guess where the event happened. They get graded on their math and accuracy of drawing. We then nervously await information from the Internet to see “who was right”!

